NEANDC(J)-160/U
INDC(JPN)-148/L

JAERI-M
91-032

PROCEEDINGS OF THE 1990 SYMPOSIUM ON NUCLEAR DATA

March 1991

(Eds.) Masayuki IGASHIRA* and Tsuneo NAKAGAWA

日本原子力研究所
Japan Atomic Energy Research Institute

JAERI-Mレポートは，日本原子力研究所が不定期に公刊している研究報告書です。
入手の問合わせは，日本原子力研究所技術情報部情報資料課（〒319-11茨城県那珂郡東海村）あて，お申しこしください。なお，このほかに財団法人原子力弘済会資料センター（〒319-11 茨城県那珂郡東海村日本原子力研究所内）で複写による実費頒布をおこなっております。

JAERI-M reports are issued irregularly.
Inquiries about availability of the reports should be addressed to Information Division Department of Technical Information, Japan Atomic Energy Research Institute, Tokai-mura, Naka-gun, Ibaraki-ken 319-11, Japan.

編集兼発行　日本原子力研究所
印　　刷　いばらき印刷㈱

JAERI-M 91-032

Proceedings of the 1990 Symposium on Nuclear Data

(Eds.) Masayuki IGASHIRA* and Tsuneo NAKAGAWA

Japanese Nuclear Data Committee
Tokai Research Establishment
Japan Atomic Energy Research Institute
Tokai-mura, Naka-gun, Ibaraki-ken

(Received February 4, 1991)

The 1990 Symposium on Nuclear Data was held at Tokai Research Establishment of Japan Atomic Energy Research Institute, on November 29 and 30, 1990. This symposium is extended to be inter-regional from previous annual Seminars on Nuclear Data, and was organized by Japanese Nuclear Data Committee and Nuclear Data Center, JAERI. In this symposium, sixteen oral presentations were made on JENDL special purpose files, group constants based on JENDL-3, recent progress of nuclear reaction theories, various topics as well as an invited talk from China. Twenty-eight papers were presented in the poster session. The proceedings contain all the papers presented at the symposium.

Keywords: Nuclear Data, JENDL-3, Special Purpose Files, Evaluation, Group Constants, Measurement, Proceedings

* Tokyo Institute of Technology

JAERI－M　91 － 032

1990年核データ研究会報文集

日本原子力研究所東海研究所シグマ研究委員会
（編）井頭　政之*・中川　庸雄

（1991年2月4日受理）

1990年核データ研究会が，1990年11月29日（木），30日（金）の両日，日本原子力研究所東海研究所で開かれた。今回の研究会は毎年行ってきた研究会を地域シンポジュウムに拡張したもので，シグマ研究委員会と原研核データセンターにより開催された。今回は，中国からの招待講演を始め，JENDLの特殊目的ファイル，JENDL－3の群定数，原子核理論の進展，その他の話題を含めて16件の口頭発表があった。また，ポスターセッションでは28件の論文が報告された。本報文集は，研究会で報告された44件の発表の論文をまとめたものである。

東海研究所：〒319 － 11 茨城県那珂郡東海村白方字白根2 － 4

＊　東京工業大学

Program Committee

Masayuki	IGASHIRA	(Chairman) (Tokyo Institute of Technology, Research Laboratory for Nuclear Reactors)
Yujiro	IKEDA	(Japan Atomic Energy Research Institute, Department of Reactor Engineering)
Tomohiko	IWASAKI	(Tohoku University, Faculty of Engineering)
Koji	OISHI	(Shimizu Construction Co. Ltd., Institute of Technology)
Norio	KISHIDA	(Century Research Center Corporation, Engineering Division)
Masayoshi	SUGIMOTO	(Japan Atomic Energy Research Institute, Department of Physics)
Yutaka	NAKAJIMA	(Japan Atomic Energy Research Institute, Department of Physics)
Tsuneo	NAKAGAWA	(Japan Atomic Energy Research Institute, Department of Physics)
Kazuki	HIDA	(Toshiba Corporation, Nuclear Engineering Laboratory)
Junji	YAMAMOTO	(Osaka University, Faculty of Engineering)

プログラム委員会

井頭　政之（委員長）（東京工業大学原子炉工学研究所）
池田裕二郎　（日本原子力研究所原子炉工学部）
岩崎　智彦　（東北大学工学部）
大石　晃嗣　（清水建設㈱技術研究所）
岸田　則生　（センチュリリサーチセンタ㈱科学システム部門）
杉本　昌義　（日本原子力研究所物理部）
中島　　豊　（日本原子力研究所物理部）
中川　庸雄　（日本原子力研究所物理部）
肥田　和毅　（㈱東芝原子力技術研究所）
山本　淳治　（大阪大学工学部）

Contents

目　　次

1. Program of 1990 Symposium on Nuclear Data

Date : November 29 and 30, 1990

Place : Meeting room in the JRR-1 building of Tokai Research Establishment, JAERI

[November 29 (Thursday)]

Speakers

10:45 - 10:50 Opening Address (JAERI) M. ISHII

10:50 - 11:55 Topics-1 Chairman: (JAERI) Y. KIKUCHI

Nuclear data activities in China

(IAE) Cai Dunjiu (60m)

11:55 - 13:00 Lunch

13:00 - 15:00 Special Purpose Files Chairman: (Toshiba) M. KAWAI

Present status of JENDL special purpose files

(JAERI) T. NAKAGAWA (20m)

JENDL activation cross section file

(JAERI) Y. NAKAJIMA (30m)

Present status of evaluation work on photonuclear reaction cross sections (CRC) N. KISHIDA (30m)

Neutron Production Data by (α,n) reaction and spontaneous fission (JAERI) Y. NAITO (30m)

15:00 - 15:10 Coffee break

15:10 - 16:45 Progress of Nuclear Reaction Theories

Chairman: (Kinki Univ.) T. OHSAWA

Review of statistical models for nuclear reactions
(NEDAC) S. IGARASI (60m)

Composite-particle emission in preequilibrium process (JAERI) A. IWAMOTO (30m)

16:45 - 17:30 Topics-2 Chairman: (Data Eng.) N. YAMAMURO

International Cooperation in nuclear data evaluation activities (Kyushu Univ.) Y. KANDA (30m)

The life devoted to nuclear data and reactor physics (Toshiba) T. MURATA (15m)

18:00 - 20:00 Reception (Akogigaura Club)

[November 30 (Friday)]

Speakers

9:00 - 10:30 Poster Session (28 papers)

10:30 - 11:55 Topics-3 Chairman: (Tohoku Univ.) M. BABA

Review of evaluation in the medium energy region
(JAERI) T. FUKAHORI (40m)

Nuclear data activities in ANL (JAERI) S. CHIBA (40m)

11:55 - 13:00 Lunch

13:00 - 14:50 Group constants of JENDL-3
Chairman: (Osaka Univ.) T. TAKEDA

Group cross-section processing method and common nuclear group cross-section library based on JENDL-3 nuclear data file (JAERI) A. HASEGAWA (25m)

One dimensional benchmark test of pricipal fissile nuclides in JENDL-3 (IAPCM) D. Tian (15m)

Analysis on FCA-HCLWR core using JENDL-3 (JAERI) T. OSUGI (30m)

Burnup calculation for the PWR spent fuels by JENDL-3 (JAERI) H. AKIE (30m)

14:50 - 15:00 Coffee break

15:00 - 15:35 Topics-4 Chairman: (JAERI) H. MAEKAWA

Nuclear data relevant to diagnostics design in a fusion experimental reactor (Univ. of Tokyo) T. IGUCHI (30m)

15:35 - 15:45 Closing Address (Data Eng.) I. OTAKE

2. Papers Presented in Oral Session

2.1 Topics-1

2.1.1 Nuclear Data Activities in China

Cai Dunjiu

Chinese Nuclear Data Center,
Institute of Atomic Energy,
P. O. Box 275 (41), Beijing 102413
P. R. China

1. Introduction

Scientific research on nuclear physics started in China during the late 1950's. At that time a research reactor and some accelerators were built in the Institute of Atomic Energy, Beijing, and some nuclear data measurements were made. Nuclear data compilation and evaluation were begun systematically only in 1975, when the Chinese Nuclear Data Center (CNDC) and the Chinese Nuclear Data Coordination Network (CNDCN) were set up in order to meet the requirements for development of nuclear energy, science, and engineering technology. Since China was not an IAEA member at that time, we could get only very few evaluated data from publications abroad and had to do our own evaluations to serve our users. Many experimental and theoretical nuclear scientists were involved in relevant work, including developing theoretical models, writing calculation codes, performing nuclear data evaluation, etc.

This situation has changed since the CNDC established contacts with IAEA / NDS, JAERI / NDC and BNL / NNDC in 1980. Especially in 1984, when the People's Republic of China became an IAEA member, international cooperation and exchange increased between the CNDC and other nuclear data centers. For example, we have participated in international cooperation in the evaluation and compilation of neutron data, nuclear structure and decay data, fission product yields, and charged particle reaction data as well as in some coordinated research programs under IAEA contracts. We obtained entire sets of evaluated neutron data of ENDF / B−4, ENDL, JENDL−2, INDL / V and quite a lot of EXFOR experi-

mental data as well as some programs from IAEA / NDS and OECD / NEA－DB. We have also sent some neutron data evaluated or measured in China to IAEA / NDS and some codes to the NEA Data Bank. It is clear that international cooperation and exchange have promoted nuclear data activities in China and also created a proper channel for us to make contributions to international nuclear data activities.

Hereafter, in accordance with the needs of nuclear data home and abroad, we will do our best to make more contributions in nuclear data activities.

2. Organizations and Objectives[1]

2.1 Chinese Nuclear Data Center (CNDC)

As mentioned above, the Chinese Nuclear Data Center was founded in 1975 by the Ministry of Nuclear Industry. At present, the CNDC has about 30 scientists and a number of support staff, and is equipped with a PDP 11 / 70 and MICRO－VAX－II computers.

The principal task of the CNDC is to function as a national center for generating, collecting, processing and disseminating nuclear data, to provide services to all nuclear data users in China, and to coordinate nuclear data activities on a national scale. So far the CNDC's activities have mainly involved the following aspects :

. working out a country wide, long－term plan on nuclear data measurement and evaluation; arranging and coordinating nuclear data activities of the CNDCN;

. studying and developing nuclear data evaluation methods; coordinating and supervising data evaluators; compiling and evaluating nuclear data;

. collecting and validating data processing programs, reports and recommended data from the network;

. maintaining and developing the Chinese Evaluated Nuclear Data Library (CENDL);

. generating multigroup constants and performing benchmark testing of CENDL;

. maintaining the data base of internationally available nucle-

ar data files; providing selective retrievals and data processing to users;

. providing nuclear data and computer program services; publishing nuclear data reports and other publications;

. convening national nuclear data meetings;

. coordinating cooperation and exchange in the nuclear data field with other national and international nuclear data organizations.

2.2 Chinese Nuclear Data Coordination Network (CNDCN)

The CNDCN is composed of the institutes and universities which are taking up nuclear data measurement and evaluation. It is organized and coordinated by the CNDC. At present, the network has about 20 members. Table 1 shows the 13 main institutions in the network which have participated in the nuclear data activities for many years.

Table 1 Main participants in CNDCN

Beijing	**Lanzhou**
Peking University	Lanzhou University
Tsinghua University	
Beijing Normal University	**Shanghai**
Institute of Applied Physics and Computational Mathematics	Fudan University
Institute of Atomic Energy	Institute of Nuclear Research
	Tianjin
Changchun	Nankai University
Jilin University	
	Wuhan
Chengdu	Wuhan University
Sichuan University	**Nanning**
	Guangxi University

All network members undertake projects under the nuclear data plan, their own capacity, and conditions established by the guidance

of the CNDC. The measured or evaluated data are provided to the CNDC. Of course, all the members of the CNDCN obtain some financial support from the Ministry of Nuclear Industry.

2.3 Working Groups

In order to assist the CNDC in its primary task on the national scale, some working groups skilled in the following specialities were organized :

Nuclear Data Measurement
Nuclear Data Calculation and Theory study
Neutron Nuclear Data Evaluation
Construction of Chinese Nuclear Data Library (CENDL)
Group Constant Generation and Benchmark Testing
Nuclear Data Processing and Computational Program
Nuclear Structure and Decay Data
Charged Particle Nuclear Reaction Data
Fission Product Yield Data
Neutron Resonance Parameter and level Density
Atomic and Molecular Data

The members of these groups come from CNDC and network institutions.
The functions of working groups are :

. To search out the proper way or method to perform a given task
. To hold symposia to exchange experiences or discuss common problems involved in these activities
. To examine, review, and recommend data values from the network.

2.4 Chinese Committee of Nuclear Data (CCND)

To strengthen the guidance of nuclear data activities in China, the Chinese Committee of Nuclear Data was established at the end of 1986.

. It is a professional consultative organization under the leadership of the body with prime responsibility for nuclear data research work in China.

. It attaches importance to the investigation of the urgent demands for nuclear data in atomic energy, nuclear science, and nuclear engineering technology development, as well as for the better understanding of the progress and achievements made in the field of international nuclear data activities.

. It is responsible for the examination of the long－term nuclear data program and phase plans, and offers key task projects and proposals of different kinds to the leading body for consideration.

. It helps the leading body to examine and approve important progress and achievements made in nuclear data research.

. It promotes its own role in such fields as external relations, nuclear technical and academic exchange at home and abroad, and takes vigorous action to promote mutual relations, intercourse, and cooperation with the organizations of like kind at home and abroad.

3. Activities on Nuclear Data Evaluation[1,2]

3.1 Nuclear Data Evaluation

In accordance with the long－term plan on nuclear data evaluation, under the organization by CNDC, a lot of scientists from network institutions have been engaged in the compilation and evaluation of nuclear data, and the research on the evaluation methods. Its contents may be summarized as follows :

3.1.1 Neutron Data for General Purpose

Based on the first version of the Chinese Evaluated Nuclear Data Library (CENDL－1)[3], we are preparing CENDL－2 and will finish it in 1991. The CENDL－2 includes file 1－5 for about 50 nuclides (or elements), which were or are being evaluated by ourselves. The neutron incident energy range is from 10^{-5} eV to 20 MeV. The nuclides include H, D, T, ^{3,4}He, ^{6,7}Li, ^{9}Be, ^{10,11}B, ^{14}N, ^{16}O, F, Na, Mg, Al, Si, P, S, Cl, ^{40}Ar, K, Ca, Ti, V, Cr, Mn,Fe, Co, Ni, Cu, Zn, Zr, Nb, Mo, ^{107,109,N}Ag, Cd, In, Sn, Sb, ^{138}Ba, Hf, Ta, W, Au, Pb, ^{235,238}U, ^{239,240}Pu, ^{241}Am, ^{249}Bk, ^{249}Cf. Among them O, F, (cooperated with LANL and ORNL) ^{241}Am (with

covariance), ^{249}Bk, ^{249}Cf were evaluated also for ENDF / B−6, ^{107,109,N}Ag (including γ production data, in cooperation with JAERI / NDC) for JENDL−3. We have taken part in the international cooperation of FENDL establishment, including the inter−comparisons of BROND, ENDF / B−6 and JENDL−3 for the file 4,5 and 6 of Fe, Cr, Ni and Pb through the comparisons of angle− integrated neutron emission spectra (EDX in CMS) and double differential cross section (DDX in LAB) at 30 and 150 degree deduced from these files with the common corresponding experimental data sets.

3.1.2 Nuclear Data for Special Purposes

a) Nuclear Structure and Decay Data (NSDD)

Initiated by the visiting of Dr. S. Pearlstein, Director of the BNL / NNDC, USA, in 1981, the CNDC has participated in the international effort on NSDD evaluation. Ten mass chains are permanently assigned to China (A = 51−55, 195−198). The Chinese NSDD evaluation group was formed in 1983 and the members are from IAE, Jilin University, Changchun, and the Institute of Nuclear Research in Shanghai.

Up to now, all useful ENSDF codes have been transplanted on MICRO−VAX−II. The data for A = 51−55, 195−198, 170,172 (total of 12 mass chains) have been evaluated and renew of some mass chains started in 1990.

b) Fission Product Yield Data (FPYD)

A group at IAE is engaged in FPYD measurement and evaluation. Before 1981, three versions of document "Evaluated Fission−Product Yield" had been issued.

After 1983, this group devoted itself to establishing the Chinese Evaluated Fission−Product Yield Library. The 1987 version of this library contains data in ENDF / B−5 format for 10 fissioning systems, they are U235T, U235F, U235HE, U238F, U238HE, Pu239T, Pu239F, Pu241T, U233T, Th232F. (T−thermal neutron, F−fast (fission) neutron, HE−14 MeV neutron). The data library on magnetic tape is available from the IAEA / NDS.

At present, this group is working on an improved and more complete data base of experimental data in EXFOR format and is studying methods to derive a best recommended set of fission yield

data, which aim at update the 1987 version data.

Besides, this group has been developing "decay heat production" research in recent years.

c) Charged Particle Nuclear Data (CPND)

The evaluation of the CPND was started in 1975. In 1983, a CPND group was organized. Its members are from the Institute of Applied Physics and Computational Mathematics (IAPCM), Sichuan University, Institute of Nuclear Research in Shanghai and IAE.

Hitherto, the twenty sets of data measured in China have been compiled in EXFOR format and sent to IAEA. The 220 sets measured data (50−1000 MeV) for the reactions induced by proton or heavy charged particles were compiled in EXFOR format cooperated with BNL / NNDC. Some activation cross sections induced by charged particles are being evaluated.

d) Neutron Activation and Dosimetry Data

Combined with measurements (77 reaction channels), the cross sections of (n,γ), (n,n'), (n,2n), (n,3n), (n,p), (n,t), (n,α) for 55 reaction channels have been evaluated.

《Compilation of Evaluation for Activation Cross Section》 −CNDC−89014, INDC (CPR)−16 has been published. The following reactions have been evaluated in an IAEA contract subject : ^{23}Na, ^{58}Fe, ^{59}Co(n,γ); ^{46,47}Ti(n,p); ^{54}Fe, ^{59}Co(n,α); ^{55}Mn, ^{59}Co, ^{115}In, ^{126}I, ^{181}Ta(n,2n) and ^{115}In(n,n'), etc.

e) Photo−Nuclear Reaction Data

The $\sigma_{\gamma,n}$ for D, Be, ^{75}As, ^{95}Zr and ^{127}I have been reevaluated. Together with the EXFOR entries, they have been sent to IAEA.

f) Atomic and Molecular (A+M) Data

The sputtering data for collisions of C, Al, Fe atoms and their ions with H, D, He atoms are being compiled and evaluated. We are also compiling the excitation cross sections of collision for He, Ne, Ar atoms with their ions, the electron impact ionization cross sections for the atoms and ions with high Z and the cross section for K−shell ionization by electron impact, etc.

3.2 Evaluation Method Research[1,2,4−14]

The three evaluation methods were usually used to generate the evaluated data :

. combine and fit available measured data by using least squares method;

. predict cross section by systematics;

. carry out a consistent theory calculation;

The related codes have been or are being developed.

3.2.1 Data Processing Method[4,5]

a) Covariance matrix construction for experimental data using the information about errors in experiments given by authors;

b) Curve fitting a spline fitting program for multi—sets of data has been developed. With which the knots can be optimized, spline order number can be chosen, the correlative data can be fitted and the covariance matrix of the fit values can be calculated; also a universal code is developed. The functions include single parameter combination, curve fitting by using orthogonal Polynomial and Legendre Polynomial as base;

c) Simultaneous evaluation based on spline fitting for multi—curves and Bayes method, several relative reaction cross sections of different nuclides, or all reaction cross sections of a nuclide can be calculated simultaneously, as a result, they are made to be consistent with each other, and the correlation between different reactions and nuclides can be calculated.

d) A code of transforming neutron emission data from ENDF / B—4,5,6 format into DDX or EDX and plotting also are being written.

3.2.2 Systematics Studies

Systematics studies on the excitation functions of the (n,γ), (n,2n), (n,3n) as well as (n,x) (x = p,d,t and ^{3,4}He) reactions have been performed. The parameterized formulae and all the parameters related have been obtained on the basis of the evaporation model with the preequilibrium mechanism and the collected data for A = 25—200 in the neutron energy range from threshold to 25 MeV.

With the formulae and parameters, the excitation function could be predicted more reliable than before for the energy regions or nuclides not measured heretofore.

3.2.3 Nuclear Data Calculation and Nuclear Theory Research[1,2,6−14]

In nuclear data evaluation, theoretical calculation plays an important role. Since the CNDCN was formed, some theorists in CNDCN have been engaged in the study of applications of various kinds of nuclear reaction theories and models, developing computer codes, and performing theoretical calculations for nuclear data values.

The main theories and methods applied to calculations of neutron nuclear data in CNDCN are shown in Table 2.

In recent years, our theoretical research on the nuclear reaction theory,calculation method and parameter and computer codes has been advanced greatly which are as follows :

. For the theoretical calculation of nuclear data on the light nuclei, a set of low rank separable nucleon−nucleon potentials has been constructed, which include different partial waves and tensor force, and has been applied to analyze D(n,n), (n,2n) reactions.

. Some efforts were made in level density parameters[8]. A new set of parameters of the Gibert−Cameron formula and back−shift formula has been gained based on more accurate recently measured data.

. The importance of the discrete level effect is discussed and a calculated framework for including the discrete level in the secondary reaction processes has been presented.

. A review of the optical model analyses in A = 40−60 mass region is given. So− called the anomaly for total cross section at the low energy is being studied[8]. A global review of phenomenological and microscopic optical potential in nuclear data evaluation of 14 elements in the neutron energy range of 0.1−24 MeV has been made. It is concluded that the microscopic optical potential based on the generalized and modified skyrme force which has analytical formalism without any free parameters, has useful value in nuclear data calculation.

. The pre−equilibrium reaction is further studied, such as adding the pick−up mechanism for complex particle (d,t,^{3,4}He) emission to improve the calculations for the (n,α), (n,d) ... reaction cross sections at the high energy region.

. To improve the agreement between the calculated results and experimental data for double differential cross sections, the effects of

the Fermi motion and the Pauli principle were taken into account in the exciton model.

. The quantum mechanical pre—equilibrium of Feshbach. Kerman and Koonin is being studied. The spin—half FKK theory and two components FKK theory have been derived.

On the basis of theories research mentioned above, many codes for the data calculations have been developed. Some of them have been sent to NEA Data Bank. Main ones are :

. MUP2 MUP2[9,10] is the second edition of an unified program for theoretical calculation of fast neutron data for medium—heavy nuclei by using the optical model, Hauser—Feshbach theory with width fluctuation correction (WHF) and pre—equilibrium (PE) statistical theory based on the exciton model and evaporation model. AUJP is an associated code of MUP2 which is used in the automatically searching for a set of optimal optical potential parameters.

Based on MUP2, CMUP code is written to calculate the cross sections of charged particle induced reactions at the energy 3—25 MeV.

. MUP3 MUP3[11] code is developed recently which is an extend code of MUP2 to calculate the neutron double differential cross section.

. UNIFY2 UNIFY2 code[12] was set up recently with the unified treatment of the pre—equilibrium and equilibrium reaction processes with the angular momentum and parity conservations and will be used to calculate nuclear data for structural materials. This code can calculate the double differential cross section for all kinds of particles (charged particles and recoiled nuclei) and γ production data in ENDF / B—6 format.

. FUP1 FUP1 is for fissile nuclides, improved based on MUP2, ASFP is its associated code used to automatically search for optimal fission parameters (including the level density and fission barrier parameters).

The direct reaction components of the inelastic scattering for 3 isolated levels of the residual nucleus by using coupled channel calculation are placed as input. These direct components are added to the calculated compound nucleus cross section and angular distribution.

Some codes have been developed for light nuclides :

. TSD TSD is based on the Faddeev equation for n+D reaction.

. ROP ROP is a unified code of optical model and R matrix calculation. DRM unified code[13] used to calculate the neutron direct inelastic scattering cross section for 1P shell nuclei with optical model and DWBA. These codes will be applied to improve the calculations for ^{6,7}Li.

. In the study of the three－body breaking up reactions, the code for the quasi－free particle scattering was developed to calculate the integral cross sections, DDX and normalization factor at any angular momentum.

Recently, CNDC is engaged in the compilation, evaluation and theoretical calculation for intermediate energy nuclear data (IEND)[14]. Based on our investigation, the nuclear reaction theories which can be easily and realistically used to calculate IEND are as follows : relativistic optical model; relativistic collective deformed DWBA approach; intranuclear cascade model and hybrid－type preequilibrium model. Some microscopic theories for IEND calculation have also been researched. Both phenomenological and microscopic nucleon relativistic optical potentials are studied. The global neutron relativistic phenomenological optical potential (RPOP) based on the available experimental data for various nuclei ranging from C to U with incident energies $E_n = 20－1000$ MeV has been obtained through automatically searching for the optimal parameters. Nucleon relativistic microscopic optical potential (RMOP) is studied by using effective lagrangian based on popular Walecka model. Through comparison between the theoretical results and experimental data, some insight into both the RMOP and RPOP have been obtained. It is concluded that both the phenomenological and microscopic relativistic optical potentials proposed by us can be used for IEND evaluation.

The evaluation of ^{56}Fe(p,n) experimental cross sections (E_p = threshold －1000 MeV) is being done and will be finished soon.

3.3 Multigroup Constant Generating and Benchmark Testing[1,2,15－17]

A group responsible for the generation of multi－group constants and benchmark testing of nuclear data was formed in 1978.

From 1978 to 1985, the main efforts of this group devoted to developing and implementing the computer programs which are as follows :

. RQCS, a program to calculate the multigroup constants for the thermal reactors. It generates the group constants for MUFT and GAM.

. KQCS, a fast reactor multigroup constant program based on the Bondarenko method, this code adjusts group constants to the temperature and composition of the reactor.

. FEONAN, it can be applied to calculate the uncollided transmitted neutron spectra and to check the total cross sections using the Broomstick experiments performed at ORNL. The checks of total cross sections for Fe, O, Na and N of CENDL－1 have been performed.

. NDP, one－dimensional diffusion program, which can be applied to calculate effective multiplication factors, spectrum indexes, and critical dimensions for the reactors;

. TDBDC, two－dimensional diffusion and burnup program, which can be used for fast reactor analysis;

. PETRC, a pertubation reactivity coefficient program, which can be applied to calculate one－dimensional or two－dimensional systems;

. ONEDANT, one－dimensional discrete ordinate Sn program, which uses the Synthetic Diffusion Method (SDM) allowing for effective accelerated convergence.

To meet the urgent needs in nuclear engineering, since 1986 we have processed large amount of the nuclear data for nuclear power, nuclear safety analysis and nuclear engineering design. Through international exchange, we have obtained many very valuable codes from ORNL / RSIC, ANL / NESC and NEA Data Bank, and based on them, we have established a program system used for nuclear engineering. Now we can provide the codes and data for the nuclear science and engineering.

1) Three program systems of group constant generating have been implemented on computer CYBER－825 at IAE. The three codes are AMPX－II, NJOY and MINX which are used in group constant generating and processing for nuclear engineering applications in China.

2) PASC－1[16] was made based on AMPX－II and in cooperation with ECN (Holland). The PASC－1 is composed of AMPX / SCALE group constant module, several transport calculation codes Sn and 1－3 dimension diffusion code CITATION. PASC－1, has been sent to NEADB. This code can be used in the design of reactors. A library including 45 and 25 group constant of 37 nuclides has been processed by PASC－1 for the fast reactor calculations.

3) Based on MINX, the CCCCPS and FRBT code systems[15] have been made for processing the interface of CCCC format library with IDX code. By using the CCCCPS code system, the 50 group constants of 47 nuclides from LIB－IV ABBN data library were processed into 46 group constants for the input of IDX. FRBT was made for 14 benchmark testing calculations. The results from FRBT calculations for 14 benchmark facilities using 46 group library are consistent with those given by CSEWG (U. S. A.).

In cooperation with ECN (Holland), the ECNJEF－1 Library[17] was set up by using NJOY－87.0, CRECTJ5, MILER, NPTXS and XLACS－2. The ECNJEF－1 Library is a 219 neutron group Library from JEF－1 in the AMPX master format. 16 files are included in this Library with 434 elements. Some problems in JEF－1 and related processing codes were met. Most of the solutions for these problems were solved. MILER－ECN version was sent to NEA Data Bank by ECN.

In addition, the theoretical analysis for Be sphere shell neutron multiplication factor is also carried out. This is a cooperation project with U. S. A. and Japan.

Now we can make the benchmark testing for the nuclear data and provide various multi－group constants for the calculations in thermal reactor, fast reactor and fission－fusion reactor and for shielding calculations.

3.4 Construction of Nuclear Data Library and Related Program Library, Management, and Service[1－3,18]

A group in CNDC is responsible for the nuclear data library and the associated program library. At present, the group has the following main tasks :

to prepare and maintain the Chinese Evaluated Nuclear Da-

ta Library (CENDL).

. to get experimental and evaluated nuclear data and computer programs from abroad through exchange.

. to improve or develop the library management, data processing and evaluation program systems.

. to compile the data measured in China in EXFOR format.

. to collect, compile and evaluate atomic and molecular data and establish such a data library in cooperation with the atomic and molecular data working group.

. to provide nuclear data and program services to Chinese users and exchange them with IAEA / NDS and other centers.

. to operate, maintain and manage the computer.

Now, the PDP 11 / 70 and MICRO－VAX－II computers are operated and used in data evaluations, data calculations and library construction successfully; The ENDF / B－6 and EXFOR code systems have been transplanted onto MICRO－VAX－II, so neutron data in EXFOR and data files in ENDF / B4－6 format can be processed; We have set up a complete program systems for nuclear data evaluation and library management.

Development of the code library. Following codes have been stored and / or checked or assessed : 20 codes made by ourselves, ～ 40 codes, used in nuclear engineering, obtained from RSIC (U.S.A.), ～ 100 codes obtained from NEADB (OECD). So far more than 100 codes have been used by the home users.

4. Progress of Nuclear Data Measurement[1,2,19－31]

Nuclear data measurements have been carried out since early in 1960′s in China. Since then some equipments for nuclear data measurement have been built. The main facilities and research subjects are listed in Table 3.

In brief, the measurement program is focused on important nuclear data for nuclear energy and nuclear technology applications, such as neutron induced nuclear fission (including fission cross section, fission neutron number, fission neutron spectra, fission product yields), fast neutron scattering and spectra (including angular distribution of scattered neutrons, double differential cross sections from neutron induced reactions), fast neutron reaction cross sections (including (n,n′), (n,2n), (n,p), (n,d), (n,α) reactions, radiative cap-

ture and γ − ray production data), charged particle reaction data, nuclear structure and decay data, neutron standards, macroscopic experiments, and atomic / molecular data.

Recently we have also participated in the research projects organized by IAEA.

In the recent years, the following measurements have been carried out :

4.1 Fast neutron scattering angular distribution and secondary neutron spectra [1,2,19−23]

. The measurements of scattering angular distributions and double differential cross sections of secondary neutrons on deuterium induced by 13.6 and 15.2 MeV neutrons have been carried out[20]. The results are shown in Figs. 1−4.

. The secondary neutron spectra of Fe, Nb and Bi at 14.2 MeV have also been measured by the associated α−particle TOF technique. The measurements of double differential cross sections on ^{6,7}Li at 14.2 MeV are under way.

. The double differential cross sections of secondary neutrons in the incident neutron energy range 8−13 MeV have been measured for ^{238}U and ^{209}Bi by both the normal and abnormal fast neutron TOF spectrometers at HI−13 tandem accelerator.[21] The normal and abnormal fast neutron TOF facilities are shown in Figs. 5 and 6. The TOF spectra of ^{12}C and ^{238}U induced by 12 and 10 MeV monoenergetic neutrons and the break−up neutrons associated with D(d,np) reaction are shown in Figs. 7 and 8 respectively. The double differential cross sections of ^{238}U and ^{209}Bi at 10 MeV neutron energy are shown in Figs. 9 and 10.

. The small angle elastic scattering cross section of fast neutrons on some nuclides have been measured by using the position sensitive fast neutron spectrometer and associated particle TOF method[22,23]. The detector consists of a long cylindrical liquid scintillator tube (50−100)× Φ(4−5)cm) with end−faces in optical contact with two photo multiplier tubes. The results of the measurements are shown in Figs. 11.1−11.4.

4.2 Double differential neutron emission cross sections of charged particle induced reactions[19,24]

For nuclear level density study, the double differential neutron emission cross sections of (p,n) reactions on ^{59}Co, ^{147}Sm and Mo isotopes have been measured[24]. The nuclear level density of the residual nuclei will be obtained after model theory analysis. The neutron emission TOF spectra, neutron energy spectra and angular distributions are shown in Figs. 12−14 respectively.

4.3 Prompt fission neutron spectra[1,2,19,25]

The prompt fission neutron spectrum measurement is being carried out at the HI−13 tandem accelerator[25]. The experimental arrangement is shown in Fig. 15. The fission chamber is composed of 103 plates of which both sides are coated with ^{238}U, and divided into 8 groups. The total weight of ^{238}U is ~ 5 g. The fission chamber is used as both detector and sample. The TOF spectrum of prompt fission neutrons of ^{238}U induced by 11 MeV neutrons is shown in Fig. 16. The data processing and further measurement are under way.

4.4 Fission product yields[1,2,19,26]

The product yields of U−238 fission induced by 11 MeV neutrons have been measured by means of the Gamma−ray spectrometry and the chemical separation of the fission product elements followed by γ and β counting. 11 MeV neutrons were produced by the D(d,n) ^{3}He reaction at the HI−13 Tandem accelerator. The neutron spectrum was measured with TOF technique in order to estimate the fission events induced by the neutron in the energy range of 2−6 MeV from D(d,np)D reaction. The yields of 39 fission chains have been obtained and the mass distribution curve is shown in Fig. 17. The mass distribution for the fission of ^{238}U with 3.0, 5.0, 8.3 and 14 MeV neutrons have also been measured.

4.5 Cross sections of fast neutron induced reactions[1,2,19,27,28]

The measurements of reaction cross sections induced by fast neutrons using the activation technique are focused on long lived and gas production reactions[28].

The following reactions have been measured : $^{109}Ag(n,2n)\ ^{108}Ag\ (T_{1/2}=127\ Y)$, $^{151}Eu(n,2n)\ ^{150m}Eu(35.8\ Y)$, $^{153}Eu(n,2n)\ ^{152g}Eu(13.33\ Y)$ and $^{159}Tb(n,2n)\ ^{158}Tb(180\ Y)$ at 14 MeV; $^{85,87}Rb(n,2n),(n,p),(n,\alpha)$ and Fe, Co, Ni & $^{115}In(n,p),(n,\alpha)$, $E_n=12-18$ MeV, $^{64}Cu(n,\alpha)\ ^{60}Co$, $^{204}Pb(n,2n)\ ^{203}Pb$ at 14 MeV; $^{23}Na(n,2n)\ ^{22}Na$, Ba(n,2n), $E_n=12-18$ MeV.

The reaction cross sections induced by charged particles have been measured, in the incident energies of 23,19.5,17 & 15 MeV for the V(d,x) reaction and at the incident energy of 17 MeV for Ni(d,x) reaction.

4.6 Radiative Capture cross section[1,2,19,29–31]

. The radiative capture cross sections have been studied with fast and thermal neutrons. The excitation function of $^{12}C(n,\gamma)$ reaction have been measured in the neutron energy range 7−14 MeV. For $E_n=9,11,14$ MeV, the γ−ray angular distributions were measured by an anticoincidence shielded NaI(Tl) spectrometer. The experimental arrangement and the results obtained are shown in Fig. 18,19. For the thermal neutrons, a device to obtain high purity thermal neutron beam has been built and the cross sections of (n_{th},γ) reaction on ^{23}Na and ^{31}P have been measured.

. The neutron capture cross sections of ^{93}Nb, ^{98}Mo, ^{169}Tm & ^{181}Ta have been measured in the neutron energy range 10−100 keV,[29]using ^{197}Au as a standard. The capture events were detected by two Moxon−Rae detectors with graphite converter. The measured result is shown in Fig. 20.3.

. The neutron radiative capture cross sections of Nb, Mo, Tb, Hf, Nd, Sm, Dy, Yb have been measured relatively to that of gold at the neutron energy range ~ 0.7−1.4 MeV, using a large liquid scintillation detector and TOF technique. The measured results are shown in Figs. 20.1−2.

. The angular distributions of discrete γ−ray lines for the interaction of 14.9 MeV neutrons with C,Al,V,Fe,Co,Nb,U have been measured[31]at a pulsed 400 KV CW accelerator using a γ−ray spectrometer. The angular distributions of ^{27}Al, $^{51}V(n,x\gamma)$ reactions are shown in Fig. 20.4.

5. Development for Future

As a national nuclear data center, the CNDC will strengthen its own activities in the near future in the following aspects :

. To develop the CENDL including updating and improving neutron nuclear data evaluation for general purpose, extending the evaluation of nuclear data for special purposes, establishing the atomic and molecular data library, etc.

. To improve and develop the methods for nuclear data evaluation, including the theoretical codes, the evaluation system, and the covariance data treatment, etc.

. To improve and develop the service system to the users, including nuclear data library management and data processing.

. To equip the Micro－VAX－II computer system provided by IAEA to improve the ability and efficiency in processing nuclear data, to make efforts to connect our computer with the international computer network of the main data centers.

. To take further steps to develop the international cooperation with other centers and institutions concerned.

CNDC, on completion of these endeavors, will be in a position to offer higher quality services within China in support of a growing nuclear industry and to play an active role in the international exchange of nuclear data.

Finally, on behalf of CNDC I wish to take this opportunity to express our gratitude to JNDC and JAERI / NDC as well as all old and new friends for their contribution to promote the cooperation with the CNDC in nuclear data activities. I hope the friendship and cooperation between us is growing day by day.

References

[1] Cai Dunjiu et al., INDC(CPR)–011 / GI, p9–32(1988).
[2] Cai Dunjiu et al., Communication of Nuclear Data Progress (CNDP), No.1,6 (1989).
[3] Cai Dunjiu et al., CENDL–1,CNDC–85010, 1986.
[4] Zhou Delin et al., CNDC–85013, 1986.
[5] Liu Tingjin et al., CNDP, No. 2, 58(1989).
[6] CNDC hsj78211–78246(1980) The Selected works on Nuclear Reaction Theories and it's Applications.
[7] Wang Shunuan, CNDP, No. 3, 32(1990).
[8] Su Zongdi et al.,
. Study of nuclear level density for Fermi gas model, to be published;
. J. Phys. G: Nucl. Phys. 14, 1485(1988).
[9] Cai Chonghai et al., CNDP, No. 3, 26–31(1990).
[10] Su Zongdi et al., Chinese Journal of Nucl. Phys. (CJNP), 11, 41(1989).
[11] Yu Ziqiang et al., CNDP, No. 1, 41(1989) & No. 2, 9(1989).
[12] Zhang Jingshang Introduction of UNIFY–2 code to be published.
[13] Zhu Yaoyin et al., CNDP, No. 1, 29(1989).
[14] Shen Qingbiao et al., IAEA Advisory Group Meeting on Intermediate Energy Nuclear Data for Applications, Vienna, Austria, 9–12 Oct., 1990
. Applied nuclear reaction theories in intermediate energy nuclear data evaluations.
. Nucleon relativistic phenomenological and microscopic optical potential.
[15] Liu Guisheng, CNDP, No. 1, 78(1989).
[16] Wang Yaoqing, J. Oppe et al., ECN–89–005(1989); CNDP, No. 3, 58(1990).
[17] Yu Peihua, H. Gruppelaar et al., NFA–LWR–90–02 & 03 (1990); ECN–89–112(89).
[18] Liang Qichang et al., CNDP, No. 3, 56(1990).
[19] Tang Hongqing et al., INDC(CPR)–011 / GI, p33–54 (1988).
[20] Shen Guanren et al., INDC(CPR)–011 / GI, p55 (1988).
[21] Qi Bujia et al., . Double differential neutron emission cross sections of ^{238}U and ^{209}Bi induced by 10 MeV neutrons;
. A new Approach to Solve Break up source neutron interference in secondary neutron spectrum measurement to be published.
[22] Qi Huiquan et al., CNDP, No. 3, 5(1990).
[23] Cao Jianhua, Ma Gonggui et al., INDC(CPR)–011 / GI, p125–139(1988).
[24] Zhou Zuying et al., INDC(NDS)–234 / L p77–89(1990).
[25] Li Anli et al., CNDP, No. 3, 20(1990).
[26] Li Ze et al., CNDP, No. 3, 16(1990).
[27] Zhao Wenrong et al., INDC(CPR)–16(1989).
[28] Lu Hanlin et al., INDC(NDS)–232 / L p33–41(1990).
[29] Xia Yijun, Wang Chunhao et al., INDC(CPR)–011 / GI, p145(1988); CNDP,No. 3, 16(1990).
[30] Mu Yunshan, Li Yexiang et al., INDC(CPR)–011 / GI, p157(88); CNDP, No. 3, 12(90).
[31] Zhou Hongyu, Yan Yiming et al., INDC(CPR)–011 / GI, p172(88); CNDP, No. 1, 17(89).

Table 2 Main theories and methods applied to neutron data calculations in CNDCN

Theory	Target	Institution
Phase Shift Analysis	H,D,T,^{3}He	Fudan University
Faddeev Equation	D	CNDC
R−Matrix Theory		Tsinghua University
Optical Model	^{6}Li,^{7}Li	Jilin University
Hauser−Feshbach Theory		
DWBA		
Quasifree Scattering	^{9}Be	IAPCM
Optical Model	Structural	CNDC
Hauser−Feshbach Theory with	Material	Nankai University
WFC and Exciton Model	fissile	Peking University
Couple Channel Calculation	nuclides	

Table 3 Facilities and research at CNDCN

Main Facilities	Research Subjects
Institute of Atomic Energy	
600 KV CW (200−500 KV)	Fission process study
2.5 MV VDG (0.3−2.5 MV)	Fast neutron spectroscopy
AVF Cyclotron (E_p～3−15 MeV,	Fast neutron reactions
E_d～4−14 MeV, E_α～8−28 MeV)	Radiative capture & γ−product.
HI−13 Tandem (HVEC,3−13 MV ± 1KV,	Nuclear structure and decay
provide p,d,α...heavy ions)	Light & heavy ion nuclear react.
Heavy Water Reactor(15 MW,	Application of nuclear technique
2.8×10^{14}n / sec.cm^2)	Atomic & molecular studies
Swimming Pool Reactor (4000KW)	
Institute of Nuclear Sci. and Tech. of Sichuan Uni.	
CW (400 KV;200 KV,～5 ns)	Fast neutron scattering
2.5 MV VDG (～1 ns)	Neutron capture γ−ray
Cyclotron (ϕ1.2 M,E_d～13.4 MeV)	Charged particle reactions
	Atomic & molecular studies
Peking University (PTNNC)	
4.5 MV VDG (0.3−4.5 MV, 1−2 ns	Nuclear reactions & nucl. structures
provide p, d,α,...Ar)	Nuclear fission
Tandem 2×7 MV (EN−18,0.5−6.5 MV)	Materials science, atomic collision
Tandem 2×1.7 MV (NEC, 5SDH−2)	Heavy ion reaction
Tsinghua University	
200 KV CW	Fast neutron scattering & reactions
Beijing Normal University	
C−W with post helix acceleration	Fast neutron spectroscopy and
(400 KV, 3.16 MH$_z$ ～ 1ns)	γ−production
Lanzhou University	
400 KV CW (3.3×10^{12} n / s)	Neutron activation reaction
Institute of Nuclear Research in Shanghai	
4 MV VDG (NEC,E_p～0.3−4 MV, ± 1KV)	Applications of nuclear technique
Tandem 2×6 MV(indigenously designed)	In−beam γ−spectroscopy
AVF Cyclotron (Φ1.2 M,E_p～3−30	Light ion and charged particle
MeV,d, α,...heavy ions)	nuclear reaction
Fudan University	
2.5 MV VDG	Application of nuclear technique
Tandem 2×3 MV (NEC)	neutron reaction (TOF, activat.)
	Atomic and molecular studies

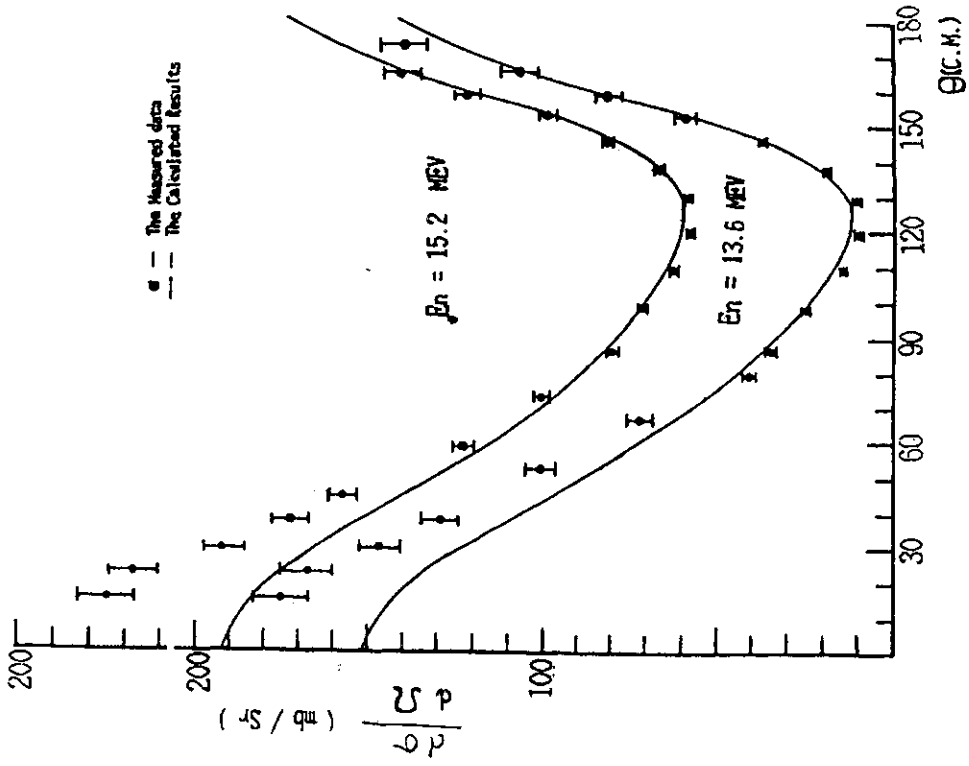

Fig. 2 Comparison of experiment and calculation for elastic angular distributions of deuterium En=13.6 MeV and 15.2 MeV

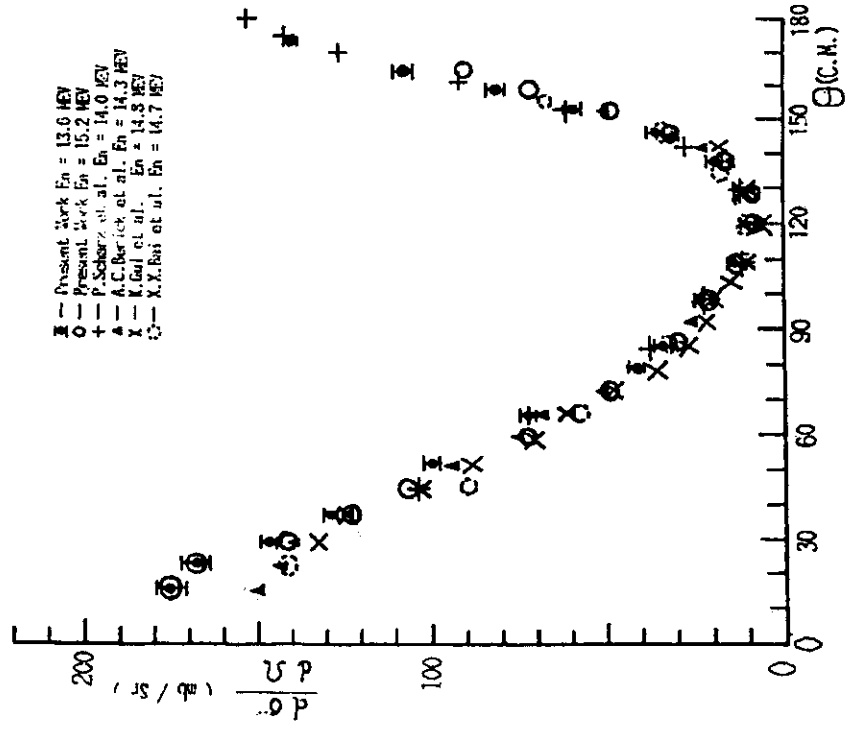

Fig. 1 Elastic scattering angular distribution from deuterium En=13.6 MeV

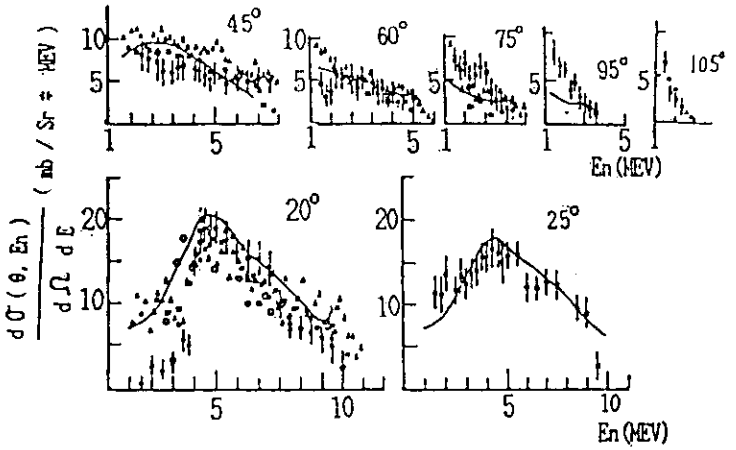

Fig. 3 Double differential cross sections from deuterium.

♦ — present work, En = 13.6 MEV. ⟵ — calcullated result, En=13.6 MEV.
O — H.Jeremie, En = 14.0 MEV. □ — M.Brullmann et al., En=14.1 MEV.
▲ — A.Takahashi et al., En=13.5-14.2 MEV.

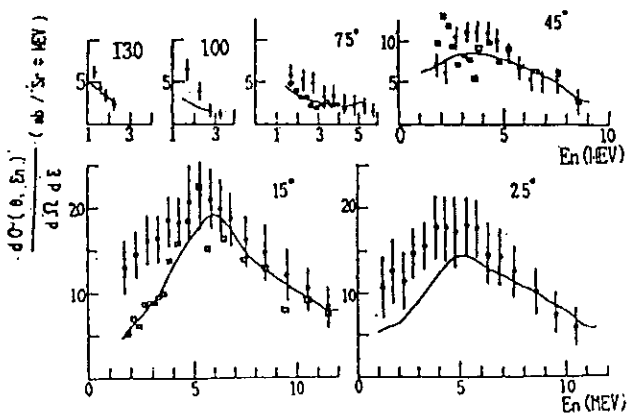

Fig. 4 Double differential cross sections from deuterium.

♦ — present work, En = 15.2 MEV.
□ — X.X.Bai et al., En = 14.7 MEV.

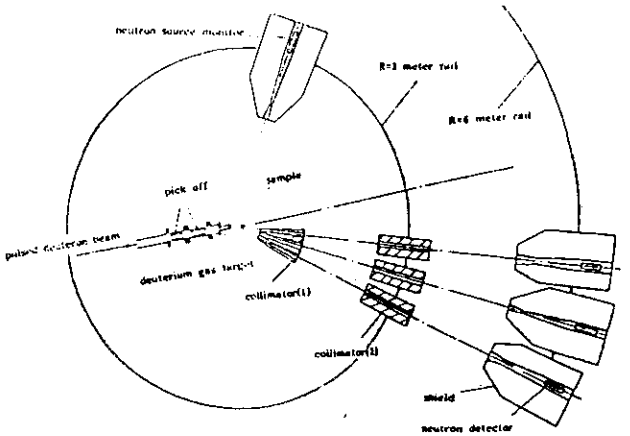

Fig. 5 The normal TOF spectrometer at the HI-13 tandem accelerator

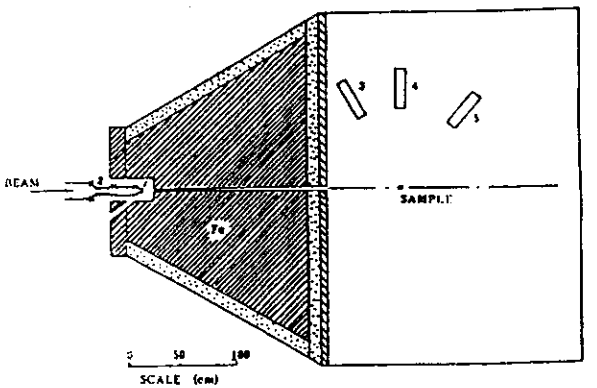

Fig. 6 The modified fast neutrons TOF spectrometer

1- neutron source 2- beam time pick-off
3,4 and 5- neutron detectors
- paraffin + lithium carbonate
- lead

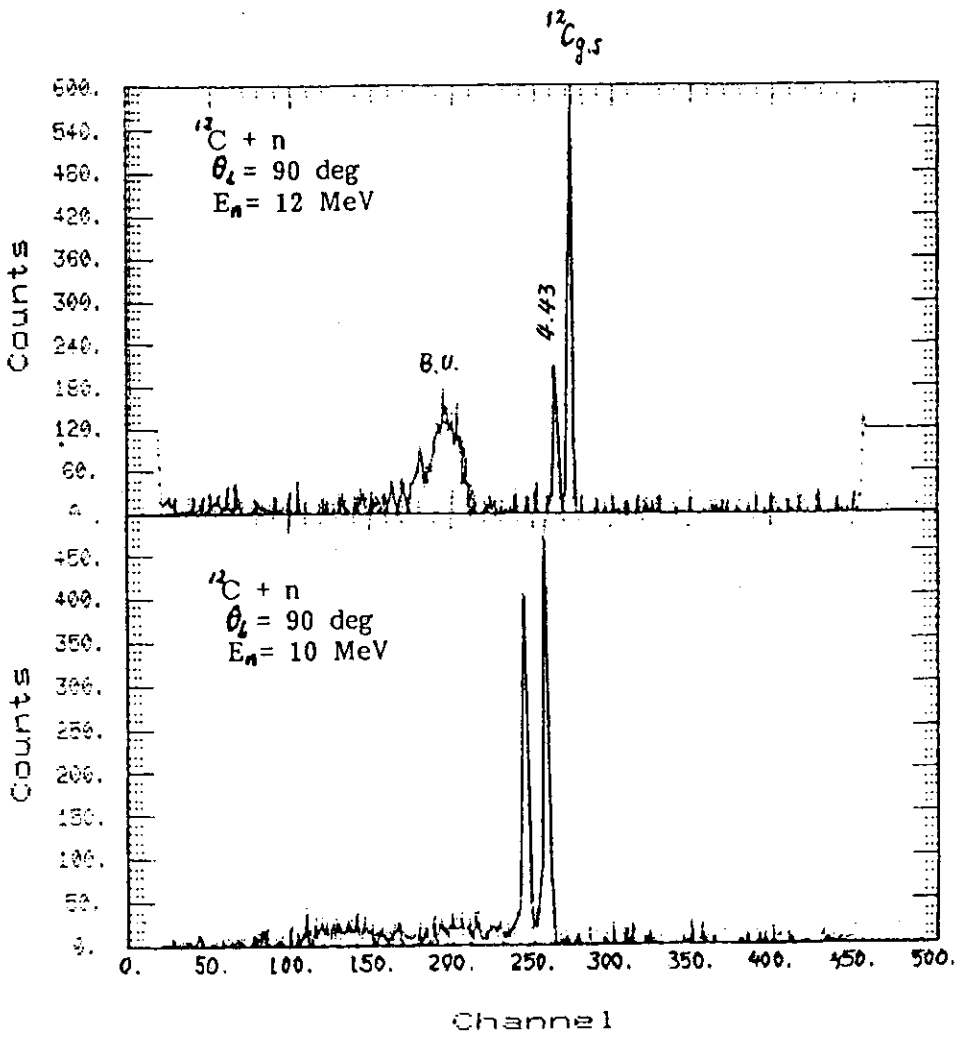

Fig. 7 Carbon scattering spectra for E_n=10 MeV and E_n=12 MeV

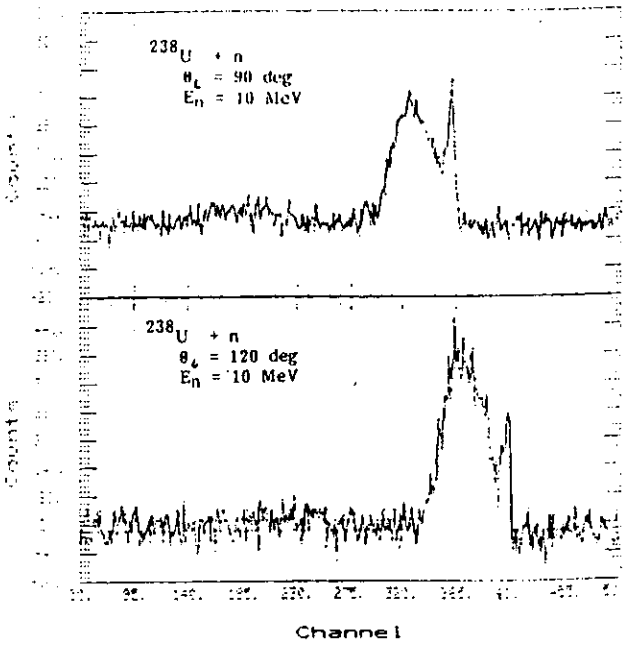

Fig. 8 Net neutron TOF spectra of ^{238}U induced by 10 MeV neutrons

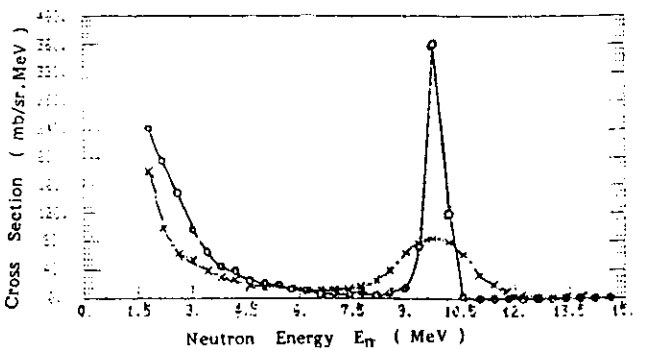

Fig. 9 Double differential neutron emission spectra of ^{238}U induced by 10 MeV neutrons at 45 degrees
—o— by using the normal TOF spectrometer
—×— by using the modified TOF spectrometer

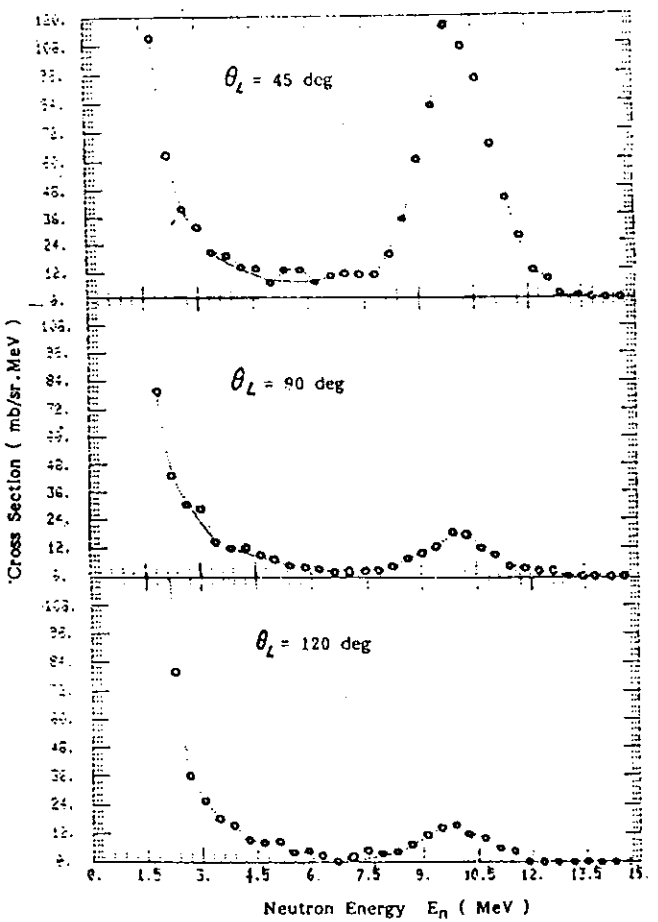

Fig.10 Double differential neutron emission spectra of ^{209}Bi induced by 10 MeV neutrons at 45, 90 and 120 degrees, respectively (by using the modified TOF spectrometer).

differential scattering cross sections for ^{27}Al and ^{16}O

scattering angles θ_{cm}		2.6	3.4	4.9	6.6	8.6
$d\sigma/d\Omega$ (b/sr)	^{27}Al	1.38	1.36	1.36	1.31	1.20
	^{16}O	1.19	1.25	1.07	1.02	1.46

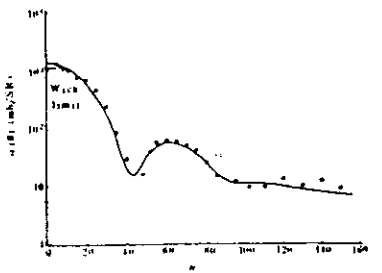

Fig.11.1 The differential scattering cross section of ^{27}Al.

■ Whisnat et al.[7]; — CC calculation.

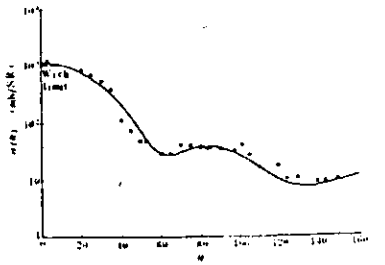

Fig.11.3 The differential scattering cross section of ^{16}O.

+ Present work; • 15 MeV[8]; — SOM calculation.

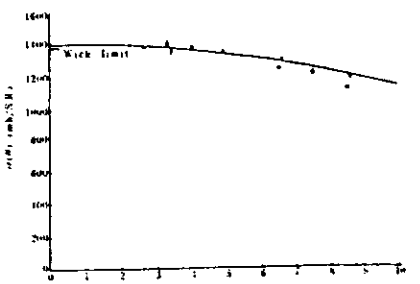

Fig.11.2 The small angle scattering cross section of ^{27}Al.

+ Present work; ◆ 14.0 MeV[8];
• 14.2 Mev [7]; — CC calculation.

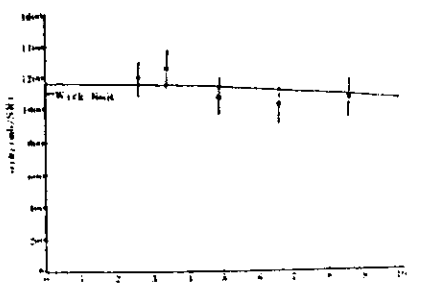

Fig.11.4 The small angle scattering cross section of ^{16}O.

• Present work; — SOM calculation.

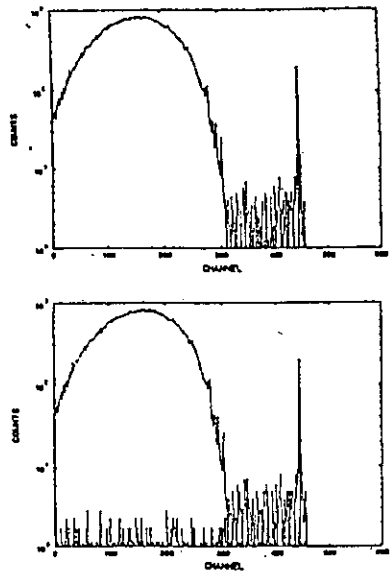

Fig.12.1 TOF spectrum of Mo97(p,n) Tc97 Ep=9MeV at 100 deg. Top: background subtracted Bottom: with and without target

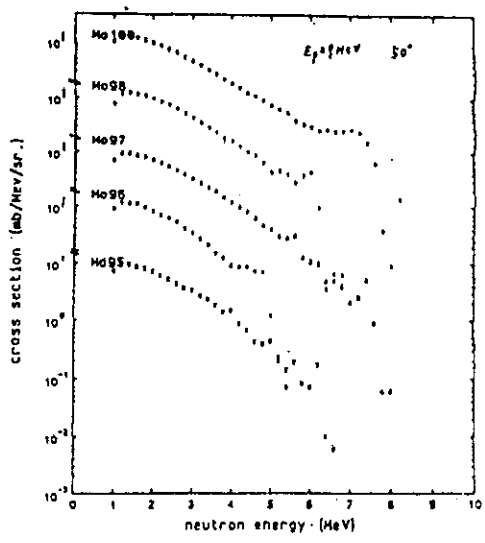

Fig.12.2 Neutron spectrum of Mo95-98,100(p,n)

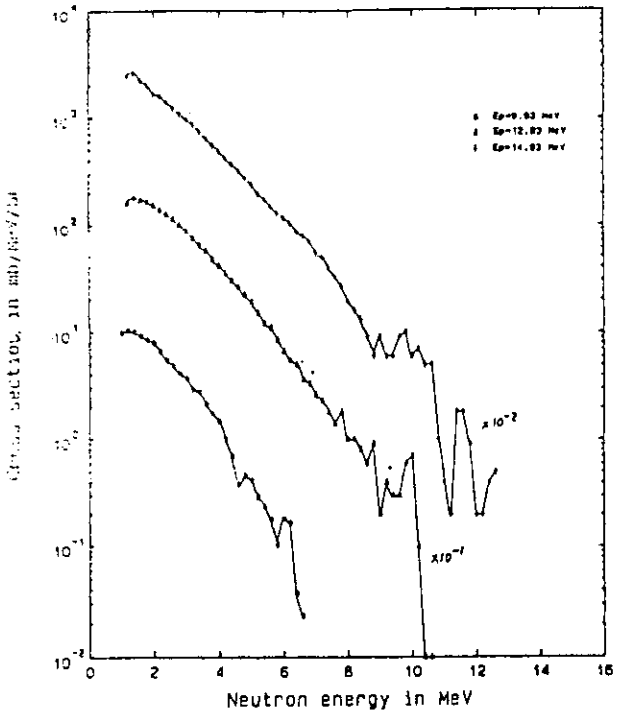

Fig.12.3 Neutron spectrum of Mo95(p,n)Tc95

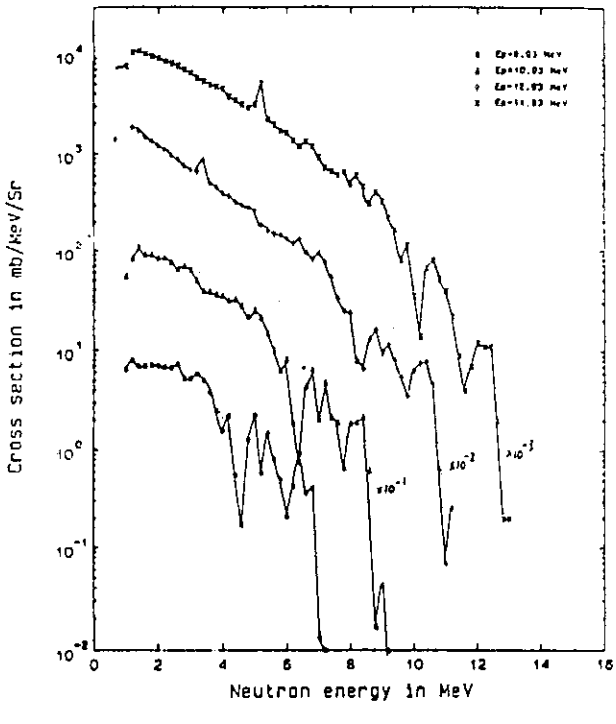

Fig.12.4 Neutron spectrum of Co59(p,n)Ni59

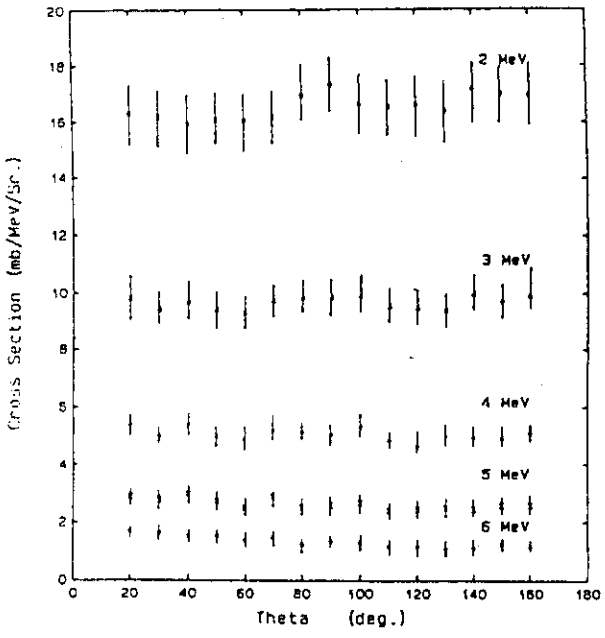

Fig.13.1 Angular distribution of Mo95(p,n)Tc95 at 15 MeV

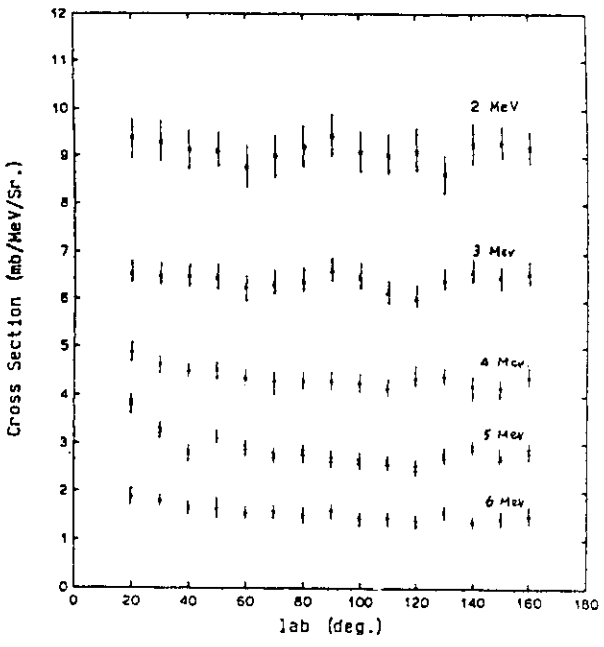

Fig.13.2 Angular distribution of Co59(p,n)Ni59 at 15 MeV

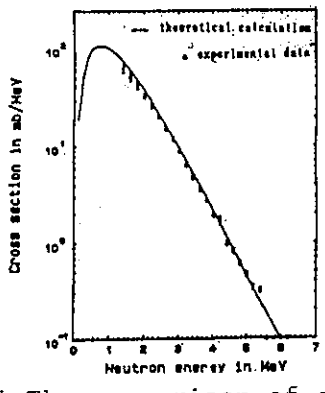

Fig.14.1 The comparison of experimental data with the theoretical calculation for 147Sm(p,n) reaction

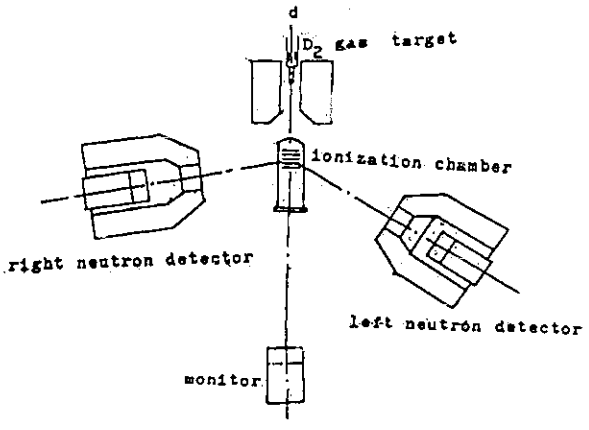

Fig. 15 The experimental set up

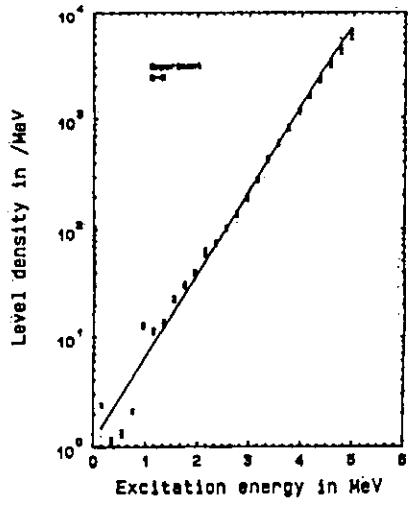

Fig.14.2

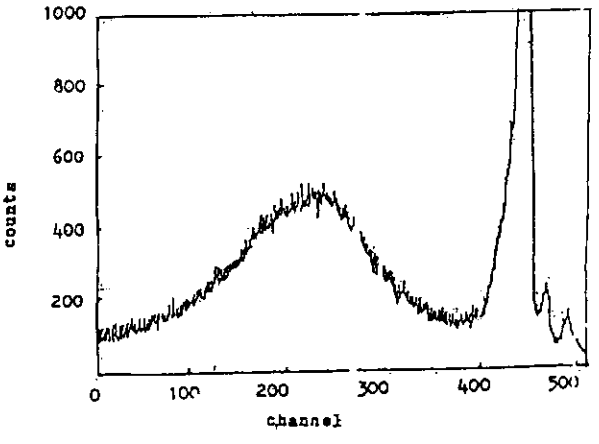

Fig. 16 Fission neutron TOF spectrum at low bias

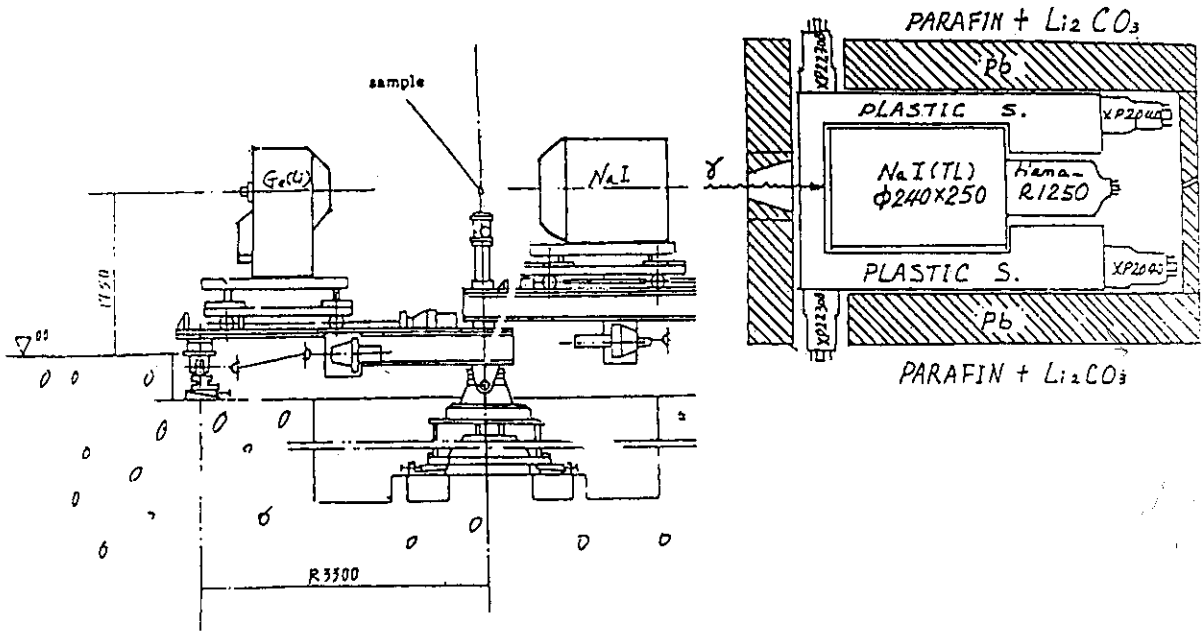

Fig. 18 Gamma-ray goniometer at the HI-13 tandem accelerator

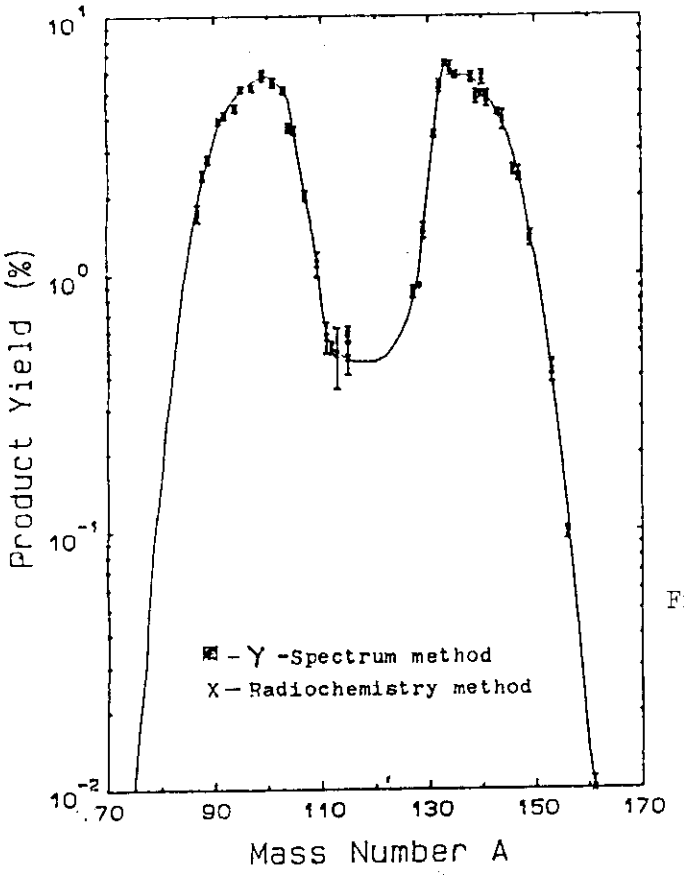

Fig. 17 Mass distribution of U-238 fission induced by 11 MeV neutron

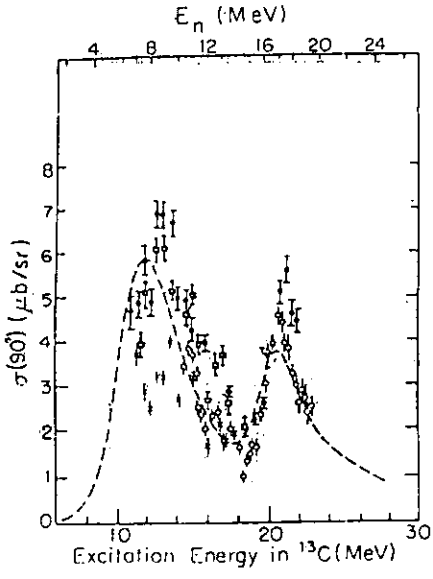

Fig. 19 The present data for the $^{12}C(n,\gamma)^{13}C$ 90° cross section are shown here along with previously published results of ref.7, 8. The direct-semidirect calculation of ref.7 is shown as the dashed line.

φ present data, • TUNL[8]

x TLU, o LANL, and --- DSD calculation[7]

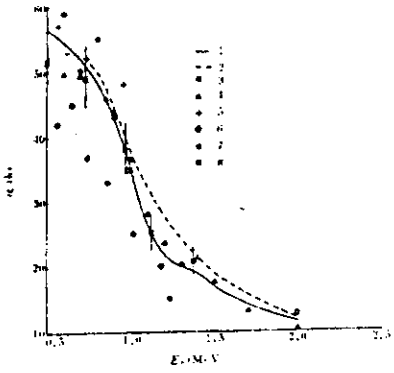

Fig.20.1 Neutron capture cross sections of natural niobium

1 Present work;calc; 2 Reffo(1982); 3 Voignier(1987); 4 Poenitz(1974); 5 Stavisskii(1961); 6 Starvisskii(1960); 7 Diven(1960); 8 Present work:exp.

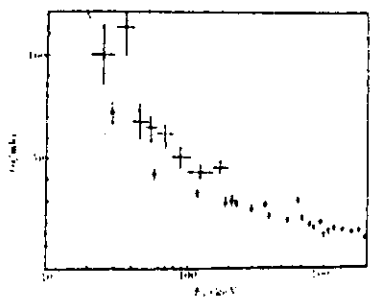

Fig.20.3 The capture cross section of ^{98}Mo

◆ present work; + Musgrove; ● Tyofinov; —— Systematics.

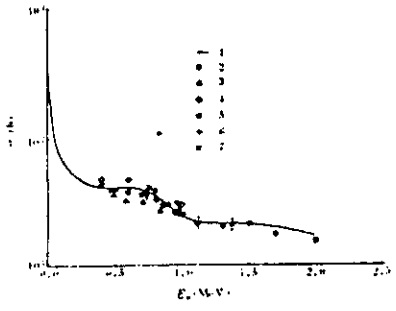

Fig.20.2 Neutron capture cross sections of natural molybdenum

1 Present work;calc; 2 Poenitz(1982); 3 Fricke(1971); 4 Diven(1960); 5 Stavisskii(1961); 6 Belanova(9160); 7 Present work:exp.

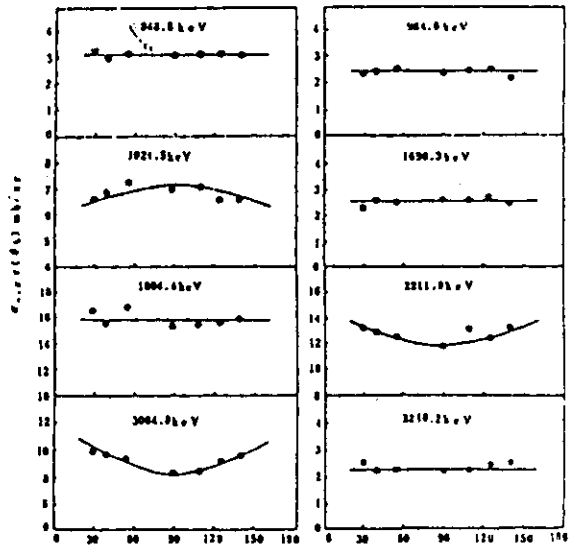

Fig.20.4 The angular distributions of differential gamma-ray cross sections for the interactions of 14.9 MeV neutrons with Al sample

2.2 Special Purpose Files

2.2.1 Present Status of JENDL Special Purpose Files

Tsuneo NAKAGAWA

Nuclear Data Center, Department of Physics
Japan Atomic Energy Research Institute
Tokai-mura, Naka-gun, Ibaraki-ken 319-11

Various kinds of JENDL special purpose files are being made by Japanese Nuclear Data Committee and Nuclear Data Center of Japan Atomic Energy Research Institute. The present status of the files is described briefly. The first version of activation cross section, dosimetry cross section, (α,n) reaction data and gas production files will be completed in 1991.

1. Introduction

It was 1985 when we made a plan of JENDL special purpose files in Japan. In the same year, an ad-hoc committee on special purpose files was organized in the Japanese Nuclear Data Committee (JNDC) and investigated needs of the files in Japan. Finally, nine special purpose files were proposed to store the following data[1].

1) Activation cross sections and decay data of radioactive nuclides.
2) Cross sections and decay data of actinide nuclides.
3) Decay data of radioactive nuclides produced by neutron induced reactions.
4) Dosimetry cross sections.
5) Gas production cross sections for damage study.
6) KERMA factors and DPA cross sections.
7) (α,n) cross sections and thick target yields.
8) Photonuclear reaction data.
9) Standard data for evaluation and experiments.

In 1986, another ad-hoc committee on post-JENDL-3 activities made proposals[2] on the nuclear data activities to be scheduled after the JENDL-3 project. The following are the proposals concerning the JENDL

special purpose files.

a) For short-term activities

Development of special purpose files for nuclear fuel cycle and fusion reactor technology.

b) For long-term activities

New activities of nuclear data evaluations should be started in the area of neutron reactions in the high energy region, charged-particle reactions and atomic & molecular reactions.

According to these proposals, the Working Group on Special Purpose Files was created in 1987. Furthermore, since the evaluation work for JENDL-3 had been finished, structure of the Subcommittee on Nuclear Data in JNDC was changed for the post-JENDL-3 activities in 1989.

At present, we are making 11 kinds of special purpose files listed in Table 1; eight files proposed by the ad-hoc committee on special purpose files excluding the standard data file, two files proposed by the ad-hoc committee on post-JENDL-3 activities and a file for fusion neutronics strongly requested from fusion neutronics community. In the next chapter, the present status of these files will be given briefly except for the activation cross-section and photon-reaction data files which will be explained in this symposium by Nakajima[3] and by Kishida[4], respectively.

2. Status of JENDL Special Purpose Files

2.1 Dosimetry cross section file

This file is to be used for neutron dosimetry in reactors and accelerators. Cross section data were mainly taken from JENDL-3. In the cases of important dosimetry cross sections whose data are not stored in JENDL-3 such as meta-stable state production cross sections, they were adopted from evaluations by Yamamuro[5] for the activation cross-section file, by Sakurai[6] and from IRDF (International Reactor Dosimetry File)[7]. Covariance matrices were taken from IRDF-85 or ENDF/B-VI, because no covariance matrix data have been evaluated for JENDL-3. Two kinds of files in the ENDF-5 format are being prepared; a pointwise data file and a group-wise data file in which cross-section data are averaged in 640 energy intervals with the same structure as IRDF.

The data are given for 42 nuclides and 57 reactions. So far the group-wise data file has been almost completed and various benchmark tests have been performed[8]. A report which describes the JENDL dosimetry

cross section file and results of the benchmark tests is under preparation. The first version of the JENDL dosimetry cross section file will be released in 1991.

2.2 Gas production cross section file

This file will be used for evaluation of damage due to the neutron induced reactions which produce gases. Therefore, it should contain the p, d, t, ^{3}He and α production cross sections of light and structural materials. All of the cross-section data were adopted from JENDL-3 for 23 isotopes or elements; ^{6}Li, ^{7}Li, ^{9}Be, ^{10}B, ^{11}B, ^{12}C, N, ^{19}F, ^{27}Al, Si, Ti, ^{51}V, Cr,^{55}Mn, Fe, Ni, ^{59}Co, Cu, Zr, Nb, Mo, ^{75}As and Se.

The numerical data have been already compiled in the ENDF-5 format. The file will be released in 1991 after adding comment data.

2.3 Actinide cross section file

The purpose of this file is to store the data for estimation of generation and depletion of actinide nuclides. According to the proposals of the ad-hoc committee on special purpose files, the capture, fission and (n,2n) reaction cross section data are stored for 73 nuclides from Pb to Es, and decay data for 127 nuclides from Tl to Fm. The data for main actinides (^{232}Th, ^{233}U, ^{235}U, ^{238}U, ^{239}Pu, ^{240}Pu and ^{240}Pu) are excluded from this file, because their total cross sections are needed to calculate their self-shielding factors. Therefore, the JENDL general purpose file is recommended for these main actinide nuclides.

The compilation of this file has not yet been started. However, JENDL-3 already covers 70 % of cross section data required. The fission and capture cross sections of transplutonium in JENDL-3 have been very much improved from JENDL-2 or other evaluated data libraries.

The present author proposes that decay data should be excluded from the actinide file and should be compiled in a large decay data file together with those for activation cross section file and for other radioactive nuclides.

2.4 (α,n) reaction data file

The (α,n) reaction data are important to estimate neutron production due to the (α,n) reaction of light or structural materials induced by the α particles emitted from heavy nuclides.

Evaluation work has been made by Matsunobu[9] for 11 elements (Li,

Be, B, C, N, O, F, Na, Al, Si and Cu) on the basis of available experimental data and theoretical calculation with ELIESE-3. Evaluated quantities are cross sections of neutron emitting reactions in the energy range from threshold energies to 15 MeV. The angular and energy distributions have been also evaluated. By compiling these data, the first version of JENDL (α,n) reaction data file will be released in 1991. After then, additional evaluation for Ar, Ca, Cr, Mn, Fe and Ni will be needed.

2.5 Decay data file

The original idea of the ad-hoc committee was to make three decay data files; for the actinide file, for the activation cross section file and for other nuclides produced by neutron induced reactions. However, it is much convenient that decay data of all radioactive nuclides are stored in one file. Therefore, the actinide cross section file and the activation cross section file will not have any decay data in them.

The decay data file will contain the data on half-life, decay mode, branching ratio, average β, γ and α energies, intensities of γ- and α-rays in the ENDF format.

The compilation work of the decay data file has not been started. However, Decay Heat Evaluation WG of JNDC has completed the JNDC FP Decay Data File version 2 which contains the decay data for 1078 nuclides in a FP mass region, and will start evaluation of decay data for actinides. We have also ENSDF as a data source. Format conversion codes from JNDC FP Decay Data File and ENSDF to the ENDF format are available. Time schedule of the JENDL decay data file will be decided by taking account of progress of the work in Decay Heat Evaluation WG.

2.6 KERMA factor and DPA cross section file

KERMA factors and DPA cross sections are required for damage study of structural materials and medical use. Iijima, Kawai and members of PKA Spectrum WG in JNDC have studied calculation methods[10] and a format[11] to store related quantities. They developed computer codes for the calculation and finished preliminary calculation for iron[12].

Two kinds of the file are probably made in order to reduce the amount of storage. The first one is a primary file to store reaction cross sections, charged-particle spectra, PKA spectra, and damage energy spectra. Another one is a secondly file for KERMA factors and DPA cross sections which can be calculated from the primary file. The data stored

in the primary file will be made based on JENDL-3 by using charged-particle spectra calculated with GNASH[13] or PEGASUS[14]. The neutron energy range is up to 20 MeV. The candidate materials for this file are ^{1}H, ^{2}H, ^{6}Li, ^{7}Li, Be, ^{10}B, ^{11}B, C, N, O, F, Na, Mg, Al, Si, P, S, Cl, K, Ca, Ti, V, Cr, Mn, Fe, Co, Ni, Cu, Ga, Ge, As, Zr, Nb, Mo, Ag, Cd, Sn, Ba, Eu, Gd, Hf, Ta, W, Au, Pb and Bi.

On the other hand, ESNIT (Energy Selective Neutron Irradiation Test Facility) project[15] started in JAERI, and KERMA factors and DPA cross-section data for 18 elements (Li, C, N, O, Na, Al, Si, K, Ca, Ti, V, Cr, Mn, Fe, Ni, Cu, Mg, Mo) are required in the neutron energy range up to 50 MeV. The evaluation work for this project has been already started and will be completed in a few years.

2.7 File for fusion neutronics

There is a requirement from fusion neutronics people for the file which stores JENDL-3 in the ENDF-6 format by explicitly giving energy-angle correlation in MF6. This work just has been started by Chiba and Yu in the Nuclear Data Center, JAERI. Now, they are compiling ^{93}Nb data as a test case. However, whole schedule of this file has not been decided yet. It will be decided by taking account of discussion at the Specialists' Meeting on Nuclear Data for Fusion Neutronics held in JAERI in this December. Fusion neutronics benchmark tests of JENDL-3 have revealed drawbacks of some nuclides at high energies. Such drawbacks will be modified at the same time.

2.8 High energy neutron data file

Test calculations were made by Hida and Iijima[16] for Fe and ^{235}U, by using GNASH and ALICE[17,18]. The ESNIT project requires also the neutron nuclear data of 19 elements (above mentioned 18 elements + H) in the energy range up to 50 MeV. The evaluation work for ESNIT is in progress by Yamamuro and Chiba. Their work will be finished in a few years. Fukahori[19] made an evaluation of Pb and Bi up to 1 GeV for the ENDF/B-VI special purpose files together with Pearlstein at BNL/NNDC. We have just started the high energy neutron data activity in Japan.

2.9 Charged-particle data file

The JNDC Charged-particle Data WG was organized in 1989. The first job was investigation of data needs. The results of the investigation

were presented by Matsunobu[20] at the 1989 Seminar on Nuclear Data. However, the scope of JENDL charged-particle file(s) has not yet been determined.

3. Concluding remarks

The present status of nine JENDL special purpose files was described briefly. Table 1 summarizes the status of the files including the activation cross section file and the photonuclear reaction file. In 1991, the first versions of dosimetry cross section, gas-production, activation cross section and (α,n) reaction-data files will be completed. In a few years, photonuclear reaction data file and files for the ESNIT project will be finished.

References

1) Iijima S., Katakura J., Nakazawa M., Kawai M., Asami T. and Nakagawa T.; "JENDL Special Purpose Data Files", JAERI-M 87-025, p.230 (1987).
2) Nakazawa M., Hasegawa A., Katakura J., Mizumoto M., Nakagawa T. and Yoshida T.; "Proposals on Post-JENDL-3 Activity Programme for Japanese Nuclear Data Committee", JAERI-M 87-025, p.9 (1987).
3) Nakajima Y. and JNDC Working Group on Activation Cross Section Data: presented in this symposium.
4) Kishida N. and JNDC Photonuclear Data Working Group: presented in this symposium.
5) Yamamuro N.: private communication (1990).
6) Sakurai K.: private communication (1990).
7) IAEA Nuclear Data Section: International Reactor Dosimetry File (IRDF)
8) Nakazawa M. and Dosimetry sub-WG: "Benchmark Test of JENDL-3 Dosimetry File", JAERI-M 90-025, p.103 (1990).
9) Matsunobu H.: private communication.
10) Iijima S. and Kawai M.: J. Nucl. Sci. Technol., 27, 375 (1990).
11) Kawai M.: private communication.
12) Iijima S. and Kawai M.: "Development of the JENDL Special Purpose File for PKA Spectra, DPA Cross Sections and KERMA Factors", JAERI-M 90-025, p.329 (1990).
13) Young P.G. and Arthur A.D.: LA-6947(1977).
14) Iijima S., Sugi T., Nakagawa T. and Nishigori T.: "Program PEGASUS", JAERI-M 87-025, p.337 (1987).

15) Kondo T., Ohno H., Mizumoto M. and Odera M.: J. Fusion Energy, 8, 229 (1989).

16) Hida K. and Iijima S.:" Neutron Cross Section Calculation for ^{56}Fe and ^{235}U in the up to 50 MeV Energy Range", JAERI-M 90-025, p.393 (1990).

17) Blann M. and Vonach H.K.: Phy. Rev., C28, 1475 (1983).

18) Blann M. and Komoto T.T.: Phy. Rev., C29, 1678 (1983).

19) Fukahori T.: presented in this symposium.

20) Matsunobu H.: "Status of the Demand for Charged Particle Nuclear Data", JAERI-M 90-025, p.167 (1990).

Table 1 Present status of JENDL special purpose files

No.	file	size	completion	comment
1	Dosimetry cross section file	57 reactions	1991	
2	Gas production data file	23 nuclides	1991	
3	Activation cross section file	1000 reactions	1991	
4	(α,n) reaction data file	11 elements	1991	
5	Photonuclear reaction data file	30 elements	in a few years	
6	KERMA factor and DPA cross section file	46 elements	not determined	< 20 MeV
	- File for ESNIT	18 elements	in a few years	< 50 MeV
7	Decay data file	not determined	not determined	
8	Actinide cross section file	73 nuclides[a]	not determined	
9	File for fusion neutronics	not determined	not determined	
10	High energy neutron data file	not determined	not determined	
	- File for ESNIT	19 elements	in a few years	< 50 MeV
11	Charged-particle data file	not determined	not determined	

a) This number is the proposal of the ad-hoc committee. Final number will be fixed later.

2.2.2 JENDL Activation Cross Section File

Y. Nakajima
Department of Physics
Japan Atomic Energy Research Institute
Tokai-mura, Ibaraki-ken 319-11

and

JNDC Working Group on Activation Cross Section Data

Evaluation on activation cross sections for the JENDL activation cross section file was initiated in 1987. All elements below z=83 were examined thoroughly from the point of the applications to all kinds of fission and fusion reactors and accelerators and were classified into three groups according to their importance for the applications. About 1,000 reaction cross sections have been evaluated for 37 and 22 elements designated as priority 1 and 2, respectively, up to 20 MeV, will be compiled in the JENDL activation cross section file and the file will be completed by March 1991. In this presentation, evaluation methods are described and evaluated results are compared with experimental data and other evaluations to show that evaluated data are reasonable and reliable.

1. Introduction

After the accomplishment of the JENDL-3 general purpose file[1], the Japanese Nuclear Data Committee has focused its efforts to the evaluation and compilation of different kinds of JENDL special purpose files. As one of them the JENDL activation cross section file was planned in 1987, the

activation cross section file was planned in 1987, the selection of elements and reactions for the file and preliminary evaluation were made in the same year. In 1988 the evaluation on 37 elements designated as the priority 1 was carried out. In 1989 the evaluation on 22 elements designated as the priority 2 was performed. About 1,000 reaction cross sections have been evaluated for 57 elements designated as the priority 1 and 2 up to 20 MeV. The file will be finalized in 1990 and will be completed by March 1991.

2. Selection of elements and reactions

There are already big activation libraries USACT-88[2] in the United States, and REAC-ECN-4[3] and UKACT1[4] in Europe. In this situation we are aiming at more accurate evaluation of important reactions to applications to fission and fusion reactors than aiming at the evaluation as many as reactions in these libraries. All elements below z=83 were examined thoroughly from the point of the applications to all kinds of fission and fusion reactors and accelerators and were classified into three groups according to their importance to the applications. The results of the classification is given in Table 1.

In the selection of the activation cross sections the following items and criteria have been employed:

(1) the half lives of target nuclides: longer than 1 day,

(2) the half lives of product nuclides: longer than 1 day.

(3) the threshold energies: lower than 18 MeV,

(4) the kind of reactions:(n,γ),(n,n'),(n,2n),(n,3n), (n,p),(n,d),(n,t),(n,np),(n,nd),(n,nt),(n,2p), (n,α),(n,^{3}He),(n,nα).

3. Evaluation methods and results

3.1 Elements with z<27(priority 1 and 2), Ga, Ge[5]

The evaluation on all nuclides of these elements with half lives longer than 1 day has been performed with the same nuclear parameters as those used in the JENDL-3 evaluation with a few exceptions. Data for the reactions which have already been evaluated in the JENDL-3 have been employed in the JENDL activation cross section file.

For some nuclides evaluated total neutron cross sections were found to have larger values than measured data below several MeV. Up to now this kind of deficiency has been found for the neutron total cross sections of ^{31}P, S, K. For these nuclides the optical potential which reproduced the measured values was searched and it was found that Moldauer potential[6] with modified parameters was appropriate. In Fig. 1 the total cross section of ^{31}P calculated with this potential is compared with JENDL-3 and the experimental data. With this potential the evaluation of activation cross sections is under way.

For the nuclides whose data have not been compiled in JENDL-3 the new evaluation has been made. These elements are Cl, Ga and Ge. An example of the evaluation on these nuclides is shown in Fig. 2. The present evaluation is in good agreement with experimental data.

3.2 Ni, As, Sr, Y, Ba, Sm, Eu, Gd, Tb, Er, Tm, Hf, W[7]

The evaluation on all stable nuclides of these elements has been performed. As all data needed are available in JENDL-3 for the nuclides which do not have isomeric states, the data in JENDL-3 were employed and compiled in the JENDL activation cross section file. Only branching ratios between the ground state and isomeric states have been calculated with GNASH[8] and then the ground state and isomeric state cross sections have been computed by combining the branching ratios and the total reaction cross section in JENDL-3.

Three examples are shown in Fig. 3 to Fig. 5. The agreement between the evaluated and measured values is satisfactory. From these figures it is proved that the present evaluation is reasonable.

3.3 Cu, Zn, Zr, Nb, Mo, Pd, Ag, Cd, In, Sn, Sb, Dy, Ho, Ta, Re, Os, Ir, Pb, Bi[7]

The evaluation on all stable isotopes of these elements has been performed. All the cross sections which satisfy the criteria described in Section 2 has been newly calculated with the GNASH code. In the evaluation global optical model parameters were used.

For neutrons, a modified Walter-Guss potential[9] was used. Walter and Guss recommended their potential to be applied above 23 in the target mass number and between 10 and 80 MeV in th neutron energy. To apply the potential below 10 MeV neutron energy, the following surface absorption term W_s(in MeV) was assumed between 0 and 20 MeV,

$$W_s = 7.71 - 14.94(N-Z)/A.$$

This was determined so that the calculated non-elastic cross sections agreed with the experimental data within 10 % uncertainty.[10]

For protons, the Perey potential[11] and Walter-Guss potential were used below 10 MeV and between 10 and 20 MeV, respectively.

For alpha particles and deutrons, the Lemos set modified by Arthur and Young[12] and the Lohr-Haeberli potential[13] were used, respectively.

For tritons and ^{3}He, the Becchetti-Greenlees potential[14] was used.

The results of the evaluation on ^{66}Zn(n,p)^{66}Cu is shown in Fig. 5. Experimental data is in good agreement with the present evaluation.

In Fig. 6 the present evaluation of ^{95}Mo(n,p)^{95}Nb is compared with the JENDL-3 evaluation and experimental data. The JENDL-3 evaluation is 10% lower than the present

evaluation and lower than the most measured data. The latest measured data by H.Liskien et al.[15] show no saturation. Although H.Lieskin et al. asserted that there was no contamination of other reactions, this behavior can be explain by the inclusion of the reaction $^{96}Mo(n,d+np)^{95}Nb$ to this reaction, because both reactions produce the same reaction product and H.Liskien et al. measured the cross sections with the activation method using natural targets. In Fig. 7 total $^{95}Mo(n,p)^{95}Nb$ cross sections + a x $^{96}Mo(n,d+np)^{95}Nb$ cross sections(where a is the abundance ratio of the natural element between ^{95}Mo and ^{96}Mo) of the present evaluation is compared with the total $^{95}Mo(n,p)^{95}Nb$ cross sections measured by H.Liskien et al. The measured cross sections are lower than the present evaluation, but the energy dependence is very similar each other and both show no saturation. The same situation exists in the reaction $^{96}Mo(n,p)^{96}Nb$, which is shown in Fig. 8, while the evaluated data are in good agreement with other measured data. This inference may be proved to be true, because the reaction which has no contribution from other reactions shows the saturated cross sections. An example is shown in Fig. 9. In this case the evaluated data are in good agreement with all measured data including the data by H.Liskien et al.

The evaluation on $^{185}Re(n,\gamma)^{186}Re$ is compared with measured data in Fig. 10. The data by Lindner et al.[16] are the cross sections corresponding to the ground state and other two sets of the data are the total capture cross sections. The evaluated values of the ground state cross section reproduced the data by Lindner et al. very well. Therefore the present evaluation is reasonable. To confirm the reliability of the present evaluation the evaluated total capture cross sections of natural Re are compared with the latest measured values by Macklin[17] in Fig. 11. The figure shows that the evaluated data reproduced the data by Macklin very well and the evaluation is reliable. The

present evaluation of the capture cross sections was performed using the CASTHY code[18]. Examples of the evaluation on the cross sections of long-lived radionuclide production are shown in Figs. 12 and 13. The cross sections of $^{206}Pb(n,2n)^{205}Pb$ are in good agreement with measured data. Evaluated values of two cross sections for $^{209}Bi(n,2n)^{208}Bi$ and $^{209}Bi(n,3n)^{207}Bi$ reproduced measured data very well.

4. Compilation format

Evaluated data have been compiled in ENDF/B-5 Format File 10. For the capture cross sections, the data in the resonance region were converted to 70 group cross sections using the CRECTJ5 code[19], were connected with evaluated pointwise cross sections at an appropriate energy, the data in the whole energy range from 10^{-5} eV to 20 MeV were set up and ave been compiled. For other reactions the usual pointwise cross section data have been compiled.

5. Summary

The scope of the JENDL activation cross section file is presented. The evaluation methods are described and a few examples of the evaluated results were compared with measured data. The present evaluated data are proved to be reasonable and reliable.

References

(1) Shibata K., et al.: JAERI 1319(1990).
(2) Mann F.: Proc. Nucl. Data for Science and Technol., ed. Igarasi S., Saikon, Tokyo, 1013(1988).
(3) Kopecky J.: Proc. of the IAEA Specialists' Meeting of Fusion Evaluated Nuclear Data Library(FENDL), INDC(NDS)-223/GF, 62(1989).
(4) Forrest R., et al.: Proc. Nucl. Data for Science and Technol., ed. Igarasi S., Saikon, Tokyo, 1061(1988).
(5) Watanabe T.: Private communication.
(6) Moldauer P.A.: Nucl. Phys., **47**, 65(1963).
(7) Yamamuro N. and Iijima S.: JAERI-M 89-129(1989) in Japanese; Yamamuro N., Iijima S. and Asami T.: To be published in JAERI-M in Japanese.
(8) Young P.G. and Arthur E.D.: LA-6974(1977).
(9) Walter R.L. and Guss P.P.: Proc. Int. Conf. Nuclear Data for Basic and Applied Science, ed. Young P.G., et al., Gordon and Breach Science Publisher, New York, Vol. 2, 1079(1986).
(10)Yamamuro N.: JAERI-M 90-006(1990).
(11)Perey F.G.: Phys. Rev., **131**, 745(1963).
(12)Arthur E.D. and Young P.G.: LA-8626-MS(1980).
(13)Lohr J.M. and Haeberli: Nucl. Phys., **A232**, 381(1974).
(14)Becchetti F.D.Jr. and Greenlees G.W.: "Polarization Phenomena in Nuclear Reactions", The University of Wisconsin Press, 682(1071).
(15)Liskien H., et al.: Appl. Rad. Isot., **41**, 83(1990).
(16)Lindner M., et al.: Nucl. Sci. Eng., **59**, 381(1976).
(17)Macklin R.L.: ibid., **97**, 239(1987).
(18)Igarasi S.: J. Nucl. Sci. Technol., **12**, 67(1975).
(19)Nakagawa T.: Private communication.

Table 1 Priority of materials required for activation file

Z	Element	Priority	Z	Element	Priority	Z	Element	Priority
1	H	1	29	Cu	1	57	La	3
2	He	2	30	Zn	2	58	Ce	3
3	Li	1	31	Ga	2	59	Pr	3
4	Be	1	32	Ge	2	60	Nd	3
5	B	1	33	As	2	61	Pm	3
6	C	1	34	Se	3	62	Sm	2
7	N	1	35	Br	3	63	Eu	1
8	O	1	36	Kr	3	64	Gd	1
9	F	2	37	Rb	3	65	Tb	2
10	Ne	3	38	Sr	2	66	Dy	2
11	Na	1	39	Y	2	67	Ho	2
12	Mg	2	40	Zr	1	68	Er	2
13	Al	1	41	Nb	1	69	Tm	2
14	Si	1	42	Mo	1	70	Yb	3
15	P	2	43	Tc	3	71	Lu	3
16	S	2	44	Ru	3	72	Hf	1
17	Cl	2	45	Rh	3	73	Ta	1
18	Ar	1	46	Pd	2	74	W	1
19	K	2	47	Ag	1	75	Re	1
20	Ca	1	48	Cd	1	76	Os	2
21	Sc	3	49	In	1	77	Ir	2
22	Ti	1	50	Sn	1	78	Pt	3
23	V	1	51	Sb	1	79	Au	3
24	Cr	1	52	Te	3	80	Hg	3
25	Mn	1	53	I	3	81	Tl	3
26	Fe	1	54	Xe	3	82	Pb	1
27	Co	1	55	Cs	3	83	Bi	1
28	Ni	1	56	Ba	1			

Priority 1: 37 elements
Priority 2: 22 elements
Priority 3: 24 elements

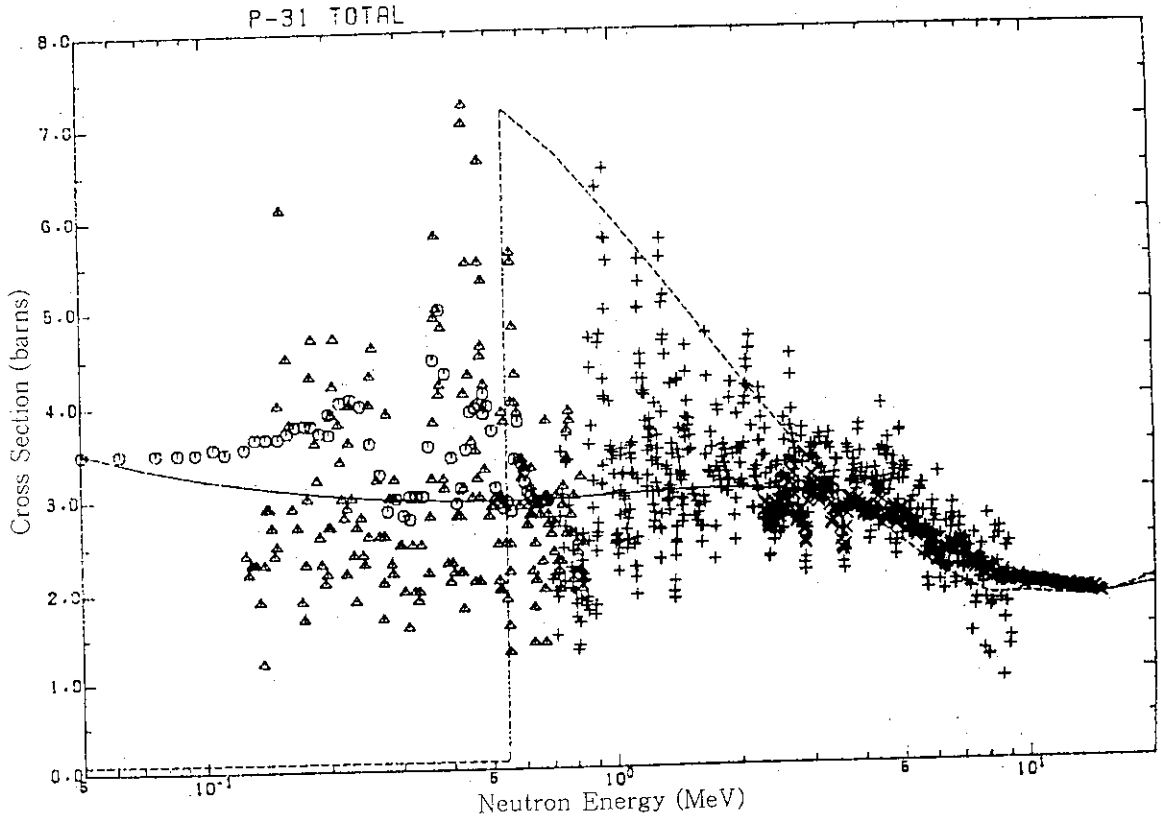

Fig. 1 Neutron total cross section of ^{31}P. Dashed line shows JENDL-3, where the contribution from the resonance regions below 500 keV is ignored in this plot. Solid line shows the neutron total cross section calculated with the Moldauer potential.

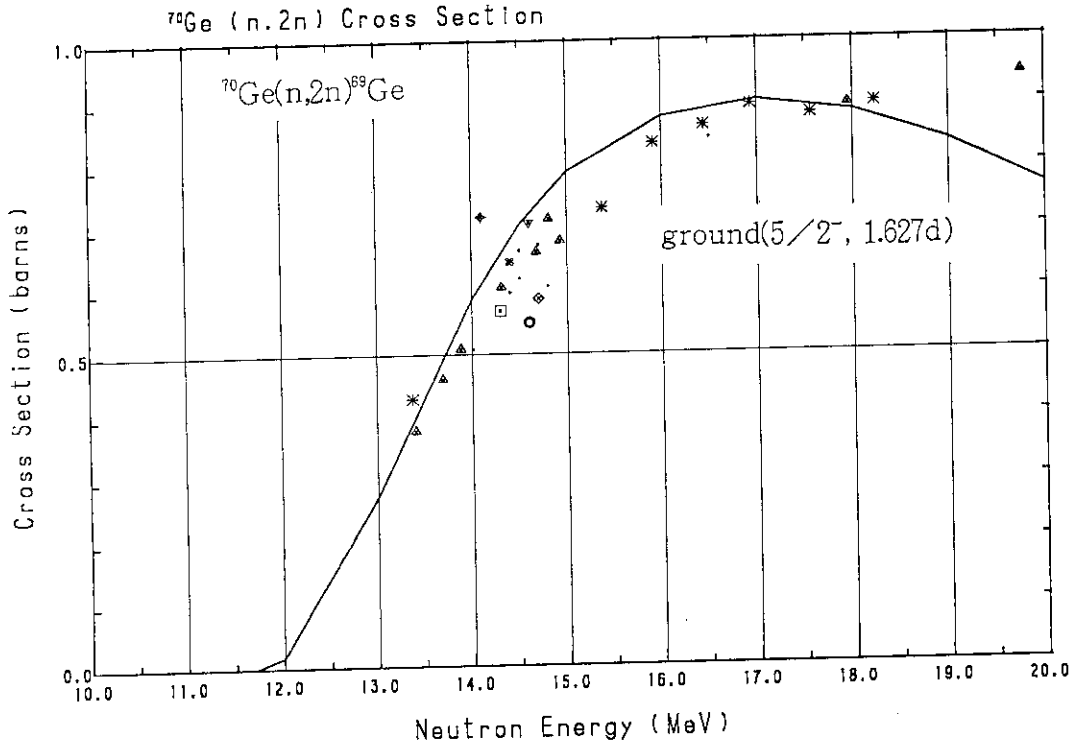

Fig. 2 $^{70}Ge(n,2n)^{69}Ge$ cross section. Line shows the present evaluation.

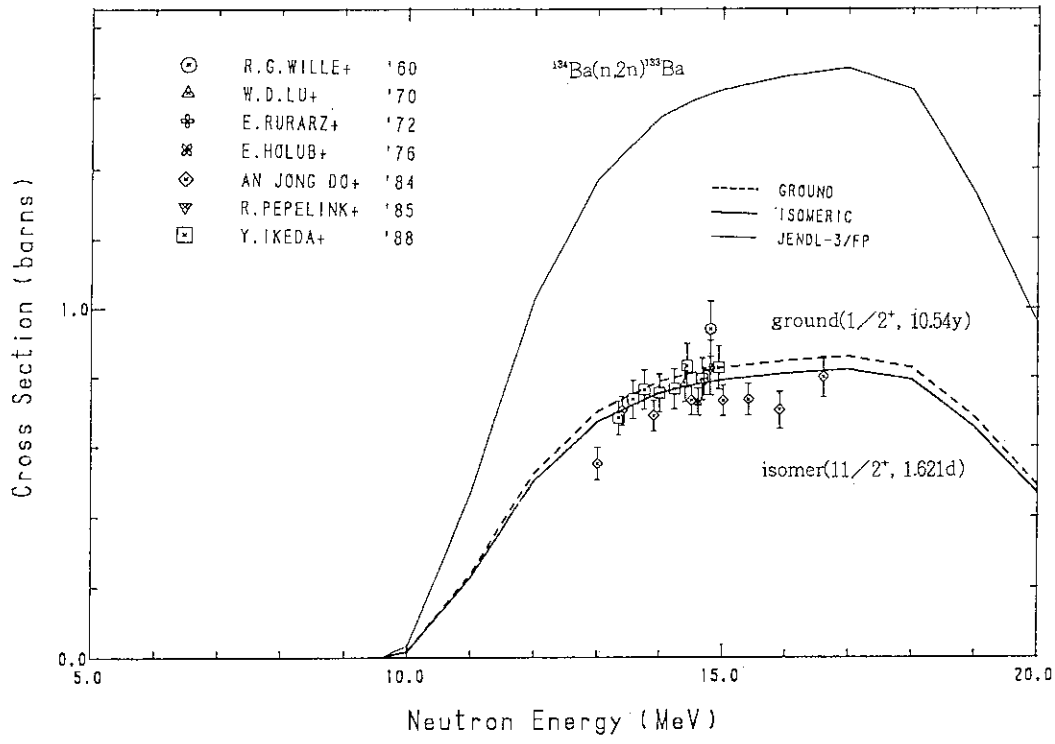

Fig. 3 $^{134}Ba(n,2n)^{133}Ba$ cross sections. JENDL-3 corresponds to the total (n,2n) cross section. Dashed and thick solid lines represent the present evaluation. Measured data are shown only for the isomeric cross sections.

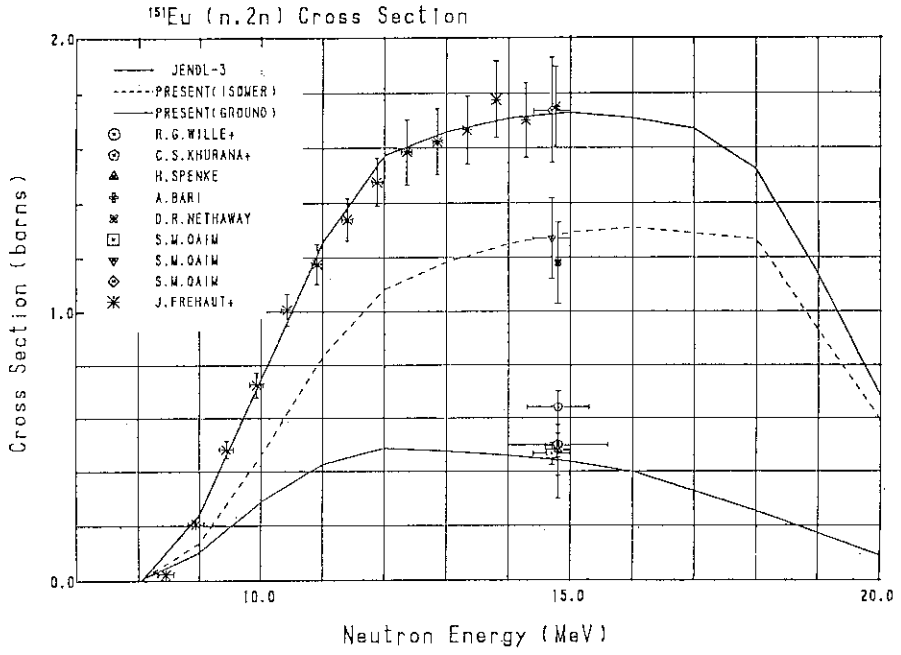

Fig. 4 $^{151}Eu(n,2n)$ cross section. The total (n,2n) cross section of JENDL-3 was shared into ground state(0^-, 12.66h) cross section and the isomeric(4^+, 36.4y) cross section according to isomeric ratio calculated with GNASH. Measured data corresponding total, isomeric and ground states can be distinguished easily from their values.

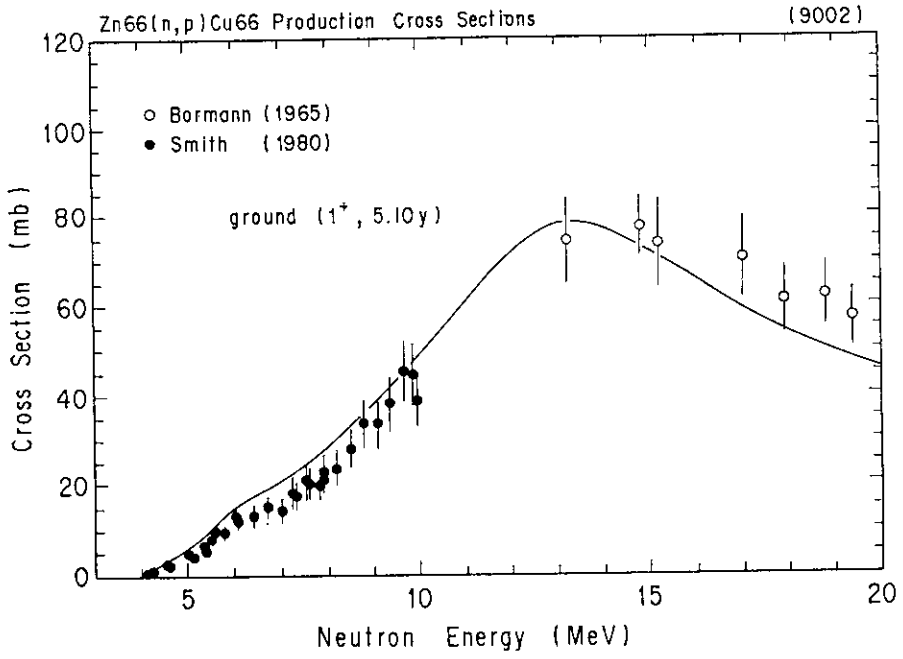

Fig. 5 $^{66}Zn(n,p)^{66}Cu$ cross section. Solid line shows the present evaluation.

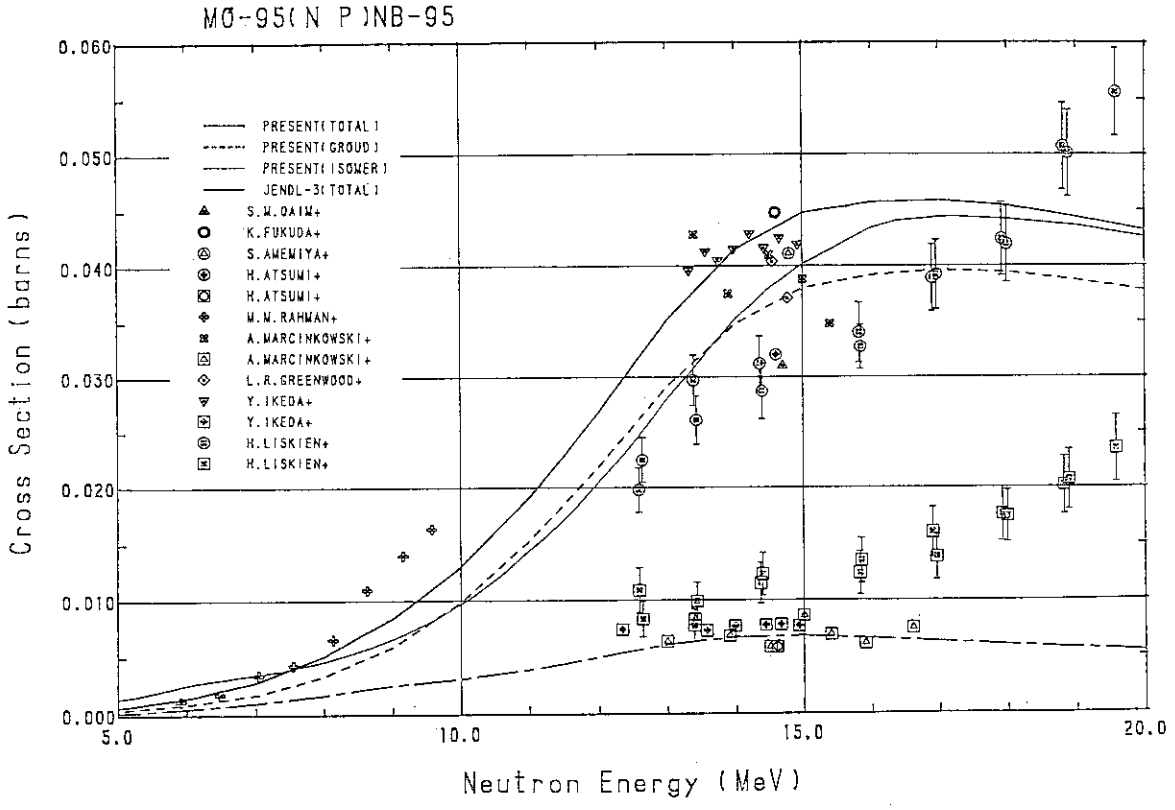

Fig. 6 $^{95}Mo(n,p)^{95}Nb$ cross sections. Symbols enclosed with a circle denote the ground state cross sections. Symbols enclosed with a square represent the isomeric cross sections. Other symbols show the total (n,p) cross sections.

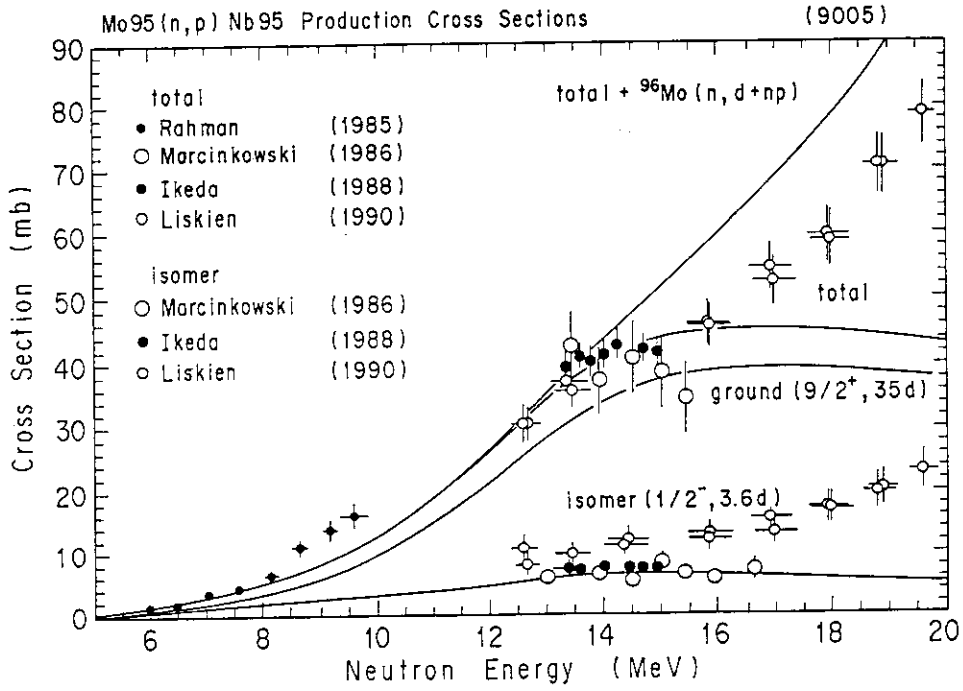

Fig. 7 $^{95}Mo(n,p)^{95}Nb$ cross section. Only the measured data corresponding to the total (n,p) cross sections and to the isomeric cross section are shown in this plot. Lines show the present evaluation.

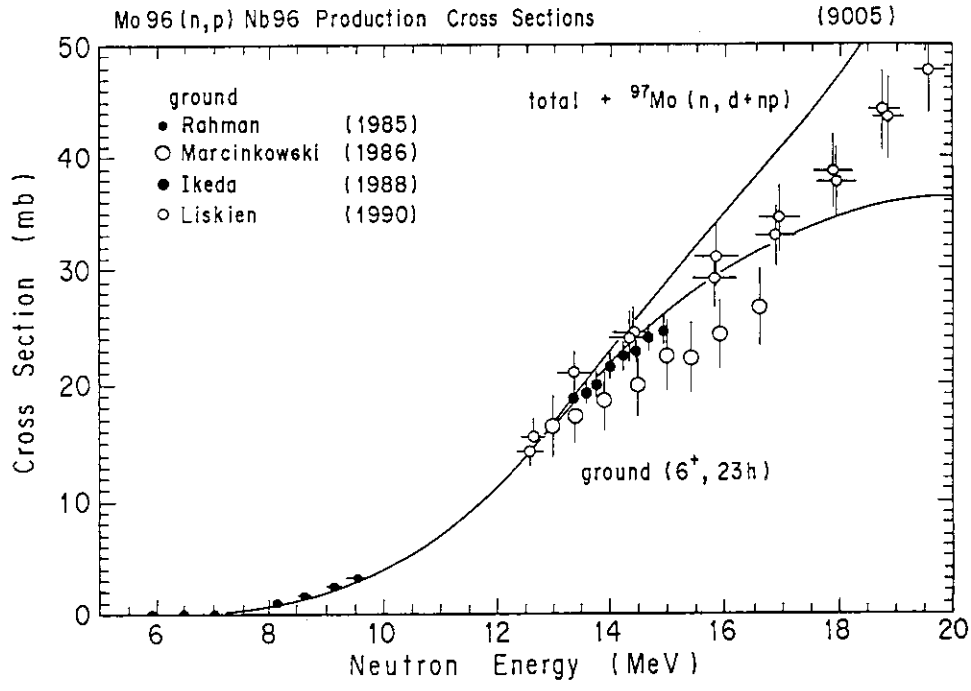

Fig. 8 $^{96}Mo(n,p)^{96}Nb$ cross section. Lines show the present evaluation.

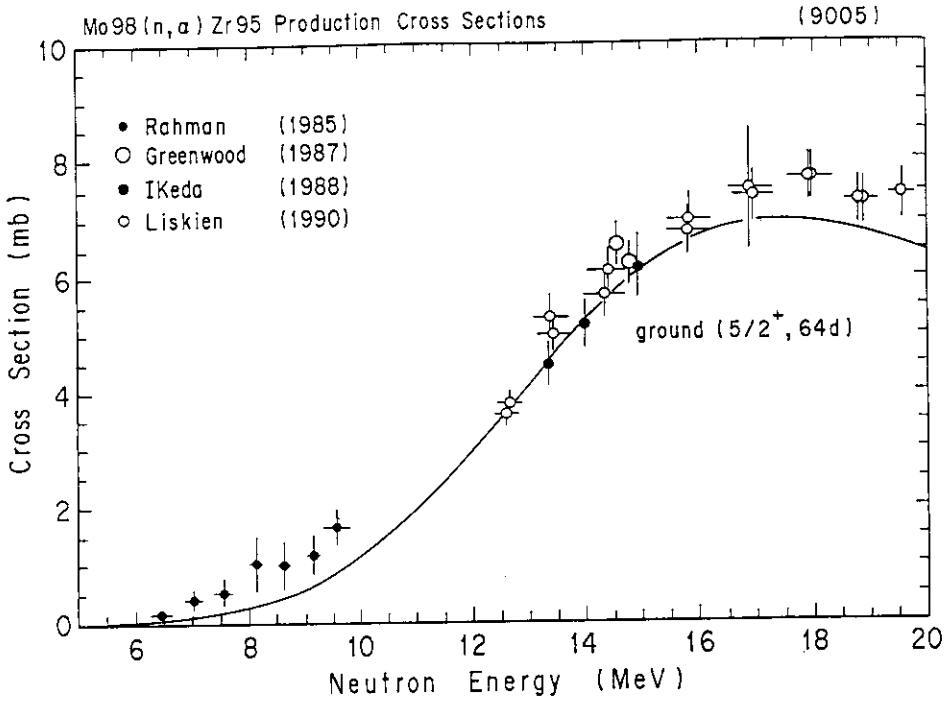

Fig. 9 $^{98}Mo(n,\alpha)^{95}Zr$ cross section. Line shows the present evaluation.

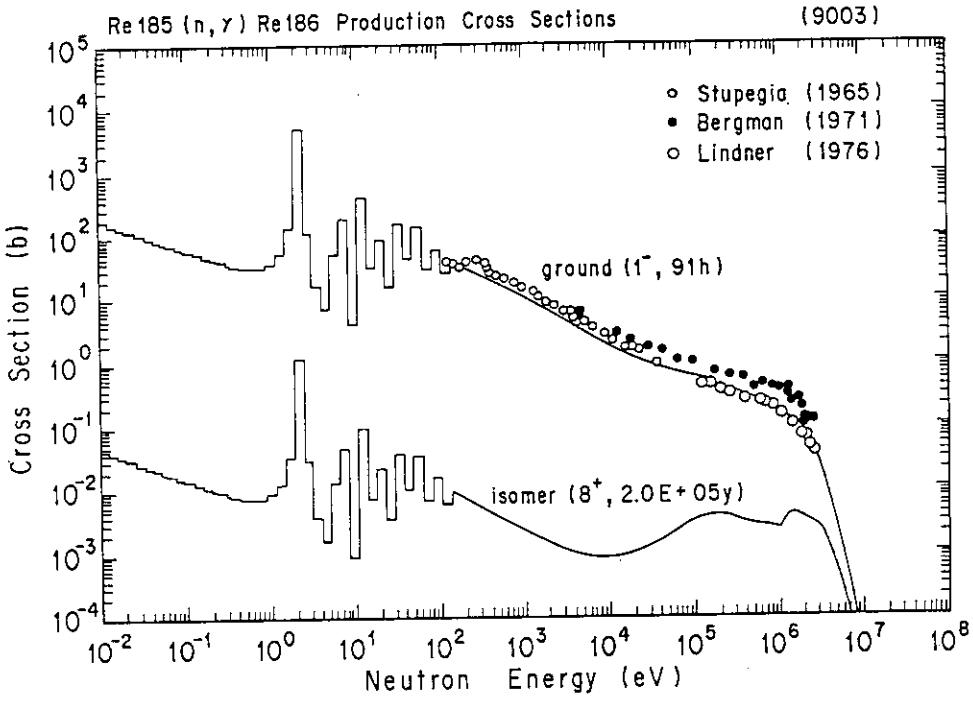

Fig. 10 $^{185}Re(n,\gamma)^{186}Re$ cross section. Lines represent the present evaluation. Measured data by Lindner et al. correspond to the ground state cross sections. Other measured data correspond to the total (n,γ) cross sections.

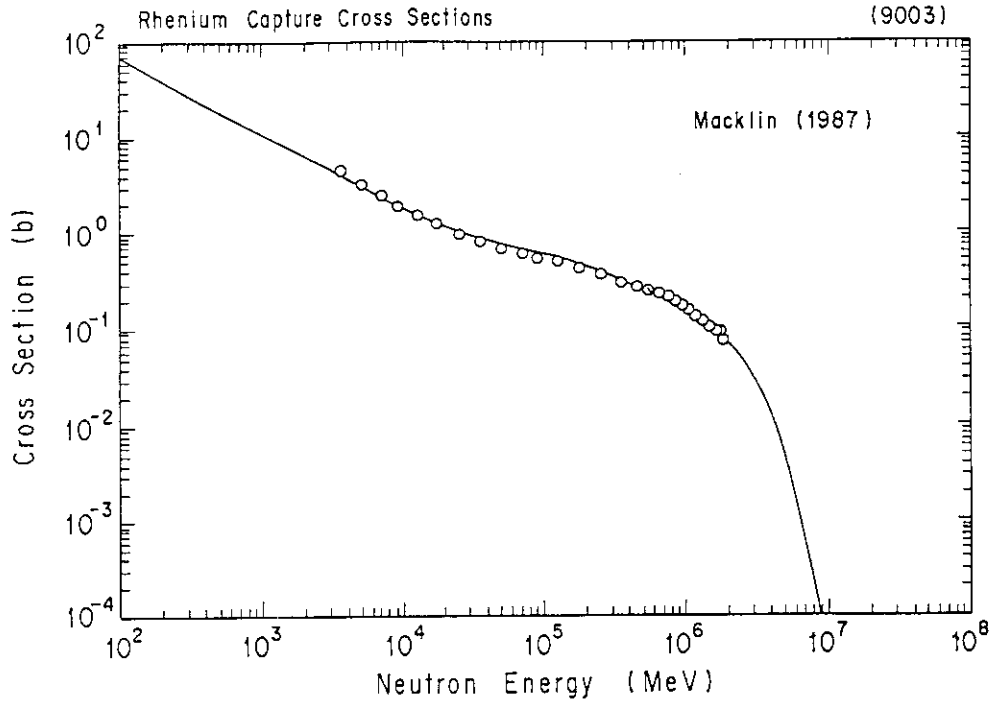

Fig. 11 Re(n,γ) cross section. Line represents the present evaluation.

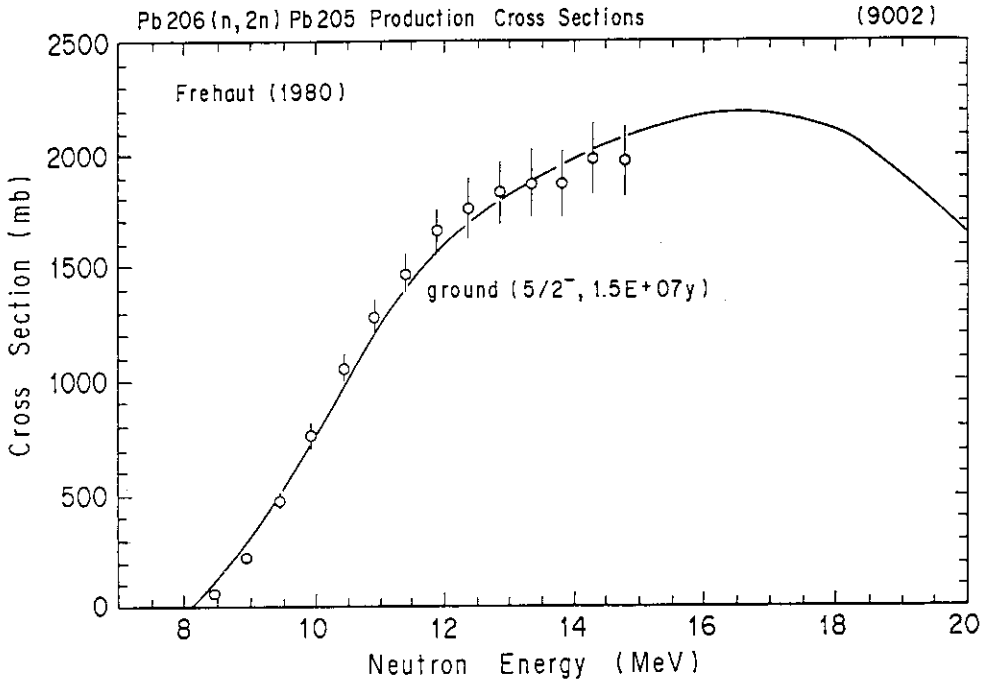

Fig. 12 $^{206}Pb(n,2n)^{205}Pb$ cross section. Line shows the present evaluation.

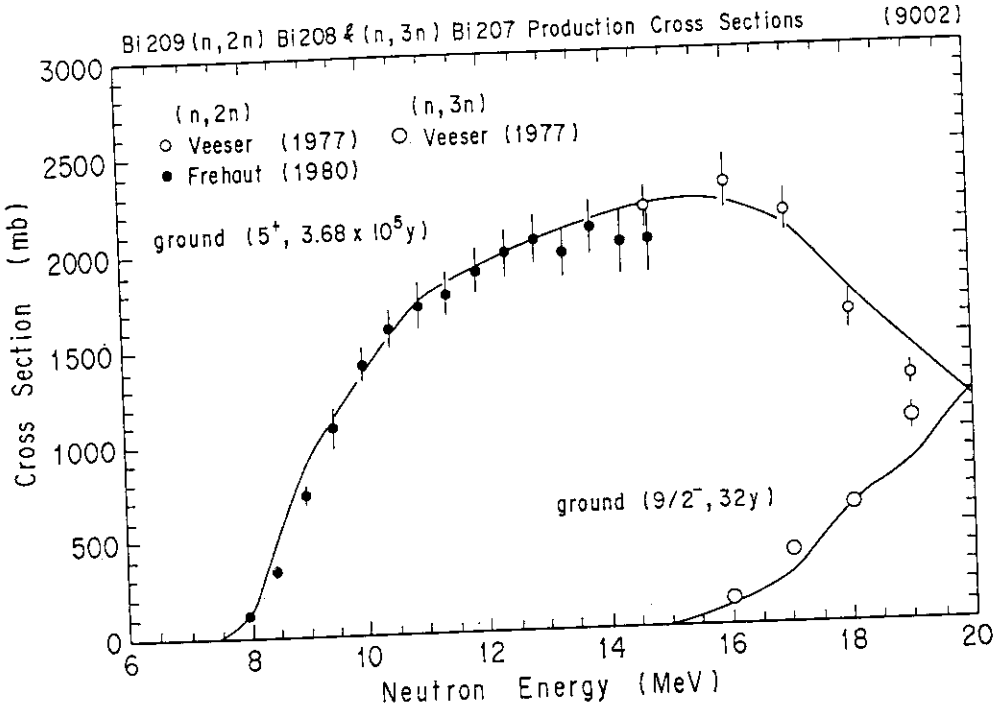

Fig. 13 $^{209}Bi(n,2n)^{208}Bi$ and $^{209}Bi(n,3n)^{207}Bi$ cross sections. Lines show the present evaluation.

2.2.3 Present Status of Evaluation Work on Photonuclear Reaction Cross Sections

Norio Kishida†
and
Photonuclear Data Working Group

Japan Atomic Energy Research Institute
Tokai-mura, Naka-gun, Ibaraki-ken, JAPAN

Evaluation work of photonuclear reaction cross sections is in progress as an activity in photonuclear data working group of JNDC. Now this group is evaluating the following nuclides: C, N, O, Al, Ti, Fe, Cu, Ta, W, Pb, Bi and U. The photonuclear reaction data file is to be construct using ENDF-VI format. We will store absorption, (γ, xn), (γ, n), $(\gamma, 2n)$ and (γ, p) cross sections up to 140 MeV in that file. In addition, we will store energy spectrum and angular distributions of emitted particles, too. Accumulation of experimental cross sections has been completed. Evaluation for photo-absorption and photoneutron excitation functions is in progress with the help of computer codes based on some theoretical model.

1. Introduction

Recently nuclear data for photonuclear reactions are required in the following two field: (1) shielding design of high-energy electron accelerators and (2) nuclear transmutation of long-lived radioactive waste produced from nuclear fuel-cycle facilities.

In the former field, it is highly desirable to perform accurately shielding design of an accelerator building in order to thin the shielding walls as much as possible. This is because designers of the accelerators are always required to reduce the cost of those construction. In high-energy electron accelerators, the shielding designers mainly analyzed behavior of electrons and bremsstrahlung photons until now. It is, however, clear that neutrons from photonuclear reactions by the bremsstrhalung photons must be also considered for the purpose of precise estimation of the influence of secondary radiations.

In the later field, the photonuclear data will be employed to estimate the precise speed of nuclear transmutation from long-lived radioactive nuclides to short-lived or stable

†Century Research Center Corp.
1–3–D17, Nakase, Chiba–shi, Chiba–ken, JAPAN

ones. Hence, the evaluated photonuclear cross sections are basic data to conclude whether a nuclear transmutation facilities can be practically realized or not.

From these demands for the photonuclear data, the working group to evaluate the nuclear data for photonuclear reaction cross sections has been organized in April, 1988 under an activity in Japanese Nuclear Data Committee(JNDC).

2. Evaluation

2.1 Object Nuclides of the Evaluation

We intend to evaluate all of the natural isotopes, several transuranic nuclei(TRU) and some fission products(FP). Unfortunately, our group does not have large man-powers, so we determined to divide the period of file construction into three periods. In the first period, the following nuclides will be evaluated by 1992: C, N, O, Al, Ti, Fe, Cu, Ta, W, Pb, Bi and U. In the second period, the following nuclides will be evaluated by 1996: H, D, Be, Na, Si, Cl, Ar, K, Ca, Cr, Ni, Sr, Mo, Sn, Cs, Pt, Au, Th, Pu and Np. In the third period, the remaining nuclides will be evaluated by 2000: We are planning to complete the primary version of the photonuclear data file within 2 or 3 years.

2.2 Contents of the Photonuclear Data File

We have determined to construct the photonuclear data file using ENDF-6 format. The following data types will be stored:

(1) total absorption cross sections(photonuclear cross sections) : $\sigma_{abs}(E_\gamma)$,

(2) photoneutron cross sections : $\sigma[(\gamma,\ n) + (\gamma,\ pn) + (\gamma,\ 2n) + \cdots]$,

(3) photoneutron yield cross sections : $\sigma[(\gamma,\ n) + (\gamma,\ pn) + 2(\gamma,\ 2n) + \cdots]$,

(4) photoproton cross sections : $\sigma[(\gamma,\ p) + (\gamma,\ pn) + (\gamma,\ 2p) + \cdots]$,

(5) photoproton yield cross sections : $\sigma[(\gamma,\ p) + (\gamma,\ pn) + 2(\gamma,\ 2p) + \cdots]$,

(6) single neutron emission cross sections : $\sigma[(\gamma,\ n) + (\gamma,\ pn)]$,

(7) double neutron emission cross sections : $\sigma[(\gamma,\ 2n) + (\gamma,\ x2n)]$,

(8) neutron energy spectra : $\dfrac{d\sigma}{dE_n}$,

(9) proton energy spectra : $\dfrac{d\sigma}{dE_p}$,

(10) neutron angular distributions : $\frac{d\sigma}{d\Omega_n}$,

(11) proton angular distributions : $\frac{d\sigma}{d\Omega_p}$,

(12) neutron DDX : $\frac{d^2\sigma}{d\Omega_n dE_n}$, and

(13) proton DDX : $\frac{d^2\sigma}{d\Omega_p dE_p}$.

In the energy region above the threshold energy of the (γ, π) reaction, experimental data scarcely exist and it is very difficult to calculate theoretical cross-sections. For this reason, we adopted 140 MeV as the maximum incident photon energy.

As for photonuclear activation cross sections, which are important quantity in the maintenance of electron accelerators, we are planning to construct the photonuclear activation data file other than the photonuclear reaction data file.

2.3 Status of Experimental Data

We collect experimental photonuclear cross sections with the help of "Photonuclear Data - Abstracts Sheets 1955 - 1983"[1] and "Atlas of Photoneutron Cross Sections Obtained with Monoenergetic Photons".[2] Reference 1 exhausts all articles related to photonuclear experiments to have been performed before 1983. Reference 2 is the compilation article collecting photoneutron excitation functions with monoenergetic photons in the giant dipole resonance region(E_γ is nearly less than 25 MeV).

We have known from both articles that the photoneutron excitation functions had been measured in the giant resonance region for almost all of the nuclides to compose structural and shielding material. But energy spectra and DDX of emitted particles were scarcely measured in the entire energy region for nearly all of the nuclides. For a quasi deuteron-effect region(E_γ is from near 25 MeV to near 140 MeV, which corresponds to the (γ, π) threshold energy), several photo-absorption and photoneutron excitation functions have been reported in the literatures[3),4)].

Anyhow we have understood that it is difficult to construct the photonuclear data files using measured cross sections only.

2.4 Present Status of Evaluation Work

Collection of experimental data have been finished for nuclides of which cross sections are being evaluated at the first period. In the giant resonance region, the photo-absorption and photoneutron excitation functions are evaluated in such a way that we fit experimental excitation curves to single or multiple Lorentz resonance curves. An example of such a

fitting analysis[5] for $^{16}O(\gamma, n)$ reaction is shown in Fig. 1. In the case of lack of or no experimental data, the excitation functions are evaluated using a systematics[6] of the giant dipole resonance. An example for $^{56}Fe(\gamma, n)$ reaction is shown in Fig. 2.

In the quasi deuteron effect region, the excitation functions are evaluated by normalizing a systematic excitation function[7] to experimental data.

Due to lack of experimental data, we stated previously that it is difficult to construct the photonuclear data files using measured cross sections only. Hence we decided to develop a computer program which calculates theoretical photonuclear cross sections such as DDX and energy spectra. Its first version[8] completed last year.

The program consists of two parts, namely, one is the calculational part of the absorption cross sections and the other is the part that calculates a decay process from excited nuclei. The absorption cross sections are derived by utilizing experimental values and those systematics. For the calculation of decay process, we adopted a random walk exciton model[9] and a statistical evaporation model[10].

Figure 3 shows comparison between the experimental[2] and calculated excitation functions for ^{75}As in the giant resonace region. The program, which we call it MCPHOTO, reproduces the ratio of (γ, n) and $(\gamma, 2n)$ cross sections very well.

Figure 4 shows comparison between the experimental[4] and calculated excitation functions of six or more neutrons emission reaction for ^{nat}Sn in the quasi deuteron effect region. The calculated result[12] by ALICE are also shown in Fig. 4 for reference. Both the calculations were performed for the ^{119}Sn target(taken as the average mass of the highly abundant ^{118}Sn and ^{120}Sn isotopes). Two codes reproduce the experimental excitation functions very well and to nearly same extent. From these results, we believe that these theoretical codes will play an important role in our evaluation work.

3. Summary

The evaluation status and plans of photonuclear data in photonuclear data working group of JNDC were briefly reviewed. The evaluation work begins just now, so the primary version data file does not complete. We strongly expect that data types other than excitation functions, especially energy spectra of emitted neutrons will be measured by a number of experimentalists.

References

1) Fuller, E. G. and Gerstenberg, H. : *NBSIR* 83–325.

2) Fultz, F. and Berman, B. : *Atom. Data Nucl. Data Tables*, **38**, 199(1988).

3) Ahrens, J., *et al. Nucl. Phys.*, **A251**, 479(1975).

4) Leprêtre, A., *et al.* : *Nucl. Phys.*, **A325**, 63(1979).

5) Murata, T. : *Private communication.*

6) Berman B. L. and Fultz S. C. : *Rev. Mod. Phys.*, **47**, 713(1975).

7) Igashira, M. : *Private communication.*

8) Kishida N. and Kadotani H. : *JAERI-memo*, **02-291**, (1990)(unpublished).

9) Gudima, K. K., Osokov, G. A. and Toneev, V. D. : *Yad. Fiz.*, **21**, 260(1975).

10) Weisskopf, V. F. : *Phys. Rev.*, **52**, 295(1937).

11) Blann, M., Berman, B. L. and Komoto, T. T. : *Phys. Rev. C* , **28**, 2286(1983).

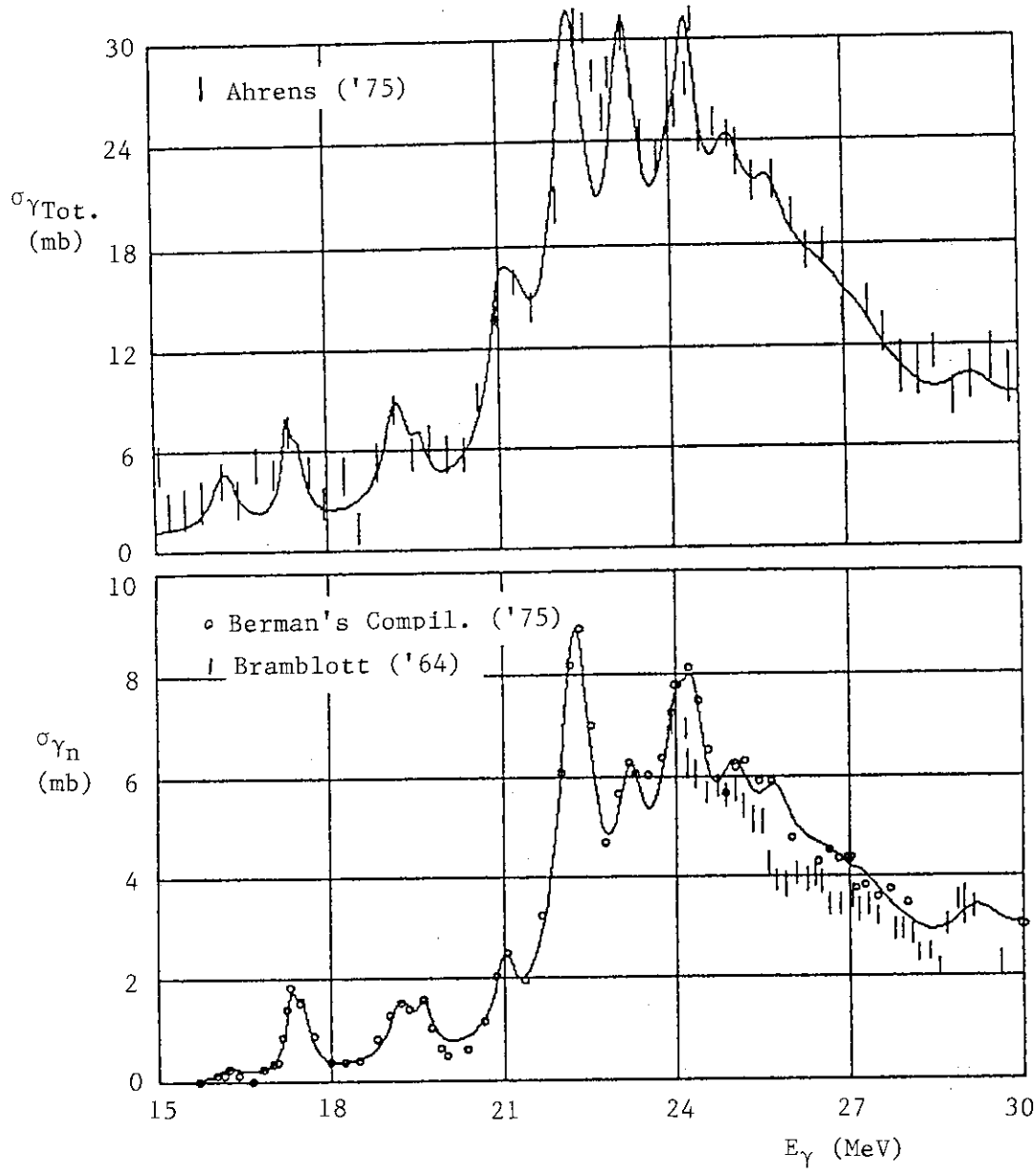

Fig. 1 Photo-absorption and photoneutron excitation functions for ^{16}O. Bars and circles represent experimental data. The solid lines are a result of multi parameter Lorentzian fitting.

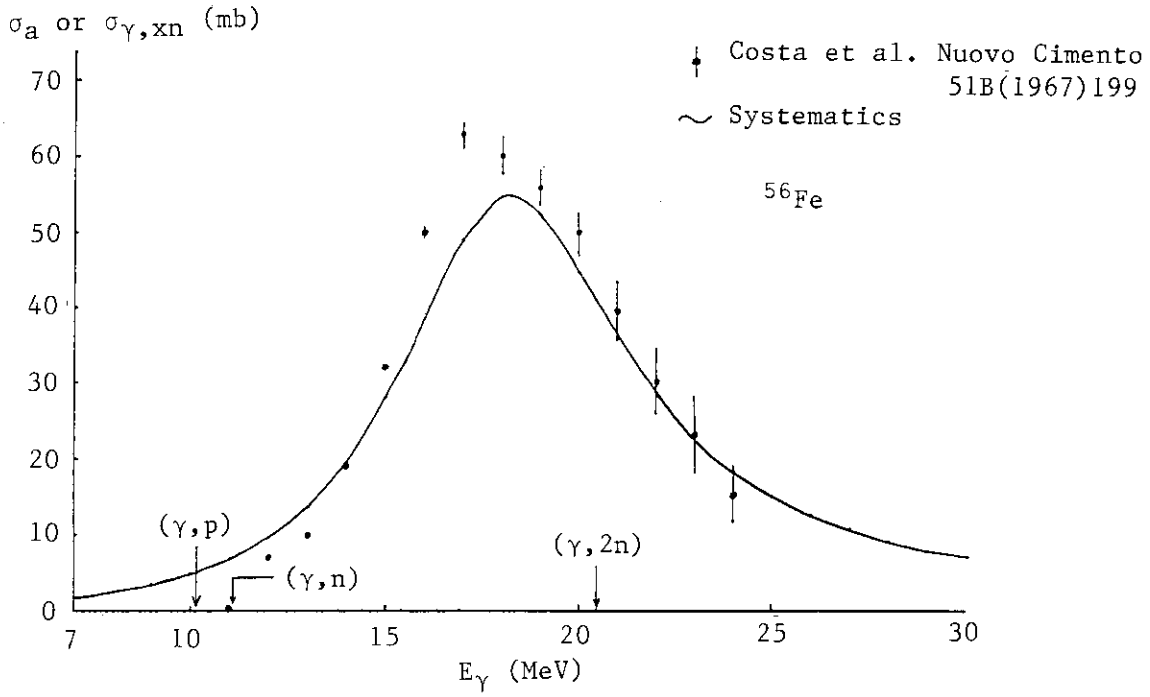

Fig. 2 Photoneutron excitation functions for ^{56}Fe. Solid circles with error bar represent experimental data and the solid line is a calculated result from the systematics of the giant dipole resonance.

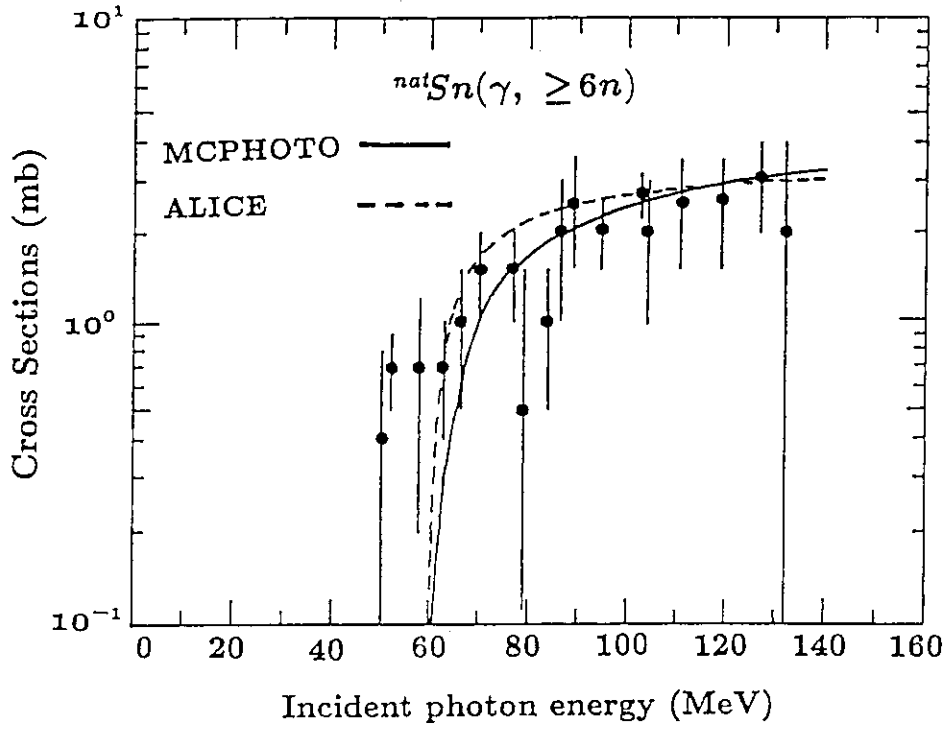

Fig. 4 Photoneutron excitation functions for ^{nat}Sn. Solid circles with error bar represent experimental data. The solid and broken lines are calculated results by MCPHOTO and ALICE code, respectively.

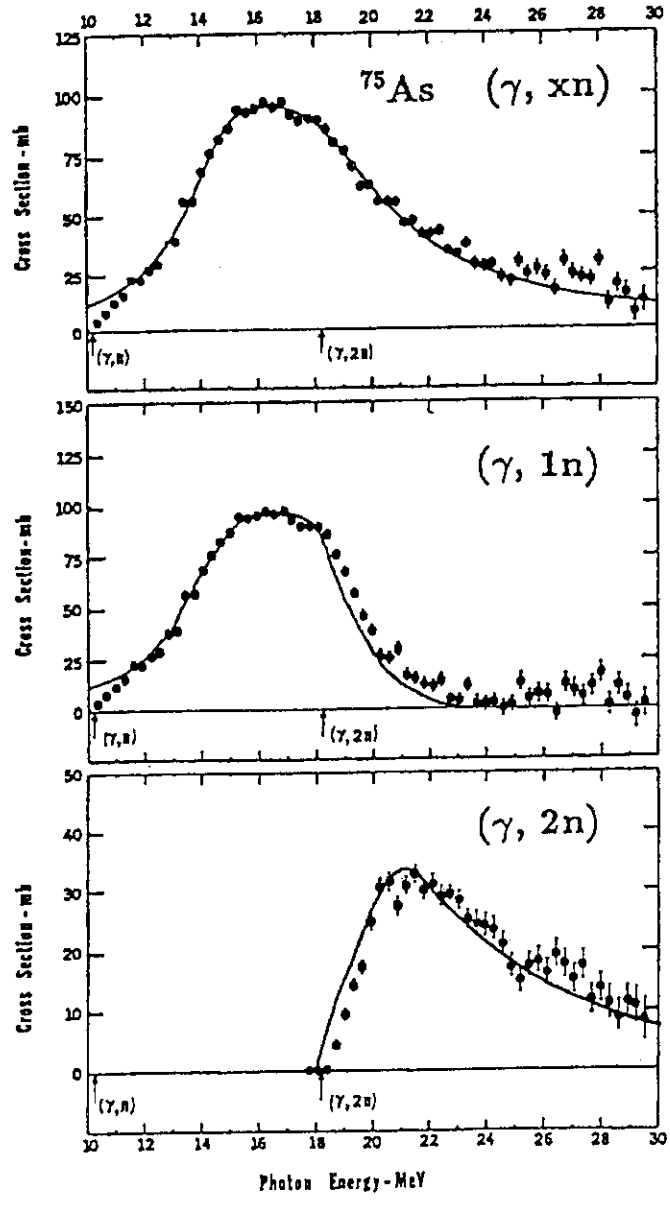

Fig。 3 Photoneutron excitation functions for ^{75}As. Solid circles with error bar represent experimental data and solid lines are calculated results by MCPHOTO code.

2.2.4 Neutron Production Data by (α,n) Reaction and Spontaneous Fission

Yoshitaka NAITO
Japan Atomic Energy Research Institute
Tokai-mura, Naka-gun, Ibaraki-ken, Japan
and
Ryuzo NAKASIMA
Hosei University
2-17-1, Fijimi, Chiyoda-ku, Tokyo, Japan

Neutron yield data by (α, n) reaction and spontaneous fission which are very important for analyzing radiation shielding safety of storage and transportation or safe handling of spent fuel, were collected and evaluated to obtain the recommended values and their accuracy. As for thick target neutron yield from (α, n) reactions, experimental data by Bair and Gomez del Campo, West and Sherwood, Jacobs and Liskien, and Stelson and McGowan were compiled in the present evaluation work. The discrepancies between them are discussed referring available evaluation works by Nakasima and Heaton et al. Neutron yield which have not been obtained experimentally were calculated using the experimental data on (α, n) excitation functions and the stopping powers published by Ziegler. As for neutron yield data from spontaneous fission, recommended values by S. Raman were adopted in the present work. Neutron energy spectra were also collected as well as neutron yields data. These data are compiled in this Data Book with theoretical explanation. Neutron generation data of many kind of materials will be obtained by using this Book.

1. Introduction

In discussing the fuel cycle problem such as storage, transportation or safe handling of the spent fuel, one of the important nuclear data is that on neutron yield produced in (α, n) reaction by α-particles and spontaneous fission of various actinide nuclides cumulated in spent fuel. These data are essential for evaluating radiation shielding safety of fuel cycle facilities and fuel transport casks. Recently, high burnup fuels are so often treated that it may be worthy to present the extensively evaluated neutron yield data in tabular form together with the detailed explanation as shown in Table 1.

The thick target neutron yield from (α, n) reaction have been measured directly by Bair and Gomez del Campo[1], West and Sherwood[2], Jacobs and Liskien[3], and Stelson and McGowan[4]. These experimental data are used preferably in the present evaluation work, although some discrepancies are seen between them as shown in Fig. 1. In adopting the recommendable values, the available evaluation works by Liskien and Paulsen[5], Nakasima[6], and Heaton et al.[7] are referred as well as those calculated by using the experimental data on (α, n) excitation functions and the stopping powers published by Ziegler[8]. However, the most of the (α, n) excitation functions at low incident energies show the resonance structure which makes the uncertainty of the calculated neutron yield large. In spite of this uncertainty, the errors of the thick target neutron yields tabulated in the present work are considered to be not so large in the most cases, since the uncertainty in the resonance region has little effect on the yield at higher incident energy where the neutron yield is much larger than that in the resonance region. Furthermore, it is expected that the uncertainty could be reduced considerably by taking the small energy mesh (interval) in numerical integration.

The data on energy spectra of neutrons from thick target (α, n) reactions are based on those measured by Jacobs and Liskien. The differential neutron yields are determined by renormalizing the integrated energy spectra to neutron yields measured by West and Sherwood or by Heaton et al..

As for neutron yield data from spontaneous fission, recommended values by S. Raman[9] are used in present work. Neutron energy spectrum of spontaneous fission is assumed to be Maxwellian whose neutron temperature is the same as that of ENDF/B-IV or -V.

The above data are compiled in a data book with theoretical explanation. This work was performed by Working Group on Evaluation for Generation and Depletion of Nuclides of JNDC.

2. Contents of the Data Book.

The contents of the Data Book for calculating neutron yield by (α, n) reaction and spontaneous fission are shown in Table 1. As shown in this Table, many data are collected under the following standpoints;

a) age measured and evaluated the data being new,

b) number of material being many on which the data have been measured and evaluated,

and

c) energy range of the data being wide.

Eighty α-emitters are selected; 41 heavy nuclides and 39 daughters of them. Forty target materials are selected; 10 nuclides, 22 elements, 7 compounds and 1 mixture

Name of target materials, energy range measured and references are shown in Table 2. As shown in this table, measured data are collected from 4 reports produced by Bair and Gomez del Campo (1979), West and Sherwood (1982), Jacobs and Liskien (1983), and Stelson and McGowan (1964), and evaluated data are collected from 3 reports produced by Liskien and Paulsen (1977), Nakasima (1982), and Heaton et al(1989).

In Fig. 1, adopted data are compared with other data. From these data, we can evaluate the integrity of adopted data. Neutron yields from spontaneous fissions are compiled from those recommended by S. Raman (1976) which are shown in Table 3. Summary data of neutron yields from spontaneous fissions and (α, n) reactions are shown in Table 4 which is a final production of present work. With this table we can easily obtain neutron yield data on many kind of α-emitters and target materials. Data for neutron energy spectra of 7 elements (B, C, O, F, Mg, Al, Si) and 2 compounds (Al_2O_3, SiO_2) are collected from the report produced by Jacobs. An example is shown in Fig. 2.

Neutron energy spectrum from spontaneous fission is expressed by following equations;

$$\phi_g^{SF} = \bar{\nu}_{SF} \cdot N_k \cdot 10^{24} \cdot \frac{\ln 2}{\tau_{1/2}} \int_{E_g}^{E_{g-1}} M(E)dE$$

$$M(E) = \frac{2}{\sqrt{\pi T^3}} E^{1/2} \exp\left(-\frac{E}{T}\right)$$

where, data on $\bar{\nu}_{SF}$ and $\tau_{1/2}(SF)$ are shown in the report by S. Raman, and neutron temperature Ts are obtained from ENDF/B-IV and -V or modified Terrell's formula. In Fig. 3, solid line shows Terrell's formula and dotted line is a modified Terrell's formula which is adopted in the present work.

Neutron yields of compounds are obtained by following simplified formula.

$$Y_M(E) = N \int_0^E \frac{\sum_i f_i \sigma_i(E')}{\sum_j N f_j S_j(E')} dE' \approx \sum_i \frac{f_i Y_i(E)}{\sum_j f_j S_j(E_0) / S_i(E_0)}$$

In this formulation, $S_j(E)/S_i(E)$ is assumed to be independent of energy. This assumption was supported by surveying the energy dependence of stopping power S(E) of each nuclide. With this formulation, (α, n) yield of compounds BN and UO_2 are obtained and compared with those of measured ones. As shown in Table 5, calculated values show a good agreement with those of measured ones.

(α, n) yields of the elements whose yields have not been measured, are able to be introduced with (α, n) cross section obtained by evaporation model and with stopping power from Ziegler's formula. The (α, n) yields obtained with such a way are compared with Heaton's data. As shown in Fig. 4, the energy dependence of (α, n) yields by present way shows similar as that of Heaton's.

Errors of (α, n) yields were evaluated. As shown in Fig. 5, estimated errors depend upon incident energy of α-particle and the values are between a few % and 20 %.

3. Conclusion

Data for calculating neutron yields were compiled. The data book will be published in near future. The (α, n) yields not measured are calculated with (α, n) cross sections which have been evaluating at Sigma committee. When more accurate (α, n) cross section will be obtained and the estimation on (α, n) yields will be more accurate, this data book will be hoped to be revised. The (α, n) yields of compounds can be estimated with the data book. We hope the estimated results will be evaluated with experimental data.

Acknowledgements

This work was performed under the leadership of Dr. S. IIJIMA. We want to pay grateful thanks for his kind advice and hope him passing away peacefully.

References

(1) J. K. Bair and J. Gomez del Campo : Nucl. Sci. Eng. **71**,18 (1979)
(2) D. West and A. C. Sherwood : Ann. Nucl. Energy **9**, 551 (1982)
(3) G. J. H. Jacobs and H. Liskien : *ibid.*, **10**, 541 (1983)
(4) P. H. Stelson and F. K. McGowan : Phys. Rev. **133**, B911 (1964)
(5) H. Liskien and A. Paulsen : Atomkernenenrgie **30**, 1 (1977)
(6) R. Nakasima : JAERI-M 82-117 (1982) (in Japanese)
(7) R. Heaton et al. : Nucl. Instr. Methods **A276**, 529 (1989)
(8) J. F. Ziegler : Press, Oxford (1977)
(9) S. Raman : Transactinium Isotope Nuclear Data (TND) Vol. 1, IAEA-189 (1976)

Table 1 Contents of the data book

Table 2 List of the (α,n) data adopted in present work

	Target	E_{th} [MeV]	Energy range [MeV]	Adopted data
1	Li	4.382	4.4～9.8	82 Heaton
2	Be	0.0	3.4～9.9	82 West, 89 Heaton
3	B	0.0	3.6～9.8	79 Bair, 89 Heaton
4	C	0.0	3.7～9.9	82 West
5	N	6.088	6.2～9.8	89 Heaton
6	O	0.0	3.4～9.8	89 Heaton
7	F	2.360	3.4～9.8	89 Heaton
8	Ne	0.0	3.6～5.2	82 Nakasima
9	Na	3.485	3.6～9.8	89 Heaton
10	Mg	0.0	3.7～9.9	82 West
11	Al	3.027	3.7～11.0	82 West, 64 Stelson
12	Si	1.736	3.7～9.9	82 West
13	^{35}Cl	6.674	6.8～10.2	82 Nakasima
14	Sc	1.736	3.4～10.2	82 Nakasima
15	^{46}Ti	4.830	5.0～10.2	82 Nakasima
16	^{51}V	2.472	5.2～10.2	82 Nakasima
17	^{50}Cr	5.358	5.8～10.2	82 Nakasima
18	Fe	1.450	4.7～9.9	82 West
19	Co	5.421	5.8～11.0	82 Nakasima, 64 Stelson
20	^{60}Ni	8.434	8.6～10.8	82 Nakasima, 64 Stelson
21	^{62}Ni	6.901	7.2～10.8	82 Nakasima, 64 Stelson
22	Cu	6.181	6.4～10.6	82 Nakasima, 64 Stelson
23	^{64}Zn	9.555	9.8～11.2	82 Nakasima, 64 Stelson
24	^{66}Zn	7.900	8.0～11.0	82 Nakasima, 64 Stelson
25	^{68}Zn	6.085	6.4～10.8	82 Nakasima, 64 Stelson
26	^{70}Zn	4.136	6.2～10.8	82 Nakasima, 64 Stelson
27	Zr	5.335	6.6～11.0	82 Nakasima, 64 Stelson
28	Nb	7.340	7.6～11.0	82 Nakasima, 64 Stelson
29	Mo	4.133	7.4～11.0	82 Nakasima, 64 Stelson
30	Pd	4.989	8.6～11.0	82 Nakasima, 64 Stelson
31	Ag	6.607	8.8～11.0	82 Nakasima, 64 Stelson
32	In	7.436	9.6～11.0	82 Nakasima, 64 Stelson
33	BeO	0.0	4.1～9.9	82 West
34	BN	0.0	4.1～6.7	82 West, 79 Bair, 89 Heaton
35	Al_2O_3	0.0	3.7～9.9	82 West, 89 Heaton
36	SiO_2	0.0	3.7～9.9	82 West, 89 Heaton
37	CaF_2	0.0	3.4～ .	89 Heaton
38	M316	0.0	4.7～9.9	82 West
39	UC	0.0	3.8～9.9	82 West
40	UO_2	0.0	3.8～9.9	82 West

Table 3 Neutron yields from spontaneous fission (The data recomended by S. Raman (1976))

Isotope	$T_{1/2}$ (S.F.) years measured	$T_{1/2}$ (S.F.) years estimated	$\bar{\nu}$ (S.F.) measured	$\bar{\nu}$ (S.F.) estimated	Neutron Yield [n/gm-sec] measured	Neutron Yield [n/gm-sec] estimated
^{235}U	$(3.5\pm0.9)\times10^{17}$			1.695		2.73×10^{-4}
^{236}U	2.0×10^{16}		1.65±0.12	1.784	4.64×10^{-3}	5.00×10^{-3}
^{237}U		6.3×10^{19}		1.872		1.66×10^{-6}
^{238}U	$(1.01\pm0.03)\times10^{16}$		2.00±0.08	1.960	$(1.10\pm0.06)\times10^{-2}$	1.08×10^{-2}
^{239}U	8.9×10^{18}			2.048		1.27×10^{-5}
^{236g}Np		6.3×10^{17}		1.783		1.59×10^{-4}
^{236m}Np		6.3×10^{17}		1.790		1.59×10^{-4}
^{237}Np	$>10^{18}$			1.873		$<1.05\times10^{-4}$
^{238}Np		2×10^{18}		1.963		5.45×10^{-5}
^{239}Np		6.3×10^{16}		2.053		1.80×10^{-3}
^{236}Pu	3.5×10^{9}		2.22±0.20	1.793	3.55×10^{4}	2.87×10^{4}
^{237}Pu		2×10^{15}		1.886		5.26×10^{-2}
^{238}Pu	$(5.0\pm0.6)\times10^{10}$		2.28±0.08	1.977	$(2.54\pm0.32)\times10^{3}$	2.20×10^{3}
^{239}Pu	5.5×10^{15}		2.24±0.11	2.069	2.26×10^{-2}	2.08×10^{-2}
^{240}Pu	$(1.33\pm0.12)\times10^{11}$		2.16±0.02	2.160	$(9.0\pm0.9)\times10^{2}$	8.95×10^{2}
^{241}Pu		2.5×10^{15}		2.250		4.94×10^{-2}
^{242}Pu	$(7.4\pm0.2)\times10^{10}$		2.15±0.02	2.340	$(1.58\pm0.04)\times10^{3}$	1.72×10^{3}
^{243}Pu		2×10^{15}		2.430		6.61×10^{-2}
^{244}Pu	$(2.5\pm0.8)\times10^{10}$		2.30±0.19	2.518	$(5.0\pm1.7)\times10^{3}$	5.46×10^{3}
^{240}Am		1×10^{15}		2.290		1.26×10^{-1}
^{241}Am	$(2.3\pm0.8)\times10^{14}$			2.383		5.69×10^{-1}
^{242g}Am		1×10^{10}		2.475		1.35×10^{2}
^{242m}Am	$(9.5\pm3.5)\times10^{11}$		2.59±0.10	2.481	$(1.5\pm0.6)\times10^{2}$	1.43×10^{2}
^{243}Am	$(3.3\pm0.3)\times10^{13}$		2.52±0.11	2.566	4.2±0.5	4.23
^{244g}Am		7.9×10^{13}		2.657		1.82
^{244m}Am		7.9×10^{13}		2.665		1.83
^{240}Cm	1.9×10^{6}			2.406		6.98×10^{7}
^{241}Cm		1.6×10^{12}		2.500		8.58×10^{1}
^{242}Cm	7.2×10^{6}		2.59±0.09	2.594	1.97×10^{7}	1.97×10^{7}
^{243}Cm		1.2×10^{11}		2.687		1.22×10^{3}
^{244}Cm	$(1.30\pm0.07)\times10^{7}$		2.76±0.07	2.780	$(1.15\pm0.07)\times10^{7}$	1.16×10^{7}
^{245}Cm		4.0×10^{12}		2.872		3.88×10^{1}
^{246}Cm	$(1.80\pm0.01)\times10^{7}$		3.0±0.2	2.964	$(9.0\pm0.7)\times10^{6}$	8.85×10^{6}

Table 4 Example of the final form of present work

α-emitter		Cm-241	Cm-242	Cm-243
Yn (SF) (n/g/sec)		8.58E+1	1.97E+7	1.22E+3
Half-life B.R. of α-decay (%) <Ea> (MeV) RaλN₀ (a/g/sec)		3.2800E+1 d 1.0 5.930 6.110E+12	1.6294E+2 d 100. 6.102 1.225E+14	2.8500E+1 y 99.76 5.813 1.905E+12
n-emitter	Neutron Yields			
Li	Yn (n/a) Yn (n/g/sec)	4.90E-06 3.00E+07	6.36E-06 7.79E+08	4.08E-06 7.78E+06
Be	Yn (n/a) Yn (n/g/sec)	1.06E-04 6.46E+08	1.15E-04 1.41E+10	9.89E-05 1.88E+08
B	Yn (n/a) Yn (n/g/sec)	2.47E-05 1.51E+08	2.63E-05 3.22E+09	2.36E-05 4.49E+07
C	Yn (n/a) Yn (n/g/sec)	1.62E-07 9.90E+05	1.93E-07 2.37E+07	1.43E-07 2.72E+05
N	Yn (n/a) Yn (n/g/sec)	0.00E+00 0.00E+00	0.00E+00*) 0.00E+00	0.00E+00 0.00E+00
O	Yn (n/a) Yn (n/g/sec)	9.12E-08 5.57E+05	1.04E-07 1.27E+07	8.36E-08 1.59E+05
F	Yn (n/a) Yn (n/g/sec)	1.51E-05 9.23E+07	1.76E-05 2.15E+09	1.37E-05 2.62E+07
Ne	Yn (n/a) Yn (n/g/sec)	--- 	--- 	---
Na	Yn (n/a) Yn (n/g/sec)	3.79E-06 2.31E+07	4.65E-06 5.69E+08	3.28E-06 6.25E+06
Mg	Yn (n/a) Yn (n/g/sec)	2.15E-06 1.31E+07	2.57E-06 3.15E+08	1.95E-06 3.71E+06

Table 5 (α,n) yields (n/α) for elements and compounds

(a) Boron and BN.

E(MeV)	Boron(exp)	Nitrogen N(exp)	BN(exp)	BN(cal)
4.0	5.64±0.30(-6)	0.0	2.53±0.12(-6)	2.44(-6)
4.5	1.05±0.06(-5)	0.0	4.70±0.23(-6)	4.55(-6)
5.0	1.56±0.09(-5)	0.0	6.98±0.33(-6)	6.75(-6)
5.5	2.06±0.12(-5)	0.0	9.22±0.44(-6)	8.92(-6)

(b) Oxygen and UO_2

E(MeV)	Oxygen(exp)	UO_2(exp)	UO_2(cal)
4.0	1.64±0.14(-8)	0.51±0.03(-8)	0.48(-8)
4.5	2.93±0.24(-8)	0.91±0.05(-8)	0.86(-8)
5.0	5.18±0.43(-8)	1.60±0.09(-8)	1.52(-8)
5.5	6.46±0.52(-8)	1.99±0.10(-8)	1.90(-8)

*) Experimental data are from Jacobs and Liskien(1983).
BN(cal)=0.433xBoron(exp), UO_2(cal)=0.294xOxygen(exp).
(-6) reads 10^{-6}.

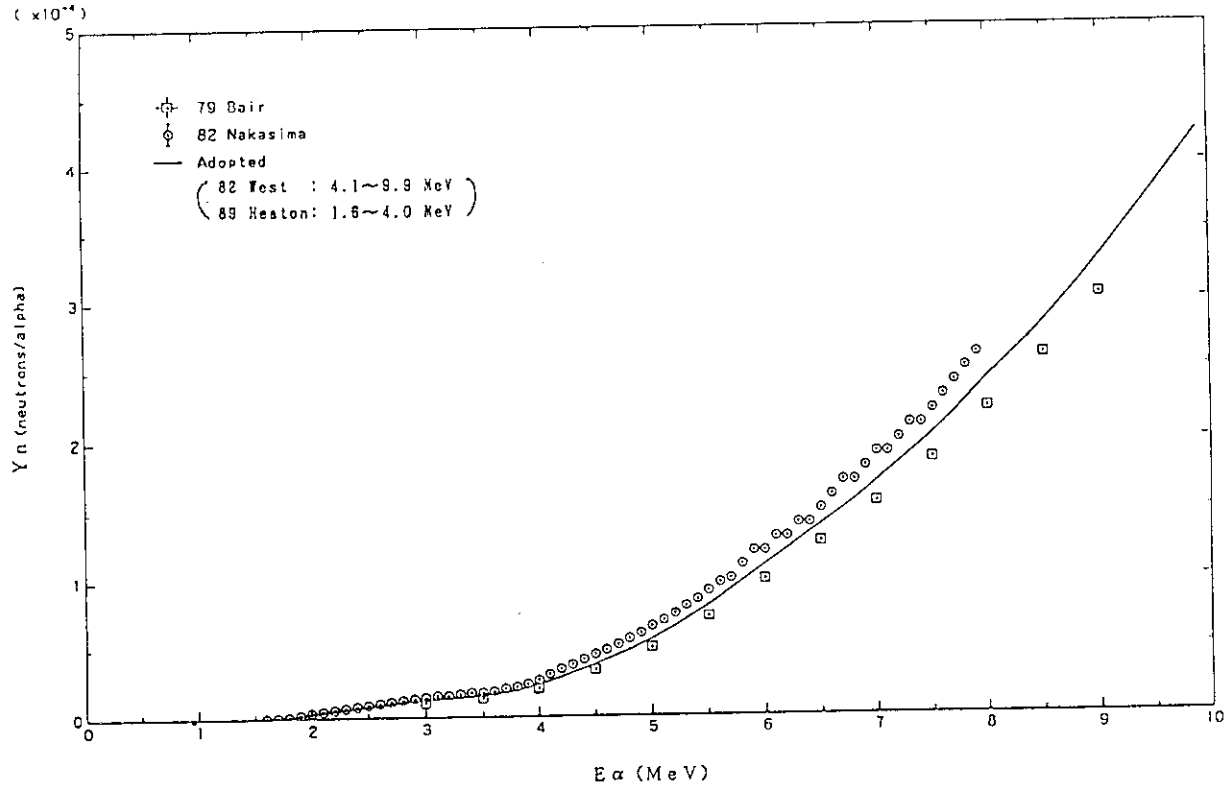

Fig. 1 Thick target neutron yields for Be(α,n) reaction

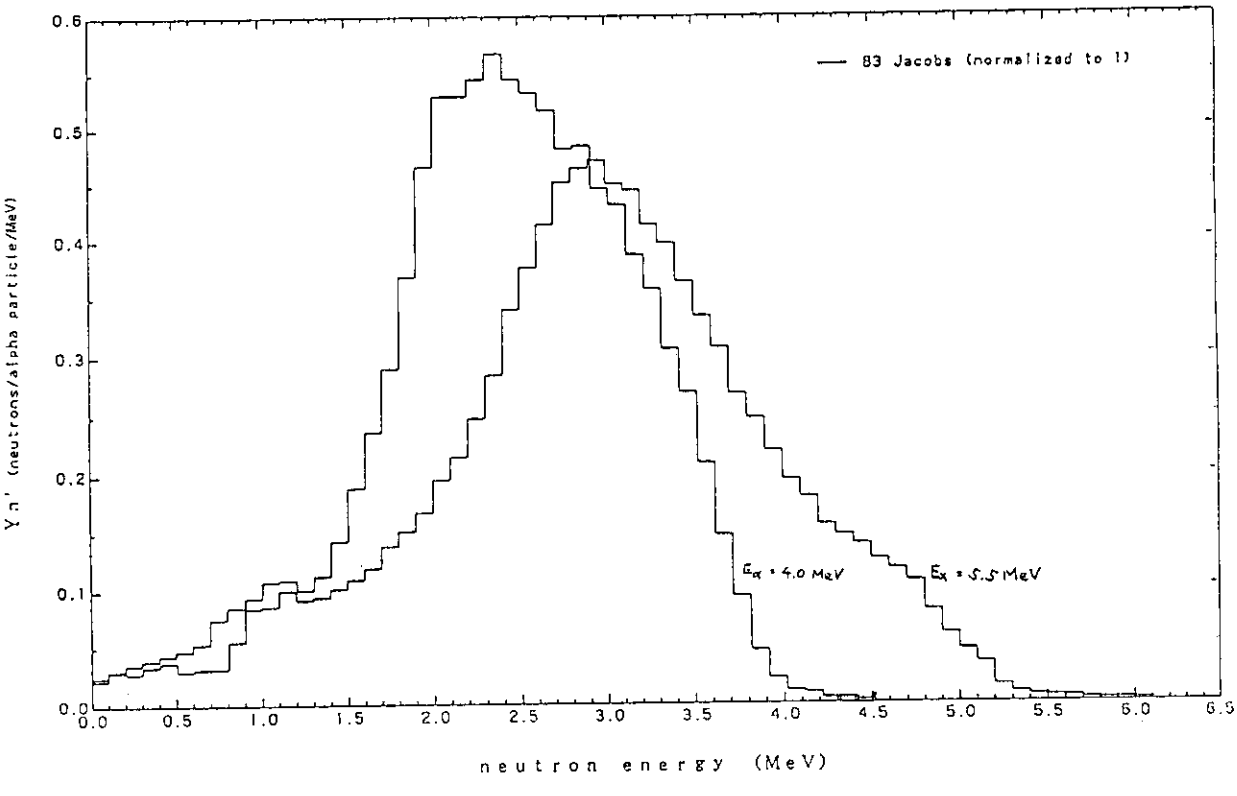

Fig. 2 Neutron energy spectrum for B(α,n)

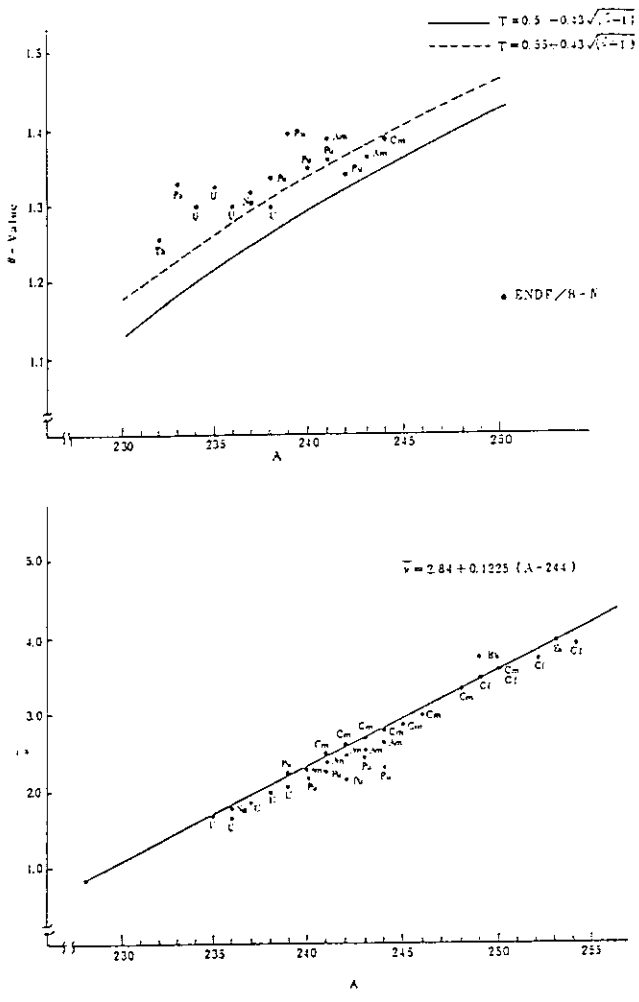

Fig. 3 Mass dependence of $\bar{\nu}_{SF}$ and T

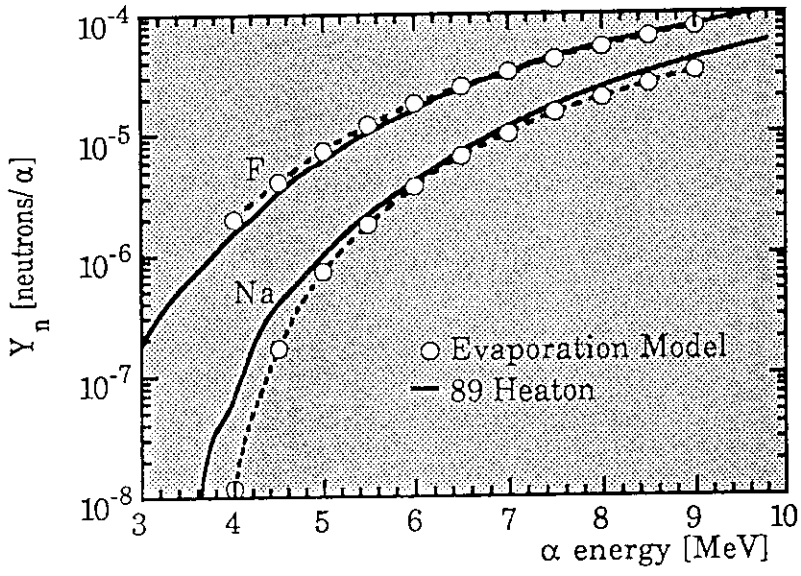

Fig. 4 (α,n) yield by evaporation model

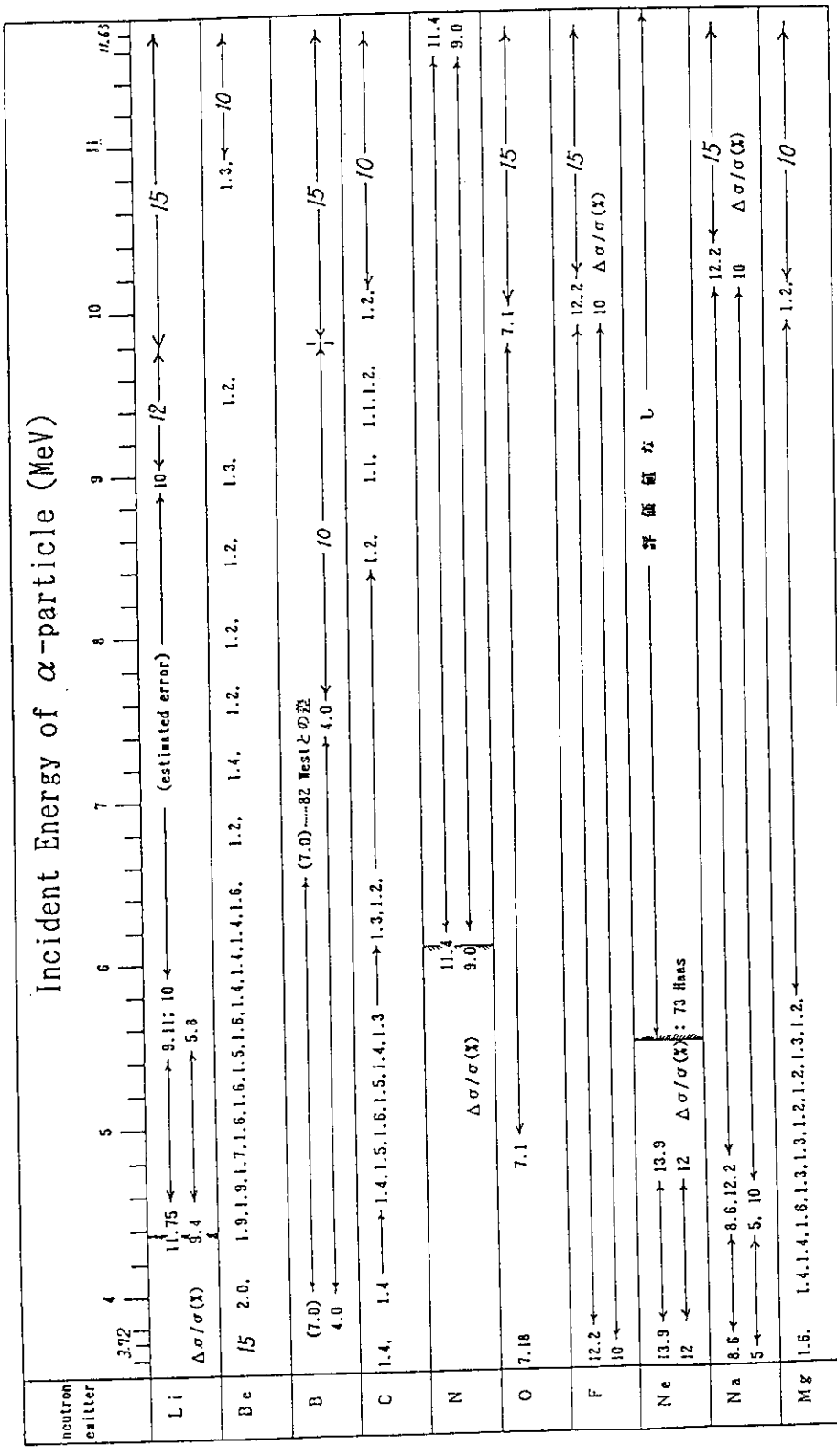

Fig. 5 Errors in the measured and evaluated neutron yields (%)

2.3 Progress of Nuclear Reaction Theories

2.3.1 Review of Statistical Models for Nuclear Reactions

Sin－iti Igarasi
Nuclear Energy Data Center
Tokai－mura, Naka－gun, Ibaraki－ken

Abstract: Statistical model calculations have been widely performed for nuclear data evaluations. These were based on the models of Hauser-Feshbach, Weisskopf-Ewing and their modifications. Since the 1940s, non-compound nuclear phenomena have been observed, and stimulated many nuclear physicists to study compound and non-compound nuclear reaction mechanisms. Concerning compound nuclear reactions, they investigated problems on the basis of fundamental properties of S-matrix, statistical distributions of resonance pole parameters, random matrix elements of the nuclear Hamiltonian, and so forth. They have presented many sophisticated results. But old statistical models have been still useful, because these models were simple and easily utilizable. In this report, these old and new models will be briefly reviwed with a purpose of application to nuclear data evaluation, and examine applicability of the new models.

1. Introduction

Statistical models for nuclear reactions have been widely used in nuclear data evaluation. Evaporation model[1,2] and Hauser-Feshbach formula[3] are particularly popular. They were formulated on the basis of the famous Bohr's hypothesis[4] on compound nuclear process. It was described as independence of formation and decay of the compound nucleus(CN), and characterized by factorization of these two factors. This simple formula was expanded recently into a triple integral[5,6] by using Gaussian Orthogonal Ensemble(GOE). In this report, a brief review on these developments from Hauser-Feshbach formula to GOE will be tried from a viewpoint of application to the nuclear data evaluation. Chronology from the 1930s to the 1980s is shown in Table 1.

In the 1950s, single particle phenomena were discovered, and were explained by using new models such as shell model[7,8], optical model[9] and direct interaction (DI) model[10]. Concepts on these are completely different from that of the old

evaporation model. Intermediate structure in resonance phenomena and precompound reactions were observed, furthermore, in the 1960s.

In background of these observation, various studies have been made to lay the theoretical foundation of CN, to combine CN and DI, and to reformulate the cross section for practical application. In particular, Moldauer[11,12,13] studied the CN cross section in terms of resonance formula. He described the cross section by using pole expansion of S-matrix. He took a statistical S-matrix which has a uniform distribution of the pole parameters. This method presented, however, a complicated cross-section formula. This may be due to unitarity of the S-matrix which does not allow any simple distribution of the pole parameters[14].

In the 1970s, there was considerable evolution in the theoretical approach on CN. Kawai et al.[15] argued the effect of DI to the cross section of CN, relaxing the unitarity condition of the S-matrix. This stimulated theoretical investigation on CN from the viewpoint of basic property of the S-matrix. Using K-matrix which secures unitarity of the S-matrix, Hofmann et al.[16,17] studied CN cross section evaluating the K-matrix parameters numerically as random variables. They examined correlations of the S-matrix parameters through those of the K-matrix parameters, and showed that one could make the S-matrix transform a new one that has the same properties as the former in the absence of DI. They obtained the CN cross section with parametrized elastic enhancement factor.

Moldauer studied numerically the distribution of the S-matrix pole parameters by using the K-matrix[18,19], and obtained some important outcome concerning the distribution of the parameters. He derived M-cancellation scheme, and formulated the CN cross section with resonance level-width fluctuation correction-factor[18,19,20] which was parametrized. Although his derivation was very complicated, this formula of the CN cross section seems to be useful for nuclear data evaluation.

More plausible, rigorous and fundamental derivation of the CN cross section has been done[5,6] recently by using Gaussian Orthogonal Ensemble (GOE) method[21,22] in which matrix elements of the nuclear Hamiltonian are random and obey Gaussian orthogonal distribution law[22,23]. Since this formula has triple integration, it is not necessarily clear from its analytical form whether or not the sum of the partial cross sections is equal to the total reaction cross section. It is very important for nuclear data evaluation that the conservation of the cross section is satisfied, and this will be shown later numerically.

In the next section, a brief survey on average cross sections, basic character of S-matrix and their relation is presented. Using these relations, the Hauser-

Feshbach formula can be derived, although the original one was obtained by the reciprocity theorem and detailed balance. No discussion on it will be done, but a short and primitive introduction for width fluctuation correction factors will be given in the section 3.

From a standpoint of nuclear data evaluation for JENDL, it is indispensable to present Moldauer model in this report. Computer codes for statistical model calculations for JENDL, which were made by the present author, were constructed based on his model as well as Hauser-Feshbach formula. In section 4, his effort will be introduced.

In section 5, modern development on CN is briefly viewed, and finally example of numerical calculation with S-matrix two-point function[5,6] is presented.

2. Average Cross Sections and S-matrix

Differential reaction cross section is given, with usual notations[24,25,26], as follows,

$$\frac{d\sigma(\alpha\to\alpha')}{d\Omega_{\alpha'}}=\frac{\pi}{k_\alpha^2}\frac{1}{(2I_1+1)(2I_2+1)}\sum_{m_{j_1}m_{I_2}}\sum_{m_{I'_1}m_{I'_2}}\Big|\frac{k_\alpha}{\sqrt{\pi}}f_{Coul}(\Omega_{\alpha'})\delta_{\alpha,\alpha'}$$

$$+i\sum_{JMjm_j}\sum_{lj'm_{j'}l'm_{l'}}(ll_1om_{I_1}\,|\,jm_j)(l'I'_1m_{l'}m_{I'_1}\,|\,j'm_{j'})$$

$$\times(jI_2m_jm_{I_2}\,|\,JM)(j'I'_2m_{j'}m_{I'_2}\,|\,JM)$$

$$\times e^{i\sigma_l^{\alpha'}}[\delta_{\alpha jl:\alpha'j'l'}-S^J_{\alpha jl:\alpha'j'l'}]e^{i\sigma_l^{\alpha}}Y_{l'm_{l'}}(\Omega_{\alpha'})\Big|^2 \qquad (2.1)$$

For reaction independent of Coulomb scattering amplitude $f_{Coul}(\Omega)$, the cross section is

$$\sigma(\alpha\to\alpha')=(\pi/k^2)\Sigma g^J\,|\,\delta_{\alpha jl:\alpha'j'l'}-S^J_{\alpha jl:\alpha'j'l'}\,|^2, \qquad (2.2)$$

Omitting trivial factors and using simple notations like $a\equiv(\alpha jlJ\Pi)$, Eq. (2.2) is presented hereafter as

$$\sigma_{ab}=|\,\delta_{ab}-S_{ab}\,|^2. \qquad (2.3)$$

Time reversal invariance of Schrodinger equation and conservation of probability flux make the S-matrix symmetric and unitary:

$$S_{ab}=S_{ba}, \qquad (2.4)$$

$$SS^+=S^+S=1. \qquad (2.5)$$

Assuming simple distribution and applying orthogonal transformation for pole parameters from R-matrix formalism[25,26], the S-matrix can be written as

$$S_{ab}=S_{ab}^{(0)}+i\sum_{\lambda}^{\Lambda}\frac{g_{\lambda a}g_{\lambda b}}{E_{\lambda}-i\frac{1}{2}\Gamma_{\lambda}-E} \tag{2.6}$$

where

$$g_{\lambda a}=e^{i\omega a}\sqrt{2P_a}\sum_{\nu}T_{\lambda\nu}\gamma_{\nu a}$$

$$\Gamma_{\lambda}=\sum_{c}|g_{\lambda c}|^2/N_{\lambda}$$

$$N_{\lambda}=\sum_{\nu}|T_{\lambda\nu}|^2\geqq 1$$

Since the number of resonances Λ is taken to be infinitely large, $S_{ab}^{(0)}$ will be assumed as a constant.

Average cross sections are defined as follows by using average and fluctuating parts of the S-matrix,

$$\langle\sigma_{ab}\rangle=\sigma_{ab}^{(D)}+\sigma_{ab}^{(C)}\ , \tag{2.7}$$

$$\sigma_{ab}^{(D)}=|\delta_{ab}-\langle S_{ab}\rangle|^2\ , \tag{2.8}$$

$$\sigma_{ab}^{(C)}=\langle|S_{ab}^{(F)}|^2\rangle\ , \tag{2.9}$$

$$S_{ab}^{(F)}=S_{ab}-\langle S_{ab}\rangle\ , \tag{2.10}$$

and

$$\langle S_{ab}\rangle=S_{ab}^{(0)}+(\pi/D)\langle g_a g_b\rangle\ . \tag{2.11}$$

3. Extension of Hauser-Feshbach Formula

Generalized transmission coefficients T_{ab} are defined[27], using the average S-matrix:

$$T_{ab}=(\langle S^{(F)}S^{(F)+}\rangle)_{ab}$$

$$=\delta_{ab}-\Sigma\langle S_{ac}\rangle\langle S_{cb}^{+}\rangle\ . \tag{3.1}$$

These relations are reduced to those for the usual optical model, if $\sigma_{ab}^{(D)}=0$, that is $\langle S_{ab}\rangle=0$ for $a\neq b$. The transmission coefficients T_a for the optical model are

$$T_a=1-|\langle S_{aa}\rangle|^2\ . \tag{3.2}$$

Formation cross section of the CN ($\sigma_c(a)$) is obtained by summing $\sigma_{ab}^{(C)}$ with respect to the exit channels b, if $\langle S_{ab}\rangle=0$ for $a\neq b$. Furthermore, it is easily seen that Eq.(3.2) is equal to the formation cross section $\sigma_c(a)$.

The evaporation model and Hauser-Feshbach formula are given symbolically by using Eq.(3.2) as

$$\sigma_{ab}^{(C)}=T_a T_b/T\ , \tag{3.3}$$

where

$$T=\sum_{c}T_c\ .$$

Original works by Weisskopf-Ewing[1] and Hauser-Feshbach[3] who introduced Eq.(3.3)

were based on the Bohr's hypothesis on the CN and detailed balance. If Eq.(3.3) is factorized by two factors and $T_a=\sigma_c(a)$ is used, one can derive Eq.(3.3). It is equivalent to a formal derivation of the Hauser-Feshbach formula based on the Bohr's hypothesis and unitarity of the S-matrix. More sophisticated and modern derivations[11,12,27] have been done by using the S-matrix. In such derivations, some correction factors were added to Eq.(3.3) depending on the assumptions concerning distribution of the pole parameters in the S-matrix.

In the region of isolated resonances ($\Gamma \ll D$), partial widths $\Gamma_c=|g_c|^2$ are distributed in accordance with a χ^2 law[28] with a degree of freedom of 1. This is called Porter-Thomas distribution, and was most used in the nuclear data evaluation for JENDL. In general, Eq.(3.3) is modified by multiplying the width fluctuation correction factor (WFCF) W_{ab}, because the partial widths fluctuate with ν (≥ 1) degrees of freedom. General formula[29,30,31] for W_{ab} in this case is

$$W_{ab}=\int_0^\infty dt \frac{1+\frac{2}{\nu_a}\delta_{ab}}{(1+\frac{2\xi_a}{\nu_a}t)(1+\frac{2\xi_b}{\nu_b}t)\prod_c(1+\frac{2\xi_c}{\nu_c}t)^{\nu_c/2}} \qquad (3.4)$$

where $\xi_a=<\Gamma_a>/<\Gamma>$. There is an important relation between W_{ab} and T_a;

$$\Sigma\, T_c\,(1-W_{ac}) = 0 \quad . \qquad (3.5)$$

This relation implies that W_{ab} is not necessarily smaller than unity for $a \neq b$, and raises the contribution from a channel with smaller T_c and reduces it from a channel with larger T_c (see Table 2).

In the region of $\Gamma \gg D$, the WFCF was discussed by many authors[15,16,17,32,33] and was given as $(1-\delta_{ab})$ with some conditions. Agassi et al.[33] mentioned that it was true, if the life-time of the CN was longer enough than equilibrium time for internal states. Vager[32] had presented it, in the strong absorption limit, with the symmetry of the S-matrix.

4. Moldauer Model

Moldauer examined the CN cross section by introducing a statistical S-matrix. It was assumed that the pole parameters of the S-matrix distributed uniformly, their statistical properties were the same outside the energy interval as in it where the energy averages of a model S-matrix were taken, and the number of resonances was infinite. He took the two-level correlation function[34] between the resonance levels, and

$$< g_{\lambda a} g_{\lambda b} > = \delta_{ab} < g_{\lambda a}^2 > \quad . \tag{4.1}$$

for level-width correlation.

His cross section formula was given as

$$\sigma_{ab}^{(C)} = < \Theta_a \Theta_b / \Theta > - M_{ab} \ , \tag{4.2}$$

where M_{ab} is a function of $< \Theta_a >$ given by an ensemble average of

$$\Theta_{\lambda a} = 2 \pi \mid g_{\lambda a} \mid^2 N_\lambda / D \quad . \tag{4.3}$$

The modified transmission coefficient $< \Theta_a >$ can be obtained by using T_a:

$$< \Theta_a > - Q \ (\Theta) \ < \Theta_a >^2 / 4 = T_a \ . \tag{4.4}$$

The two-level correlation is included in the factor $Q\ (\Theta)$ which is connected with the factor M_{ab}.

Moldauer's formula Eq.(4.2) is completely different from Eq.(3.3), because of M_{ab}. He investigated the reason behind the differences by taking account of the unitarity of the S-matrix[18,19]. The factor M_{ab} can be given with the S-matrix pole parameters, and is related with the factor $Q\ (\Theta)$, if the direct reaction is negligibly small[12].

$$M_{ab} = Q \ (\Theta) \ < \Theta_a >^2 / 4 \ . \tag{4.5}$$

It can be further expressed[18] by summing the exit channels b as

$$\sum_b M_{ab} = 2 \pi D^{-1} < N_\lambda \mid g_{\lambda a} \mid^2 > - T_a \ . \tag{4.6}$$

The first term in the right hand side of Eq.(4.5) is given as follows, by using the unitarity of the S-matrix;

$$2 \pi D^{-1} < \mid g_{\lambda a} \mid^2 > = T_a \ (1 - T_a)^{-1/2} \ . \tag{4.7}$$

Since $N_\lambda \geqq 1$, this relation implies that ΣM_{ab} becomes infinity, if $T_a \fallingdotseq 1$. Hence, there may be some channels with large values of M_{ab}, $Q\ (\Theta)$ and $< \Theta_a >$. Table 3 shows an example of $Q\ (\Theta)$ and $< \Theta_a >$. In comparison with T_a in Table 2, the modified transmission coefficients $< \Theta_a >$ are generally larger than the formers. It means probably that Eq.(4.2) gives subtraction between large values of two terms for some channels with large $< \Theta_a >$. In fact, effect of Q-factors did not clearly appear in numerical calculations[35].

Using a simple model in which plural equivalent channels were taken account of Moldauer investigated M-cancellation[18]. He showed with numerical investigations that the channel-channel correlations from the S-matrix unitarity and the level-level correlations conspired to cancel large non-Hauser-Feshbach terms. Finally, he presented the following formula[20] with effective degrees of freedom ν_c for χ^2 distribution of T_c:

$$\nu_c = 1.78 + (T_c^{1.212} - 0.78) \exp (- 0.228 T) . \tag{4.8}$$

$$\sigma_{ab}^{(C)} = \frac{T_a T_b}{T}\left(1+\frac{2}{\nu_a}\delta_{ab}\right)\times\int_0^\infty dx \prod_c \left(1+\frac{2T_c}{\nu_c T}x\right)^{-\delta_{ac}-\delta_{bc}-\nu_c/2} \quad . \tag{4.9}$$

This must be one of the applicable formulas for nuclear data evaluation.

5. Some Other Modern Formulas

Kawai et al.[15] studied the effect of DI to the CN reactions. Since DI brought a complicated correlation $<g_{\lambda a} g_{\lambda b}> \neq 0$ for $a \neq b$, they rewrote the S-matrix as follows,

$$S_{ab}(E) = <S_{ab}> + i \sum_{\lambda} \hat{g}_{\lambda a}(E)\, \hat{g}_{\lambda b}(E) / (\varepsilon_\lambda - i(\Gamma_\lambda/2) - E) . \tag{5.1}$$

They assumed $<\hat{g}_{\lambda a}\hat{g}_{\lambda b}> = 0$, and gave the following characteristics to the pole parameters:

(1) fluctuations of total width Γ_λ were omitted,

(2) energy dependence of $\hat{g}_{\lambda a}$ was neglected partly,

(3) real and imaginary parts of $\hat{g}_{\lambda a}$ were the uncorrelated random variables with normal distribution law.

Using these properties, they derived the relation,

$$<S_{ab}^{(F)} S_{cd}^{(F)*}> = X_{ac}X_{bd} + X_{ad}X_{bc} , \tag{5.2}$$

which was proposed by Vager[32], as an extension of Satchler's factorization[27], in order to keep the symmetry of $S_{ab}^{(F)}$ when the effect of DI to the CN was taken. Combining Eq.(5.2) with Eq.(3.1), the CN cross section can be obtained;

$$\sigma_{ab}^{(C)} = (1+\delta_{ab})\, T_a T_b / T, \quad \text{if} \quad \Gamma >> D. \tag{5.3}$$

In their derivation of these equations, they did not use the unitarity of the S-matrix, but the average unitarity Eq.(3.1). Hence, their theory brought up the matter of investigations of the unitarity of the S-matrix.

Tepel et al[16] and Hofmann et al[17], for example, studied the CN cross section using the K-matrix to avoid difficulty about the pole expansion of the S-matrix. They tried several numerical calculations assuming the K-matrix parameters to be random variables. Their CN cross section may be written below;

$$\sigma_{ab}^{(C)} = X_a X_b W_{ab} / X , \tag{5.4}$$

where $X = \sum_c X_c$, and

$$W_{ab} = 1 + \delta_{ab}(W_{aa} - 1) . \tag{5.5}$$

Summing up this on b and combining with Eq.(3.1),

$$T_a = X_a + (X_a^2/X)\cdot(W_{aa} - 1) . \tag{5.6}$$

This should be solved by iteration.

Tepel et al. gave

$$W_{aa} = 1 + 2\ (1 + T_a^{1/2})^{-1}\ , \tag{5.7}$$

and Hofmann et al. did, with the arithmetic mean $<T>$ of all T_a;

$$W_{aa} = 1 + 2\ (1 + T_a^{0.3+1.5T_a/T})^{-1} + 2\ ((T_a - <T>)/T)^2\ . \tag{5.7'}$$

These should be also examined whether or not they are applicable to the nuclear data evaluation.

The most exciting development of the CN cross-section formula has been made by Heidelberg group[5,6]. Their theory is based on the Gaussian Orthogonal Ensemble initiated by Wigner[21,22,23]. They made the S-matrix whose pole parameters were functional variables of matrix elements of the Hamiltonian which were assumed to follow the Gaussian orthogonal distribution law. Since their derivation is very complicated and hard, only the CN cross-section formula is presented here. It is a little modified from the S-matrix two-point function which is published in the original papers[5,6]:

$$\sigma_{ab}^{(c)} = \frac{T_a T_b}{8}\int_0^\infty d\lambda_1 \int_0^\infty d\lambda_2 \int_0^1 d\lambda \frac{\lambda(1-\lambda)\,|\lambda_1-\lambda_2|}{[\lambda_1(1+\lambda_1)\lambda_2(1+\lambda_2)]^{1/2}(\lambda+\lambda_1)^2(\lambda+\lambda_2)^2}$$

$$\times \prod_c \frac{1-T_c\lambda}{(1+T_c\lambda_1)^{1/2}(1+T_c\lambda_2)^{1/2}} \left\{\delta_{ab}(1-T_a)\left(\frac{\lambda_1}{1+T_a\lambda_1}+\frac{\lambda_2}{1+T_a\lambda_2}\right.\right.$$

$$\left.+\frac{2\lambda}{1-T_a\lambda}\right)^2 + (1+\delta_{ab})\left[\frac{\lambda_1(1+\lambda_1)}{(1+T_a\lambda_1)(1+T_b\lambda_1)}\right.$$

$$\left.\left.+\frac{\lambda_2(1+\lambda_2)}{(1+T_a\lambda_2)(1+T_b\lambda_2)}+\frac{2\lambda(1-\lambda)}{(1-T_a\lambda)(1-T_b\lambda)}\right]\right\} \tag{5.8}$$

Table 4 shows examples of numerical calculation. Sum of the two cross sections σ_{ce} and σ_{in} for three options agrees with each other. This agreement is one of the important check-points for nuclear data evaluation, because the total cross section calculated with the optical model should be equal to the sum of the partial cross sections. As three fold integration must be done in GOE calculations, undesirable cumulative errors may be larger than those for the other two cases. Therefore, this point should be carefully taken into account.

Another important point is CPU-time for the calculation. For GOE, it is 30-40 times larger than the Hauser-Feshbach calculation with or without WFCF. Although these matters must be resolved, Eq. (5.8) is surely one of the applicable tools.

6. Concluding Remarkes

Development of the statistical model for nuclear reaction was briefly reviewed from the standpoint of the nuclear data evaluation. Since too many interesting and applicable papers existed, only a few were presented in this review.

For the nuclear data evaluation, the Hauser-Feshbach and Moldauer models have been widely used. Moldauer developed his theory by assuming a uniform distribution of the S-matrix pole parameters. Although Eq.(4.2) was complicated and has difficulty, his final formula, Eq.(4.8), may be useful for application.

After Kawai et al. studied the effect of DI to CN with loose unitarity of the S-matrix, this problem has been investigated by many authors. Most of them took the K-matrix to keep the unitarity of the S-matrix, and formulated the CN cross sections by applying the unitary transformation to the S-matrix. In this review, only the CN cross sections proposed by Tepel et al. and Hofmann et al. were introduced.

Finally, a rigorous and magnificent formula presented by the Heidelberg group was introduced. Some examples of the numerical calculations were shown, and compared with the Hauser-Feshbach with and without WFCF. Because this formula is a triple integration, there may be some problems to be resolved in order to apply to the nuclear data evaluation.

References

1) V.F.Weisskopf and D.H.Ewing: Phys. Rev. 57, 472 (1940)
2) J.Blatt and V.F.Weisskopf: Theoretical Nuclear Physics, p.365 Wiley, New York, 1952
3) W.Hauser and H.Feshbach: Phys. Rev. 87, 366 (1952)
4) N.Bohr: Nature 137, 344 (1936)
5) J.J.M.Verbaarschot, H.A.Weidenmuller and M.R.Zirnbauer: Phys. Rep. (Phys. Lett. C) 129, 367 (1985)
6) J.J.M.Verbaarschot: Ann. Phys. 168, 368 (1986)
7) M.G.Mayer: Phys. Rev. 75, 1969 (1949)
8) O.Haxel, J.H.D.Jensen and H.E.Suess: Phys. Rev. 75, 1766 (1949)

9)H. Feshbach, C. E. Porter and V. F. Weisscopf: Phys. Rev. 96, 448 (1954)
10)N. Austern: Direct Nuclear Reaction Theories, Wiley, New York, 1970
11)P. A. Moldauer: Phys. Rev. 123, 968 (1961)
12)P. A. Moldauer: Phys. Rev. 135, B642 (1964)
13)P. A. Moldauer: Rev. Mod. Phys. 36, 1079 (1964)
14)C. A. Engelbrecht and H. A. Weidenmuller: Phys. Rev. C8, 859 (1973)
15)M. Kawai, A. K. Kerman and K. W. McVoy: Ann. Phys. 75, 156 (1973)
16)J. W. Tepel, H. M. Hofmann and H. A. Weidenmuller: Phys. Lett. 49B, 1, (1974)
17)H. M. Hofmann, J. Richert, J. W. Tepel and H. A. Weidenmuller:
Ann. Phys. 90, 403 (1975)
18)P. A. Moldauer: Phys. Rev. C11, 426 (1975)
19)P. A. Moldauer: Phys. Rev. C12, 744 (1975)
20)P. A. Moldauer: Nucl. Phys. A344, 185 (1980)
21)H. A. Weidenmuller: Nuclear Structure 1985, Proc. Niels Bohr Centenniel Conf., Copenhagen, 1985, R. Broglia et al. (ed.), p. 213 (1985)
22)J. E. Lynn: Theory of Neutron Resonance Reaction, Clarendon Oxford (1968) p. 177
23)T. A. Brody, J. Flores, J. B. French, P. A. Mello, A. Pandey and S. S. M. Wong:
Rev. Mod. Phys. 53, 385 (1981)
24)J. M. Blatt and L. C. Biedenharn: Rev. Mod. Phys. 24, 258 (1952)
25)A. M. Lane and R. G. Thomas: Rev. Mod. Phys. 30, 257 (1958)
26)E. Vogt: Rev. Mod. Phys. 34, 723 (1962)
27)G. R. Satchler: Phys. Lett. 7, 55 (1963)
28)C. E. Porter and R. G. Thomas: Phys. Rev. 104, 483 (1956)
29)L. Dresner: Proc. Int. nat. Conf. on Neutron Interaction with the Nucleus, Columbia Univ. 1957, CU-175, p. 71 (1957)
30)J. E. Lynn: Theory of Neutron Resonance Reaction, Clarendon Oxford (1968) p. 230
31)H. Gruppelaar and G. Reffo: Nucl. Sci. Eng. 62, 756 (1977)
32)Z. Vager: Phys. Lett. B36, 269 (1971)
33)D. Agassi, H. A. Weidenmuller and G. Mantzouranis:
Phys. Rep. (Phys. Lett. C) 22, 145 (1975)
34)F. Dyson: J. Mat. Phys. 3, 166 (1962)
35)S. Igarasi: J. Nucl. Sci. Technol. 12, 67 (1975)

Table 1 Chronology on development of statistical model

Years	Events and Related Matters
1934	E. Fermi and others observed big resonance in slow neutron capture cross section
1936	N. Bohr presented the concept of compound nucleus (CN) Many experiments on slow neutron capture resonances Breit and Wigner gave resonance cross section formula
1937	Many works on generalization of resonance formula, and on relation with CN concept; Bethe・・・・・・・・ $\Gamma \langle D$ Weisskopf・・・・ $\Gamma \rangle D$
1940	Weisskopf and Ewing presented evaporation formula
1949	Shell model proposed
1950	Butler observed stripping reaction with deuteron
1951	Wolfenstein proposed a formula for inelastic scattering cross section calculation
1952	Barschall measured neutron total cross sections, and observed systematics in their gross structure Hauser and Feshbach expanded the Wolfenstein's formula

Table 1 (Continued)

Years	Events and Related Matters
1954	Feshbach, Porter and Weisskopf analysed the neutron total cross sections with optical model
1956	Wigner studied level spacing distribution with Hamiltonian matrix of random variable
1956	Porter and Thomas presented χ^2 distribution law for partial level width
1957	Dresner calculated level width fluctuation correction effects Lane and Lynn also studied the fluctuation correction
1960	Ericson predicted statistical fluctuations in non－averaged cross sections
1960	Anderson and Wong observed isobaric analog states
1962	Sidorov observed precompound reactions
1963	Holbrow and Barschall measured also precompound processes
1964	Moldauer formulated compound nuclear cross sections based on statistical S－matrix
1965	Robson gave theory on isobaric analog resonances
1966	Griffin analysed precompound nuclear reactions

Table 1 (Continued)

Years	Events and Related Matters
1967	Feshbach et al. (FKL) formulated intermediate structure of nuclear cross sections
1970	Austern fomulated direct inter－action theory
1971	Vager showed relation between symmetry of S－matrix and elastic enhancement factor
1973	Engelbrecht and Weidenmuller showed difficulty of S－matrix pole parameter distribution law due to its unitality They studied also the effect of direct interaction Kawai et al. (KKM) investigated direct interaction effect to compound nuclear process
1975	Hofmann et al. and others studied compound nuclear cross section numerically using K－matrix Agassi et al. formulated nuclear reactions with random matrix Moldauer studied numerically M－cancellation scheme
1977	Gruppelaar and Reffo reviewed width fluctuation correction
1978	Kretschmer and Wangler obtained experimentally $W_a = 2.09 \pm 0.14$
1979	Mello studied fluctuation cross sections with ensemble of S－matrices

Table 1 (Continued)

Years	Events and Related Matters
1980	Feshbach et al. (FKK) formulated the statistical theory of multi−step compound and direct reactions
1981	Brody et al. reviewed random−matrix physics
1985	Mello et al. applied information theory to nuclear reactions
	Verbaarschot et al. formulated one−point and two−point S−matrices with GOE of random Hamiltonian

Table 2 Example of W_{ab}: 1st Level of Cr-52(2+) : E=1.5 MeV

J	Π	l_a	l_b	T_a	T_b	W_{ab}
0.5	+	0+	2−	0.949	3.29−4	0.950
0.5	+	0+	2+	0.949	9.06−4	0.937
0.5	−	1−	1+	0.131	3.54−3	0.754
1.5	+	2−	0+	0.544	0.653	0.501
1.5	+	2−	2−	0.544	3.29−4	1.040
1.5	+	2−	2+	0.544	9.06−4	1.053
1.5	−	1+	1−	0.157	3.17−3	0.756
1.5	−	1+	1+	0.157	3.54−3	0.750
2.5	+	2+	0+	0.382	0.653	0.509
2.5	+	2+	2−	0.382	3.29−4	1.159
2.5	+	2+	2+	0.382	9.06−4	1.152
2.5	−	3−	1−	7.12−3	3.17−3	0.583
2.5	−	3−	1+	7.12−3	3.54−3	0.569

Table 3 Example of Q^J: 1st level of Cr-52(2+) : E=1.5 MeV

J	Π	l_a	l_b	Θ_a	Θ_b	Q^J
0.5	+	0+	2−	1.65	3.29−4	1.031
0.5	+	0+	2+	1.65	9.04−4	1.031
0.5	−	1−	1+	0.140	3.54−3	1.806
1.5	+	2−	0+	0.666	0.852	1.100
1.5	+	2−	2−	0.666	3.29−4	1.100
1.5	+	2−	2+	0.666	9.04−4	1.100
1.5	−	1+	1−	0.170	3.17−3	1.773
1.5	−	1+	1+	0.170	3.54−3	1.773
2.5	+	2+	0+	0.438	0.876	1.164
2.5	+	2+	2−	0.438	3.29−4	1.164
2.5	+	2+	2+	0.438	9.06−4	1.164
2.5	−	3−	1−	7.14−3	3.17−3	1.969
2.5	−	3−	1+	7.14−3	3.54−3	1.969

Table 4a Comparison of cross sections Fe-56 E_n=3.0 MeV (5 levels)

	H−F	Fluc.	GOE
σ_{ce} (b)	0.34492	0.66114	0.56719
σ_{in} (b)	1.1669	0.85069	0.94340
Time (sec)	0.10	0.17	3.79

Table 4b Comparison of cross sections Cr-52 E_n=3.0 MeV (5 levels)

	H−F	Fluc.	GOE
σ_{ce} (b)	0.37647	0.67530	0.59086
σ_{in} (b)	0.93778	0.63895	0.72261
Time (sec)	0.10	0.15	2.96

2.3.2 Composite Particle Emission in Preequilibrium Process − Reminiscing Work Done in Collaboration with the Late Dr. Kichinosuke Harada −

A. Iwamoto
Japan Atomic Energy Research Institute
Tokai-mura, Naka-gun, Ibaraki-ken

Works on light particle emission in preequilibrium nuclear reaction which were done in collaboration with the late Dr. Kichinosuke Harada are reviewed. Basic idea for the formalism for emission of composite particle is given first, followed by the numerical calculations for energy spectra under this formalism. Secondly, we will discuss the formalism for the energy-angle double differential cross section which takes into account the conservation of the linear momentum explicitly. This formalism is applied to both the nucleon and composite particle emission in numerical calculations.

1. Introduction

Dr. Kichinosuke Harada, certainly one of the most prominent nuclear physicists in our age, died on 9 February 1990 at his home in Yono City. He was 59 years old. He gained his reputation early by his work on alpha decay theory, which clarified an important role of nuclear pairing for the process and is now regarded as classic. Since then, he had been a very active and energetic physicists at Japan Atomic Energy Research Institute and even after his retirement, he never lost his interest in this field. We cannot forget, however, his achievements as director of the Department of Physics of JAERI. He successfully constructed JAERI Tandem Accelerator in spite of many difficulties. He brought together and nurtured many physicists at JAERI. He was also active as chairman of Sigma committee and contributed much to the nuclear data community. I personally learned much from him through our collaboration on theoretical nuclear physics, which lasted more than 15 years. It is impossible to describe all of his activities here, even if we limit his contribution to theoretical nuclear physics only and thus I will focus on one of our works briefly. Our collaboration was done mainly in the field of nuclear fission and heavy ion reactions, but for several years we were involved in the theory of preequilibrium nuclear reactions. I will choose this as the topic of this meeting.because this field is also important in the nuclear data activity,

Exciton model has been used widely as a practical tool to calculate the energy spectra of light particles emitted in the nuclear reaction which leaves the residual nucleus in its continuum state. It works rather well for the nucleon emission induced by nucleons or light composite particles. Typical examples are nucleon inelastic and charge-exchange reactions .

For the case of composite-particle induced reactions, such as (α,p) or (α,n) reaction, the situation is nearly the same if we can assume that the incident particle breaks up into nucleons in the field of target nucleus, although there is some ambiguity as to what is the initial exciton number. The situation is quite different for the composite-particle emission reactions, such as (p,α) and (n,α), because we have to arrange several nucleons to form the composite particle in this case. We thought some existing models had problems and thus formulated a new model for the reaction, which will be described in Sec.2.

As to the angular distributions in the exciton model, there was a model of fast particle at that time. The model took into account of the change of the direction of momentum for the particle in the continuum in the framework of exciton model. The nucleon-nucleon collision in this model is treated by free N-N scattering and thus the effects of Fermi motion and Pauli blocking were not taken into account. To remove such defects and to get results that reproduce experimental angular distributions better, we developed a new formalism of exciton model in which correct kinematics, as well as the Fermi motion effect and the Pauli blocking effect,is taken into account. This new model and related problems will be discussed in Sec.3.

Finally in Sec.4, we will give a brief summary of our works .

2. Mechanism of composite particle emission in exciton model

Original exciton model is formulated [1] assuming statistical distribution of nucleons and Fermi-gas model. Therefore, we have to extend the formalism in order to apply it to the emission of composite particles such as α particle. One method to achieve this is a preformed alpha model.[2] in which α particles are assumed to be preformed in the ground state of the target nucleus . Alpha particle in this model is treated as α-exciton and the amount of pre-formed α is treated as a parameter. One problem of this model is that the value of this parameter determined from fitting to data is too large compared to the microscopic calculation of α spectroscopic factor for the ground-state wave functions. Another problem is the difficulties for reproducing the high momentum component of α spectra.. To reproduce the data, it is necessary to assume that preformed α have moderate amount of high energy component, which is hard to justify because α is believed to be weakly bound in the target nucleus. Other models which do not assume the preformed α is either conceptually hard to justify or the calculated results differ from the data so much. Therefore, we developed a new model which could overcome difficulties mentioned above.[3,4]

The basic emission rate expression W for the particle x from n-exciton state is given by

$$W_n^{(x)}(\varepsilon) = \frac{2s+1}{\pi^2 \hbar^3} \mu_x \varepsilon \sigma_{abs}^{(x)} \frac{\omega(p-n_x,h,U)}{\omega(p,h,E)} \quad , \qquad (1)$$

where s is the spin, μ the reduced mass and ε is the energy of the emitted particle. Capture cross section for the particle x is denoted by $\sigma_{abs}^{(x)}$ and ω is the level density formula for a fixed particle and hole numbers. Symbol p stands for the particle number, h the hole number and n_x is the number of constituent nucleons for the particle x which is 1 for nucleon emission and 4 for α emission. The excitation energy of the compound nucleus is E and that of the residue is U. Our concern is the factor n_x, which reduces the probability for composite particle drastically because the reduction of particle number for the residual nucleus causes a drastic reduction of the level density.of the residue. On the other hand, the experimental (p,a) cross section, for example, has far more larger than the results calculated by eq.(1). It means that the naive application of the exciton model is unsuccessful for composite particle emission.

Our idea is to change the expression (1) to the one given by

$$W_{n(l,m)}^{(x)}(\varepsilon) = \frac{2s+1}{\pi^2\hbar^3}\mu\varepsilon\sigma_{abs}^{(x)}F_{l,m}(\varepsilon)\frac{\omega_{n(l,m)}^{*}(U)}{\omega(p,h,E)} \quad , \tag{2}$$

where $F_{l,m}(\varepsilon)$ is the formation factor for the composite particle and $\omega_{n(l,m)}^{*}(U)$ is the level density for the residue after the particle emission. The meaning of l and m are the followings: Equation (1) means that the composite particle x, whose number of the constituent particles is n_x, is formed from the nucleons in particle state In eq.(2), on the other hand, we assume that the composite particle is formed from l-particles above the Fermi level and and m-particles below and $l+m=n_x$. It represents a process of pick-up type reaction where m particles are picked-up not from excitons but from unexcited single-particle levels. In the case of α emission, n_x is 4 and we show in Fig.1 an illustration of 4 processes which lead to α emission. In the figure, the process (d) is normal exciton-model process calculated by eq.(1). Other three processes are new and they are included in eq.(2).

The formation factor F represents the possibilities to form the particle of energy ε from the configuration that l-particles are above the Fermi level and m below. Thus it can be calculated by the overlap integral between the wave function of the compound nucleus and the wave function of the particle-plus-residue, i.e., spectroscopic factor. This calculation was done in terms of the harmonic oscillator wave function [5], but it required a large scale numerical calculations, because there are so many components. We developed an alternative method of calculating this F in which we can calculate it by the classical phase space integration base on the Fermi-gas model. We can get closed form expressions for $F_{l,m}(\varepsilon)$ in this model, although the expressions are length one. The important feature of F is that

$$\sum_{l+m=n_x} F_{l,m}(\varepsilon) = 1 \qquad (3)$$

holds for any ε. In Fig.2, we show this formation factor for α emission. From this figure, we see that when the emission energy is high, most of α emitted are composed of 4 particles above the Fermi level, i.e., a normal exciton process. But as energy decreases, the pick-up type components become more important and below a fixed energy, only pick-up type components contribute..

The emission rate expression (2) was incorporated into the standard exciton model formalism and numerical calculations were done for many preequilibrium reactions. Among them, we will show in Fig.3, the proton induced reactions on ^{197}Au [4]. The calculations were done only for the preequilibrium component of the energy spectra and thus we should add the equilibrium component to compare with the experimental data. As is shown in the figure, we could get an overall qualitative agreement with the data although we didn't include any fitting parameter. Especially, the high energy component of alpha and triton particles are reproduced well. Though the high energy component of deutron and ^{3}He is not well reproduced, cause of which might be a direct pick-up process which is not included in the exciton model, the relative ratio of the cross section was well reproduced. The calculations were done for many reactions and we could get similar quality of fitting to data.

From these calculations, we demonstrated the importance of the pick-up type reactions in the high energy spectra of composite particles. The formulation for the process was done in line with the standard exciton model picture, without introducing the pre-formed composite particles.

3. Refinement of the double differential cross section

To calculate the angular distributions in preequilibrium reactions, an generalization of exciton model was proposed [6,7]. In that model, the original master equation which determines the evolution of the probability was written in the form,

$$\frac{d}{dt}q(n\Omega t) = \sum_m \int d\Omega'\, q(m\Omega' t) w_{m\to n}(\Omega'\to\Omega) - q(n\Omega t)\left\{\sum_m \int d\Omega' w_{n\to m}(\Omega\to\Omega') + W_n\right\}, \qquad (4)$$

where $q(n\Omega t)$ is the probability that the state is in n-exciton state at time t and the direction of the "fast" particle is Ω. $w_{m\to n}(\Omega'\to\Omega)$ represents the transition rate from the m-exciton state to the n-exciton state associated with the change of the direction of the particle $\Omega'\to\Omega$. W_n represents the total emission rate of the particle.

As eq.(4) shows, the quantity $w_{m\to n}(\Omega'\to\Omega)$ is independent of the energy of the "fast" particle and its angular dependence is calculated from the uniform distribution for the s-wave free nucleon-nucleon scattering in the center-of-mass coordinate. In this respect, the effect of the Fermi motion of nucleons in the target nucleus is neglected and no Pauli blocking effect is taken into account. In order to include these effects, we should include the energy of the "fast" particle as a dynamical variable as well as the scattering direction. Thus we extended the formalism of the generalized exciton model as follows [8]:

We extended the master equation (1) to the form

$$\frac{d}{dt}q(n\Omega\varepsilon t) = \sum_m \int d\Omega' \int d\varepsilon'\, q(m\Omega'\varepsilon' t) w_{m\to n}(\Omega'\varepsilon'\to\Omega\varepsilon) - q(n\Omega\varepsilon t)\left\{\sum_m \int d\Omega' \int d\varepsilon' w_{n\to m}(\Omega\varepsilon\to\Omega'\varepsilon') + W_n\right\} , \tag{5}$$

where $q(n\Omega\varepsilon t)$ is the probability that the state is in n-exciton state at time t and the direction and energy of the "fast" particle are Ω and ε. Accordingly, $w_{m\to n}(\Omega'\varepsilon'\to\Omega\varepsilon)$ is generalized to the transition rate associated with the change of energy as well as the direction for the "fast" particle. By the inclusion of ε as a new variable, we could introduce the Fermi motion and Pauli blocking effects in the transition rate expression.

In Fig.4, we show the change of the shape of energy spectra for the incident nucleon of 62 MeV after the collision of the Fermi-gas of the target nucleus. The shapes of the spectra after n-th collision are shown by curves with circled n. Whereas the spectra after the first collision is wide and direct-reaction like, they change to statistical like after several collisions.

With this generalized transition rate expression, we solved the master equation (5). By the use of the Legendre polynomial expansion technique, the numerical calculation is simplified much. From the solution of eq.(5), the energy-angle double differential cross section is obtained directly without any fitting parameter. In Fig.5, we show one of the results of numerical calculations based on the formalism [8]. It is a proton angular distribution induced by 62 MeV proton on ^{209}Bi. As is seen in the figure, our results are rather good except for the backward angles and angles near zero degree. Main reason for the discrepancy in backward angle is that the high momentum components in nuclear Fermi motion is not taken into account fully in the Fermi-gas model we adopted. In other words, the many body correlation of the target nucleus is important to the backward cross section. In fact, when we replace the Fermi-gas distribution used to calculate $w_{m\to n}(\Omega'\varepsilon'\to\Omega\varepsilon)$ by the momentum distribution of harmonic oscillator wave function [9], we got a much enhanced

backward cross section. It is caused because by confining nucleons in a single-particle potential, the momentum distribution of nucleons is spread to higher energies and the collision of the incident particle with these high-momentum component produces a backward components. The problem of the discrepancy near zero degree is another problem and complete solution is not yet achieved.

We also formulated a double differential cross section for the emission of composite particles. In this case, due to the averaging procedure used in the formalism, the calculated results reproduce the data well, including backward angels and near zero degree angels. One example is given in Fig.6 for the 62 MeV ^{209}Bi(p, α) reaction [8] where we could get an overall good reproduction of the data.

4. Summary and conclusions

In Secs.2 and 3, we reviewed our works on the exciton model. What we added as new knowledge to this field are: 1) Exciton model can be generalized to the composite particle emission naturally and it can reproduce the main feature of the data without any fitting parameter. Physically important process in this model is the pick-up type reaction which occurs in relatively small exciton state. 2) Generalized exciton model can be extended to calculate the energy-angle double differential cross section, in which the Fermi motion and the Pauli blocking effects are properly taken into account. This formalism can be applied also to the double differential cross section for the composite particle emission.

There are several problems left which should be solved in future, e.g., the problem of deutron energy spectra mentioned in Sec.2 and the most forward angular distribution mentioned in Sec.3. Also interesting is the preequilibrium particle emission in heavy ion reactions. A trial was done [10] and the results were promising. But it needs more studies before the method becomes a standard one like the exciton model in light ion reactions.

References

[1] J.J. Griffin, Phys.Rev.Lett.**17** (1966)478.

[2] L. Milazzo Colli and G.M. Braga Marcazzan, Riv.Nuovo Cimento **3** (1973)535.

[3] A. Iwamoto and K. Harada, Phy.Rev.C**26** (1982)1821.

[4] K. Sato, A. Iwamoto and K. Harada, Phys.Rev.C**28** (1983)1527.

[5] I. Tonozuka, A. Iwamoto and K. Harada, JAERI-M **83-057** (1983)

[6] G. Mantzouranis, D. Agassi amd H.A. Weidenmüller, Phys.Lett.**57B** (1975)220.

[7] J.M. Akkermanns, Phys.Lett.**82B** (1977)20.

[8] A. Iwamoto and K. Harada, Nucl.Phys.**A419** (1984)472.

[9] K. Sato, Phys.Rev.C**32** (1985)647.

[10] A. Iwamoto, Phys.Rev.C**35** (1987)984.

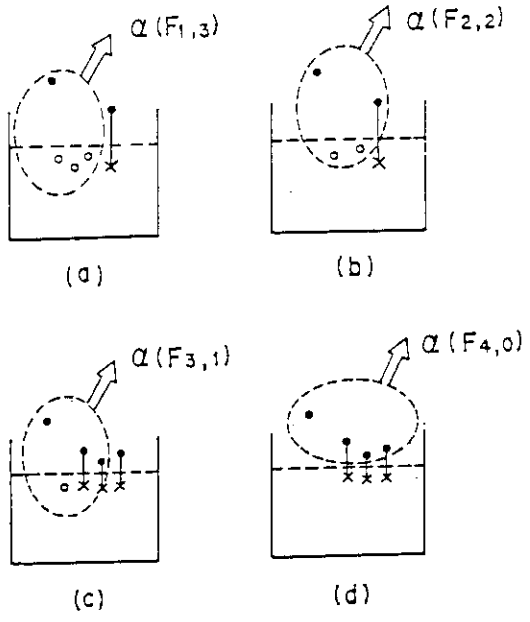

Fig. 1 Illustration of the processes for alpha particle emission. Processes (a),(b),(c) are pick-up type reactions.

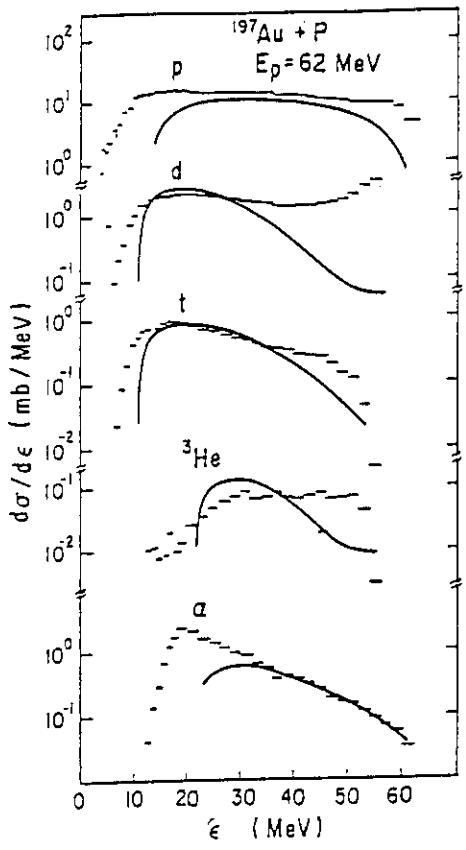

Fig. 3 Angle-integrated energy spectra for (p,d), (p,t), (p,^{3}He) and (p,α) reactions on ^{197}Au induced by 62 MeV proton. Data (dots) and our calculations (solid lines) are shown.

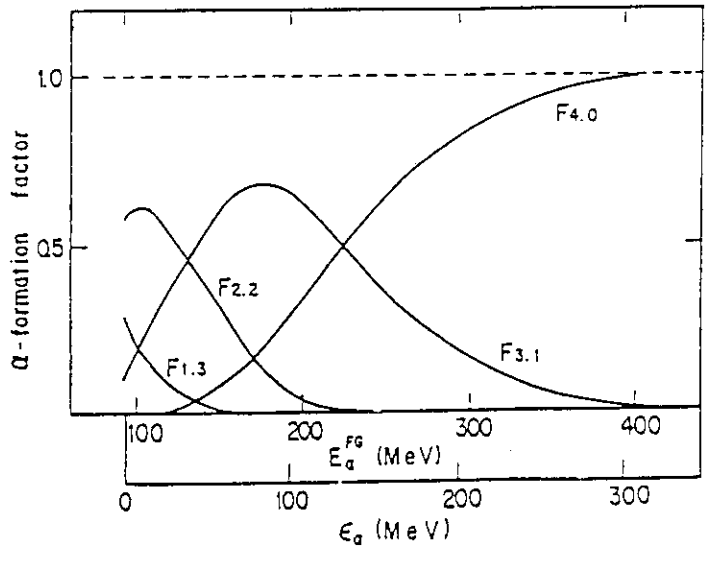

Fig. 2 The alpha particle formation factor F as a function of the alpha energy ε_α.

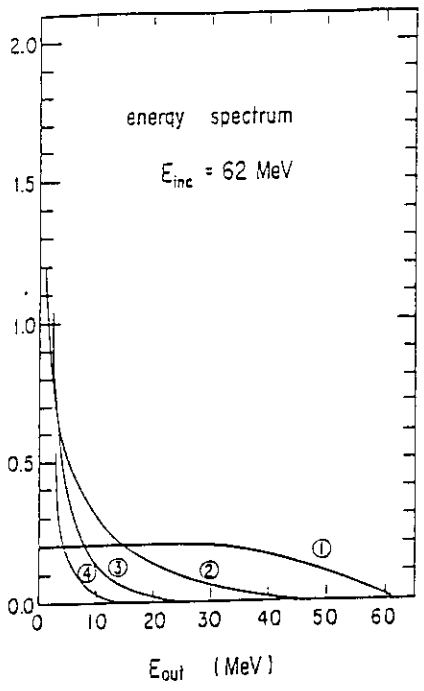

Fig. 4 Shapes of the energy spectra after collisions with the nucleons of the target for 62 MeV incident nucleon. The numbers circled specify the number of collisions.

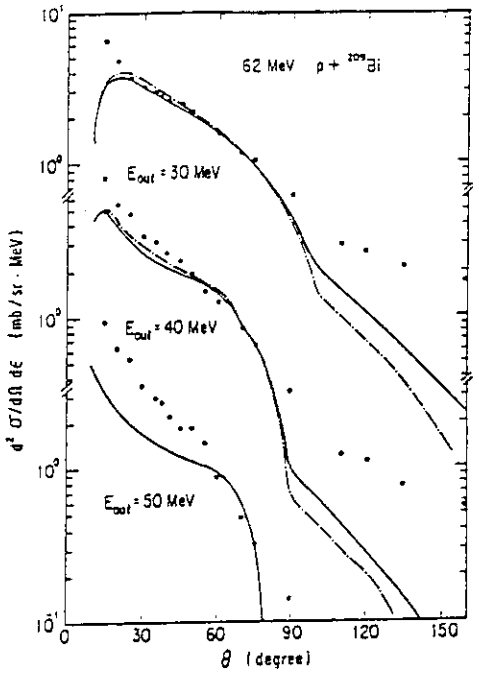

Fig. 5 Double differential cross sections for (p,p') reaction induced by 62 MeV proton on ^{209}Bi. Data (dots) and two types of our calculations (solid and dot-dashed lines) are shown.

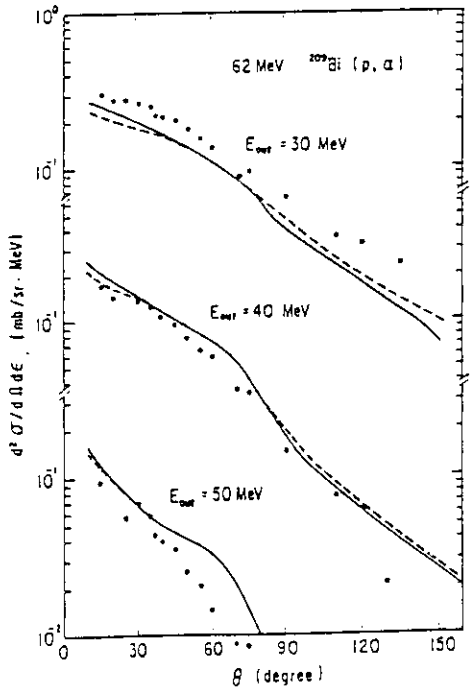

Fig. 6 Double differential cross sections for (p,α) reaction induced by 62 MeV proton on ^{209}Bi. Data (dots) and our calculations (solid line) are shown.

2.4 Topics-2

2.4.1 International Cooperation in Nuclear Data Evaluation Activities

Y. Kanda
Department of Energy Conversion Engineering,
Kyushu University
Kasuga, Fukuoka 816, Japan

A history of international cooperation of nuclear data community is briefly reviewed and the present activities are outlined. Detailed description concerned can be found in the reports of Igarasi[1] and Kikuchi[2].

In 1964, the network of nuclear data information exchange was established by connecting the following four data centers: The USA National Nuclear Data Center at Brookhaven National Laboratory, USA, The NEA Data Bank at Saclay, France, The USSR Nuclear Data Center at the Fiziko-Energeticheskij Institut, Obninsk, Soviet Union, and the IAEA Nuclear Data Section at Vienna, Austria. Japan belongs to the NEA Data Bank Group as a member country of OECD. One of the main cooperative activities is the compilation and publication of CINDA, the Computer Index of Neutron Data which contains bibliographical references to neutron nuclear data. Numerical data of the references listed in CINDA can be obtained in a common exchange format called EXFOR. CINDA and EXFOR data have been valuably used in the nuclear data evaluation.

There are four main nuclear data evaluation projects in the OECD countries; the JENDL in Japan, the ENDF/B in USA, and JEF and DFF in Western Europe. They have inherent and individual histories. However, they have the same object. It has been discussed for several years that the evaluators in these projects cooperate to produce a common nuclear data file. As a result, agreement was reached in October 1989 to establish a Working Group on Evaluation Cooperation sponsored by the NEA Committee on Reactor Physics (NEACRP) and the NEA Nuclear Data Committee (NEANDC). The working group selected following six high priority tasks;

1) intercomparison of evaluations for ^{52}Cr, ^{56}Fe and ^{58}Ni
2) generation of covariance files for ^{56}Fe and ^{nat}Fe

3) actinide data in the thermal energy range
4) ^{238}U capture and inelastic scattering cross sections
5) ^{239}Pu fission cross section from 1 to 100 keV
6) delayed neutron data benchmarking

They are progressing by organizing individually the six sub-working groups. A few reports on their outcome will be presented in International Conference on Nuclear Data for Science and Technology held on 13–17 May 1991 at Jülich, Federal Republic of Germany.

References

[1] S. Igarasi, "Iternational Cooperation on Nuclear Data Evaluation", J. Atom. Ener. Soc. Japan, **31**, 912 (1989) (In Japanese)
[2] Y. Kikuchi, "International Cooperation on Nuclear Data Evaluation (II)", J. Atom. Ener. Soc. Japan, **32**, 167 (1990) (In Japanese)

2.4.2 The Life Devoted to Nuclear Data and Reactor Physics － Shungo Iijima (Sept. 22, 1930 ～ Nov. 14, 1990)

Toru Murata
Nuclear Engineering Laboratory
Toshiba Corporation
4-1 Ukishima-cho, Kawasaki-ku, Kawasaki,
210, Japan

Dr. S. Iijima

Shungo Iijima died of pneumonia caused by lung cancer on November 14, 1990 at the age of 60. His death was great sad to all those who engaged in nuclear data and reactor physics in Japan.

After graduation from master course of Faculty of Science, Gakushuin University, he entered doctor course of Faculty of Science, The University of Tokyo and studied theoretical nuclear physics. On 1959, he found employment with Nippon Atomic Industry Group, and engaged in researches on reactor physics and nuclear data evaluation. He was a member of Japan Nuclear Data Committee from the establishment of the committee.

In the field of reactor physics, his early works were studies on light water reactor criticality and resonance absorption, which was done during his stay at ORNL in 1962. He also had interests on thermal neutron scattering law and lattice dynamics.

After these works, he engaged in nuclear design of fast breeder reactor and made nuclear data set for

the design. He finished up the data set by analyzing the experimental results of JAERI Fast Critical Assembly. Wth the data set, nuclear design of the experimental fast reactor "JOYO" was made successfully. As a private companies' project, he promoted the analysis of experimental results of "MOZART Program" for the nuclear design of the prototype fast reactor "MONJU" and also "JUPITER Program" for the conceptual study of the demonstration fast reactor, which programs were conducted by PNC. At the final stage of reactor physics research, he studied feasibility of burning TRU using fusion reactor,and obtained the conclusion that a fusion reactor would burn the amounts of TRU discharged from several tens of LWRs.

In the field of nuclear data, Shungo Iijima was one of the most energetic promoter of the nuclear data activity in Japan. He had good abilities of nuclear physics and reactor physics, and more than anything else, had strong interest in nuclear data evaluation.

For JENDL, he played an important part in the evaluation such as fission products, structural material and thermal neutron scattering law. As working group leader, he established,for fission product nuclides, the systematic method of cross section evaluation, and was awarded with the technical prize by Atomic Energy Society of Japan in 1976. He prepared doctral thesis about a study on parameters of fast neutron cross section calculation for fission product nuclides, and took a degree of doctor of engineering in 1983. For the evaluation works of JENDL-2, some evaluaters were awarded with the special prize by Atomic Energy Society of Japan in 1985, he was nominated as one of main contributors. In the course of JENDL evaluation, he played important roles to assist some troubled evaluaters and to organize to solve problems such as discrepancy between preliminary evaluated values and

integral data.

In addition to JENDL evaluation, his activity of nuclear data was directed toward the areas other than nuclear reactor, such as nuclear fuel cycle,particle accelerator and medical use. He investigated these area as leader of the task force, and made foundation of the present working group activity of Nuclear Data Evaluation Committee of JNDC.

His passing was a great loss to us all.

List of Shungo Iijima's Main Publications
(For simplification, names of co-author are omitted.)

1) 三組理論を用いた直方体原子炉の臨界計算：原子力学会誌 1(1959)412
2) Resonance Absorption and the Resonance Disadvantage Factor : Nucl.Sci.Eng.17(1963)42
3) One-Phonon Coherent Scattering of Slow Neutrons from Polycrystalline Aluminum : J.Nucl.Sci.Technol.3(1966)160
4) On the Coherent Scattering of Slow Neutron from Heavy Water : ibid.4(1967)625
5) Point Dipoleモデルによる理想ウルツ型結晶の格子力学 :日本応用物理学会誌38(1969)645
6) Analysis of FCA Critical Experiments and its Application to JOYO Nuclear Design : Proc.Int.Conf.on Fast Reactor Phy.,Tokyo(1973),p.1344
7) Evaluation of Design Methods by Analysis of Mockup Experiments : ibid.p.371
8) Analysis of Doppler Experiments : ibid.p.984
9) 常陽モックアップ実験の解析 : JAERI-1228 (1973),p.183
10) Evaluation of Fission Product Nuclear Data for 28 Important Nuclides: Proc.on Nuclear Cross Section and Technology Washington(1975) : vol1,p.320
11) 核分裂生成物からの崩壊熱：原子力学会誌 17(1975)3
12) 核データの利用と現状（熱中性子炉）：原子力工業 22(1976)13
13) Numerical Study on Applicability of Benoist's Diffusion Coefficient to Sodium Void Reactivity: J.Nucl.Sci.Technol.13(1976)464
14) Evaluation of Neutron Cross Section of 27 Fission Product Nuclides Important for Fast Reactor : ibid.14(1977)161
15) Status of Fast Neutron Reaction Cross Sections of Fisson Products : IAEA-213,vol1,279(1978)
16) Problems Encountered in the Evaluation of Fission Product Neutron Cross Sections : JAERI-M-8163,p167(1979)

17) Angular Distributions of Resonance Neutron Scattering from Fe-56 :
J.Nucl.Sci.Technol.17(1980)474
18) Neutron Total Cross Section for Iron around Resonance Valley near 24keV :
ibid.17(1980)477
19) Evaluation of Fission Product Neutron Cross Section in Japan and
their Applications: Trans.Am.Nucl.Soc.38(1981)656
20) Revisions Recommended for Preliminary JENDL-2 Based on Benchmark Test Results :
JAERI-M-9523,p60(1981)
21) Neutron Cross Section of 28 FP Nuclides Adopted in JENDL-1 : JAERI-1268 (1981)
22) Fission Product Model for BWR Lattice Calculation Code :
J.Nucl.Sci.Technol.19(1982)96
23) Integral Test of JENDL Neutron Cross Sections for Structural Material and
Fission Products :JAERI-M-9999,p183(1982)
24) 核分裂生成物高速中性子断面積の理論計算におけるパラメタに関する研究：
東京工業大学博士論文（1983）
25) Systematics of Neutron fotal Cross Sections of Fission Product Nuclei and
Optical Model Fit: J.Nucl.Sci.Technol.20(1983)77
26) Extension of Fission Product Model for Use in Lattice Calculation of
Thorium Fueled BWR : ibid.20(1983)523
27) Systematics and Determination of Level Density Parameters of Fission Product
Nuclei : ibid.21(1984)10
28) A Review of the Theory of Sensitivity and Uncertainty Analysis :
JAERI-M84-010,p82(1984)
29) Evaluation of FP Cross Section for JENDL-2 : Proc.of Int.Conf.on Nuclear
Data for Basic and Applied Sci.SantaFe(1985),vol2,p.1627
30) Fission Product Cross Section Evaluation,Integral Test and Adjustment Based on
Integral Data : JAERI-M86-080,p30(1986)
31) Simplified Method for Calculation of Neutron Capture Transformation Effects of
Fission Products on Decay Power : J.Nucl.Sci.Technol.23(1986)914
32) 原子炉構造材のガス生成中性子反応基礎データ : 原子力学会誌28(1986)285
33) JENDL Special Purpose Data File : JAERI-M87-025,p230(1987)
34) Usage of Nuclear Data Library and Proposal to JENDL : ibid.p217
35) Program PEGASUS,A Precompound and Multi-step Evaporation Theory Code for
Neutron Threshold Cross Section Calculation: ibid.p337
36) Fission Product Cross Section Integral Tests and Adjustment Based on
Integral Data : JARI-M88-065,p148(1988)
37) Activation of Structural Material duc to Recoil Protons in Light Water Reactor :
ibid.p330

38) Calculation of Double Differential Cross Sections for Structural Materials by PEGASUS Code : ibid.p486
39) Fission Product Model for lattice Calculation of High Conversion Boiling Water Reactor : Nucl.Technology 80(1988)263
40) Evaluation and Integral Tests of FP Nuclear Data for JENDL-3 : Proc.of Int.Conf.on Nuclear Data for Sci.and Technol.,Mito(1988),p.569
41) Evaluation of Neutron-Induced Cross Sections of Cr,Fe and Ni : ibid.p.627
42) Activation of Structural Materials due to Recoil Protons in Light Water Reactor: ibid.p.999
43) Activation of Structural Materials due to Recoil Protons in Light Water Reactor: J.Nucl.Sci.Technol.26(1989)874
44) JENDL Special Purpose Data Files and Related Nuclear Data : JAERI-M89-126,p148(1989)
45) Activation Cross Section Data File (1) : JAERI-M89-129 (1989)
46) 核燃料サイクル用核データ；現状と問題点 : 原子力学会誌 31(1989)1083
47) 評価済み核データライブラリーＪＥＮＤＬ－３ : ibid.31(1989)1190
48) 原子炉崩壊熱とその推奨値：日本原子力学会「原子炉崩壊熱基準」研究専門委員会報告（1989）
49) Simplified Method of Calculation of PKA Spectra,DPA Cross Section and KERMA Factor for Medium and Heavy Weight Nuclides: J.Nucl.Sci.Technol.27(1990)375
50) Spectrum-Averaged One-Group Cross Sections of Actinides Based on JENDL-3 : ibid.27(1990)572
51) Thermal Reactor Benchmark Test of JENDL-3 : JAERI-M90-025,p5(1990)
52) JENDL-3 FP Data File : ibid.p53
53) Development of the JENDL Special Purpose Data File for PKA Spectra,DPA Cross Sections and KERMA Factors: ibid.p329
54) Neutron Cross Section Calculation for Fe-56 and U-235 in the Energy Range up to 50 MeV : ibid.p393
55) One-Group Actinide Cross Section Set Based on JENDL-3 and Calculation of U-232 Production in Light Water Reactors: ibid.p403
56) ＦＰ崩壊熱感度係数および崩壊熱不確かさ計算のためのＢＡＳＩＣプログラム : JAERI-M90-197 (1990)
57) Simple Fitting Formula of He Stopping-Powers between 2 and 10 MeV and the Thick Target(alpha,n)Yields for Chemical Compounds: to be publ.in J.Nucl.Sci.Technol.
58) Evaluation of O-17(n,alpha)C-14 Cross Section : to be publ.in J.Nucl.Sci.Technol.
59) Fission Product Decay Power--AESJ Recomendation : to be submitted to Int.Conf on Nuclear Data for Technol.(1991,Julich)

2.5 Topics-3

2.5.1 Review of Evaluation in the Medium Energy Region

Tokio FUKAHORI

Nuclear Data Center, Japan Atomic Energy Research Institute,
Tokai-mura, Naka-gun, Ibaraki, 319-11 Japan

Medium energy nuclear data in the 1-1000 MeV range is necessary to accelerator shielding design, spallation neutron sources, medical isotope production, radiation therapy, and space applications. For the design of fission and fusion reactors, the nuclear data files for neutrons below 20 MeV are available and well evaluated. Nuclear data for protons and data in the medium energy region, however, have not been prepared completely. In this paper, the evaluation of neutron and proton induced nuclear data in the medium energy region has been reviewed using the example of ^{208}Pb and ^{209}Bi.

1. Introduction

Many applications, such as spallation neutron sources for radioactive waste treatment, accelerator design, medical isotope production, radiation therapy, the effects of space radiation on astronauts and their equipments, and the cosmic history of meteorites and other galactic substances, need medium energy nuclear data in the 1-1000 MeV range. For the design of fission and fusion reactors, the nuclear data files for neutron below 20 MeV are well evaluated such as JENDL-3[1], ENDF/B-VI[2], and so on. Nuclear data for proton and data in the medium energy region, however, have not been prepared completely, except those for iron[3].

Evaluation in the medium energy region might be performed by using theoretical calculation codes or based on experimental data. The calculation codes usable at the medium energy are HETC[4] using Monte Carlo techniques based on intranuclear cascade model[5], ALICE[6] and GNASH[7] using evaporation and preequilibrium theory, and PNEM[8] using systematics for neutron emission cross sections. They were compared by Pearlstein[9] in calculated results and running time. ALICE has been modified to ALICE-P by Pearlstein[3] and for this study the 1989 version of ALICE[10] was modified to ALICE-P. The modifications consist mainly of changes in optical model

parameters and the calculation of inverse cross sections. The ALICE-P variables and parameters referred to this report are same in the ALICE.

In this paper, the evaluation of neutron and proton induced nuclear data has been reviewed using the example of ^{208}Pb and ^{209}Bi evaluation with mainly ALICE-P and nuclear systematics. A methodical search for the best ALICE-P parameters have been carried out. ALICE-P has default options for the mass formula, level density formula, mean free path, exciton starting points for preequilibrium calculation and some systematics for nucleon emission spectra. The combination of these options and parameters was compared with the Pearlstein's systematics for neutron emission spectra. Experimental data of fission cross section for several isotopes near lead in the energy range from 50 MeV to 9 GeV were reviewed, and new systematics for the fission cross section was derived.

2. Consideration of Mass Calculations

ALICE-P code has a default option for mass calculation. The calculated results for isotope production cross sections could not reproduce most parts of the experimental data, especially at threshold energies. On the other hand, the ten latest mass formula have been introduced in the Atomic Data and Nuclear Data Tables (vol.39, No.2 (1988)). The comparison of the ten mass values and the binding energies calculated by using them were performed as well as the ALICE-P options. The comparison of the mass values calculated by Pape & Antony[11], Dussel et al.[12], Moller & Nix[13], Moller et al.[14], Comay et al.[15], Stapathy & Nayak[16], Tachibana et al.[17], Spanier & Johannson[18], Janecke & Masson[19], and Masson & Janecke[20] with the experimental data of Wapstra et al.[21] was performed for all mass ranges using as criteria for suitability the chi-square, the largest ratio different between mass formula and Wapstra mass, and availability to predict mass values and binding energies necessary for ALICE-P calculations.

The mass formulas of Moller & Nix, and Moller et al. have larger chi-square values than the others. The small difference between the values of mass formula and Wapstra was given by Pape & Antony, Dussel et al., Comay et al. and Janecke & Masson. The results of the mass values near Bi, which are the isotopes necessary for ALICE-P calculation of proton induced reactions in a ^{209}Bi target, i.e. Z=76-84, 22 isotopes for each Z, are almost satisfied except for those masses of Pape & Antony. The calculated results of the binding energies compared with those calculated from the Wapstra's

show the values of Pape & Antony, and Satpathy & Nayak are not acceptable. The mass formulas of Pape & Antony, Dussel et al., Moller & Nix, Spanier & Johannson, and Masson & Janecke are not acceptable since they can not predict all binding energies needed. From the above discussion, the predicted values of Janecke & Masson is closer to Wapstra's than the others and can reproduce the experimental data.

3. The Sensitivities of Parameters

ALICE-P has default options but a lot of options can be selected by users. However, it is difficult to decide what values are suitable to the individual problems. The options except mass formula in order to adjust or get the final values for evaluation still remains to be selected. Firstly, the sensitivities of the options and parameters were considered by using the experimental data of neutron double differential cross sections (DDX) and angular integrated neutron emission spectra (SDX) for ^{209}Bi[22] and ^{208}Pb[23-28]. The summary of these parameters are in Table 1. The considered parameters were level density parameter (a=A/PLD), and exciton starting points (TD, EX1, EX2) and the calculated multiplier of mean free path (1.0+COST) in ALICE-P. The formulations of level density, which were Fermi Gas Model, the method of Ramamurthy[29] and Liquid Drop Model, were compared, and the difference of results calculated by ALICE-P, the systematics of Kalback-Mann[30,31] and Pearlstein was examined.

The results of comparison between three methods for level density illustrate that the differences are very small, especially the results of the Ramamurthy's and the liquid drop model are almost same in this case. The formulation of level density does not affect the results at least in the case of targets in the lead region and high proton incident energies. The results of comparison between three values of level density parameter (a=A/PLD) for three method, are similar to each other. Although the calculated results tend to have smaller gradient with smaller PLD, they have similar shapes and the difference is only a few percents. The calculations of DDX and SDX are not sensitive to the choice of level density parameter.

The effect of different initial exciton number (TD) is that the shape of cross section depends on the TD value and the gradient of curve is smaller while the TD value is smaller. The shape of TD=3.0 is the most suitable to experimental data. The examination results of the dependence on neutron fraction to initial exaction number (EX1) for TD=3.0 show the larger

value of EX1 gives larger neutron emission cross section. It is reasonable since EX1 is the fraction of neutrons. However, the effect is not very big.

For the correction factors to ALICE-P calculation for the calculated mean free path multiplier (1.0+COST), larger values of COST gives a flatter shape and this parameter influences the shape. The shape for COST=0.0 seems to be the best fit to experimental data.

The angular distributions using the systematics of Kalback-Mann and Pearlstein were compared with the ALICE-P calculation and experimental data in Fig.1. The results of the Kalback-Mann systematics have a similar overall shape to the ALICE-P calculation. The systematics of Pearlstein gives much closer values to measured cross sections than the others.

The similar study has been performed by comparing the results with the experimental data of isotope production cross sections for $^{209}Bi^{32-40)}$. As the result of comparison between three methods for level density, the differences are small, except for the low incident energy region of (p,n) reaction. However, the Ramamurthy and liquid drop model give similar results even for the (p,pxn) reactions with large x values. The choice of level density formula does not affect the results of (p,xn) reactions, and the effect continues to (p,pxn) reactions with larger x values and probably higher multiplicity particle emission reactions. The results of comparison between three values of level density parameter for three methods, show that they have similar shapes and the difference is only a few percents, although the calculates cross sections tend to have smaller gradient in smaller PLD. The isotope production cross section is not sensitive to level density parameter although the results for more particle emission give the rather big differences, about 5%.

The difference from initial exciton number is shown in Fig.2. In the case of (p,xn) reaction cross section larger values give sharper peaks and the values of cross sections decrease according to the energy increase rapidly. The peak values are smaller while the TD is smaller. In the case of (p,pxn), the situation is similar, except the peak values are larger with smaller TD with small x values. The shape of TD=3.0 is the most suitable to them. Figure 3 shows the dependence of neutron fraction to initial exciton number for TD=3.0. The larger value of EX1 gives larger (p,xn) cross section and smaller (p,pxn) cross sections.

The larger value of the calculated mean free path multiplier gives larger cross sections in the case of less particle emission and smaller in

that of more particle emission. In the case of (p,pxn), the peak energy shifts with increasing COST value, especially higher x values. This parameter affects to the shape and useful to change the fraction of isotope production cross sections, such as that of (p,xn) and (p,pxn) cross sections according to x value.

The results by using systematics of Kalback-Mann and Pearlstein were compared with the ALICE-P calculation. Three methods give much close values of isotope production cross section.

4. The Study of New Systematics for Fission Cross Section

The calculation of fission cross section by ALICE-P takes a lot of time. Researching experimental data of fission cross section for several isotopes at the energy range from 50 MeV to 9 GeV, and parameter search of fitting equations to reproduce the experimental data have been performed. For the fitting equation, the following was selected.

$$S = P(1)*[1-\exp\{-P(2)*(Ep-P(3))\}] \qquad (1)$$

where S is the fission cross section in mb, Ep is the proton energy in MeV, and P is the fitting parameter. In attaching pictorial meanings to the parameters in eq.(1), P(1) is the saturating cross-section, P(3) is the apparent threshold energy, and P(2) is the saturating rate. The experimental data and the fitted results are summarized in Tables 2 and 3, for ^{208}Pb and ^{209}Bi, respectively. The fitted results are summarized in Table 4 by using the experimental data[41-55].

Based on above parameterization, a study of creating systematics was carries out. For the parameters P(i), the following systematics was considered, since they are almost on the linear line as the function of Z^2/A in semi-log plot;

$$P(1) = A^{2/3}*\exp[Q(1)*Z^2/A+Q(2)] \qquad (2\text{-}1)$$
$$P(2) = A^{2/3}*\exp[Q(3)*Z^2/A+Q(4)]*10^{-3} \qquad (2\text{-}2)$$
$$P(3) = A^{2/3}*\exp[Q(5)*Z^2/A+Q(6)] \qquad (2\text{-}3)$$

where Q(i) are fitting parameters, Z is the atomic number, and A is the mass number. The factors Z^2/A and $A^{2/3}$ physically mean proton form-factor and surface terms, respectively. The weighting function was chosen unity

(equal weight), since the results of parameters (P(i)) for each isotope were obtained from much different number of measurements and the parameter errors were not according to them.

The fitted results except for W were used for the systematics study of eqs.(2), since the result for W did not appear to be part of the same systematics. The result of systematics and chi-square per freedom are shown in Table 5. Figure 4 shows the systematics with the best fit parameters. In Figs. 5 and 6 the fission cross sections for ^{208}Pb and ^{209}Bi calculated by systematics are shown. The systematics gives the good agreement with the experimental data below 1 GeV. The neutron induced fission was found to be about 1/2 proton induced fission in the case of ^{209}Bi. Therefore, in generating the neutron library, the fission cross section was taken to be 1/2 the proton induced value.

5. Calculated Results

Based on previous discussions, the nuclear data of ^{208}Pb and ^{209}Bi for proton and neutron incident reaction at the energy region 10^{-5} eV to 1 GeV were calculated by using ALICE-P and systematics. For the neutron incident data below 20 MeV, ENDF/B-VI data[56] were adopted. For proton and for neutron above 20 MeV, the total (for neutron), elastic and reaction cross sections are calculated by the ALICE-P optical model[3]. Elastic scattering angular distributions are based on a diffraction model[57] amended for relativistic effects and empirical fits to high energy data. The calculated results that make up the final evaluation together with experimental data are shown in Figs. 7-14.

6. Conclusion

The ALICE-P calculation was performed using values discussed above. The calculations using systematics of Pearlstein have good overall agreement with the magnitude and shape for the DDX and SDX experimental data. The study of systematics for fission cross section in the region of $29<Z^2/A<33$ have been performed. The systematics can reproduces the experimental data below 1 GeV. With this systematics, the fission cross sections, which do not have experimental data, can be obtained below 1 GeV in this mass region.

At this time, ALICE-P, Pearlstein's systematics and systematics for fission cross section are useful to calculated and/or evaluated the medium energy data. However, more investigation for the theoretical and

systematics calculations is necessary to evaluate nuclear data satisfying many applications. It might he optical model potential, level density formula, creating more suitable model and systematics, etc.

Acknowledgements

The author is grateful to Sol Pearlstein for cooperating this study and to Marshall Blann for valuable discussions about the physical modelling used in the ALICE code. This work was supported by JAERI, the DOE Office of Energy Research and carried out under the aegis of the JAERI/DOE Cooperation in Research in the Area of Nuclear Physics.

References

1. K. Shibata et al., JAERI-1319 (1990).
2. ENDF/B-VI, to be published.
3. S. Pearlstein, J. Astrophys., 346 (1989) 1049.
4. HETC, Code Package CCC-178, ORNL-4744 (1977).
5. H.W. Bertini, Phys. Rev., 188 (1969) 1711.
6. M. Blann, CODE ALICE/85/300, UCID-20169.
7. P.G. Young and E.D. Arthur, LA-6947 (1977).
8. S. Pearlstein, Nucl. Sci. Eng., 95 (1987) 116.
9. S. Pearlstein, BNL-NCS-52155 (1988).
10. M. Blann, CODE ALICE/89, Private Communication (1989).
11. A. Pape et al., Atomic Data and Nuclear Data Tables, 39 (1988) 201.
12. G. Dussel et al., ibid., 39 (1988) 205.
13. O. Moller and J.R. Nix, ibid., 39 (1988) 213.
14. P. Moller et al., ibid., 39 (1988) 225.
15. E. Comay, I. Kelson and A. Zidon, ibid., 39 (1988) 235.
16. L. Stapathy and R.C. Nayak, ibid., 39 (1988) 241.
17. T. Tachibana et al., ibid., 39 (1988) 251.
18. L. Spanier and S.A.E. Johannson, ibid., 39 (1988) 259.
19. J. Janecke and P.J. Masson, ibid., 39 (1988) 265.
20. P.J. Masson and J. Janecke, ibid., 39 (1988) 273.
21. A.H. Wapstra, G. Audi and R. Hoekstra, ibid., 39 (1988) 289.
22. A.M. Kalend et al., Phys. Rev., C28 (1983) 105.
23. N.S. Birjukov et al., International Conf. at Jurmal in 1987, p.284.

24. K. Harada et al., Phys. Rev., C36 (1987) 834.
25. M.M. Meier et al., LA-11518-MS or Nucl. Sci. Eng., 102 (1989) 310.
26. M.M. Meier et al., LA-11656-MS (LANL) (1989).
27. M.M. Meier et al., Int. Conf. Nucl. Data for Basic and Applied Sci., Santa Fe (May 13-17, 1985), Rad. Eff., Vol.2, p.1415.
28. D. Filges et al., KFK-3779 (1984).
29. V.S. Ramamurthy et al., Nucl. Phys., A398 (1983) 544.
30. C. Kalback, Phys. Rev., C37 (1988) 2350.
31. C. Kalback and F.M. Mann, Phys. Rev., C23 (1981) 112.
32. Y.L. Beyec and M. Lefort, Nucl. Phys., A99 (1967) 131.
33. P.J. Daly and P.F.D. Shaw, Nucl. Phys., 56 (1964) 322.
34. K. Miyano et al., Nucl. Phys., A230 (1974) 98.
35. C. Birattari et al., Nucl. Phys., A166 (1971) 605.
36. W.R. Pierson and N. Sugaman, Phys. Rev., B133 (1964) 384.
37. R.E. Bell and H.M. Skarsgrad, Can, J. Phys., 34 (1956) 745.
38. K. Miyano et al., J. Phys. Soc. Japan 45 (1978) 1071.
39. J. Wing and J.R. Huizenga, Phys. Rev., 128 (1962) 280.
40. E.T. Hunter and J.M. Miller, Phys. Rev., 115 (1959) 1053.
41. V.S. Bychenkov et al., Sov. J. Nucl. Phys., 17 (1974) 496.
42. H.M. Steiner, J.A. Jungerman, Phys. Rev. 101 (1956) 807.
43. J. Jungerman, Phys. Rev., 79 (1950) 632.
44. L.G. Jodra and N. Sugarman, Phys. Rev., 99 (1955) 1470.
45. V.A. Kon'shin et al., Sov. J. Phys., 2 (1966) 489.
46. R. Brandt et al., Rev. Phys., Appl., 7 (1972) 243.
47. J. Hudis and S. Katcoff, Phys. Rev., 180 (1969) 1122.
48. J. Hudis and S. Katcoff, Phys. Rev., C13 (1976) 1961.
49. E.S. Matusevichand et al., Sov. J. Nucl. Phys. 7 (1968) 708.
50. B.A. Bochagov et al., Sov. J. Nucl. Phys., 28 (1978) 291.
51. L.A. Vaishnene et al., Z. Phys., A302 (1981) 143.
52. G. Remy et al., Nucl. Phys., A163 (1971) 583.
53. Par L. Kowalski et al. Le Journal De Physique, 24 (1963) 901.
54. H.A. Khan and N.A. Khan, Phys. Rev., C29 (1984) 2199.
55. R. Antanasijevic, Z. Todorovic and M. Juric, Z. Phys., 269 (1974) 385.
56. C.Y. Fu et al., Atomic Data and Nuclear Data Tables, 16 (1975) 409.
57. S. Pearlstein, Nucl. Sci. Eng., 49 (1972) 162.

Table 1 The summary of examined parameters

	LDOPT	PLD	TD	EX1	EX2	COST	IADST	ESYS
Level Density (Fermi Gas Model)								
	0*	9.0*	3.0*	0.82*	1.18*	0.0*	1*	250*
	0*	8.0	3.0*	0.82*	1.18*	0.0*	1*	250*
	0*	10.0	3.0*	0.82*	1.18*	0.0*	1*	250*
Level Density (Ramamurthy)								
	1	9.0*	3.0*	0.82*	1.18*	0.0*	1*	250*
	1	8.0	3.0*	0.82*	1.18*	0.0*	1*	250*
	1	10.0	3.0*	0.82*	1.18*	0.0*	1*	250*
Level Density (M-S Liquid Drop Model)								
	2	9.0*	3.0*	0.82*	1.18*	0.0*	1*	250*
	2	8.0	3.0*	0.82*	1.18*	0.0*	1*	250*
	2	10.0	3.0*	0.82*	1.18*	0.0*	1*	250*
Exciton Starting Points (TD=3.0)								
	0*	9.0*	3.0*	0.82*	1.18*	0.0*	1*	250*
	0*	9.0*	3.0*	0.90	1.10	0.0*	1*	250*
	0*	9.0*	3.0*	0.70	1.30	0.0*	1*	250*
Exciton Starting Points (TD=5.0)								
	0*	9.0*	5.0	1.20	1.80	0.0*	1*	250*
	0*	9.0*	5.0	1.10	1.90	0.0*	1*	250*
	0*	9.0*	5.0	1.30	1.70	0.0*	1*	250*
Excit on Starting Points (TD=7.0)								
	0*	9.0*	7.0	1.60	2.40	0.0*	1*	250*
	0*	9.0*	7.0	1.80	2.20	0.0*	1*	250*
	0*	9.0*	7.0	1.40	2.60	0.0*	1*	250*
Calculated Multiplier of Mean Free Path								
	0*	9.0*	3.0*	0.82*	1.18*	0.0*	1*	250*
	0*	9.0*	3.0*	0.82*	1.18*	0.5	1*	250*
	0*	9.0*	3.0*	0.82*	1.18*	1.0	1*	250*
Systematics								
ALICE-P	0*	9.0*	3.0*	0.82*	1.18*	0.0*	1*	900
Kalback-Mann	0*	9.0*	3.0*	0.82*	1.18*	0.0*	3	900
Pearlstein	0*	9.0*	3.0*	0.82*	1.18*	0.0*	1*	50

* ALICE-P and PEND6 default values. PEND6 is the compilation code from the calculated results of ALICE-P to ENDF-6 format.
LDOPT : the selection of the level density formula.
PLD : input valuable for level density parameter (a=A/PLD).
TD : exciton starting point.
EX1 : the fraction of neutron for particle exciton.
EX2 : the fraction of proton for particle exciton.
COST : the multiplication factor for the calculated mean free path (1.0+COST).
IADST : the selection of the systematics for particle emission spectra.
ESYS : the border energy to use Pearlstein's systematics. Above ESYS [MeV], Pearlstein's systematics is automatically choosen in the code PEND6.

Table 2 Experimental data and fitted results for Pb-208

POINT	X	D	D-ERROR	ref.	FIT	FIT-ERROR
1	7.000E+01	1.380E+01	8.000E-01	41	1.439E+01	1.766E-02
2	1.000E+02	3.660E+01	1.600E+00	41	3.387E+01	3.743E-02
3	1.500E+02	4.600E+01	6.000E+00	45	5.985E+01	9.763E-02
4	1.550E+02	6.230E+01	2.600E+00	41	6.207E+01	7.769E-02
5	2.000E+02	7.550E+01	3.100E+00	41	7.945E+01	1.068E-01
6	2.800E+02	1.060E+02	1.100E+01	45	1.013E+02	1.284E-01
7	3.600E+02	1.000E+02	5.000E+01	45	1.152E+02	1.850E-01
8	3.900E+02	1.300E+02	1.500E+01	45	1.190E+02	1.548E-01
9	5.900E+02	1.440E+02	1.800E+01	46	1.330E+02	1.939E-01
10	6.000E+02	1.340E+02	1.800E+01	43	1.334E+02	2.104E-01
11	6.000E+02	1.440E+02	2.000E+01	52	1.334E+02	1.957E-01
12	6.600E+02	1.210E+02	2.000E+01	45	1.352E+02	2.444E-01
13	1.000E+03	1.320E+02	1.300E+01	51	1.390E+02	2.524E-01
14	1.000E+03	1.420E+02	1.400E+01	51	1.390E+02	2.347E-01
15	2.000E+03	1.390E+02	2.000E+01	52	1.397E+02	2.454E-01
16	2.900E+03	1.490E+02	2.300E+01	46	1.397E+02	2.289E-01
17	3.000E+03	1.350E+02	2.600E+01	52	1.397E+02	2.526E-01

VARIANCE = 8.63
CHISQUARE PER DEG OF FREEDOM= 0.922

Table 3 Experimental data and fitted results for Bi-209

POINT	X	D	D-ERROR	ref.	FIT	FIT-ERROR
1	7.000E+01	5.190E+01	3.400E+00	41	5.522E+01	6.925E-01
2	1.000E+02	1.034E+02	6.500E+00	41	8.496E+01	7.461E-01
3	1.320E+02	1.250E+02	6.250E+01	42	1.111E+02	9.419E-01
4	1.400E+02	9.300E+01	4.650E+01	45	1.168E+02	1.360E+00
5	1.500E+02	1.030E+02	1.200E+01	45	1.236E+02	1.325E+00
6	1.540E+02	1.450E+02	7.250E+01	42	1.262E+02	9.665E-01
7	1.550E+02	1.364E+02	4.900E+00	41	1.268E+02	1.034E+00
8	1.580E+02	1.470E+02	7.350E+01	42	1.287E+02	9.772E-01
9	1.760E+02	1.570E+02	7.850E+01	42	1.393E+02	1.001E+00
10	1.820E+02	1.470E+02	7.350E+01	42	1.426E+02	1.095E+00
11	1.920E+02	1.470E+02	7.350E+01	42	1.478E+02	1.131E+00
12	2.000E+02	1.589E+02	6.900E+00	41	1.518E+02	1.069E+00
13	2.170E+02	1.730E+02	8.650E+01	42	1.595E+02	1.013E+00
14	2.320E+02	1.550E+02	7.750E+01	42	1.657E+02	1.148E+00
15	2.420E+02	1.500E+02	7.500E+01	44	1.695E+02	1.191E+00
16	2.520E+02	1.750E+02	8.750E+01	42	1.730E+02	1.021E+00
17	2.620E+02	1.900E+02	9.500E+01	42	1.764E+02	9.368E-01
18	2.800E+02	1.660E+02	1.100E+01	45	1.819E+02	1.056E+00
19	2.880E+02	2.020E+02	1.010E+02	42	1.841E+02	8.594E-01
20	3.020E+02	1.870E+02	9.350E+01	42	1.878E+02	9.086E-01
21	3.030E+02	1.600E+02	8.000E+01	44	1.881E+02	1.060E+00
22	3.360E+02	1.970E+02	9.850E+01	42	1.955E+02	8.027E-01
23	3.550E+02	1.600E+02	8.000E+01	44	1.992E+02	9.398E-01
24	3.730E+02	1.700E+02	8.500E+01	44	2.022E+02	8.383E-01
25	3.900E+02	1.700E+02	1.500E+01	45	2.048E+02	7.932E-01
26	4.270E+02	1.900E+02	9.500E+01	44	2.096E+02	6.203E-01
27	4.500E+02	2.000E+02	1.000E+01	44	2.121E+02	5.375E-01
28	4.500E+02	2.200E+02	1.100E+01	44	2.121E+02	4.886E-01
29	4.500E+02	2.100E+02	4.000E+01	46	2.121E+02	5.119E-01
30	4.800E+02	2.140E+02	2.000E+01	45	2.148E+02	4.417E-01
31	5.640E+02	2.190E+02	2.000E+01	45	2.201E+02	2.905E-01
32	5.900E+02	2.150E+02	1.075E+01	45	2.213E+02	2.604E-01
33	5.900E+02	2.170E+02	2.500E+01	46	2.213E+02	2.580E-01
34	6.000E+02	2.200E+02	3.000E+01	46	2.217E+02	2.050E-01
35	6.000E+02	2.160E+02	8.000E+00	47	2.217E+02	2.088E-01
36	6.600E+02	2.180E+02	2.000E+01	45	2.236E+02	1.609E-01
37	1.000E+03	2.900E+02	4.000E+01	46	2.273E+02	1.306E-01
38	1.000E+03	2.620E+02	5.000E+01	48	2.273E+02	1.445E-01
39	1.000E+03	2.900E+02	4.000E+01	49	2.273E+02	1.306E-01
40	2.000E+03	2.700E+02	4.000E+01	46	2.278E+02	1.445E-01
41	2.000E+03	2.550E+02	4.000E+01	48	2.278E+02	1.530E-01
42	2.000E+03	2.700E+02	4.000E+01	49	2.278E+02	1.445E-01
43	2.900E+03	2.270E+02	3.300E+01	46	2.278E+02	1.719E-01
44	3.000E+03	2.130E+02	4.000E+01	48	2.278E+02	1.832E-01
45	5.000E+03	2.800E+02	4.000E+01	46	2.278E+02	1.394E-01
46	5.000E+03	2.800E+02	4.000E+01	49	2.278E+02	1.394E-01
47	9.000E+03	2.700E+02	4.000E+01	46	2.278E+02	1.445E-01
48	9.000E+03	2.700E+02	4.000E+01	49	2.278E+02	1.445E-01

VARIANCE = 26.1
CHISQUARE PER DEG OF FREEDOM= 0.941

Table 4 The summary of fitted parameters and their corrilation

Isotopes	P(1)	P(2)	P(3)*1.E+3
Ta-181	24.5 +- 2.5 -0.31 -0.75	190.0 +- 19.0 -0.34	1.52 +- 0.01
W	66.1 +- 0.1 0.00 -0.44	50.1 +- 4.6 0.08	1.67 +- 0.04
Re	33.7 +- 1.1 0.12 -0.66	140.0 +- 7.0 0.16	1.51 +- 0.07
Pt	62.8 +- 0.1 0.15 -0.53	94.4 +- 0.6 0.30	2.44 +- 0.02
Au-197	83.0 +- 8.3 0.01 -0.61	70.0 +- 7.0 0.23	3.61 +- 0.03
Pb-206	141.0 +- 0.1 0.20 -0.33	51.1 +- 0.2 0.42	10.80 +- 0.07
Pb-207	134.0 +- 0.1 0.20 -0.37	47.3 +- 0.1 0.36	6.97 +- 0.05
Pb-208	145.0 +- 0.2 0.05 -0.59	49.9 +- 0.1 0.50	5.31 +- 0.01
Bi-209	217.0 +- 0.5 0.00 -0.43	36.6 +- 1.2 0.46	7.82 +- 0.13

Table 5 The results of the systematics study

Parameters	fitted results
Q(1)	5.75637E-01 +- 3.90613E-04
Q(2)	-1.72680E+01 +- 2.95076E-02
XI	9.99627E-01
Q(3)	5.49152E-01 +- 6.18542E-04
Q(4)	-1.94530E-01 +- 6.12872E-02
XI	1.22823E-02
Q(5)	-4.56190E-01 +- 7.05967E-03
Q(6)	1.52102E+01 +- 1.84684E-01
XI	1.35614E-01

NOTE : The corrilations between Q(1) and Q(2), Q(3) and Q(4), and Q(5) and Q(6) have values of 1.00.

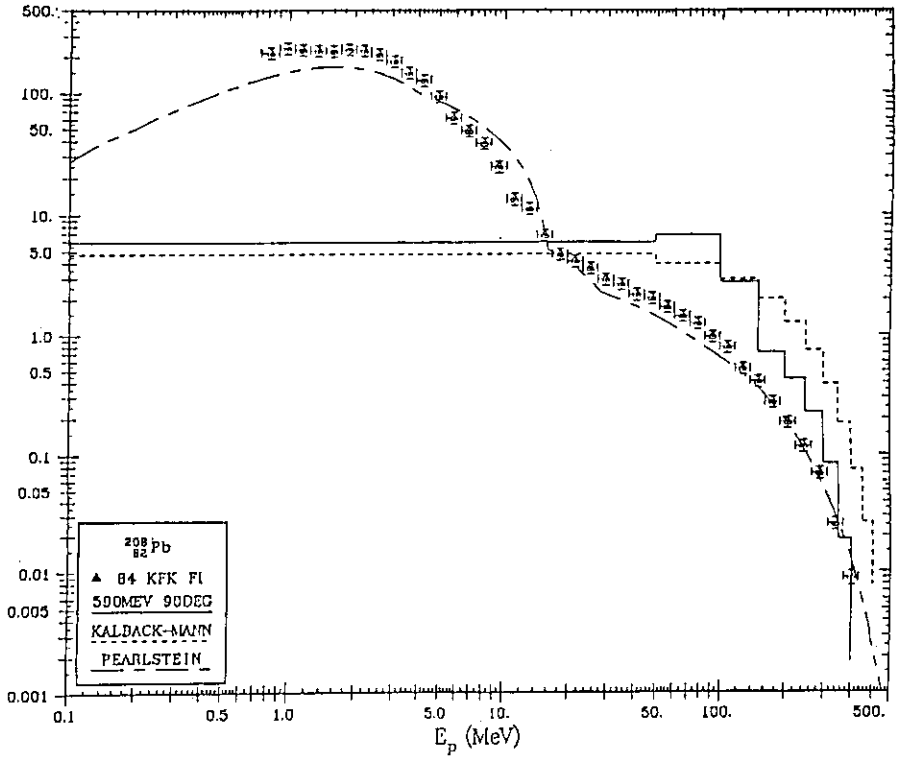

Fig. 1 Difference between the ALICE-P calculation and the two systematics comparing with the experimental data of DDX at 590 MeV and 90 deg. for natural lead.

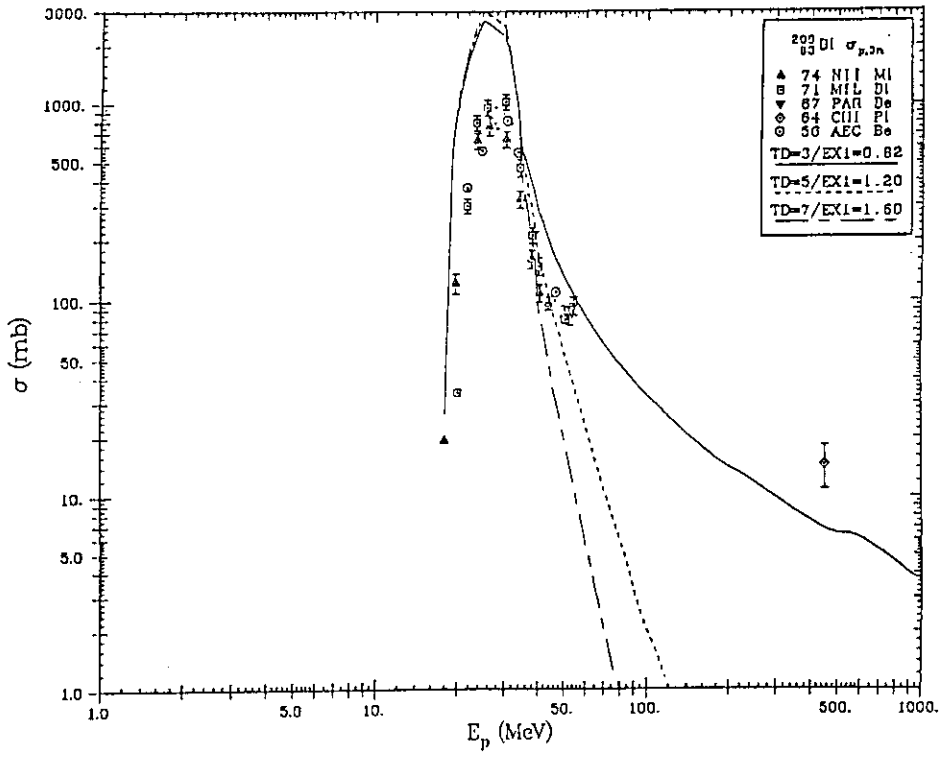

Fig. 2 Difference between the exciton starting points comparing with the experimental data of Bi-209 (p,3n) reaction.

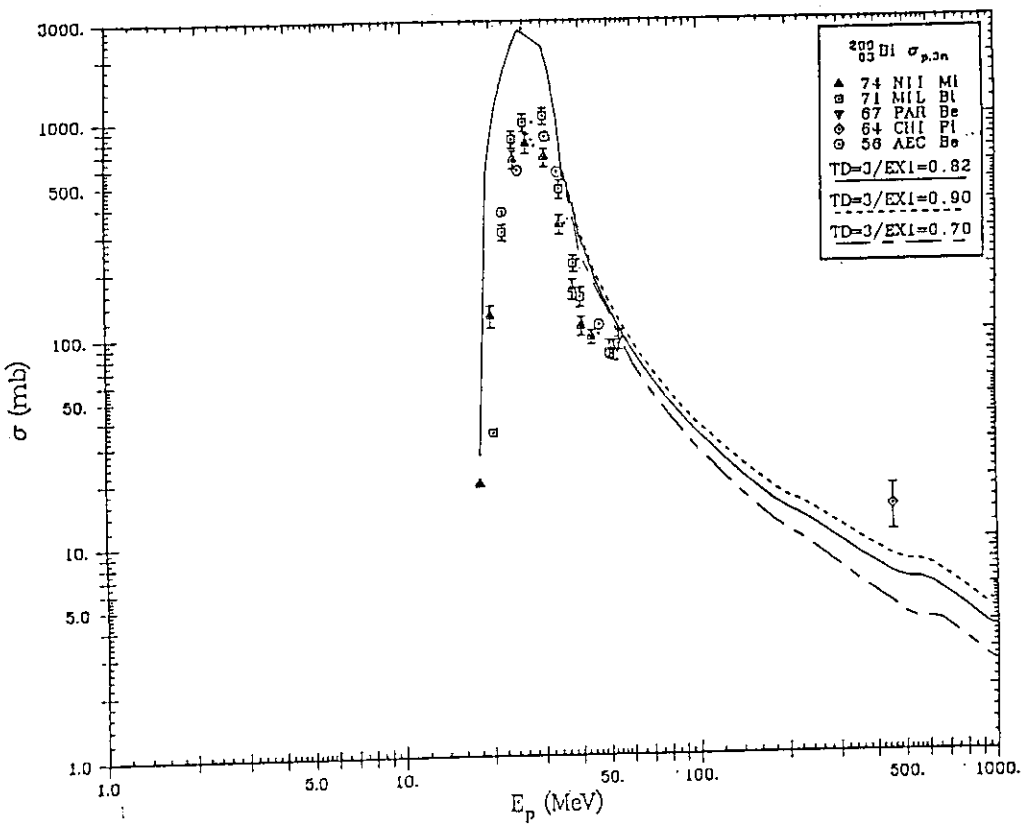

Fig. 3 Difference between the neutron fraction for the exciton starting points comparing with the experimental data of Bi-209 (p,3n) reaction.

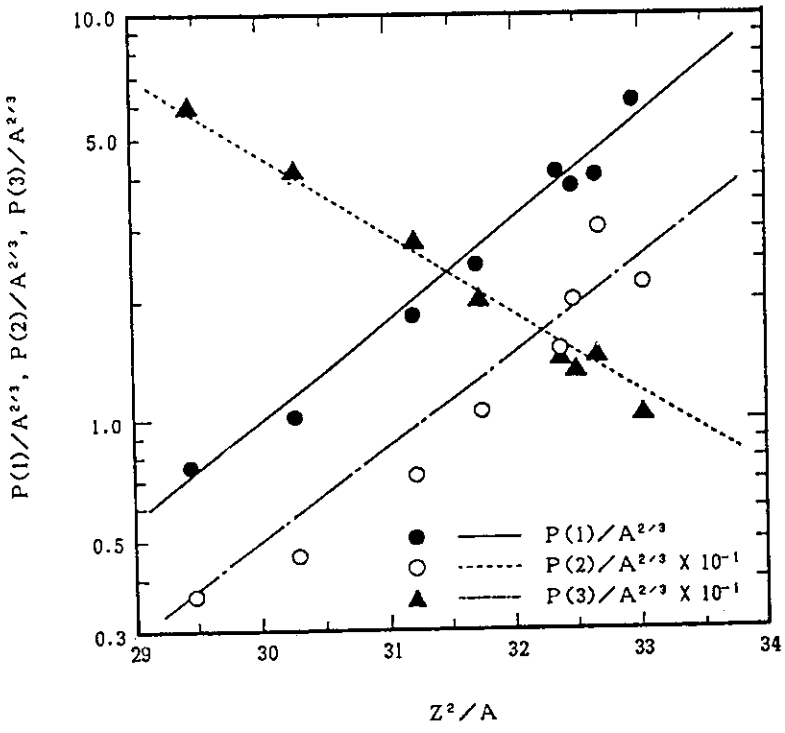

Fig. 4 Fitted results for parameters of fission cross section.

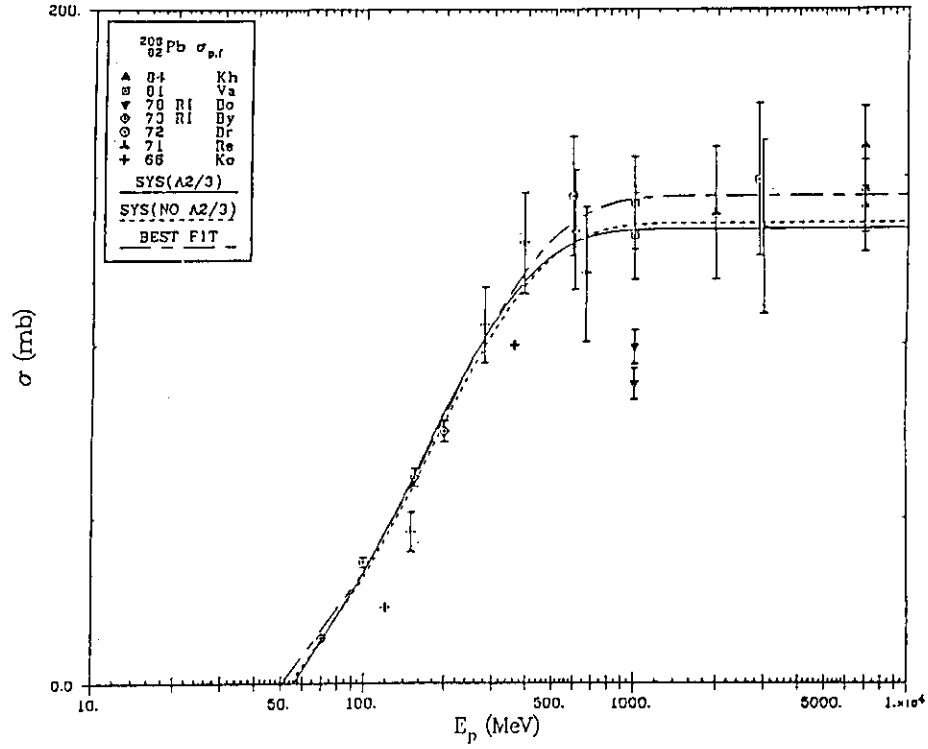

Fig. 5 Calculated results for Pb-208 fission cross section using the systematics.

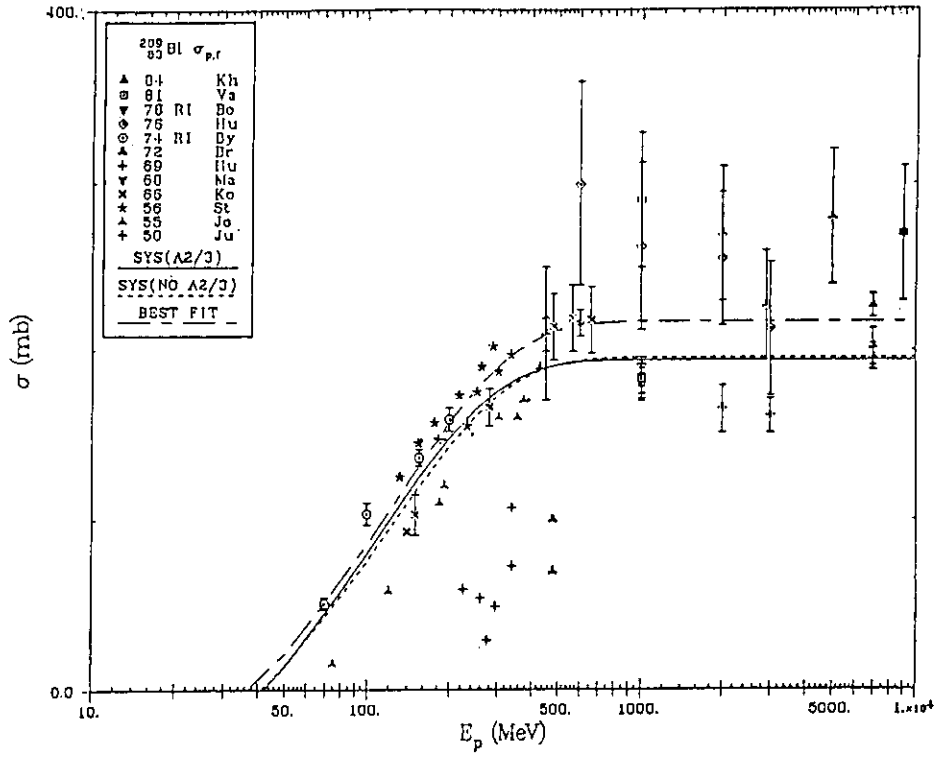

Fig. 6 Calculated results for Bi-209 fission cross section using the systematics.

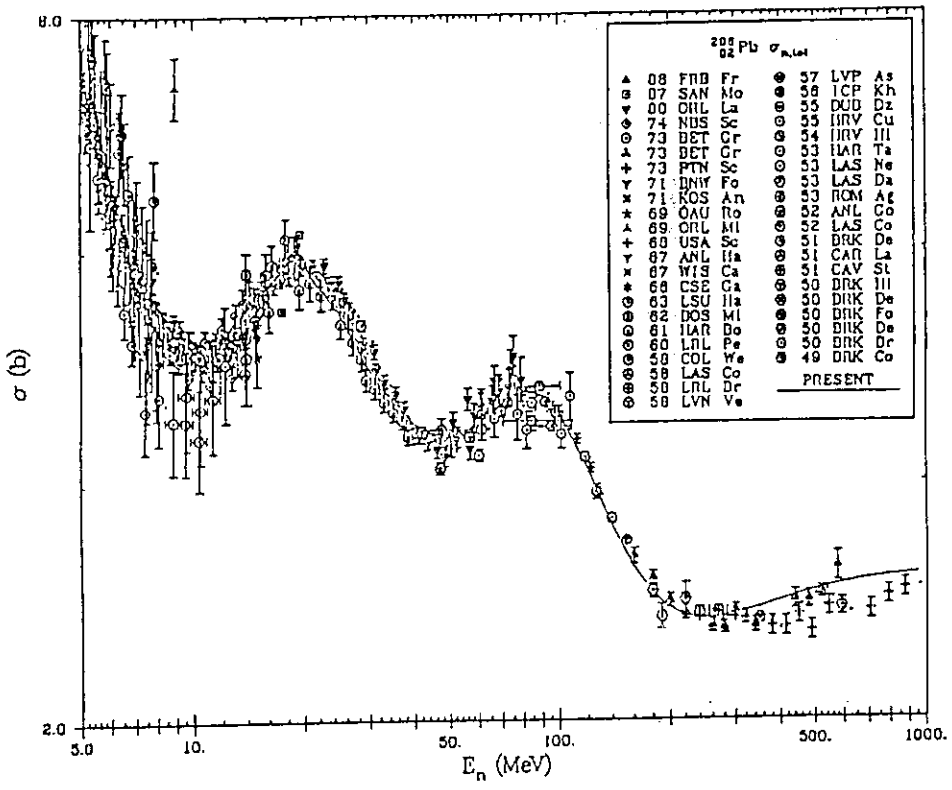

Fig. 7 Evaluated result for Pb-208 (n,tot) cross section.

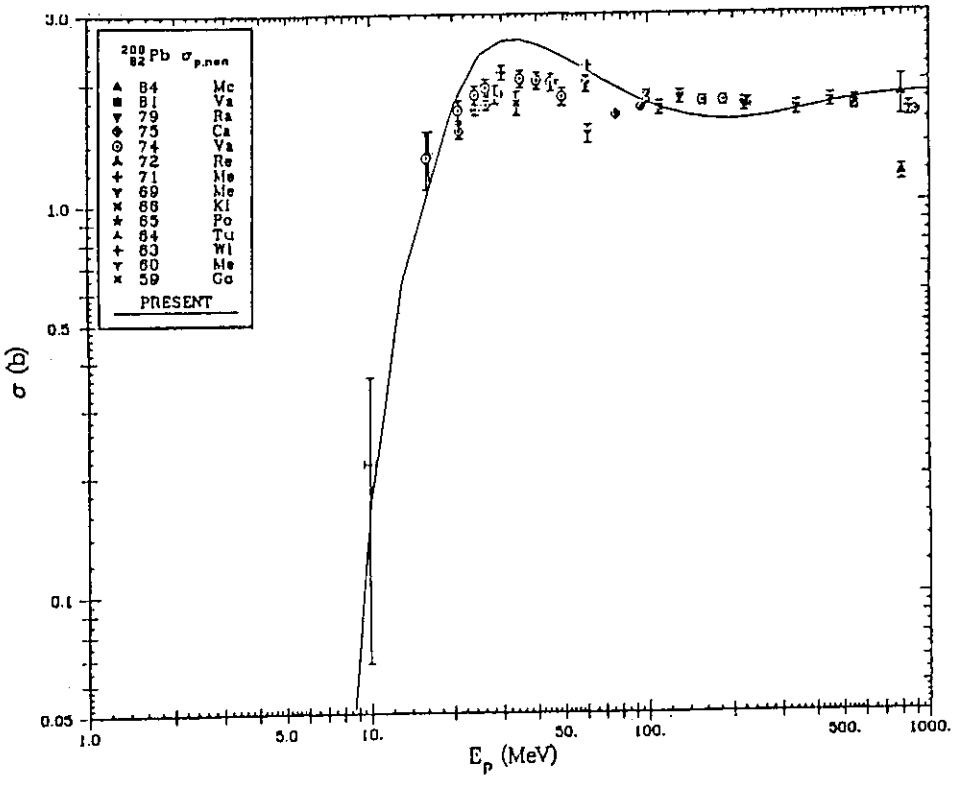

Fig. 8 Evaluated result for Pb-208(p,non) cross section.

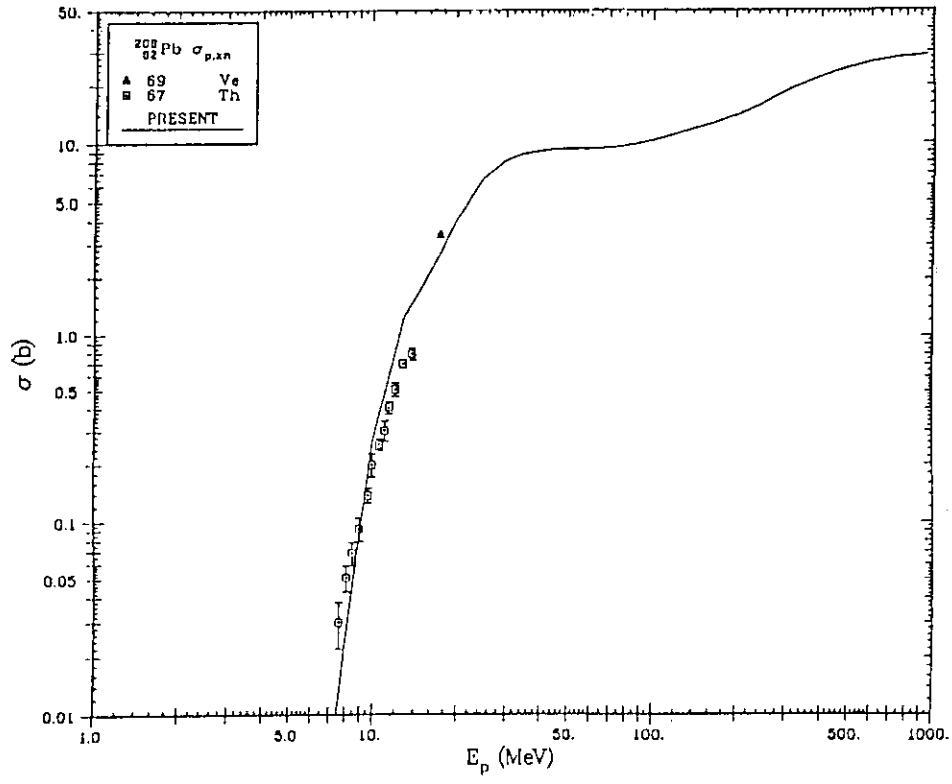

Fig. 9 Evaluated result for Pb-208 (p,xn) cross section.

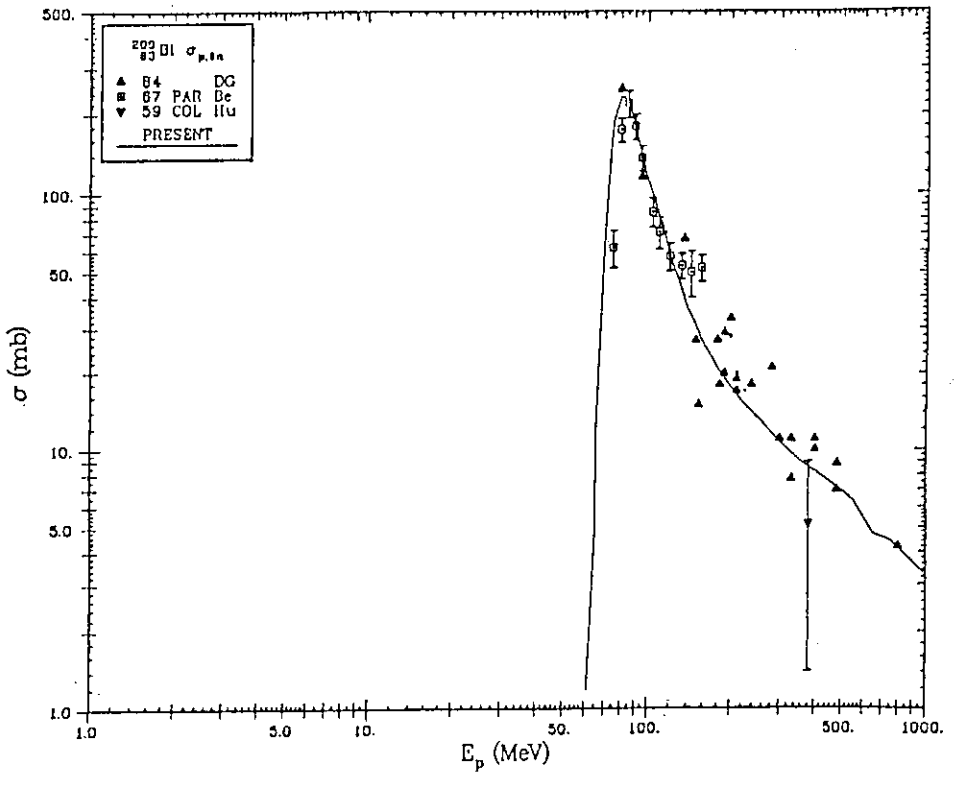

Fig. 10 Evaluated result for Bi-209 (p,8n) cross section.

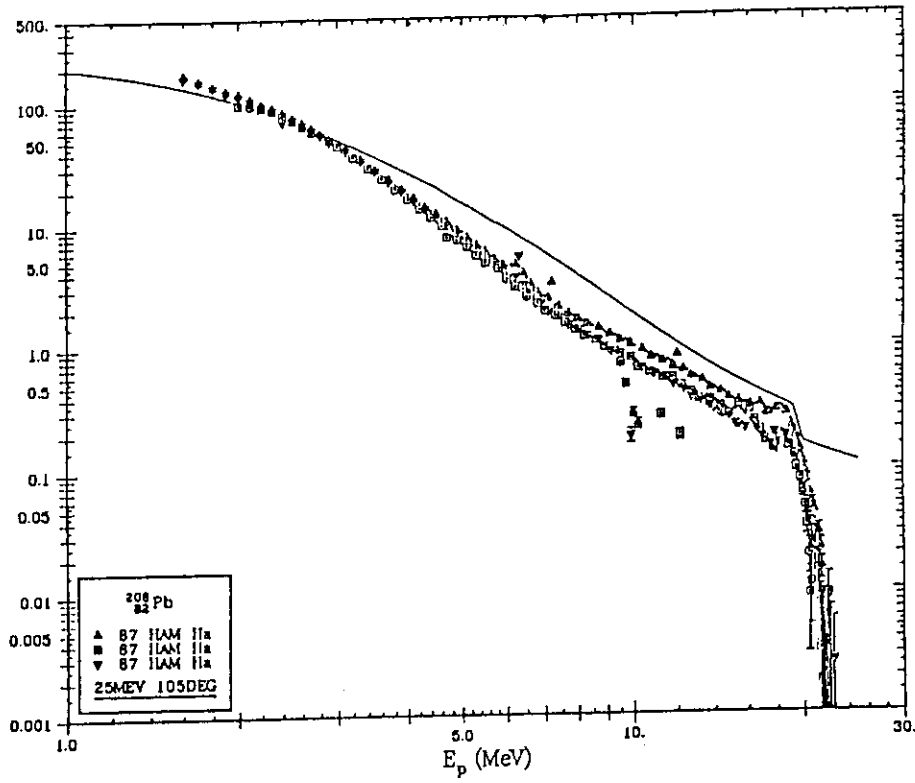

Fig. 11 Evaluated result for Pb-208 DDX of neutron at 25 MeV and 105 deg.

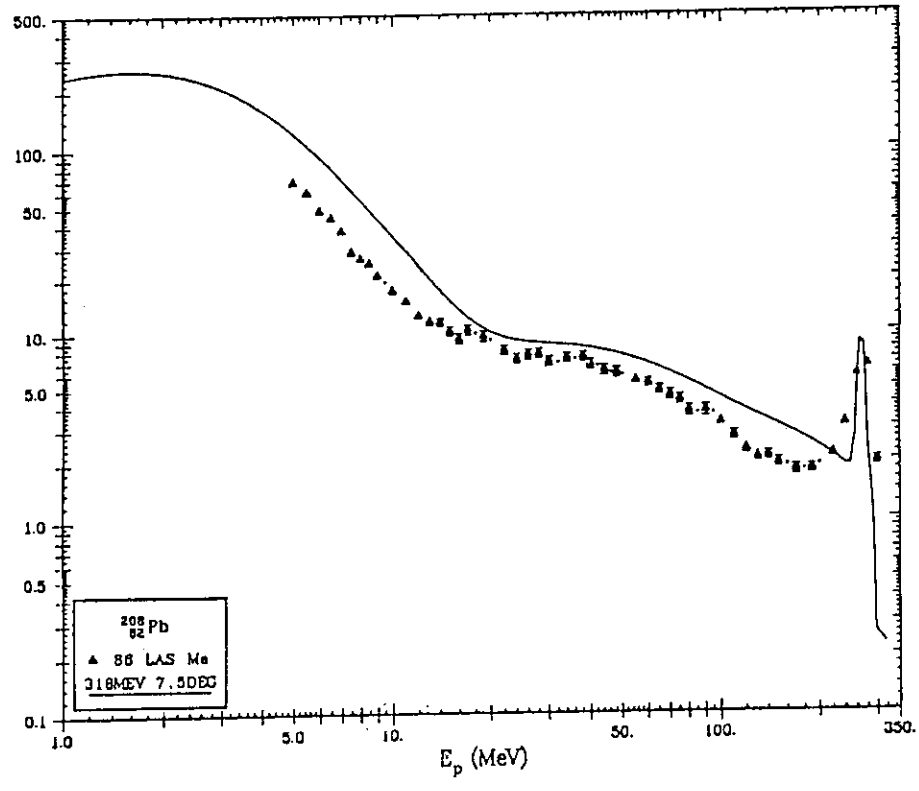

Fig. 12 Evaluated result for Pb-208 DDX of neutron at 318 MeV and 7.5 deg.

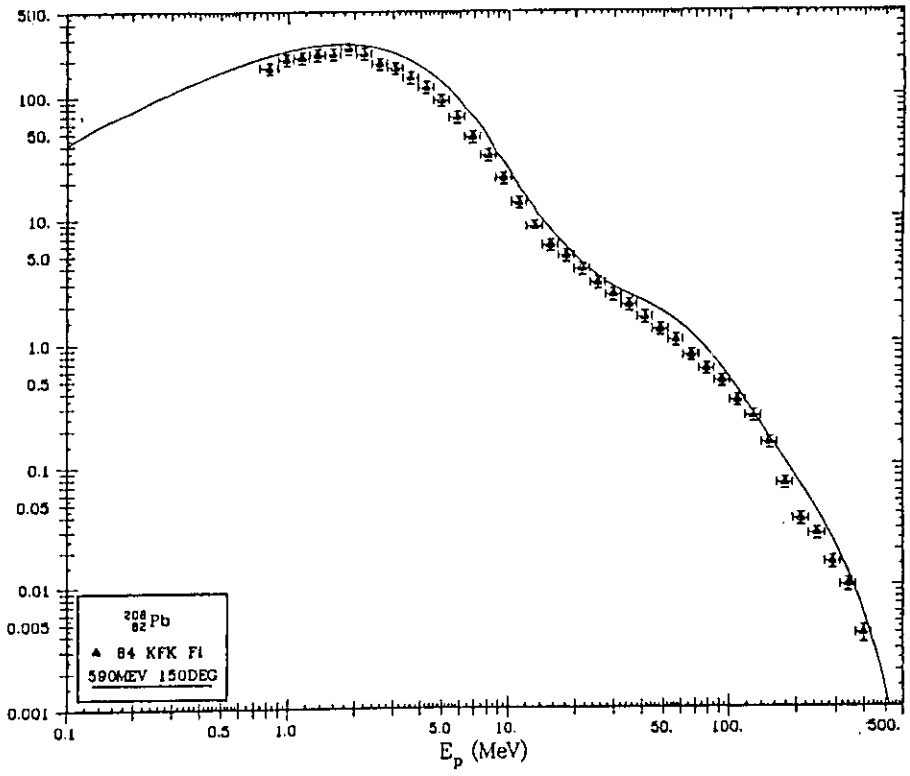

Fig. 13 Evaluated result for Pb-208 DDX of neutron at 590 MeV and 150 deg.

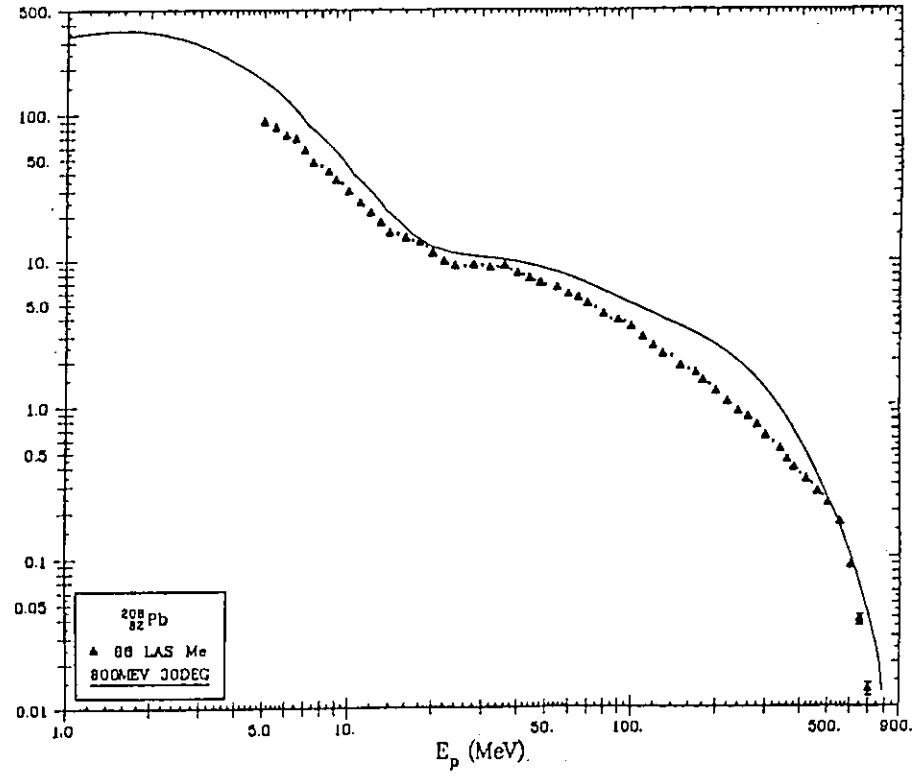

Fig. 14 Evaluated result for Pb-208 DDX of neutron at 800 MeV and 30 deg.

2.5.2 Nuclear Data Activities in ANL

Satoshi CHIBA

Japan Atomic Energy Research Institute

Tokai-mura, Naka-gun, Ibaraki-ken

This paper describes some of the experiences the author had during his 18-month stay in the Fast Neutron Generator (FNG) facility of Argonne National Laboratory. Emphases will be placed on the neutron scattering experiments, theoretical analyses, and a puzzle about the least-squares method.

1. Introduction

In FNG, they have a 3.5-MV tandem Dynamitron accelerator which is basically 100% used for neutron cross section measurements. This group, led by Dr. Alan B. Smith, has been producing an enormous amount of experimental information for more than 20 years, and the results are documented in ANL/NDM reports which accumulate to more than a meter thick!! The main experimental activities might be divided into three categories now: measurements of the neutron scattering cross sections, activation cross sections and fission cross sections.

In this paper, their activities will be briefly described placing emphases on neutron scattering experiments and analyses, taking an example of elemental indium. The later part of this paper will describe an interesting puzzle in applying the least-squares method in the real nuclear data evaluation. Interested readers will get a concrete idea of their activities if they refer to ANL/NDM reports.

2. Experimental Facilities

Deuterons and protons can be accelerated up to 7MeV by using 3.5-MV tandem Dynamitron accelerator. By a double buncher system, these beam can be pulsed into a bunch length of less than 1ns. Neutrons can be produced by the $D(d,n)^3He$ or $^7Li(p,n)$ reaction, the former is used mainly above 4MeV, and the later below 3MeV. Scattered neutrons are detected

by the ten-angle neutron TOF spectrometer (12.5cm dia. by 1.25cm thick NE213) with flight paths of 5m which covers an angular range from 20 to 160 degrees[1], or by an array of four NE213 detectors at a flight path of 15m but at a fixed angle of 80 degrees. Figure 1 shows an example of the neutron spectrum produced by scattering 8-MeV neutrons by ^{58}Ni sample, measured with the longer flight path. Although the scattering angle is fixed to 80 degrees, this set-up can give a great deal of information on the structure and dynamical properties about n + target system. The data are corrected for the effects of flux attenuation, multiple scattering, angular resolution and effective scattering center by the Monte-Carlo method before an extensive theoretical analysis is started.

3. Examples of the experimental and theoretical results

Figure 2 shows the neutron elastic scattering cross sections of elemental indium mainly measured by the authors[2]. The data are given in the laboratory coordinate system. Curves indicate the results of the optical-statistical model calculations. Parameters of this model are given as follows:

$$J_V = (433.4 - 3.7 \cdot E)\ MeV \cdot fm^3, \quad (1)$$
$$r_V = (1.258 - 0.003 \cdot E)\ fm, \quad (2)$$
$$a_V = 0.6404\ fm, \quad (3)$$
$$J_W = (41.8 + 2.9 \cdot E)\ MeV \cdot fm^3, \quad (4)$$
$$r_W = (1.305 - 0.003 \cdot E)\ fm, \quad (5)$$
$$a_W = 0.3798\ fm, \quad (6)$$

where J, r and a denote volume-integrals per nucleon, radius parameter and diffuseness parameter, respectively, and subscripts v and w denote real and imaginary parts, respectively. These parameters were determined by a comprehensive parameter search procedure using ABAREX code[3], while the spin-orbit term was fixed to a standard set; V_{so}=5.5MeV, r_{so}=1.0fm and a_{so}=0.65fm. This potential was extensively used in the evaluation of the neutron nuclear data of elemental indium[4]. Besides, we have investigated the bound state properties of n + ^{115}In system by extraporating this potential into the bound state region by applying the dispersion relation of the optical model potential[5]:

$$J_V(E) = J_{HF} + \frac{P}{\pi}\int_{-\infty}^{+\infty} \frac{J_W(E')}{E-E'} \cdot dE', \qquad (7)$$

where J_{HF} is the Hartree-Fock component of the real potential, and P denotes principal-value integral. By assuming some properties on J_W that are implied from the nuclear matter theory (e.g., J_w is continuous and symmetric about the Fermi energy E_F, J_w is proportional to $(E-E_F)^2$ in the vicinity of the Fermi energy, etc.), and that J_{HF} depends on the neutron energy in linear fashion, we can calculate the real potential volume-integrals in the bound state region. ^{115}In consists of 49 protons and 66 neutrons. Therefore, one might expect that near the middle of the N=50-80 shell which is consisting of $d_{5/2}$, $g_{7/2}$, $h_{11/2}$, $s_{1/2}$ and $d_{3/2}$, the low-spin states, $s_{1/2}$ and $d_{3/2}$, would have little population because the pairing force favors high spin states, and that their binding energies might be reasonably predicted by this extrapolation. By taking the single-particle energies measured by the (d,p) reaction, and supplementing them for missing levels by the shell model calculation[2], we can construct the "average" single-particle binding energies (BE) for these shells. The results are summarized in the following table:

Table 1 Required and predicted potential well depth for the bound states of n + ^{115}In system

State	BE (MeV)	Well Depths Required (MeV)	Well Depths Predicted (MeV)
$s_{1/2}$	6.6	45.1	45.8
$d_{3/2}$	6.3	44.7	46.0
$h_{11/2}$	5.9	46.8	46.2
$g_{7/2}$	10.3	48.7	43.8
$d_{5/2}$	10.1	47.9	43.9

where the "Required" well depth denotes a shell model potential depth to reproduce the measured binding energies, meanwhile the "Predicted" well depth stands for the extrapolated well depth from the optical model potential of Eqs. (1) ~ (6) and the dispersion relation Eq. (7). In the present results, the $h_{11/2}$, $d_{3/2}$ and $s_{1/2}$ shells are considered to be fairly good "single" particle states, and therefore the present model can predict the required potential depth well. On the contrary, the present model

could not predict the hole state energies for $d^{-1}_{5/2}$ and $g^{-1}_{7/2}$ shells. This indicates that these hole states are not true single hole states, and have an occupational probability sufficiently different from unity that the Pauli excluaion principle which is not taken into consideration in the present calculation becomes an important factor. However, it should not be forgotten that the analysis is not very clear in this example because of the odd-odd property of the compound system.

4. A Puzzle about the least-squares method

Suppose we have two data points for a single physical quantity x as follows and want to calculate an average of them by using the least-squares method:

Table 2 Sample data and uncertainties

Data	value	random err. (percent)	common err. (percent)
x_1	1.5	10.0	20.0
x_2	1.0	10.0	20.0

Covariance matrix can be easily calculated as:

$$V = \begin{bmatrix} 1.5^2 \cdot (0.1^2+0.2^2) & 1.5 \cdot 1.0 \cdot 0.2^2 \\ 1.5 \cdot 1.0 \cdot 0.2^2 & 1.0^2 \cdot (0.1^2+0.2^2) \end{bmatrix} = \begin{bmatrix} 0.1125 & 0.06 \\ 0.06 & 0.05 \end{bmatrix} \tag{8}$$

The least-squares condition reads:

$$\chi^2 = (D - AX)^+ \cdot V^{-1} \cdot (D - AX) = minimum \tag{9}$$

where D ≡ data vector = $(1.5,1.0)^+$, A ≡ design matrix = $(1.0,1.0)^+$, and X ≡ solution vector = $(\langle x \rangle)$. From this condition, the least-squares solution is given as:

$$\langle x \rangle = (A^+V^{-1}A)^{-1} \cdot A^+V^{-1}D = \frac{(V_{22}-V_{12}) \cdot x_1+(V_{11}-V_{12}) \cdot x_2}{(V_{22}-V_{12})+(V_{11}-V_{12})}$$

$$= \frac{(0.05-0.06) \cdot x_1+(0.1125-0.06) \cdot x_2}{(0.05-0.06)+(0.1125-0.06)}$$

$$= -0.2353 \cdot x_1 + 1.2353 \cdot x_2 = 0.882 \tag{10}$$

$$\partial x = \sqrt{(A^{+}V^{-1}A)^{-1}} = 0.218 \tag{11}$$

Therefore, the least-squares solution is 0.88 ± 0.22 !?!

The following may be natural questions:

Is this answer right?
If not, what is wrong?
What is the correct answer?
What is the meaning of the negative weight (-0.235) assigned to x_1?

After this problem was pointed out by Peelle in 1987, several people have joined the discussion to answer these questions[6]. Although a unique answer is not still achieved which satisfies all who participate in the discussion, the following is a conclusion that the author and D.L. Smith, i.e., Argonne group, have reached finally: In the nuclear data measurements, the cross sections are usually obtained by measuring many factors, and the results are given by multiplying or dividing these factors. For example, the scattering cross section is given very generally in the following way;

$$\frac{d\sigma}{d\Omega} = \frac{Y}{Y_s} \cdot \frac{N_s}{N} \cdot \frac{\varepsilon_s}{\varepsilon} \cdot \frac{A}{A_s} \cdot \frac{d\sigma_s}{d\Omega}, \tag{12}$$

where subscript s denotes "standard", Y, N, ε and A stand for background-subtracted counting yield, number of atoms in a sample, detection efficiency and correction factor for finite sample size effects including that of the fluence factor, respectively. Each of these factors is a result of one or more measurements, and therefore has an uncertainty. Usually, the associated uncertainties are given relatively, e.g., we know the detection efficiency within 5% and the sample thickness is known to 1%, etc. If we believe these relative errors, and if we recall the fact that the "uncertainties" in a measurement of physical constants actually denote a "diffuseness" of the results around the true value, these %-error should be multiplied to the true value of the quantity to be measured, not to the result of a single experiment which in common is not equal

to the true value. Furthemore, result of a single measurement may have a serious bias against the true value. The whole idea is that as well as the measured "result", the reported "uncertainties" themselves have uncertainties if they are obtained by multiplying the %-error to the error-affected "results" of a single experiment. The reason of the negative weighting can thus be traced to a fallacious calculation of the covariance matrix which led to $V_{22} < V_{12}$, as given in Eqs. (8) and (10). According to this policy, the covariance matrix should be calculated by assuming a true value of the results ($\langle x \rangle$) which we are trying to get!! Fortunately, we can proceed without knowing the true value as in the following:

$$Cov(x) = \begin{bmatrix} \langle x \rangle^2 \cdot (0.1^2 + 0.2^2) & \langle x \rangle^2 \cdot 0.2^2 \\ \langle x \rangle^2 \cdot 0.2^2 & \langle x \rangle^2 \cdot (0.1^2 + 0.2^2) \end{bmatrix}$$

$$= \langle x \rangle^2 \cdot \begin{bmatrix} 0.05 & 0.04 \\ 0.04 & 0.05 \end{bmatrix} \tag{13}$$

$$\therefore \langle x \rangle = \frac{(V_{22}-V_{12}) \cdot x_1 + (V_{11}-V_{12}) \cdot x_2}{(V_{22}-V_{12}) + (V_{11}-V_{12})} = 0.5 \cdot 1.5 + 0.5 \cdot 1.0$$

$$= 1.250 \pm 0.265. \tag{14}$$

Of course, we do not think this method is universally correct. Moreover, generally this method requires an iterative procedure. However, it is known in most cases that this iteration converges fairly quickly, so usually only two or three iterations are required[7]. Anyway, this puzzle clearly showed us that if we apply the least-squares method to correlated data, the covariance matrix should be very carefully prepared. Otherwise, it will lead to an unphysical "negative" weighting of the data. We encountered the same situation in evaluation of $^{115}In(n,n')^{115m}In$ reaction cross section, where result of the least-squares method looked too small compared with the existing body of the experimental data. We applied the present method, and the results became much more reasonable[4].

In the present report, only a brief explanation could be given on this puzzle. The discussion among the participants to this puzzle actually accumulates to a bundle of letters of more than 10cm!! Unfortunately, not all of the participants to this puzzle agree with our method, and many alternative methods are also suggested[6,8]. For example, if we take the logarithm of the data ($y_i = \ln(x_i)$, i=1,2) and

apply the least-squares method to the transformed data (y), the result becomes $\langle x \rangle \equiv e^{\langle y \rangle} = 1.23 \pm 0.26$; nothing is strange. However, this logarithmic method can be used only to positive quantities. Futhermore, is the modern statistics not able to give a unique answer to this simplest problem? The puzzle, therefore, is still open for discussion to the readers.

Acknowldgement

The author is grateful to the FNG stuff for their hospitality and helps during his stay, especially to Drs. Alan B. Smith, Donald L. Smith, Peter T. Guenther, Robert D. Lawson and James W. Meadows. Helps from accelerator operating crew are also acknowledged. This work was supported by JAERI, the DOE Office of Energy Research and carried out under the aegis of the JAERI/DOE Cooperation in Research in the Area of Nuclear Physics.

References

1. Smith, A., Guenther, P., Larson, R., Nelson, C., Walker, P. and Whalen, J.: Nucl. Instr. Methods 50 277(1967).
2. Chiba, S., Guenther, P.T., Lawson, R.D. and Smith, A.B.: "NEUTRON SCATTERING FROM ELEMENTAL INDIUM, THE OPTICAL MODEL, AND THE BOUND-STATE POTENTIAL", ANL/NDM-116 (1990).
3. Moldauer, P.A.: Nucl. Phys. A344 185 (1980).
4. Smith, A.B., Chiba, S., Smith, D.L., Meadows, J.W., Guenther, P.T., Lawson, R.D. and Howerton, R.J.: "EVALUATED NEUTRONIC FILE FOR INDIUM", ANL/NDM-115 (1990).
5. Satchler, G.R.: "DIRECT NUCLEAR REACTIONS", Clarendon Press (1983).
6. Peelle, R.W., Perey, F.G., Zhao, Z., Fröhner, F.H., Muir, D.W., Vonach, H.K., Smith, D.L. and Chiba, S.: Private communications.
7. Chiba, S. and Smith, D.L.: to be published.
8. Smith, D.L.: "NUCLEAR DATA UNCERTAINTIES", (temporary title), to be published as NEUTRON PHYSICS AND NUCLEAR DATA IN SCIENCE AND TECHNOLOGY, VOL. 4, NEA, OECD.

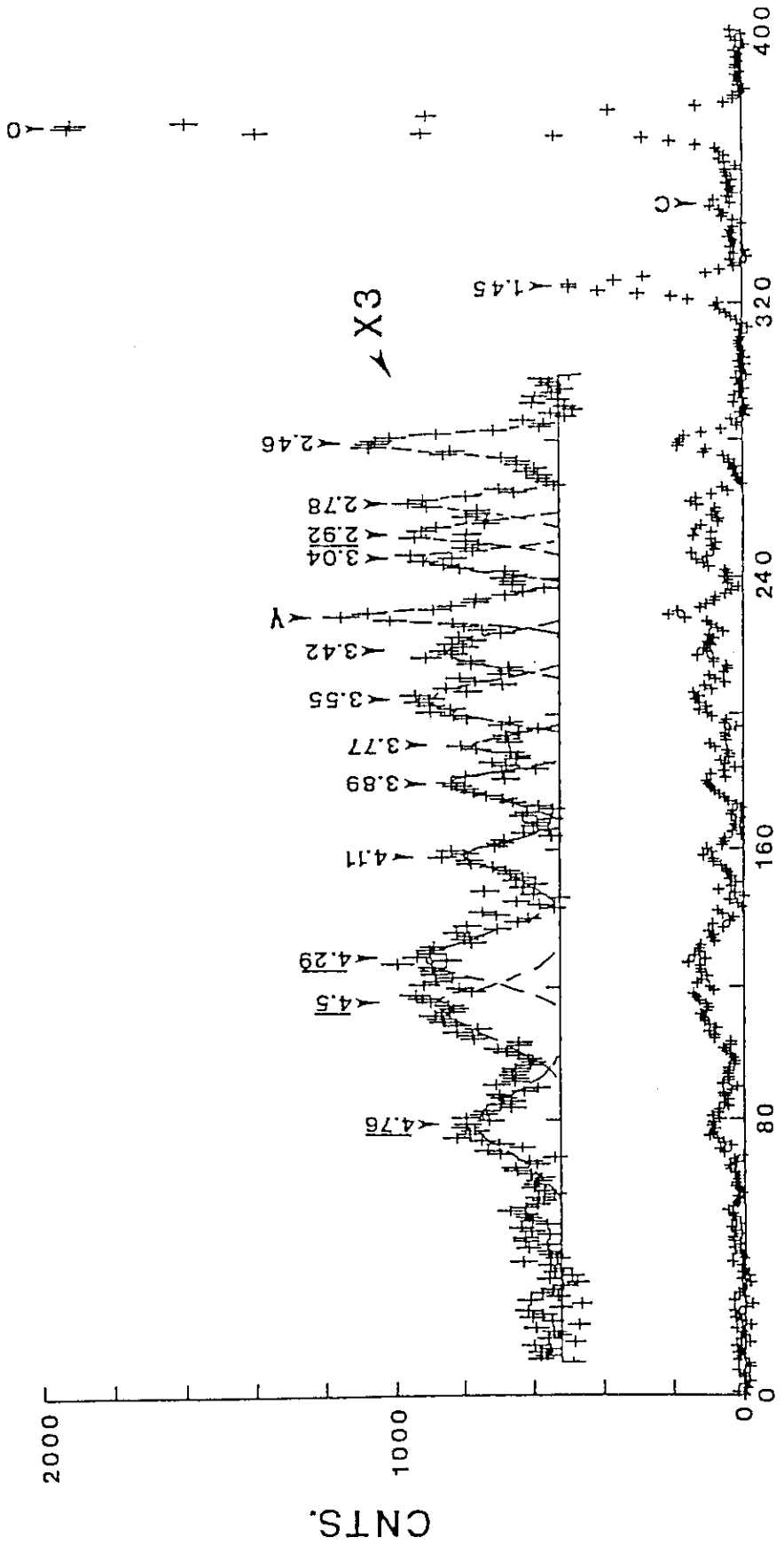

Fig. 1 Neutron time-of-flight spectrum produced by scattering 8-MeV neutrons from ^{58}Ni at 30 degrees

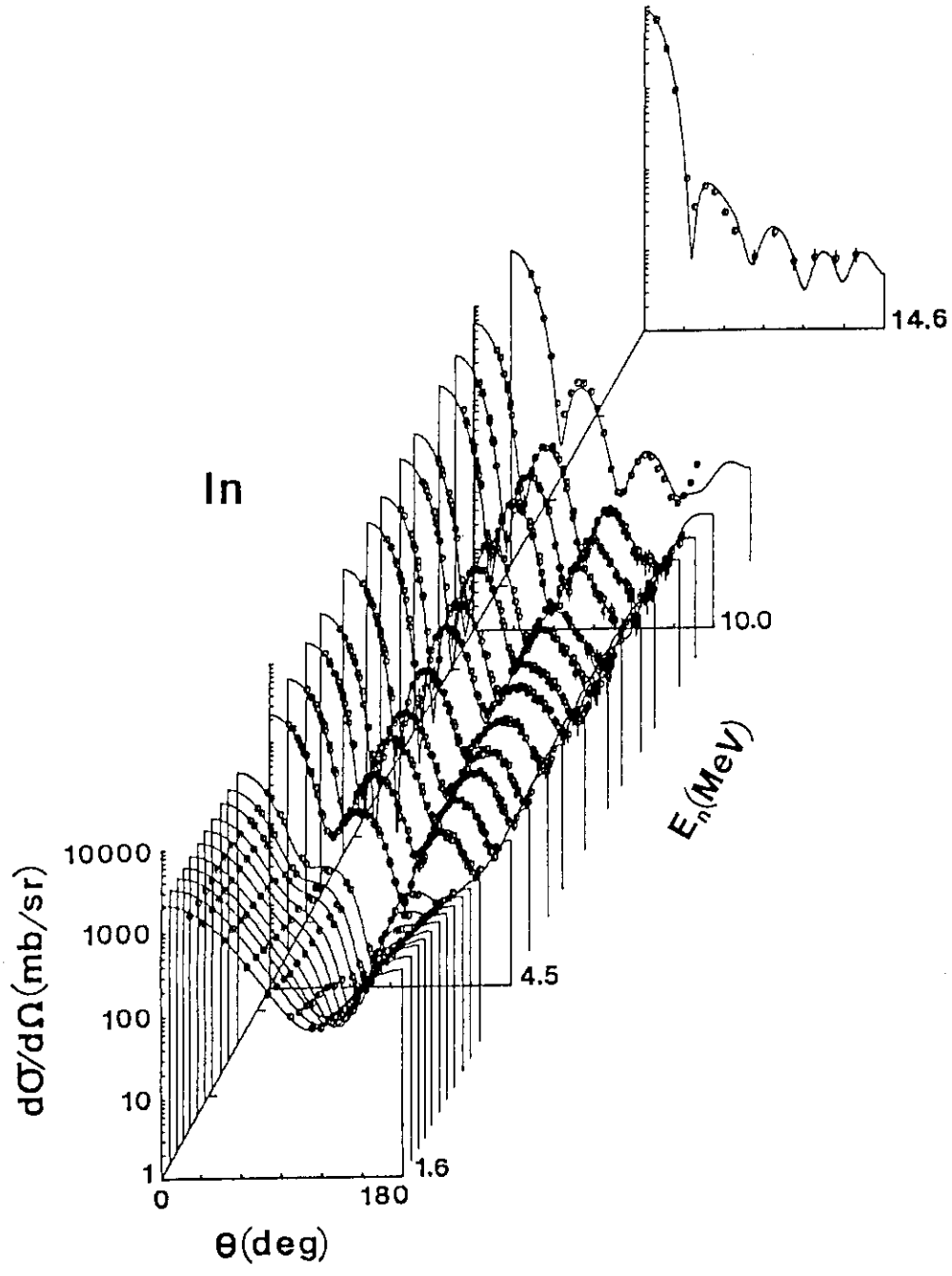

Fig. 2 Neutron elastic scattering cross sections of elemental indium[2)]

2.6 Group Constants of JENDL-3

2.6.1 Group Cross-section Processing Method and Common Nuclear Group Cross-section Library Based on JENDL-3 Nuclear Data File

Akira HASEGAWA

Shielding Laboratory, Department of Reactor Engineering

Tokai Research Establishment,
Japan Atomic Energy Research Institute,
Tokai-mura, Naka-gun, Ibaraki-ken, 319-11 Japan

abstract

A common group cross-section library has been developed in JAERI. This system is called "JSSTDL-295n-104γ (neutron:295 gamma:104) group constants library system", which is composed of a common 295n-104γ group cross-section library based on JENDL-3 nuclear data file and its utility codes. This system is applicable to fast and fusion reactors. In this paper, firstly outline of group cross-section processing adopted in Prof. GROUCH-G/B system is described in detail which is a common step for all group cross-section library generation. Next available group cross-section libraries developed in Japan based on JENDL-3 are briefly reviewed. Lastly newly developed JSSTDL library system is presented with some special attention to the JENDL-3 data.

keywords: group constants library, JSSTDL system, JENDL-3, group cross-section processing, fast reactor, fusion reactor, nuclear data

1. Introduction

Evaluated nuclear data library, as one of the representatives of JENDL-3/1/, is doomed to be used primally in reactor engineering through the group cross-section library, i.e., group constants. Today, calculation codes which are not using group-constants directly such as MCNP MonteCarlo code are sometimes used, but most frequently traditional group constants are used as standard neutronics analysis in nuclear power industries. Group cross-section processing is closely coupled not only with the the nuclear data file but also with the neutronic calculation code to be used. The group cross-section processing is a way for bridging over the nuclear data and reactor engineering.

Recently the third version of JENDL is released officially after the several times of revisions by the feedback information from the benchmark tests. Up to now several group constants libraries have been generated and used in Japan.

In this paper, we first give the outline of group cross-section processing in detail adopted in Prof. GROUCH-G/B processing code system/2/. As described earlier, group

processing is tightly coupled with the nuclear calculation code to be used, but the methodology is not so quite different for the other nuclear codes. In chapter 2, it is included that pre-processing: generating point-wise cross-sections in linear-linear interpolable scheme from the original JENDL-3 file using the codes of resonance reconstruction and Doppler broadening, group averaging process and post-processing: making up some specific group cross-section library. In chapter 3, available group constants libraries processed from JENDL-3 are briefly shown. In chapter 4, a common cross-section library JSSTDL-295n-104γ system is presented. We put stress here on the point why this system is developed(i.e., developing target) and outline of the system. In chapter 5, some comments on the data in JENDL-3 are described especially for the problems encountered in the processing of group constants generation.

2. Outline of group cross-section processing

Generally evaluated nuclear data file is compiled from two principles, i.e., data should be given as simple as possible and as complete as possible. For example, the real complex world of cross-sections are usually represented by hundreds of resonance parameters at most. This is a typical example for simpliness and completeness. Resonance reconstruction is one of the main target of the processing. Group averaging process is another target. Group library compilation is also necessary. Processing out-line is shown in Fig. 2.1.

Starting from original JENDL-3 library, processing is divided into the following three steps, i.e., pre-processing, processing, post-processing.

2.1 Pre-processing: In the pre-processing stage, generating point-wise cross-sections in tabular form at desired material temperature is the main problem. In this tabular form, the data should be given in linear-linear interpolable scheme in energy and cross-sections. The process proceeds as follows, firstly all cross-section data represented by ENDF/B general interpolation scheme are converted to linear-linear interpolable form. Next resonance reconstruction processing is made according to the specified resonance formulae and additional floor cross-sections. Generated point-wise cross-sections up to here is only for zero degree in Kelvin. To reflect the Doppler broadening between the nuclei and materials, additional processing is required, i.e., bootstrapping kernel broadening method is used starting from zero degree in Kelvin cross-section data. In this stage, LINEAR /3/, RECENTJ /4/ and SIGMA1 /5/ codes are used.

2.1.1 LINEAR: In the evaluated nuclear data file, data are represented in the tabular form with general interpolation scheme as shown in Table 2.1 in order to define a real cross-section world in the simplest way.

Table 2.1 Interpolation Scheme

1	CONSTANT	Constant cross section between tabulated energies
2	LINEAR-LINEAR	Linear variation in cross section and energy
3	LINEAR-LOG	Linear variation in cross section, log in energy
4	LOG-LINEAR	Log variation in cross section, linear in energy
5	LOG-LOG	Log variation in cross section, log in energy

Thus real cross-sections are represented as a function of energy connected by several piece-wise energy intervals where a specified interpolation scheme is applied. If we used this original representation, the processing becomes rather complicated according to the different interpolation schemes. In fact, up to ten years ago we used general interpolation scheme directly in the processing code. In such processing, numerical instability is inevitable. To assure the accuracy, we had to increase the point number of the integration or tolerance for the convergence of numerical integration. It took long calculation time but relatively poor calculation results were obtained.

Today at first step, we convert all cross-sections in general interpolation scheme to linear-linear interpolation data. Succeeding process keeps this criteria; i.e. all data are linear interpolable. Therefore numerical integration in the group averaging process becomes quite simple and relatively error free. On the contrary, generated data points becomes very huge. Imagine that, if complete 1/v cross section require only two points for all energy region if log-log scheme is used, but more than several hundreds points should be necessary for lin-lin case depending on the required accuracy. However, more merits are appreciated than the cost-up by the increasing of data storage. Even though, minimum data points are generated from this code by the binary division method comparing a true value calculated from general interpolation method and a lin-lin interpolated value from the generated data. At the same time, thinning processing is also applied. So minimum data points are generated within the required accuracy.

2.1.2 RECENTJ: For some light element such as H, C, O has no resonance parameters in the evaluated nuclear data file, because resonance structure is quite simple, i.e., all data are represented as point-wise basis. But for structure nuclides (Fe,Cr,Ni,etc.) or heavy nuclides (U, Pu fuel elements) so many resonances are observed, data are given as a set of resonance parameters. In Fig. 2.2, very complicated cross-section are shown. In this figure more than hundred thousand data points is drawn, but it is only represented by several hundred resonance parameters at most in the evaluated data file. Usually we cannot construct real cross-sections only from the resonance parameters, the difference between the real cross-section and constructed ones only from the resonance parameters are stored in the cross-section data part (FILE3: ENDF FILE category) as back-ground cross section, thus this part(FILE3) can be negative cross sections in some case.

It is necessary to reconstruct the resonance cross-sections in lin-lin form from resonance parameters(FILE2) and back-ground cross-sections(FILE3). This range is divided into two distinct energy rage; i.e., resolved resonance and unresolved resonance regions. This part is very sensitive for the processing, because different evaluated files has some differences in definition (ex. J-unknown state, two resolved resonance region, adoption of Reich-Moor parameters, energy range mismatch between isotopes in natural element). And technically very difficult and deep consideration is required for the code development for back-ground cross section treatment, isotopic treatment of resonance parameters and resonance formulae allowed to be used.

For the user's side, processing for the generation of required cross sections is very difficult task. For some case, it takes more than one hour in CPU time using the mainframe computer(FACOM-M/780) in JAERI. And several times, generated cross section exceeds more than 200000 points. It not only requires huge storage space but also affects the later processing.

Resolved Resonance: In this range all resonances are resolved and cross-sections are uniquely determined. Allowable resonance formulae are shown in Table 2.2.

Table 2.2 Resonance Formulae

1	SLBW	Breit-Wigner single-level parameter
2	MLBW	Breit-Wigner multilevel parameter
3	RM	Reich-Moor parameters
4	AA	Adler-Adler parameters

At the early stage of the evaluated nuclear data file, mainly SLBW is used. But in the shape fitting of the real cross-section, errors is relatively large. To overcome the shortage of SLBW, today, MLBW is more often used than before. But it takes more and more computation time due to the calculation of interference between levels. RM is deactivated in ENDF/B-5 format, but recently some nuclides are evaluated by this formulae (for ex. JENDL-3 Pu-239), due to the possibilities more physical resonance shape reconstructions and physical explanations. From now on, this formulae should play an important role. But the code accepting this formula is not so popular and it takes much time to reconstruct the cross sections.

Processing is performed by binary division algorithm using the resonance energy grid data to generate the resonance shape. Selecting from any adjacent two resonance energy grid data (i.e., peak value of cross-section), a rough fine grid is determined considering resonance width. For each of the rough grid, binary division method is applied and data points are generated within the required accuracy. Thus any resonance structure can be reproduced within the required accuracy. In this case, energy presentation accuracy is very

important, because usual 6 digits representation (for example 1PE11.5) is not enough in some case. Seven digit representation is required.

Unresolved Resonance: In this energy range, as opposed to the resolved range cross section, they are not determined uniquely from the resonance parameters, instead statistically averaged cross section is represented by parameters. Thus cross-section shape is represented as rather smoothed curves. We cannot know the real cross-section in any particular energy point. Instead we can observe only expectation values determined from resonance width at the requesting energy point. From these physical meaning, calculation of self-shielding factors becomes difficult.

Only permitted formula in this range is SLBW, with an option of energy dependence of resonance width. At the cross-section reconstruction, interpolation of resonance parameters are not allowed. Always cross-sections out-side the resonance energy grid should be calculated by the interpolation of the grid cross-sections. Some old code violate this criteria.

2.1.3 SIGMA1: Up to now, point-wise cross section of zero degree in Kelvin is generated. Room temperature is about 300 K, reactor operation temperature is more than several hundreds K and in the accident stage temperature may exceed 2000 K. So we must know the cross-section shape in these temperatures, to simulate reactor behavior exactly. Doppler effect between the nuclei and materials surrounding plays an important role for the resonance cross-section shape as seen in Fig. 2.3. Peak narrow resonance is considerably broadened by Doppler effect. Thus this affects self-shielding factors.

There are two methods for this processing. One is the kernel broadening method, which solve directly Doppler broadening equation using point-wise cross section table in linear-linear interpolation. This method applies to any reaction and to any temperatures. But calculation cost is rather expensive. SIGMA1 uses this method/5/. But this cannot applied to unresolved data. The other is ψ -χ method/6/. Starting from resonance parameters, using precalculated weight tables and fitting routines, Doppler broadened cross-section is defined. The calculation cost is quite cheap, however, this method is only applicable for SLBW resonance formula. Thus this method is used in unresolved range self-shielding factor calculation in the group averaging process.

This pre-processing is quite important for the group averaging process. A decade years ago, we processed all these processing in a group averaging process code. In that case, so many numerical calculation options had been used to assure the numerical integration accuracy due to the different interpolation schemes.

2.2 Group constants processing:

Group averaging process is the main-part of the group cross-section processing. In this processing, main problems are effective cross-section calculation (i.e., self-shielding factor calculation) and scattering matrices generation. This processing and the post-processing are used for making up some specific group cross-section library. For the processing, we discuss the problems along with our processing code Prof. GROUCH/G-B(MACS-N) /2/.

2.2.1 Self-shielding Factor: In strong absorbing media effective cross-section is decreased due to the flux distortion by it's absorption when considering energy range is wider than a resonance. In the resonance region, this effect is very large. Therefore it is called resonance self-shielding effects.

Under the condition of constant collision density, flux is inversely proportional to total cross-section. Thus effective cross-sections are defined by group averaged cross-section whose weighting flux is inversely proportional to the sum of total cross-section and back-ground cross-section, where back-ground cross-section is defined by per atom of the total cross-section other than the nuclide considered. Self shielding factor (f-factor) is defined as the ratio of effective cross section and infinite dilution cross-section, where the latter is the effective cross-section when back-ground cross-section is infinite; i.e., no flux distortion case.

$$self\ \ shielding\ \ factor \equiv \frac{<\sigma_{eff}>_g^r}{<\sigma_\infty>_g^r} \tag{1}$$

$$<\sigma_x>_g^r = \frac{\int_{E_g}^{E_{g-1}} \sigma^r(E)\,\phi_x(E)\,dE}{\int_{E_g}^{E_{g-1}} \phi_x(E)\,dE}$$

$$\phi_x(E) = \frac{\phi_0(E)}{(\sigma_t(E)+\sigma_0)^k}$$

where

$k = 0$: *no self-shielding* (*for* $<\sigma_\infty>$)
$k = 1$: *self-shielded scalar flux*
$k = 2$: *self-shielded current*

r : *reaction*

g : *group*

$\phi_0(E)$: *Energy dependent weighting spectrum*

A set of f-factors parameterized by back-ground cross-section (σ_0) and material temperature (T) is called f-table. Using this f-table, effective cross-sections of any nuclides in some material region can be calculated quite simply by the table interpolation method.

In the averaging process, numerical calculation is very difficults to obtain the accurate results if the data represented as general interpolation scheme. Today all of the cross section data is represented in linear-linear interpolation as stated before. Integration is performed analytically using given data points both for weighting flux and cross-section in our code, thus no numerical instability is observed and accuracy is quite satisfactory. In this processing, double precision representation is necessary for energy variables to distinguish very narrow resonances and to account their contribution to the averages.

Cross sections are defined uniquely in the smooth cross-section part and resolved resonance region. Thus group averaging process described above is applied to these region. But in the unresolved resonance region, integration cannot be performed by eq. (1). Because cross-section in this region is defined by some statistic averages of resonance parameters. For the self-shielding factor calculation, there are two methods. One is analytical method using ψ - χ function, which is already mentioned in the pre-processing, the other is a stochastic method which is called as ladder method, i.e., simulating the pseudo resonances generated statistically from random sampling of resonance energy and resonance width. For these generated resonances, processing is the same as the resolved one. UNRESR/7/ adopts former method, TIMS-1/8/ adopts latter method. In our code, former method is used. The result is somewhat different between the code due to the calculation model. There are no true value for this range.

Physically the cross-section in upper part of resolved resonances and lower part of unresolved resonances should be continuous. But generated cross-sections from evaluated data file sometimes differ more than 30 %. Data evaluation and data definition still be necessary in this region.

Typical f-table values are shown in Fig. 2.4.

2.2.2 Group Transfer Matrices Calculation: For all reactions exiting neutron, group transfer matrices should be calculated. Group transfer matrices are calculated from following data;

Angular Distribution(FILE4) in CMS or Lab,
Energy Distribution(FILE5) in Lab,
Angle-Energy Correlated Distribution(FILE6) in CMS or Lab.

Usually in two body collision, correlated distribution should be given, i.e., angular and energy distribution are not independent. For elastic scattering and discrete inelastic scattering, only angular distribution is used, energy distribution is automatically calculated by collision theory. Emitted neutrons from break-up reaction in light elements like Li,Be or from continuum level of inelastic scattering requires FILE6 angle-energy correlated distribution. But in JENDL-3, FILE6 data representation is abandoned completely, although in JENDL-3PR1&2 some data had been evaluated in FILE6(ENDF-5 Format). For primally nuclides in ENDF/B-VI, FILE6 data are supplied. From now on processing of FILE6 becomes very important. In Japan no data processing code has the capability for FILE6 data of ENDF/B-6 FORMAT/9/.

Numerical integration method is used for this calculation. For higher P l moment calculation, numerical instability is sometimes appeared. High precision Gauss Integration method is used to overcome the difficulty in our code. Even though, significant differences are born due to the bit length of the computer machine used.

Processing for this part is completely dependent on the neutronics code to be used. For fast reactor calculation, Legendre expansion method is mainly used. On the other hand, as seen in the fusion neutronics case, to treat the angular distribution more rigorously, i.e., free from the negative fluxes due to the truncation error of finite Legendre expansion, DDX(Double Differential Cross-section) type data processing is required.

3. Available group cross-section libraries based on the JENDL-3 Nuclaer Data file

All group-cross-section libraries used in the JENDL-3 benchmark test are summarized in Table 3.1. Group constants library is completely dependent to the neutronic calculation code to be used. Since benchmark test fields for JENDL-3 has been expanded quite wide and main contributing energy range is quite different from fields to fields, different group cross-section processing systems and neutronic calculation systems have been used. For major benchmark test fields, more than two group-constants libraries are produced and used.

Table 3.1 Group Constants library used in JENDL-3 Benchmark-test

Test item	Group Constants	Processing System
FBR	JFS-3-J3	TIMS-PGG
LWR	SRAC-LIB	SRAC,TIMS-PGG
	WIMS-LIB	NJOY
	MGCL	MGCL-ACE
Shielding	JSSTDL-295	PROF/GROUCH-G/B(MACSN)
	SSL-90J3	RADHEAT-V4
	FSXLIB	NJOY
Fusion Neutronics	FSXLIB	NJOY
	FUSION-J3	PROF/GROUCH-G/B(MACSN)
	DDXLIB3.J3	PROF-DD

4. JSSTDL-295n-104γ common group cross-section library

This is a common group cross-section library developed in JAERI by the author under the cooperation of working group on Standard Group Constants affiliated by the Committee of Group Constants of JNDC(Japanese Nuclear Data Committee). This work was promoted by the Nakazawa Committee's recommendation /10/ deserted to the JNDC (Action for the Post JENDL-3 Project of JNDC, 1986) defining the working frame of JNDC after JENDL-3 project was completed. In the recommendation, it was written that JNDC should supply immediately commonly usable group cross-section library for primary data users such as fast or fusion reactor designers when JENDL-3 is released. Such a system has been requested for many years by various nuclear data users, particularly nuclear design group. Up to now shielding and criticality calculations have been performed in different calculation paths using the different group constants libraries, i.e., in different group structures and data sources due to the characteristics of the calculations involved. Finer group structure is inevitably necessary for the shielding calculation but relatively coarse group structure is sufficient for the criticality calculations. Hence there have been many requests for supplying a common library applicable both for the criticality and shielding calculations. Users are also very keen for using the latest nuclear data.

Responding to these requests, specifications of the common group constants were decided. In Table 4.1 specification of JSSTDL system is shown. Most users insist to maintain their own group structure which has been so far used. Therefore a universal group structure was decided to cover almost all group structures used in Japan, as seen in Table

4.2 ~ 3, so as to produce their own required group structure library from a master library. It was also decided to prepare a library for design codes most frequently used such as ANISN, DOT or MORSE. Resonance self-shielding factors were also considered for primary reactions. Scattering matrices were calculated up to P5 components and were stored independently for elastic and inelastic scatterings so as to use the different self-shielding factors. For secondary γ production cross sections, data are stored for the following 4 reactions, i.e., total, capture((n,γ) MT:102 only), fission(MT:18), other than capture and fission ((n,n'),(n,p),(n,α),...), to reflect self-shielding factor for capture and fission reactions in neutrons. Gamma transport cross-section are generated by GAMLEG-JR/11/.

A utility routine was developed to enhance portability of this system to other sites or machines. Routines for group collapsing and for generating region dependent macro-scopic cross sections were also developed and released with the library.

Up to now, 63 nuclides were processed and stored for JSSTDL library from JENDL-3 general purpose file. Gamma data are furnished for 32 nuclides out of 63 processed nuclides. Almost all nuclides available of γ production data in JENDL-3 were processed. For the processing of JENDL-3 neutron and γ production cross-section, Prof.GROUCH-G/B /2/ system and its utility codes were fully used.

This library system has been fully applied for the benchmark test of JENDL-3. We confirmed the applicability of this system to the fast reactor calculations both for criticality and shielding and also to the fusion neutronics calculations. This system: 295n-104γ JSSTDL library is now available through JNDC Nuclear Data Center with the associated utility codes in FORTRAN source. The package includes also 100n-40γ library for the users of shielding field.

For future plan, more nuclides will be processed and stored according to the user's requests not only from JENDL-3 but also from ENDF/B-VI or ENDL data files. Gamma production data are relatively poor in JENDL-3 because not so many nuclides are evaluated. The requests for the nuclides not available in JENDL are very strong for some γ production data. We are now starting for making a complete set of the neutron and gamma coupled group constants library of JENDL-3 by substituting γ production data not available in JENDL-3 for the data from the other data files.

5. Comments on the JENDL-3 data processing

Now cost of the processing of group constants became more and more expensive. Since more and more accuracy is requested from the users, the data stored in the evaluated nuclear data file become more and more complex. The data amount of the evaluated data file were increasing rapidly with version up.

Especially, for resonance parameters, in these days, MLBW (Multi Level Breit Wigner) representation is not a special formulae and some nuclides use RM (Reich-Moor) resonance formulae. Though the fitted results of the cross sections by these formulae are extremely good and physically meaningful, these advanced method consume so much computation time. And energy boundary of resolved resonance region become shifting higher due to the smooth connection for self-shielding factor value in unresolved part. Many new levels are included as resolved levels. Therefore, for example for U-238 of JENDL-3, we spend more than 10 hours of CPU time by FACOM M-780 machine to generate 5 different temperature point -wise cross-sections data(Doppler broadened point cross-section). This cost is tremendous for our usual computation sense. Some one says that resonance processing requires once in a life of the evaluated files, therefore it is not a serious problem. But we usually process original file repeatedly according to the user's request for the processing accuracy. At the same time required storage of the generated point-wise data became huge. We must think about the evaluated data file philosophy i.e. give the data as simple as possible.

For inelastic scattering, in order to give much agreements for the DDX shape of outgoing neutron, pseudo level representation are frequently used in the light element data of JENDL-3. The cost of processing also increased by this pseudo level inclusion. We must think about the rational data representation for the industry use.

In JENDL-3, for the threshold reaction of many body break-up process, energy distribution is given in tabular-form and some special form data (triangular distribution between 1 and 2 eV) representation is given for the threshold point. The next (the second) energy distribution data is given relatively higher energies than the threshold. This gives some odd results for the fast breeder spectra or DDX spectra calculated by JENDL-3 data, some bump is appeared around 1 ~ 2 eV(please see the presentation made by Mr. Tian /12/).

J-unknown state assignments, this is a trick made by an invalid J number assignments to indicate J-unknown state, which have been a local definition valid only for JENDL-2, is completely removed. This local assignments had been the largest problematic problem in JENDL-2.

6. Conclusion

One year is not yet passed since the JENDL-3 is officially released, though, we have already several group cross-section libraries available for us. Of course all of them are not yet openly available in user's hands, but we have some feeling that fairly freely we can use these libraries by the time not so late from now. Users are very keen the latest data. Many experiences are reported as to the applicability of the JENDL-3 data.

JSSTDL system is just the requested one from the user's side. To accept user's common requests for the group-constants, such as applicable to widely used transport code,

consistent with user's required group-structures, the latest nuclear data source,..., JSSTDL library system was developed and released through JNDC Nuclear Data Center.

Today JENDL-3 is a common treasure for all of the persons involved in nuclear industries of JAPAN. Therefore we should take care of JENDL-3 as a common knowledge for all of the persons involved. The contact point between industry side persons and nuclear physics side persons is the group constant. We hope that JSSTDL library system becomes a platform for the users of JENDL-3 and the discussions on the problems encountered in JENDL-3 are going on with this library.

References

/1/ Shibata K., Nakagawa T., Asami T., et al. :"Japanese Evaluated Nuclear Data Library, Version-3 -JENDL-3-",JAERI-1319 (1990).
/2/ Hasegawa A. :"Development of a Processing Code System Prof. GROUCH-G/B", unpublished work (1986).
/3/ Cullen D.E.:"Program LINEAR",UCRL-50400,Vol.17,Part A,(1979).
/4/ idem:"Program RECENT",UCRL-50400,Vol.17,Part C,(1979);
RECENT-J is a modified version in JAERI.
/5/ idem:"Program SIGMA1",UCRL-50400,Vol.17,Part B,(1979).
/6/ Schenter R.E., Baker J.L. and Kidman R.B. :"ETOX", BNWL-1002, (1969).
/7/ MacFarlane R.E., Muir D.W. and Boicourt R.M. :"NJOY UNRESR module", LA-9303-M, Vol. 1 (1982).
/8/ Takano H, et al.: "TIMS-1", JAERI-1267, (1980).
/9/ Rose R.F. :"Description of ENDF/6 Format", private communication, BNL,(1989).
/10/ Nakazawa M. et al.: "Proposal on Post-JENDL-3 Activity Programme for Japanese Nuclear Data Committee",JAERI-M 87-025 pp9 (1987).
/11/ Koyama K. et al. :"RADHEAT-V3",JAERI-M 7155 (1977).
/12/ Tian D.F. et al. :"One-Dimensional Benchmark Tests of Principal Fission Nuclides in JENDL-3", proceedings of the 1990 Seminar on Nuclear Data (1990).

Table 4.1 Group cross-section library processing specification

Group structure	neutron:295 gamma:104
Weighting spectrum	Maxwellian from 1.0E-5 to 0.3224 eV the rest is 1/E.
Resonance reconstruction tolerance	0.1%
Self-shielding factor	
Temperature grid	300 600 900 2100 Kelvin
σ_0 grid	0 0.1778 1 10 10^2 10^3 10^4 10^5 10^6 barn
Self-shielding factor reaction	total, elastic, capture, fission.
Anisotropic Pl order	5

Table 4.2 Neutron group boundaries considered in JSSTDL system

Library name	groups
JSD-100	100
JSD-1000	100
BERMUDA-121	121
FNS-125	125
VITAMIN-C	171
VITAMIN-J(E+C)	175
GICX-42	42
ABBN-25	25
JFS-New	70
GAM-123(fast only)	92
MGCL-137(fast only)	91
WIMS-69(fast only)	28

Table 4.3 Gamma group boundaries considered in JSSTDL system

Library name	groups
CSEWG-94	94
LANL-12	12
STEINER-21	21
STRAKER-22	22
LANL-48	48
LANL-24	24
BERMUDA-36	36
HONEYCOMB-15	15

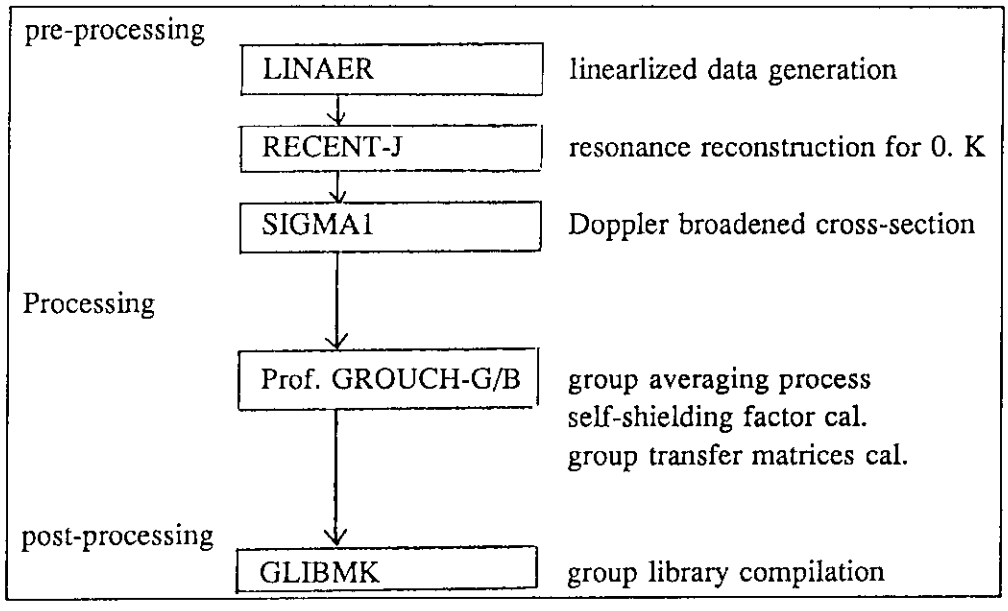

Fig. 2.1 Processing out-line for group cross-section library generation

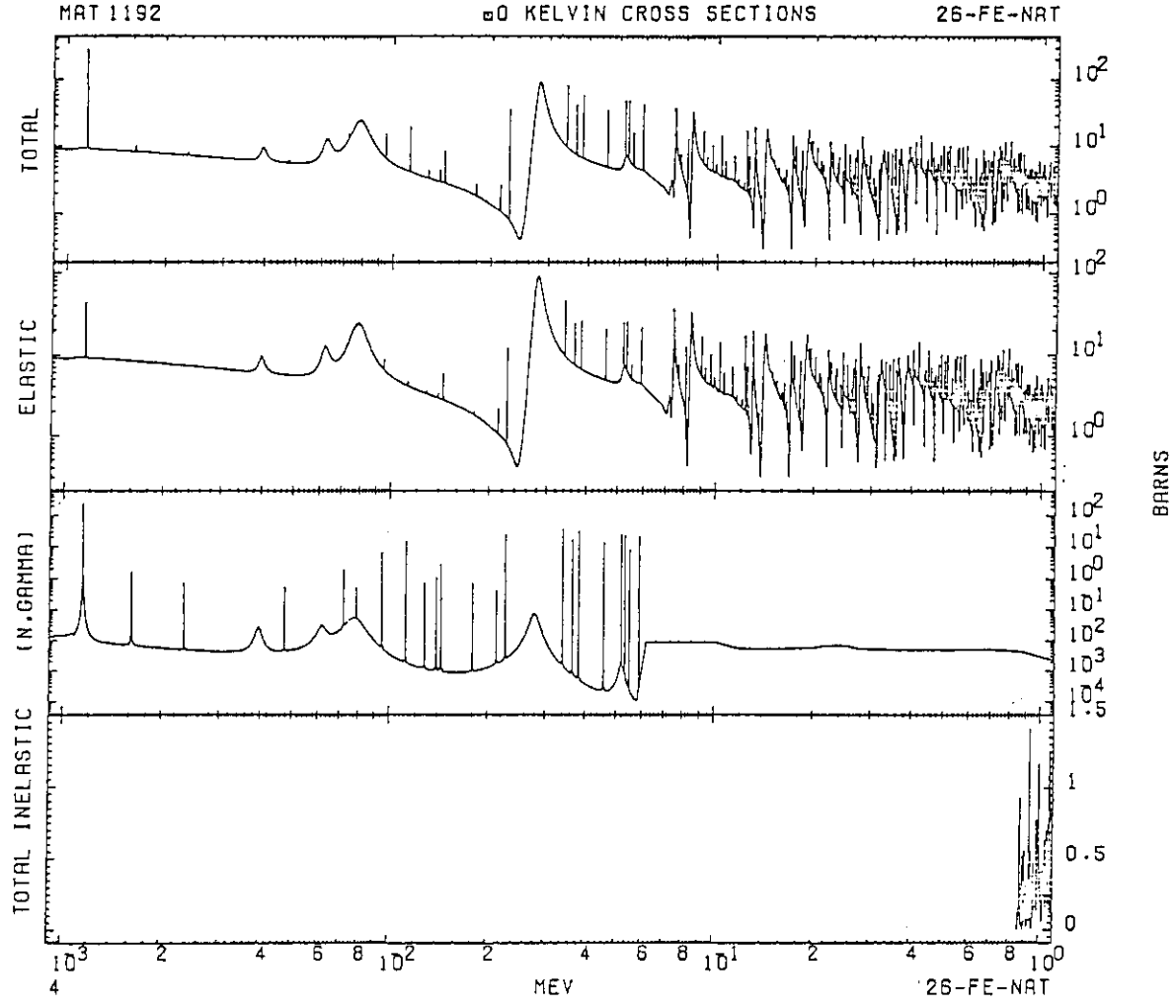

Fig. 2.2 Cross-section of natural iron (generated by ENDF/B-IV data)

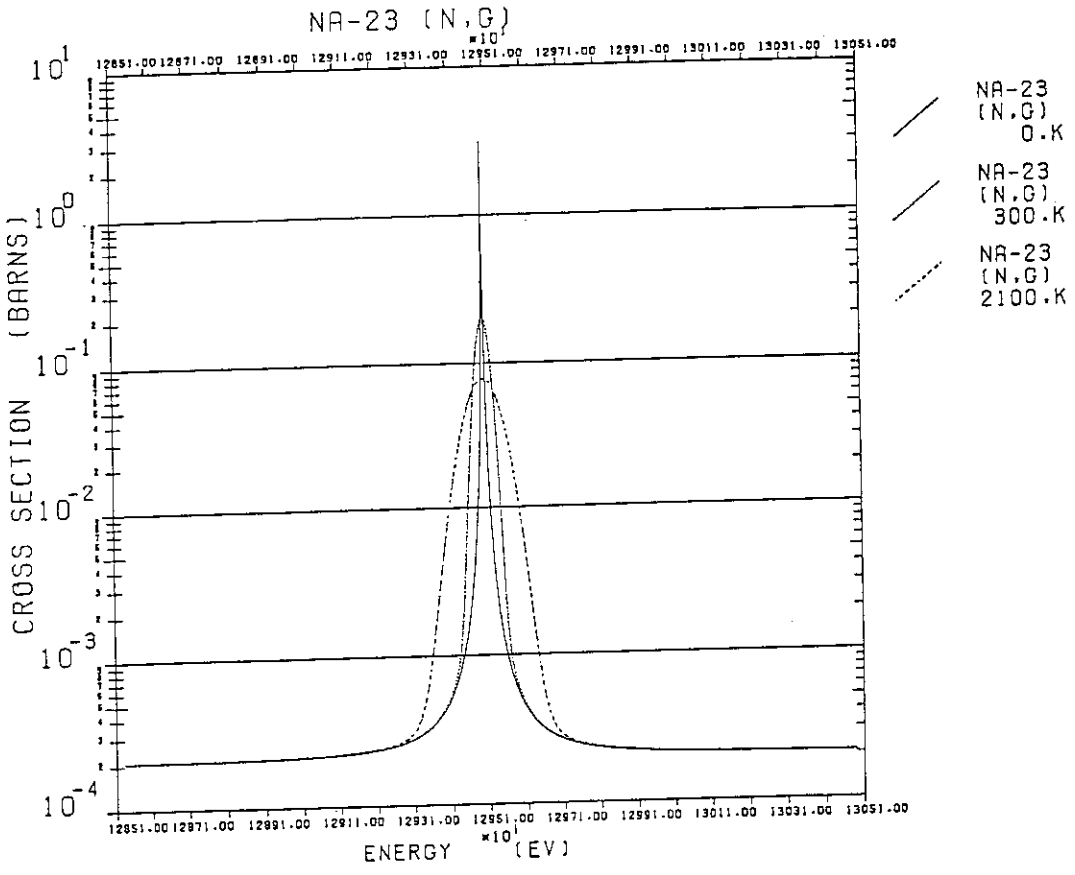

Fig. 2.3 Doppler broadened Na capture cross-section for 12.95 keV resonance

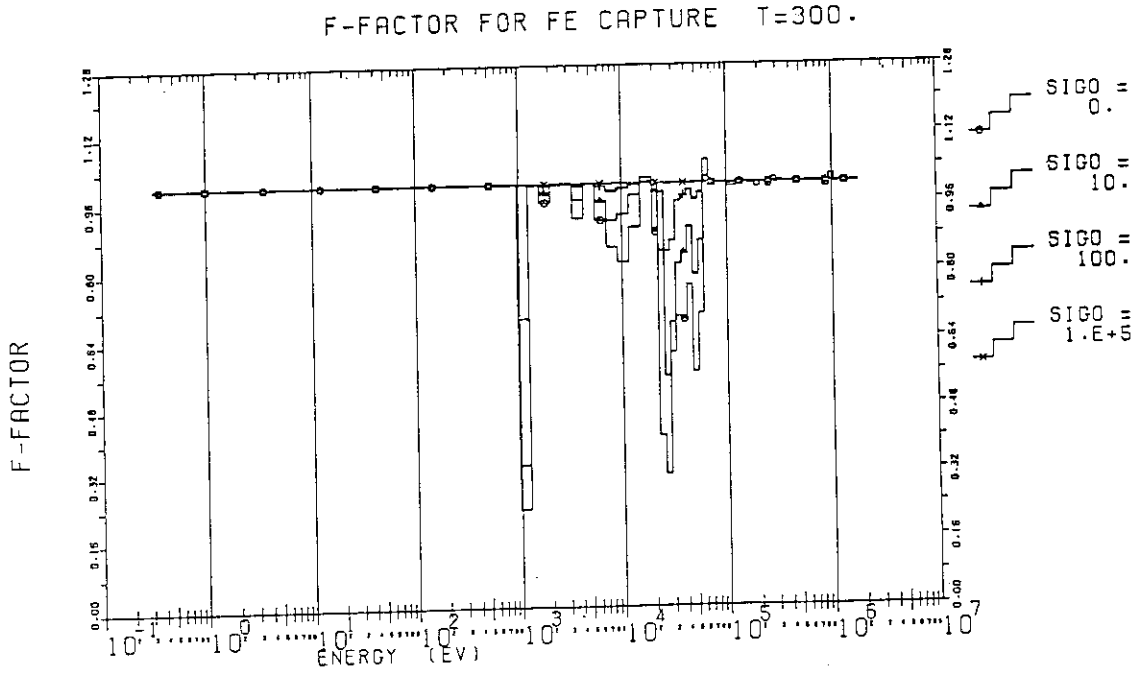

Fig. 2.4 Self-shielding factor for capture reaction of natural iron (generated by ENDF/B-IV data)

2.6.2 One Dimensional Benchmark Test of Principal Fissile Nuclides in JENDL-3

Dongfeng TIAN, Akira HASEGAWA,
Tsuneo NAKAGAWA, and Yasuyuki KIKUCHI

ABSTRACT

As one of the Benchmark tests of JENDL-3, criticality calculations have been performed on 9 small critical Benchmark assemblies for fast reactor, such as JEZEBEL, JEZEBEL-Pu, FLATTOP-Pu, THOR, GODIVA, FLATTOP-25, BIG TEN, JEZEBEL-23, and FLATTOP-23. These assemblies have the characteristics of simple geometry and very high enriched cores consisting of single fissile nuclide such as ^{233}U, ^{235}U and ^{239}Pu. All calculations are performed by one-dimensional S_n Code ANISN (S_{16},P_5) with JSSTDL-295 group cross section library. From this benchmark test, following problems are pointed out: (1). inadequacy of δ function energy distribution representention adopted in JENDL-3 at the threshold energy point for the continuum inelastic scattering, (n,2n), (n,3n) (n,4n) and charged particle emitting reaction. (2). ^{233}U data of JENDL-3 reproduces K_{eff} nearly 2.1% over prediction. χ data is suspected to this over prediction. reevaluation is requested. (3) as to ^{235}U and ^{239}Pu data, no problem is pointed out.

1. Introduction

The benchmark tests of JENDL-3 on the 9 simple critical benchmark assemblies for fast reactor, such as JEZEBEL, JEZEBEL-Pu, FLATTOP-Pu, THOR,GODIVA, FLATTOP-25, BIG TEN, JEZEBEL-23, and FLATTOP-23[1](listed in Table 1). Because these assemblies have the characteristics of simple geometry and very high enriched cores consisting of single fissile nuclide such as ^{233}U, ^{235}U and ^{239}Pu, they are suitable to check nuclear data applicability directely.

All calculations were performed by one dimensional transport code -- ANISN (S_{16},P_5) with JSSTDL-295 group cross section libary. Testing items ars as follows: criticality, central spectrum indices, and leakage spectra.

2. Benchmark Testing Results

(1) A Probelm from Triangular Energy Distribution of Secondary Neutrons in JENDL-3

When the original data of JENDL-3 were used, the calculated central neutron spectra for all the benchmark assemblies have one large peak near 1 eV like the dotted line as shown in Figure 1. It is not thought a normal phenomena. Such strange peak can not be explained physically. Now it has been proved that the large "strange peak" is caused by the triangular energy distribution of secondary neutrons in JENDL-3.

In File 5 of JENDL-3, for the threshold reactions of some nuclides listed in Table 2, their secondary neutrons were described by arbitrary tabulated function (LF=1)[2]. At the threshold energy point, the shape of energy distribution is like a triangular as shown in Figure 2. At the second energy point, the energy distribution is given as shown in Figure 3.

When the data are processed to group constant, as you know,

it is necessary to interpolate the energy distributin between the two energy points mentioned above. The shape of interpolated energy distribution will be like the solid line in Figure 4. It is obvious that such energy distribution is never reasonable. Naturally it is imaginable that it must make the group transfer matrix like the dotted line in Figure 5. That means much more neutrons will be transfered to the region below 1 eV artificially like the dotted line in Figure 1.

This is the reason to the "strange peak" in the calculated central neutron spectra. Till now the modification of JENDL-3 has been performed. The revised data also has been released as JENDL-3 Rev 1. Now the "strange peak" will be disappear in neutronics calculations (like the solid line in Figure 1) if the JENDL-3 Rev 1 data are used.

(2) One Dimensional Benchmark Testing Results of JENDL-3 Rev. 1

Table 3 showes the calculated K_{eff} table for the 9 benchmark assemblies mentioned above. Here we can find the data of ^{239}Pu and ^{235}U seems no probelm, but there must exist some probelm in the data of ^{233}U. Also the calculated spectrum indices listed in Table 4 show some probelm from the data of ^{233}U. Here we will only discuss about the data of ^{233}U.

The ν and σ_f data of ^{233}U in JENDL-3 are almost same as the JENDL-2 data. But the fission spectra are much different between the two libaries (see Figure 6). Though the difference is thought from the Maxwellian spectrum used in JENDL-2 and Madland Nix spectrum used in JENDL-3, the fission spectrum of ^{233}U seems too hard to be accepted. Some numerical test has been done to check the effect from fission spectrum (see Table 4). The results demonstrates that the fission spectrum is very sensitive for criticality calculations.

3. Discussions

Based on our results and analysis, some discussions will given as follows:

(1) When the arbitrary tabulated presentation (LF=1) is adopted for threshold reaction, it will be unsuitable to use the triangular energy distribution for secondary neutrons. In other words, it will not be a simple and easy method.

(2) the fission spectra of ^{233}U in JENDL-3 are too hard to be accepted.

(3) the fission cross section of ^{233}U seems higher ?

(4) the fission spectrum data should be paid more attention.

Till now this work is still being carried on. The final conclusions will be given shortly.

REFERENCES

[1] Cross Section Evaluation Working Group Benchmark Specifications, November 1974, BNL 19302 (ENDF-202)

[2] R. Kinsey: Data Formats and Prosedures for the Evaluated Nuclear Data File, ENDF, October 1979 (ENDF-102)

Table 1 One dimensional calculating models of some benchmark assemblies for fast reactor

SPECIFICATIONS	CORE RADIUS (cm)	ISOTOPES	DENSITY NUCLEI/b-cm	INNER AND OUTER REFLECTOR RADIUS (cm)	ISOTOPES	DENSITY NUCLEI/b-cm
JEZEBEL	6.385	^{239}Pu ^{240}Pu ^{241}Pu Ga	0.037050 0.001751 0.000117 0.001375	--	--	--
JEZEBEL-Pu	6.599	^{239}Pu ^{240}Pu ^{241}Pu ^{242}Pu Ga	0.029940 0.007880 0.001210 0.000160 0.001380	--	--	--
FLATTOP-Pu	4.533	^{239}Pu ^{240}Pu ^{241}Pu Ga	0.036740 0.001860 0.000120 0.001380	4.533 , 24.13	^{235}U ^{238}U	0.000340 0.047740
THOR	5.310	^{239}Pu ^{240}Pu Ga	0.036180 0.001940 0.001330	5.310 , 29.88	^{232}Th	0.030050
GODIVA	8.741	^{234}U ^{235}U ^{238}U	0.000492 0.045000 0.002498	--	--	--
BIG TEN	30.48	^{234}U ^{235}U ^{238}U	0.000050 0.004840 0.042680	30.48 , 45.72	^{235}U ^{238}U	0.000100 0.047970
FLATTOP-25	6.116	^{234}U ^{235}U ^{238}U	0.000490 0.044490 0.002700	6.116 , 24.13	^{235}U ^{238}U	0.000340 0.047740
JEZEBEL-23	5.983	^{233}U ^{234}U ^{235}U ^{238}U	0.046710 0.000590 0.000010 0.000290	--	--	--
FLATTOP-23	4.317	^{233}U ^{234}U ^{235}U ^{238}U	0.046710 0.000590 0.000010 0.000280	4.610 , 24.13	^{235}U ^{238}U	0.000340 0.047740

Table 2 Nuclides and reactions in JENDL-3 whose secondary neutrons are described by the triangular distributions

NUCLIDE	REACTION TYPE
^{2}H	(n,2n)
^{9}Be	(n,2n), (n,2n′ α)
Ni	(n,2n), (n,3n), (n,n′ α), (n,n′ p)
^{58}Ni	(n,2n), (n,n′ α), (n,n′ p)
^{60}Ni	(n,2n), (n,n′ α), (n,n′ p)
^{61}Ni	(n,2n), (n,n′ α), (n,n′ p), (n,n′)
^{62}Ni	(n,2n), (n,n′ α), (n,n′ p), (n,n′)
^{64}Ni	(n,2n), (n,3n), (n,n′ α), (n,n′ p), (n,n′)
^{90}Zr	(n,2n), (n,n′ α), (n,n′ p), (n,n′)
^{91}Zr	(n,2n), (n,3n), (n,n′ α), (n,n′ p), (n,n′ d), (n,n′)
^{92}Zr	(n,2n), (n,3n), (n,n′ α), (n,n′ p), (n,n′ d), (n,n′ t), (n,n′)
^{94}Zr	(n,2n), (n,3n), (n,n′ α), (n,n′ p), (n,n′ d), (n,n′)
^{96}Zr	(n,2n), (n,3n), (n,n′ α), (n,n′ p), (n,n′)
Mo	(n,2n), (n,3n), (n,n′ α), (n,n′ p), (n,n′ d), (n,n′)
^{92}Mo	(n,2n), (n,n′ α), (n,n′ p), (n,n′)
^{94}Mo	(n,2n), (n,3n), (n,n′ α), (n,n′ p), (n,n′ d), (n,n′)
^{95}Mo	same as above
^{96}Mo	same as above
^{97}Mo	same as above
^{98}Mo	same as above
^{100}Mo	same as above
Cd	same as above
Sb	(n,2n), (n,3n), (n,n′ α), (n,n′ p), (n,n′ d), (n,n′ t), (n,n′)
^{121}Sb	same as above
^{123}Sb	same as above
^{232}Th	(n,2n), (n,3n), (n,n′)
^{233}U	(n,2n), (n,3n), (n,n′)
^{234}U	(n,2n), (n,3n), (n,n′)
^{235}U	(n,2n), (n,3n), (n,4n), (n,n′)
^{236}U	(n,2n), (n,3n), (n,n′)
^{239}Pu	(n,2n), (n,3n), (n,4n), (n,n′)
^{240}Pu	(n,2n), (n,3n), (n,n′)
^{242}Pu	(n,2n), (n,3n), (n,n′)

Table 3 K_{eff} (C/E) of one dimensional calculating results

ASSEMBLY	CORE	C／E of K_{eff}
JEZEBEL	^{239}Pu	1.0001
JEZEBEL－PU		0.9963
FLATTOP－PU		0.9974
THOR		0.9985
GODIVA	^{235}U	1.0066
BIG TEN		1.0038
FLATTOP－25		1.0033
JEZEBEL－23	^{233}U	1.0206
FLATTOP－23		1.0175

Table 4 Effect from fission spectra of JENDL-2 and JENDL-3

Using fission spectrum of JENDL−3		
	JEZEBEL−23	FLATTOP−23
C/E of K_{eff}	1.0206	1.0175
Average fission energy E_f	2.25 MeV	2.25 MeV
$\sigma_f(Na^7)/\sigma_f(U^5)$	1.0192	1.0300
$\sigma_f(U^8)/\sigma_f(U^5)$	1.0619	1.0696
Using fission spectrum of JENDL−2		
	JEZEBEL−23	FLATTOP−23
C/E of K_{eff}	1.0163	1.0076
Average fission energy E_f	2.01 MeV	2.01 MeV
$\sigma_f(Na^7)/\sigma_f(U^5)$	0.9700	0.9831
$\sigma_f(U^8)/\sigma_f(U^5)$	0.9357	0.9455

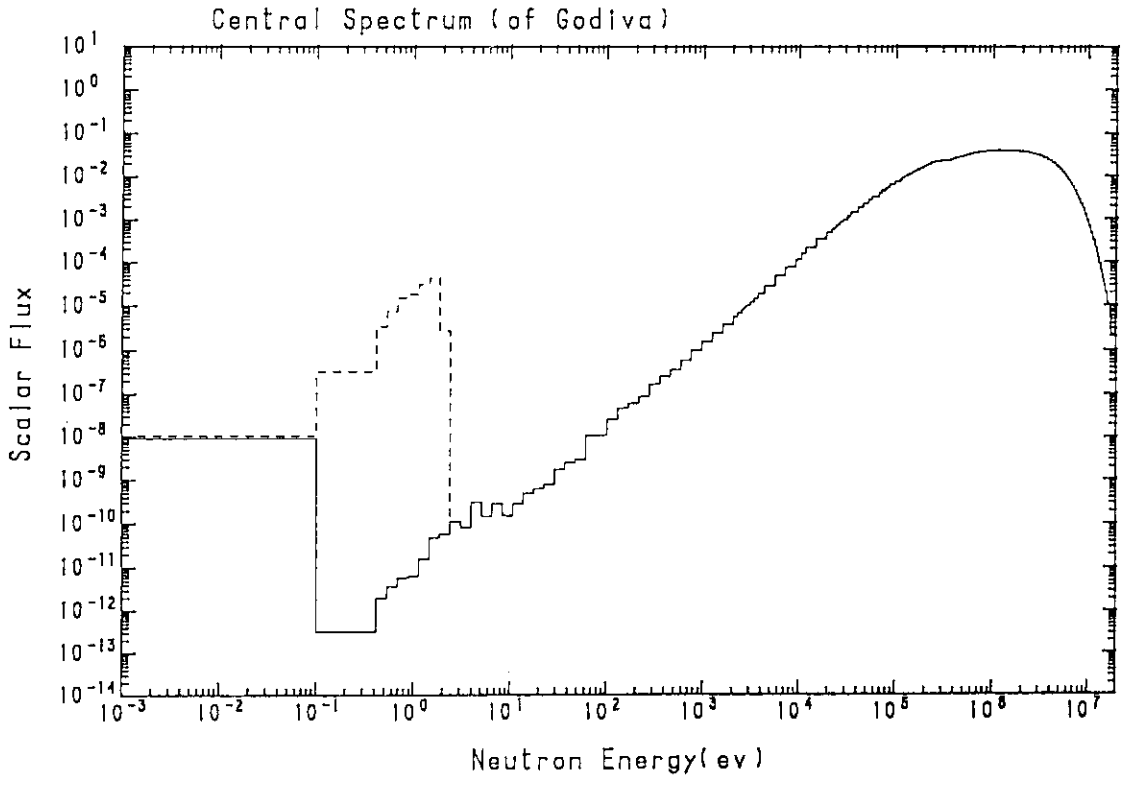

Fig. 1 Calculated neutron central spectrum of GODIVA

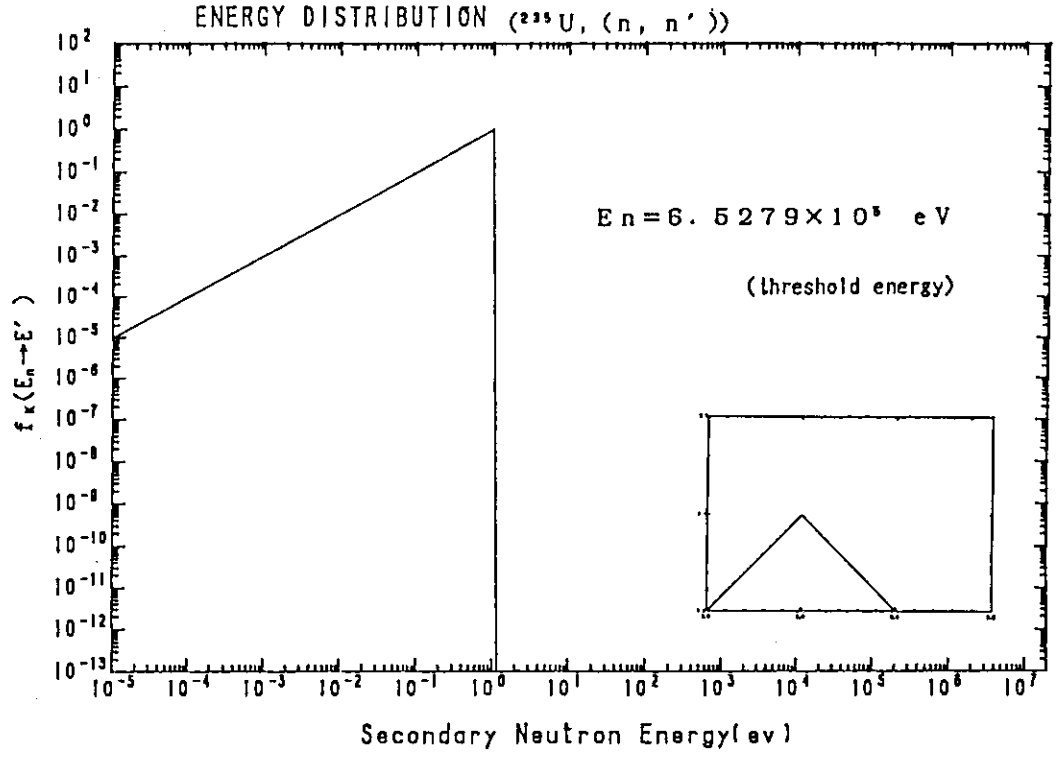

Fig. 2 The partial energy distribution at the threshold energy in File 5 of JENDL-3

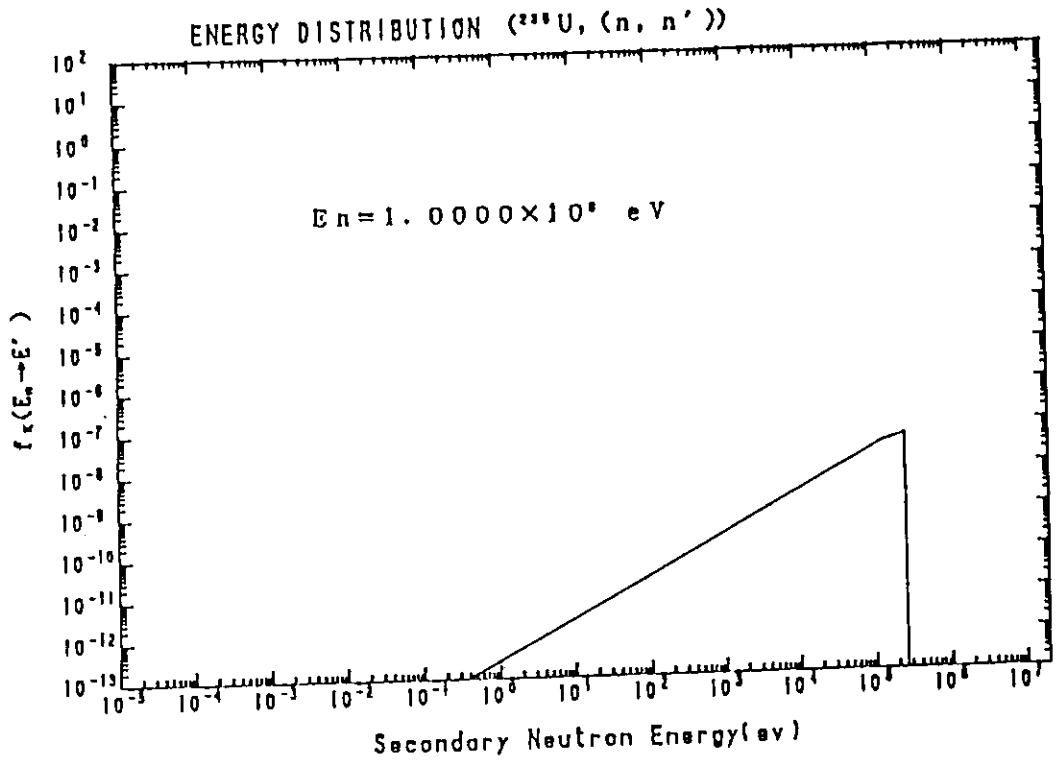

Fig. 3 The partial energy distribution at the second energy point in File 5 of JENDL-3

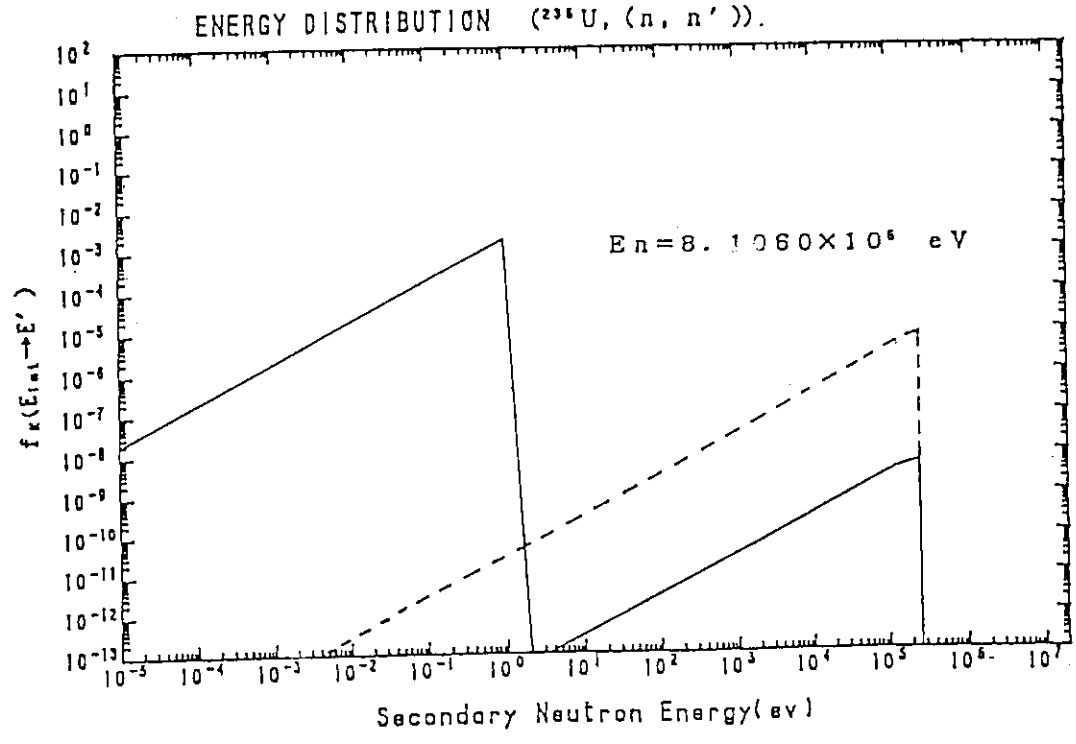

Fig. 4 The interpolated partial energy distributions at E_n = 0.8106 MeV

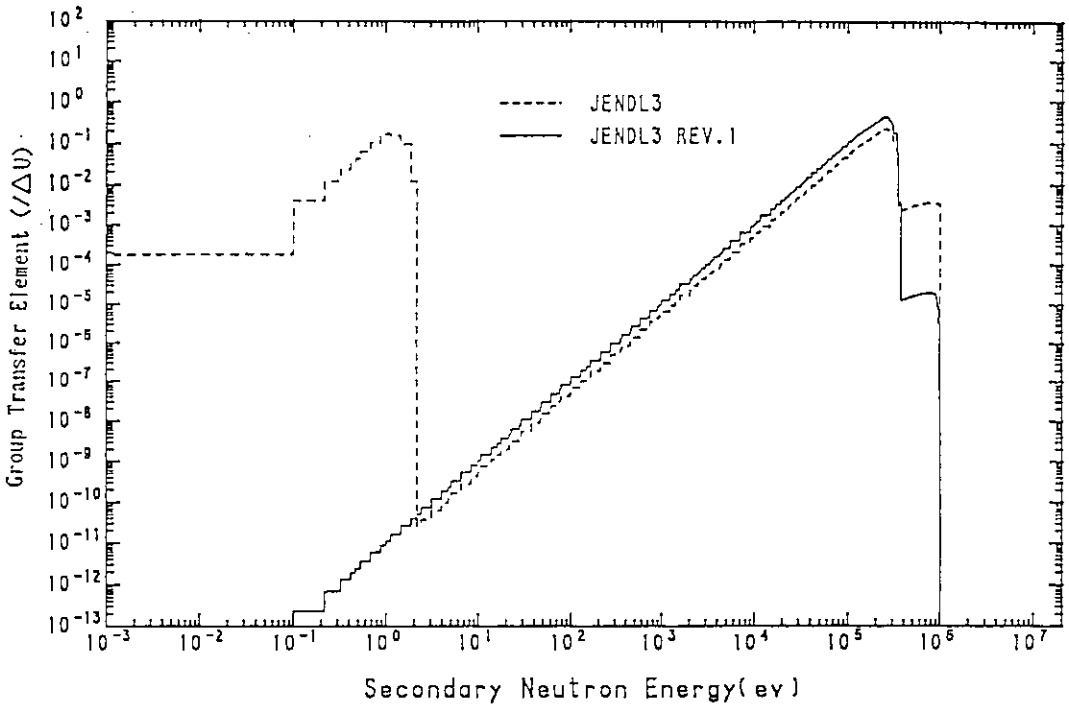

Fig. 5 The group transfer elements of 131st group, (n,n') of ^{235}U (JSSTDL-295 structure)

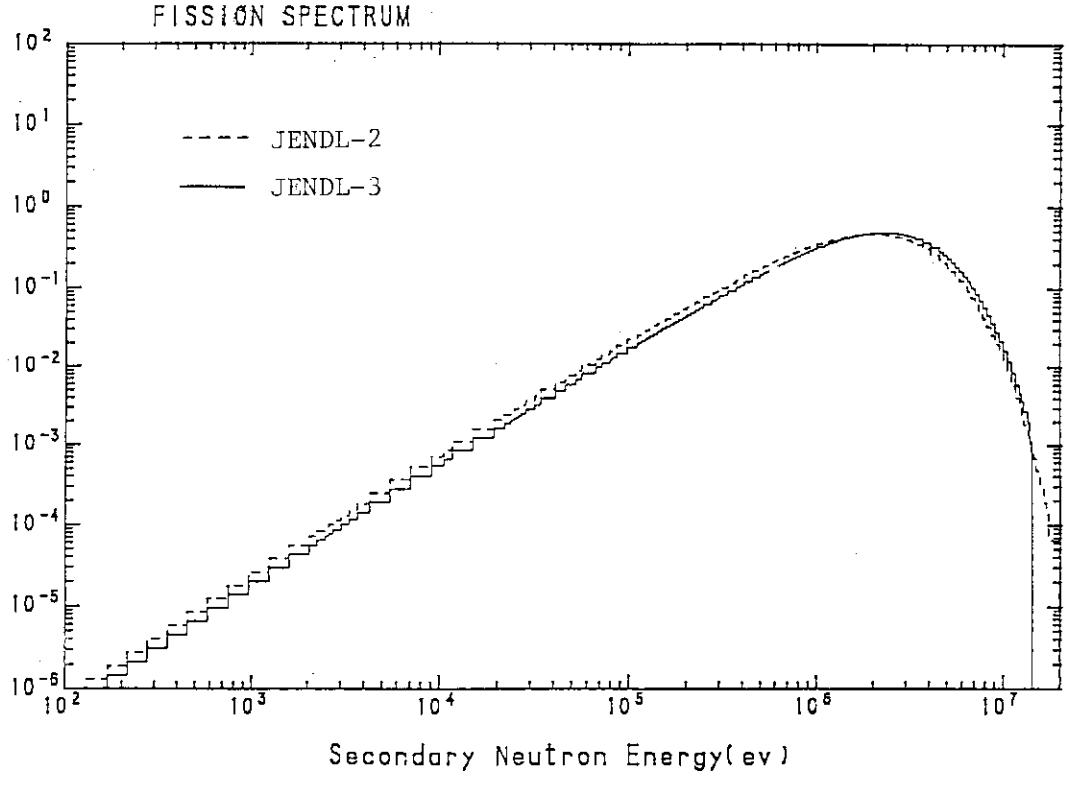

Fig. 6 Fission spectrum of JENDL-2 and JENDL-3

2.6.3 Analysis on FCA-HCLWR Core Using JENDL-3

Toshitaka OSUGI and Mutsumi NAGATANI

Japan Atomic Energy Research Institute
Tokai-mura, Naka-gun, Ibaraki-ken, 319-11 JAPAN

Benchmark calculation on the FCA-HCLWR core is carried out to examine the availability of JENDL-3 to the HCLWR core. Analysis is made by using the SRAC code system and the SRACLIB-JENDL2 or -JENDL3. The calculated items are the infinite multiplication factor, reaction rate ratio and sample reactivity worth. Calculated values with JENDL-2 and JENDL-3 are compared. Trend in C/E values are also discussed.

1. Introduction

A series of experiments were carried out at the Fast Critical Assembly (FCA) in Japan Atomic Energy Research Institute (JAERI) to investigate the reactor physics characteristics of the High Conversion Light Water Reactor (HCLWR) core. The experimental program consists of two phases : Phase-1 with enriched uranium core and Phase-2 with plutonium core (Ref.1). The FCA facility has high flexibility in the selection of fuel and moderator compositions, since the combination of plate-type solid materials can be varied easily. It is, therefore, suitable to examine the effects of the fuel materials, fuel enrichment or moderator voidage states on the reactor physics characteristics. In the FCA-HCLWR experiments, three uranium cores and five plutonium cores were constructed. Moderator voidage states were simulated in detail using foamy polystyrene plates of different densities (Ref.2).

Analysis on FCA-HCLWR core has been made to establish "DATA & METHOD" for the reactor physics calculation of the HCLWR or intermediate neutron energy reactor. Through this analysis with the Japanese Evaluated Nuclear Data Library, Version-2 (JENDL-2) (Ref.3), we found some discrepancies be-

tween the calculation and experiment. To explain these discrepancies and to examine the availability of the JENDL-3 (Ref.4), the FCA-HCLWR data have been re-analized (Ref.5).

In this paper, comparisons of the calculated results between JENDL-2 and JENDL-3 are made for the infinite multiplication factor, reaction rate ratio and sample reactivity worth. Analysis was made by using the SRAC code system (Ref.6) and SRACLIB-JENDL3 (Ref.7).

2. Comparisons of calculated results between JENDL-2 and JENDL-3

2.1 Neutron spectrum and diffusion constant

To grasp general features, the neutron spectrum and diffusion constant calculated by JENDL-2 and JENDL-3 are compared. The JENDL-3 adopts harder fission spectra for fissionable nuclides. To examine this effect on neutron spectrum, the difference in cell averaged neutron spectra of plutonium fueled cell is shown in Fig.1. Figure 2 shows relative difference in cell effectve diffusion constants calculated by JENDL-2 and JENDL-3.

2.2 Infinite multiplication factor

In order to examine the criticality of the HCLWR core, the infinite multiplication factor (K-inf) was measured with "buckling method" for the uranium cells (Ref.8) or with "reactivity-reaction rate method" for the plutonium cells (Ref.9). With JENDL-2 we observed about 1% discrepancies in Calculation/Experiment (C/E) values between uranium and plutonium cells.

Figure 3 shows difference in K-inf values calculated by JENDL-2 and JENDL-3 as a function of atomic number ratio of hydrogen to heavy metal (H/HM). For the uranium cells (EU05 and EU06A cells), the JENDL-3 gives larger K-inf values than the JENDL-2 does in the normal moderator voidage states (H/HM = 2.0 for EU05 cell and H/HM = 1.2 for EU06A cell), and smaller K-inf values in higher voidage states. The K-inf values calculated by JENDL-3 are larger than those by JENDL-2 for the plutonium cells (Pu08 cell). These differences increase with decreasing H/HM value (increasing

moderator void ratio of the cell or hardening neutron spectrum).

The discrepancies in C/E values between uranium and plutonium cells enlarge to about 2% in the case of JENDL-3. Nuclide-wise difference in K-inf values are shown in Fig.4 for the plutonium cells.

2.3 Reaction rate ratio

To evaluate the spectrum index or conversion ratio of the HCLWR core, the reaction rate ratios of F28/F25 (fission of uranium-238 to uranium-235) and C28/F25 (capture of uranium-238 to fission of uranium-235) were measured by using micro-fission chambers or activation foils (Refs.10 and 11). Calculations with JENDL-2 overpredict these ratios for both of the uranium and plutonium cells.

The JENDL-3 gives larger F28/F25 or C28/F25 values than the JENDL-2 does from 3.6% to 7.2% or from 0% to 1.4%, respectively, depending on the neutron spectrum as shown in Fig.5. Differences in C28/F49 (capture of uranium-238 to fission of plutonium-239) values calculated by JENDL-2 and JENDL-3 are also shown in Fig.5. To show the nuclide-wise contribution to these reaction rate ratios, the cell averaged one-group micro-constants are shown in Fig.6 for plutonium-239 and uranium-235, 238.

2.4 Sample reactivity worth

Most current-day HCLWR designs employ the boron carbide (B4C) , either of natural isotopic composition or enriched B-10 contents, as the control material. The reactivity worth of B4C in the HCLWR core is considered to be much different from that of the convensional LWR due to the difference in neutron spectrum. We measured the reactivity worths of the B4C sample with different B-10 contents and hafnium sample as one of the alternatives to B4C (Refs.12 and 13). The calculated worths of these absorber materials with JENDL-2 show underprediction to experimental ones. There is, however, no dependence on B-10 content in C/E values.

The JENDL-3 gives slightly larger sample worths of plutonium, which

are used as reference, than the JENDL-2 does. There are not much differences in calculated worth ratios of B4C/Pu between JENDL-2 and JENDL-3 as shown in Fig.7. The JENDL-3 gives larger worth ratios of Hf/Pu than the JENDL-2 does from 8% to 14% depending on the neutron spectrum. Underpredictions of Hf/Pu worth ratio by the JENDL-2 calculation are much improved in the case of JENDL-3. The test calculation, in which the Hf cross-section of JENDL-3 are replaced with that of JENDL-2, shows that this improvement is not due to the Hf cross-section itself but due to the hard neutron spectrum of JENDL-3.

3. Conclusion

Integral data of the FCA-HCLWR were re-analized using newly evaluated data library JENDL-3. The calculated results by JENDL-3 were compared with those by JENDL-2, and were summarized as follows :

(1) The discrepancies in C/E values of K-inf between uranium and plutonium cells enlarge from 1% to 2% by JENDL-3,
(2) Overpredictions by JENDL-2 for the reaction rate ratios of C28/U25 or F28/U25 were not improved by JENDL-3,
(3) Underpredictions of Hf/Pu worth ratio by JENDL-2 were much improved,
(4) The JENDL-3 gives almost same worth ratios of B4C/Pu as the JENDL-2 does.

References

1) OSUGI T., et al. : in Proc. of International Reactor Physics Conference, Jackson Hole, Wyoming, U.S.A., Sep. 19-22, 1988, Vol.II, II-361 (1988)
2) OSUGI T., et al. : in Proc. of International Conference on the Physics of Reactors : Operation, Design and Computation, Marseille, France, Apr. 23-27, 1990, Vol.3, PI-93 (1990)
3) NAKAGAWA T. (Ed.) : JAERI-M 84-103 (1984)
4) SHIBATA K., et al. : JAERI 1319 (1990)

5) OSUGI T., et al. : 1990 Annual Meeting of the Atomic Energy Society of Japan, B34 (1990)
6) TSUCHIHASHI K., et al. : JAERI 1302 (1986)
7) TAKANO H., et al. : Private communication (1990)
8) OSUGI T., et al. : J. Nucl. Sci. Technol., Vol.26(5), pp.477-491 (1989)
9) SAKURAI T. et al. : 1990 Annual Meeting of the Atomic Energy Society of Japan, B33 (1990)
10) OBU M., et al. : J. Nucl. Sci. Technol., Vol.26(11), pp.993-1001 (1989)
11) OBU M., et al. : 1989 Annual Meeting of the Atomic Energy Society of Japan, C29 (1989)
12) OKAJIMA S., et al. : J. Nucl. Sci. Technol., Vol.27(10), pp.950-959 (1990)
13) OKAJIMA S., et al. : JAERI-M 90-042 (1990)

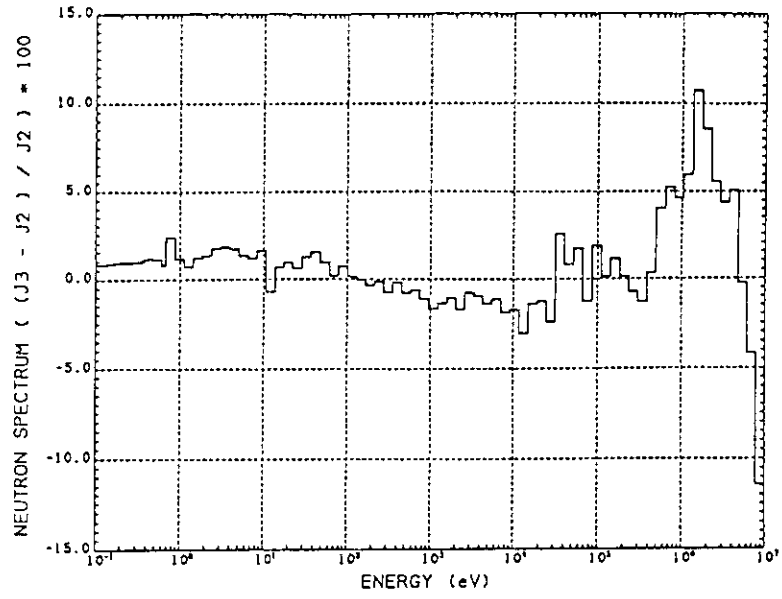

Fig. 1 Relative difference in cell averaged neutron spectra calculated by JENDL-2 and JENDL-3 in Pu08 cell

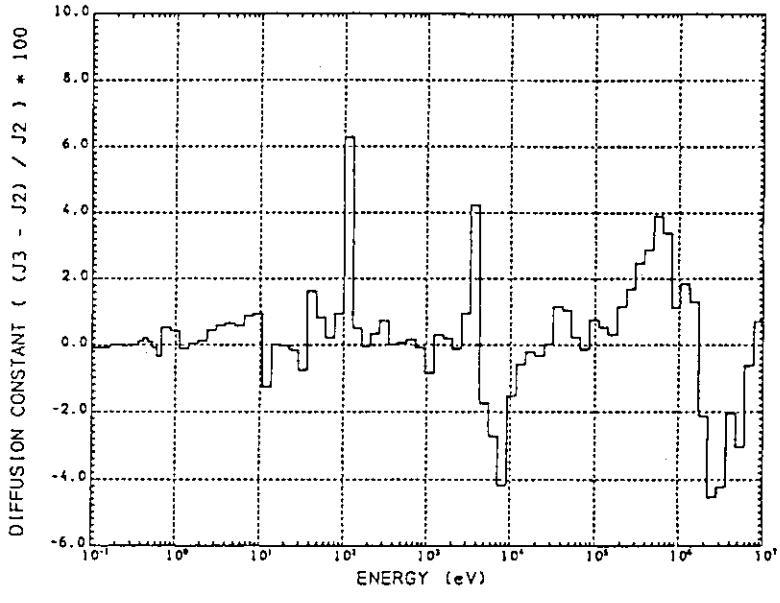

Fig. 2 Relative difference in cell averaged diffusion constants calculated by JENDL-2 and JENDL-3 in Pu08 cell

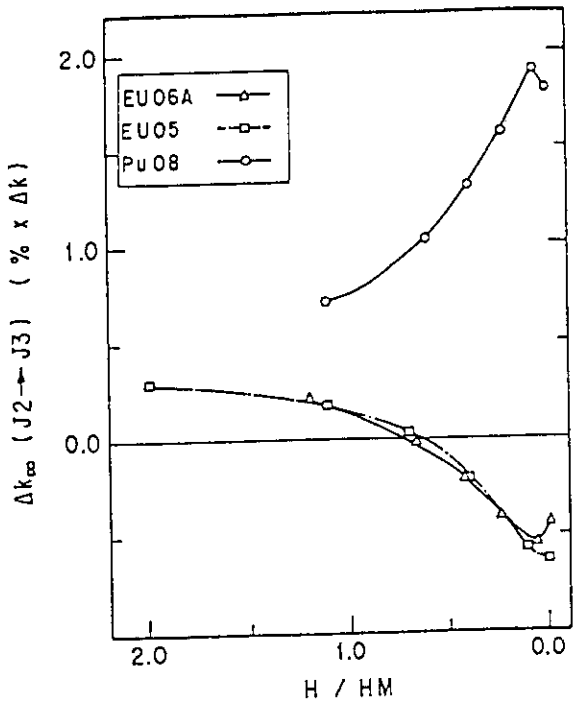

Fig. 3 Difference in infinite multiplication factors calculated by JENDL-2 and JENDL-3

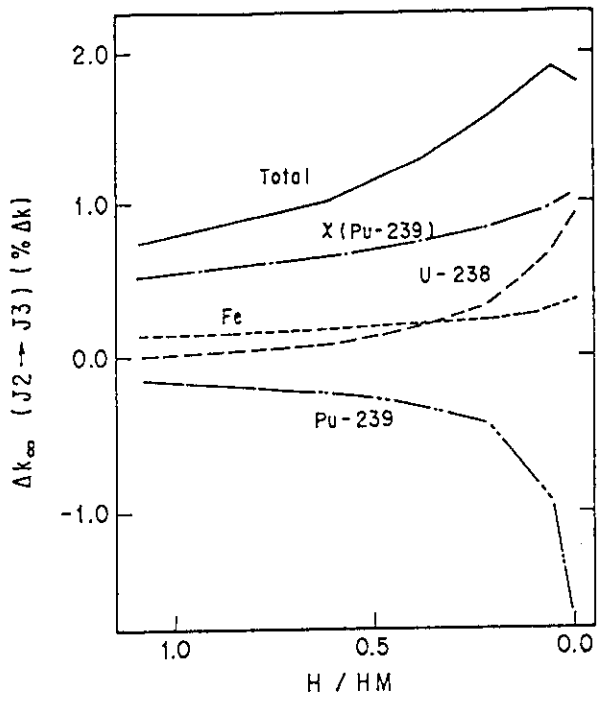

Fig. 4 Nuclide-wise difference in infinite multiplication factors calculated by JENDL-2 and JENDL-3 for the Pu08 cell

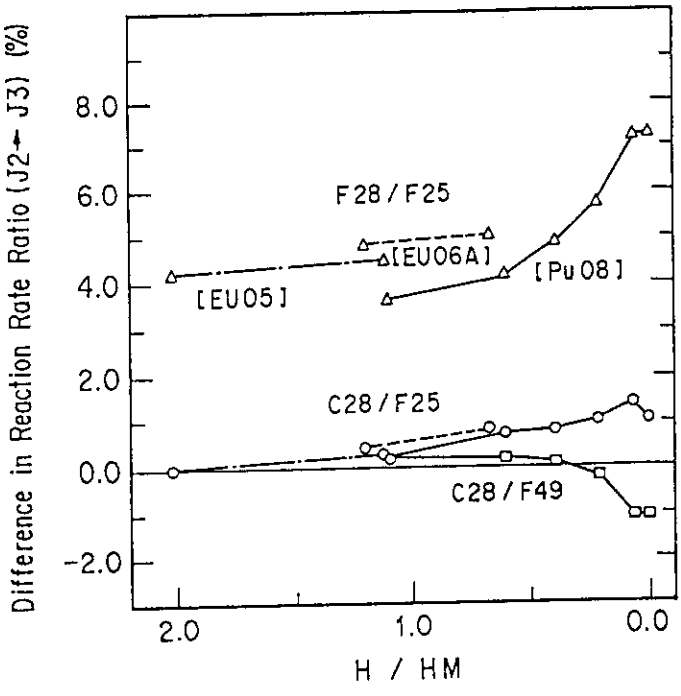

Fig. 5 Relative difference in reaction rate ratios calculated by JENDL-2 and JENDL-3

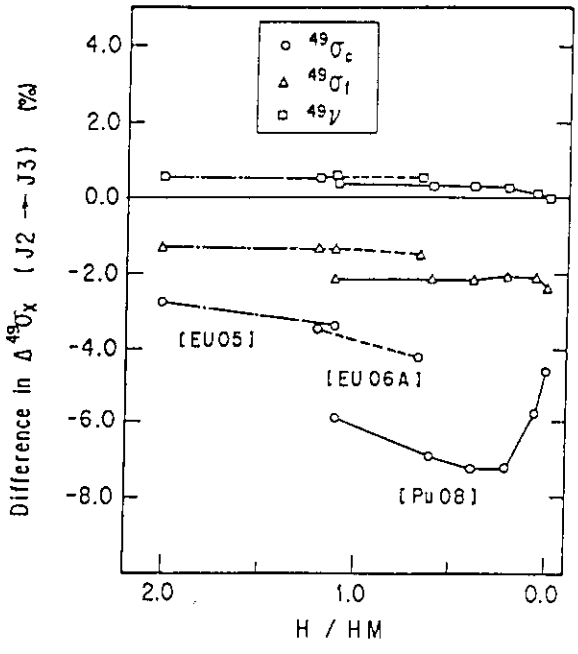

(a) Plutonium-239

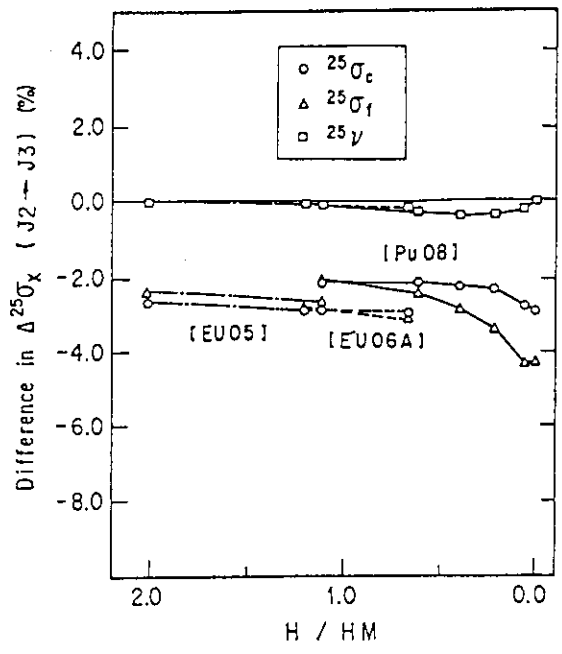

(b) Uranium-235

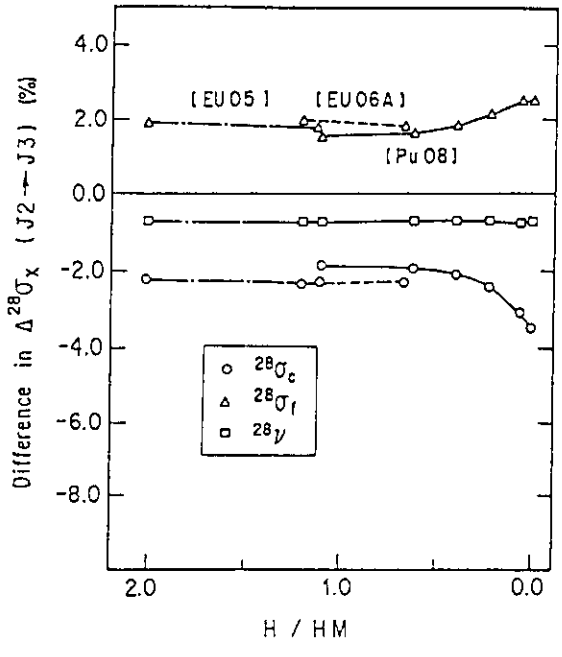

(c) Uranium-238

Fig. 6 Cell averaged one-group constants

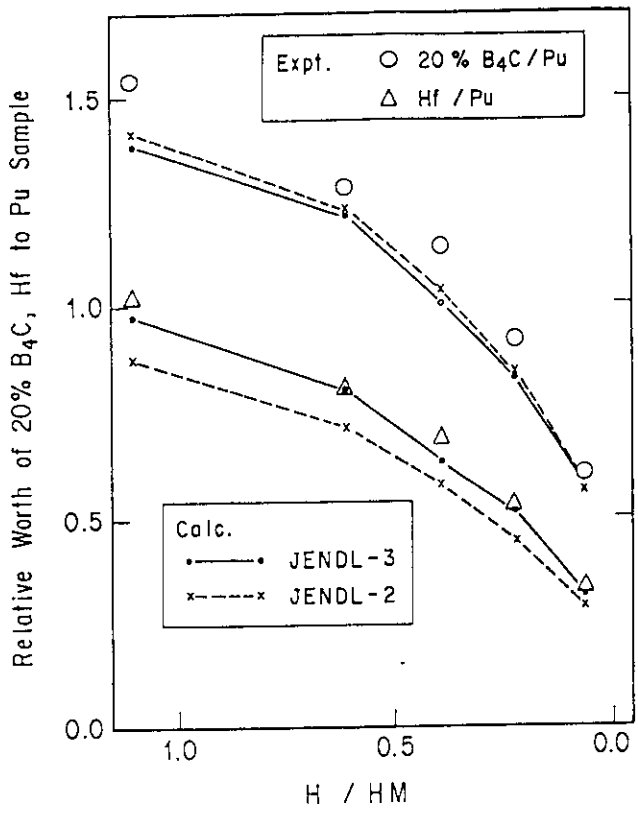

Fig. 7 Comparison between the experimental and calculated worth ratios of 20%B4C/Pu of Hf/Pu

2.6.4 Burnup Calculation for the PWR Spent Fuels by JENDL-3

H.Akie, H.Takano and K.Kaneko*

Reactor Engineering Department, JAERI,
Tokai-mura, Naka-gun, Ibaraki-ken, 319-11

Burnup calculations for PWR spent fuels were made by the SRAC-FPGS system with the different data libraries based on JENDL-2, -3 or ENDF/B-V. The estimated amounts of uranium and plutonium isotopes with these libraries agreed well with one another, and also with the experiment. By comparing the results obtained by JENDL-2 with those by JENDL-3, the large differences were found in the concentrations of U-232 and Np-237. To predict accurately the buildup of U-232, reliable evaluation for minor cross sections such as capture of Pu-236 is needed. The JENDL-3 library improved the prediction accuracy as compared with that by the JENDL-2 library. For the calculation of Np-237 amount, (n,2n) cross section of U-238 becomes important. The calculated amounts of Am-243 and Cm-244 with ENDF/B-V library differed from those with JENDL-2 or JENDL-3. In this case, Pu-242 capture cross section of ENDF/B-V is different from others.

1. Introduction

The view point of fuel cycle(fuel reprocessing, refabrication, waste management, etc.) is indispensable in the present atomic energy development. One of the important area for this purpose is the exact prediction of nuclide compositions in nuclear reactor fuels based on calculation, not only for the advanced reactors but also for the existing reactors. For the correct prediction, an accurate method for burnup calculation is required, and at the same time reliable nuclear data evaluation is an essential part, for minor actinides and fission products as well as for major nuclides like uranium and plutonium isotopes. Recently, destructive measurements for nuclide composition of PWR spent fuels were made by Nakahara et al.[1]. In the present study, the burnup calculations were performed by the SRAC-FPGS[2] system with the use of

---

* *The Japan Research Institute, Ltd.*

three different nuclear data of JENDL-2, JENDL-3 and ENDF/B-V.

2. Measurements of PWR Spent Fuels

Destructive analysis of nuclides was carried out for the PWR spent fuels of 11 different burnup histories. The burnup rates of the fuels were from 7 to 39 GWd/t. Here the burnup rates in GWd/t were converted from the number of fission per initial metallic atom in per cent(%FIMA), that were obtained from the measured data of Nd-148/U and Pu/U atom ratios. The measurements for the isotopes of uranium, neptunium, plutonium, americium, curium and 20 fission products were performed by mass spectrometry, α ray and γ ray spectrometry. All of the measured data were normalized to the values at 5 years after the irradiation.

3. Burnup Calculation

3.1 SRAC-FPGS System

In the present study, the burnup calculations were performed by the SRAC-FPGS system. The FPGS-3[3] is the code for nuclide depletion and generation calculation and is based on the DCHAIN code[4]. In the analysis by the FPGS-3, concentrations of about 160 nuclides are obtained by solving build up and decay of more than 1000 nuclides. In the SRAC-FPGS calculation, the SRAC code[5] calculates neutron spectrum and effective cross sections of the nuclides in a fuel lattice, and depletion calculation for a given burnup period is made by the FPGS-3 with the effective cross sections prepared by the SRAC. The FPGS code then gives nuclide concentration changes to the SRAC, for the calculation of spectrum and cross sections of the next burnup step.

3.2 Libraries

Three different SRAC libraries based on JENDL-2, JENDL-3 and ENDF/B-V were used for the comparison between nuclear data files. The library SRACLIB-JENDL2 was generated based on JENDL-2 but for several minor nuclides such as U-232 and Cs-134, that the data are not evaluated in JENDL-2 library. The SRACLIB-ENDFB5 is the library based on ENDF/B-V. However, the major nuclear data for U-238, Pu-239, Pu-240 and Pu-241 were not released, therefore, they were taken from JENDL-2. The third library was produced totally based on JENDL-3.

4. Results and Discussion

The amount of nuclides calculated by the SRAC-FPGS were compared with the measured results and also with the values calculated by the widely used burnup code ORIGEN-2[6]. In general, estimations by JENDL-2, JENDL-3 and ENDF/B-V agree well with one another and also with the experiment. Figure 1 shows that the calculation/experiment(C/E) values of U-235 amount obtained by the SRAC-FPGS are slightly overestimated as burnup rate increases. Amounts of U-238 and plutonium calculated with the SRAC-FPGS agree well with those measured(Figs.2 and 3), though the ORIGEN2 results are underestimated for the case of plutonium. Improved predictions of the SRAC-FPGS are also found in the C/E values of Sb-125 and Eu-154, that the ORIGEN2 overestimated remarkably as shown in Fig.4.

For some minor nuclides such as U-232, Np-237, Am-243 and Cm-244, prediction accuracies by the SRAC-FPGS are not so good as the cases of uranium and plutonium. Furthermore, large differences are found in the calculated amounts of these minor nuclides by the different data libraries.

4.1 U-232

Uranium-232 has γ active daughter nuclides such as Tl-208 and Bi-212. There can be difficulties in fuel reprocessing, when uranium fuels are recycled. The generation paths of U-232 are complicated as in Fig.5. To predict accurately the buildup of U-232, reliable data for minor cross sections such as (n,2n) of Np-237 and capture of Pu-236 are needed. Table 1 summarizes the one group cross sections for the fuel of burnup rate of 8 GWd/t. It is observed that the ENDF/B-V data for Np-237 (n,2n) reaction is smaller than the others. The large discrepancy is also observed in the capture cross section of Pu-236 between JENDL-2 and the other libraries. The SRAC group cross sections of Pu-236 capture(Fig.6) show the different data evaluation of JENDL-2 from JENDL-3 or ENDF/B-V. Figure 7 shows the C/E values of the fraction of U-232 to the quantity of initial uranium. It can be seen that JENDL-3 gives a little underestimation, while JENDL-2 and ENDF/B-V show considerable underprediction. The large capture cross section of JENDL-2 for Pu-236 leaded to the difference between the U-232 amounts estimated by JENDL-2 and JENDL-3, while the difference between JENDL-3 and ENDF/B-V is caused by the (n,2n) cross section of Np-237.

4.2 Np-237

Neptunium-237 is one of the most important transuranium(TRU) waste nuclides because of its generation rate in the LWR fuel, long half life and large hazard. In Fig.8, the C/E values of Np-237 obtained by JENDL-2 give little overestimation, and those by JENDL-3 show slight underestimation. As can be observed in Fig.5, large part of Np-237 is generated by the (n,2n) reaction of U-238 in the LWR fuel. The U-238 (n,2n) cross section of JENDL-2 is larger than that of JENDL-3 as shown in Table 1. In Fig.8, the prediction accuracy of Np-237 itself is not so bad as the case of U-232, but the amount of Np-237 largely contribute to the accuracy of the calculation of U-232, Pu-238, etc.

4.3 Am-243 and Cm-244

These are also important TRU waste nuclides. Figures 9 and 10 show the C/E values of the amounts of Am-243 and Cm-244. Underestimations are seen for all the data libraries. The difference between ENDF/B-V and JENDL is caused by the difference in Pu-242 capture cross section(Table 1). The difference in cross sections at the large resonance at 2.7eV is the cause(Fig.11). For the accurate predictions of these nuclides, both exact treatment of nuclide generation chain, including the branching reactions(Fig.5), and the reliable capture cross section data for plutonium, americium and curium are required.

5. Summary

The calculated results of burnup analysis for PWR spent fuels show that the differences among JENDL-3, JENDL-2 and ENDF/B-V are small, except for U-232, Np-237(Pu-238), Am-243 and Cm-244. For the better estimation of U-232 and Np-237, the data for reactions of Np-237 (n,2n) Pu-236 capture and U-238 (n,2n) are important. The difference of Pu-242 capture cross section between ENDF/B-V and JENDL leaded to the differences in the estimations of Am and Cm.

Generally, prediction of compositions for PWR spent fuels by SRAC-FPGS system is satisfactory in comparison with that of ORIGEN2, especially for Pu and some FPs.

References

(1) NAKAHARA, Y., et al.: *Radiochimica Acta*, 50, 141 (1990).
(2) TAKANO, H., et al.: Private communication, (1988).

(3) IHARA, H., et al.: Private communication, (1988).
(4) TASAKA, K.: *JAERI* 1250, JAERI (1977).
(5) TSUCHIHASHI, K., et al.: *JAERI* 1302, JAERI (1986).
(6) CROFF, A.G.: *ORNL*-5621, ORNL (1980).

Table 1 One group cross sections (barns) for the fuel of 8 GWd/t burnup

Libraries	Pu-236 (n, γ)	Np-237 (n,2n)	Np-237 (n, γ)	U-238 (n,2n)	Pu-242 (n, γ)	Am-243 (n, γ)	Cm-244 (n, γ)
JENDL-2	373.6	8.53E-4	35.4	4.49E-3	28.9	51.8	12.4
JENDL-3.	18.5	6.80E-4	36.4	3.00E-3	28.8	51.2	13.6
ENDF/B-V	18.8	3.44E-4	32.6	—	32.4	51.1	12.1
ORIGEN2-82	20.4	1.06E-3	32.9	5.53E-3	31.8	50.2	13.7

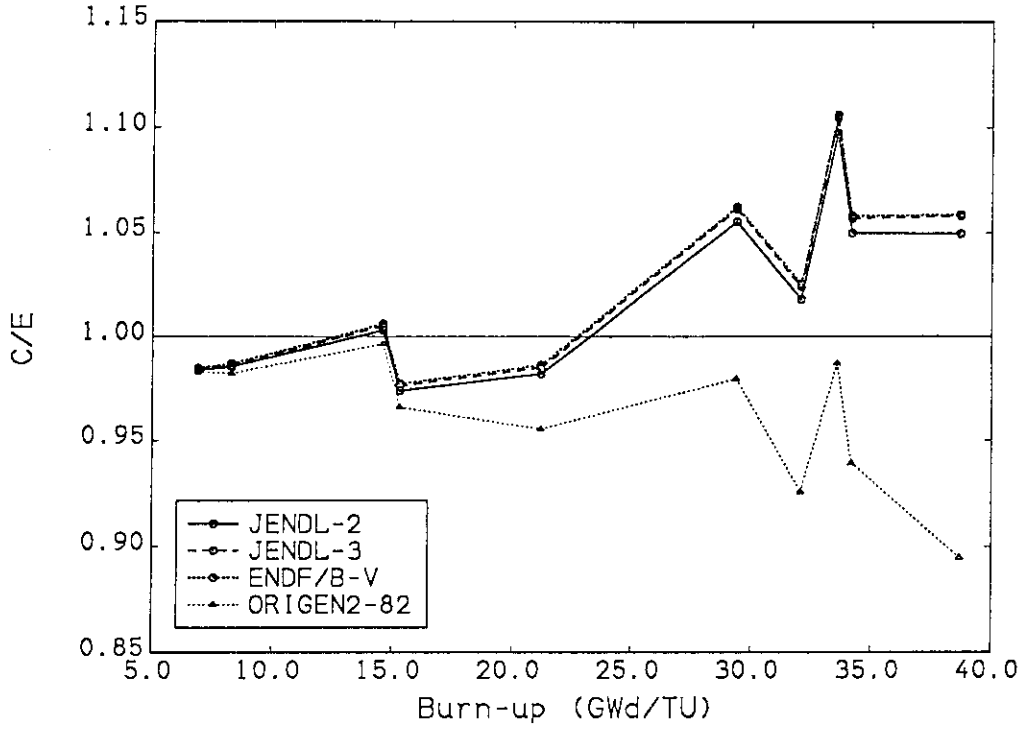

Fig. 1 C/E values of U-235 concentrations obtained by SRAC-FPGS

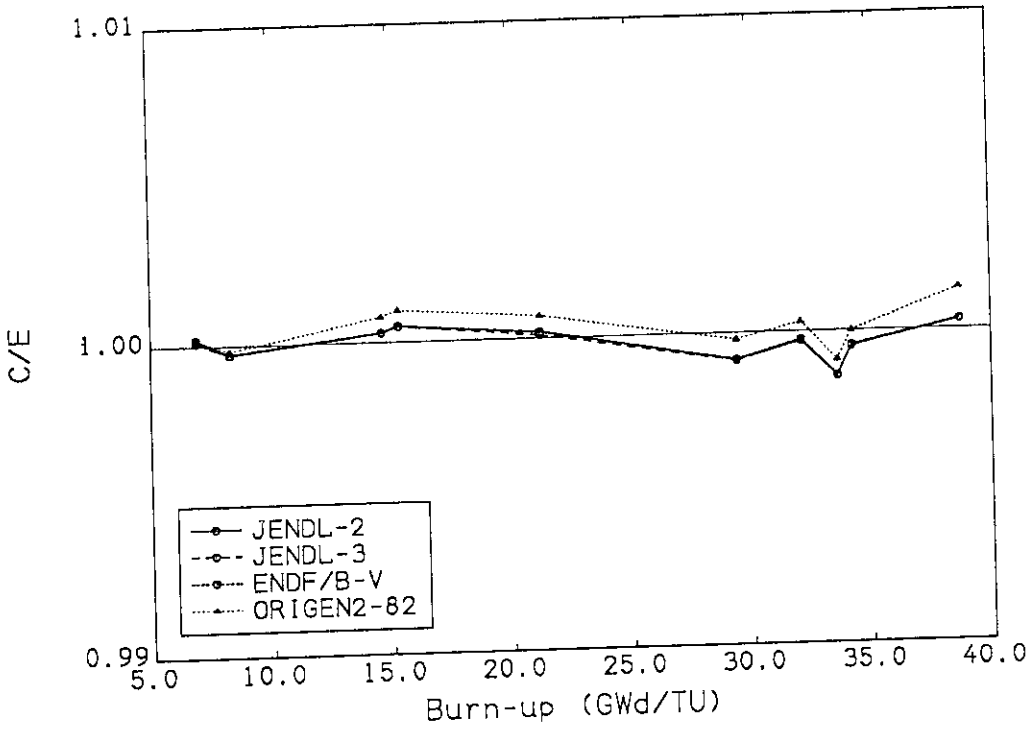

Fig. 2 C/E values of U-238 concentrations obtained by SRAC-FPGS

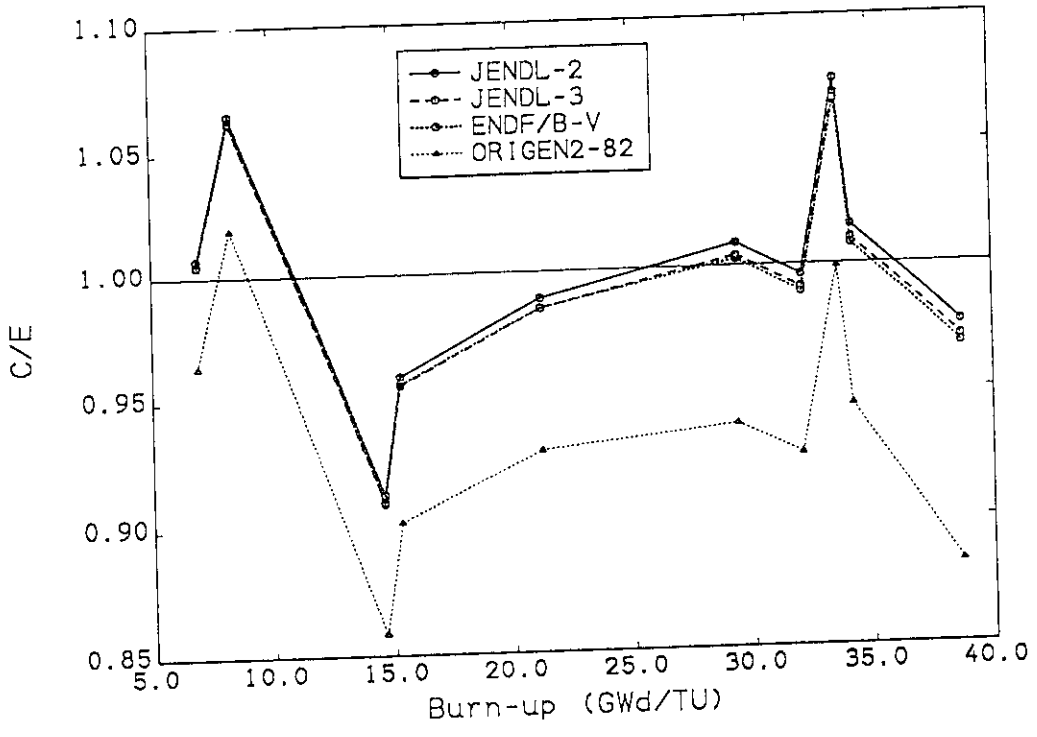

Fig. 3 C/E values of Pu concentrations obtained by SRAC-FPGS

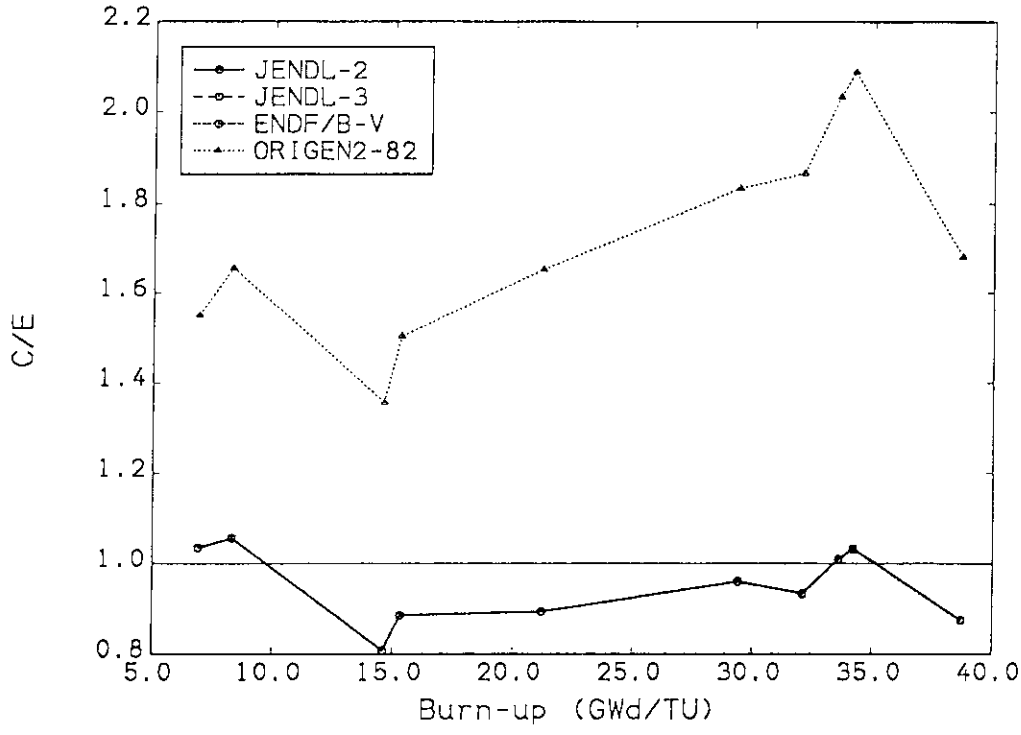

Fig. 4 Quantities of Eu-154 in PWR fuels obtained by SRAC-FPGS(C/E)

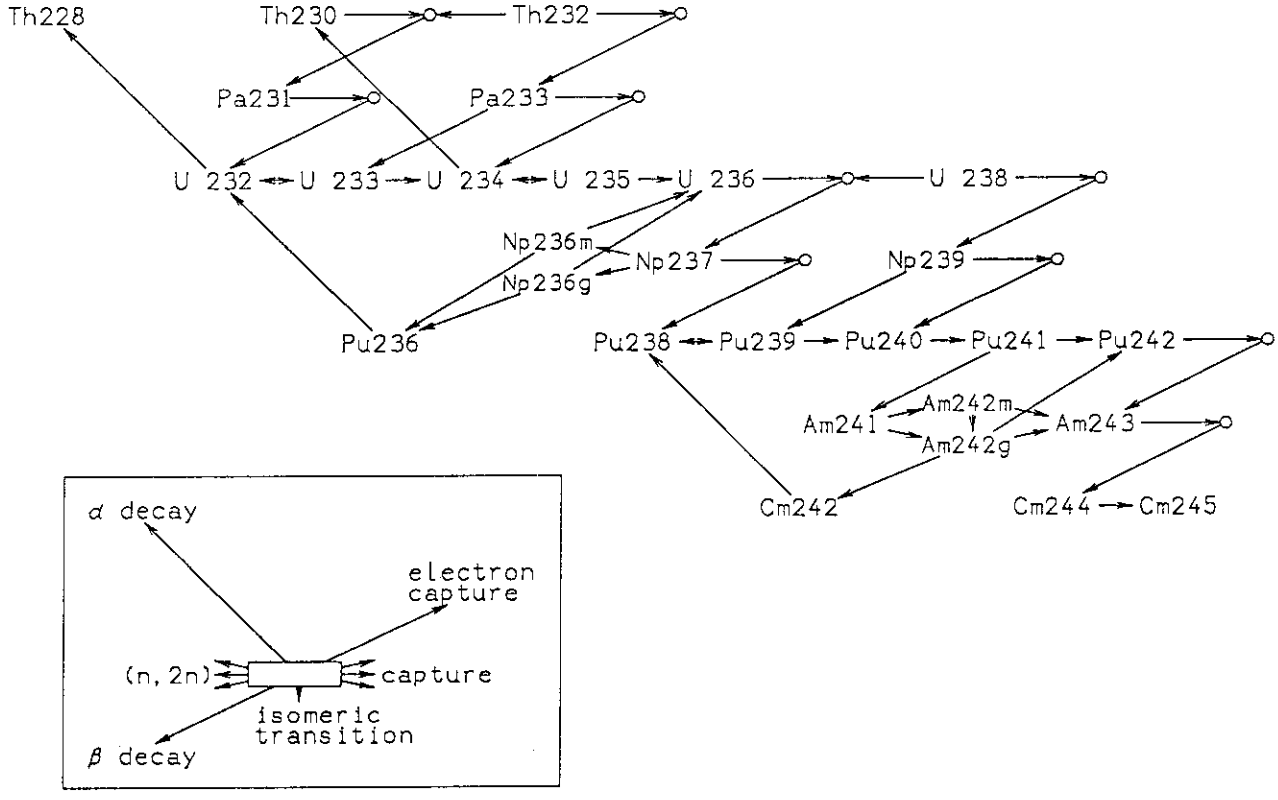

Fig. 5 Production chains of actinide nuclides

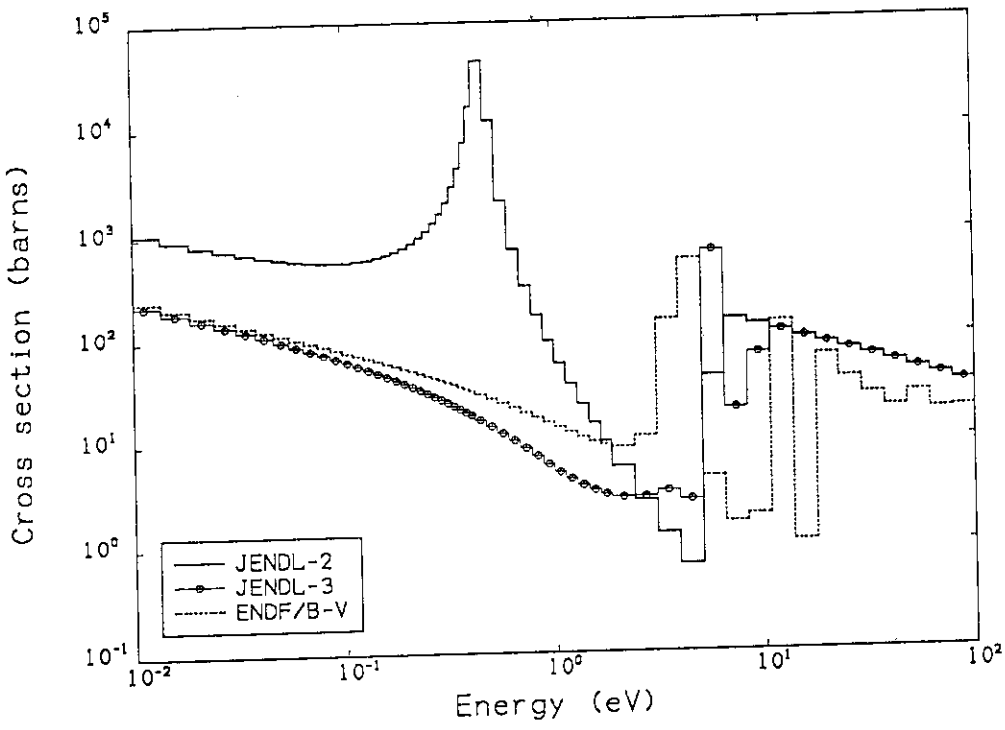

Fig. 6 Capture group cross sections of Pu-236 in the SRAC system

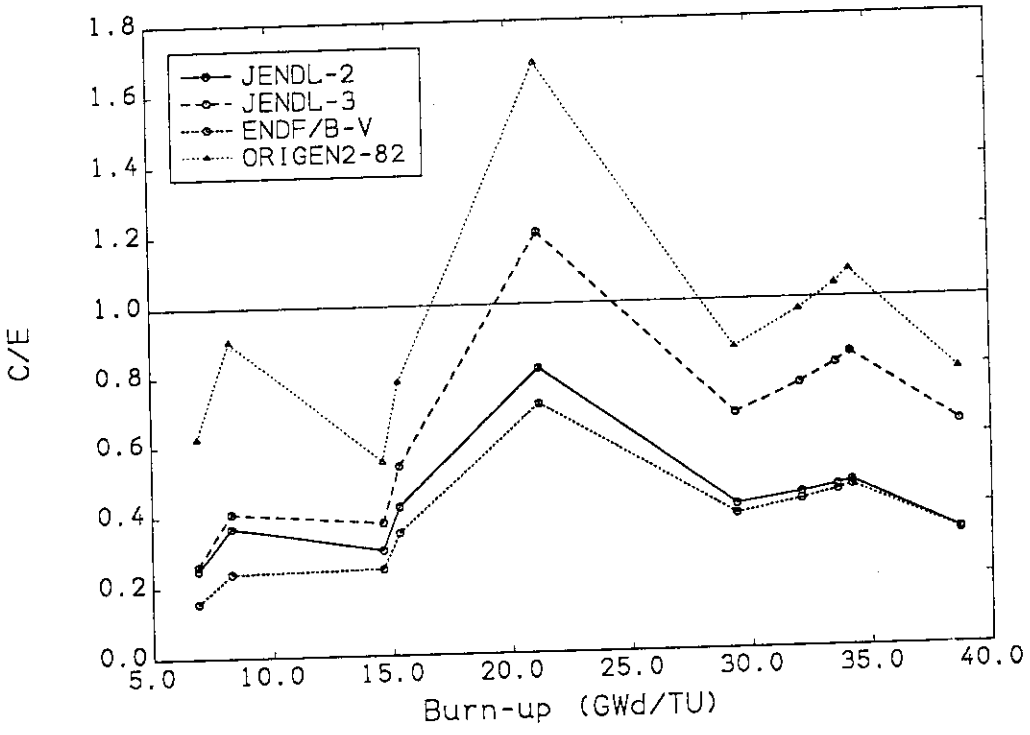

Fig. 7 Fractions of U-232 to initial U calculated by SRAC-FPGS(C/E)

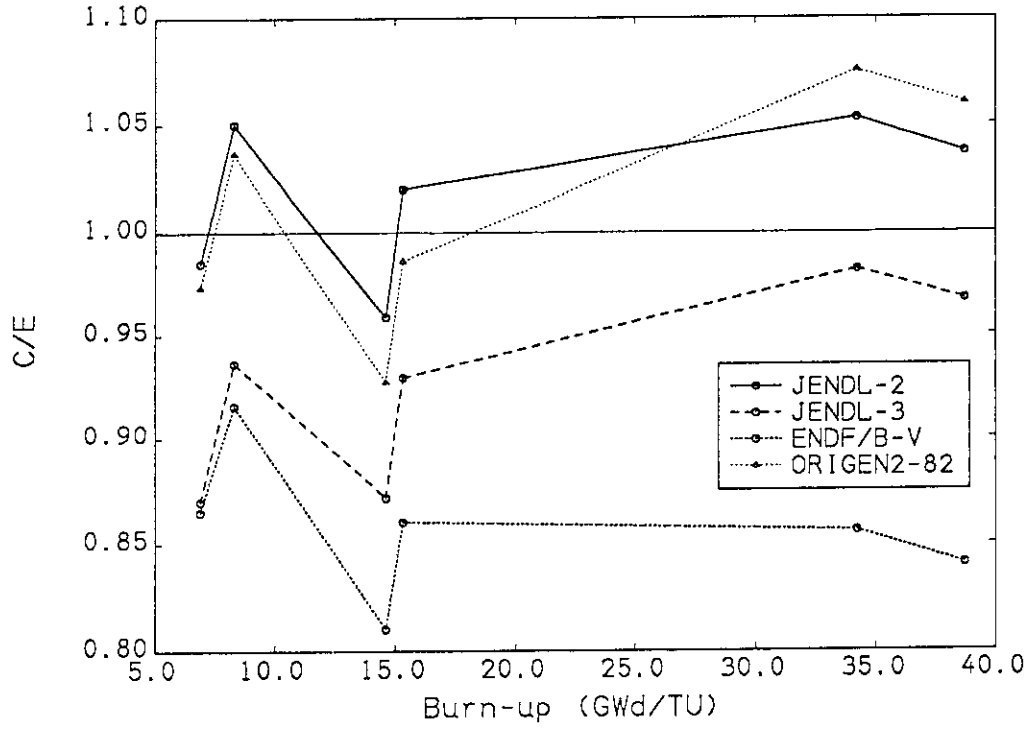

Fig. 8 Fractions of Np-237 to initial U calculated by SRAC-FPGS(C/E)

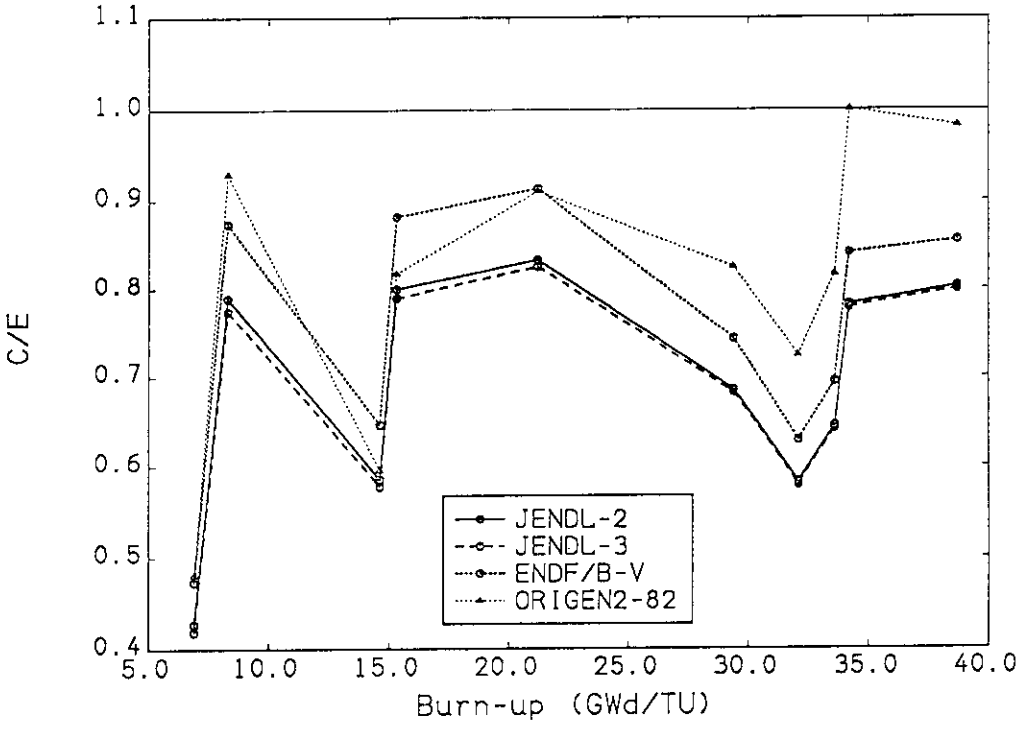

Fig. 9 C/E values of the amounts of Am-243 calculated by SRAC-FPGS

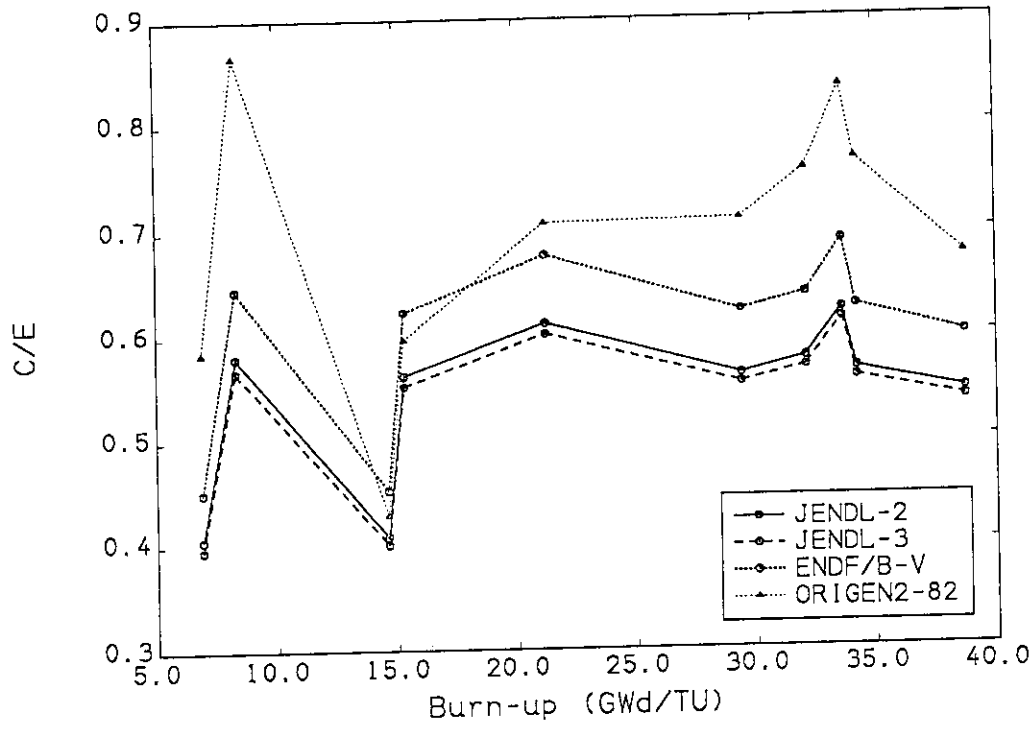

Fig. 10 C/E values of the amounts of Cm-244 calculated by SRAC-FPGS

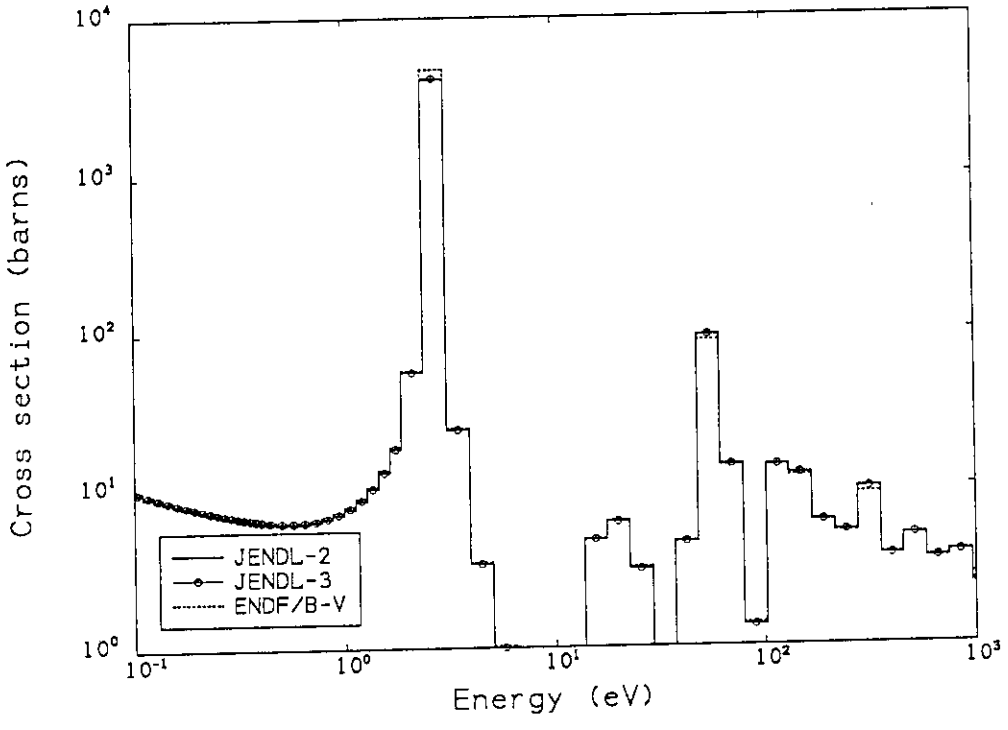

Fig. 11 Capture cross sections of Pu-242 (SRAC libraries)

2.7 Topics-4

2.7.1 Nuclear Data Relevant to Diagnostics Design in Fusion Experimental Reactor

Tetsuo Iguchi

Department of Nuclear Engineering, University of Tokyo,
7-3-1 Hongo, Bunkyo-ku, Tokyo, JAPAN

Nuclear data needs and application area relevant to burning plasma study are reviewed, mainly based on the results of ITER diagnostics conceptual design works. In particular, some topics are given on fusion reaction cross sections, activation cross sections for plasma diagnostics, cross section data related to radiation damage of diagnostic instruments and neutron transport calculation for diagnostics designs.

1. Introduction

The ITER conceptual design activity has been just completed in November 1990, and given us a clear image on the 'Fusion Experimental Reactor'. This makes it possible to consider a more concrete design of diagnostic systems for nuclear burning plasma closely matched with the reactor specification. In addition, starting with a large scale deuterium plasma experiment at JT-60U of JAERI in 1991, nuclear burning plasma study in Japan will be greatly encouraged.

So far, there were several good reviews on nuclear data requirements mainly for fusion power reactor designs, but this review are concentrated on the nuclear data needs and application area relevant to the burning plasma diagnostics, which have been made clear through ITER diagnostics conceptual design works.

2. Outline of ITER diagnostics conceptual design

To fulfill the ITER mission of providing a physics and technology data base for a demonstration fusion reactor, the proposed diagnostics

are categorized into three; i)for safety, plasma control and plasma performance in the high radiation technology phase, ii)for plasma optimization and physics understanding during the preceding physics phase, and iii) further planned diagnostics such as on-line monitoring of blanket nuclear performance. As an example, the candidated set of diagnostics required for i) is shown in Table 1 with the plasma parameters to be measured. Through three times of the specialists meeting on ITER diagnostics attended by the total number of about 60 participants from Japan, EC, USA and USSR, the design specification of each diagnostic systems were defined, including machine-interface requirements and port-space sharing between diagnostics. Fig.1 shows the result of machine integration on the present diagnostic systems with a bird's-eye view of ITER. The principal tasks on the ITER diagnostics R&D program were also considered as listed in Table 2. [1] From these items, there are found many kinds of nuclear data need and application area relevant to the burning plasma diagnostics. Here are presented some topics briefly on fusion reaction cross sections, activation cross sections for plasma diagnostics, cross section data related to radiation damage of diagnostic instruments and neutron transport calculation for diagnostics designs.

3. Fusion reaction cross section data

Fusion reaction cross section data on light ions are essentially important in application to the burning plasma diagnostics. At present, the reactions of interest are as follows;

(1) $d + d \rightarrow n(2.449MeV) + {}^3He(0.820MeV)$ [50%]
$\rightarrow p(3.022MeV) + t(1.011MeV)$ [50%]
$\rightarrow {}^4He + \gamma(23.8MeV)$ [10^{-5}%]

(2) $d + t \rightarrow n(14.032MeV) + {}^4He(3.558MeV)$ [100%]
$\rightarrow {}^5He + \gamma(16.6MeV)$ [7×10^{-3}%]

(3) $d + {}^3He \rightarrow p(14.640MeV) + {}^4He(3.713MeV)$ [100%]
$\rightarrow {}^5Li + \gamma(16.5MeV)$ [3×10^{-3}%]

(4) $t + t \rightarrow {}^4He + 2n + 11.332MeV$

(5) $p + d \rightarrow {}^3He + \gamma(5.5MeV)$ [100%]

In these reactions, neutron diagnostics are extensively used to obtain the informations on fusion power, plasma ion temperature/density etc. through the measurement of total neutron yield, neutron emission

profile and neutron energy spectrum. To realize this, it is clear that the fusion reaction cross section must be accurately known over the whole particle energy range, which will be from 0.2keV to several MeV, corresponding to all kinds of plasma operating phases. The present accuracy on the important fusion cross section such as $d(t,n)^4He$ and $d(d,n)^3He$ reactions is said to be better than 5% in the energy range between 20keV and 120keV.[2] However, in the lower and/or the higher energy region, the accuracy of the fusion cross section data seems to be still uncertain. From the viewpoint of plasma diagnostics, it will be necessary to reevaluate the existing fusion cross section data and improve their accuracy into $\pm 3\%$.

The escaping charged fusion product diagnostic is also useful to study the mechanism of high energy particle confinement and loss in the burning plasma although this measurement will be very difficult under the high radiation environment. For the d-^3He reaction, which is sometimes used as minority ion in ICRF heating, the 14.7MeV fusion product proton flux escaping from the plasma can be measured. However, it is reported that the cross section data of $^3He(d,p)^4He$ reaction has a large uncertainty around $\pm 50\%$ at low energies.[3]

Very energetic γ-rays produced in fusion reactions are recently being used for many kinds of plasma diagnostic purposes such as assessments of fusion reactivities in D/H/^{3}He plasmas, concentration of some impurities in the plasma, non-fusion neutron production, etc. The relevant reactions for this γ-ray diagnostic are;
$D(p,\gamma)^3He$ $E\gamma$ = 5.5MeV, $T(p,\gamma)^4He$ $E\gamma$ =19.7MeV, $D(d,\gamma)^4He$ $E\gamma$ =23.8MeV, $D(t,\gamma)^5He$ $E\gamma$ =16.6MeV, $D(^3He,\gamma)^5Li$ $E\gamma$ =16.4MeV in fusion reactions, $^{12}C(^3He, p\gamma)^{14}N$ $E\gamma$ = 5.1MeV, $^{12}C(d, p\gamma)^{13}C$ $E\gamma$ = 3.1MeV, 3.8MeV, $^{12}C(p, p'\gamma)^{12}C$ $E\gamma$ = 4.4MeV, $^{16}O(p, p'\gamma)^{16}O$, $E\gamma$ = 6.1MeV, 7.0MeV, $^9Be(p, \alpha\gamma)^6Li$ $E\gamma$ = 3.5MeV in nuclear reactions with impurity ions and $^7Li(p, \gamma)^8Be$, $^{11}B(p,\gamma)^{12}C$, $^{13}C(p,\gamma)^{14}N$, $^{15}N(p,\gamma)^{16}O$, $d(\alpha,\gamma)^6Li$, $^6Li(\alpha,\gamma)^{10}B$, $^7Li(\alpha,\gamma)^{11}B$, $^9Be(\alpha,n_1\gamma)^{12}C$ in resonant capture reactions induced by the pellet or beam injection. These reactions will be necessary to evaluate the cross section data and its γ-ray branching ratio.[4]

Another topic is concerned with the use of spin-polarized d-t and d-^{3}He fuels, which may increase the fusion reactivity by 50% and deviate the angular distributions of the reaction products. Some systematic experiment is needed to check these theoretical predictions.[5]

4. Some activation cross section data for plasma diagnostics

There are some candidates of activation reactions to measure neutron, γ-ray and α-particle for plasma diagnostics. As a new neutron yield monitor, the fluid activation system has been proposed in ITER, based on $^{16}O(n,p)^{16}N$, $^{17}O(n,p)^{17}N$ and $^{9}Be(n,\alpha)^{6}He$ reactions. Photonuclear reactions with threshold energy such as $^{12}C(\gamma,\alpha n)^{7}Be$, $^{58}Ni(\gamma,2n)^{56}Ni$, etc. can be used to assess the energy and intensity of runaway electrons caused by disruption.(Table 3.) The use of the alpha activation reactions such as $^{10}B(\alpha,n)^{13}N$, $^{14}N(\alpha,\gamma)^{18}F$, etc. will be the most promissing and practical method to obtain the energy information of the escaping α particle from the burning plasma.(Table 4) These can be regarded as new fusion dosimetry technique in a wide sense. It is hoped to establish an evaluated library for these activation cross section data.[6],[7]

5. Cross section data for radiation damage of diagnostic instruments

One of the most important R&D issues in ITER diagnostics is to assess the radiation effects on the diagnostic components inside or close to the first wall of the tokamak, such as vaccuum windows, reflectors, ceramics for electrical isolation, fiber optics, cabling and vacuum feedthroughs, plasma facing sensors, etc. In particular, the databases on the performance of diagnostic components in radiation fields must be established to provide a basis for diagnostic selection, design and integration on the tokamak device. It will be the first consideration to develop the database format, which should be optimized to support enginnering needs, accessibility and update of the data. For example, the concept of the DPA cross sections and KERMA factors may be useful to express the permanent radiation effect and the transient radiation induced noise on the diagnostic components, respectively.

6. Neutron transport calculation for diagnostics designs

The development of good neutron and gamma transport codes is also ranked as one of the most important R&D issues for the ITER diagnostic design. A mixture of 1-D, 2-D and 3-D modelling codes, qualified by actual measurement, will be necessary, supported by good cross section

libraries. At present, four basic types of neutronic information are required; 1) Accurate assessment of the collimation developed for the neutron diagnostics, including backscattering from the central mass of material, 2) Calculations of neutron and gamma spectra at the location of micro-fission chambers and nuclear activation samples, 3) Shielding capability required for a non-fusion product detector configuration, including the impact of any direct streaming, 4) Nuclear heating or noise induced in the detection system. These calculational modellings are needed to be sufficiently detailed because the accuracy of the calculational results will be directly reflected to the assesment of plasma performance. It is not too much to say that 'Fusion Neutronics' is the key to success in the burning plasma diagnostics.

7. Summary

Through the conceptual design works in ITER diagnostics, nuclear data needs and application area relevant to burning plasma study have been briefly reviewed. In this research field, the usefulness of nuclear data and neutronics will be directly reflected to the plasma physics and engineering. With the progress of the engineering design activities of ITER and the d-d plasma experiment at JT-60U, some special purpose nuclear data library for burning plasma diagnostics is expected to be compiled and established.

References

(1) V. Mukhovatov et al., 'ITER DIAGNOSTICS' IAEA ITER Documentation series No.33 (1990).
(2) N. Jarmie et al., Nucl. Instrum. Meth. in Phys. Res., B10/11, 405(1985).
(3) W.W. Heidbrink et al., Nucl. Fus. 23, 917(1983)
(4) G. Sadler et al, Proc. 14th Europ. Conf. on Contl. Fus. Plasma Heat. 11D/3, 1232(1987).
(5) B.J. Micklich et al., Nucl. Technol./Fusion 5, 162(1984).
(6) O.N. Jarvis et al. JET-P(87)50 (1987).
(7) F.E. Cecil et al., Rev. Sci. Instrum. 57(8), 1777(1986).

Table 1 Candidate set of diagnostics required for safety, control and performance

Plasma parameter	Candidate diagnostics	Comments
1) Plasma current	Magnetics	Need to develop methods of measuring steady-state fields
2) Plasma position and shape	Magnetics	See above
	Neutron camera	Needs validation
3) q(r) (current density)	Magnetics	$l_i(t)$; see above
	Motional Stark effect†	Needs diagnostic neutral beam
	Faraday rotation	Severe access limitations
	Reflectometry	Needs R&D to demonstrate feasibility
4) Electron density	Interferometry	Line-averaged; limited chord number
	Thomson scattering	Radial profile; limited time points
	Reflectometry	Radial profile; density fluctuations are issues
5) Ion/electron temperature	Neutron spectrometry	Core plasma ($r< 2a/3$) at DT phase
	Neutral particle analysis	Plasma periphery; needs diagnostic neutral beam
	CHERS	Needs diagnostic neutral beam and radiation resistant optics
	Thomson scattering	$T_e(r)$ profile; limited time points
	ECE	Suitable for T_e. Issues: harmonic overlap and supra-thermal emission
6) D/T density	*Neutral particle analysis*	Edge plasma; improves with neutral beam
	Neutron spectrometry	Core plasma; issue: S/N for DD neutrons
	Visible spectroscopy	Edge plasma; needs radiation resistant optics
7) Fusion power	Neutron yield monitor	Calibration methods need further development
8) Confined α-particles	Collective Thomson scattering	Needs validation on existing tokamaks and development of 1.5 THz radiation source
	CHERS	Needs diagnostic neutral beam
	Neutral particle analysis	Needs diagnostic neutral beam
9) Escaping α-particles	γ-spectroscopy	Needs R&D to demonstrate feasibility
	Thermocouples	Slow response time
	Faraday cups	Needs R&D to demonstrate feasibility
	Bolometers	Needs R&D to demonstrate feasibility
10) Divertor plasma	*Visible spectroscopy*	Needs radiation resistant optics
	Laser induced fluorescense	Needs R&D to demonstrate feasibility
	Langmuir probes	Severe erosion problems
	Reflectometry	Complicated plasma geometry
11) Erosion rate	*Visible spectroscopy*	See above
	Tile markers	Needs R&D to demonstrate feasibility
12) Heat loads	Thermocouples	Slow response time
	IR monitor	Needs radiation resistant optic
13) Helium concentration	*CHERS*	Needs dedicated neutral beam
	Residual gas analyzers	Relation to He density in the plasma is uncertain
14) Radiative loss	Bolometers	Limited access; low S/N ratio
15) Impurity content	*VUV spectroscopy*	For divertor view; access problematic
	X-ray spectroscopy	Key issue: radiation hardening of crystals
	Visible spectroscopy	Needs radiation resistant optics
16) Runaway electrons	ECE	Suitable in principle; needs validation
	X-ray monitor	Analysis of likely capability is required
17) Disruption precursors	Magnetics	Possible but not universal
	ECE	T_e fluctuations; uncertain
	Neutron camera	n_iT_i fluctuations; uncertain
	Bolometers	Radiation increase; not universal
18) Edge localized modes (ELMs)	D(T)-light monitor	Needs radiation resistant optics
	Reflectometry	Suitable in principle; needs validation
	Langmuir probes	Severe erosion problems
	Magnetic probes	Need probes with good time response

† Diagnostics shown *in italics* are additional ones for the physics phase

Table 2 ITER diagnostics R&D tasks

Radiation Effects on Components
Develop vacuum windows for diagnostics
Develop reflectors for diagnostics
Radiation sensitivity of ceramics
Radiation properties of fiber optics
Radiation hard dispersive and reflective methods
Data-base development for components in high radiation fields
Radiation capability of cabling
Radiation sensitivity of specific diagnostic hardware
New and Significantly Modified Diagnostic Methods
New fusion product techniques
Dual-polarization reflectometry for electron density and magnetic field profile studies
Source for collective scattering of fast ions
New Calibration Methods
In-situ calibration technique for 14 MeV neutrons
Hot source calibration of the ECE diagnostics
New Diagnostic Components
Many examples are given in the Plan
Studies of New Methods on Operating Fusion Experiments
Provides funding to operating groups for installation of test diagnostic equipment on their devices
Development of Diagnostic Computer Codes
Neutron transport codes
Analysis codes for the magnetic diagnostics
Interpretive diagnostic codes
Development of Computer Methods for Real-Time Data-Handling
Reliability Studies of Operating Equipment

Table 3 Photonuclear activation reactions

Target	Reaction	Product	Threshold (MeV)	$T_{1/2}$	E_γ (keV)	%
^{12}C	γ,x(x=α+n)	^{7}Be	26.3	53.3 d	477.56	10.3
^{58}Ni	γ, p	^{57}Co	8.2	270.0 d	122.07	85.6
	γ, n	^{57}Ni	12.2	37.0 h	1377.62	84.9
	γ, np	^{56}Co	19.6	77.3 d	846.75	99.99
	γ, 2n	^{56}Ni	22.5	6.1 d	158.30	99.00
	γ, 2np	^{55}Co	29.5	18.0 h	931.50	75.00
^{62}Ni	γ, np	^{58}Co	20.0	70.8 d	810.75	99.45
^{54}Fe	γ, np	^{54}Mn	20.4	312.2 d	834.81	99.97
^{56}Fe	γ, np	^{52}Mn	20.9	5.7 d	1434.43	100.00
^{55}Mn	γ, n	^{54}Mn	10.2	312.2 d	834.81	99.97
^{52}Cr	γ, n	^{51}Cr	12.0	27.7 d	320.07	9.83
^{50}Cr	γ, np	^{48}V	21.6	15.97 d	983.50	100.00

Table 4 Escaping α-activation reactions

Reaction	Q value (MeV)	$T_{1/2}$	σ (mb)[a]	Comment
$10B(\alpha,n)13N$	+ 1.06	9.9 min	10 [12]	e^+, no γ
$14N(\alpha,\gamma)18F$	+ 4.4	110 min	5 [13]	e^+, no γ
$25Mg(\alpha,p)28Al$	− 1.2	2.2 min	—	1.78 MeV γ
$27Al(\alpha,n)30P$	− 2.6	2.5 min	3 [14]	e^+, 1% γ
$29Si(\alpha,p)32P$	− 2.4	14 days	—	e^-, no γ
$30Si(\alpha,p)33P$	− 2.9	25 days	—	e^-, no γ
$41K(\alpha,n)44Sc$	− 3.4	3.9 h	—	e^+, 1.15 MeV γ

[a] The values of the cross sections are rough averages over the energy range from about 1–3 MeV.

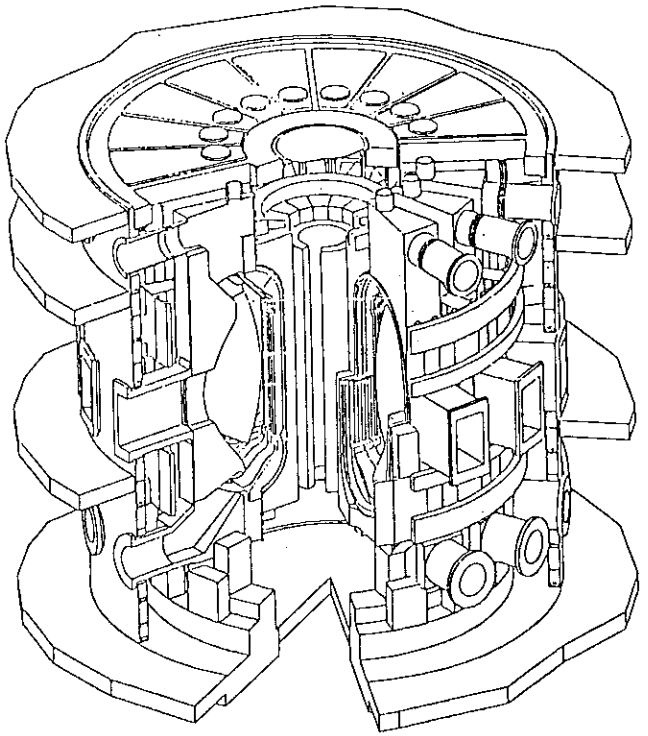

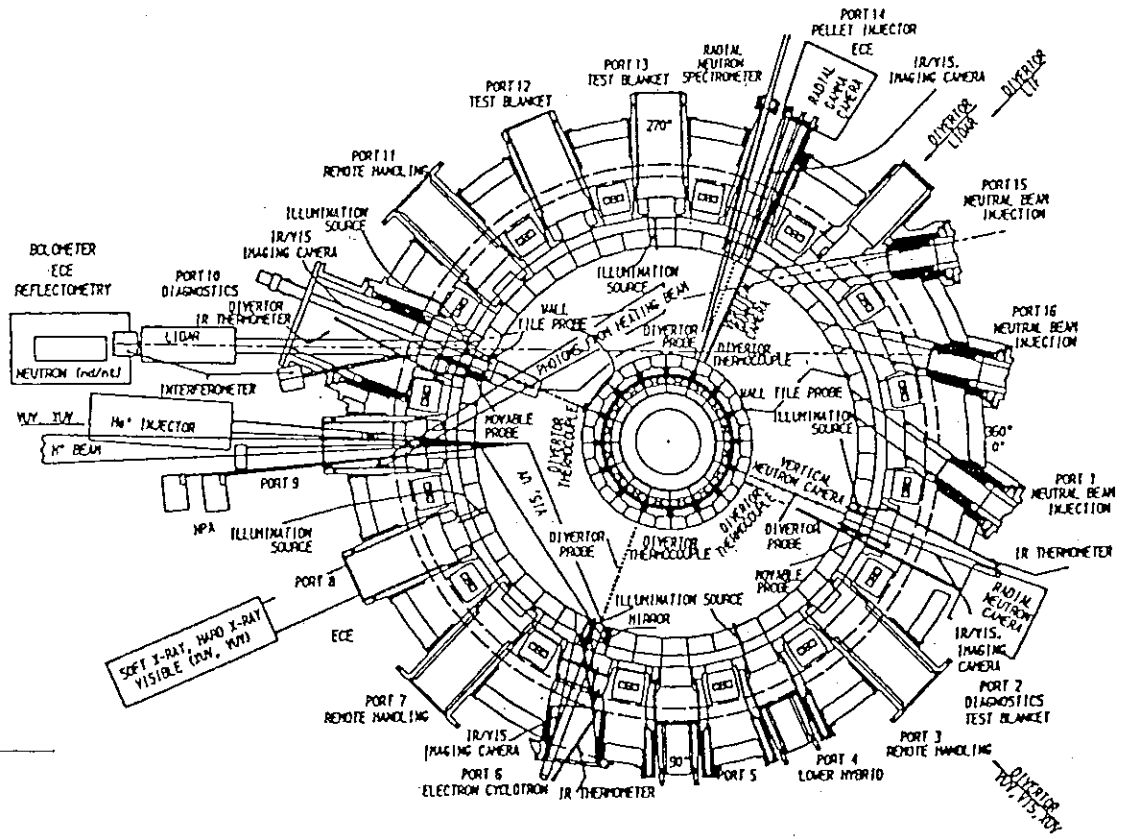

MAIN PARAMETERS OF ITER DEVICE

Plasma major radius, R (m)	6.0
Plasma minor radius, a (m)	2.15
Elongation (at 95% flux surface)	2.0
Toroidal field on axis (at R= 6 m), B_T (T)	4.85
Maximum field at the TF winding, B_{max} (T)	11.2
Nominal plasma current, I_p (MA)	22
Nominal fusion power, P_{fus} (GW)	1

Fig. 1 ITER and machine integration on the diagnostic systems

3. Papers Presented in Poster Session

3.1 Absolute Measurement of Neutron Capture Cross Sections with BGO Scintillators

Katsuhei Kobayashi, Shuji Yamamoto and Yoshiaki Fujita
Research Reactor Institute, Kyoto University
Kumatori-cho, Sennan-gun, Osaka 590-04 Japan

For the absolute measurement of capture cross sections by the linac time-of-flight method, a total absorption gamma-ray detector which is composed of 12 bricks of BGO scintillators (5 x 5 cm^2, 7.5 cm thick) was prepared. At first, with the BGO scintillation detectors, determination of the capture detection efficiency and absolute measurement of neutron flux incident upon the sample were carried out. Then, the experimental results were applied to the cross section measurement for the $^{197}Au(n, \gamma)^{198}Au$ and $Sb(n, \gamma)$ reactions in the energy region between 0.01 and 1.0 eV, by using the $^{10}B(n, \alpha \gamma)$ reaction as a well known standard reference cross section.

Since the result of the $^{197}Au(n, \gamma)^{198}Au$ cross section showed a good agreement with the existing measurements and the evaluated data ENDF/B-V, it was verified that the BGO detection system could be used for the absolute measurement of capture cross sections. Then, the detectors were applied to the $Sb(n, \gamma)$ cross section measurement, whose data were not always enough in quality and quantity.

1. Introduction

The neutron radiative capture process is great importance not only in understanding of the physical phenomena but also in many aspects of nuclear reactor design and the associated fuel cycles. Neutron capture gamma-ray spectroscopy has become

useful for the practical applications, especially in the time-of-flight experiment using a pulsed neutron source. For the determination of the number of capture events, it is necessary to employ the detection method which is independent on the cascade mode of nuclei or on the energy spectrum of the prompt gamma-rays, that is, the method which the detection efficiency for capture gamma-rays should not be affected by the cascade mode. From these points of view, a number of neutron capture gamma-ray detectors have been developed, such as NaI(Tl) and various types of organic and/or inorganic scintillation detectors[1].

The principle of this type of capture gamma-ray detector is to collect all prompt gamma-radiation energies emitted in neutron capture. An ideal detector is a type of 4π geometry around the sample, and so large that the whole radiation energies corresponding to sum of the neutron binding energy and kinetic energy of the incident neutron can be absorbed. A liquid scintillation tank of about 3000 liters meets the qualifications and it is often used for the capture measurements, since the gamma-rays can be totally absorbed and the detection efficiency approaches to 100 %. However, the discrimination level of this detector has to be usually set high, for example, at 2.5 MeV, because of troublesome background pulses in the low pulse height region. Then, the absolute determination of the number of capture events with the scintillation tank is not reliable enough for measurement of capture cross sections.

Bismuth germanate, $Bi_4Ge_3O_{12}$ (BGO) scintillator has a high density and a high stopping power for gamma-rays. Accordingly the volume of the scintillator to absorb the major part of capture gamma-rays can be smaller than the liquid scintillation tank. Then, the scintillator has been expected to be usuable for a gamma-ray spectroscopy[2-4]. Moreover, advantageous point

to employ the BGO detection system is able to use the $^{10}B(n,\alpha\ \gamma)$ reaction as a standard for the measurement of neutron flux impinging on the capture sample[5].

This paper describes how to make the absolute measurements for the $^{197}Au(n,\gamma)^{198}Au$ and Sb(n,γ) reactions and the results obtained by using the BGO detetion system in the linac neutron time-of-flight method.

2. BGO Detector

A $Bi_4Ge_3O_{12}$(BGO) scintillator has a high specific weight of about 7.13 g/cm^3 and it is intended to be applied to measurement of capture gamma-rays as a total absorption detector. We have prepared 12 bricks of BGO scintillators, each size 5 x 5 cm^2 and 7.5 cm thick, and assembled a scintillation bank to have a through hole 2 x 2 cm^2, as shown in Fig. 1. Total volume of the BGO scintillators is 2.25 liters and corresponds to about 1/1000 of that of a large liquid scintillation tank. Neutron beams are let through the hole to a capture sample placed at the center of the assembly. The inside of the hole was covered with enriched lithium-6 tiles of ^{6}LiF 3 mm thick, to absorb neutrons scattered by the capture sample. Moreover, the BGO detection system is installed in a lead shield of 10 cm wall thickness to reduce background from the surroundings.

Some of the characteristics of this BGO detector, such as measurement and calculation of capture gamma-ray spectra from Fe and Au, detection efficiency for gamma-rays and sensitivity to neutrons scattered by the capture sample, were measured and reported in the previous paper[5].

3. Experimental Method

3.1 Sample

As a capture sample in the present experiment, at first, gold was selected to investigate the application of the BGO detector to the absolute measurement of capture cross sections, because the $^{197}Au(n,\gamma)^{198}Au$ reaction is one of the well known standard cross sections[6]. The gold sample was a metallic plate of 1.8 x 1.8 cm^2 and the thickness was 0.7160 g/cm^2. Secondly, this BGO detector was used for the absolute measurement of the $Sb(n,\gamma)$ reaction, whose experimental data have not always been enough in quality and quantity. The antimony sample was powder and packed in a 0.2 mm thick aluminum case 1.8 x 1.8 cm^2 and 5 mm thick. The sample thickness was 1.843 g/cm^2.

Neutron flux impinging on a capture sample was measured by the $^{10}B(n,\alpha\gamma)$ reaction, whose cross section data are well known as a standard[6]. Boron-10 powder, whose enrichment was 90.4 %, was also put in a 0.2 mm thick aluminum case 1.8 x 1.8 cm^2 and 8 mm thick, and the ^{10}B sample thickness was 1.102 g/cm^2.

3.2 Experimental Arrangement

Capture cross section measurements in the neutron energy region between 0.01 and 1.0 eV were made by the time-of-flight (TOF) method using the 46 MeV electron linear accelerator (linac) at the Research Reactor Institute, Kyoto University (KURRI). The experimental arrangement is shown in Fig. 2. The flight path used in the experiment is in the direction of 135 degree to the linac beam. The neutron collimation system was mainly composed of B_4C, Li_2CO_3 and Pb materials, and tapered from about 12 cm diameter at the entrance of the flight tube to 1.5 cm at the detector.

Burst of fast neutrons were produced from the water-cooled

photoneutron target, which was made of 12 sheets of Ta plates 4.8 cm in diameter with an effective thickness of 3 cm[7]. This target was set at the center of an octagonal water tank, 30 cm diameter and 8 cm thick, to moderate the neutron energies.

The experimental parameters and conditions are summarized in Table 1. In order to prevent overlap of thermal neutrons produced by the previous linac burst, the pulse repetition rate was set to be low as 50 in 12.7 m TOF measurement. Neutron flux incident upon the capture sample was measured in the TOF method by using the $^{10}B(n,\alpha\gamma)$ reaction as a standard reference cross section[6]. The neutron intensity during the experiment was monitored with a BF_3 counter which was inserted into the TOF beam.

4. Capture Measurement

In order to make an absolute measurement of neutron capture events, at first, we selected samarium as a capture sample, 1.8 x 1.8 cm^2 and 0.5 mm thick plate. Compound nucleus of samarium has a capture cascade with high gamma-ray multiplicity. Therefore, in the measurement of capture gamma-rays from the samarium sample, missing the detection of capture events is very rare, as we described before[5]. Then, we can assume that the detection efficiency $\varepsilon_{Sm}(E_o)$ appeared in Eq.(1) is equal to unity;

$$C_{Sm}(E_o) = \varepsilon_{Sm}(E_o)\, Y_{Sm}(E_o)\, \phi(E_o) = Y_{Sm}(E_o)\, \phi(E_o), \quad (1)$$

where the subscript "Sm" is for samarium, E_o means thermal neutron, C is counting rate, Y is capture yield, and ϕ is neutron flux. Samarium has a very large capture cross section to thermal neutrons, and a Sm sample is, therefore, "black" for impinging thermal neutrons. Then, Eq.(1) is rewritten as

$$C_{Sm}(E_o) = \phi(E_o). \quad (2)$$

The cross section of the $^{10}B(n,\alpha\gamma)$ reaction for thermal neutrons is so large that the ^{10}B sample of about 1.102 g/cm^2 thickness becomes black to the incident neutrons. Then, the following relation is also derived:

$$C_B(E_o) = \varepsilon_B(E_o)\, Y_B(E_o)\, \phi(E_o) = \varepsilon_B(E_o)\, \phi(E_o) , \quad (3)$$

where the subscript "B" means ^{10}B. From Eqs.(2) and (3), the detection efficiency $\varepsilon_B(E_o)$ is given as

$$C_B(E_o)/C_{Sm}(E_o) = \varepsilon_B(E_o) = \varepsilon_B . \quad (4)$$

It has to be noted that the $\varepsilon_B(E_o)$ is constant at any other neutron energies, because the $^{10}B(n,\alpha\gamma)$ reaction emitts 480 keV gamma-ray only at any incident neutron energies. On the other hand, at the first s-wave big resonance of 4.9 eV for Au, the capture yield is also close to unity. Then, the following relation with gold can be given;

$$C_{Au}(E_R) = \varepsilon_{Au}(E_R)\, Y_{Au}(E_R)\, \phi(E_R) = \varepsilon_{Au}(E_R)\, \phi(E_R), \quad (5)$$

where E_R means resonance energy and $\phi(E_R)$ can be obtained by the flux measurement using the $^{10}B(n,\alpha\gamma)$ reaction. Since the BGO detector is thought to be a total energy absorption detector, the detection efficiency with gold measurement can be constant at any energy E,

$$\varepsilon_{Au} = \varepsilon_{Au}(E_R) . \quad (6)$$

The capture events at neutron energy E are obtained from the following Au and ^{10}B measurements;

$$C_{Au}(E) = \varepsilon_{Au}\, Y_{Au}(E)\, \phi(E) , \quad (7)$$

$$C_B(E) = \varepsilon_B\, Y_B(E)\, \phi(E) . \quad (8)$$

Then, the capture yield $Y_{Au}(E)$ can be derived as

$$Y_{Au}(E) = \frac{C_{Au}(E)}{C_B(E)} \cdot \frac{\varepsilon_B}{\varepsilon_{Au}}\, Y_B(E) , \quad (9)$$

by using a standard cross section for the $^{10}B(n,\alpha\gamma)$ reaction[6].

5. Experimental Results and Discussion

Making use of a total absorption BGO detector for capture gamma-ray measurement, firstly, absolute measurement of the neutron capture cross section of gold was made in the neutron energy region between 0.01 and 1.0 eV using the linac TOF method. The result is given in every 0.11 lethargy width and illustrated in Fig. 3. The experimental uncertainties are 3 to 4 % which are mainly derived from the statistical error of about 2 to 3 %. The present measurement for the $^{197}Au(n,\gamma)^{198}Au$ reaction is in very good agreement with the existing measured and evaluated data. Then, it could be considered that the BGO detector can be verified to be applicable to the absolute measurement of capture cross sections by detecting prompt capture gamma-rays using the linac TOF method.

Secondly, the BGO detector was used to measure the cross section for the Sb(n,γ) reaction at energies between 0.01 and 1.0 eV. Statistical error was about 3 % at lower energies and about 5 % at higher energies, and the total uncertainties were up to 4 to 6 %. The present result is illustrated in Fig. 4, comparing with the existing data. Koester's value[8] at 0.025 eV agrees with the present data. The evaluated curve of JENDL-3 recently released[9] shows a general agreement with the present measurement, although the present values seem to show some structure and deviate a little from the evaluated curve in the energy region between 0.1 and 0.5 eV. This discrepancy would be investigated in future, although similar tendency is observed in the neutron total cross section of Sb measured by the authors very recently.

References

1) R. E. Chrien(Ed.): "Neutron Physics and Nuclear Data in

Science and Technology", Vol.3, Neutron Radiation Capture, OECD/NEA, Pergamon Press (1984).
2) D. J. Wagner, N. R. Roberson and H. R. Weller: Nucl. Instr. Meth., A234, 109 (1985).
3) S. A. Wender, G. F. Auchampaugh, H. Hsu, P. T. Debeves, S. F. LeBrun and S. D. Hoblit: Nucl. Instr. Meth., A258, 225 (1987).
4) R. Alba, G. Bellia and A. Del Zoppo: Nucl. Instr. Meth., A271, 553 (1988).
5) S. Yamamoto, Y. Fujita, T. Shibata and S. Selvi: Nucl. Instr. Meth., A249, 484 (1986).
6) IAEA Technical Series No.227, "Nuclear Data Standards for Nuclear Measurements", IAEA, Vienna (1983).
7) K. Kobayashi, G. Jin, S. Yamamoto, K. Takami, Y. Kimura, T. Kozuka and Y. Fujita: Annu. Rep. Res. Reactor Inst., Kyoto Univ., Vol.22, 142 (1989).
8) L. Koester et al.: Zeitsch. f. Phys., A323, 359 (1986).
9) Japanese Evaluated Nuclear Data Library, Version-3, -JENDL-3- JAERI 1319 (1990).

Table 1 Typical experimental parameters and conditions.

Linac operation:	
pulse height	30 μ sec
pulse repetition	50 Hz
average current	~60 μ A
electron energy	30 MeV
Capture γ detector	BGO detector (12 bricks) assembly
Neutron monitor	BF_3 counter in TOF beam
Flight path	12.7 $\pm$ 0.1 m
Time analyzer (channel width & No. of channel):	
capture measurement	0.25 to 4 μ sec / channel 1024 or 2048 channels
neutron monitor	0.08 μ sec / channel 2048 channels

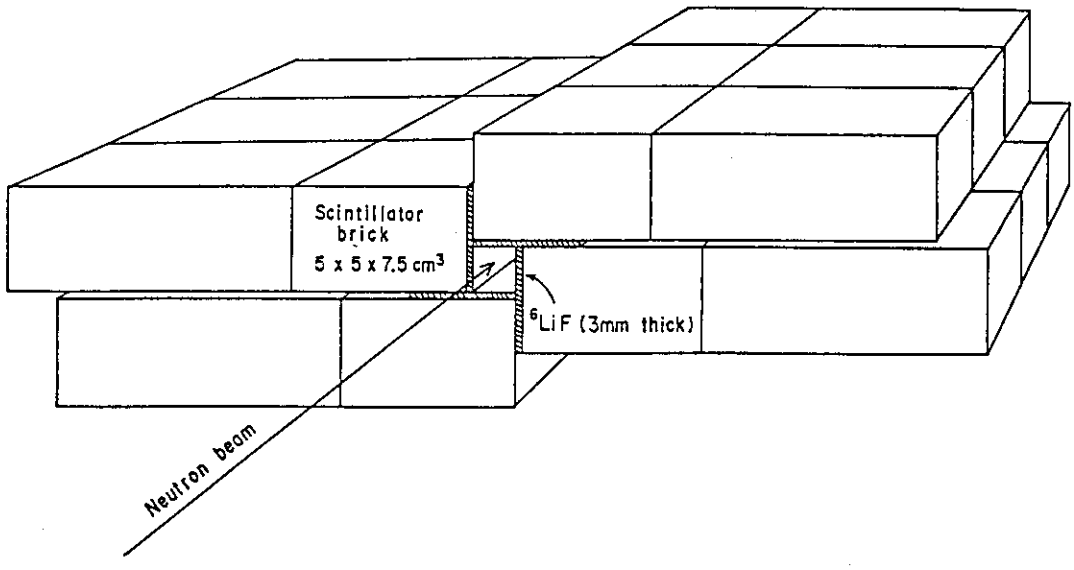

Fig. 1 BGO detector assembly.

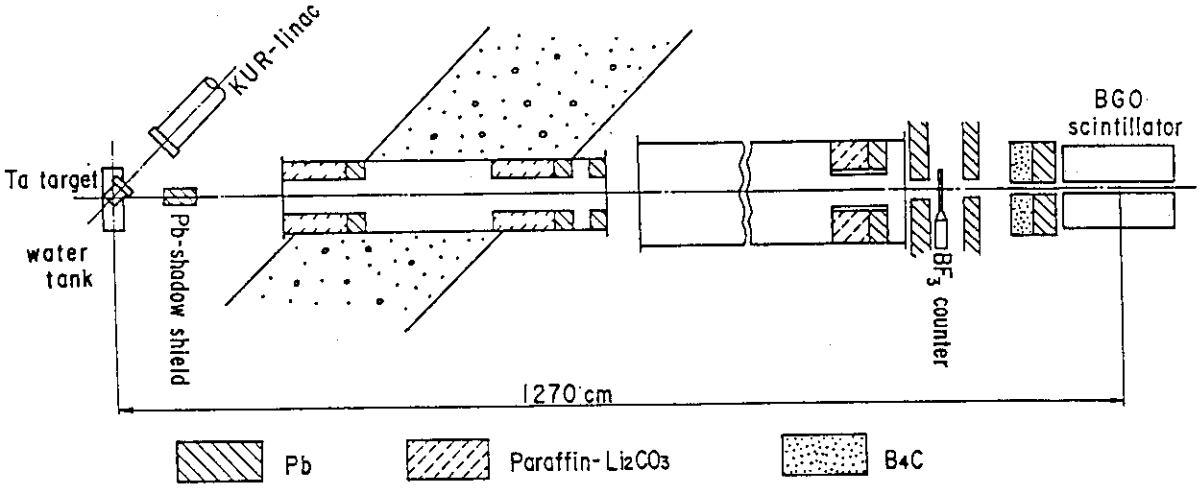

Fig. 2 Experimental arrangement for the capture cross section measurement.

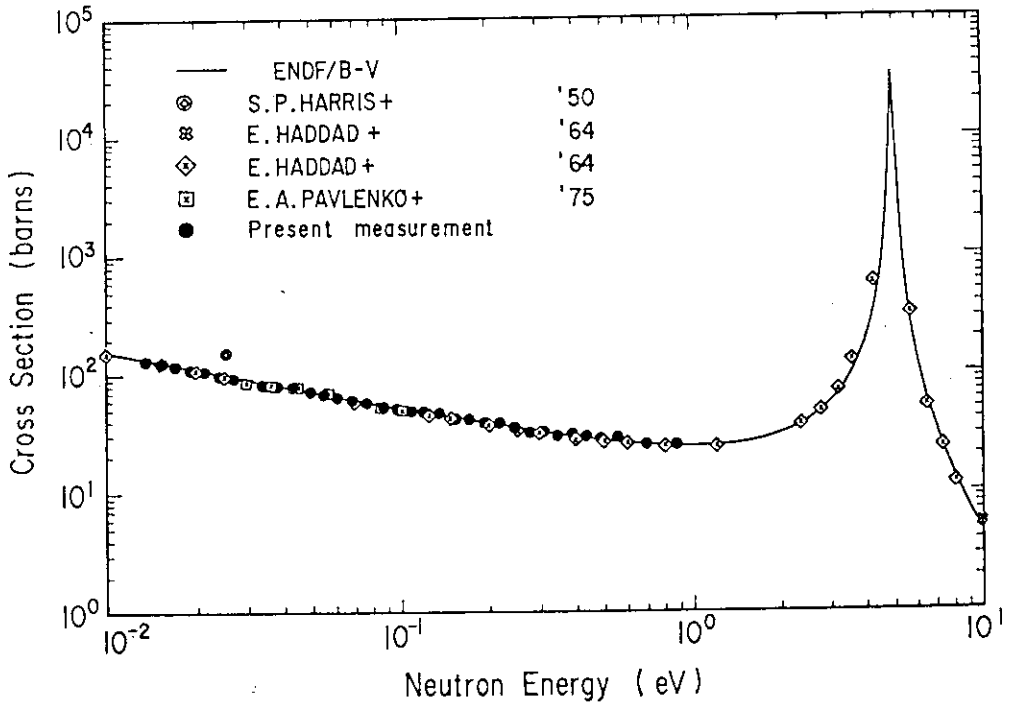

Fig. 3 Capture cross section for the $^{197}Au(n,\gamma)$ reaction.

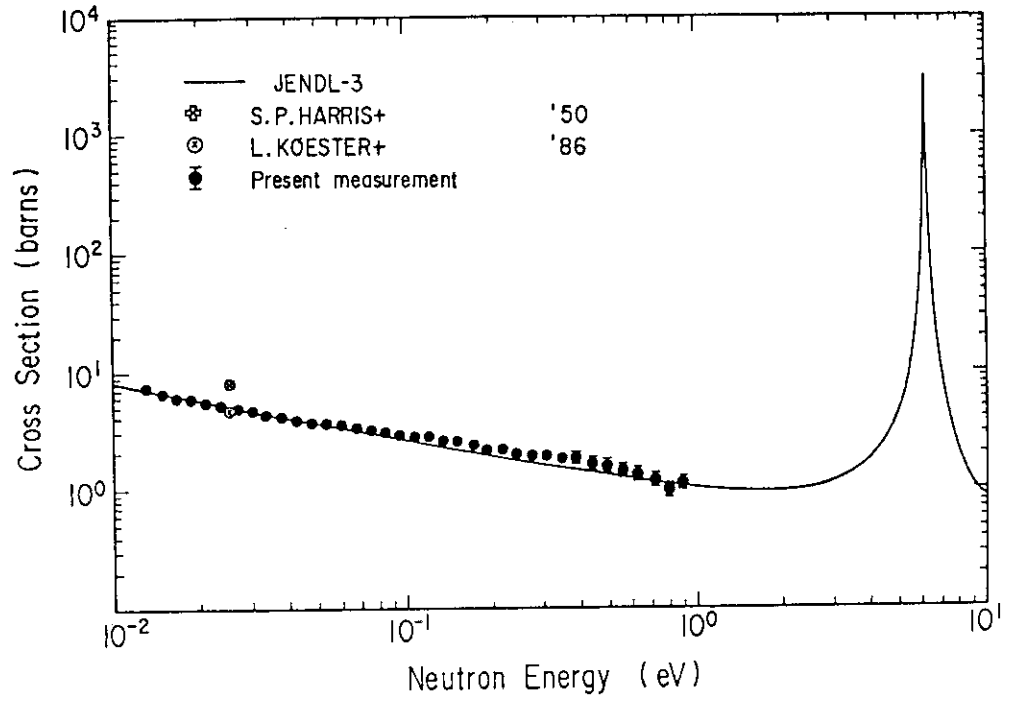

Fig. 4 Capture cross section for the Sb(n,γ) reaction.

3.2 Measurements of the Neutron Capture Cross Section of the Fission Product ^{137}Cs

Hideo HARADA, Hisashi WATANABE,
Tokai Works, Power Reactor and Nuclear Fuel Development Corp.
Tokai-mura, Ibaraki-ken, 319-11
Toshiaki SEKINE, Yuichi HATSUKAWA, Katsutoshi KOBAYASHI,
Department of Radioisotopes, Japan Atomic Energy Research Institute
Tokai-mura, Ibaraki-ken, 319-11
Toshio KATOH,
Department of Nuclear Engineering, Nagoya University
Furo-cho, Chikusa-ku, Nagoya, 464-01

Abstract

To obtain fundamental data for the research of the transmutation of long-lived radioactive waste, the cross section of the reaction ^{137}Cs(n, γ)^{138}Cs has been measured by means of an activation method . First, the thermal neutron capture cross section, including a contribution of epithermal neutrons, was obtained relative to that of the ^{59}Co(n,γ)^{60}Co reaction. A target of about 0.4 MBq of ^{137}Cs was irradiated together with a Co flux monitor at JRR-4 in JAERI. The samples were purified chemically and their γ-ray spectra were measured with a HPGe detector of 90 % relative efficiency. The resulting activity ratios between ^{138}Cs and ^{137}Cs and neutron flux data gave the cross-section value of 0.250$\pm$ 0.013 b. This value is twice as large as that of the previous work by D. C. Stupegia (J. Nucl. Energy, A12, 16 (1960)). Second, another set of irradiations, using a Cd thermal neutron shield, were carried out to separate the contributions from thermal and epithermal neutrons. The cross section for 2,200 m/s neutrons, σ_0, was 0.25$\pm$ 0.02 b and the resonance integral, I_0, was 0.36$\pm$0.07 b. This result is consistent with the cross section obtained in our first experiment. It is found that the resonance integral of the reaction has been overestimated in evaluations: I_0=0.499 b in ENDF/B-V and I_0=0.680 b in JENDL-3.

[1] Introduction

The nuclide ^{137}Cs is one of the most important fission products in the radioactive waste management. The accurate cross section of the $^{137}Cs(n, \gamma)^{138}Cs$ reaction is necessary for the research of the neutron utilized transmutation.[1] There has been no measurement of the cross section of the $^{137}Cs(n, \gamma)^{138}Cs$ reaction since Stupegia measured the thermal neutron capture cross section first in 1960; he obtained the value of 0.110 ± 0.033 b with a NaI(Tl) spectrometer by an activation method.[2] In this seminar, details of the measurements of the thermal neutron cross section and resonance integral of ^{137}Cs are given; the cross sections were measured by taking advantage of a highly efficient Ge detector and fast electronics; further, a chemical separation process is introduced to enhance the sensitivity of activity measurement.

[2] Measurement of the thermal neutron cross section of the $^{137}Cs(n, \gamma)^{138}Cs$ reaction

The thermal neutron capture cross section was measured relative to that of the $^{59}Co(n,\gamma)^{60}Co$ reaction. About 0.4 MBq of ^{137}Cs was used as a target. Three μl of CsCl solution containing the radioactivity was put into a small polyethylene bottle and evaporated to dryness. The target was irradiated together with a flux-monitor wire of 0.475 w% Co/Al-alloy (0.76 mm in diameter) during a 10 min period in the T-pipe of the JRR-4 reactor at JAERI. The irradiation position is characterized with a thermal neutron flux of 4×10^{13} n/cm^2/s and an epithermal index in the Westcott convention[3], $r\sqrt{T/T_0}$, of 0.02.

About 15 min after irradiation, a chemical procedure for purification of the irradiated ^{137}Cs target was started. Two ml of water containing 2 mg of zeolite (natural mordenite) was poured into a polyethylene bottle. The zeolite absorbing Cs was separated from the solution by filtration and washed with water and then with a small amount of acetone. Most of the ^{24}Na and ^{38}Cl activity was eliminated.

About 30 min after irradiation, the measurement of the ^{137}Cs sample was started. For the observation of weak transitions of ^{138}Cs in the strong γ-ray field of ^{137}Cs, a HPGe detector of 90% efficiency and a fast ADC (450 MHz) were used. Fig.1 shows the block diagram of the high-rate gamma spectroscopy system. The digital pulse height signals were accumulated through a CAMAC interface in a histogram memory; the pulse height data with 4K channels were dumped at intervals of 600 s into a floppy disk.

Fig.2 shows a γ-ray spectrum of the irradiated and purified ^{137}Cs sample. In the spectrum, the γ-rays of ^{138}Cs can be seen at 1010, 1436 and 2218 keV besides the 662 keV γ-ray of ^{137}Cs. Figure 3 shows the decay curves of the ^{138}Cs γ–lines. The data are well fitted with a single exponential curve. Table 1 shows half-life values of ^{138}Cs determined from those γ–lines in each of four runs. The weighted mean is 33.1 ± 0.6 min. This value is in good agreement with the experimental one reported by Ehrenberg and Amiel.[4] These facts indicate that the ^{138}Cs γ lines are free from contamination of other radioactivities.

The reaction rate of ^{137}Cs was deduced from the activity ratio of ^{138}Cs to ^{137}Cs. The thermal neutron capture cross section was obtained by dividing the reaction rate by the thermal neutron flux measured with a flux monitor Co. The relation between the activity ratio and the capture cross section can be expressed by

$$\sigma = \frac{A_2}{A_1} \cdot \frac{\lambda_1}{\phi(1 - e^{-\lambda_2 T_{IR}})} \cdot \quad \text{---(1)}$$

Symbols are defined as follows:

A : Activity at the end of neutron irradiation

λ : Decay constant

ϕ : Thermal neutron flux

T_{IR} : Period of neutron irradiation.

The subscripts 1 and 2 refer to ^{137}Cs and ^{138}Cs, respectively. The nuclear data used are summarized in Table 2.[4),(5),(6)]

The second column in Table 3 shows the thermal neutron fluxes determined from ^{60}Co radiactivities produced in the flux monitors; the cross section value of 37.18 b[7)] was taken for the ^{59}Co(n,γ)^{60}Co reaction. Table 3 also shows the measured cross section for each ^{138}Cs γ-ray obtained from four runs. The errors of the cross section do not include the errors of the nuclear data in Table 2. A weighted mean of 0.250 ± 0.013 b has been obtained as the thermal neutron cross section. This is 2.3 times larger than that of the previous work by D. C. Stupegia.[2)]

[3] Measurement of the cross section at 2,200 m/s and resonance integral

The resonance integral of the ^{137}Cs(n, γ) ^{138}Cs reaction was measured together with its 2,200-m/s neutron cross section. One possibility for the cause of the discrepancy between our result given in sect. [2] and Stupegia's is a difference in neutron spectrum, if the resonance integral is very large. An experimental data of the resonance integral is also needed for the feasibility study of nuclear transmutation, when the epithermal range of neutrons is used.

About 0.4 MBq of ^{137}Cs was irradiated together with Co, Au and Mo flux monitors by using the pneumatic tube equipped with a movable Cd shield at JRR-4. Fig.4 shows the schematic diagram of the pneumatic tube. Irradiations were carried out with and without the Cd shield during a period of 10 or 2 min.

Chemical procedures and γ-ray measurements were the same as the previous ones mentioned in sect. [2]. Fig. 5 shows γ-ray spectra obtained at Run 2 for the ^{137}Cs samples irradiated with and without a Cd shield. In both the spectra, γ-rays from the ^{138}Cs were observed. Since the production of the ^{138}Cs was much reduced in irradiation with a Cd shield, the 1436-keV γ-ray, which is the strongest in the γ-rays of ^{138}Cs, was used for the radioactivity determination. The γ-ray intensities observed for the ^{137}Cs samples and the flux monitors were reduced to the radioactivities at the end

of the irradiation, refering to the nuclear data listed in Tables 2 and 4. The radioactivity of ^{138}Cs was determined relative to that of ^{137}Cs, as described previously.

The reaction rate, R, over σ_0 (cross section for 2,200 m/s neutrons) is expressed by the following equations.

$$R/\sigma_0 = \phi_1 + \phi_2 \times s_0 G_{epi} \quad \text{for irradiation without a Cd shield} \quad \text{--- (2)}$$

$$R'/\sigma_0 = \phi_1' + \phi_2' \times s_0 G_{epi} \quad \text{for irradiation with a Cd shield} \quad \text{--- (3)}$$

where $\phi_1^{(\prime)}$, $\phi_2^{(\prime)}$ are free parameters determined by the flux monitors; $\phi_1^{(\prime)}$ and $\phi_2^{(\prime)}$ are approximately the thermal and epithermal neutron fluxes, respectively. The s_0 is defined by

$$s_0 = \sqrt{\frac{4}{\pi}} \times \frac{I_0'}{\sigma_0} \qquad \text{--- (4)}$$

where I_0' is the reduced resonance integral. Parameters for eq. (2)～(4) are listed in Table 5. Fig. 6 shows the relation between $R^{(\prime)}/\sigma_0$ and $s_0 G_{epi}$ measured for Co, Au and Mo flux monitors. As indicated by eq. (2) and (3), good linear relationship can be seen in Fig. 6 for both irradiations with and without a Cd shield.

The thermal neutron fluxes $\phi_1^{(\prime)}$ and epithermal neutron fluxes $\phi_2^{(\prime)}$ in each of irradiation conditions were deduced from the fitted lines. Table 6 shows the results of neutron flux determinations and the cross sections of the reaction ^{137}Cs(n, γ) ^{138}Cs. The weighted means of the thermal cross section σ_0 (for 2200 m/s neutrons) and the resonance integral I_0 (including the 1/v part) are $\sigma_0 = 0.25 \pm 0.02$ b and $I_0 = 0.36 \pm 0.07$ b, respectively.

This result is consistent with the cross section obtained in our first experiment. In Table 7, the measured value I_0 is shown together with recent evaluations(ENDF/B-V and JENDL-3).[9] It is found that the resonance integral of the reaction has been overestimated in evaluations.

[4] Conclusion

The neutron capture cross section of ^{137}Cs, which is one of the most important nuclide for the management of radioactive waste, has been studied for the research of the neutron-utilized transmutation. First, the thermal neutron capture cross section was measured relative to that of the ^{59}Co(n,γ)^{60}Co reaction. The value obtained, 0.250 ± 0.013 b, is twice as large as that of the previous work by D. C. Stupegia[2]. Next, the neutron capture cross section for 2,200 m/s neutrons, σ_0 , and the resonance integral, I_0 , were measured. The results are $\sigma_0 = 0.25 \pm 0.02$ b and $I_0 = 0.36 \pm 0.07$ b. This result is consistent with the cross section obtained in our first experiment. It is found that the resonance integral of the reaction has been overestimated in recent evaluations.[9]

References

(1) Harada, H., Watanabe, H., Sekine, T., Hatsukawa, Y., Kobayashi, K.,Katoh, T.: J. Nucl. Sci. Tech., 27,577 (1990).

(2) Stupegia, D. C.: J. Nucl. Energy, A12, 16 (1960).

(3) Westcott, C. H., Walker, W. H., Alexander, T. K.:Proc. 2nd Geneva Conf., Vol. 16, 70(1958).

(4) Ehrenberg, B., Amiel, S.:Phys. Rev. C16, 618 (1972).

(5) Carlson, G. H., Talbert, W. L., McConnell, J. R.: ibid., C9, 283 (1974).

(6) Lederer, C. M., Shirley, V.S.: Table of Isotopes, (7th ed.), (1978), John Wiley & Sons.

(7) Mughabghab, S. F., Divadeenam, M., Holden, N. E.: Neutron Cross Sections, Vol. I, Part A, (1981), Academic Press.

(8) Matsuoka, H., Sekine, T.: JAERI-M 9552 (1981) (in Japanese).

(9) Nakagawa, T.: private communication.

Table 1 Experimental half-life of ^{138}Cs

Run No.	Half-life (min)		
	1,010 keV	1,436 keV	2,218 keV
1	34.4±5.2	32.9±1.3	34.2±3.4
2	33.1±5.3	33.4±2.1	30.1±9.3
3	37.1±4.9	33.7±1.1	26.5±2.5
4	32.5±3.9	33.8±1.1	32.1±3.4
	34.1±2.4	33.5±0.6	30.0±1.7

Weighted mean=33.1±0.6 (min)

Table 2 Nuclear data used in the present work

Nuclide	$T_{1/2}$	E_γ (MeV)	γ-intensity
^{60}Co	5.271 yr	1.173	1.00
		1.332	1.00
^{137}Cs	30.17 yr	0.662	0.85
^{138}Cs	33.4 min	1.010	0.284
		1.436	0.750
		2.218	0.161

Table 3 Experimental results of thermal neutron flux and cross section

Run No.	Neutron flux (10^{13} $n/cm^2 \cdot s$)	Cross section (barn)		
		1,010 keV	1,436 keV	2,218 keV
1	3.7±0.2	0.286±0.023	0.251±0.014	0.271±0.019
2	3.8±0.2	0.282±0.026	0.258±0.016	0.235±0.033
3	3.9±0.1	0.264±0.020	0.248±0.014	0.205±0.015
4	3.8±0.1	0.277±0.021	0.250±0.014	0.223±0.016
		0.276±0.017	0.250±0.013	0.230±0.014

Weighted mean=0.250±0.013 (barn)

Table 4 Neutron flux monitors and nuclear data used for the determination of radioactivities

Material of wire	Diameter of wire (mm)	Radio nuclide	Half-life	Detected γ-ray		
				Energy (keV)	Intensity (%)	Gγ
0.475w% Co/Al	0.76	^{60}Co	5.271y	1173	100	0.995
				1332	100	0.996
0.061w% Au/Al	0.51	^{198}Au	2.696 d	412	95.5	0.995
Mo	0.51	^{99}Mo	66.02 h	141	89.0	0.908

Table 5 Data used for the determination of $\phi_1^{(')}$ and $\phi_2^{(')}$

Nuclear reaction	σ_0 (b)	s_0	G_{epi} †
^{59}Co(n, γ)^{60}Co	37.2	1.83	1.00
^{197}Au(n, γ)^{198}Au	98.8	17.02	1.00
^{98}Mo(n, γ)^{99}Mo	0.130	53	0.85

† Values for the wires listed in Table 4

Table 6 Results of neutron flux determinations and the cross sections of the reaction ^{137}Cs(n,γ)^{138}Cs

Run	Irradiation Type	Period	ϕ_1 or ϕ_1' (10^{13}cm^{-2}s^{-1})	ϕ_2 or ϕ_2' (10^{13}cm^{-2}s^{-1})	^{137}Cs(n, γ)^{138}Cs reaction R/R'	s_0	σ_0 (b)
1	no Cd shield	2 m	3.15±0.12	0.124±0.012	9.8±0.8	0.89±0.35	0.279±0.021
	with Cd shield	10 m	0.234±0.017	0.111±0.004			
2	no Cd shield	10 m	2.96±0.18	0.093±0.014	8.2±0.9	1.69±0.60	0.234±0.018
	with Cd shield	10 m	0.220±0.015	0.095±0.004			
					Averaged	1.09±0.30	0.253±0.022

Table 7 Comparison of resonance integrals for the ^{137}Cs(n,γ)^{138}Cs reaction

I_0	Resonance integral[1] (b)
Present work	0.36±0.07
ENDF/B-V	0.499
JENDL-3	0.680

[1] The Cd cutoff energy is 0.5 eV.

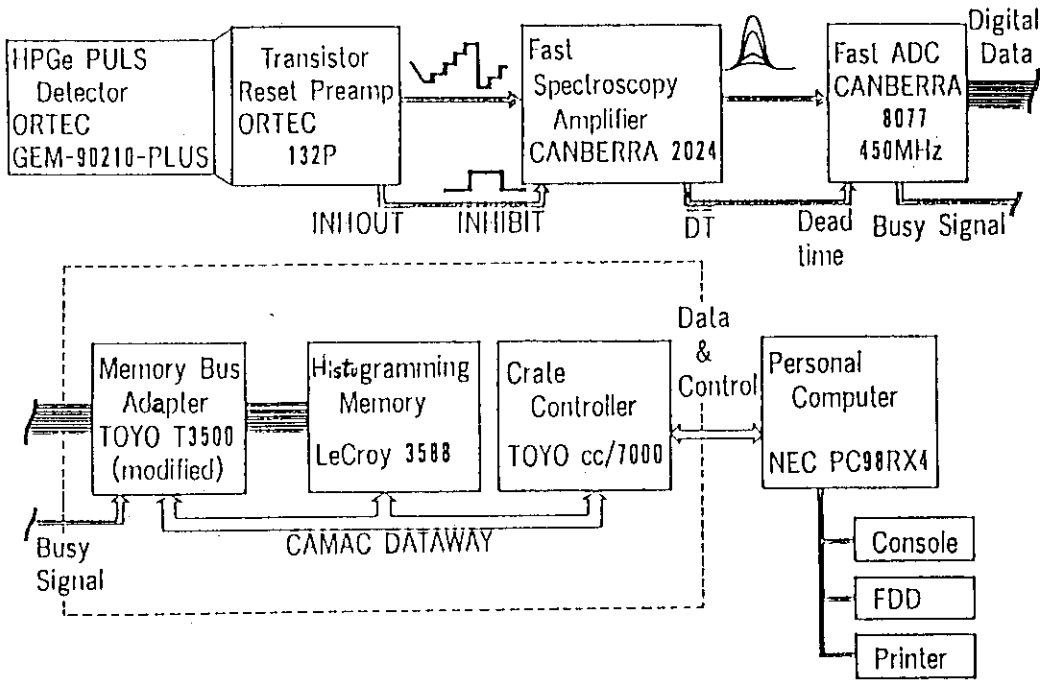

Fig. 1 High count rate spectroscopy system

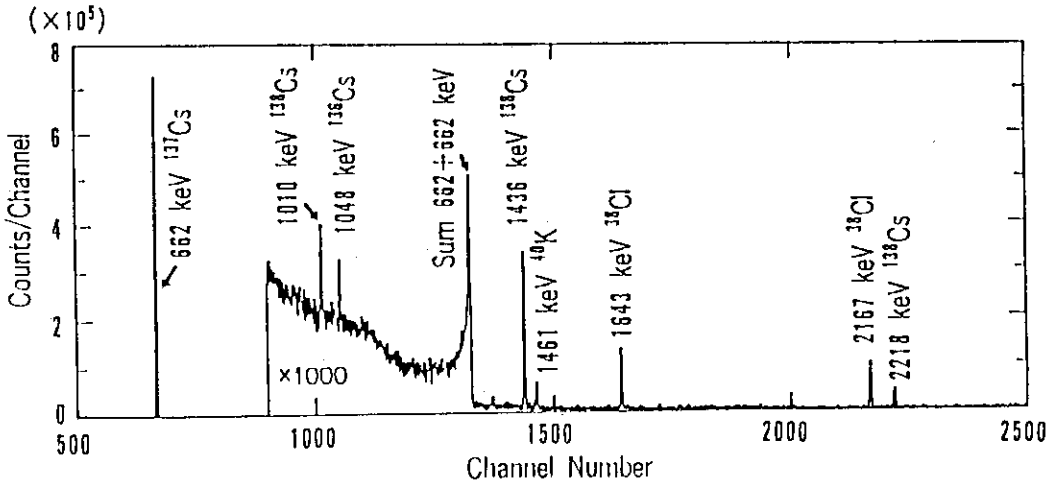

Fig. 2 Gamma-ray spectrum obtained from neutron-irradiated and chemically purified ^{137}Cs sample in 10-min measurement

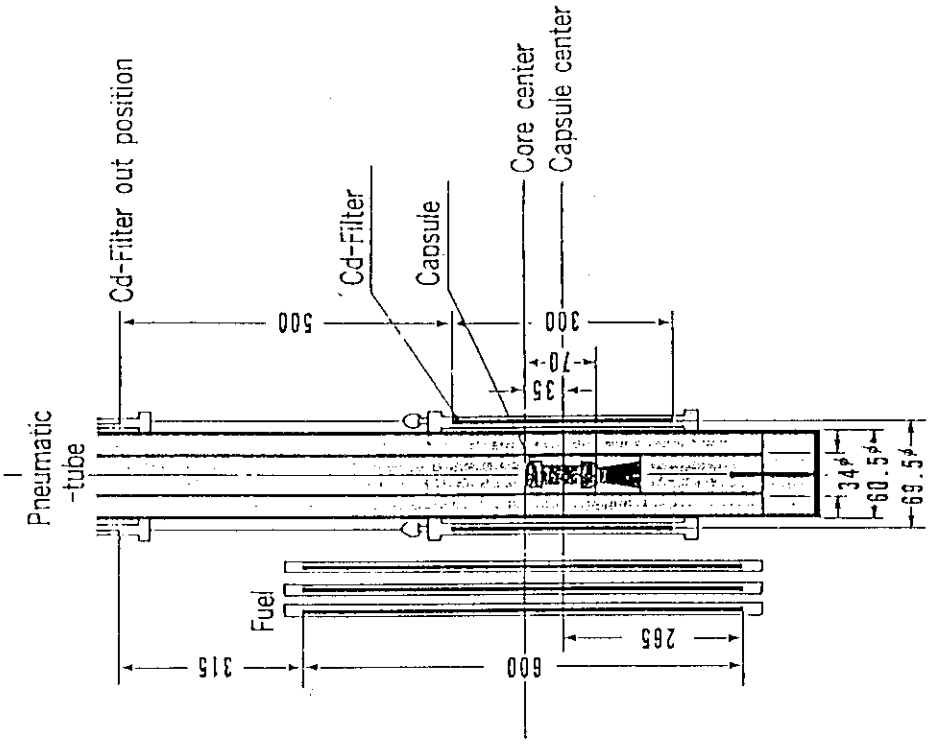

Fig. 4 Schematic diagram of the pneumatic tube at JRR-4

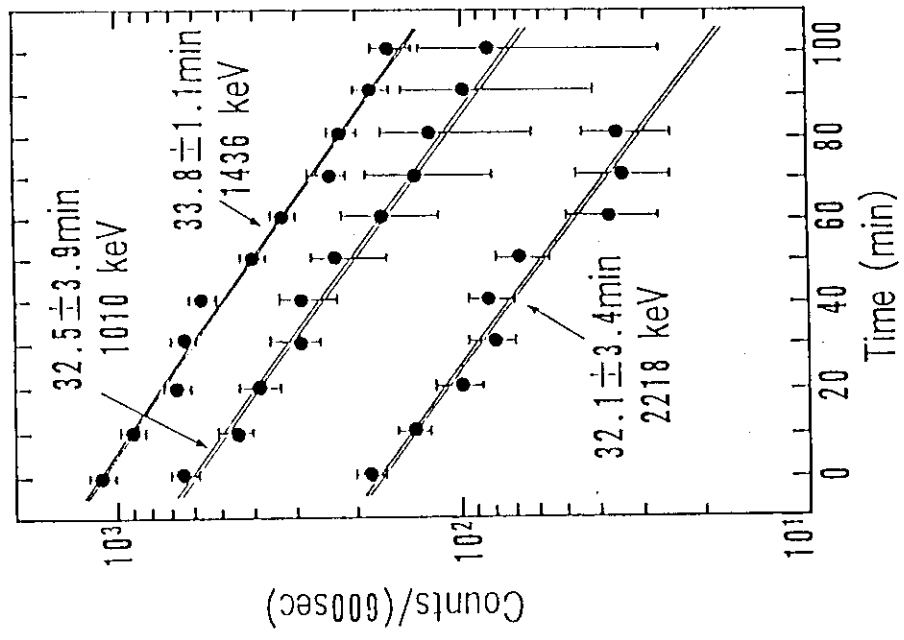

Fig. 3 Decay curves of ^{138}Cs γ-rays obtained in Run 4

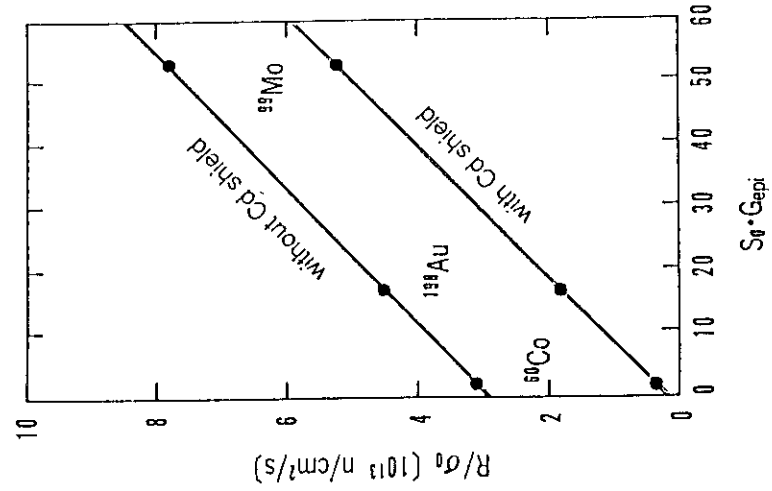

Fig. 6 Plot of R/σ_0 against s_0G_{epi} for neutron-flux monitors irradiated with and without a Cd shield.

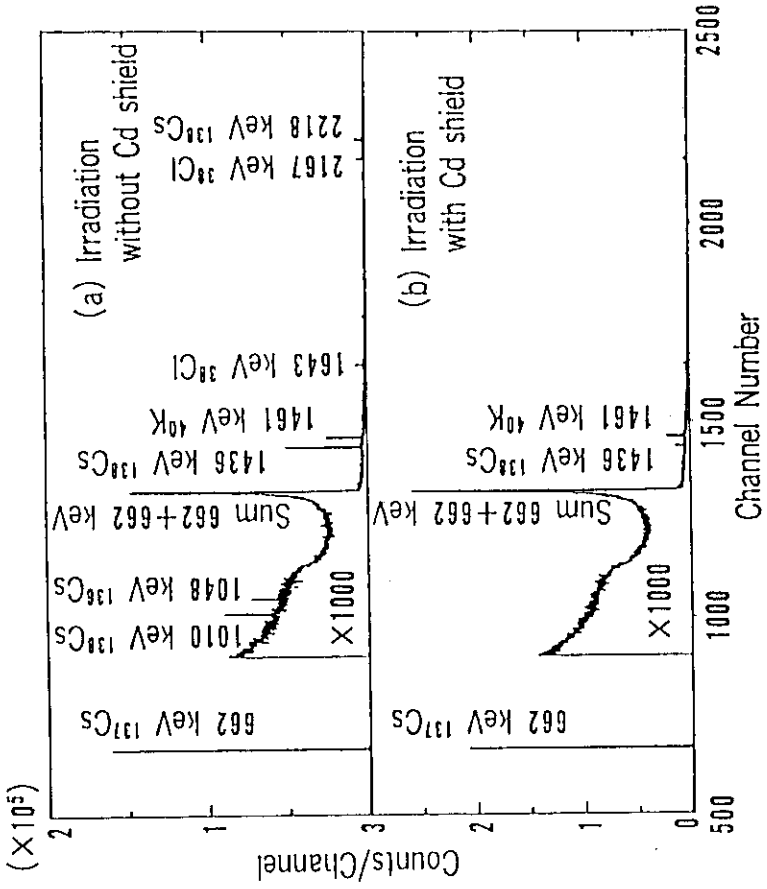

Fig. 5 γ-ray spectra of ^{137}Cs samples irradiated with and without a Cd shield, and purified chemically. Measurements were started 30 min after irradiation, and their counting periods were 30 min.

3.3 Evaluation of Cross Sections for the Dosimetry Reactions of ^{93}Nb

Naoteru Odano, Shin Iwasaki and Kazusuke Sugiyama

Department of Nuclear Engineering
Tohoku University
Aramaki-Aza-Aoba, Aoba-ku
Sendai, 980 Japan

Cross sections for ^{93}Nb(n,n')^{93m}Nb and ^{93}Nb(n,2n)^{92m}Nb reactions were evaluated using nuclear model calculation and experimental data. In this study, the ELIESE-GNASH joint program, the Hauser-Feshbach code with preequilibrium correction, was used for calculation of the cross sections and particle emission spectra. The input parameters for the nuclear model code were adjusted to reproduce the recent experimental data. To establish reliable excitation functions for the dosimetry application, the cross section were evaluated with their uncertainties and covariance matrices from the results of the nuclear model calculation and recent experimental data using a generalized least squares program, GMA.

The fission spectrum averaged cross sections calculated from the evaluated cross sections were compared with the recent integral experiments. The degree of agreement for both the reactions was good.

1. Introduction

The ^{93}Nb(n,n')^{93m}Nb and ^{93}Nb(n,2n)^{92m}Nb reaction are of importance for dosimetry applications. Specifically, the ^{93}Nb(n,n')^{93m}Nb reaction is considered as reaction for measurement of fast neutron fluence by activation in pressure vessel of light water reactor. Its threshold energy of 30 keV and half life of ^{93m}Nb (13.6 year) are suitable for the fluence monitor. On the other hand, the ^{93}Nb(n,2n)^{92m}Nb reaction cross section is interest as a monitor for fusion reactor dosimetry application because of a hale life of the produced ^{92m}Nb (10.15 day) and its high threshold energy, about 9 MeV.

In spite of the importance of the ^{93}Nb(n,n')^{93m}Nb reaction, experimen-

tal data of the cross section is still sparse and the uncertainties of the data are large due to the difficulty of the activity measurement. We intended to improve the present status of the reaction cross section using theoretical calculation /1/. In this paper, evaluation of the two pertinent reaction cross sections were described.

2. Nuclear Model Calculation

2.1 Nuclear Model Codes

In this study, a joint program of ELIESE /2/ and GNASH /3/ (EGNASH/4/), and DWUCK /5/ code were used for the calculation of the neutron induced reaction cross sections and particles emission spectra. EGNASH was a main code in this study. The code is a statistical nuclear model code and includes preequilibrium correction by exciton model. The code provides reaction cross sections and spectra (emission of neutron, γ-ray and charged particles) resulting from particle induced reactions. The transmission coefficients for the GNASH code were prepared by ELIESE which is implemented in EGNASH. The DWUCK code, distorted wave Born approximation code, was used to calculate the direct inelastic scattering cross sections. The contribution of the direct inelastic scattering cross sections were taken into account in the calculation of EGNASH code.

2.2 Parameters for the Nuclear Model Codes

Input parameters for the nuclear model codes were carefully chosen and adjusted to reproduce the reaction cross sections and particles emission spectra. In the nuclear model calculation, the optical model potential parameter, level density parameter and data for discrete level were important as input parameters.

A optical model potential parameter set by Smith (ANL) /6/ was adopted for the calculation. For checking of the adopted parameter set, the so-called "SPRT" data, i.e., the s- and p-wave neutron strength functions, scattering radius and total cross section, were compared with experimental data.

In the original EGNASH code, the Gilbert-Cameron's level density formula /7/ was used. In this study, energy dependence of level density parameter

developed by Ignatyuk /8/, which is effective for the nucleus in the neighborhood of the closed shell was newly implemented /1/. The energy dependence of the level density parameter can be expressed by the following formula,

$$a(U) = a\{1+f(U)dW/U\}, \qquad (1)$$

where "U" is the excitation energy and "a" is the asymptotic value for the Fermi gas parameter occurring at higher energies. The term dW denotes the shell correction term and evaluated by the mass formula by Cameron and Elkin /9/. The term f(U) owes the energy dependence of the parameter by $f(U)=1-\exp(-0.05)$.

The discrete level data (spin and parity of discrete levels, and γ-ray decay scheme) was found to be important input data in the present calculation. The data for ^{93}Nb was taken from the evaluation by Demanins /10/. The data of the reference 11 was used for the other nuclei.

2.3 Discussion on the Result of the Nuclear Model Calculation

The calculated excitation functions of the ^{93}Nb(n,n')^{93m}Nb, ^{93}Nb(n,2n)^{92m}Nb, ^{93}Nb(n,2n)$^{92m+g}$Nb, ^{93}Nb(n,α)^{90m}Y and ^{93}Nb(n,α)$^{90m+g}$Y were compared with their experimental data. The excitation function of the ^{93}Nb(n,n')^{93m}Nb reaction is slightly lower than the experimental data in the energy range from 2 MeV to 4 MeV. The excitation function of the isomeric state production cross section via (n,2n) reaction is higher than the experimental data above 16 MeV while the excitation function agrees with the experimental data below 16 MeV. The sum of production of the isomeric state and the ground state is somewhat higher from threshold energy to 12 MeV. For (n,α) and (n,γ) reaction, the calculated cross sections reproduced the experimental data in acceptable level.

The particle emission spectra were calculated around 14 MeV, and also compared with experimental data. The agreement was rather good.

Thus, by using theoretical model codes, a consistent data set of neutron induced reaction cross sections for ^{93}Nb was obtained. The two pertinent cross sections were reproduced by the model calculation, though the degree of agreement with experimental data is still insufficient from the view point of the dosimetry application. In order to obtain reliable dosimetry cross sections, an evaluation was performed using a generalized least

square method taking into account the result of the nuclear model calculation in addition to the experimental data because the experimental data were too scarce.

3. I Evaluation of Cross Sections

3.1 Evaluation Procedure

A pascal version of GMA code /12/, Gauss-Markov-Aitken least squares nuclear data evaluation program, was used for evaluating the cross sections with their uncertainties and covariance matrices. The program evaluates cross sections by 0-order spline fitting. Because of the peculiarity of the 0-order spline function, all experimental data used in the evaluation must be converted at energy grid determined in advance. The energy grid was chosen considering the distribution of experimental data. As the first step, the experimental data were surveyed. Some experimental data were rejected because the data were inconsistent with the other experimental data. In the GMA calculation, the result of the present theoretical calculation was treated the same as the experimental data. The uncertainties and correlations of the experimental data were appropriately assumed from the literatures. The uncertainty of result of the theoretical calculation was assumed 7.5 % for each reactions.

3.2 The ^{93}Nb(n,n')^{93m}Nb Reaction Cross Section

In the evaluation of the (n,n') reaction cross section, weight of the experimental data by Wagner /13/ in the vicinity of 8 MeV and Ryves's /14/ data at 14 MeV was reduced in order to avoid unnatural structure in the excitation function. The evaluated result were shown in Fig.1 with experimental data used in this evaluation. The evaluated correlation matrix was illustrated in Fig.2. Variance of the present evaluated result was 3 % in the energy range from 2 to 6 MeV. In the other energy range, the variance was 7.5 %. The present evaluation reasonably follows the experimental data below 6 MeV. Comparing with the other evaluation of JENDL Dosimetry File seemed to be overestimation in the energy range between 4 to 6 MeV, while present result agrees with IRDF-90.

3.3 The $^{93}Nb(n,2n)^{92m}Nb$ Reaction Cross Section

For the evaluation of the (n,2n) reaction cross section, 32 experimental data (178 energy points) and the result of theoretical calculation were used as input data. The uncertainties and correlations of each experimental data were assumed from the description of the EXFOR. The evaluated result was shown in Fig.3 with experimental data. Fig. 4 illustrates the correlation matrix of the evaluated cross section. Variance of the present evaluated result was 0.7 % around 14 MeV. In the other energy range, the variance was 2 to 7 %. Because of the lack of the experimental data around 12 MeV, present evaluated result is lower than recent evaluated data files, the IRDF-90 and JENDL Dosimetry File. Because present evaluation follows the present theoretical calculation which is lower than the IRDF-90 and JENDL Dosimetry File around 12 MeV.

4. Fission Spectrum Averaged Cross Section

To validate the present evaluated result, the fission spectrum averaged cross sections were calculated. For the $^{93}Nb(n,n')^{93m}Nb$ reaction, the ^{252}Cf fission spectrum evaluated by Mannhart /15/ was taken for the fission neutron field. The average cross section was compared with experimental data /16-22/ and average cross sections calculated using the other evaluated cross section. The average cross section calculated using present evaluated result, 145 mb, agreed with recent integral experiment as shown in Table 1.

For the $^{93}Nb(n,2n)^{92m}Nb$ reaction, thermal fission spectrum of ^{235}U of the ENDF/B-VI was taken as the fission field. The calculated average cross section was shown in Table 2 with experimental data /23-25/ and the calculation using the other evaluated data. Comparing with IRDF-90, the present average cross section was slightly lower than that of IRDF-90 because of the lower cross section of the present evaluation around 12 MeV. The response function of $^{93}Nb(n,n')^{93m}Nb$ reaction in ^{235}U fission neutron field has high sensitivity in the energy range from 10 to 12 MeV. The present average cross section is much lower than that of JENDL Dosimetry File. This attributed to the low cross section of the present evaluation all energy range. Comparing with recent experimental data of the average cross section by Williamson /25/, the present result is lower than the experimental data by 7 %.

5. Conclusion

The cross sections of dosimetry reaction of ^{93}Nb, the ^{93}Nb(n,n')^{93m}Nb and ^{93}Nb(n,2n)^{92m}Nb reaction, were evaluated based on the nuclear model calculation and statistical method using GMA, the generalized least square code. For the ^{93}Nb(n,n')^{93m}Nb reaction, the evaluated result reasonably follows the experimental data. The ^{93}Nb(n,2n)^{92m}Nb reaction cross section, however, is slightly lower than the other evaluated libraries around 12 MeV. Comparison of average cross sections in a Li(d,n) neutron field /26/ which was produced by Dynamitron accelerator, Tohoku University, will be performed to check the validity of present evaluation. Differential measurement at the energy range above 6 MeV for ^{93}Nb(n,n')^{93m}Nb, and abound 12 MeV for ^{93}Nb(n,2n)^{92m}Nb, respectively, are required to evaluate the cross sections more precisely.

Acknowledgement

The authors would like to thank Dr. N.Yamamuro of Data Engineering for his useful discussions on the nuclear model codes, and Dr. T.Nakagawa of JAERI for offering EXFOR data and various codes, and Dr. Y.Sugimoto of JAERI for providing GMA code.

References

1. N.Odano, S.Iwasaki and K.Sugiyama, The Seventh ASTM-EURATOM Symposium on Reactor Dosimetry, Strasbourg, France, 27-31 August 1990 (to be published), and NETU-54, Research Report of Department of Nuclear Engineering, Tohoku University (1990).
2. S.Igarashi, J. Nucl. Sci. Tech., Vol.12, p.67 (1975).
3. P.G.Young and E.D.Arthur, LA-6947 (1977).
4. N.Yamamuro, JAERI-M 88-140 (1988).
5. P.D.Kunz, "DWUCK", University of Colorado Report (1974).
6. A.B.Smith, P.T.Guenther and R.D.Lawson, ANL/NDM-91 (1985).
7. A.Glibert and A.G.W.Cameron, Can. J. Phys., 43, 1446 (1965).
8. A.V.Ignatyuk, INDC(CCP)-233/L (1985).
9. A.G.W.Cameron and R.M.Elkin, Can. J. Phys., Vol.43, p.1288 (1965).
10. F.Demanins, U.Abbondano and F.Raicich, Report INFN(REP)-014/88, Instit-

uto Nazionale de Legnaro, Annual Report 1987 (1988).
11. C.M.Lederer and V.S.Shirley, "Table of Isotopes, Seventh Edition", John Wiley & Sons, Inc., (1978).
12. W.P.Poenitz, BNL-NCS-51363, p.249 (1981). Modified by M.Sugimoto of JAERI for PC (Pascal) Version.
13. M.Wagner, G.Winkler, H.Vonach and H.Liskien, Proc. Int. Conf. Nucl. Data for Science and Technology, Mito, Japan, May 30 - June 3, 1988, p.1049 (1988).
14. T.B.Ryves and P.Kolkowski, J. Phys. G., Vol.7, p.529 (1981).
15. W.Mannhart, IAEA-TECDOC-410, p.158 (1987).
16. F.Hegedus, Swiss Report EIR-Bericht 195, 1971.
17. K.Kobayashi and I.Kimura, NEANDC(J)-61U, 1979.
18. K.Sakurai, Nucl. Instr. Methods, 187, 649 (1981).
19. W.G.Alberts, R.Hollnagel, K.Knauf, M.Matzke, W.Pessara, Proc. of the 4th ASTM-EURATOM Symposium on Reactor Dosimetry, NBS, 1983.
20. J.G.Willias, C.O.Cogburn, L.M.Hodgson, S.C.Apple, E.D.McGarry, G.P.Lamaze, F.J.Schima, JW Rogers, R.J.Gehrke, J.D.Baker and F.J.Wheeler, Proc. of the 6th ASTM-ERATOM Symposium on Reactor Dosimetry, ASTM STP 1001, p.235 (1989).
21. W.G.Alberts, U.Schotzig and H.Siegert, ibid., p.223 (1989).
22. T.G.Williamson, T.A.Ayers, W.L.Hammersten, G.P.Lamaze and F.J.Schima, ibid., p.229 (1989).
23. B.Strohmaier, S.Tagesen and H.Vonach, Physics Data, 13-2, p.62 (1980).
24. B.Strohmaier, Ann. Nucl. Energy, 16, p.461 (1989).
25. I.Kimura, K.Kobayashi and T.Shibata, J. Nucl. Sci. Tech., 8, p.59 (1971).
26. A.Fabry, Rep. BLG-465 (1972).
27. T.G.Williamson and G.P.Lamaze, The Seventh ASTM-EURATOM Symposium on Reactor Dosimetry, Strasbourg, France, 27-31 August 1990 (to be published).
28. J.R.Dumais, S.Iwasaki, S.Tanaka, N.Odano and K.Sugiyama, ibid., and NETU-55, Research Report of Department of Nuclear Engineering, Tohoku University (1990).

Table 1 The ^{252}Cf fission spectrum averaged cross section of the $^{93}Nb(n,n')^{93m}Nb$ reaction.

Reference	Average Cross Section (mb)	
Hegedus (1971) /16/	155 ± 55	Experiment
Kobayashi (1979) /17/	164 ± 12	
Sakurai (1981) /18/	177 ± 40	
Alberts (1983) /19/	149 ± 10	
Williams (1989) /20/	151 ± 5	
Alberts (1989) /21/	145 ± 5	
Williamson (1989) /22/	144 ± 5	
Strohmaier (1980) /23/	158 ± 16	Calculation
Strohmaier (1989) /24/	155	
IRDF-90 (1990)	143	
JENDL Dosimetry File (1990)	149	
Present Work(1990)	145	

Table 2 The ^{235}U fission spectrum averaged cross section of the $^{93}Nb(n,2n)^{92m}Nb$ reaction.

Reference		Average Cross Section (mb)	
Kimura (1971) /25/	(1)	0.432 ± 0.033	Experiment
Kimura (1971) /25/	(2)	0.402 ± 0.034	
Fabry (1971) /26/		0.47 ± 0.03	
Williamson (1990) /27/		0.433 ± 0.001	
Strohmaier (1989) /24/	(3)	0.44	Calculation
Strohmaier (1989) /24/	(4)	0.43	
IRDF-90 (1990)	(5)	0.412	
JENDL Dosimetry File(1990)	(5)	0.478	
Present Work (1990)	(5)	0.404	

Comments: (1) reactor spectrum.
(2) fission plate.
(3) NIST fission spectrum was used for the calculation.
(4) ENDF/B-V fission spectrum was used for the calculation.
(5) ENDF/B-VI fission spectrum was used for the calculation.

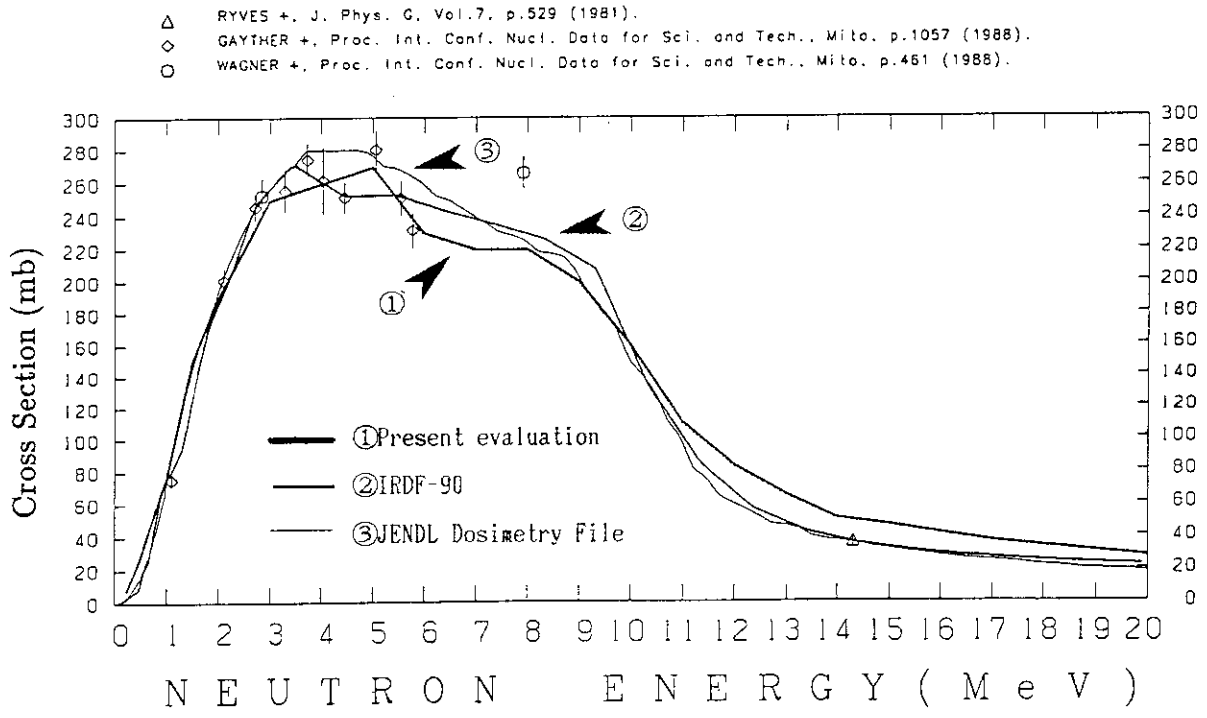

Fig. 1 The evaluated $^{93}Nb(n,n')^{93m}Nb$ reaction cross section.

Correlation matrix of the result: DIFF. INELASTI DIFF. INELASTI

		1	2	3	4	5	6	7	8	9	10	11	12	13	14	15	16	17	18	19	20	21	22	23	24	25
1	0.25[MeV]	1000																								
2	0.50[MeV]	95	1000																							
3	0.75[MeV]	95	95	1000																						
4	1.00[MeV]	81	81	81	1000																					
5	1.50[MeV]	95	95	95	81	1000																				
6	2.00[MeV]	98	98	98	237	98	1000																			
7	2.50[MeV]	103	103	103	273	103	318	1000																		
8	3.00[MeV]	78	78	78	148	78	173	196	1000																	
9	4.00[MeV]	106	106	106	313	106	362	420	221	1000																
10	5.00[MeV]	95	95	95	214	95	249	286	159	325	1000															
11	6.00[MeV]	99	99	99	270	99	313	362	194	416	282	1000														
12	7.00[MeV]	95	95	95	81	95	98	103	78	106	95	99	1000													
13	8.00[MeV]	87	87	87	77	87	93	98	104	102	90	95	87	1000												
14	9.00[MeV]	95	95	95	81	95	98	103	78	108	95	99	95	87	1000											
15	10.00[MeV]	95	95	95	81	95	98	103	78	106	95	99	95	87	95	1000										
16	11.00[MeV]	95	95	95	81	95	98	103	78	106	95	99	95	87	95	95	1000									
17	12.00[MeV]	95	95	95	81	95	98	103	78	106	95	99	95	87	95	95	95	1000								
18	13.00[MeV]	95	95	95	81	95	98	103	78	106	95	99	95	87	95	95	95	95	1000							
19	14.00[MeV]	88	88	86	73	88	88	93	71	96	87	90	86	79	86	88	88	86	88	1000						
20	15.00[MeV]	95	95	95	81	95	98	103	78	106	95	99	95	87	95	95	95	95	95	88	1000					
21	16.00[MeV]	95	95	95	81	95	98	103	78	106	95	99	95	87	95	95	95	95	95	86	95	1000				
22	17.00[MeV]	95	95	95	81	95	98	103	78	106	95	99	95	87	95	95	95	95	95	88	95	95	1000			
23	18.00[MeV]	95	95	95	81	95	98	103	78	106	95	99	95	87	95	95	95	95	95	86	95	95	95	1000		
24	19.00[MeV]	95	95	95	81	95	98	103	78	106	95	99	95	87	95	95	95	95	95	88	95	95	95	95	1000	
25	20.00[MeV]	95	95	95	81	95	98	103	78	106	95	99	95	87	95	95	95	95	95	86	95	95	95	95	95	1000

Fig. 2 Correlation matrix of the evaluated $^{93}Nb(n,n')^{93m}Nb$ reaction cross section.

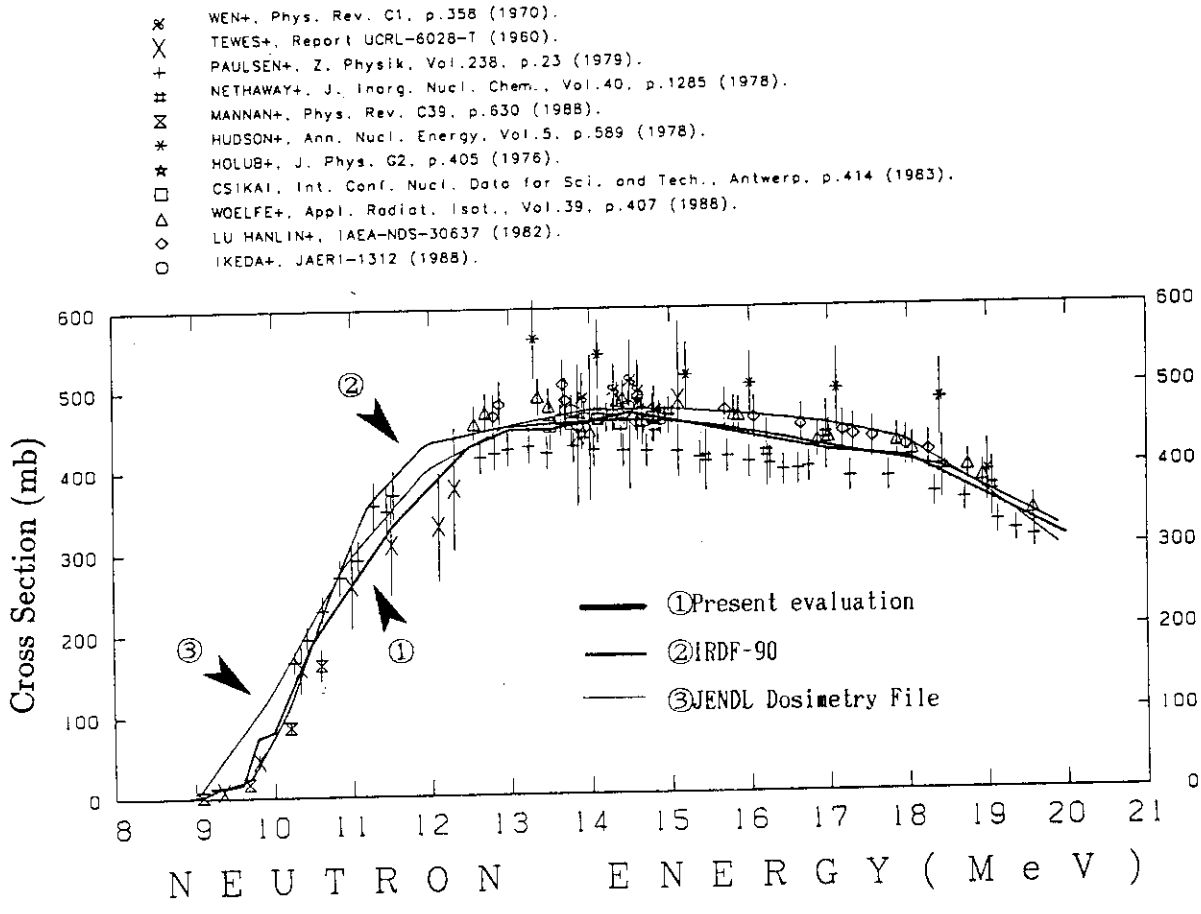

Fig. 3 The evaluated $^{93}Nb(n,2n)^{92m}Nb$ reaction cross section.

Correlation matrix of the result:ODANO+ 1990 EVAL ODANO+ 1990 EVAL

		1	2	3	4	5	6	7	8	9	10	11	12	13	14	15	16	17	18	19
1	9.20[MeV]	1000																		
2	9.40[MeV]	421000																		
3	9.60[MeV]	17	141000																	
4	9.80[MeV]	43	37	141000																
5	10.00[MeV]	35	48	32	291000															
6	10.50[MeV]	39	33	26	33	331000														
7	11.00[MeV]	43	38	15	37	29	451000													
8	11.50[MeV]	43	36	15	37	29	46	471000												
9	12.50[MeV]	33	28	11	29	22	49	47	481000											
10	13.00[MeV]	35	29	12	29	23	72	67	68	951000										
11	13.50[MeV]	31	26	11	26	21	54	51	52	103	1241000									
12	14.00[MeV]	36	30	13	31	24	66	62	64	113	149	5841000								
13	14.50[MeV]	34	29	12	29	23	63	59	61	111	143	571	8031000							
14	15.00[MeV]	36	30	13	31	24	66	62	64	113	149	584	999	8031000						
15	16.00[MeV]	35	29	12	30	24	81	74	77	137	200	170	204	193	2041000					
16	17.00[MeV]	33	27	12	28	22	69	64	66	124	172	154	181	172	181	2181000				
17	18.00[MeV]	31	25	11	26	21	58	55	56	114	144	141	163	155	163	188	1711000			
18	19.00[MeV]	34	28	12	28	23	72	66	68	124	164	148	178	168	178	213	182	1551000		
19	20.00[MeV]	32	26	11	27	22	48	46	47	84	95	88	100	98	100	125	109	96	1141000	

Fig. 4 Correlation matrix of the evaluated $^{93}Nb(n,2n)^{92m}Nb$ reaction cross section.

3.4 Measurements of Double-differential Neutron Emission Spectra of ^{238}U and ^{232}Th at Incident Energy of 18 MeV

S.Matsuyama, M.Baba, T.Ito, K.Maeda, N.Ito, H.Nakamura and N.Hirakawa
Department of Nuclear Engineering, Tohoku University
Aoba, Aramaki, Aoba-ku, Sendai 980, Japan

Double-differential neutron emission spectra of ^{238}U and ^{232}Th have been measured for 18 MeV incident neutron energy using Tohoku university Dynamitron time-of-flight spectrometer. The results of neutron emission spectra of both nuclides show marked difference from evaluated nuclear data in the energy region above about 8 MeV. The angular distributions of the continuum neutrons show forward rise in the higher energy region, and reproduce fairy well with Kalbach-Mann systematics.

1. Introduction

The neutron emission spectra for fast neutron interaction with ^{238}U and ^{232}Th are important nuclear data for the design of accelerator-breeder reactors and for the research of nuclear reaction mechanism of fissioning nuclides. However no data are available at the incident energy higher than 14 MeV.

The emission neutrons from these nuclides consist of those by scattering and fission. In the high-energy neutron induced reaction, fission neutrons will account for larger fraction of emitted neutrons through multiple-chance-fissions. Therefore in the model calculation of neutron emission, competition between scattering and fission processes should be considered in strict manner. The data of neutron emission spectra are expected as reference data for the theoretical calculations/1/.

2. Experiments and Data Analyses

The experiments were carried out employing time-of-flight technique using Tohoku university 4.5 MV Dynamitron accelerator as the pulsed neutron generator. The experimental technique and the data analysis are almost the same as those in previous studies/2,3,4,5/. In this study, a post-acceleration beam chopper/4/ was applied in order to improve overall energy resolution.

Primary neutrons of 18 MeV were obtained via the d-T reaction at the

emission angle of 0 degree by bombarding a Ti-T metallic target with pulsed deuteron beam about 1.5 nsec duration at 2 MHz repetition rate. The energy spread of primary neutrons was less than 400 keV. In order to minimize the background due to parasitic neutrons, we employed a virgin Ti-T target. Because of higher deuteron beam energy than in 14 MeV measurements, parasitic neutrons were produced significantly by bombardment of contaminant elements in Ti-T target, i.e., carbon and deuteron, with deuteron beam. They distorted the observed neutron emission spectra in energy region lower than a few MeV.

The scattering samples were metallic cylinders of elemental uranium and thorium, 2 cm in dia. and 5 cm long, and encapsulated in thin aluminum containers. They were placed 12 cm from the target.

Emitted neutrons were detected by a NE213 liquid scintillator, 14 cm in dia. and 10 cm thick, located about 4 m from the sample. Two separate neutron-gamma pulse shape discriminators, biased at 3 and 0.6 MeV of proton, were used to suppress gamma-ray backgrounds. The high-bias and low-bias systems provided the data, respectively, for energy region above around 5 MeV and lower energy region. The detector was connected to a standard time-of-flight circuit consisting of a constant-fraction timing-discriminator and a time-to-amplitude converter. The time resolution of the present system was about 2.5 nsec.

Energy dependence of detector efficiency was determined by the time-of-flight measurements of fission neutrons from ^{252}Cf for the region lower than 4 MeV and the calculation using O5S code for higher energy region. The absolute value of the cross section was determined referring the standard n-p scattering cross section.

Another NE213 scintillation detector, 2" in dia and 2" long, was used for neutron monitor to provide the normalization between sample-in and sample-out runs.

The neutron emission spectra of both elements were measured at several angles between 30 and 120 degree. For each measurement, remote-controlled sample-changer was used to change the samples without stopping the beam.

The raw data were corrected for the effects of 1)sample-out background, 2)sample activity, 3)finite sample size and 4)parasitic neutrons. Sample-out backgrounds were measured with the empty can in sample position. Backgrounds due to sample activity were found to be significant and subtracted as flat backgrounds. The influence of finite sample-size and para-

sitic neutrons was estimated by Monte-Calro calculations using a program "SYNTHIA"/6/. This code provides "Real" and "Ideal" spectra which are these, respectively, with and without multiple-scattering and flux attenuation, considering energy-angular distributions of neutrons out-going from sample. Ratio of "Ideal" and "Real" spectra served the correction factor for each neutron energy. The data used in the calculation were taken from JENDL-3. However, as shown later, the neutron emission spectra in JENDL-3 were largely different from experiments. Therefore to make correction adequate, neutron emission spectra were modified using experimental data and Kalbach-Mann (K-M) systematics/7/ in the manner described in the next section.

In the actual correction, "Ideal" and "Real" spectra were calculated both for primary 18 MeV neutrons and for parasitic neutrons. The intensity and the spectrum of parasitic neutrons were determined by measuring the source spectra before and after scattering experiments. In order to consider their time dependence due to accumulation of contaminant elements, "Real" spectra for parasitic neutrons were evaluated by interpolation between the two simulated spectra corresponding to each source spectrum. "Real" spectra for parasitic neutrons were added to "Real" spectra for primary 18 MeV neutrons in order to simulate observed neutron emission spectra which were distorted with the effects of 3) & 4). Figure 1 shows the typical simulated spectra in comparison with the raw data and the correction factors.

3. Results and Discussion

Typical neutron emission spectra of ^{238}U and ^{232}Th are shown in Figs.2 and 3, respectively, compared with the data derived from JENDL-3 and ENDF/B-IV. The neutron emission spectra of these elements are very similar with each other while contribution of fission neutrons are much less for ^{232}Th.

The experimental spectra of ^{238}U show marked forward rise in the continuum region above 8 MeV and disagree with JENDL-3 in this region since pre-equilibrium component is lacking in JENDL-3. The data derived from ENDF/B-IV, which represents the pre-equilibrium component employing pseudo-levels, still underpredict around 11 MeV.

The neutron emission spectra of ^{232}Th have similar tendency with those of ^{238}U. The experimental data are traced better by JENDL-3 compared with ENDF/B-IV. Nevertheless in the region above 8 MeV, there still exists

discrepancy between experimental spectra and the data from JENDL-3. This difference will be attributed primarily to the lack of angular dependence of emission spectra in JENDL-3

The angular distributions of continuum neutrons of ^{238}U and ^{232}Th are illustrated in Figs.4 and 5, respectively, compared with the calculations based on the systematics proposed by Kalbach-Mann (K-M)/7/ and Kalbach/8/. The fraction of pre-compound reaction was derived by fitting the angle-integrated experimental spectrum with the superposition of exciton spectrum/9/, cascade-neutron emission spectrum/10/ and fission spectrum. The calculated spectra are shown in Figs.6 and 7. In the calculation, the contribution of fission neutrons are assumed to be isotropic spectrum with the shape given by JENDL-3. The K-M systematics reproduces the experimental results better than the Kalbach systematics while it has been pointed out that the K-M systematics overemphasize the forward rise of the angular distributions for non-fissionable nuclides(see Fig.8/5/). Similar results were observed for 14 MeV incident neutrons. The fact that the results of ^{232}Th have similar tendency with those of ^{238}U will imply that the scattered neutrons from these nuclides have forward rise steeper than for light elements, since fission neutrons from ^{232}Th are much less than those from ^{238}U.

4. Summary

We have measured double-differential neutron emission spectra of ^{232}Th and ^{238}U for incident energy of 18 MeV and derived 1)the double-differential neutron emission cross section and 2)the angular distribution of continuum neutrons. The emission spectra of ^{238}U derived from JENDL-3 greatly under predict the continuum neutrons. The spectra of ^{232}Th are traced generally by JENDL-3 data but differ in the continuum region in forward angle. The angular distribution of continuum neutrons are traced well by K-M systematics for both nuclides.

Reference

1. H.Kalka et.al. ;Proc.Int.Conf. "Nucl. Phys.", Gaussig,1987, ZfK-646 p.24(1988)

2. M.Baba et.al. ;Proc.Int.Conf. "Nucl. Data for Sci. & Technol.",1988, Mito, p.253(1988)

3. M.Baba et.al. ;J.Nucl.Sci.Technol., 27(7) p.601(1990)

4. M.Baba et.al. ;JAERI-M, 90-025, p.383

5. M.Baba et.al. ;Proc.Int.Conf. "Nucl. Data for Sci. & Technol.",1988, Mito, p.291(1988)

6. T.Sakase ;private communication

7. C.Kalbach & F.M.Mann ;Phys.Rev., C23(1) p.112(1982)

8. C.Kalbach, ;Phys.Rev., C37(6) p.2350(1988)

9. M.Blann & F.M.Lanzafame;Nucl.Phys., A142 p.559(1970)

10. M.LeCouteur & D.W.Lang ;Nucl.Phys., 13 p.32(1959)

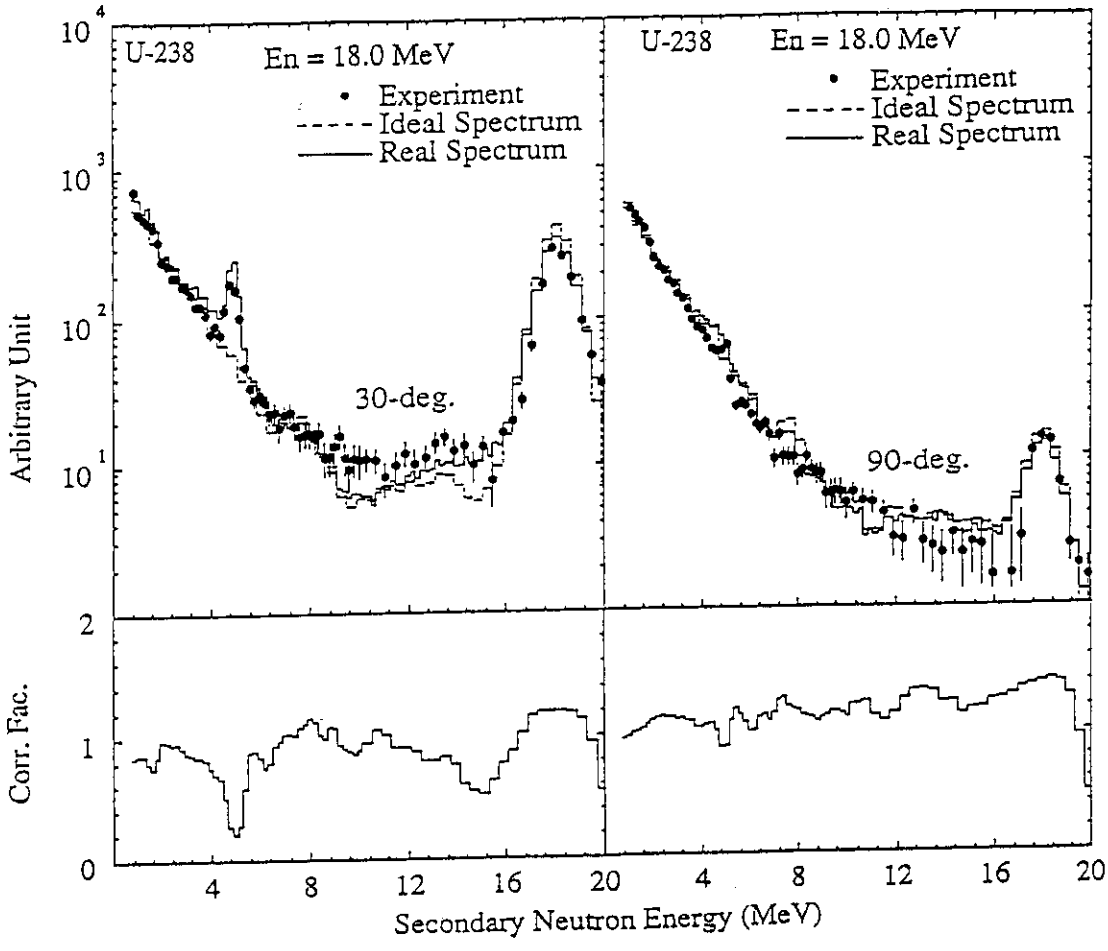

Fig. 1 Calculated and observed neutron emission spectra, and correction factors for sample-size effect.

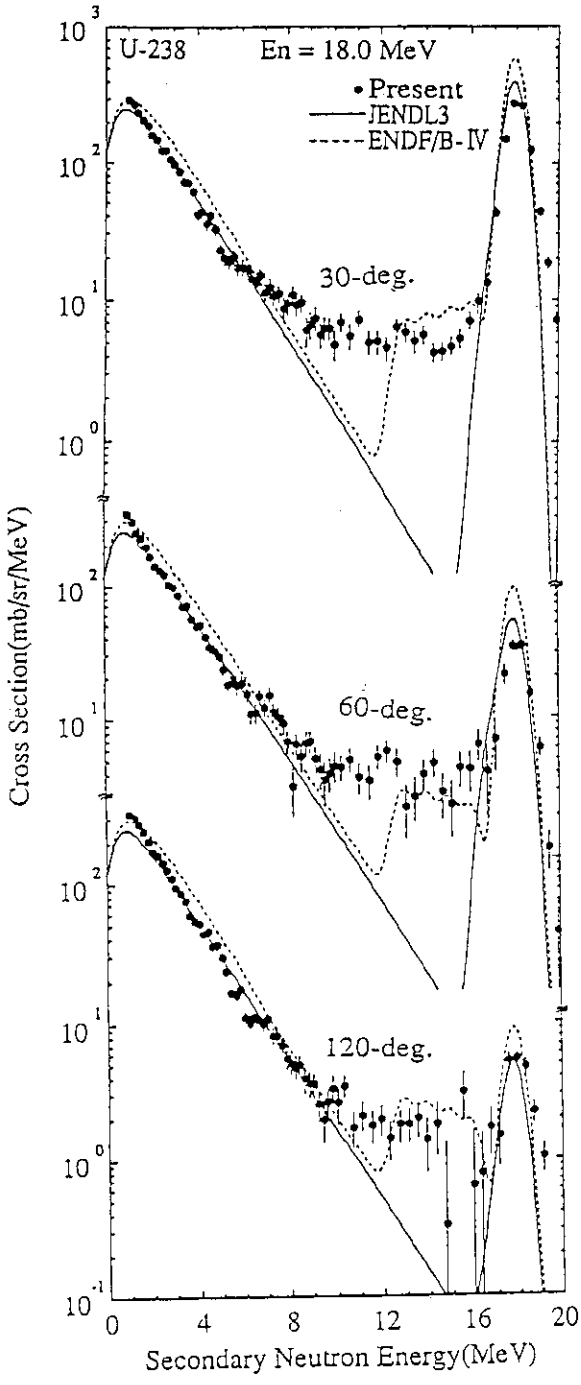

Fig. 2 Neutron emission spectra of ^{238}U for the incident energy of 18 MeV

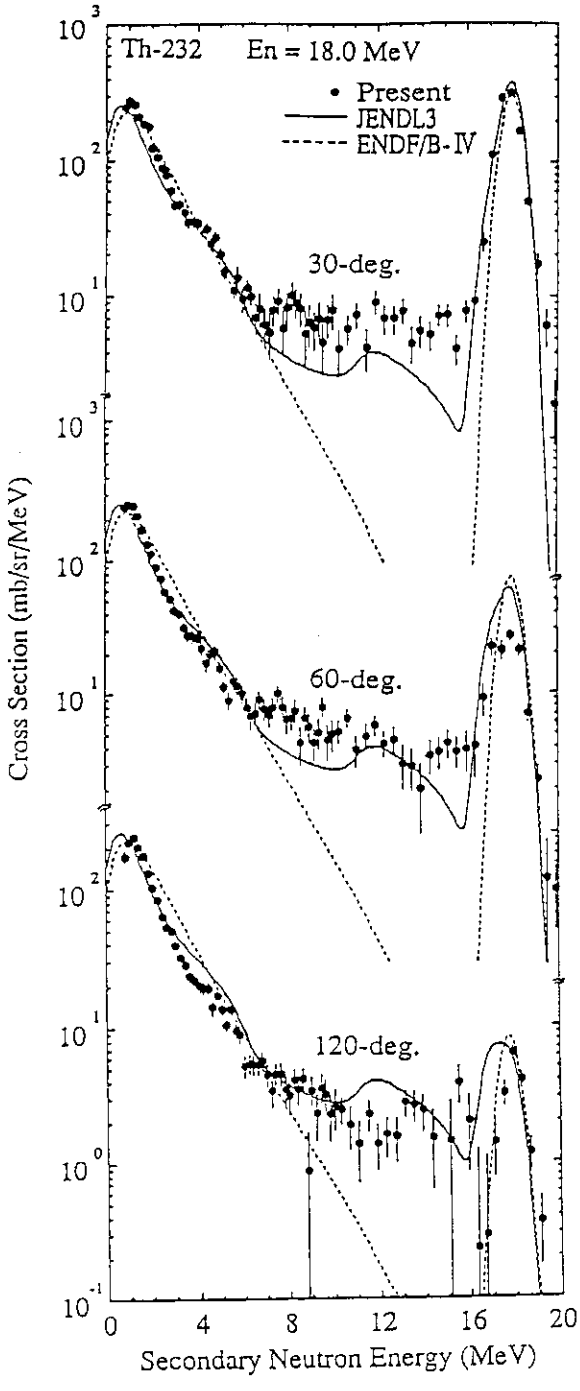

Fig. 3 Neutron emission spectra of ^{232}Th for the incident energy of 18 MeV

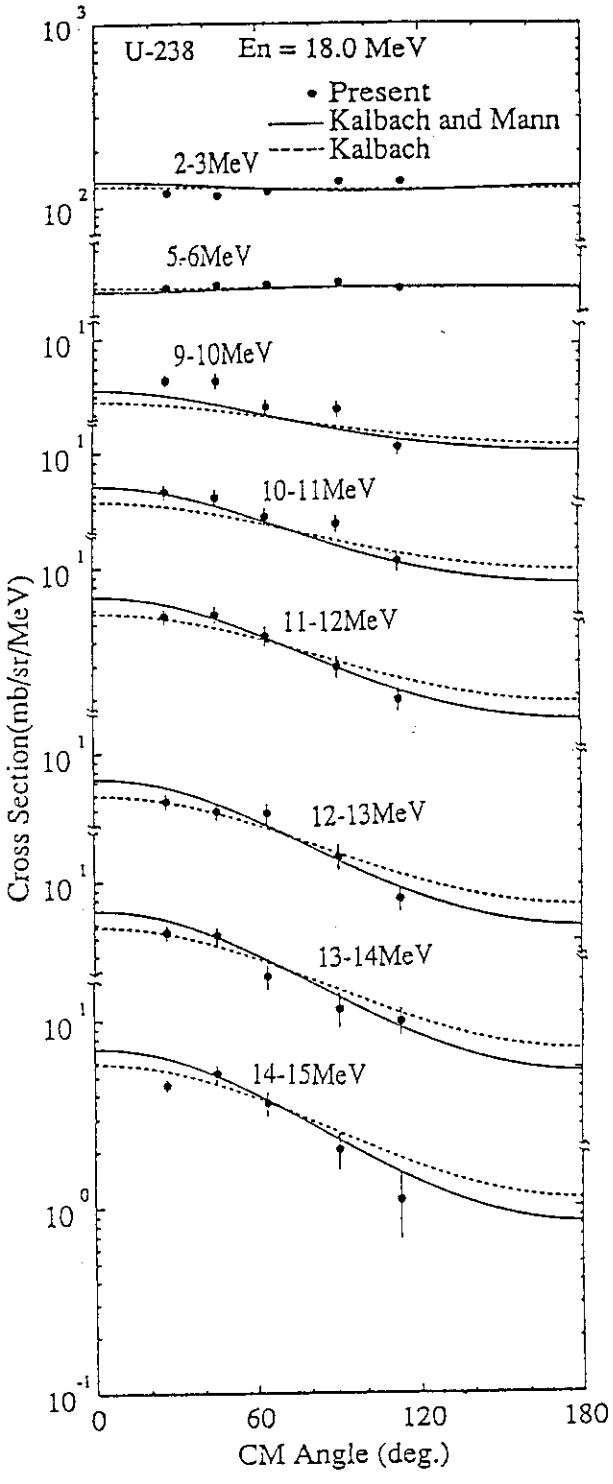

Fig. 4 Angular distribution of secondary neutrons from ^{238}U.

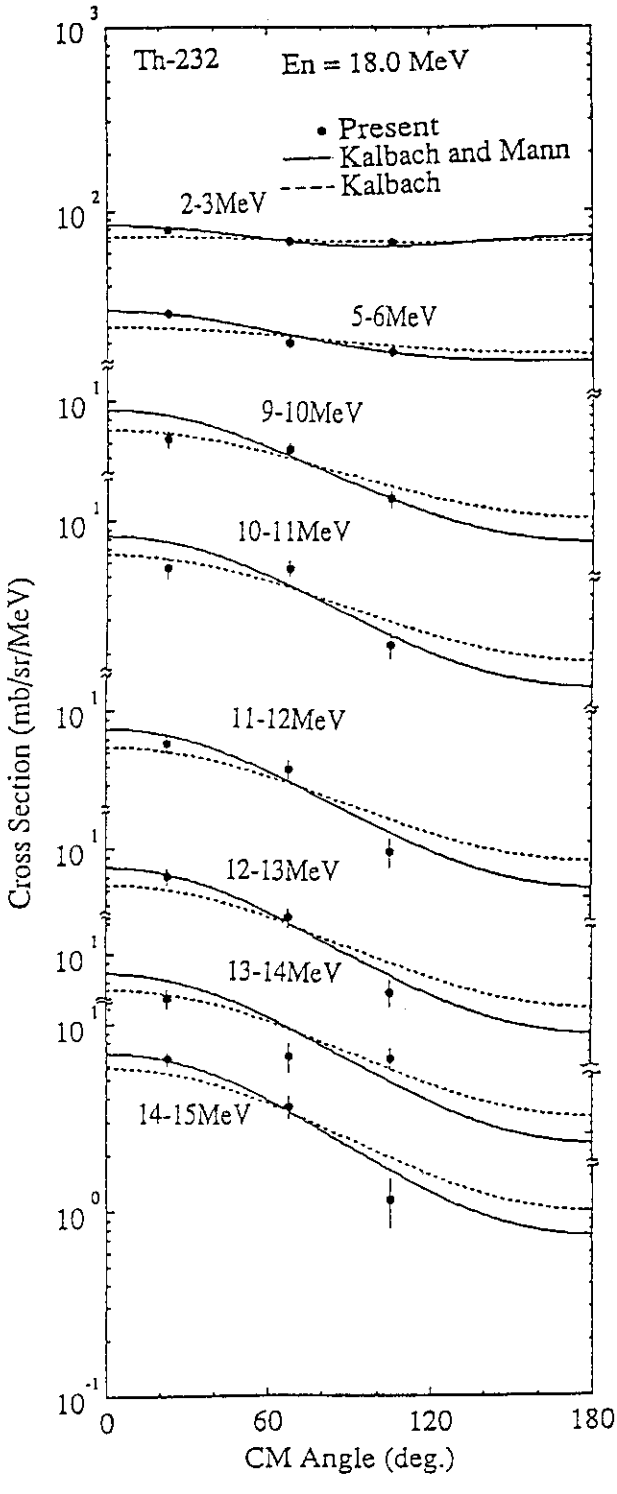

Fig. 5 Angular distribution of secondary neutrons from ^{232}Th.

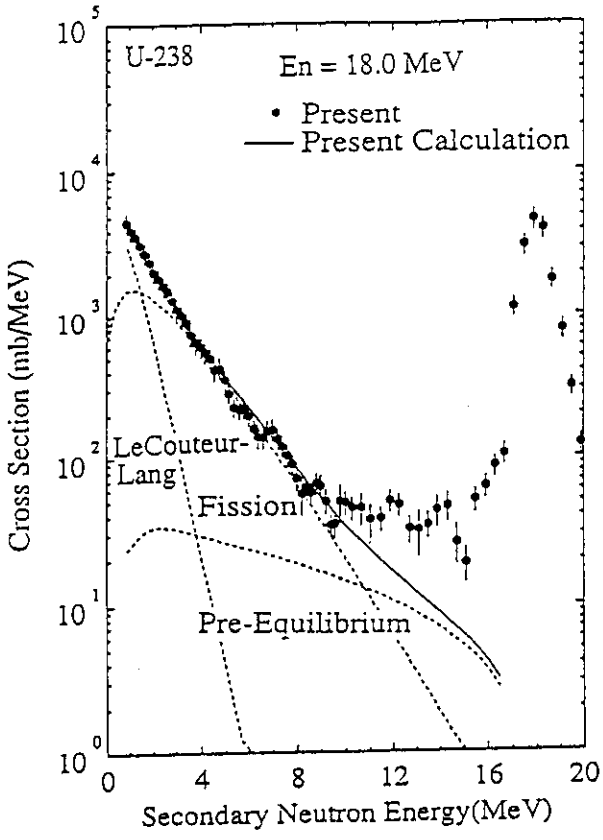

Fig. 6 Angle integrated neutron emission spectrum of ^{238}U.

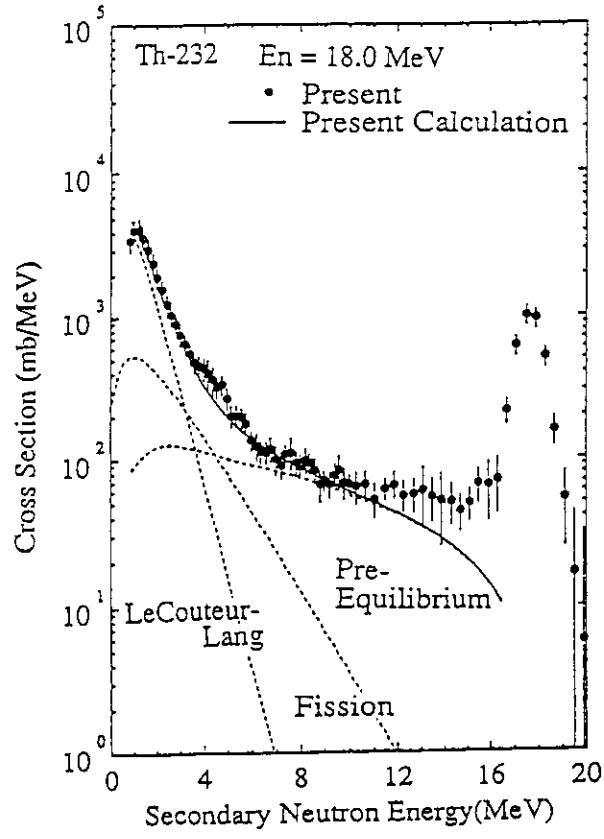

Fig. 7 Angle integrated neutron emission spectrum of ^{232}Th.

3.5 Measurement of Double Differential Neutron Emission Cross Sections at 14.1 MeV for Ti, Mo, Sn and Sb

Masami Gotoh and Akito Takahashi

Department of Nuclear Engineering,
Faculty of Engineering, Osaka University
2-1, Yamada-Oka, Suita, Osaka

Abstract

Double differential neutron emission cross sections at incident neutron energy of 14.1 MeV were measured for 16 angle-points from 15 deg to 160 deg in the laboratory (LAB) system for Ti, Mo, Sn and Sb, using a fixed 8.3 m TOF facility at OKTAVIAN. The secondary neutron energy region covered in the experiments is from 1 MeV to 15 MeV. Statistics and energy resolutions of obtained data are satisfactory. The results of experiments are compared with evaluated nuclear data files, and some discrepancies were found. We also performed theoretical calculations of neutron emission spectra for compound and precompound nuclear processes, and also calculated angular distributions using the Kalbach & Mann and the Kumabe systematics. In graphs, comparisons with evaluated data and results of calculations are shown.

1. Introduction

Double differential neutron emission cross section (DDX) is secondary neutron distribution data with respect to secondary neutron energy and scattering angle. DDXs at the incident neutron energy of 14.1 MeV are important in fusion application for the estimation of primary knock-on atom spectra and kerma factors as well as for the neutronics calculations of blankets, shielding materials and structures. Experimental DDXs data have been also used for the assessment of nuclear reaction models for evaluation works. Up to now many experimental data around 14 MeV have been accumulated for many nuclei[1], but data for other nuclei are still requested. In other energy region, data remain still so scarce that extrapolation based on theoretical nuclear model has to be done for evaluation works.

This paper shows DDX data at En=14.1 MeV for Ti, Mo, Sn and Sb recently measured at OKTAVIAN. Ti is considered as constituent of first wall material in fusion reactor. Mo is expected to be a divertor plate. Sn is a candidate of superconductors. So accurate experimental data are requested. Sb is one of the elements which consist of compound semiconductors. As for such elements that will compose semiconductors, experimental DDX data as well as evaluate data are scarce.

2. Experiment

Using the time of flight facility (8.3 m neutron flight path) with a liquid scintillator of NE213(25.4 cm diam.x 10 cm thick) at OKTAVIAN[2], the experiments were carried out. The neutron flight path is constructed in 85 deg against the deuteron beam line. A shadow bar, collimator and pre-collimator are set up along the flight path to shield direct and room-scattered neutrons. The pulsed D-T neutron source of OKTAVIAN is operated with <2 ns pulse width at FWHM and 1 MHz repetition frequency. As scattering samples, cylindrical metal rods with 3 cm in diameter and 7 cm in length were used. For changing the scattering angle, a sample is moved around the TiT target. Other details of our experimental method are described elsewhere.[3] The calibration of DDX values is done in usual way: cross sections of hydrogen elastic scattering which are measured for 7 angles(20-50 deg in the LAB system) with a 1.5 cm diam. x 3.0 cm long polyethylene sample, are normalized to be equal to the corresponding differential cross sections given in ENDF/B-IV.[4] For multiple scattering corrections, the MUSCC3 code[5] was used by adopting evaluated data; JENDL-3[6] for Ti,Mo and Sb, ENDL75[7] for Sn. The energy resolution of the experiment was $\pm$ 0.25 MeV at En'=14 MeV, and $\pm$ 0.02 MeV at En'=1.1 MeV.

3. Results and Discussions

Graphs of DDX data are given in Fig.1-8, for only two angles each element due to the limitation of paper, compared with evaluated nuclear data files which are also used for multiple scattering corrections. The experimental data in the LAB system are once converted to those in the center-of-mass (C.M.) system and integrated over scattering angles to obtain neutron emission spectra(EDX; Energy Differential neutron emission Cross section). As the result of comparison with evaluated data, some descrepancies are found especially for discrete inelastic

scatterings by the direct processes. Evaluated spectra of compound nuclear processes of the whole elements are agreeable with experimental neutron emission spectra in the low energy region 1-5 MeV. Disagreements between experiments and evaluated data in the 5-10MeV region have been resolved by the SINCROS-II[8] calculation, which treated properly the compound and precompound nuclear processes, as shown in Fig.9-12. Agreements are good for angular distributions between experimental ADX(Angular Differential neutron emission Cross section) data and calculations using two systematics of the Kalbach & Mann[9] and the Kumabe[10], as shown in Fig.13-16. In the following, we discuss details for individual elements.

3.1 Titanium

The peak around 14 MeV corresponds to elastic scattering, and the broad peak at around 10 MeV in the 50 deg data correspond to the collective excitation by the direct process. The scattering sample is composed of 5 isotopes (natural sample). Taking energy resolution (< 0.4 MeV at outgoing neutron energy around 10 MeV) into consideration, the broad peak contains several discrete inelastic scatterings with different excitation cross sections of 5 isotopes. The Q-values of 5 isotopes distribute within the range from -3.5 MeV to -4.2MeV. Cross Sections of these levels are very underestimated in the evaluated data JENDL-3. Calculations based on the DWBA method with useful parameters are required for future evaluations. We show the data only for 50 deg and 120 deg, due to the page limitation of the paper. Shapes of neutron emission spectra, except for discrete inelastic scatterings, are well estimated in JENDL-3. However with respect to angular distributions, some disagreements appear. In the region of En'=3 MeV to 8 MeV, spectra are underestimated in forward angles and significantly overestimated in backward angles.

The result of calculation for neutron emission spectrum except the direct process, using the SINCROS-II, shows good agreement with the experimental data in the 1-9 MeV energy region. The calculation was only done for ^{48}Ti(abundance raio:73.7%) because discrete level data of Z=20 for other isotopes are not available, and we considered that the neutron emission spectra of other isotopes, except the direct process, are not so different. Used level density parameters are shown in Table1. The parameters are determined by neutron emission spectra and charged particle emission cross sections. In determining a daughter nucleus of alpha particle emission reaction(except for compound nucleus of even-even), we have been pointed out the necessity to consider another

parameter.[11] As for the angular distributions shown in Fig.13, both of the Kalbach & Mann and the Kumabe systematics give good agreements with experiment, and considerable difference between the two cannot be found.

3.2 Molybdenum

As shown in graphs, almost the same thing with Ti can be said with respect to the peaks from direct processes, since the scattering sample contains 7 isotopes. Q-values of discrete inelastic scatterings distribute in the range from -1.4 MeV to -3.4 MeV. The drastic underestimation of discrete (n,n') reactions in JENDL-3 is seen. The model which was used for the evaluation work should be changed; in the evaluation for inelastic scatterings in JENDL-3, the spherical optical model and the statistical model are used. In the region of En'=4-9 MeV, the spectra of all angles are underestimated, and this tendancy is more significant in forward angles. In this energy region, experimental data have angular distributions, which tend to become larger in forward angles. Below 4 MeV, where secondary neutrons by the Mo(n,2n) reaction are dominant, good agreements are seen in whole angles. The result of calculation (used level density parameters are taken from SINCROS-II) shows fairly good agreement with experimental EDX data in the 1-9 MeV region. For angular distributions shown in Fig.15, the results with the Kumabe's systematics look better than those with the Kalbach & Mann's systematics.

3.3 Tin

The peaks around 14 MeV corresponds to elastic scattering, which is well estimated in ENDL75. In the 5-13 MeV region of outgoing neutron energy, we can see structures by direct inelastic scattering. Q-values of a broad peak seen in EDX in the C.M. system in Fig.11 are ranged from -1.9 MeV to -3.1 MeV. A bump in the 5-10 MeV may be attributed to possibile excitation of the low energy octapole resonance by the direct process. In ENDL75, no estimations of discrete inelastic scatterings by the direct process are performed. Besides, the shape of spectra is different in the 5-13 MeV range. However, considering that it passed over 10 years since the evaluation for Sn was done, the disagreement can be understood.

The results of calculation for EDX shows good agreement with our experimental data. Used level density parameters are taken from SINCROS-II. The calculation is carried out for major 8 isotopes, and other 3 isotopes were ignored because abundance rates are below 1%. About the angular distributions shown in Fig.11,

slight disagreements are observed in lower energy region.

3.4 Antimony

We see the elastic peaks around 14 MeV, the discrete inelastic scattering peaks (Q= -1.0 to -4.0 MeV), and structures in the En'=5-11 MeV; the situation is almost the same with Sn. Except discrete inelastic scatterings by the direct process, evaluated nuclear data are rather agreeable with the experimental data. In detail, underestimation can be found above 3 MeV in forward angles and overestimation in backward angles. This is because that experimental data have angular distributions but the evaluated data neglect angular distributions.

The results of calculation (used level density parameters are from SINCROS-II) shows fairly good agreement with our data. For angular distributions, calculation shows smaller values in the 1-3 MeV region. The result of EDX calculation gives slightly smaller values below 3 MeV. Similary disagreements can be seen for Sn. These cannot be inproved by the change of the Kalbach constant.

4. Conclusion

Double differential neutron emission cross sections (DDX) at En=14.1 MeV for 15-160 deg angle-points have been measured with satisfactory energy resolution and counting statistics for Ti, Mo, Sn and Sb. Compared with evaluated data, some descrepancies were found. With respect to discrete excited states by inelastic scatterings, underestimations in JENDL-3 are pointed out for all elements. For elastic scatterings of 4 elements, agreements are seen especially in forward angles (below 40 deg). Fairly good agreements are seen in continuum neutron emissions by the compound nuclear process. To the precompound nuclear process, underestimations were pointed out except for Sb. Some problems still remain in angular distributions.

Angle-integrated neutron emission spectra in the C.M. system were deduced by integrating DDXs over the scattering angle. The results of calculations for compound and precompound nuclear processes using SINCROS-II gave good agreements with the experimental data. As for angular distributions, good agreements could be seen for Ti and Mo. Especially for Ti, both of the Kalbach & Mann and the Kumabe systematics gave good results. For Mo, the calculation using the Kumabe systematics shows better agreement. For Sn and Sb, overestimations in lower energy regios were seen. Within the present study, better agreements were seen in lighter elements like Ti(Z=22) than heavier elements like Sn and Sb(Z=50,51).

Reference

(1) Takahashi,A.,et al.,J.Nucl. Sci. and Technol.,16,1-15 (1979)
(2) Sumita, K.,et al.,Nucl.Sci. and Eng.,106,249-265 (1990)
(3) Takahashi,A.,et al.,J.Nucl. Sci. and Technol.,25,215-232 (1988)
(4) ENDF/B Summary documentation, BNL-NCS-17451 (1975)
(5) Ichimura, E.,Takahashi, A.,OKTAVIAN Rep.,A-87-02, Osaka Univ. (1987)
(6) JENDL Compilation Group (Nuclear Data Center, JAERI), JENDL-3
(7) LLNL Nuclear Data Libaries, Private Communication by R.J.Howerton
(8) YAMAMURO, N.,JEARI-M,90-006 (1990)
(9) Kalbach,C.,Mann, F.M.G., Phys.Rev.,C23,1121 (1981)
(10) Kumabe, I.,et al., Nucl. Sci. and Eng.,104,280-287 (1990)
(11) YAMAMURO, N.,Private communucation at Nuclear Data Sysmposium (1990)

Table 1 Level density parameters for Ti-48 used in the SINCROS-II

	Ca	Sc	Ti
45	10.5		
46			8.0
47		7.0	8.9
48		6.8	7.5
49			8.0

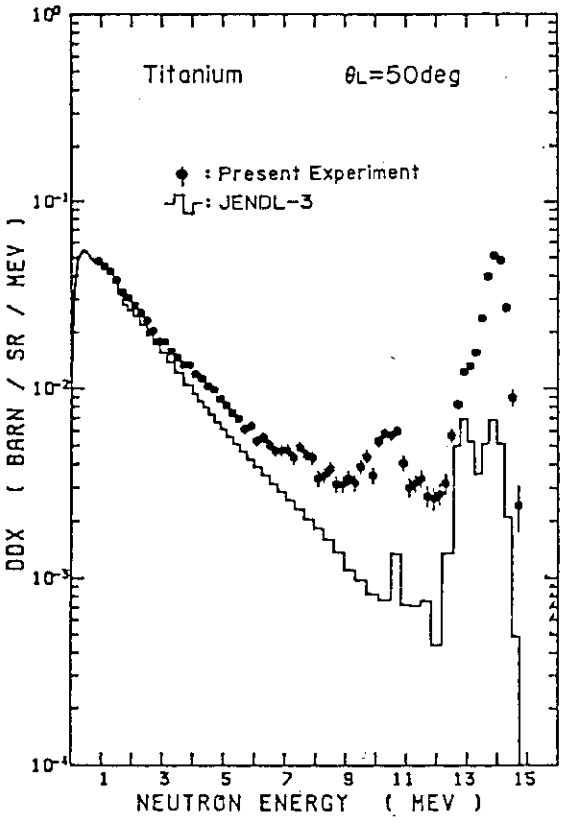

Fig. 1 DDX at 50 deg for Ti

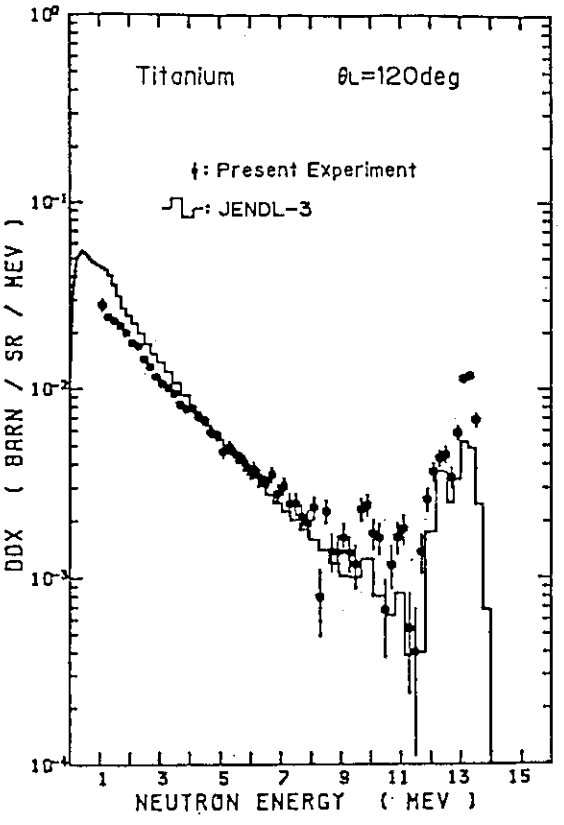

Fig. 2 DDX at 120 deg for Ti

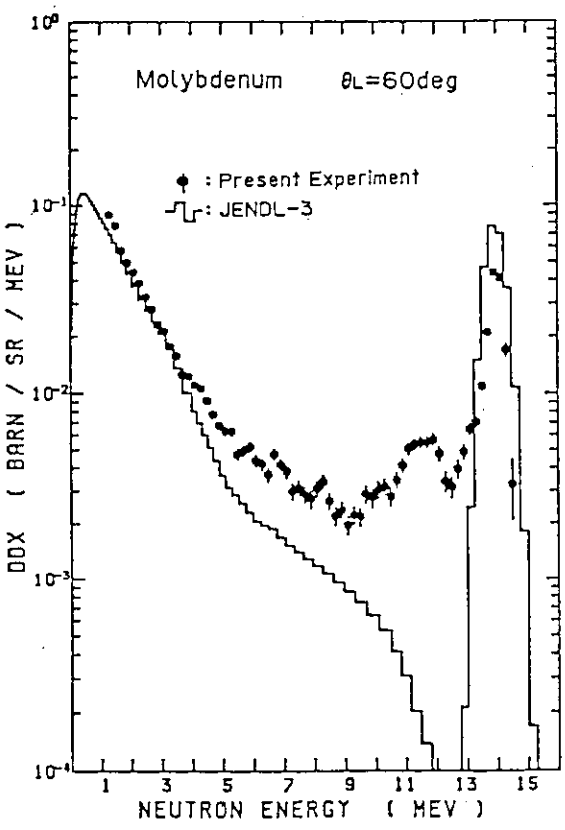

Fig. 3 DDX at 60 deg for Mo

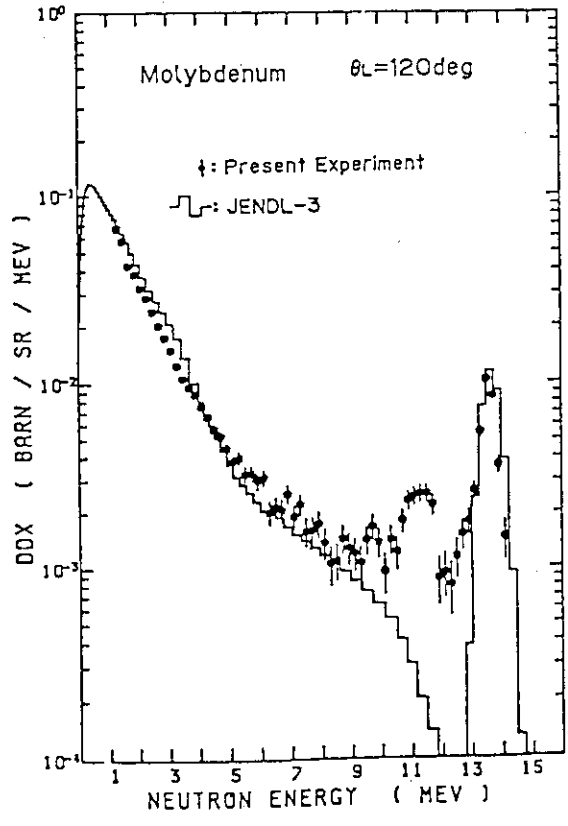

Fig. 4 DDX at 120 deg for Mo

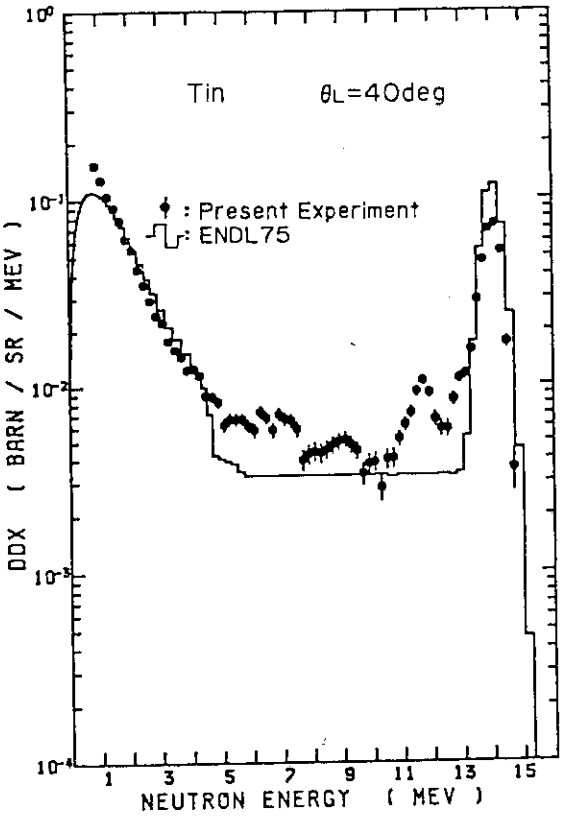

Fig. 5 DDX at 40 deg for Sn

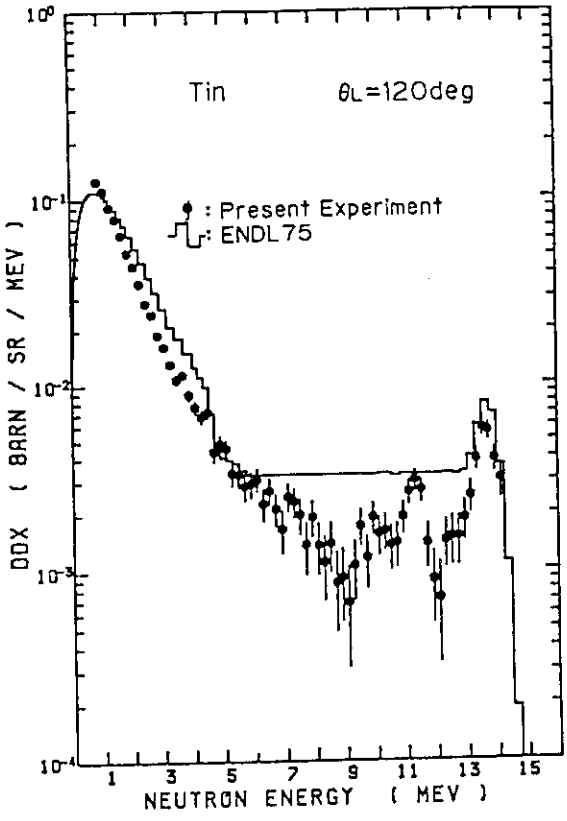

Fig. 6 DDX at 120 deg for Sn

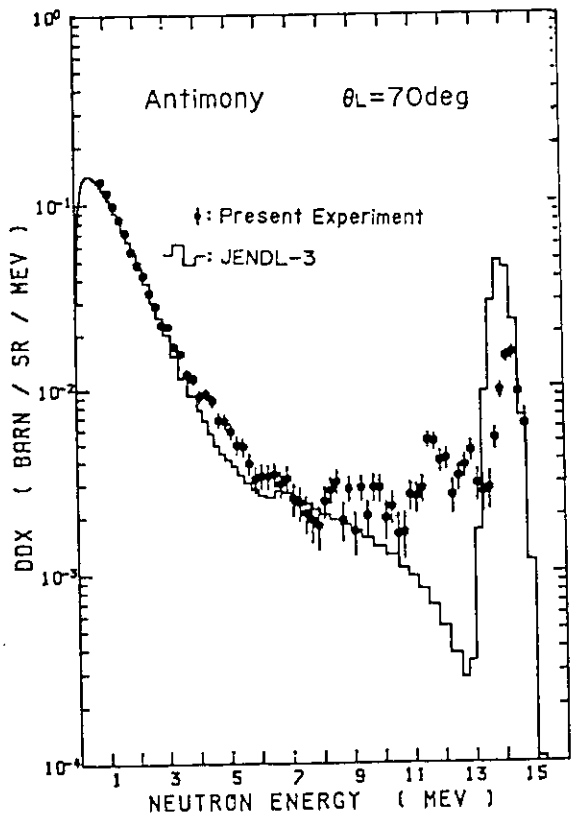

Fig. 7 DDX at 70 deg for Sb

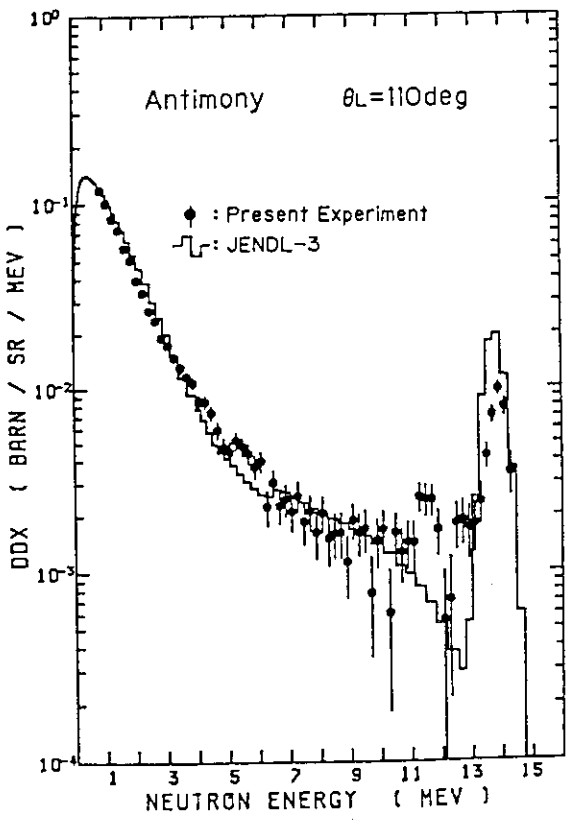

Fig. 8 DDX at 110 deg for Sb

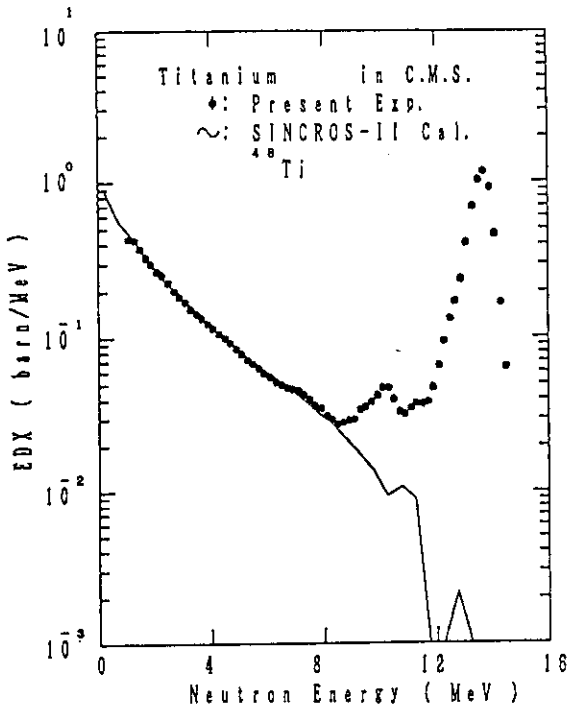

Fig. 9 EDX for Ti compared with SINCROS-II calculation

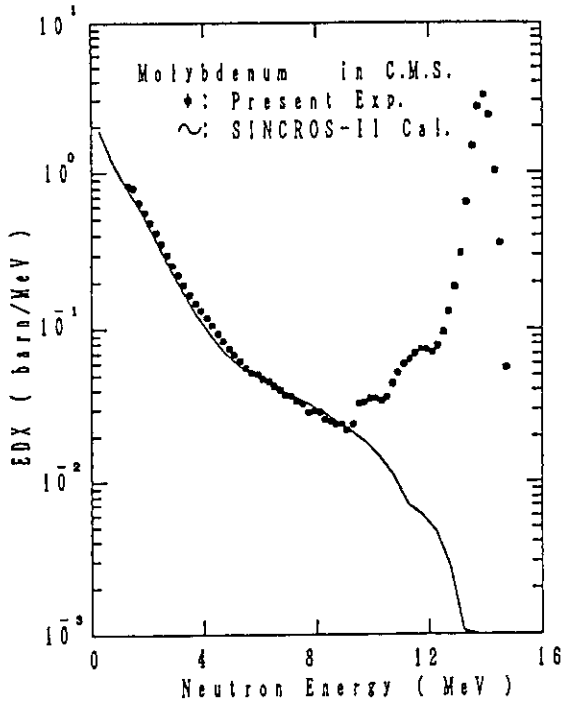

Fig. 10 EDX for Mo compared with SINCROS-II calculation

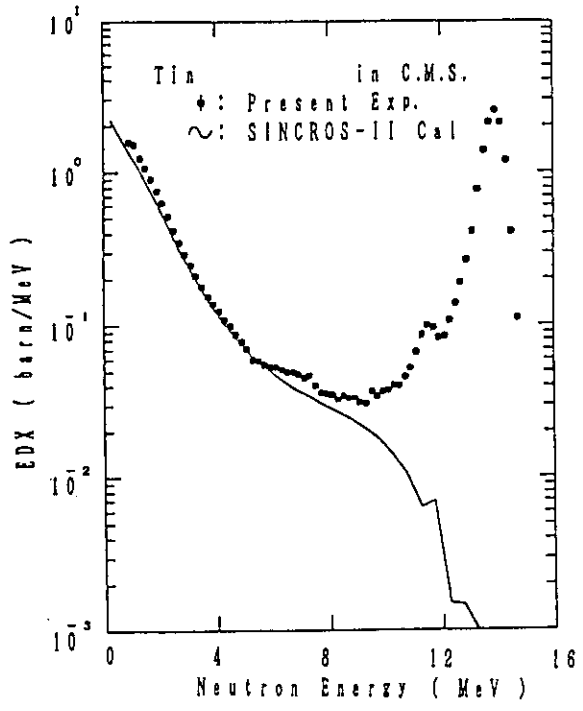

Fig. 11 EDX for Sn compared with SINCROS-II calculation

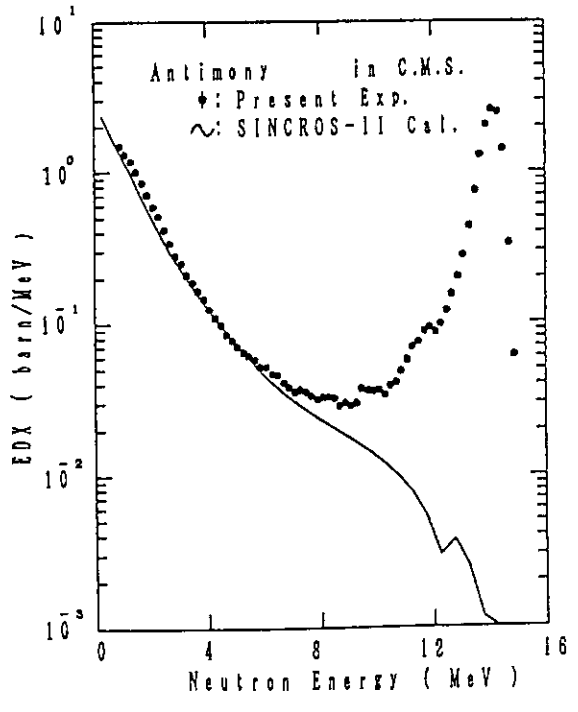

Fig. 12 EDX for Sb compared with SINCROS-II calculation

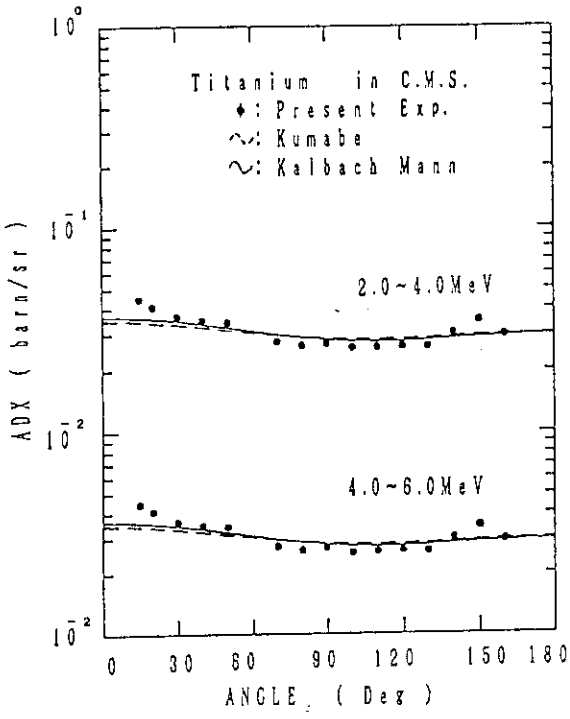

Fig. 13 ADX for Ti compared with SINCROS-II calculation

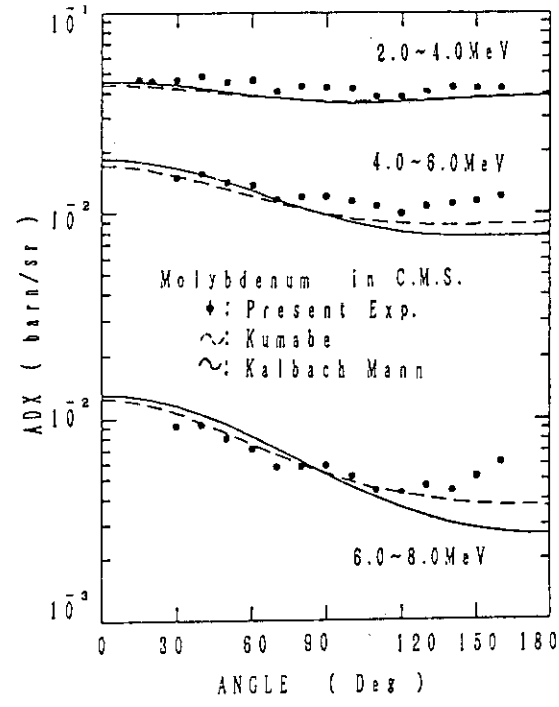

Fig. 14 ADX for Mo compared with SINCROS-II calculation

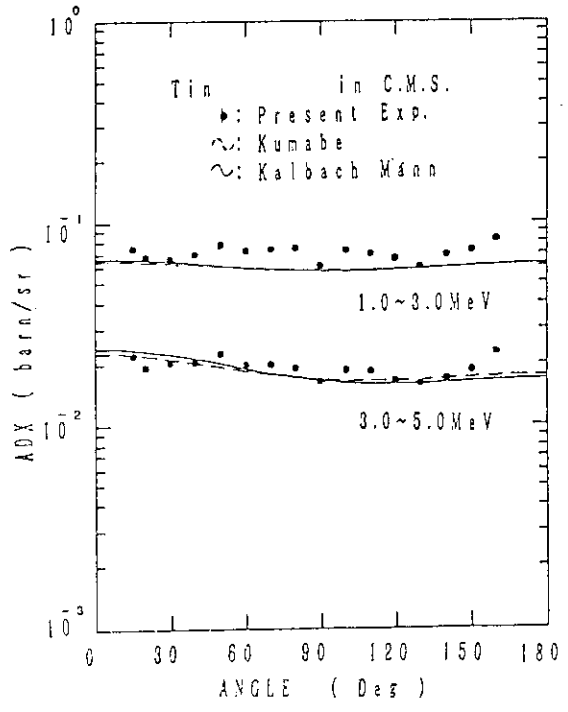

Fig. 15 ADX for Sn compared with SINCROS-II calculation

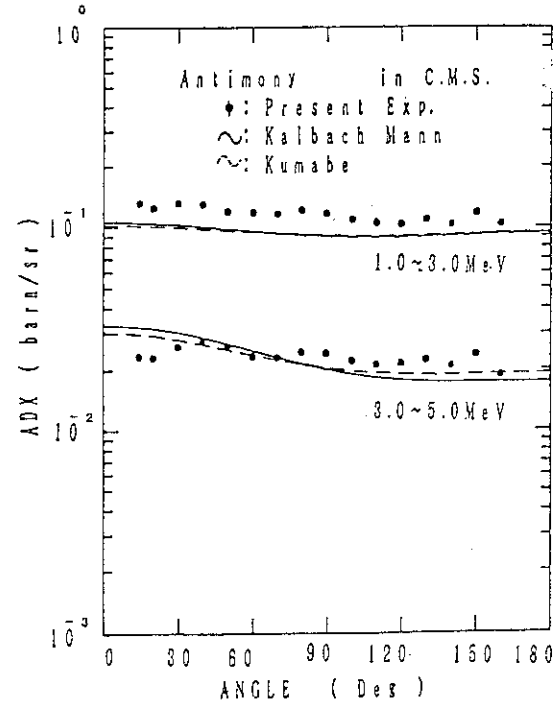

Fig. 16 ADX for Sb compared with SINCROS-II calculation

3.6 Fast Neutron Spectrum Measurement from Thorium Scatterer Using Associate Particle Method

S. A. HAYASHI, C. ICHIHARA
Research Reactor Institute, Kyoto University
Kumatori-cho, Sennan-gun, Osaka 590-04

J. YAMAMOTO
Dep. Nuclear Engineering, Fac. Engineering, Osaka University
2-1 Yamada-oka, Suita 565

S. KANAZAWA, I. KIMURA
Dept. of Nuclear Eng., Fac. of Eng., Kyoto University
Yoshida-honmachi, Sakyo-ku, Kyoto 606

Abstract

A fusion-fission hybrid reactor system based on a thorium material have been studied for an insurance of a future fuel. We have been conducting integral experiments to examine the nuclear data of thorium and to characterize the hybrid system. Neutron spectrum from a thorium slab scatterer, the size of which was 20.3 cm × 35.6 cm × 26.7 cm rectangular prism piled with 2-inches-square thorium plates, was obtained by a time-of-flight method using an associated particle method. The associated alpha signals from a thin plastic scintillator were used to trigger the time analyzer. Thorium scatterer was set 43.8 cm from the tritium target and 37.5° with respect to the D^+ beam axis. Scattered neutrons were detected with a 5 cm dia. × 5 cm thickness liquid scintillator by the help of *an n*-γ discrimination technique. The detector efficiency was determined by the combination of the measured neutron spectrum from a lead scatterer with the similar detection technique and the theoretically calculated one used with O5S Monte Carlo code. The measured spectrum from thorium was compared with the calculated one with MCNP code and JENDL-3 data file. General shape of the spectra agreed in the measured and calculated results.

1. INTRODUCTION

On the view of the provision of energy resources, thorium element to be converted to 233-uranium is one of the effective selections for a fuelling of fission reactors in the future[1]. The feasibility to convert natural thorium to 233-uranium should be searched in a system of a thorium-loaded fusion-fission hybrid reactor. Some groups have been carried out an experiment of a combination with 14 MeV neutron source and thorium material[2-4]. In this stage, there are much differences between measured and calculated results because these are not sufficient in both accuracies[5].

This study is to fundamentally analyze the system of fusion-fission hybrid reactor which consists of D-T fusion source combined with 233-uranium and thorium materials. The purpose of this study is to examine nuclear data and to obtain the characteristics of the thorium-loaded blanket in a fusion-fission hybrid reactor[6].

A series of the experimental studies consists of the following themes: (1) A determination of the D-T source characteristics, (2) Th(n,$2n$) reaction cross section measurement, (3) neutron spectrum and (4) reaction rate distribution measurements in simulated thorium-loaded blankets.

The simulated piles of fusion-fission hybrid blankets based on a thorium fertile material consist of thorium plates and beryllium or stainless steel sheets. A 14 MeV source used here is the D-T neutron source installed in the Kyoto University Critical Assembly (KUCA) building at the Research Reactor Institute, Kyoto University. For determination of a fast neutron spectrum, there are several methods in or from a pile, such as a multi-foil activation method, an unfolding method of proton recoil spectrum and a neutron time-of-flight (TOF) method.

In this report, the neutron spectrum from the thorium-loaded blanket pile combined with the 14 MeV neutron source was measured by the TOF technique using an associated particle method and these results were analyzed with a Monte Carlo calculation. Because the pulse width of the accelerator is wider than 200 nsec, the TOF method using the associated particle method instead of a pulsed neutron technique was

obliged to carry out. This method is based on the neutron TOF method triggered with an alpha particle which is emitted from the D-T reaction.

2. EXPERIMENTAL ARRANGEMENT

The thorium scatterer, 20.3 cm × 35.6 cm × 26.7 cm rectangular prism, was piled with thorium plates, 5.08 cm square × 1.27 cm and 0.32 cm thick, on a grid plate of a critical assembly. The 14 MeV source from D-T reactions with a 300 kV insulated-transformer-type accelerator with a duoplasmatron ion source installed in the KUCA building, which was already described in another report[7]. The operational condition of this accelerator is as following: pulse width 200 nsec, average beam current 15 μA and beam energy about 210 keV. The angular neutron spectrum was measured by the TOF technique using the associated particle method. The experimental arrangement is shown in **Fig. 1.** The experimental principle is based on that the associated α-particle occurred from the D-T reaction is detected with a thin plastic scintillator and the neutron from the same reaction is detected with a liquid scintillator at the 7 m flight path station in coincidence with the α-signals. These signals of alpha and neutron work as the start and stop signals for a time analyzer. The electronic block diagram of the TOF experiment is shown in **Fig. 2.**

a) Alpha detection

A plastic scintillator, NE 102A 2.54 cm dia. × 0.03 cm thickness, was selected for the detection of alpha particle emitted from the D-T reaction, because of the consideration on its fast time response, large effective area, and radiation durability. The alpha signals from the plastic scintillator were used for the trigger of the time analyzer.

b) Neutron detection

Two neutron detection systems were adopted. One is a main neutron detector of 5.08 cm dia. × 5.08 cm thick liquid scintillation counter, NE 213, which was set on neutron beams at the 7 m station. The other is a neutron monitor of 3.81 cm dia. × 3.81 cm thick liquid scintillation counter, NE 213, set at 230 cm position from the scatterer.

When 14 MeV neutrons entered directly into the main neutron detector, the time distribution of n-γ discrimination is shown in Fig. 3, and the n-γ discrimination level was adjusted so as to observe neutrons whose energies were higher than 1 MeV.

c) TOF electronics

The main neutron detector was arranged in the position of the scatterer in stead of that of 7 m flight path station, and all electronics of detection systems including the n-γ discrimination circuits were examined by the TOF method triggered with associated α-signals. The time spectrum of neutrons correlated to alpha was presented with a good S/N ratio as shown in Fig. 4. The space dependent neutrons correlated to alpha was checked and, at the center of correlated neutron beam the thorium scatterer was set 43.8 cm from the tritium target and 37.5° with respect to the D^+ beam axis.

3. RESULTS AND DISCUSSION

The time spectrum obtained with the time analyzer is converted to the neutron spectrum with the helps of the detector efficiency and some corrections. This neutron spectrum reflects the steady state spectrum emitted from the scatterer. The detector efficiency was determined by the combination of the measured neutron spectrum from a lead scatterer with the similar detection technique and the theoretically calculated one with O5S Monte Carlo code. The neutron spectrum calculation was performed by the continuous energy Monte Carlo code, MCNP[8] code using the data contained in JENDL-3[9] file. In this calculation the neutron flux was reduced from the events crossed through the spherical surface restricted to the conical angles between 100° and 110°. The neutron spectra from the thorium scatterer are shown in Fig. 5. General shape of the spectra agreed in the measured and calculated results. But there are some discrepancies in the several resonances between calculated and experimented spectra, these reasons may come from the statistical errors of experiment or the unsatisfied accuracy of the data file. The improved measurement is scheduled with larger detectors and fast detection

circuits, etc.

ACKNOWLEDGEMENTS

The present work has been partially supported by a Grant-in-Aid for Fundamental Research of the Ministry of Education, Government of Japan, and undertaken within the framework of the Visiting Researchers Program at the Kyoto University Critical Assembly (KUCA). The authors wish to thank the staff of the KUCA for their assistance in the experiment and analysis.

References

1) H. A. Bethe : "*The Fusion Hybrid*", Nuclear News, **21**, p. 41, (May 1978).

2) E. Greenspan : "*Fusion-Fission Hybrid Reactors*", Advances in Nuclear Science and Technology, **16**, p. 289, Plenum Press (1984).

3) L. F. Hansen, *et al.* : Nucl. Sci. Eng., **72**, 35 (1979).

4) V. R. Nargundkar, *et al.* : Fusion Tech., **14**, 354 (1988).

5) A. Kumar, *et al.* : Fusion Tech., **15**, 1430 (1989).

6) I. Kimura (*ed.*) : "*The Fundamental Study of Thorium-Loaded Hybrid Reactor*", Research Result Report of Grant-in-Aid. Ministry of Education, Science and Culture, Japan (May 1990).

7) C. Ichihara, *et al.* : "*Characteristics of KUCA Pulsed Neutron Generator*", KURRI-TR-240 (1983).

8) F. Briesmeister (*ed.*) : "*MCNP-A General Monte Carlo Code for Neutron and Photon Transport*", LA-7396-M, Rev. 2, (1986).

9) K. Shibata *et al.* : "*Japanese Evaluated Nuclear Data Library, Version-3*", -JENDL-3-, JAERI 1319, (1990).

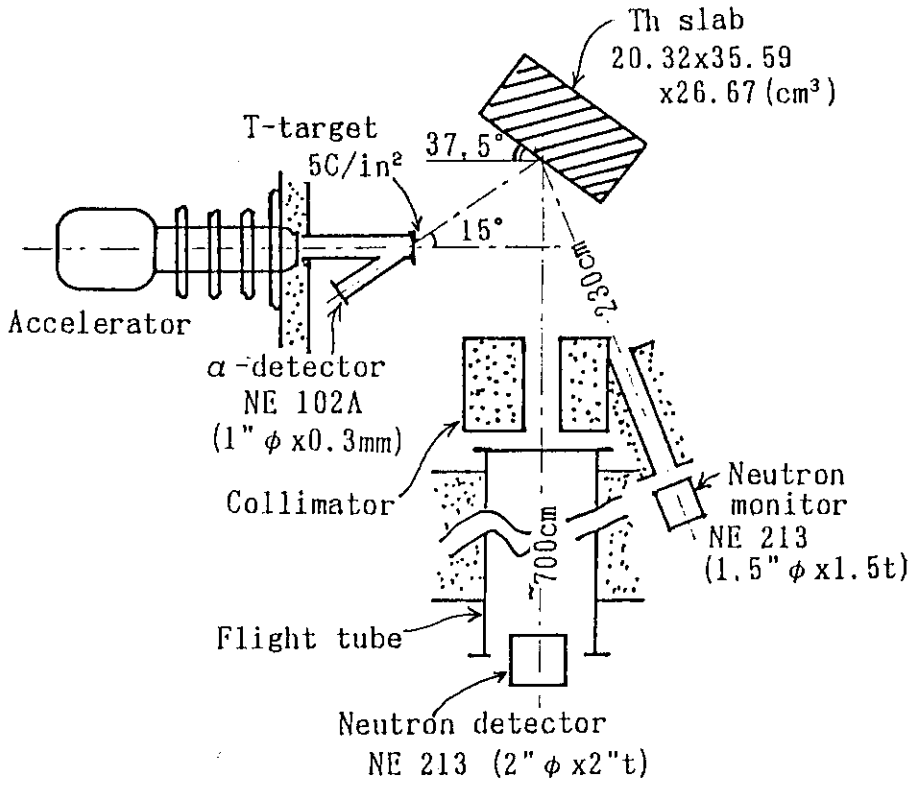

Fig. 1 Experimental arrangement of TOF method using associated particle technique.

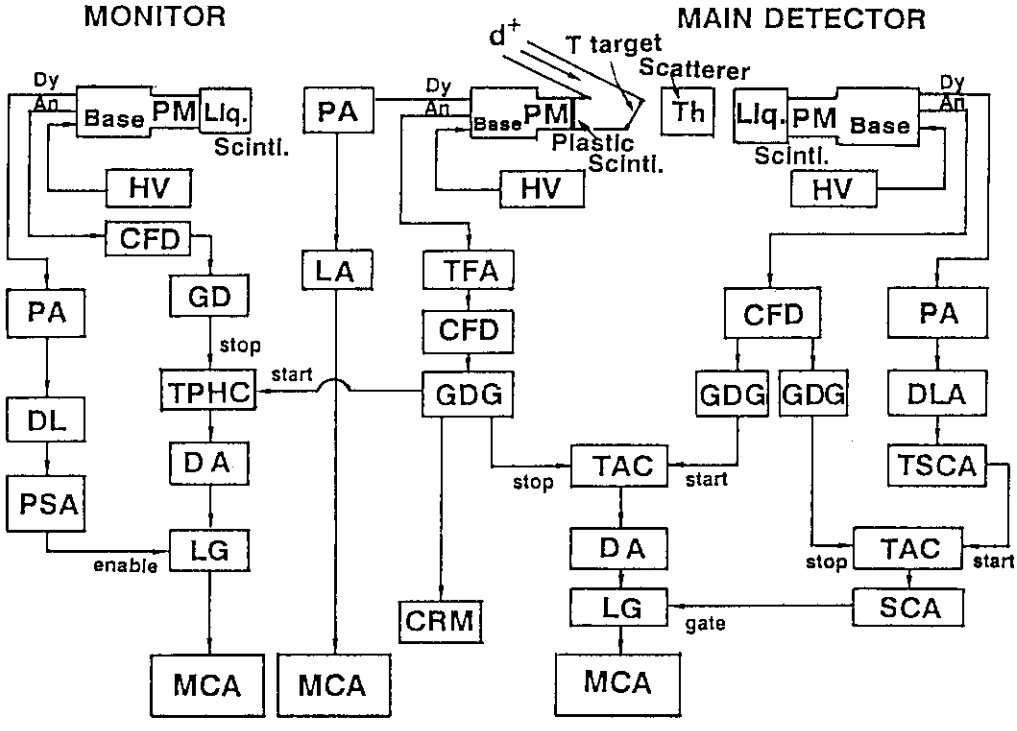

Fig. 2 Electronic block diagram of TOF method using associated particle technique.

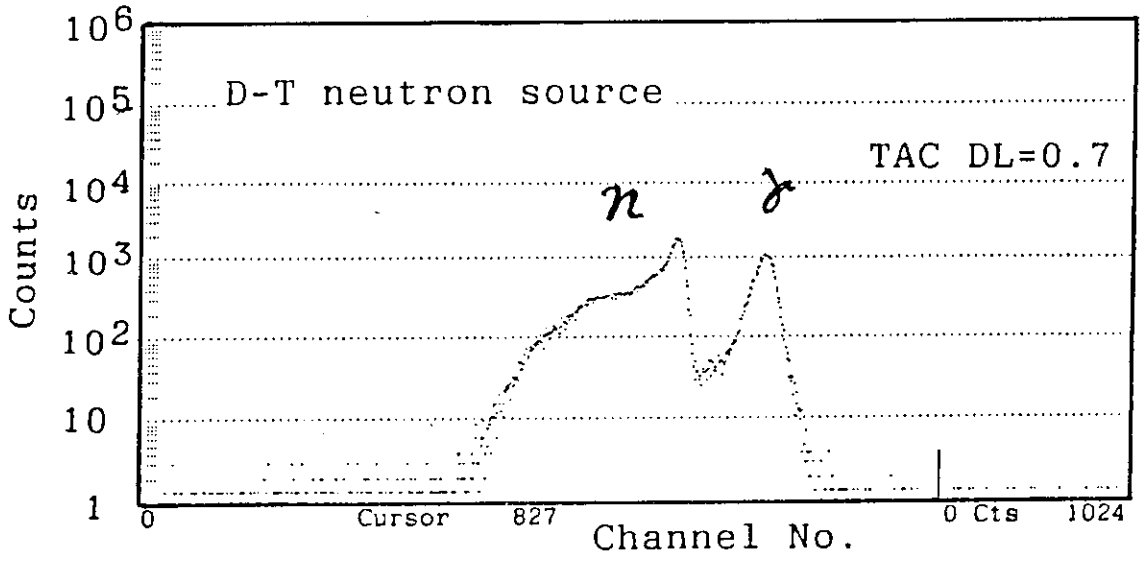

Fig. 3 Time distribution for n-γ discrimination of main neutron detector bombarded with 14 MeV neutrons.

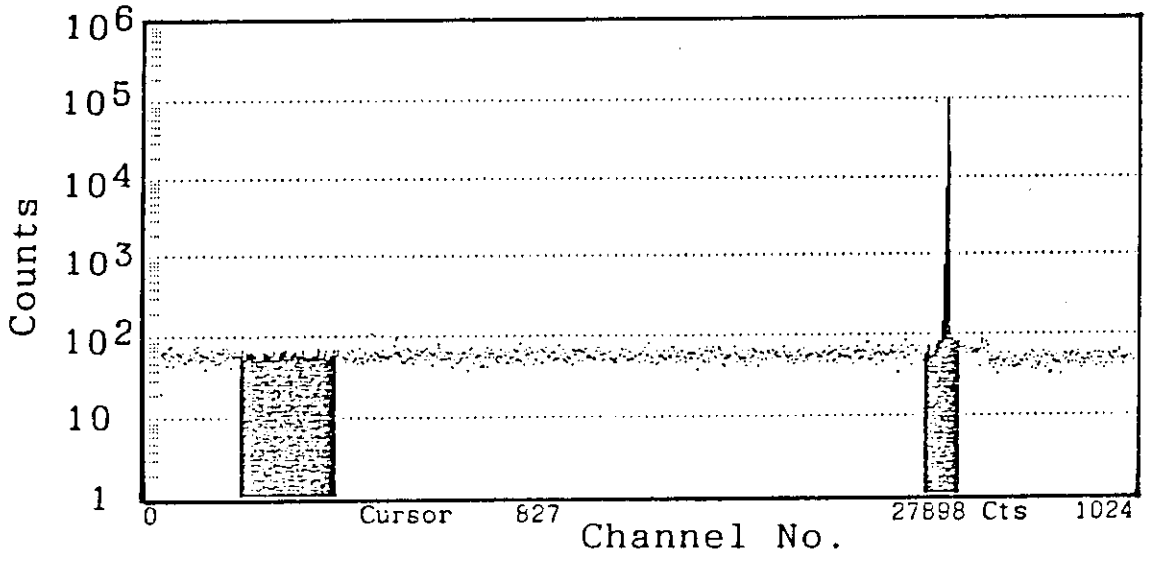

Fig. 4 Time spectrum of main neutron detector bombarded with 14 MeV neutrons.

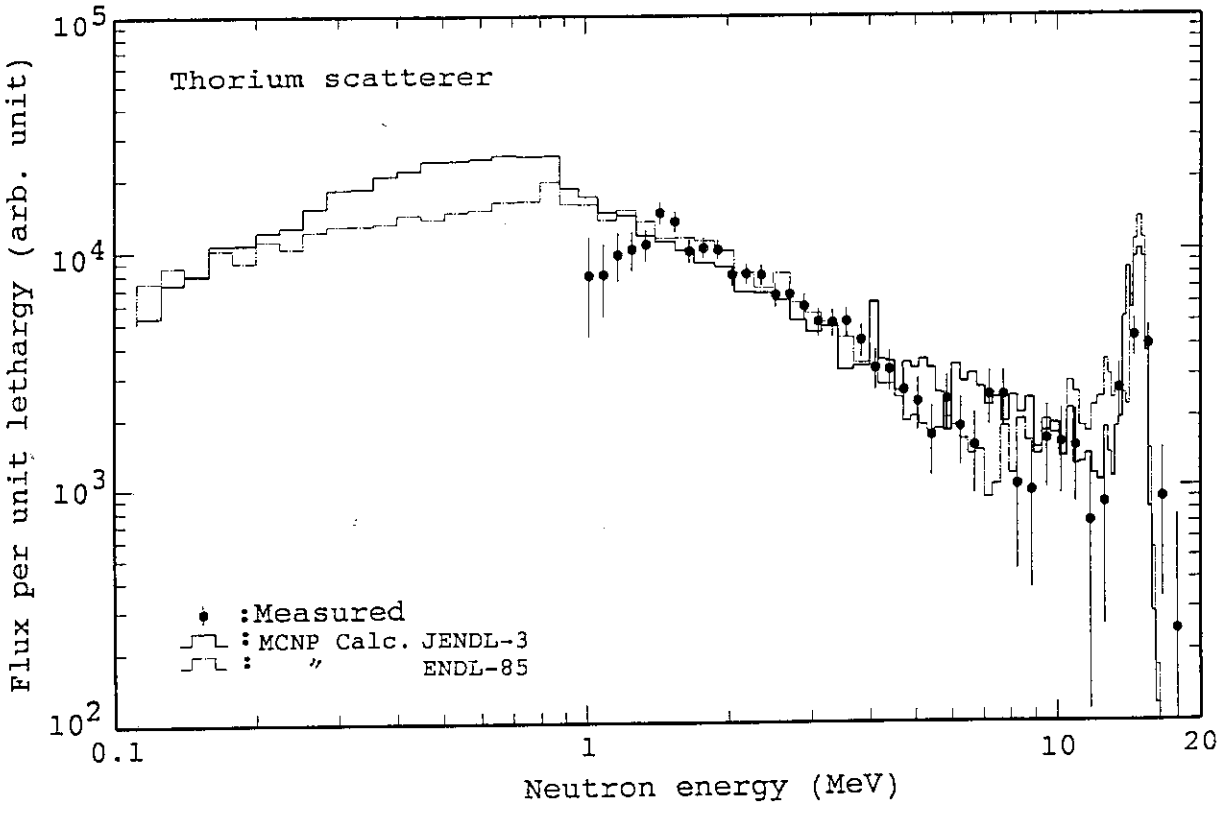

Fig. 5 Comparison of calculated and experimented neutron spectra from Thorium scatterer.

3.7 Measurement of ^{232}Th(n,2n)^{231}Th Reaction Cross Section with 14 MeV Neutrons

Hiroshi Chatani
Research Reactor Institute, Kyoto University,
Kumatori−cho, Sennan−gun, Osaka, 590−04, JAPAN

Itsuro Kimura
Department of Nuclear Engineering, Kyoto University,
Yoshida, Sakyo−ku, Kyoto, 606, JAPAN

Abstract

The cross section for the ^{232}Th(n,2n)^{231}Th reaction was measured by using a neutron generator at the Kyoto University Critical Assemblies (KUCA). We used the ^{27}Al(n,α)^{24}Na reaction cross section (117.3mb) as a reference. The present result, (1177±79)mb for the (14.7±0.1)MeV neutrons agrees with the evaluated values in ENDF/B−V,VI and ENDL−86 within an experimental error, but is much larger than the newly evaluated value in JENDL−3.

1. Introduction

Because of the emission of very high energy gamma rays from a daughter nuclide ^{208}Tl, it is very important for fuel reprocessing and for fabrication of ^{233}U fuel to evaluate the ^{232}U accumulation in thorium loaded reactors. One of main reactions to produce ^{232}U is ^{232}Th(n,2n)^{231}Th. This reaction is also important from the neutron multiplication by ^{232}Th. Therefore precise cross section data for this reaction are strongly requested for the design of a fusion−fission hybrid reactor with a thorium blanket or an accelerator breeder with a thorium target. However there exist considerably large discrepancy in measured[1][2] and evaluated values for this reaction. We measured this cross section at 14.7MeV with a neutron generator at KUCA[3] and the result was compared with evaluated values (JENDL−3 , ENDF/B−V,VI and ENDL−86) and earlier measured ones.

2. Experimentals

2.1 Irradiation

The neutrons were generated by the D−T reaction with a Ti−T target bombared by a deuteron beam 212 keV in energy and about 20 μA in average beam current.

We made three polyethylene packs of thorium nitrate powder sample about 500mg in weight. The three thorium nitrate samples were sandwiched with aluminum foils 0.5mm

thick used for neutron fluence monitoring and were attached on an aluminum holder. The distance between the Ti−T target and the front surface of the thorium nitrate samples was 1.6cm as shown in Fig.1. Time dependent neutron flux was monitored with a moderator type neutron dose rate meter located about 2m from the Ti−T target. We irradiated the thorium nitrate samples by 14MeV neutrons for sbout 7.5 hours.

2.2 Characterization of Neutron Environments

Average neutron energy was experimentally determined by the reaction ratio of $^{90}Zr(n,2n)^{89m+g}Zr$ and $^{93}Nb(n,2n)^{92m}Nb$. Four zirconium and five niobium foils were irradiated at the position 4.4cm apart from the Ti−T target as shown in Fig.2. From the obtained reaction ratio 1.67±0.04 and the data taken by Ikeda et al.[4], the average neutron energy became 14.7±0.1 MeV.

The cross section for the $^{27}Al(n,\alpha)^{24}Na$ reaction was determined by the interpolation of the Dosimetry File of ENDF/B−V and its value was 117.3mb at 14.7 MeV.

The flux distribution and energy spectrum of the neutrons in the thorium nitrate samples were calculated by a Monte Carlo code, MCNP. In this calculation we used the measured source neutron spectrum at OKTAVIAN[5] as an input spectrum. The calculated neutron flux distribution agrees with the measured values by using the $^{27}Al(n,\alpha)^{24}Na$ reaction as shown in Fig.3. In Fig.4, the calculated neutron spectrum averaged in two thorium nitrate samples behined the Ti−T target is compared with the source spectrum. From this figure, it can be seen that the distortion of the neutron spectrum in the thorium nitrate samples is negligible.

2.3 Chemical purification

Since the irradiated thorium nitrate samples contain various radioactive nuclides, thorium must be purified before its radioactivity measurement. Two irradiated thorium nitrate samples which were more closely located to the Ti−T target were mixed and chemically purified[6]. The chemical procedures are shown in Fig.5. The quantity of the recovered thorium after the purification was determined by the neutron activation analysis method in comparison with a known weight thoria sample. The recovery ratio was about 50%.

2.4 Radioactivity measurement

The gamma rays from all of the radioactive nuclides generated in this experiments were measured with a pure germanium (HPGe) detector. Absolute full energy peak efficiencies of the detector were calibrated with standard gamma ray sources made by IAEA and Amersham Co. Corrections were achieved for random, chance and summing coincidences.

A typical gamma ray spectrum of a purified thorium sample after irradiation is shown in Fig.6. The sum counts of triplet photo peaks at 81, 82 and 84 keV was plotted in Fig.7 and the half life became very close to the literature value[7].

For the absolute measurement of ^{231}Th activity, the sum counts of the triplet photo peaks were used. Calibration for the triplet peaks was carried out by making use of 90% enriched uranium−aluminum alloy foils which contained ^{231}Th in the secular equilibrium as shown in Fig.8. The advantages of this method are (1) Gamma ray intensity of ^{231}Th is unnecessary, (2) Correction of coincidence summing effect at 84keV is not considered and so on. The correction for the self absorption of gamma rays was determined by the gamma ray attenuation curve which was obtained by using 5 uranium−aluminum alloy foils shown in Fig.9. The efficiency change by geometrical area of the purified thorium sample was also corrected using the method by Kushelevski et al.[8](Fig.10)

3. Results and discussion

Uncertainties associated with this experiment were estimated as shown in Table 1. The present obtained value of the cross section for the ^{232}Th(n,2n)^{231}Th reaction at 14.7±0.1 MeV is tabulated in Table 2. Present result is close to those of earlier measurements[1][9] except that of Prestwood et al.[2], and evaluated value of ENDF/B−V and VI in the experimental error. However the evaluated value in JENDL−3 is much smaller than the present data. Fig.11 shows the comparison with representative values.

References

(1) Karius H., Ackermann H. et al., J.Phys.G:Nucl.Phys., Vol.5, No.5 (1979) pp.715−721.
(2) Prestwood R.J. and Bayhurst B.P., Phys.Rev., Vol.121,No.5 (1961) pp.1438−1441.
(3) Ichihara C. et al., KURRI−TR−240,"Characteristics of KUCA Pulsed Neutron Generator", (1983).
(4) Ikeda Y. et al., JAERI−1312 (1988).
(5) Yamamoto J., Private communication.
(6) Hyde K. et al., NAS−NS 3004 (1960).
(7) Brown E. et al., "Table of Isotopes (7th. ed.)", ed. Lederer C.M. et al., (Wiley, New York),(1978).
(8) Kushelevski A.P. and Alfassi Z.B., Nucl.Instr.Meth., 131,(1975) pp.93−95.
(9) Butler J.P. and Santry D.C., Can.J.Chemistry, Vol.39 (1961) pp.689−696.
(10) Perkin J.L. and Coleman R.F., J.Nucl.Energy, Vol.14 (1961) pp.69−75.

Table 1 Uncertainties associated with the experiment.

Source of error	Resulting uncertainty (±%)
Th sample	
Counting statistics	0.37
Recovery of Th	1
Efficiency of HPGe for 84keV	1.2
Self absorption	1.8
Neutron fluence monitor	
Counting statistics	0.15
Purity of Al foils	0.56
Efficiency of HPGe for 1.37MeV	3.1
Flux distribution	5
Others	2
Total	6.7

Table 2 Cross sections for the $^{232}Th(n,2n)^{231}Th$ reaction to 14 MeV neutrons.

Author	Cross section (mb)
Present (1990)	1177± 79 (14.7±0.1MeV)
Butler J.P. et al. (1961)[9]	1230± 60 (14.47MeV)
Perkin J.L. et al. (1961)[10]	1200± 50 (14.1±0.3 MeV)
Prestwood R.J. et al. (1961)[2]	1400±140 (14.68±0.26 MeV)
Karius H. et al. (1979)[1]	1049± 99 (14.79±0.19 MeV)
JENDL−3	873± 4 (14.7 MeV)*
ENDF/B−V,VI	1098± 33 (14.7 MeV)*
ENDL−86	1076± 22 (14.7 MeV)*

* Interpolated value

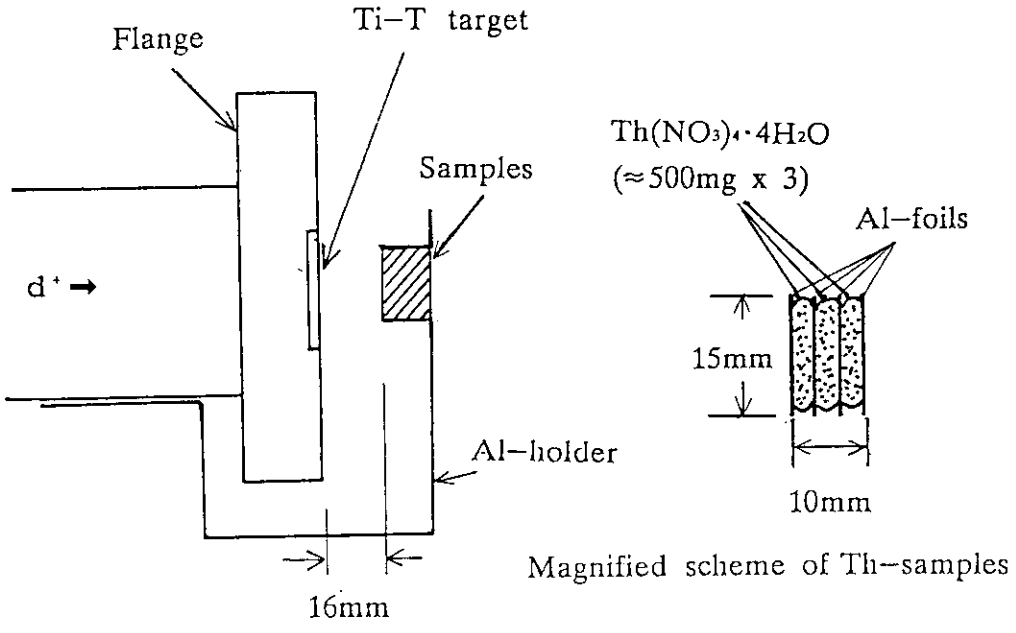

Fig. 1 Experimental arrangement for irradiation of Th samples.

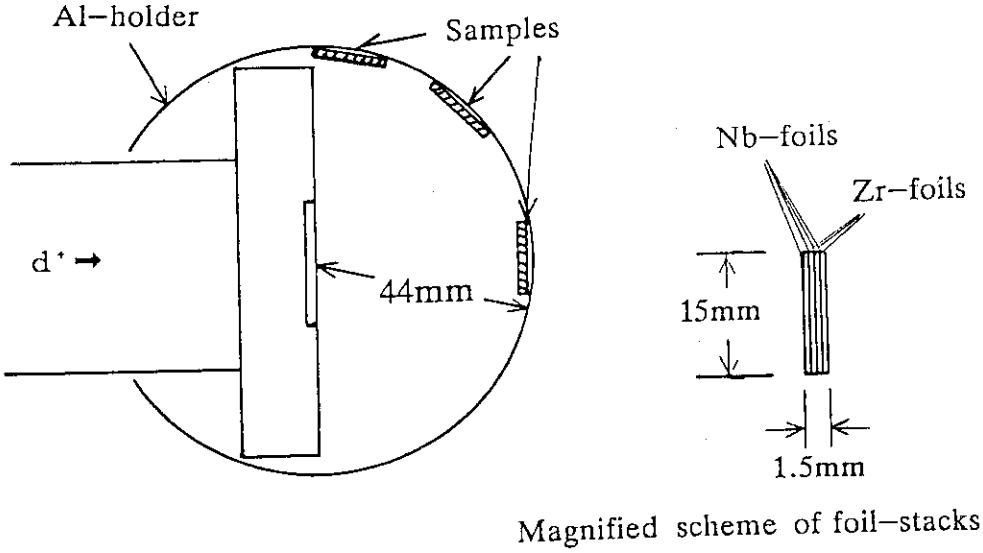

Fig. 2 Experimental arrangement for irradiation of Zr and Nb foils.

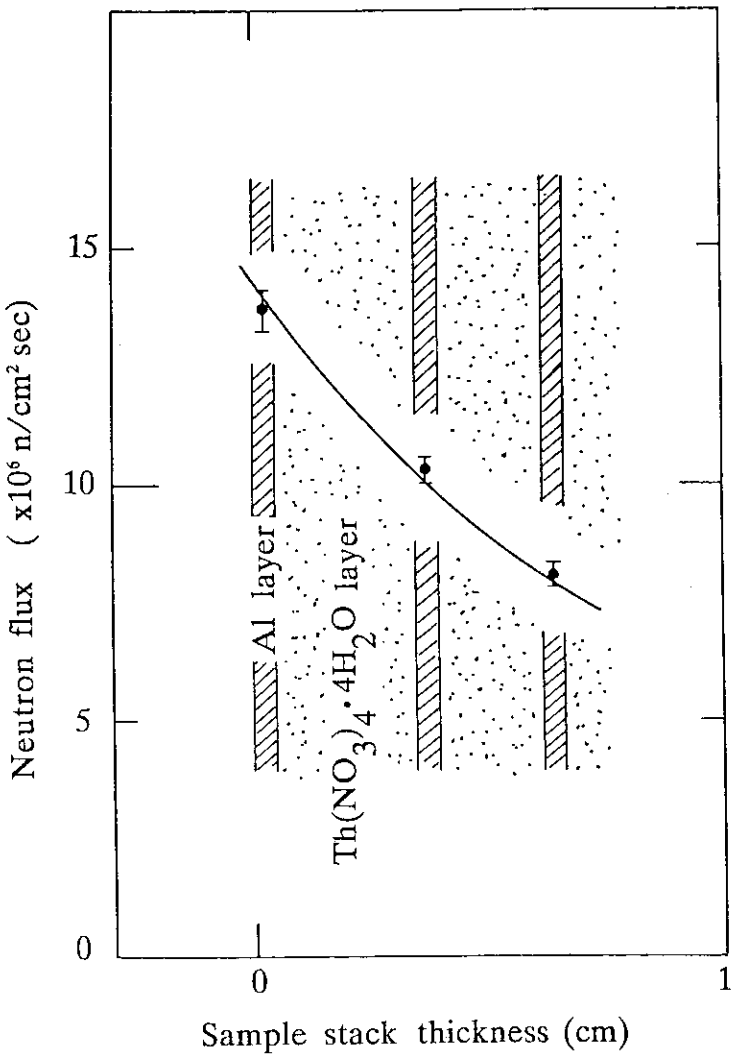

Fig. 3 Neutron flux distribution in Th samples. Solid circles are experimental values using the $^{27}A(n,\alpha)^{24}Na$ reaction, solid line is relative values calculated by MCNP.

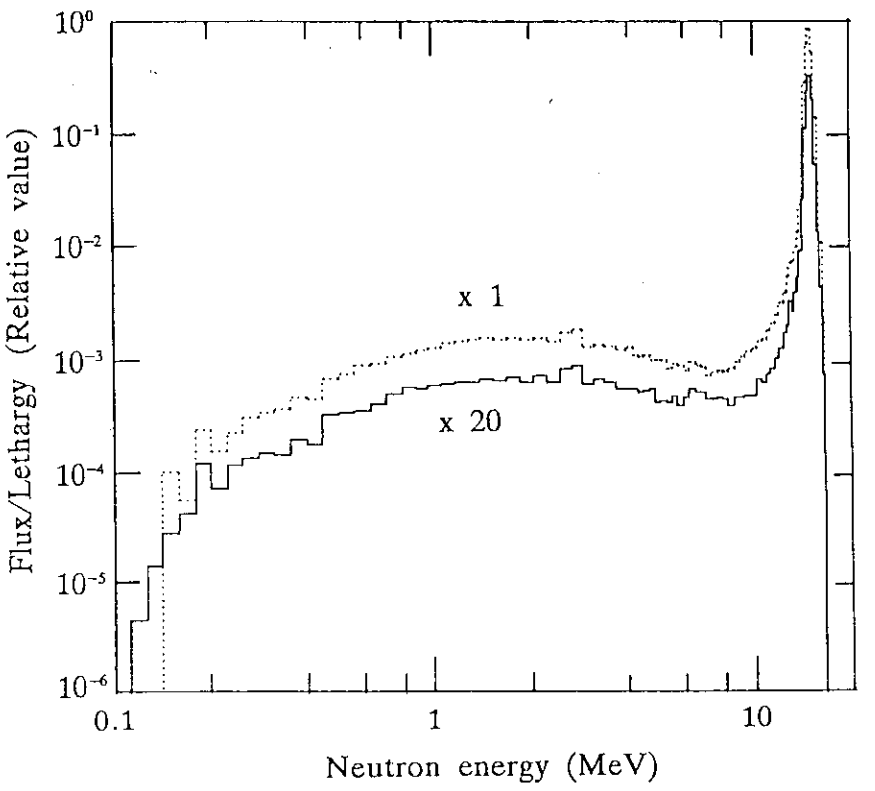

Fig. 4 Neutron energy spectra. The dotted line is the input spectrum, and the solid line is the averaged spectrum in the two packs of $Th(NO_3)_4 \cdot 4(H_2O)$ samples calculated by MCNP.

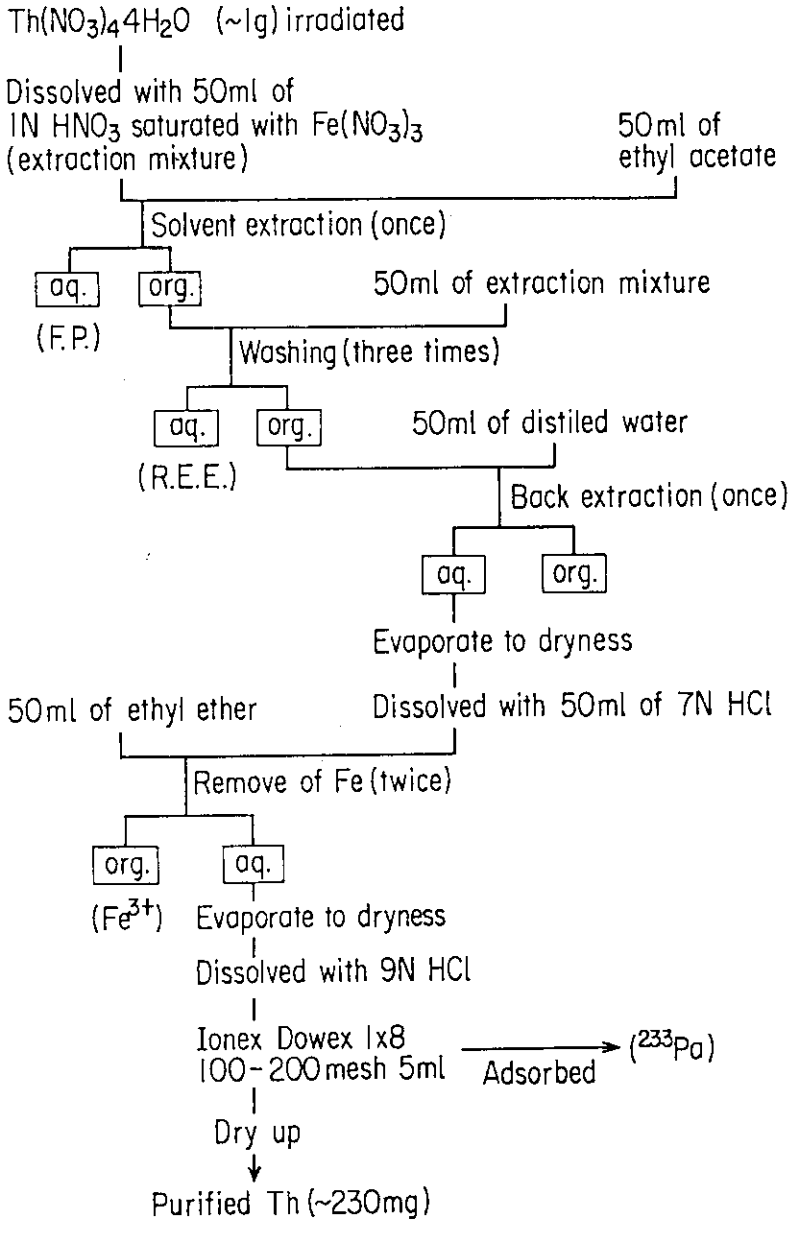

Fig. 5 Chemical purification procedures of irradiated thorium nitrate.

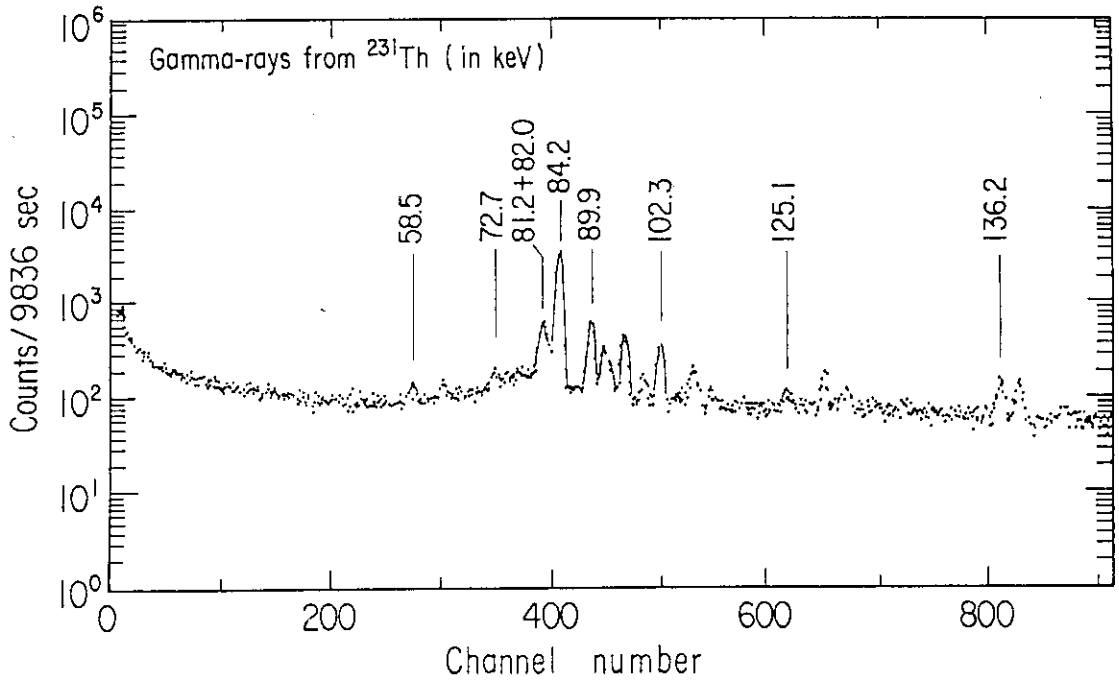

Fig. 6 Typical gamma ray spectrum of purified Th sample.

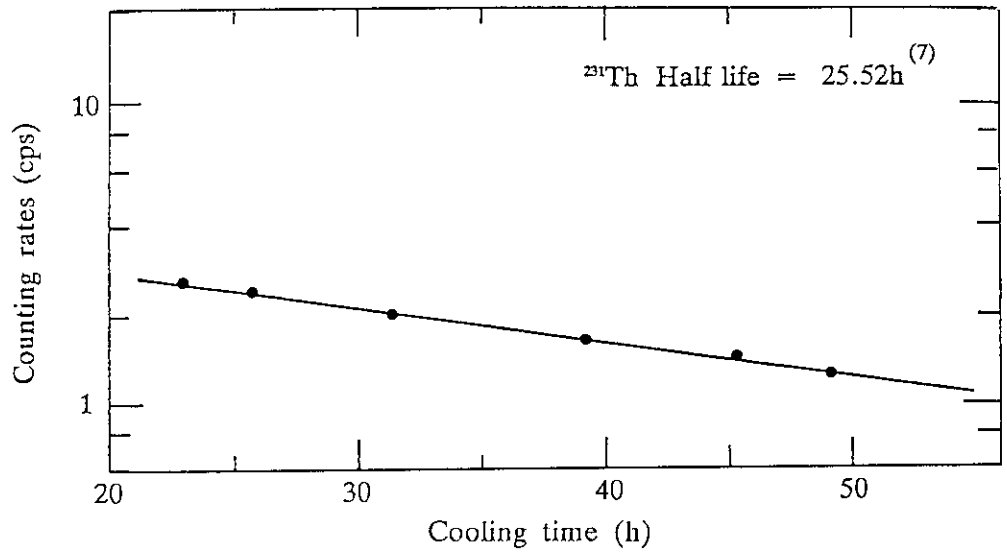

Fig. 7 Time dependent counts rates around 84 keV triplet photo peaks. The solid circles are experimental values, the statistical errors are included in the circles, and the solid line is the literature value[7].

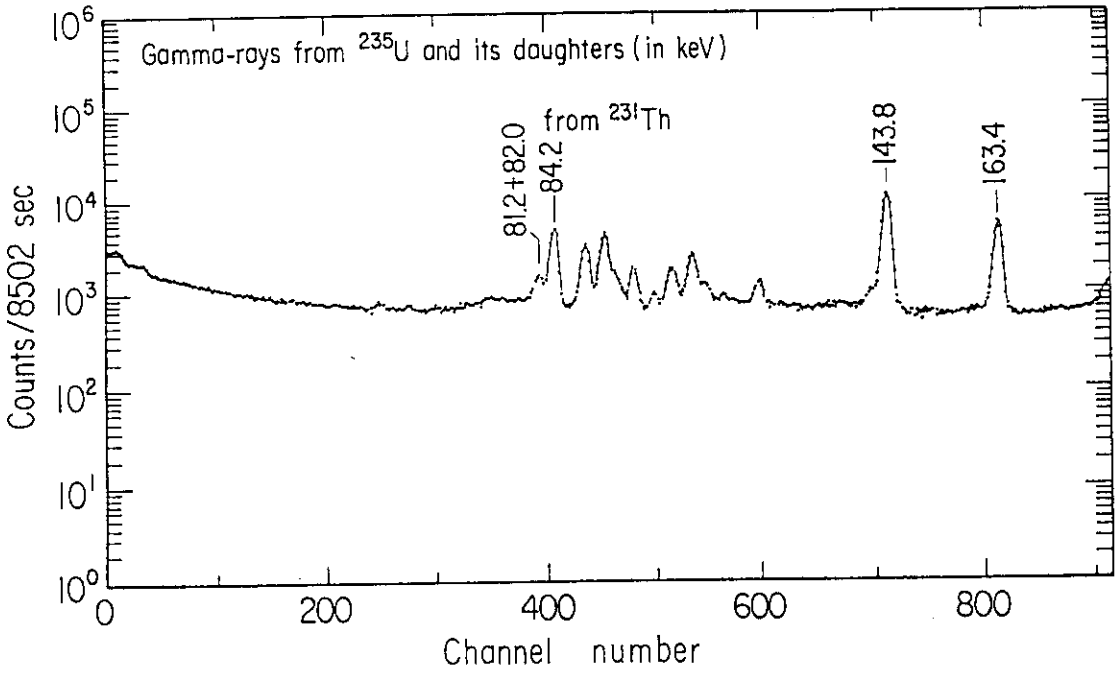

Fig. 8 Typical gamma ray spectrum of a 90% enriched U-Al alloy foil.

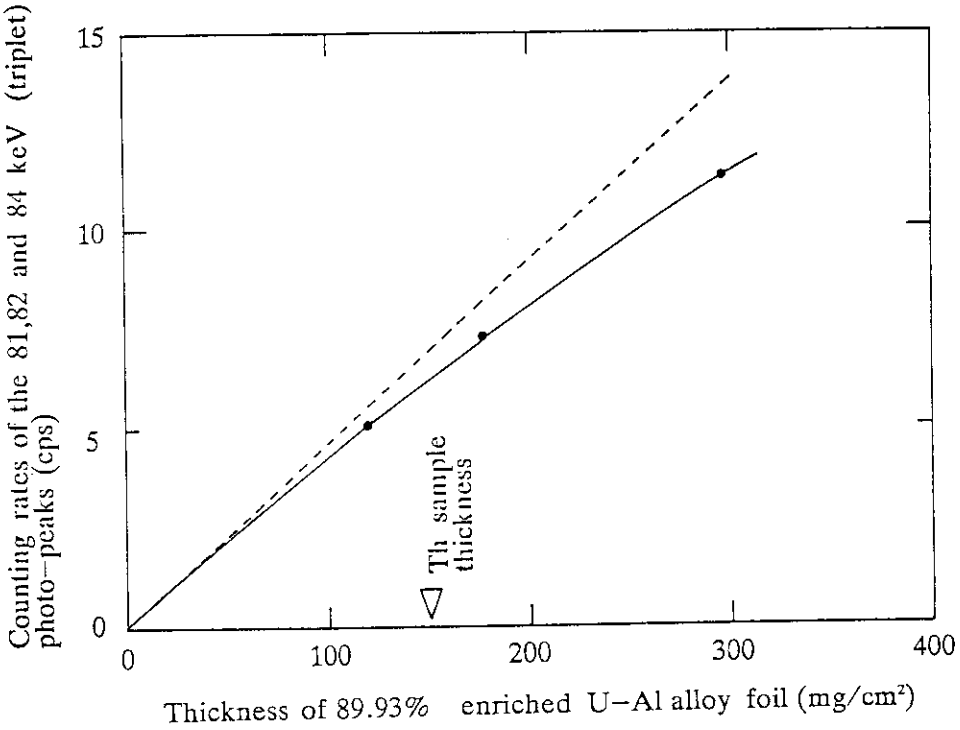

Fig. 9 Self attemuation curve for the 84 keV gamma ray, measured with 2, 3 and 5 sheets of U-Al alloy foils. Solid line is the best fitted curve by a quadratic equation, broken line is the differential one at 0 mg/cm^2. Thickness of the purified Th sample is indicated by a triangle.

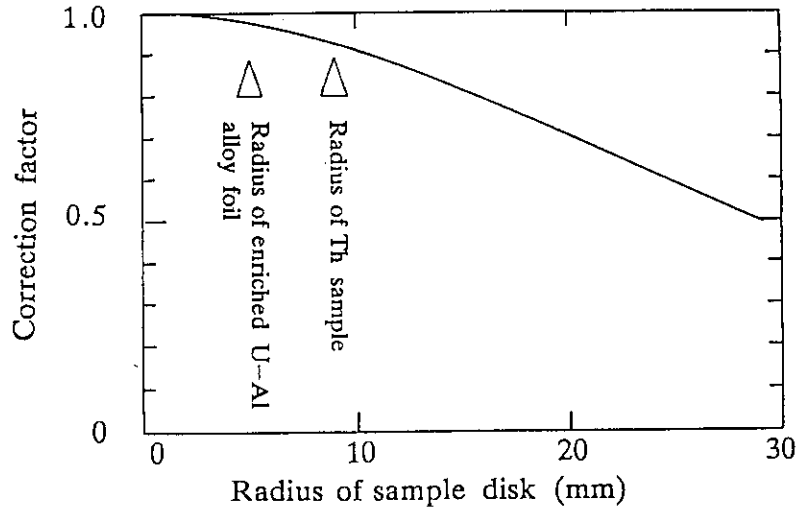

Fig. 10 Efficiency correction for disk source with 84 keV gamma rays. Two triangles indicate the radii of 90% enriched U-Al foil and purified Th sample.

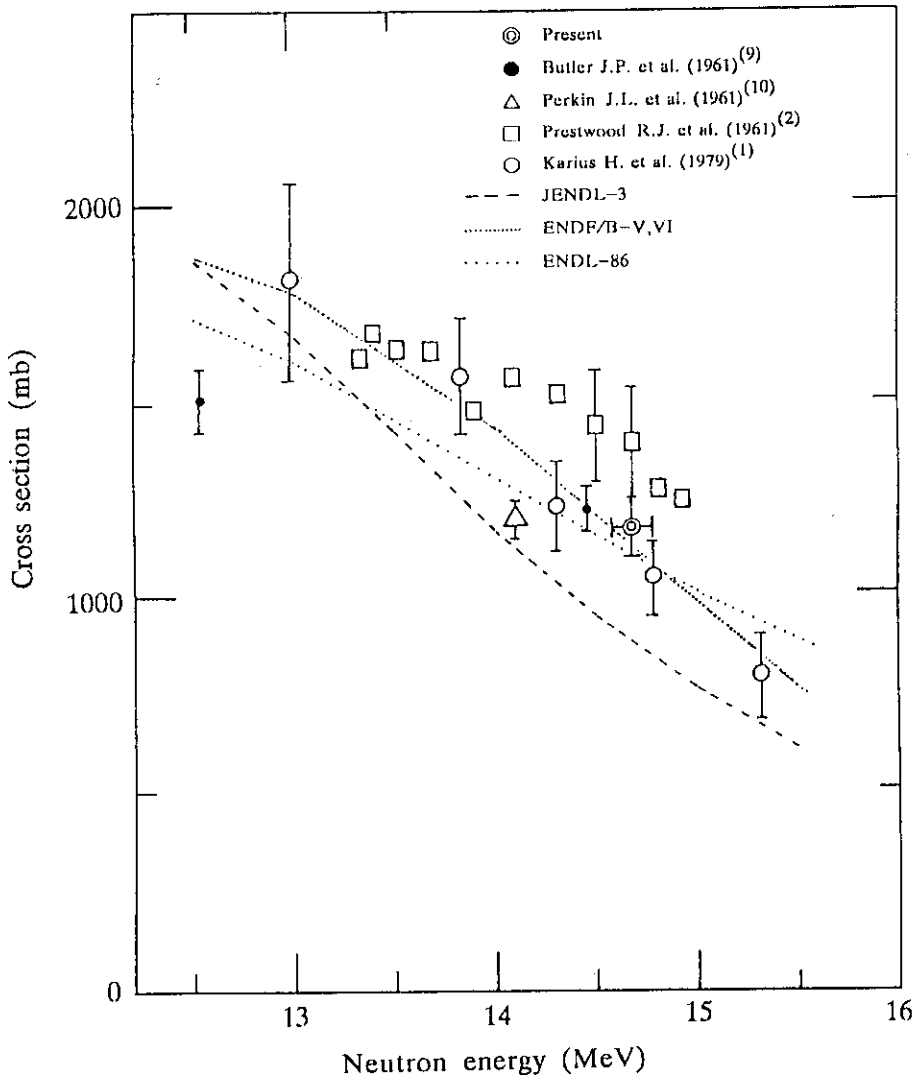

Fig. 11 Cross section data of the $^{232}Th(n,2n)^{231}Th$ reaction.

3.8 Gamma-ray Production Cross Sections with 14 MeV Neutrons for 8 Elements from Z = 22 to 29

Takuzo Takayama ,Yoshiyuki Ohta ,Junji Yamamoto,
Akito Takahashi and Kenji Sumita

Department of Nuclear Engineering, Osaka University
2-1 Yamada-oka ,Suita 565

Gamma-ray production cross sections from (n,n'γ) reactions by 14 MeV neutrons were measured with regard to energy differential cross sections and production ones for discrete gamma-rays, using the D-T neutron source OKTAVIAN of Osaka University. Results were obtained for 8 natural elements; Ti, V, Cr, Mn, Fe, Co, Ni and Cu. The measured cross sections were compared with the calculations by SINCROS-II and the gamma-ray data evaluated in the currently used nuclear data file of JENDL-3.

1. Introduction

Nuclear data for gamma-rays produced by the interactions of high energy neutrons around 14 MeV are one of the important data for the design works of D-T fusion reactors in order to calculate the amount of heating and shielding for gamma-rays. Most of the measured elements are structural materials of fusion reactors. The present work is to check the gamma-ray production cross sections in the nuclear data file of JENDL-3. The file is the first version of a JENDL series in which the gamma-ray production cross sections are evaluated. For vanadium and cobalt, however, the evaluations are not compiled in JENDL-3.

The energy differential cross sections were measured at the emission angles of 125°, 90° and 45° with respect to the incident neutrons. In this paper, the measured data at 125° are presented to be compared with the differential cross sections, which are provided

from the individual reactions of (n,n'),(n,2n), (n,p),(n,n'p) and so on and have been compared with the cross sections calculately by SINCROS-Ⅱ. We have compared with JENDL-3.

The production cross sections of discrete gamma-rays were obtained from the integration of the augular distributions, which were measured at 6 angular points from 30° to 150° between the emission gamma-rays and the incident neutrons.

2. Experiment

Experimental method was a conventional one[1][2]. Fig.1 shows an experimental layout for the measurement of energy differential cross sections. An NaI detector of 5" in diameter was surrounded by iron, lead and polyethylene to eliminate the neutron background. A shadow bar was set to shield the neutrons which generated and came directly from a tritium target. Samples were either disks of 10 cmdiam. x 2.5 mm-t, as shown in Fig.2 or squares of 10 cm x 10 cm x 10 mm-t. The sample was located at the positions where the emission angles were 45°, 90° and 125° in the laboratory system, respectively. The energy spectra were measured in the gamma-rays energy range from 700 keV to 10 MeV. The pulse height spectra were unfolded by the FERDOR code.[3] The efficiency and the response functions of the NaI detector were determined with the caluculations by the Monte Carlo method. They were in good agreement with the experimental results.

Figure 3 shows a layout for the measurement of discrete gamma-rays. Angular distributions of the discrete gamma-rays were analyzed with a Ge detector all. The discrete gamma-rays were measured in the gamma-rays energy range from 500 keV to 3 MeV. Samples were hollow cylinderso f 30 mm-c.d. x 26 mm-i.d. x 70 mm-long, as shown in Fig.4. The angular distributions of the discrete gamma-rays for natural manganese were shown in Fig.5.

The neutron fluence at the sample position for each run was determined with aluminum and niobium foils activated by $^{27}Al(n,\alpha)^{24}Na$ and $^{93}Nb(n,2n)^{92}Nb$ reactions, respectively. The relative yield of the source neutrons was monitored run by run with an NE213 liquid scintilation counter. The correction of multiple scattering has been

done using a neutron and photon Monte Calro transport code MCNP[4] as well as the correction of attenuation for not only the incident neutrons in the sample but also the produced gamma-rays . The factors of the corrections were less than about 5 %.

The error bars in the energy differential cross sections denote the statistical errors. The errors of the measured values were taken to be less than about 10 %. The error sources were the estimation of neutron production at the D-T neutron source, and the efficiency of Ge detector which were used to measure the neutron fluences at the samples positions.

3. Calculation of gamma-ray production cross sections

After the calculations of energy differential cross sections for secondary neutrons from inelastic scattering, the gamma-ray production cross sections could be obtained. As for the energy differential cross sections of gamma-rays, the calculations agreed with the measurements in the case that the calculated ones[5]. For vanadium and cobalt, the gamma-ray nuclear data of which are not evaluated in JENDL-3, the calculational results were in good agreement with the experimental values.

The kalbach normalization factors (F2 parameters) used in the calculation were shown in Table 1. The level density parameters of Z = 25 to 29 were taken from the ref.(6). The gamma-ray level skim were produced from ENSDF[7].

4. Data presentation and comparison

The C/E values of production cross sections are shown in Fig.6, where the value at 125° for every measured element was obtained from the integration of the energy differential cross sections over the energy range from 700 keV to 10 MeV. The calculated cross sections by SINCROS-Ⅱ agreed with the measured ones except nickel.(Z=28) The JENDL-3 evaluations for iron and nickel have overestimated by about 80 %. The C/E values of JENDL-3 are systematically lareger than 1.0.

In the comparison of the energy differential cross sections between the measurements, the calculations and the evaluations, the

results are summarized as follows:

For titanium, chromium, and iron the evaluations overestimated the measurements in the every range between 2 MeV to 6 MeV, where the gamma-rays from the inelastic scattering mainly contributed to the measured energy spectra. Figure 7 shows the energy differential cross sections for chromium. The secondary neutron distribution is shown in Fig.8, JENDL-3 evalution underestimates the measurement in the range between 8 MeV to 12 MeV. The calculation, however, agrees with the experimental values by accuratly calculating the secondary neutrons from the inelastic scattering.

For copper and manganese there was no marked distinction between JENDL-3 and the calculations. The JENDL-3 evaluation is fair agreement with the experimental value as shown in Fig.9.

The production cross sections of vanadium and cobalt could be successfully estimated by the use of SINCROS-Ⅱ. The result of cobalt is shown in Fig.10. for the gamma-rays and in Fig.11 secondary neutrons. It was reported that the evaluated values in JENDL-3 for vanadium and cobalt were not in agreement with the experimental values of the double-differential cross sections of secondary neutrons[4].

The reaction channels of nickel are characterized by two mainly reactions, (n,n') and (n,p), for the incident neutron energies between 2 MeV to 10 MeV. In Fig.12, considerable discrepancy between the measurement and the evaluation can be found in the energy range from 2 to 6 MeV. The cause of the disagreement is now investigated by calculating the secondary protons from the (n,p) reaction.

Table 2 lists the production cross sections of discrete gamma-rays for copper. In this paper, we skipped the discussion on these production cross sections for 5 elements ; manganese, iron, cobalt, nickel and copper. Most of the calculated values, however, agreed with the experimental values.

5. Concludind remarks

Using the SINCROS-Ⅱ, the gamma-rays production cross sections could be estimated for the eight elements based on the acculate calculations of the energy differential cross sections for the

secondary neutron emissions. The gamma-rays from the (n,n'γ) reaction were dominant in the gamma-ray energy spectra from 2 MeV to 10 MeV, so that it was essential determine the emission cross sections of secondary neutrons from inelastic scattering. The numerical data of energy differential cross sections and production cross sections will be listed in another report including the additional the elements; aluminium, silicon, niobium, molybdenum, tantalum, tungsten, lead and bismuth. It will contain the comparisons of the experimental data with the JENDL-3 evaluations and calculations using SINCROS-Ⅱ.

References

(1)Yamamoto, J., et al.: Differential Cross Sections for Gamma-Ray Production by 14 MeV Neutrons, JAERI-M88-065,P.374 (1988).

(2)Murata, I., et al.: DIFFERENTIAL CROSS SECTIONS FOR GAMMA-RAY PRODUCTION BY 14 MeV NEUTRONS WITH SEVERAL ELEMENTS IN STRUCTUAL MATERIALS,Proc.Int.Conf.Nuclear.Data for Sci.and Technol.,p.275 (1988).

(3)Kendrick, H. and Spering, M.,: An Introduction to the Principles and Use of the FERDOR Unfoldind Code, GA-9882, General Atomic Company (1970)

(4)Los Alamos Radiation Transport Group (X-6): MCNP-Monte Carlo Neutron and Photon Transport Code, LA-7396-M,Rev.,LANL (1981)

(5)Takahashi, A.,et al.: DOUBLE DIFFERENTIAL NEUTRON EMISSION CROSS SECTIONS AROUND 14 MEV, OKTAVIAN Report A-87-01 (1987)

(6)YAMAMURO, N.: A NUCLEAR CROSS SECTION CALCULATION SYSTEM WITH SIMPLIFIED INPUT-FORMAT VERSION Ⅱ, JAERI-M90-006 (1987).

(7)EWBANK, W.B.,SCHMORAK, M.:Evaluated nuclear structure data file, ORNL-5054/R1, (1978)

Table 1 F2 parameters.

Nuclei	F2
Ti-48	0.40
V-51	6.50
Cr-52	1.00
Mn-55	0.30
Fe-56	0.50
Co-59	0.50
Ni-58	1.60
Ni-60	1.50
Cu-63	0.70
Cu-65	0.70

Table 2 Production cross sections of discrete gamma-rays for copper.

Energy (keV)	Reaction	Exp. (barn)	Cal. (barn)	C/E
669.6	$^{63}Cu(n,n')^{63}Cu$	19.4±1.8	49.45	5.79±0.54
881.0	$^{63}Cu(n,n')^{63}Cu$	19.2±1.8	35.60	1.83±0.17
898.9	$^{63}Cu(n,n')^{63}Cu$	26.8±2.4	14.93	0.60±0.05
962.1	$^{63}Cu(n,n')^{63}Cu$	127.5±10.4	128.14	1.03±0.08
978.0	$^{65}Cu(n,n')^{65}Cu$	21.7±2.0	7.17	0.39±0.04
1116.0	$^{63}Cu(n,n')^{63}Cu$	63.0±5.2	40.87	1.09±0.09
1162.3	$^{63}Cu(n,n')^{63}Cu$	62.3±5.2	2.68	0.86±0.07
1172.9	$^{63}Cu(n,n'p)^{62}Ni$	140.8±11.5	149.5	1.03±0.08
1327.0	$^{63}Cu(n,n')^{63}Cu$	100.0±8.2	99.6	1.18±0.10
1412.0	$^{63}Cu(n,n')^{63}Cu$	21.3±1.9	20.34	0.85±0.08
1482.0	$^{65}Cu(n,n')^{65}Cu$	40.7±3.5	52.74	1.75±0.15
1861.0	$^{63}Cu(n,n')^{63}Cu$	30.5±2.7	16.89	0.60±0.05

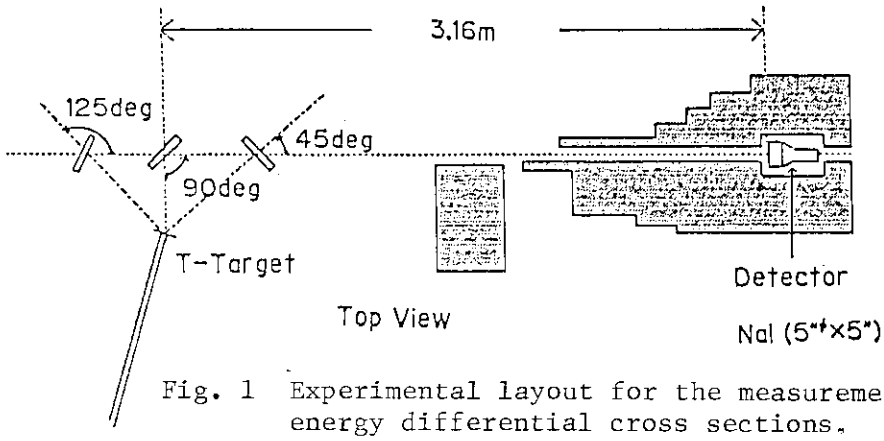

Fig. 1 Experimental layout for the measurement of energy differential cross sections.

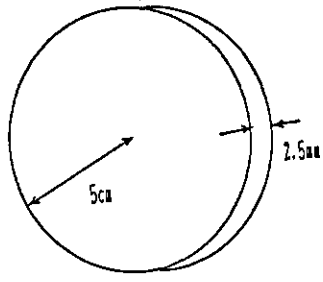

Fig. 2 Sample for measurement of differential cross sections.

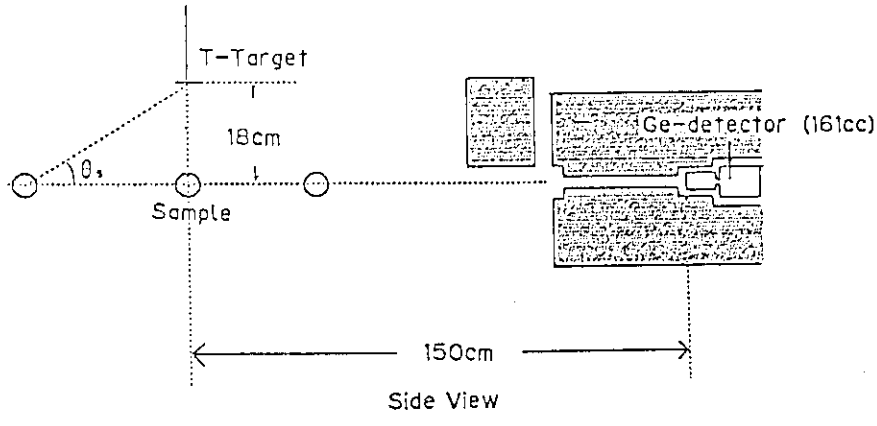

Fig. 3 Experimental layout for the measurement of discrete gamma-rays.

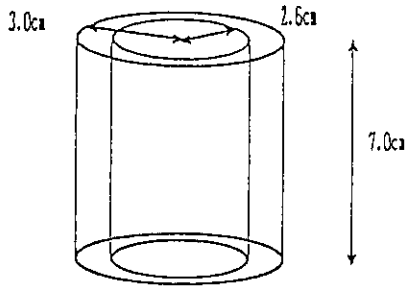

Fig. 4 Sample for measurement of discrete gamma-rays.

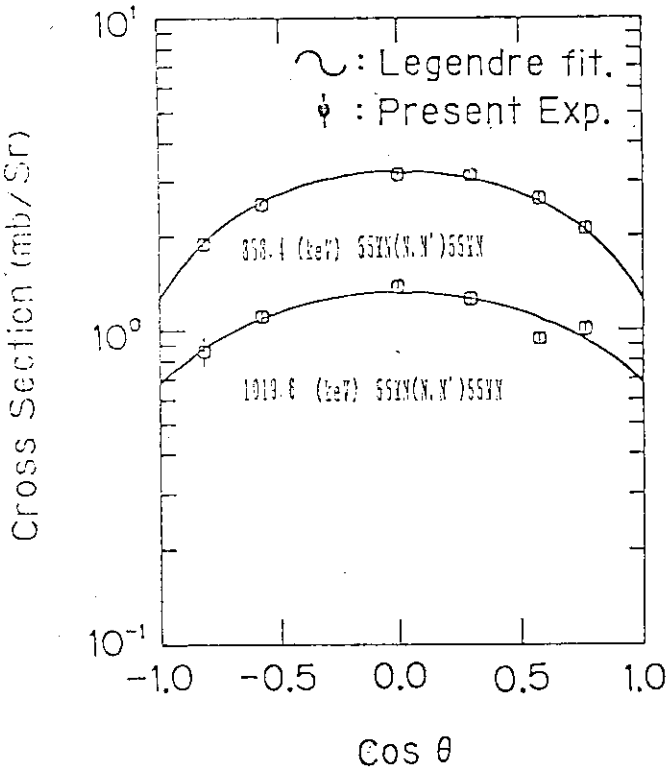

Fig. 5 Angular distributions of the discrete gamma-rays for natural manganese.

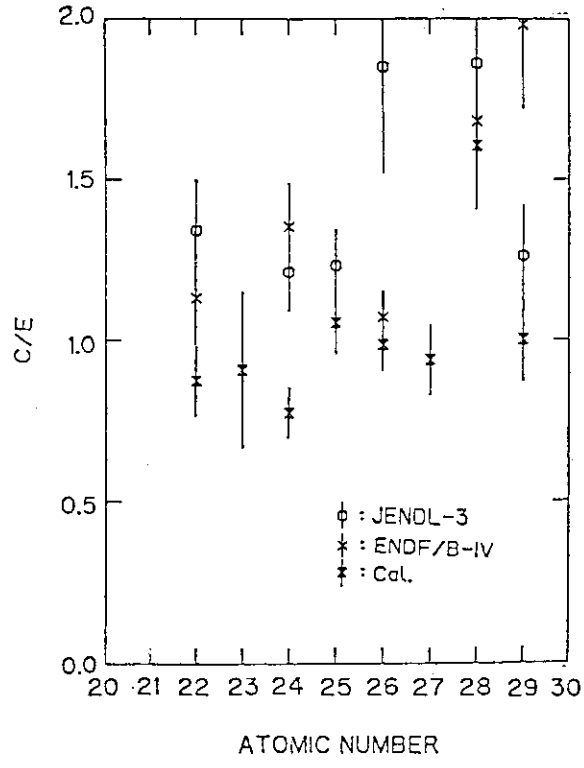

Fig. 6 C/E values of production cross sections.

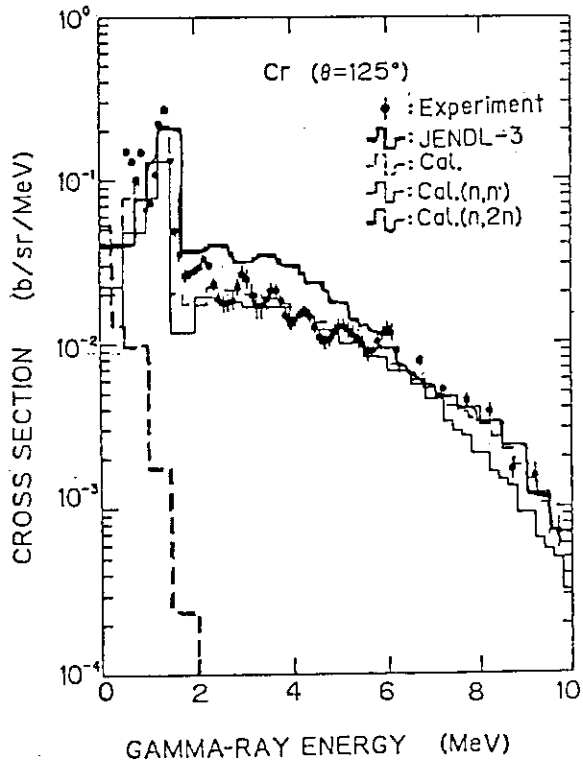

Fig. 7 Energy differential cross sections of gamma-rays for chromium.

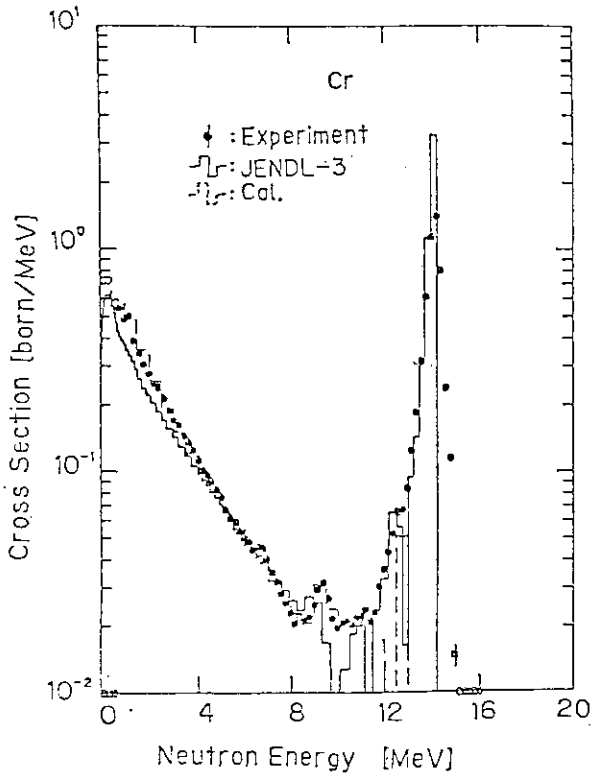

Fig. 8 Emission cross sections of secondary neutrons energy spectra for chromium.

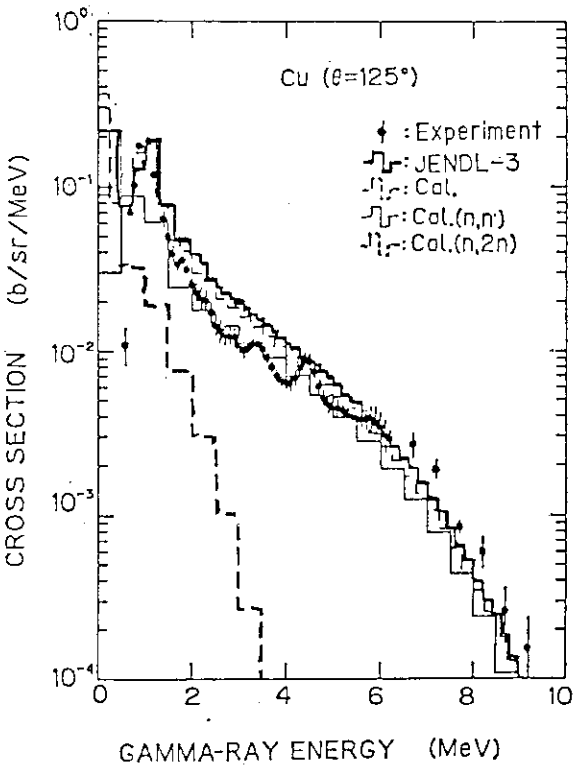

Fig. 9 Energy differential cross sections of gamma-rays for copper.

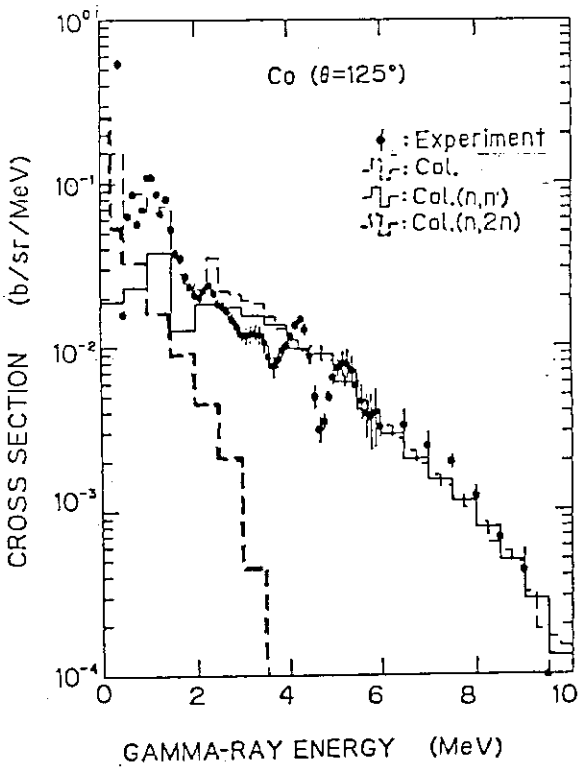

Fig. 10 Energy differential cross sections of gamma-rays for cobalt.

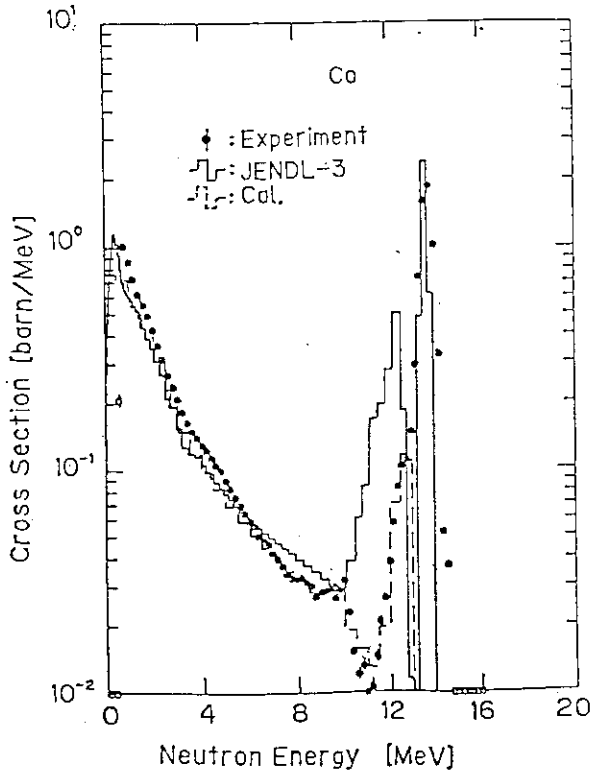

Fig. 11 Emission cross sections of secondary neutrons energy spectra for cobalt.

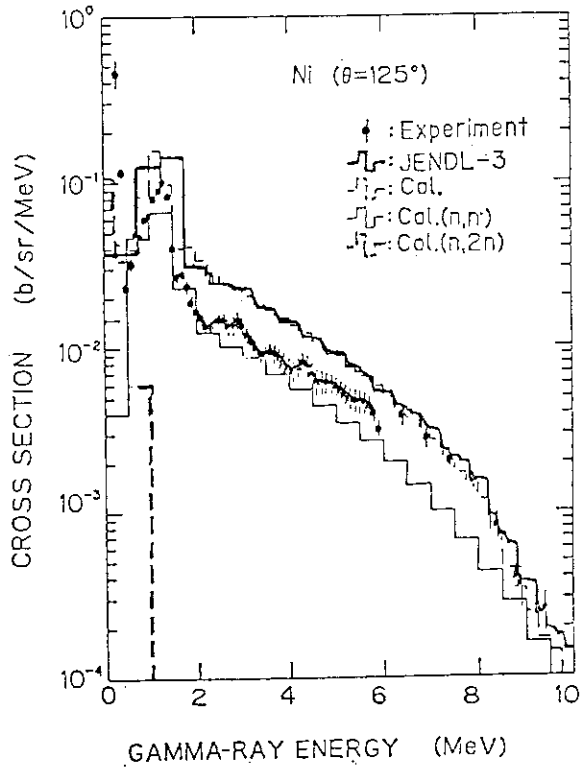

Fig. 12 Energy differential cross sections of gamma-rays for nickel.

3.9 Measurement of Formation Cross Sections of Short-lived Nuclei Production by 14 MeV Neutrons (IV)

T. Kobayashi, A. Taniguchi, T. Ikuta, K. Kawade,
H. Yamamoto, T. Katoh, *T. Iida and *A. Takahashi
Department of Nuclear Engineering, Nagoya University
*Department of Nuclear Engineering, Osaka University

Neutron activation cross sections of short-lived nuclei with half-lives between 21 s and 7 min have been measured at neutron energy of 13.4 to 14.9 MeV by the activation method for the 15 reactions; $^{19}F(n,p)$, $^{25}Mg(n,p)$, $^{29}Si(n,p)$, $(n,n'p)$, $^{50}Ti(n,p)^{m+g}$, $^{54}Cr(n,p)$, $(n,n'p)$, (n,α), $^{64}Ni(n,\alpha)$, $^{69}Ga(n,\alpha)$, $^{87}Rb(n,2n)^{m}$, $(n,\alpha)^{m}$, $^{86}Sr(n,p)^{m}$, $^{87}(n,n'p)^{m}$, and $^{107}Ag(n,p)^{m}$.

1. Introduction

Neutron activation cross section data around 14 MeV have become important from the viewpoint of fusion reactor technology, especially for calculations on radiation damage, nuclear transmutation, induced activity and so on. Cross sections for the reactions leading to short-lived nuclei were measured by the activation method.

2. Experiment and results

Experiments were performed at the Intense 14-MeV-Neutron Source Facility (OKTAVIAN) of Osaka University. For the activation of samples, pneumatic tubes were set at 6 directions (0°, 50°, 75°, 105°, 125° and 155°) for the incident deuteron beam direction. The distances between the T-target and the irradiation points were 15 cm. The induced activities were measured with two Ge detectors(12%, 16%) at an equivalent distance of 5 cm. The effective neutron energies were determined by the Zr/Nb method(1). The errors are estimated to be about 50 keV. The neutron flux at the irradiation points was monitored by using two aluminum foils (purity:99.2%, 1 cm × 1 cm × 0.2 mm^{t}). The reference reaction for the flux measurement was the $^{27}Al(n,p)^{27}Mg(9.46\ min)$ reaction, which was determined referring to the standard $^{27}Al(n,\alpha)^{24}Na$ reaction (ENDF/B-V). Separated isotopes or natural samples were used for irradiation. The samples were between 30 and 190 mg

in weight (size : 1 cm × 1 cm).

In Table I, measured reactions and associated data(2) of the half-live ($T_{1/2}$), the γ-ray energy ($E\gamma$), the absolute intensity in photons per disintegration($I\gamma$) are listed together with the Q values.

Corrections were made for time fluctuation of neutron flux, thickness of samples, self absorption of γ-ray, sum-peak effect of γ-ray and contribution of low energy neutrons below 10 MeV. The details of the corrections are described elsewhere (3). The total errors (δt) were derived by combining the experimental (δe) and the error of nuclear data (δr) in quadratic:

$$\delta t^2 = \delta e^2 + \delta r^2.$$

Estimated major sources of the errors are listed in TableⅡ. Accuracies of the obtained cross-sections were around 3.5% in case of the good statistics. The results are listed in Table Ⅲ and some of them are shown in Fig.1.

The authors with to express their sincere thanks to Prof. K. Sumita for his support to this work and messrs. H. Sugimoto, M. Datemichi and S. Yoshida for the operation of the OKTAVIAN accelerator. We wish to thank Dr. T. Nakagawa of the JAERI Nuclear Date Center. This work was performed under the construction between Nagoya University and Japan Atomic Energy Institute (JAERI).

References

(1) Lewis, V. E., Zieba, K. J.: Nucl. Instr. and Meth. 174(1980)141.
(2) Browne, E., Firestone, R. B., Shirley, V. S.: Table of Radioactive Isotopes "John Wiley & Sons, New York (1986).
(3) Kawade, K., Yamamoto, H., Yamada, T., Katoh, T.,Iida, T., and Takahashi, A.: JAERI-M 90-171 (1990).
(4) Miyahara: private communication(1990).

Table 1 Reactions and decay parameters

Reaction[a]	$T_{1/2}$	Eγ (keV)	Iγ (%)	Q(MeV)[b]
$^{19}F(n,p)^{19}O$	26.91s	197.1	95.9(21)	-4.04
$^{25}Mg(n,p)^{25}Na$	59.6s	585.0	12.96(71)	-3.05
$^{29}Si(n,p)^{29}Al$	6.56m	1273.4	91.3	-2.90
$(n,np)^{28}Al$	2.241m	1779.0	100	-12.33
$^{50}Ti(n,p)^{50m+g}Sc$	1.710m	523.8	88.7(18)	-6.11
$^{54}Cr(n,p)^{54}V$	49.8s	834.8	97.1(17)	-6.26
$(n,np)^{53}V$	1.61m	1006.2	90(2)	-12.37
$(n,\alpha)^{51}Ti$	5.76m	320.1	93.0(4)	-1.56
$^{64}Ni(n,\alpha)^{61}Fe$	5.98m	298.0	22.2(28)	-2.53
$^{69}Ga(n,\alpha)^{66}Cu$	5.10m	1039.4	9.12(14)[c]	2.58
$^{87}Rb(n,2n)^{86m}Rb$	1.017m	556.1	98.19(1)	-10.48
$(n,\alpha)^{84m}Br$	6.0(m)	424.3	100(10)	-1.49
$^{86}Sr(n,p)^{86m}Rb$	1.017m	556.1	98.19(1)	-1.55
$^{87}Sr(n,np)^{86m}Rb$	1.017m	556.1	98.19(1)	-9.98
$^{107}Ag(n,p)^{107m}Pd$	21.3s	214.9	69.0(20)	0.53
$^{27}Al(n,\alpha)^{24}Na$[d]	14.959h	1368.6	99.994(3)	-3.13
$^{27}Al(n,p)^{27}Mg$	9.46m	843.8	72.0(4)[c]	-1.83

[a] (n,np) means [(n,d)+(n,n'p)+(n,pn)].

[b] Q(n,n'p) is given here. Q(n,d)=Q(n,n'p)+2.225MeV.

[c] taken from ref.4.

[d] Standard reaction(ENDF/B-V) used in this work.

Table 2 Principal sources of uncertainty in the measured cross sections

Experimetal error (δe)	
Source of error	Uncertainty(%)
Counting statistics	0.5 - 40
Sample mass including purity	0.1
Neutron flux fluctuation	<0.1
Gamma-peak area evaluation	0.5
Detector efficiency	1.5(Eγ>300 keV), 3(300 - 80 keV), 5(Eγ<80 keV)
Efficiency calibration at 0.5 and 5 cm	1.0
Correction for true coincidence sum	<0.3
Correction for random coincidence sum	<0.4
Correction for sample thickness	0.2 - 0.6
Correction for self-absorption of γ-rays	0 - 0.2
Correction for low energy neutrons	0 - 5
Secondary reference cross section for $^{27}Al(n,p)^{27}Mg$	0.5 (only statistics)

Error of nuclear data (δr)	
Source of error	Uncertainty(%)
Reference cross section for $^{27}Al(n,\alpha)^{24}Na$(ENDF/B-V)	3.0
Absolute γ-ray intensity	0 - 13
Half-life	0 - 5

Table 3 Activation cross sections of short-lived nuclei

En(MeV)	$^{19}F(n,p)^{19}O$	$^{25}Mg(n,p)^{25}Na$	$^{29}Si(n,p)^{29}Al$	$^{29}Si(n,np)^{28}Al$
14.87	17.8(10)mb	62.6(49) mb	130.8(47) mb	24.7(10) mb
14.58	18.6(10)	63.7(50)	131.6(47)	17.9(8)
14.28	19.4(10)	67.3(54)	131.7(49)	13.2(6)
13.88	19.5(10)	63.3(49)	132.7(48)	10.3(5)
13.65	20.8(11)	63.4(49)	130.6(47)	8.6(4)
13.40	22.7(12)	62.0(48)	125.6(45)	6.0(3)

En(MeV)	$^{50}Ti(n,p)^{50m+g}Sc$	$^{54}Cr(n,p)^{54}V$	$^{54}Cr(n,np)^{53}V$	$^{54}Cr(n,\alpha)^{51}Ti$
14.87	14.4(8) mb	21.3(13) mb	3.3(5) mb	13.2(5) mb
14.58	13.5(7)	21.6(14)	3.2(5)	12.8(5)
14.28	13.0(7)	20.8(16)	1.5(4)	12.1(6)
13.88	12.0(7)	17.5(12)	1.4(3)	11.7(5)
13.65	10.6(6)	13.4(10)	0.7(3)	11.0(5)
13.40	10.2(6)	15.0(11)	0.5(2)	10.3(4)

En(MeV)	$^{64}Ni(n,\alpha)^{61}Fe$	$^{69}Ga(n,\alpha)^{66}Cu$	$^{87}Rb(n,2n)^{86m}Rb$	$^{87}Rb(n,\alpha)^{84m}Br$
14.87	6.0(8) mb	20.7(14) mb	527(18) mb	0.81(11) mb
14.58	5.5(8)	21.7(15)	559(20)	0.69(12)
14.28	5.1(8)	19.6(20)	508(18)	0.77(20)
13.88	4.5(6)	23.5(16)	460(16)	0.59(10)
13.65	3.7(6)	24.0(17)	478(17)	0.52(11)
13.40	3.0(4)	22.0(14)	463(16)	0.49(9)

En(MeV)	$^{86}Sr(n,p)^{86m}Rb$	$^{87}Sr(n,np)^{86m}Rb$	$^{107}Ag(n,p)^{107m}Pd$
14.87	12.9(6) mb	4.3(3) mb	7.3(8) mb
14.58	13.2(7)	3.4(3)	7.4(8)
14.28	12.1(7)	2.2(2)	7.9(9)
13.88	12.7(6)	1.8(2)	7.2(7)
13.65	11.1(6)	1.1(1)	7.3(7)
13.40	10.1(5)	0.3(1)	7.7(8)

* Error of neutron energy is estimated as about 50 keV.

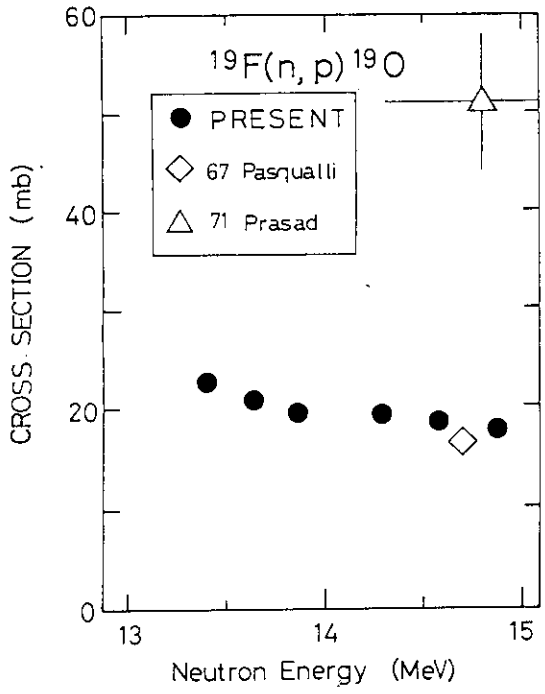

Fig. 1(1) Cross section of $^{19}F(n,p)^{19}O$

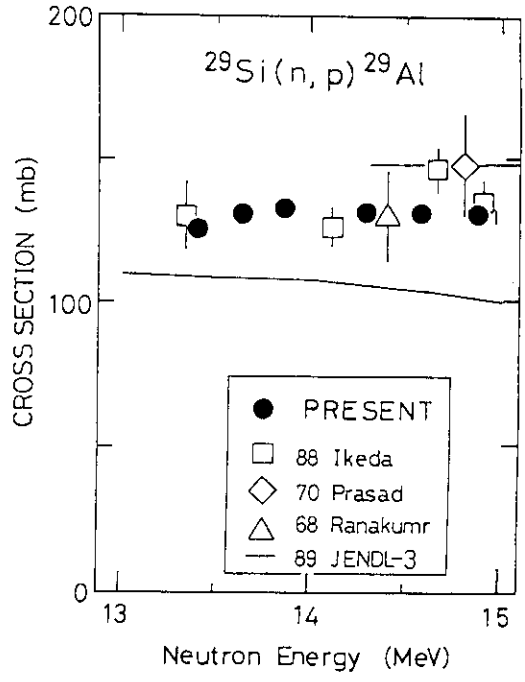

Fig. 1(2) Cross section of $^{29}Si(n,p)^{29}Al$

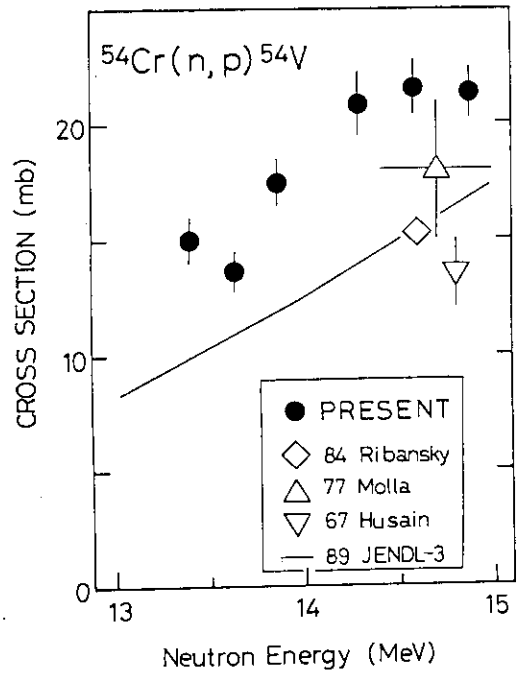

Fig. 1(3) Cross section of $^{54}Cr(n,p)^{54}V$

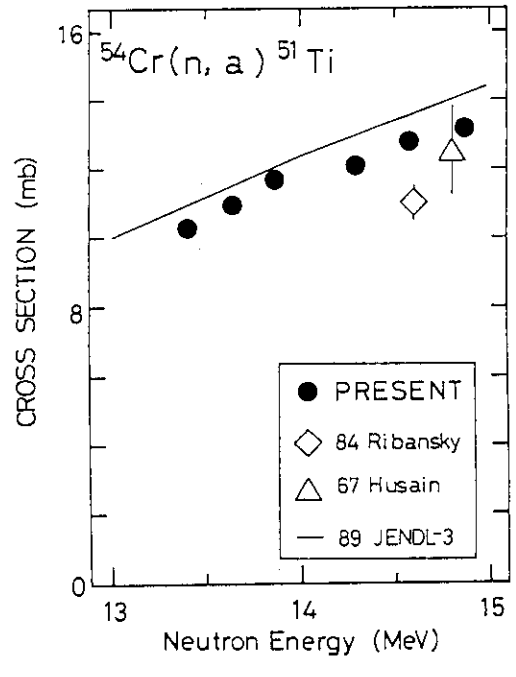

Fig. 1(4) Cross section of $^{54}Cr(n,\alpha)^{51}Ti$

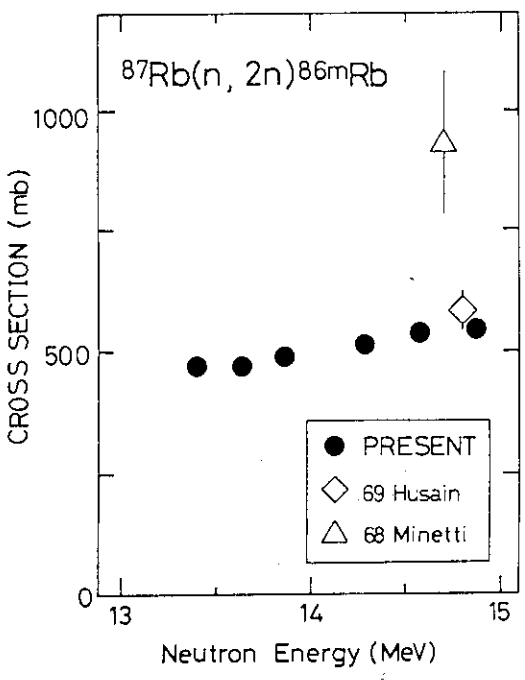

Fig. 1(5) Cross section of $^{87}Rb(n,2n)^{86m}Rb$

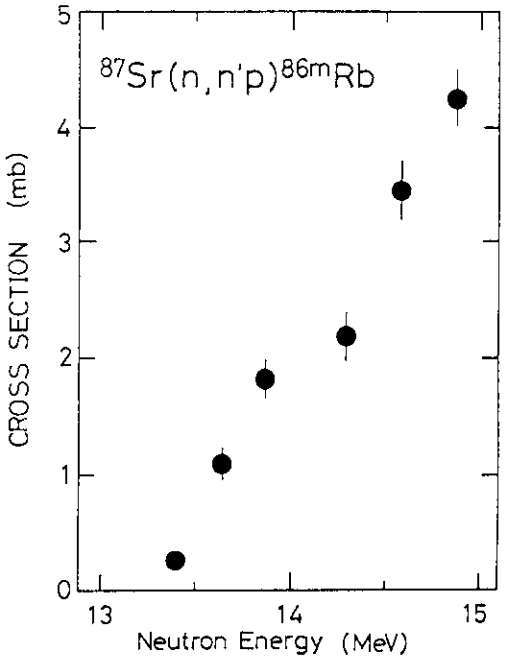

Fig. 1(6) Cross section of $^{87}Sr(n,n'p)^{86m}Rb$

3.10 Measurements of Long-lived Activation Cross Sections by 14 MeV Neutrons at FNS

Yujiro Ikeda, Donald L. Smith* , Anil Kumar** and Chikara Konno

Japan Atomic Energy Research Institute
**Argonne National Laboratory
* University of California, Los Angeles

Abstract: Several long-live activation cross sections at 14.8 MeV have been measured by using the FNS facility in order to provide experimental data meeting the requirement in the radioactive wastes disposal assessment in the D-T fusion reactor. The measurements were conducted under two international collaborations. Measured data were compared with data available in the literature and discussed in terms of accuracy needed for the requirement.

1. Introduction

An endeavor to arrive at sufficient accuracy in the nuclear data for long-lived activation cross section have been initiated a few years ago as the IAEA-CRP[1] to satiety the nuclear data needs from radioactivity waste disposal assessment. Since at the time, significant efforts have been devoted on the experimental measurement, the theoretical prediction and the evaluation. One experiment for this purpose has been proposed in the framework of the JAERI/US collaborative program on fusion neutronics.[2] This experiment was related with a systematic verification of the induced radioactivity calculation codes and activation cross section data libraries currently available.[3,4] The other experimental program was an inter-laboratory collaboration[5] was proposed by Dr. D. L. Smith at ANL under a support by the IAEA-CRP, which included different neutron sources, d-Be at ANL[6], T-p at LANL[7] and D-t at FNS, JAERI[8]. In this collaboration, it was expected that cross sections of concerned cover the neutron energy range from several MeV to 14 MeV. ANL was responsible to deliver the sample package to other facilities and to measure the activities after irradiation. The measurement of cross sections at 14 MeV was carried out at FNS, JAERI as a part of this collaboration :

the package with an identical set of samples were irradiated along with the other package which had been sent to back to ANL for counting there.

This report describes the experiments at FNS in some detail and gives a preliminary results so far of some cross sections at 14 MeV, reactions of which include $^{27}Al(n,2n)^{26}Al$, $^{109}Ag(n,2n)^{108m}Ag$, $^{151}Eu(n,2n)^{150m}Eu$, $^{153}Eu(n,2n)^{152m}Eu$, $^{159}Tb(n,2n)^{158}Tb$ and $^{179}Hf(n,2n)^{178m2}Hf$. Some of data have still remained in waiting to be measured because of significant large interfering radioactivities with modest long half-life, which are out of scope of the present task.

2. Experiment

2.1 Long-lived activity production reactions investigated

The reactions, half-lives of products, natural abundances, γ-ray - branching ratios, atomic mass are given in Table 1. Decay data were taken from the Table of Isotopes.[9] The long-lived radioactivities with half-lives from 10 to 10^6 years were concerned in this experiments. And also the radioactivities which associate the g-ray emission were the objects in this measurements. The other β-emitter of ^{63}Ni and ^{49}V are subjected in the future task.

2.2 Irradiation configuration

Samples for both programs of JAERI/USDOE collaboration and ANL/LANL/FNS inter-laboratory collaboration were irradiated simultaneously with 14 MeV neutrons for 4 days (8 hours irradiation per a day). It resulted in 1.7×10^{17} neutrons of total neutron yield at the DT target.

For the JAERI/USDOE program, four set of foil packages were placed at angles of 0°, 45°, 90° and 135° with respect to the incident d+ beam, distances of which was about 30 mm from the D-T source. This configuration enabled to provide cross section data at energy range from 13.5 to 15.0 MeV. Since the sample package was considerably thick and significant decreasing flux distribution was expected in the sample, multiple thin Nb foils were inserted in the sample package For the neutron flux monitor. Neutron flux at each sample was monitored with the $^{93}Nb(n,2n)^{92m}Nb$ reaction. The neutron fluence at the samples was estimated to range $1 - 2 \times 10^{15}/cm^2$.

The two sample packages for the inter-laboratory collaboration were placed at identical positions of 7 cm distances from D-T source. The nominal fluence on the irradiated sample was about 2×10^{14} n/cm^2. This fluence was much less than that expected because of poor tritium target performance. Neutron fluence in the sample package was monitor by some dosimetry foils of Ni, Ti and Fe, reactions to be used of

which were $^{58}Ni(n,p)^{58}Co$ (T1/2=70.8d), $^{46}Ti(n,p)^{46}Sc$ (T1/2=83.6d) and $^{54}Fe(n,p)^{54}Mn$ (T1/2=312d). However, these reaction cross section have rather low threshold energies below 14 MeV so that large contribution of low energy neutrons to the total reaction rate seemed very significant. In such a case, well defined neutron spectrum should be known to correct that low energy contribution. For this purpose, analytical calculation of the spectrum was separately carried out. In order to simplify the neutron fluence determination, Nb foils were attached on both front and rear surfaces of the package. Since cross section of $^{93}Nb(n,2n)^{92m}Nb$ has threshold energy around 10 MeV, quite accurate flux of 14 MeV was derived. From the Nb foil activation results, neutron fluxes on the front and the rear surface were 7.30 x 10^8 / cm^2•sec and 4.15 x 10^8 h/cm^2•sec, respectively.

2.3 Gamma-ray counting

More than 1.5 year after irradiation, g-ray counting has started by using a high detection efficiency Ge detector (115 % relative to 3" x 3" NaI(Tl)). Gamma-ray spectrum was analysed by GENIE code system provided by CANBERRA. The detector efficiency was calibrated by standard γ-ray sources. The uncertainty of data for efficiency is about 3 % at present moment although it was very tentative one.

3. Results

From summary peak counts, reaction rates of concern were derived with necessary corrections, e. g. decay constant, cooling time, collection time, detector efficiency, natural abundance of the target material, γ-ray branching ratio, sample weight, self-absorption of γ-ray, neutron flux fluctuation during irradiation, and so forth.

The cross section were preliminary obtained from the reaction rates divided by neutron flux determined by $^{93}Nb(n,2n)^{92m}Nb$ reaction rate. In Table 2. present data are summarized along with data available.

3.1 $^{27}Al(n,2n)^{26}Al$

Present measurement gave 44 ± 5 mb for the cross section at 14.9 MeV. This value is very close to the data reported by Iwasaki[10] and slightly higher than data reported by Sasao.[11] Still measurements of the activities at the other angles are underway.

3.2 $^{151}Eu(n,2n)^{150m}Eu$

The reaction of $^{151}Eu(n,2n)$ produces. Two isomers of ^{150}Eu with half-lives of 35.8 years and 12.6 hours. From the decay schem of ^{150}Eu, there is no isomeric transition so that activities are treated as independent reaction products. In this study, we to used on

the cross section of production for ^{150}Eu with 35.8y half-live.

Only two cross section data has been reported previonsely by Qaim [12] and Nethaway [13]. They gave cross sections of 1,270 ± 149 b and 1,180 ± 150 b at 14.7 and 14.8 MeV, respectively. Recent summary of IAEA-CRP showed available in the report [1]; 1,209 ± 28 at 14.77 MeV measured by IEA Beijing, 1,090 ± 84 at 14.9 MeV by KRI Leningrard. These data showed somewhat cowerfgency around 1,200 barns.

The present data of 1,127 ± 66 mb at 14.9 MeV gives a good agreement with those reported within experimental errors. Meanwhile we have carried out the measurement using separated isotopes (enriched ^{151}Eu samples) before. This measurement gave cross sections rauging from 1,034 to 1,130 mb at the energies 13.5 to 14.9 MeV. Both experimental data are in quite good agreements each, although the sample configuration, neutron field and Ge detectors used were different.

Thus, we may conclude that the this reaction cross section data 14 - 15 MeV could be convergented in early time. One thing should be mentioned is that the IRK evaluation seems a little bit higher than those measured. However, if they evaluate again using how data, it would be consistent one.

3.3 ^{153}Eu(n,2n)^{152m}Eu

Reaction of ^{153}Eu(n,2n) produce three state of ^{152}Eu ; one is isomeric state decaying to the ground state with 96 min half-live, the other isomer with half-life of 9.3h which disintegrates to both ^{152}Sm and ^{152}Gd and the O the is the ground state with half-live of 13.2 years which disintegrates to the ^{152}Gd with β decay.

Since the isomeric state of 96 min de excites with 100 % isomeric transitions to the ground state the cross section has bean obtained for the ^{153}Eu(n,2n)$^{152m1+g}$Eu ; Although there have been a lot of cross section measurements for the products of 96 min and 9.3 hr, only one data was avaireble for the 13.2 years production by Qaim [10] before IAEA-CRP report has appeared. It gave 1,542 ± 138 mb.

In the summary report of IAEA-CRP, we found the data of 1,544 mb at 14.77 MeV by Beijing; 1,740 mb at 14.7 MeV by KRI Leningrad. IRK vienna gave evaluation of 1,442 mb at 14 - 15 MeV. These are rather scattered around 1,500 mb. Meanwhile, at FNS, we measured cross section by using enriched sample of ^{153}Eu, resulted in from 1,300 to 1,410 mb around 14 MeV.

Note that the natural Europium has as mentioned two isotopes with mass number of 151 and 153, so that we have to be careful in the correction for the (n,γ) contribution for the ^{152}Eu production. Natural abundance of ^{151}Eu is so high about 48 % that you can not neglect the (n,γ) contribution when you use the natural Eu sample. The case is in the present measurement giving 1,975 ± 98 mb at 14.9 MeV without any correction for the (n,γ) contribution. Apparently considerbl amount of (n,g) reaction suffered the reaction rate determination. An attempted was made to correct (n,γ) fraction on the

^{152}Eu production. Using the neutron spectrum calculated by the MORSE-DD code and ^{151}Eu(n,γ)^{152}Eu reaction cross section taken from JENDL-3 dosimetry file, contribution was deduced to be 40 % to the total reaction rate. However, we have to considered the self-shielding effects for the very large capture g reaction in the sample. The fraction of 40 % seems too high to be used as the correction factor.

It is complicated that it is very hard to arrive at reasonably accurate corrections for the ^{152}Eu production cross section. Concludiegly, the use of enriched ^{153}Eu sample is highly recommended.

The status of the cross section seems a little bit controvertial, because of, as mentioned, rather scattered experimental data.

3.4 ^{159}Tb(n,2n)$^{158m+g}$Tb

Terbium-158 has two states, one isomeric state deexciting through 100 % isomeric transition with half-life of 10.5 sec and the ground state decaying with 150 year half-life. The isomer is so short life that cross section is given as ^{159}Tb(n,2n)$^{158m+g}$Tb. Natural abundance of ^{159}Tb is 100 % so that there is no interference (n,γ) contribution to ^{158}Tb products.

Two experimental data have been reported by Qaim [12] and Prestwood[14] before IAEA-CRP report. They are 1,801 mb at 14.7 MeV and 1,930 mb at 14.8 MeV, respectively. In the IAEA-CRP report, one experimental data and one evaluation are given by IAE Beijing to be 1,968 mb at 14.77 MeV and by IRK Vienna to be 1,930 mb at 14 - 15 MeV. Those data seem very close each other. The present data measured at FNS gives a cross section of 1,600 mb at 14.9 MeV. The value is considerable lower them those previously reported even though the experimental errors are taken into account. The data should be check in the successive counting.

3.5 ^{179}Hf(n,2n)^{178m2}Hf

Abundances of ^{179}Hf and ^{177}Hf are 13.7 % and 18.6 %, respectively. In general, it is expected that ^{177}Hf(n,g) reaction contributes to produce ^{178}Hf. However, the state of 178m2Hf of interest in this study is a high spin state (16+), so that capture reaction to this state must be very inhibited. We assume that contribution of the (n,g) reaction is negligible.

No data has been reported so far before IAEA-CRP summary. Only Harwell reported an experimental data; 5.9 ± 0.6 mb at 14.8 MeV. One calculation has been given by Oxford/LANL to be 2.9 mb at 14 MeV.

Present measurement showed the value of 6.6 ± 0.8 mb at 14.9 MeV very close to that of Harwell.

3.6 ^{109}Ag(n,2n)^{108m}Ag

No experimental data for the cross ^{109}Ag(n,2n)^{108m}Ag (T1/2=127y) has been

reported before IAEA-CRP report. In the IAEA-CRP report three experiments and one evaluation have been given ; 230 ± 7 mb at 14.77 by IAE Beijing, 263 ± 20 mb by Debrecen and 208 ± 37 mb by KRI Leningrad ; 665 ± 73 mb by IRK vienna.

As long as the half-live of 127 ± 7 year is used, the present experiment gives cross section of 191 ± 14 mb. This value is very close to the other experimental values, whereas it is three times as much as smaller them that of evaluation by IRK. This large difference between experimental data and the evaluation should be attributed to the wrong half-live data for the deduction of experimental data.

4. Present Summary

In this report, the preliminary cross section data for six reactions of $^{27}Al(n,2n)^{26}Al$, $^{151}Eu(n,2n)^{150m}Eu$, $^{153}Eu(n,2n)^{152m}Eu$, $^{159}Tb(n,2n)^{158m+g}Tb$, $^{179}Hf(n,2n)^{178m2}Hf$ and $^{107}Ag(n,2n)^{108m}Ag$ are given.

The countings of activities are still underway to arrive at sufficient statistics.

Aknowledements

Author would like to express their sincere thank to the members of the FNS facility for their opperation of accelerator.

References

1. INDC(NDS)-232/L, "Activation Cross Sections for the Generation of Long-Lived Radionuclides of Importance in Fusion Reactor Technology", Proc. of an IAEA Consultants' Meeting, Argonne National Laboratory, 11th - 12th. Sept 1989
2. T. Nakamura, et al. ;" Present Status of the Fusion Neutron Source(FNS)," Proc. 4th Symp. on Accelerator Sci. Technol., RIKEN, Saitama, 24 - 26 November 1982, pp 155- 156.
5. J. W. Meadows, et. al. "A Search for Activation Produced by Fast-Neutron Irradiations of Copper, Silver, Europium, Terbium and Hafnium", Proc. of an IAEA Consultants' Meeting, Argonne National Laboratory, 11th - 12th. Sept 1989.
6. D. L. Smith and J. W. Meadows; ANL/NDM-95, Argonne National Laboratory (986).
7. R. C. Haight "Activation with an Intense Source of Monoenergetic Neutrons in the Range 8-14 MeV", Proc. of a Specialists' Meeting on "Neutron Activation Cross Section for Fission and Fusion Energy Applications", Argonne National Lab., USA,

13th-15th sept. 1989 pp95-97

8. T. Nakamura, M. A. Abdou, "Overview of JAERI/USDOE Collaborative Program on Fusion Blanket Neutronics Experiments", Tokyo, Japan 1988, Fusion Eng. Design, 9, 303 (1989).
9. C. M. Ledere and V. S. Shirley;"Table of Isotopes," 7th edition, John Wiley &Sons, Inc., New York (1978).
10. S. Iwasaki, J. R. Dumais and K. Sugiyama,"Measurement of the Cross Section for $^{27}Al(n,2n)^{26}Al(T_{1/2}=7.16x10^{5}Y)$ reaction with Activation Technique around 14 MeV," Proc. Int'l. Conf. on Nuclear Data for Sci. and Technol., May 30-June 3, 1988, Japan.
11. M. Sasao et al.,: IPPJ-805, Inst. Plasma Phys., Nagoya Univ. (1987), and Phys. Rec. C, 35 (6) 2327 (1987).
12. S. M. Qaim; Nucl. Phys./A 224, 319(1974).
13. D. r. Nethaway; Nucl. Phys./A 190, 635(1972).
14. R. J. Prestwood; Phys. Rev. C. 30, 823(1984).

Table 1 List of objective reactions and associated decay of reaction products

	Reaction	Half-Lite	Abundance	γ-ray Energy(keV)	γ-ray Branching	Final Spin State
1	$^{27}Al(n,2n)^{26}Al$	$(7.16\pm0.32)\times10^{5}$y	100	1808.65	99.76±0.04	5^+
2	$^{94}Mo(n,p)^{94}Nb$	$(2.03\pm0.16)\times10^{5}$y	9.3	871.10	100.0	6^+
3	$^{109}Ag(n,2n)^{108m}Ag$	127±7y	48.17	434.0	90.5	6^+
4	$^{151}Eu(n,2n)^{150}Eu$	35.8±1.0y	47.9	333.96	94±3	$(4,5^-)$
5	$^{153}Eu(n,2n)^{152m2+g}Eu$	13.2±0.3y	52.0	344.3	27.2±0.4	8^-
6	$^{159}Tb(n,2n)^{158m+g}Tb$	150±30y	100	944.2	43±3	3^-
7	$^{158}Dy(n,p)^{158m+g}Tb$	150±30y	0.1	944.2	43±3	3^-
8	$^{179}Hf(n,2n)^{178m2}Hf$	31±1y	13.7	325.56	94.1±0.3	16^+
9	$^{182}W(n,n'\alpha)^{178m2}Hf$	31±1y	26.3	325.56	94.1±0.3	16^+
10	$^{193}Ir(n,2n)^{192m2}Ir$	241±9y	62.7	316.5	82.9	(9^+)
				(decay of ground state of ^{192}Ir to ^{192}Pt)		
11	$^{187}Re(n,2n)^{187m}Re$	2×10^{5}y	62.6	137	10.0	(8^+)
				(decay of ground state of ^{186}Re to ^{186}Os)		
12	$^{209}Bi(n,2n)^{208}Bi$	$3.68\pm0.04\times10^{5}$y	100	2615	100	(5^+)
				(Natural Background Subtraction is carfully needed)		
Others						
13	$^{48}Ti(n,\alpha)^{45}Ca$	165.1±0.7d	73.7	12.47	3×10^{-6}	$(7^-/2)$ β-emitter
14	$^{37}Cl(n,2n)^{36}Cl$	3×10^{5}y	no - γ-ray	$\beta^-(98.1)$, EC(1.9), $\beta^+(0.0017\%)$		
15	$^{93}Nb(n,n')^{93m}Nb$	13.6±0.3y	100	30.4		
16	$^{94}Mo(n,2n)^{93g}Mo$	^{93m}Nb				

Table 2 Cross section data measured and present status for long lived activation products

Reaction	Status	Laboratory	Energy (MeV)	Cross Section(mb)
$^{27}Al(n,2n)^{26}Al$	*	Tohoku Univ.	14.7	40.6 ± 4.4
	*	Nagoya Univ.	14.8	35 ± 7
	5)	**JAERI/USDOE**	**14.9**	**44 ± 5**
$^{109}Ag(n,2n)^{108m}Ag$	1)	IAE Beijing	14.77	230±7
	1)	Debrecen	14.50	263±20
	3)	IRK, Vienna	14 - 15	665±73
	2)	**ANL/LANL/JAERI**	**14.8**	**191 ± 7**
	1)	KRI Leningrad	14.9	208±37
$^{179}Hf(n,2n)^{178m2}Hf$	2)	Harwell	14.8	5.9±0.6**
	2)	IAE Beijing	14.2 - 14.8	- - - - - -
	4)	Oxford/LANL	14	2.9
	2)	**ANL/LANL/JAERI**	**14.8**	**6.0 ± 0.3**
$^{151}Eu(n,2n)^{150m}Eu$	1)	IAE Beijing	14.77	1219±28
	3)	IRK, Vienna	14 - 15	1325±94
	1)	KFA Julich	9.6 -10.6	1325±94
	2)	**ANL/LANL/JAERI**	**14.8**	**1127 ± 55**
	1)	KRI Leningrad	14.9	1090±84
$^{153}Eu(n,2n)^{152g}Eu$	2)	ANL/LANL/JAERI	10,14 and D-Be	- - - - - -
	1)	IAE Beijing	14.77	1544±42
	3)	IRK, Vienna	14 - 15	1442±60
	1)	KRI Leningrad	14.9	1740±145
$^{159}Tb(n,2n)^{158g}Tb$	2)	KFA Julich	8.6 - 10.6	- - - - - -
	1)	IAE Beijing	14.77	1968±56
	2)	**ANL/LANL/JAERI**	**14.8**	**1600 ± 88**
	3)	IRK, Vienna	14 - 15	1930±49

1) measurement performed for CRP
2) measurement in progress for CRP
3) evaluation of existing data performed for CRP
4) calculation performed for CRP
5) measurement of JAERI-USDOE collaboration
* measurement performed outside of CRP
** preliminary value

3.11 Activation Cross Section Measurement at Neutron Energies of 11.0, 12.0 and 13.2 MeV Using $^{1}H(^{11}B,n)^{11}C$ Neutron Source at JAERI

Y. Ikeda, C. Konno, M. Mizumoto, K. Hasegawa, S. Chiba, Y. Yamanouchi and M. Sugimoto

Japan Atomic Energy Research Institute,
Tokai-mura, Ibaraki-ken 319-11, Japan

Abstract: Some activation cross sections at neutron energies of 11.0, 12.0 and 13.2 MeV have been measured by the foil activation technique using a novel neutron source via. $^{1}H(^{11}B,n)^{11}C$ reaction at JAERI. The experimental procedure is described and the data obtained are discussed by comparing with cross sections in JENDL-3 Dosimetry File. Applicability of the present neutron source to the foil activation technique is also noted.

1. Introduction

The deficiency in experimental data of neutron cross sections at the energy region between 10 MeV and 13 MeV has been often stressed. This shortage in the experiments has been mainly due to the lack of the appropriate monoenergetic neutron sources. A use of the reaction of $^{1}H(t,p)n$ has been reported at LANL.[1] The availability is not sufficient to conduct a program to provide systematic data. So far, only a cross section measurement for the $^{58}Ni(n,p)^{58}Co$ and $^{60}Ni(n,p)^{60}Co$ has been reported by Vonach.[2] Recently, use of $^{1}H(^{11}B,n)^{11}C$ reaction to generate monoenergetic neutrons from 10 to 13 MeV has been investigated in JAERI by using the TANDEM heavy ion accelerator.[3] This source with significant low background neutrons was applied successfully in the secondary γ-ray production measurement.[4,5]

Utilizing this particular neutron source, we have carried out activation cross section measurements to provide data at energies of 11.0, 12.0 and 13.2 MeV for several important reactions in the dosimetry application.

2. Experiment

2.1 Reactions investigated

The reactions investigated in the present experiment are listed in Table 1 along with associated decay data of the product radioisotopes.[6] They are very important reactions for the dosimetry application where the accurate cross sections are needed. In particular, reaction of $^{27}Al(n,\alpha)^{24}Na$ is used as a standard for the cross section determination experiments. The reactions of $^{90}Zr(n,2n)^{89}Zr$ and $^{93}Nb(n,2n)^{92m}Nb$ are the most promising monitor reaction for the 14 MeV neutron flux. The reactions of $^{47}Ti(n,p)^{47}Sc$, $^{64}Zn(n,p)^{64}Cu$ and $^{115}In(n,n')^{115m}In$ are the spectral indices for the first neutrons with relatively low threshold energies. They are selected as the objective reactions, cross sections of which are to be measured in this program, from a view point of the importance in the dosimetry. Considerably large improvement in the accuracy of the cross sections around 10 -14 MeV region is highly anticipated from the present experiments.

2.2 Neutron source and irradiation

The monoenergetic neutrons were generated by bombarding the hydrogen gas target with ^{11}B beam energy of which were from 50 to 68 MeV by using the TANDEM accelerator at JAERI. Three different irradiations were conducted changing the energy of the incident ^{11}B beam. To subtract contributions of the parasitic neutrons produced in the structural materials of the target assembly to the total reaction rate, irradiation run without of ^{1}H gas in the target cell was carried out for each irradiation time. Irradiation usually lasted for 10 hours for both gas in and gas out runs. Typical neutron spectrum emitted from the target to the forward direction in the run at the beam energy of 64 MeV is illustrated in Fig. 1, which corresponds to the mean neutron peak energy of 12.4 MeV.

The size of the irradiation sample was 20 mm in diameter and 1 mm in thickness. Sample foils were stacked into a package in the orders of; Al/Zr/Nb/In for the irradiation at 13.2 MeV, and Al/Ti/Nb/Zn/In for the irradiations at 12.0 and 11.0 MeV. Two gold foils for neutron flux monitor were attached on rear and back sides of each package. The sample package was placed at a distance of about 100 mm from the center of the target cell. Neutrons incident into the foil package from the side of Al foil. In order to reduce the effect from the neutrons scattered by the materials surrounding the irradiation samples, sample was supported by a thin wire.

2.3 Activation measurement and cross section determination

After irradiation, reaction rates were derived from γ-ray counts measured with Ge detector performing necessary corrections. A correction factor for the neutron flux fluctuation during the irradiation was obtained from the output data of neutron flux monitor recorded in a chart. Net reaction rates were finally obtained by subtracting the data for irradiation with gas out from that with gas in, the beam current of which was adjusted to be equal to one with gas in.

As the flux monitor, the $^{197}Au(n,2n)^{196}Au$ reaction was employed due to its considerably large reaction cross section and rather flat response around energy from 10 to 14 MeV as shown in Fig. 2. The cross section data for this reaction was taken from JENDL-3 Dosimetry File.[7] The neutron flux at neutron energy corresponding to estimated one from the kinematics of $^{1}H(^{11}B,n)^{11}C$ reaction were determined from the reaction rates of $^{197}Au(n,2n)^{196}Au$ at both front and rear positions of the foil package and corresponding cross sections values. For the determination of the flux, no contribution of the low energy neutrons below the neutron peak of interest were taken into account because of rather high threshold energy of the $^{197}Au(n,2n)^{196}Au$ reaction.

Cross sections for the reaction of interest were obtained by using reaction rates and the neutron fluxes determined by the monitor reaction. At present moment, no contribution of the low energy neutron component in the incident neutron spectrum to the net reaction rate was considered due to insufficient data concerning the neutron spectrum. Further investigation is needed to correct for this item. However, it is expected that the $^{115}In(n,n')^{115m}In$ is the only one required significantly the correction for the low energy component because of its low threshold energy at 0.33 MeV. Other reaction have a relaxation from this condition due to their higher effective threshold energies.

Major experimental errors are summarized in Table 2. The error in the γ-ray counting statistics dominated overall uncertainty because the neutron flux level was not so high in comparison with the available D-T and D-D neutron sources. Furthermore, size of sample should be as concise as possible in order to keep the accuracy of the neutron flux and energy.

3. Results and discussion

Cross sections obtained in the present experiment are summarized in Table 3.

Figures 3.1 to 3.7 show the cross sections measured along with available data previously reported. Individual cross sections are discussed below.

3.1 $^{27}Al(n,\alpha)^{24}Na$

The present data are in a good agreement with data in JENDL-3 within experimental errors. In particular, the data at 13.2 MeV gives reasonably a good consistency with a value of the main body of data at 14 MeV region previously reported, as shown in Fig. 3.1. Since this reaction cross section at 14 MeV region has been believed to be in a satisfactory accuracy, the present result ensures us the reliability of the present experimental procedure.

3.2 $^{47}Ti(n,p)^{47}$

Two data at 11.0 and 12.0 MeV measured in the present experiment give slightly larger values than those in JENDL-3 and ENDF/B-V. However, the measured data show a reasonable smooth connection with the data around 14 MeV region measured at FNS.[8] On the other hand, Mannhart[9] reported that the cross sections below 8 MeV to the threshold should be considerably lower by 10 -20 % than ENDF/V-B evaluation. Concerning the reverse trend of the cross section between the different energy ranges, data at energy region from 8 to 10 MeV is highly required. A experimental data at 9.5 MeV is now processing.

3.3 $^{48}Ti(n,p)^{48}Sc$

Contrary to $^{47}Ti(n,p)^{47}$, data at 11.0 and 12.0 MeV are lower than those in JENDL-3 and ENDF/B-V as shown in Fig 3.3. Since this reaction is often used for the dosimetry purpose and the cross section should be reliable, further examination is needed in both experiment and evaluation.

3.4 $^{64}Zn(n,p)^{64}C$

Figure 3.4 shows the result for this reaction. Only one point data at 11.0 MeV was measured in the present experiment. The data is in a very good agreement with that in JENDL-3 Dosimetry file. As it is clearly given in Fig. 3.4, the data around 14 MeV region measure at FNS are considerably lower that those in the JENDL-3 Dosimetry File. This result encourage us to measure the data at energy from 12 to 13 MeV using the present neutron source.

3.5 $^{90}Zr(n,2n)^{89}Zr$

Data at one energy point at 13.2 MeV gives a little smaller value than that in JENDL-3. Nevertheless, significant consistency with the data measure at FNS is found as shown in the Fig. 3.5. Concerning the systematic in the data both measured by us, we

have very much confidence in the data accuracy. To confirm the validity of the evaluation, measurement of cross section at 12.5 MeV is hopefully required.

3.6 ^{93}Nb(n,2n)^{92m}Nb

Since there are a large number of experimental data available around 14 MeV region, reasonable convergence could be expected in the evaluation. However, The present data at 11.0, 12.0 and 13.2 MeV are systematically lower than those of JENDL-3 Dosimetry file as shown in Fig. 3.6. This result suggests to make a reevaluation of this cross section including the present data.

3.7 ^{115}In(n,n')^{115m}In

The data measured are shown in Fig. 3.7. The data are systematically much higher by 20 % than those in JENDL-3 and ENDF/B-V evaluations. This large discrepancy is definitely due to the neglect of the correction of low energy neutrons to the total reaction rate in the experimental data processing. It is considered that the contribution of the low energy neutrons to the reaction rate should be significantly large owing to the low threshold energy at 0.33 MeV for this particular reaction. Unfortunately, there was no experimental data for the source neutron spectrum below 3 MeV. In order to correct for the low energy neutron contribution, we have to perform a more precise source neutron characteristics experiment. Another approach is to calculated the spectrum by using a Monte Carlo Calculation with a precise model of the target structure.

4. Summary

Though there are considerably large numbers of data in the energy region from 13.5 to 15 MeV, data below 13 MeV were very limited, as shown in Figs. 3.1 to 3.7. The present data supplemented significantly the data needed in this particular energy region. In summary, it is demonstrated that the monoenergetic neutron source via. ^{1}H(^{11}B,n)^{11}C is very powerful to provide experimental data in the deficient region, even the activation technique is applied. Further measurements on the other important reactions are planed to be done in the future.

Acknowledgements

Authors wish to express their sincere thank to the operation crew of the TANDEM accelerator at JAERI.

References

1. R. C. Haight "Activation with an Intense Source of Monoenergetic Neutrons in the Range 8-14 MeV", Proc. of a Specialists' Meeting on "Neutron Activation Cross Section for Fission and Fusion Energy Applications", Argonne National Lab., USA, 13th-15th sept. 1989 pp95-97.
2. H. Vonach and M. Wagner,"Neutron Activation Cross-Section of ^{58}Ni and ^{60}Ni for 8-12 MeV Neutrons", ibid. pp165-176.
3. S. Chiba, et al.,"The ^{1}H(^{11}B,n)^{11}C Reaction as a Practical Low Background Monoenergetic Neutron Source in the 10 MeV Region," Nucl. Instr. & Methods, A281 581 (1989).
4. K. Hasegawa and M. Mizumoto,"Detector System for Gamma-ray Production Cross Section Measurement and Data Analysis," JAERI-M 89-042 (1989) in Japanese.
5. M. Mizumoto et al., Proc. Int. Conf. on Nucl. Data for Sci. and Technol., Mito, (1988) pp197-200.
6. C. M. Ledere and V. S. Shirley;"Table of Isotopes," 7th edition, John Wiley &Sons, Inc., New York (1978).
7. JENDL-3 Dosimetry File, to be published.
8. Y. Ikeda, et al.,"Activation Cross Section Measurement for Fusion Reactor Structural Materials at Neutron Energy from 13.3 to 15.0 MeV Using FNS Facility," JAERI-1312 (1988). (1988).
9. W. Mannhart, D. L. Smith and J. W. Meadows, "Measurement of the ^{47}Ti(n,p)^{47}Sc Reaction Cross Section", Proc. of a Specialists' Meeting on "Neutron Activation Cross Section for Fission and Fusion Energy Applications", Argonne National Lab., USA, 13th-15th sept. 1989 pp121-134.

Table 1 Reactions investigated and associated decay data

Reaction	Abundance(%)	Half-life	γ-ray energy(keV)	Branching ratio(%)
$^{27}Al(n,\alpha)^{24}Na$	100	15.02 h	1368	100
$^{47}Ti(n,p)^{47}Sc$	7.32	3.35 d	159.4	68.0
$^{48}Ti(n,p)^{48}Sc$	73.99	43.7 h	983.5	100
$^{64}Zn(n,p)^{64}Cu$	48.89	12.70 h	511.0	35.8
$^{90}Zr(n,2n)^{89}Zr$	51.46	78.4 h	909.2	99.87
$^{93}Nb(n,2n)^{92m}Nb$	100	10.15 d	934.46	99.15
$^{115}In(n,n')^{115m}In$	95.77	4.3 h	336.2	46.7
$^{197}Au(n,2n)^{196}Au$ *	100	6.183 d	355.65	87.7

* Flux monitor reaction

Table 2 Experimental errors

Items	Estimated error(%)
Reaction rate	
. γ-ray counts Statistics	1.0 - 13
. Detector efficiency	2.0
. γ-ray self-absorption	0.5
. Foil weight	0.1
. Neutron flux fluctuation	0.5
. Others	0.2
Neutron flux	
. Cross section of the monitor	not considered
. Reaction rate of the monitor	3 - 4
Overall for cross sections	4 - 14

Table 3 Cross sections obtained

Reactions	Cross sections (mb)		
	11.0 MeV	12.0 MeV	13.2 MeV
$^{27}Al(n,a)^{24}Na$	102.4 ± 4.7	118.5 ± 4.3	125.1 ± 6.9
$^{47}Ti(n,p)^{47}Sc$	148 ± 20	154 ±14	------
$^{48}Ti(n,p)^{48}Sc$	36.0 ± 2.2	44.3 ± 2.0	------
$^{64}Zn(n,p)^{64}Cu$	289 ± 17	------	------
$^{90}Zr(n,2n)^{89}Zr$	-------	------	305 ±17
$^{93}Nb(n,2n)^{92m}Nb$	219 ±12	345 ±13	444 ±23
$^{115}In(n,n')^{115m}In$	285 ±16	213 ±16	111 ± 6
$^{197}Au(n,2n)^{196}Au$ *	1970	1795	1549

* Flux monitor Reaction.
Cross sections values were taken from JENDL-3 Dosimetry File.

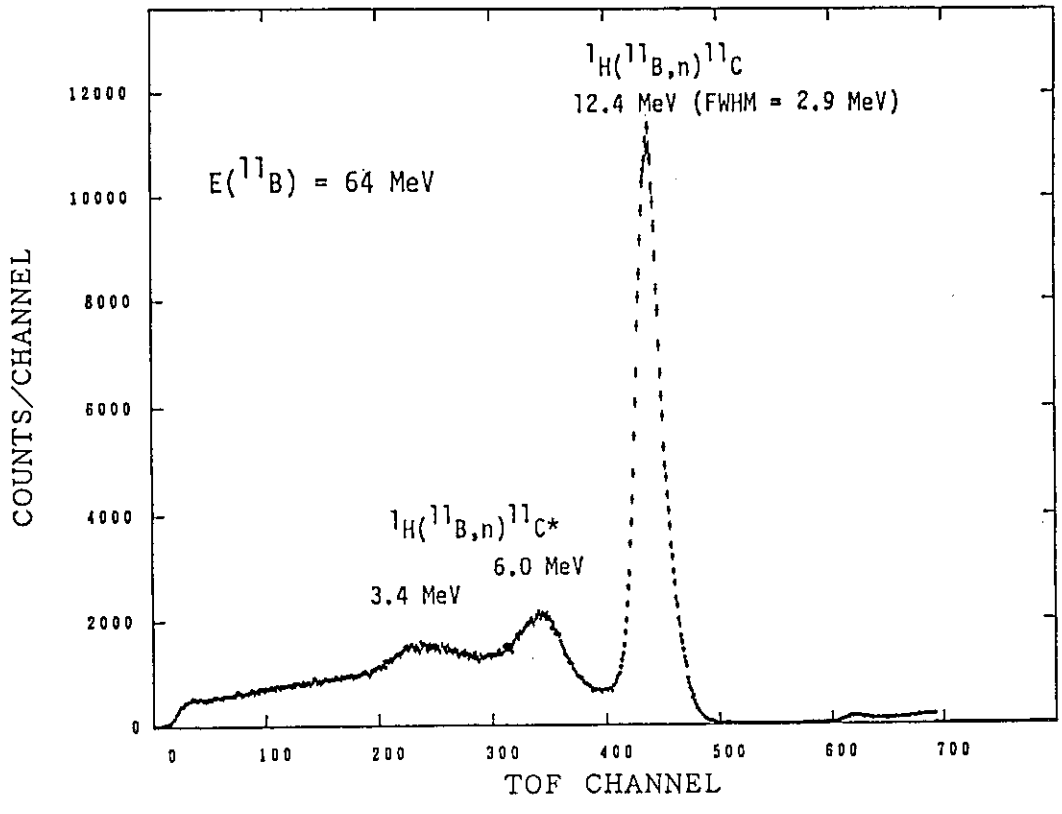

Fig. 1 TOF neutron spectrum at 0° with incident ^{11}B energy of 64 MeV. This figure is taken from Ref. 3.

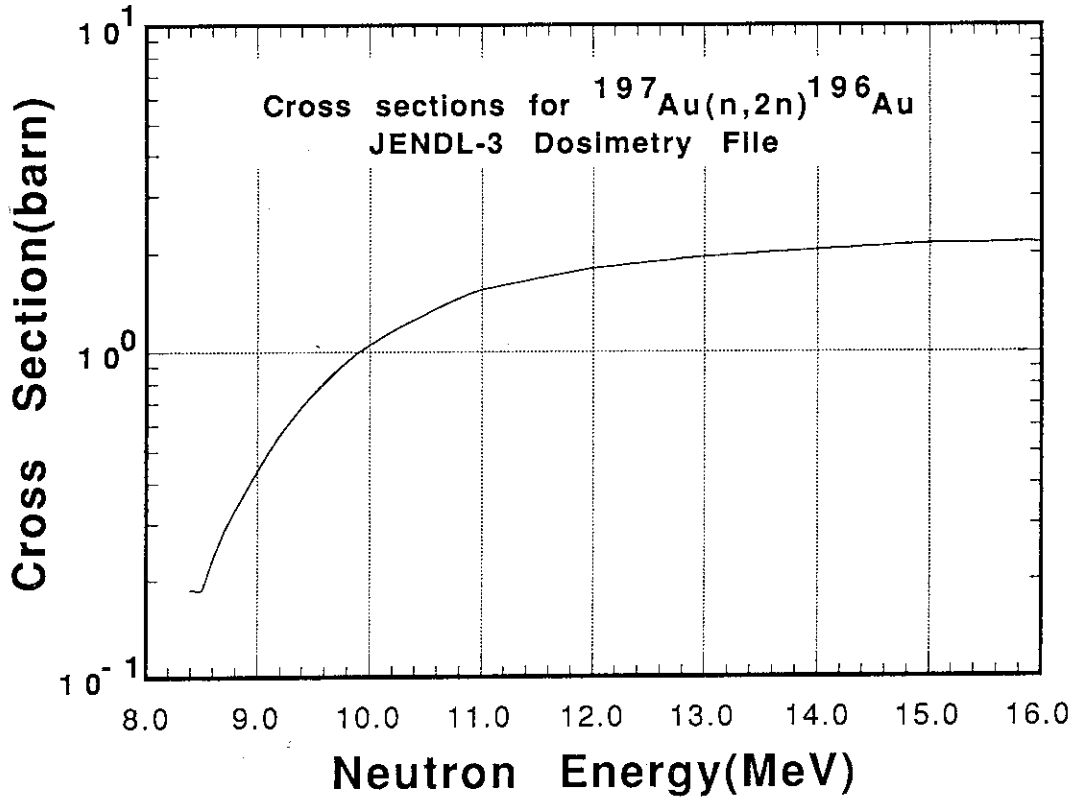

Fig. 2 Cross section curve of $^{197}Au(n,2n)^{196}Au$ reaction. Data are taken from the JENDL-3 Dosimetry File.[7]

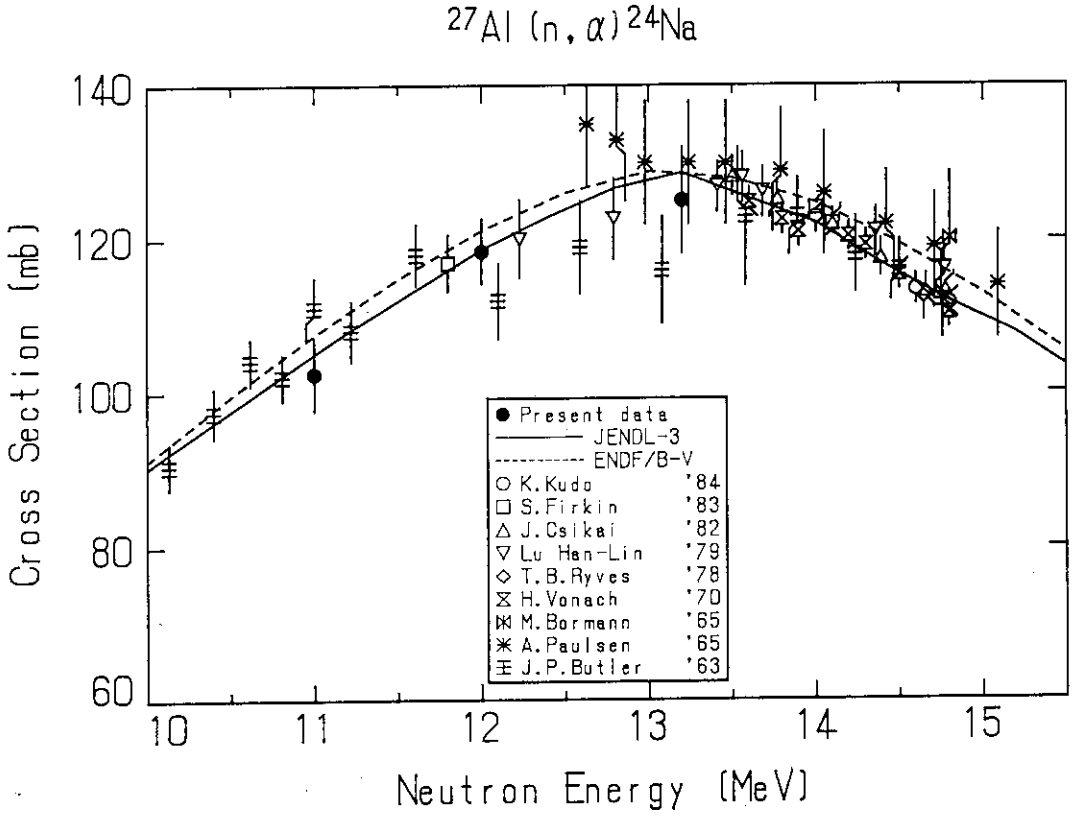

Fig. 3.1 Cross sections of $^{27}Al(n,\alpha)^{24}Na$ reaction.

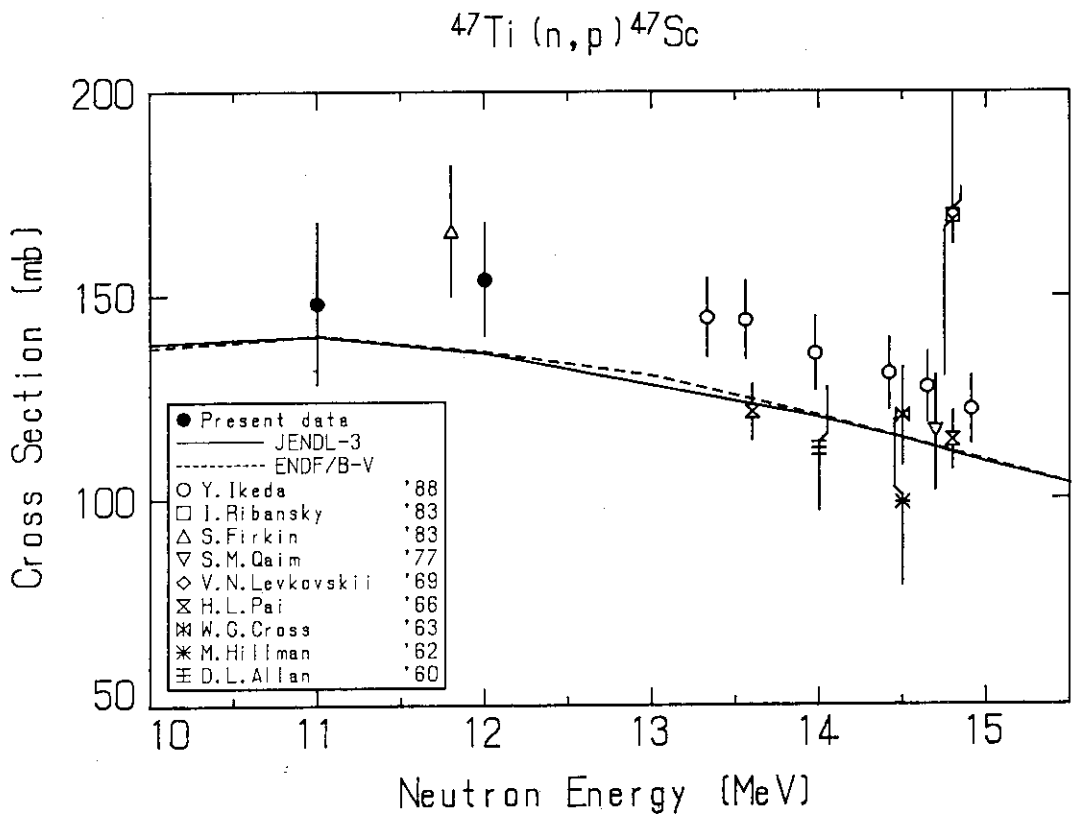

Fig. 3.2 Cross sections of $^{47}Ti(n,p)^{47}Sc$ reaction.

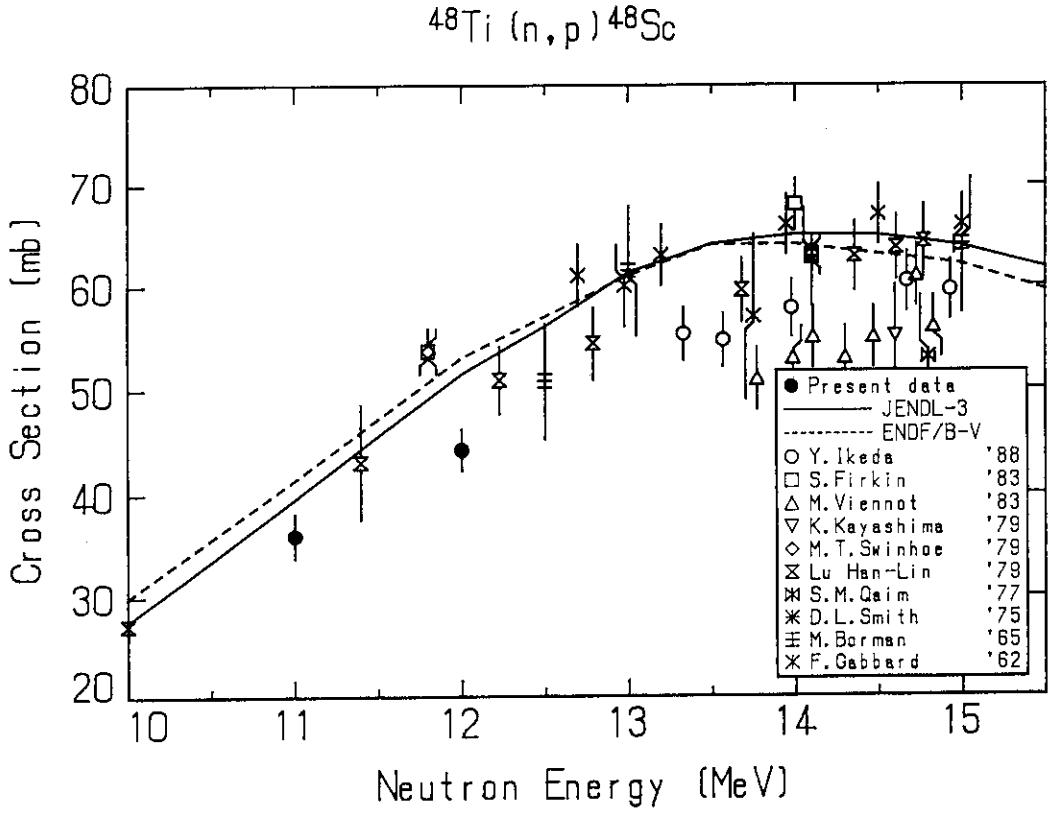

Fig. 3.3 Cross sections of $^{48}Ti(n,p)^{48}Sc$ reaction.

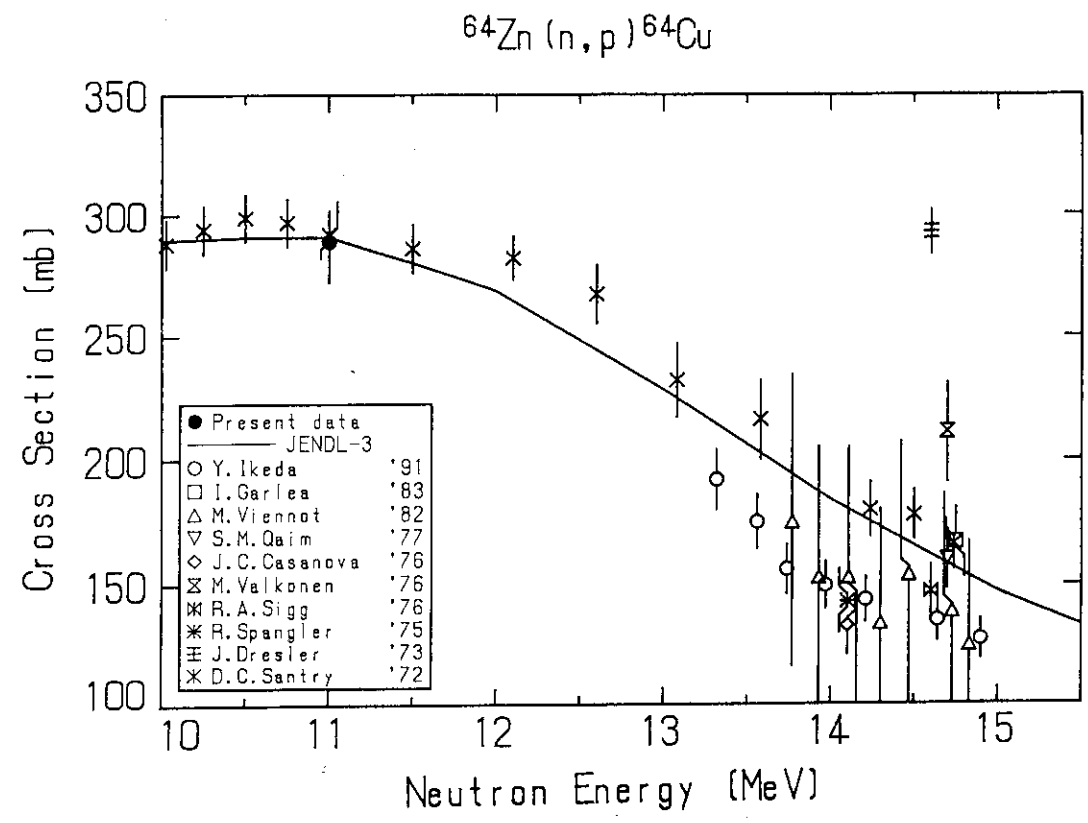

Fig. 3.4 Cross sections of $^{64}Zn(n,p)^{64}Cu$ reaction.

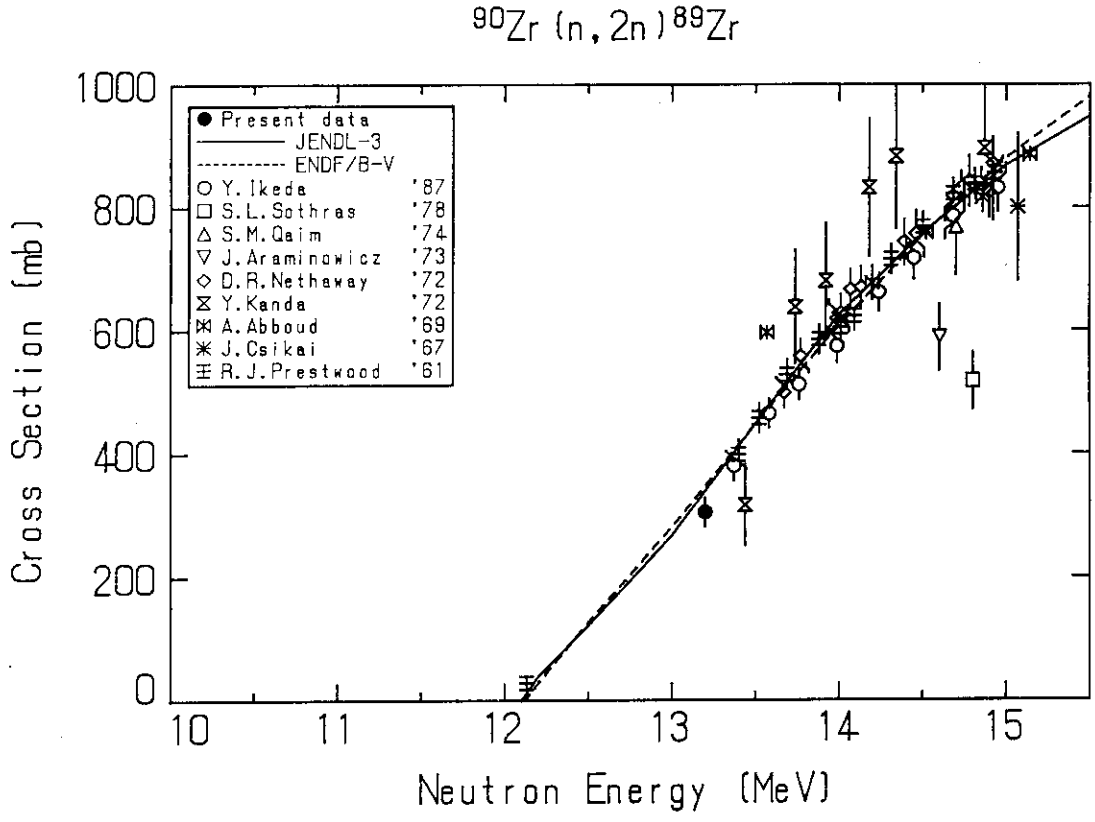

Fig. 3.5 Cross sections of $^{90}Zr(n,2n)^{89}Zr$ reaction.

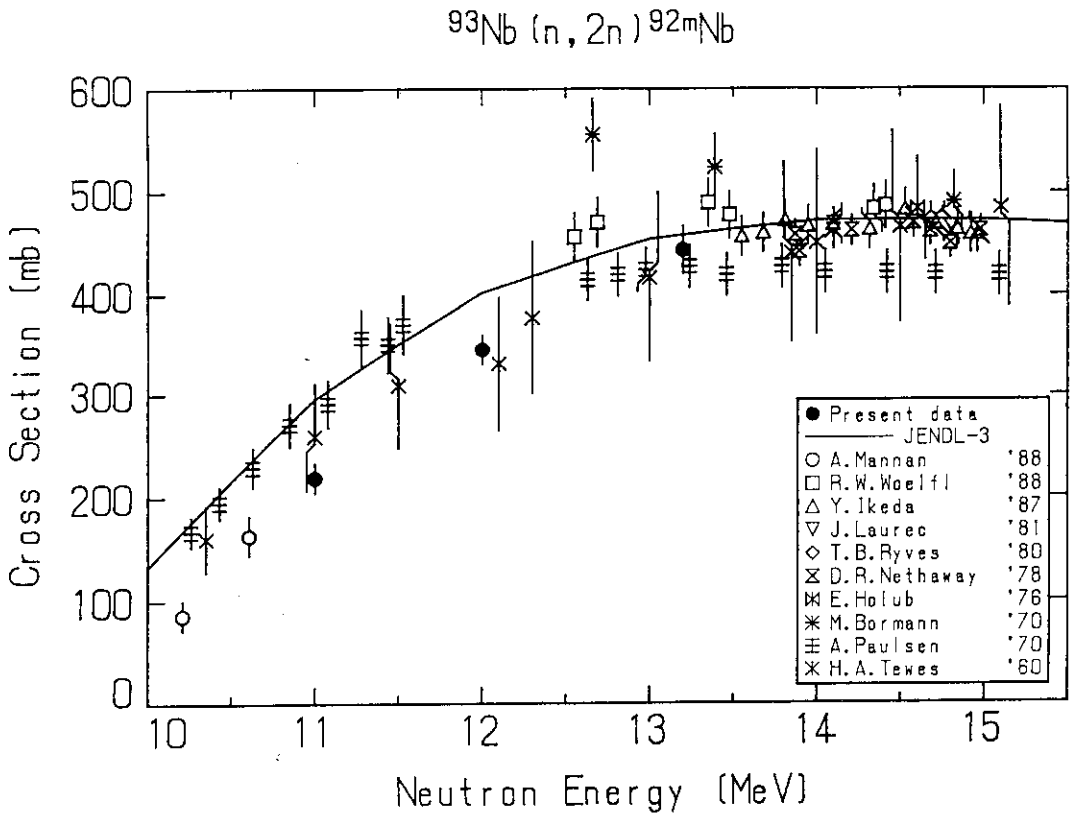

Fig. 3.6 Cross sections of $^{93}Nb(n,2n)^{92m}Nb$ reaction.

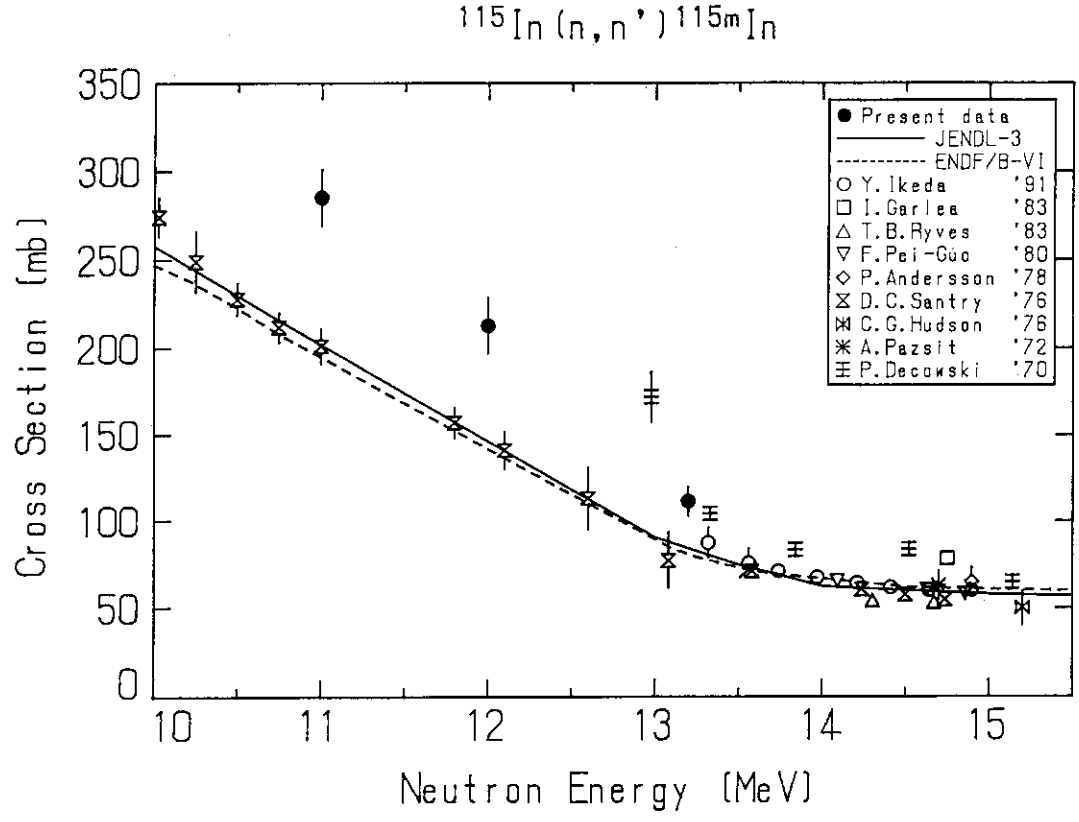

Fig. 3.7 Cross sections of $^{115}In(n,n')^{115m}In$ reaction.

3.12 Secondary Charged Particle Spectrometer Based on Two-dimensional E-TOF Analysis (II)

Seiji Ogino and Akito Takahashi
Department of Nuclear Engineering, Osaka Unversity

This paper shows a spectrometer technique for measuring energy spectral data of neutron-induced secondary charged particles -i.e, proton and alpha-particle, etc.- by analyzing energy (E) and Time-of-Flight (TOF) of charged particles in the two-dimensional E-TOF domain. Major problem in the measurement is how to decrease the backgrounds caused by neutron-induced charged particles and gamma-rays which are produced in the detector itself and coming from surrounding structural materials of the spectrometer. By reducing the backgrounds mostly by the pulse shape discrimination technique , we could measure energy spectra of neutron-induced secondary charged particles , with considerable accuracy.

INTRODUCTION

Energy spectral data for neutron-induced secondary charged particles are basic nuclear data for the estimation of the damage and nuclear heating in materials under high fluence of fast neutron fields. In general, the measurement of secondary charged particle spectrum is difficult, and experimental data are therefore scarce. Most of the available data have been measured with a quadrupole spectrometer based on the E-ΔE analysis[1)2)]. With this spectrometer an intense neutron-source like RTNS-II and complicated techniques are required to attain sufficiencies in statistics, energy resolution and particle separation . New spectrometer techniques based on other principles are therefore expected for laboratories having less intense neutron sources. The spectrometer based on two-dimensional E-TOF analysis[4)] is

one of the expected techniques for measuring neutron-induced secondary charged particles.

EXPERIMENT

Between the secondary charged particle energy(E) and the time-of-flight(TOF), we have the following relation

$$T=L\cdot\sqrt{M/2E} \qquad (1)$$

where M , E , T and L are the mass , the energy , the time-of-flight of secondary charged particle and the length between a sample and a detector. Caluculated contours of two-dimensional E-TOF distributions of various charged particles are shown in Fig.1. If the spectrometer has sufficient energy resolution, good time resolution, enough counting rates and no backgrounds, we can separately detect different charged particles and their spectra which appear on the contours in Fig.1. In actual experimental conditions , however , the separabilyty of charged particles becomes poorer due to insufficiencies of energy resolution, time resolution and counting statistics.

Few of backgrounds may be accumulated over the contours. In other words, one merit of the two-dimensional analysis is attributed to the fact that the background counts out of the contours can be automatically separated.

After separating contours of charged particles for protons, α-particles and so on , we can obtain the energy spectral data for each particle by integrating proper count events along the TOF-axis or the E(pulse height)-axis. With short flight path and insufficient energy resolution, the difference between the two spectra becomes small. We can say ,in our experimental conditions , that the energy spectrum data obtained from the pulse height channel was better than that deduced from the TOF channel.

The block diagram of the measuring system is shown in Fig.2. We measure two-dimensional contours of energy(E) and time-of-flight (TOF) gating the signals with logic signals from two parallel pulse shape discrimination circuits.

Schematic view of the experimental equipment is shown in Fig.3. Shielding materials and a charged particle detector are arranged in a 1mϕ × 1m long vacuum vessel. A rotary pump evacuates air in the

vessel in the ～1mTorr pressure range . For a charged-particle emitter with irradiation of 14MeV neutrons, an aluminum sample with 15μm thick ×6cm diam. was used. A CsI(Tl) scintillator with 2mm thick × 5cm diam. was used for the charged particle detector. An NE102 plastic scintillator was also used for test runs; in this case the pulse shape discrimination was impossible, so that the NE102 plastic scintillator was unsuitable for a charged particle detector in the field containing relatively high level gamma-rays .

The flight path between the sample and the detector was about 50cm. Major problem in the measurement is how to decrease the backgrounds caused by neutron-induced charged particles and gamma-rays produced in the detector itself and coming from surrounding structural materials of the spectrometer.

Reduction of the gamma-ray background was successfully achieved by the pulse shape discrimination technique of analyzing rise-time(RT) distributions of signals induced by charged particles and gamma-rays. The results of two-dimensional energy(E)-rise time(RT) distributions are shown in Fig.4 and Fig.5 , respectively for the cases before and after separating gamma-rays. These results show that drastic reduction of gamma-rays-origined backgrounds is possible by the pulse shape discrimination technique for the CsI(Tl) detector.

Reduction of the charged particle background can be achieved by setting the detector as far from the neutron-source as possible and by using the shadow bar shield between the neutron source and the detector; however, this arrangement also reduces the solid angle for detecting charged particles from the sample. In order to seek an optimum set of mixed materials and their arrangement, many background runs by changing the configurations have been tried . The two-dimensional RT-TOF analyses have been also used for the optimization.

The best reduction of backgrounds was obtained with the iron + lead + polyethylene shielding set, as indicated in Fig.3.

RESULTS AND DISCUSSIONS

An example of measured results of two-dimensional E-TOF distributions is shown in Fig.6, where ①, a straight line, shows

signals induced by direct 14MeV neutrons, ② shows a curve of signals induced by protons and ③ shows a curve of signals induced by alpha particles. Further reduction of back grounds is required to measure clearly the alpha particle contour; which is shown in the following.

Rejecting proton-signals by the pulse shape discrimination, the measurement for α-particles was made, and the measured result (foreground) is shown in Fig.7, where signals induced by direct 14MeV neutrons are shown with ① , contour of signals by the $^{27}Al(n,\alpha)$ alph a-particles with ② and contour of signals by neutron-induced alpha-pa rticles at the vacuum wall with ③. These results show that the rejection of proton signals is necessary to measure clearly the alpha-particle trajectory curve.

Energy differential cross section from the Al(n,xp) reaction which were obtained from the pulse height channel (integrated along the TOF axis) are shown in Fig.8, compared with the Grimes' experiment [2] and the calculation using SINCROS-Ⅱ [3] ; agreements among the three results are good.

Energy differential cross sections for the Al(n,xα) reaction are shown in Fig.9 compared with the Grimes' experiment[2] and the calculation using SINCROS-Ⅱ [3]. The presently measured spectrum is softer than that of the Grimes' and gives relatively good agreement with the calculation.

CONCLUSION

In order to measure energy spectrum data for neutron-induced secondary charged particles , a new type spectrometer based on the two-dimensional E-TOF analysis has been tested. Major problems of reducing backgrounds were almost solved by the pulse shape discrimination technique after many background test runs. The present system can be applied to measure cross sections and spectra of secondary charged particles, calibrating with the recoil proton peaks in the E-TOF domain by the elastic scatterings of hydrogen in a thin polyethylene sample at various angles between the incident and the out-going-particle directions. With improvements after the 1st report[4], the present spectrometer can be used for measuring (n,xp) and (n,xα) spectral data of other nuclide than ^{27}Al.

Reference

1) Grimes,S.M.,et al.,Phys. Rev., C17 508 (1978)

2) Grimes,S.M.,et al.,NSE:62,187-194(1977)

3) Nobuhiro YAMAMURO ,JAERI-M 90-006 (1990)

4) Ogino, S., Takahashi, A., JAERI-M 90-025 (1990)

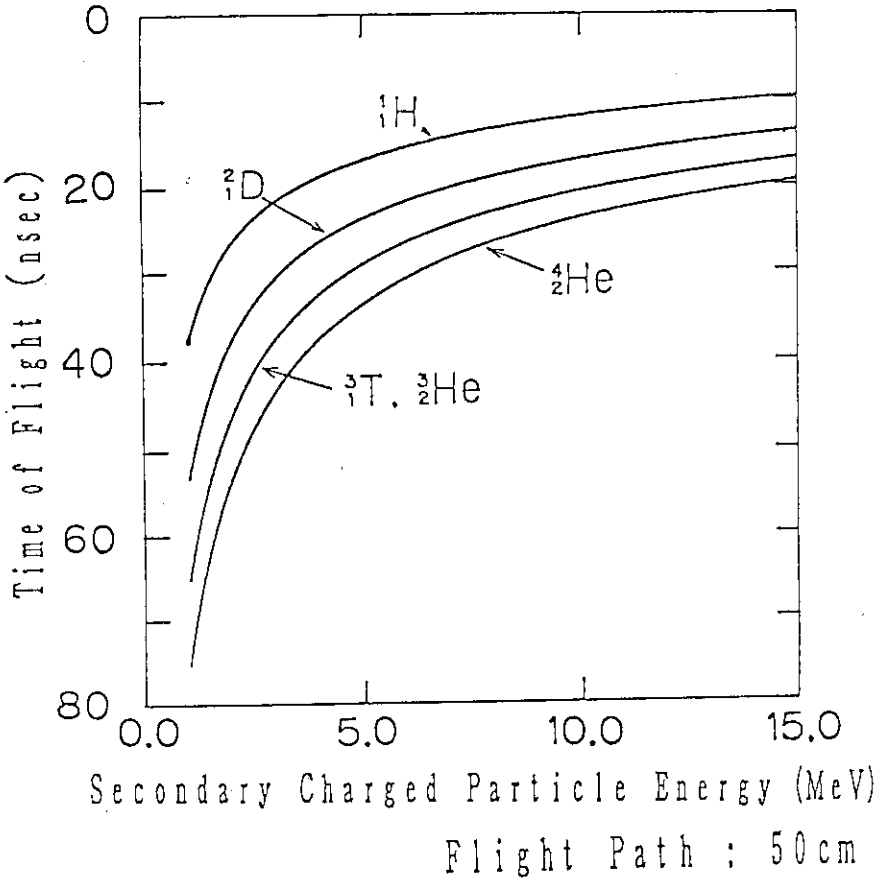

Fig. 1 Two-dimensional contours of secondary charged particles

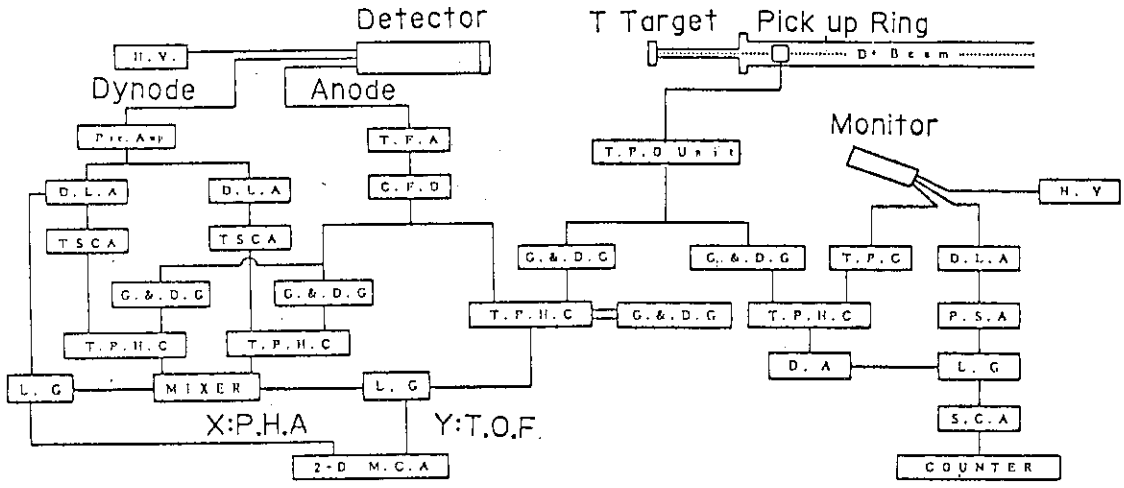

Fig. 2 The block diagram of the measuring system

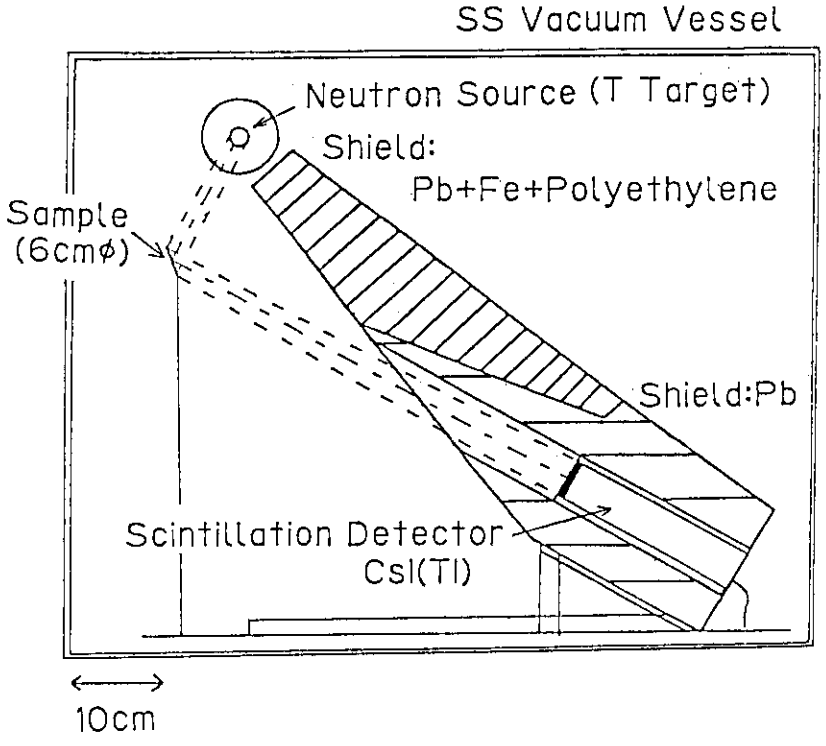

Fig. 3 Schematic view of E-TOF experiment

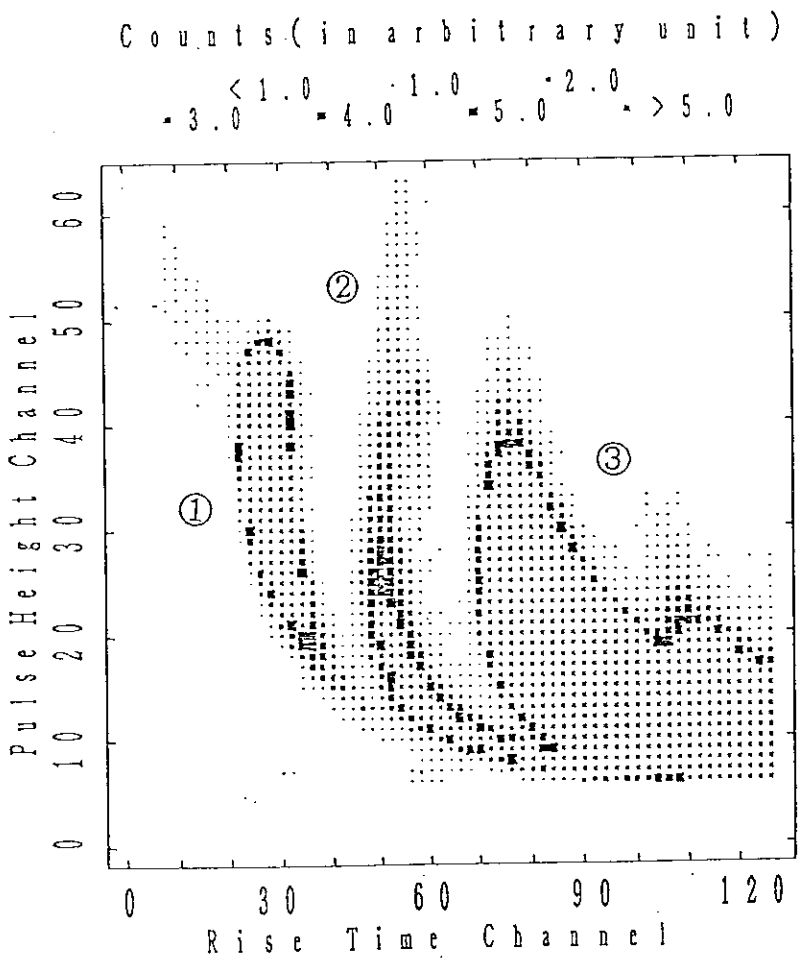

Fig. 4 Two-dimensional energy(E)-rise time(RT) distribution for charged particles and gamma rays: ① shows α-particles ② protons, and ③ gamma rays.

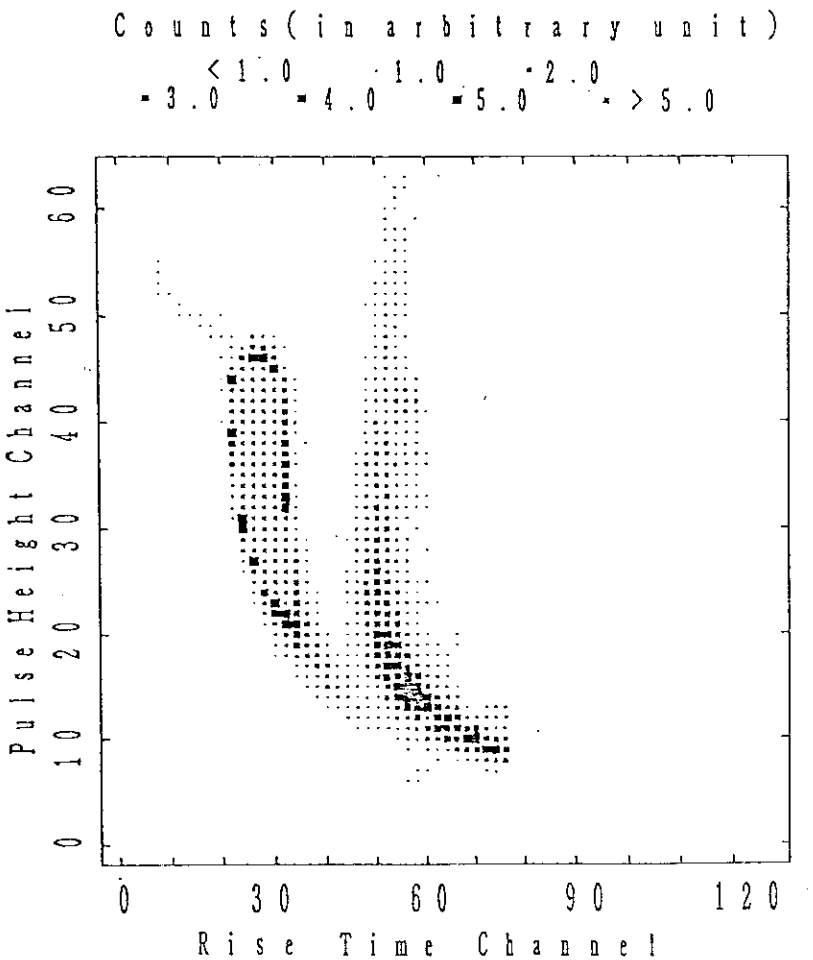

Fig. 5 Two-dimensional energy(E)-rise time(RT) distributions after the pulse shape discrimination: this shows that reduction of gamma rays could be completely achieved.

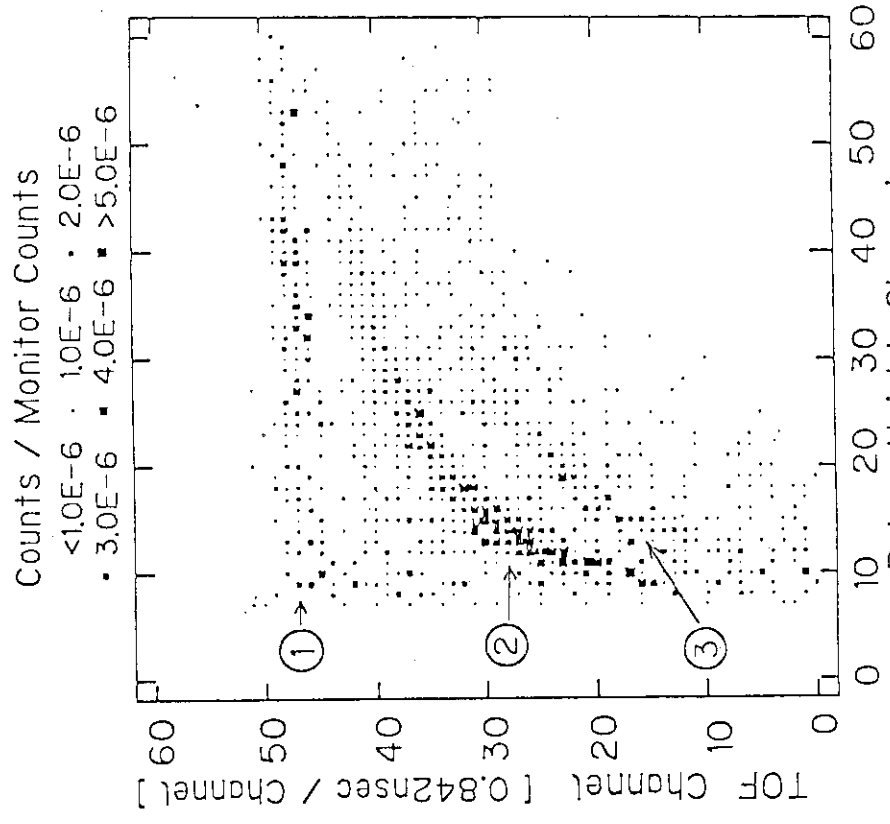

Fig. 6 Two-dimensional E-TOF distribution for secondary charged particles, for Al sample with En=14 MeV: ① shows the direct 14 MeV neutron-induced protons and α-particles ② the ^{27}Al(n,xp) protons, and ③ the ^{27}Al(n,xα) α-particles.

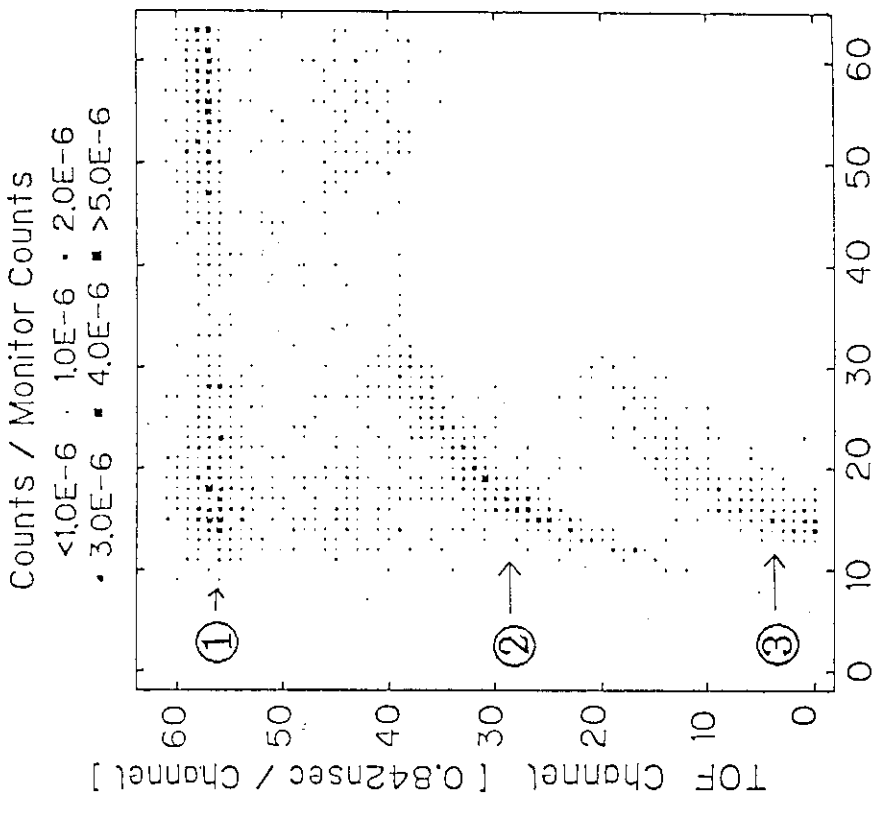

Fig. 7 Two-dimensional E-TOF distribution (fore grounds) for secondary α-particles for Al sample with En=14 MeV after the reduction of protons and gamma rays by the pulse shape discrimination.

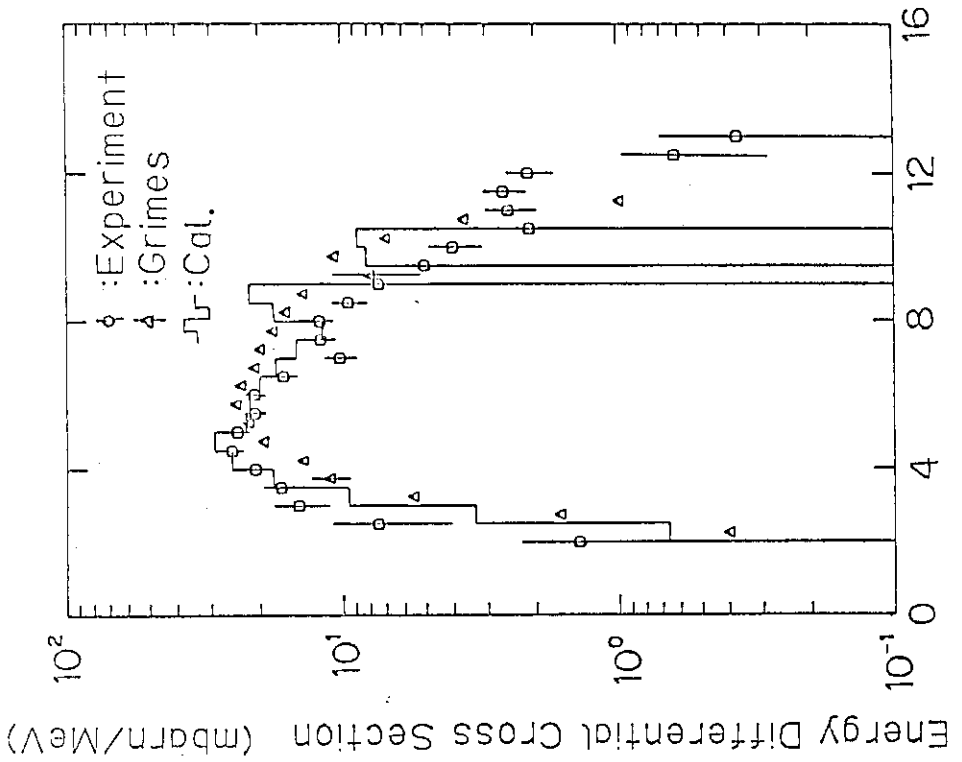

Fig. 9 EDX for ^{27}Al(n,xα) with En=14 MeV (open circles) Grimes' experiment with En=15 MeV (triangles) and the calculation using SINCROS-II.

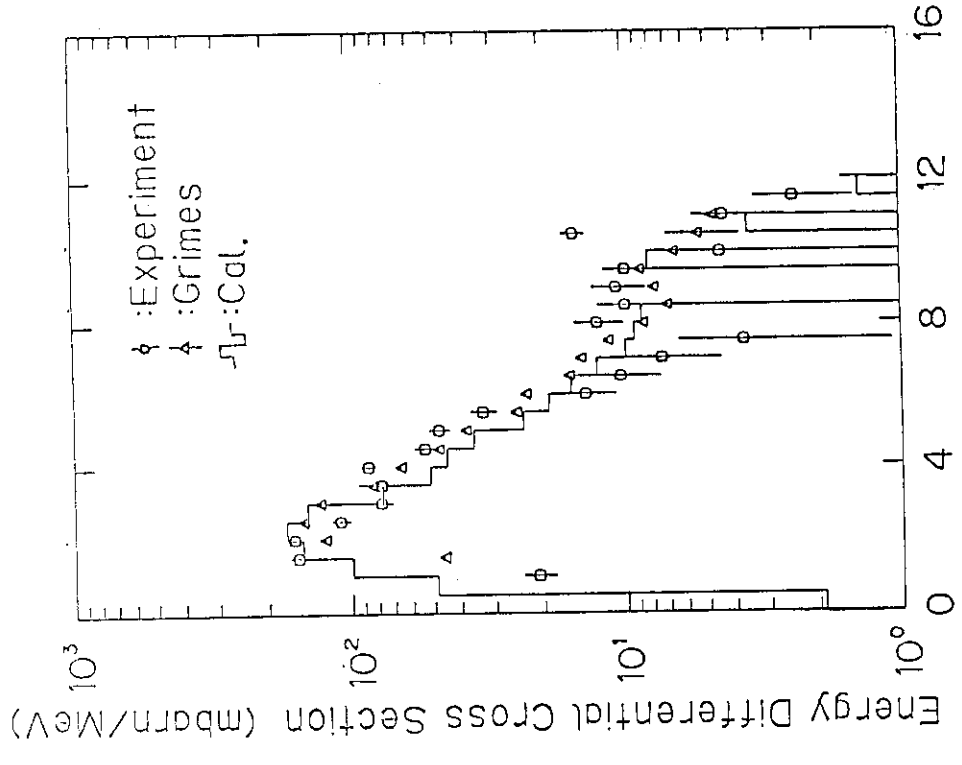

Fig. 8 EDX for ^{27}Al(n,xp) with En=14 MeV (open circles) Grimes' experiment with En=15 MeV (triangles) and the calculation using SINCROS-II.

3.13 Measurement of Neutron-induced Charged-particle-emission Reaction Cross Section Using Gridded Ionization Chamber

N.Ito, M.Baba, S.Matsuyama, K.Sugino, and N.Hirakawa

Department of Nuclear Engineering, Tohoku University,
Aoba, Aramaki, Aoba-ku, Sendai 980, Japan

A gridded ionization chamber (GIC) having large geometrical efficiency, ~2π, has been developed for measurements of neutron-induced charged-particle emission cross section. Test experiments proved the proper operation of GIC with complete charge collection even if the gas pressure was over 10 atm.. GIC was applied successfully to proton and α emission cross section measurements for nickel at the several MeV and 15 MeV incident neutron energies with the results in good agreement with the previous data and evaluations. The construction of GIC and the experimental technique are presented in this paper.

1. Introduction

Double-differential cross sections for neutorn-induced charged-particle emission reaction are important for estimation of radiation damage and nuclear heating in structural materials of fission and fusion reactors. Direct measurements of secondary charged-particles are, however, difficult because of low counting rate and high background. Various experimental devices have been developed for measurements; however, they have poor geometrical efficiency and require very long data acquisition time.

A gridded ionization chamber (GIC) is advantageous to detection of emitted charged-particles owing to high geometrical efficiency near to 2π, with capability of energy-angle determination. This type of chambers have been used successfully for measurement of triton angular distribution for the ^{6}Li(n,t) reaction for incident energies lower than 1 MeV[1] and fission fragments detection[2]. However there have been no application to high energy charged particles.

We have developed GIC appropriate for measurements of (n,xα) cross section up to ~14 MeV incident energies and (n,p) cross section in several MeV incident energies. The performance of the chamber was tested to confirm the applicability to high energy particles, and applied successfully to measurements of Ni(n,p) and Ni(n,α) cross section at several MeV incident

energies and of α-particle energy spectra from Ni(n,xα) reaction at 15 MeV neutron energy.

2. Gridded Ionization Chamber

The schematic view of GIC is shown in Fig.1; if charged-particles emitted from sample on cathode electrode are stopped by chamber gas between cathode and grid, the anode and cathode signals, P_a and P_c respectively, are represented by the following equations[2];

$$P_a = E\left(1 - \sigma\frac{\bar{x}}{d}\cos\theta\right) \sim E \qquad (1)$$

$$P_c = E\left(1 - \frac{\bar{x}}{d}\cos\theta\right) \qquad (2)$$

where

E, θ = energy and emission angle of emitted particle, respectively, in laboratory system

σ = grid inefficiency

$\bar{x}$ = distance from the beginning to the center of gravity of the charge distribution of the trace

d = spacing between cathode and grid.

Since σ can be very small (several %), anode signal represents approximately particle energy, and simultaneously the emission angle (θ) can be determined by dealing with P_a and P_c according to equations (1) and (2).

Figure 2 shows the construction of 4π-GIC fabricated in this work, which consists of two chambers with common cathode. This chamber withstands the gas pressure up to 13 atm. to be applicable to α-emission reaction for incident neutron energies up to ~14 MeV; with that pressure, detectable maximum proton energy is about 6.7 MeV with a gas mixture of Kr-CO_2. The electrodes are made of heavy metals, tantalum and tungsten, to reduce backgrounds produced by fast-neutron bombardment. In addition, the chamber is equipped with shield electrodes outside each anode to reduce backgrounds from chamber wall, and guard-ring electrodes around each grid to reject events due to long-range particles by means of anti-coincidence operation with anode or cathode signal. Three sample foils can be set up between two cathode plates of tantalum; and foil to be measured can be changed from outside the chamber. To reduce electronegative impurities such as oxygen or water vapor, the chamber is evacuated before gas filling. High voltages can

be applied to all the electrodes to achieve high electric field required for complete charge collection.

3. Test Experiments

We confirmed proper operation of GIC by measuring triton spectrum from the $^{6}Li(n_{th},t)$ reaction and proton spectrum from the H(n,p) reaction which exhibit well established energy and angular distribution.

(1) Saturation Property

We studied the saturation property of the charge collection for tritons and protons. Figure 3 shows typical anode spectrum for the $^{6}Li(n_{th},t)\alpha$ reaction; peaks for tritons and α-particles are seen clearly. Figure 4 shows the triton-peak channels as a function of ε_c/P, where ε_c is a field strength between cathode and grid and P is a gas pressure. The field strength higher than 0.22 kV/cm/(kgf/cm^2) proved to be sufficient to give saturation for tritons. For protons, Fig.5 shows typical anode spectrum for the H(n,p) reaction at 4.4 MeV incident neutron energy, and Fig.6 shows proton-edge channels shown in Fig.5 versus electric field; this result indicate the saturation is achieved also for protons in the similar field strength for tritons.

(2) Energy Resolution and Responses

The intrinsic energy resolution of GIC was estimated to be better than 45 keV from triton peak of anode spectrum shown in Fig.3: this energy resolution will be good enough for study of charged-particle emission reactions. Figure 7 shows a comparison of experimental results with simulation calculations for anode and cathode responses for the H(n,p) reaction, where energy loss of proton in the polypropylene sample and the effect of grid inefficiency were considered in the simulation. The experimental results agree with the calculation except for lower energy region where large backgrounds due to neutron reactions with the detection gas disturb the measurements.

Therefore, the test experiments ensured that proper operation of the chamber was achieved even at the high pressure over 10 atm. by employing adequate electrode potential and gas purity.

4. Ni(n,p) and Ni(n,α) cross section measurements

This chamber has been utilized successfully for proton and α emission cross section measurements for nickel at several MeV and 15 MeV of incident neutron energies.

(1) Experimental Procedure

To reduce backgrounds, neutron beam was collimated within sample-foil diameter (25 mm) by 10 ~ 15 cm copper collimator as shown in Fig.8. Natural nickel foil of 5 μm thick and tungsten foil of 50 μm thick was used for sample-in and sample-out measurements, respectively; normalization between each measurement was made by flux measurements using NE213 detector (1"ϕ x 1") located on the beam axis. As a detection gas, a mixture of Ar-CO_2 or Kr-CO_2 was used with optimal pressure for each particle type and particle energy.

Figure 9 illustrates the electronics block diagram; anode and cathode pulse height data are stored by two parameter data acquisition system. For α-particle detection, guard-ring signal was used to reject events by long-range protons with anti-coincidence operation. The shaping time constant of 2 μsec. was found appropriate for each spectroscopy-amplifire of anode and cathode signal. Energy scale for pulse height spectra of anode and cathode signal was calibrated using triton-peak channel from the $^{6}Li(n_{th},t)$ reaction or proton-edge channel from the H(n,p) reaction.

Data accumulation of about 3 hours was sufficient for each measurement to provide adequate counting statistics. Figure 10 shows two-dimensional spectrum, anode versus cathode signal, for Ni(n,p) cross section measurement at 5.0 MeV neutron energy. The straight and curved lines shown in Fig.10 correspond to 0-deg. and 90-deg. emission angles, respectively; events from the Ni(n,p) reaction distribute between these lines. In low energy region, there are large backgrounds which will be attributed to the $^{16}O(n,\alpha)$ reaction; however, these are not of so serious problem since two parameter data processing greatly reduces the backgrounds. Two dimensional pulse-height spectrum was translated into double-differential cross section according to the equations (1) and (2), using the absolute normalization factor determined by scattered proton yield from polypropylene sample.

(2) Results and Discussion

Figure 11 shows double-differential Ni(n,p) cross section at En = 4.3 and 5.0 MeV; peaks corresponding to low-lying exited states of ^{58}Co are seen. Energy- and angle-integrated cross sections obtained in this work are in good agreement with JENDL-3 and ENDF/B-IV evaluations as listed in Table 1.

Figure 12 shows double-differential α-particle spectra for natural nickel at 15 MeV neutron energy, compared with the angle-integrated spectrum for enriched ^{58}Ni by S.M.Grimes et al.[3]. The present data at 60-deg.

are in good agreement with those of S.M.Grimes et al. while these at 26-deg. show small disagreement in higher energy region which indicates anisotropic α emission. For lower neutron energy, no data are available for direct spectrum comparison; then average α-particle energies are compared in Fig.13 with the data by Paulsen et al.[4] and Grimes et al.[3]; the present results at En = 5.0 and 6.0 MeV agree with the results by Paulsen et al. within experimental error, while the present results at En = 15MeV are angle dependent and generally greater than those of Grimes et al.. The cross sections of the Ni(n,α) reaction obtained in this work are in good agreement with previous data and evaluations as shown in Fig.14.

5. Conclusion

We have developed GIC which will be useful for measurements of charged-particle emission cross section because of its large efficiency. Test experiments confirmed complete charge collection even if the gas pressure was over 10 atm.. GIC developed in this work provide very "efficient" measurements of proton and α-particle emission cross sections. This technique will be applied for various secondary charged particle measurements with improvements to get higher reliability.

Acknowledgment

The authors wish to thank Messrs. T.Takahashi, K.Komatsu and T.Nagaya for their supports in fabrication of GIC.

References

1) H.-H.Knitter et al., Nucl.Sci.Eng., 83 229 (1983).
2) C.Budtz-Jorgensen et al., Nucl.Instr. and Meth. A258 209 (1987).
3) S.M.Grimes et al., Phys.Rev., C19 2127 (1979).
4) A.Paulsen et al., Nucl.Sci.Eng., 78 377 (1981).
5) E.Wattecamps et al., Proc.Int.Conf. Nuclear Data for Science and Technology, Antwerp, Belgium, 156 (1982).

Table 1 Ni(n,p) cross section obtained in the work compared with that of JENDL-3 and ENDF/B-IV

Neutron energy (MeV)	Experiment (mb)	JENDL-3 (mb)	ENDF/B-IV (mb)
4.3	269 ± 8	273	289
5.0	305 ± 10	323	320

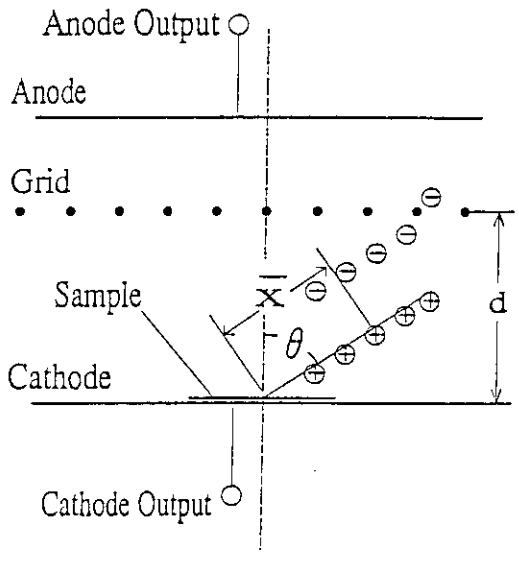

Fig. 1 Schematic view of the gridded ionization chamber; $\bar{x}$ is the distance from the beginning to the center of the charge distribution.

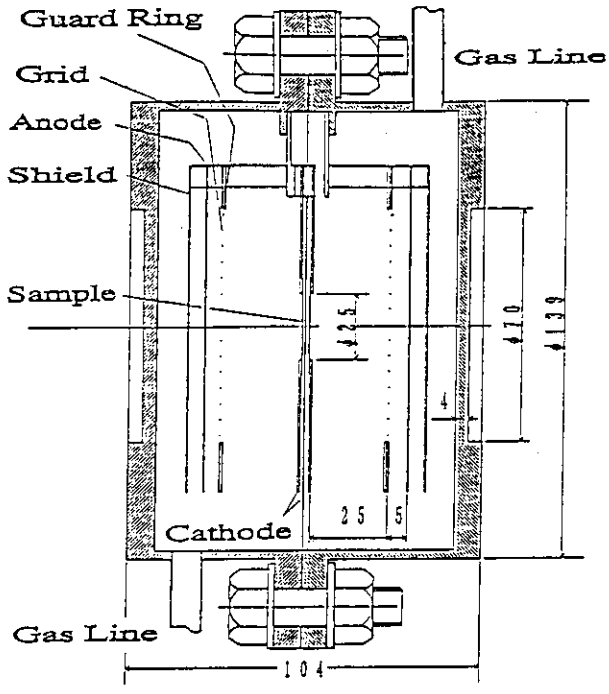

Fig. 2 Design of the gridded ionization chamber developed in this work.

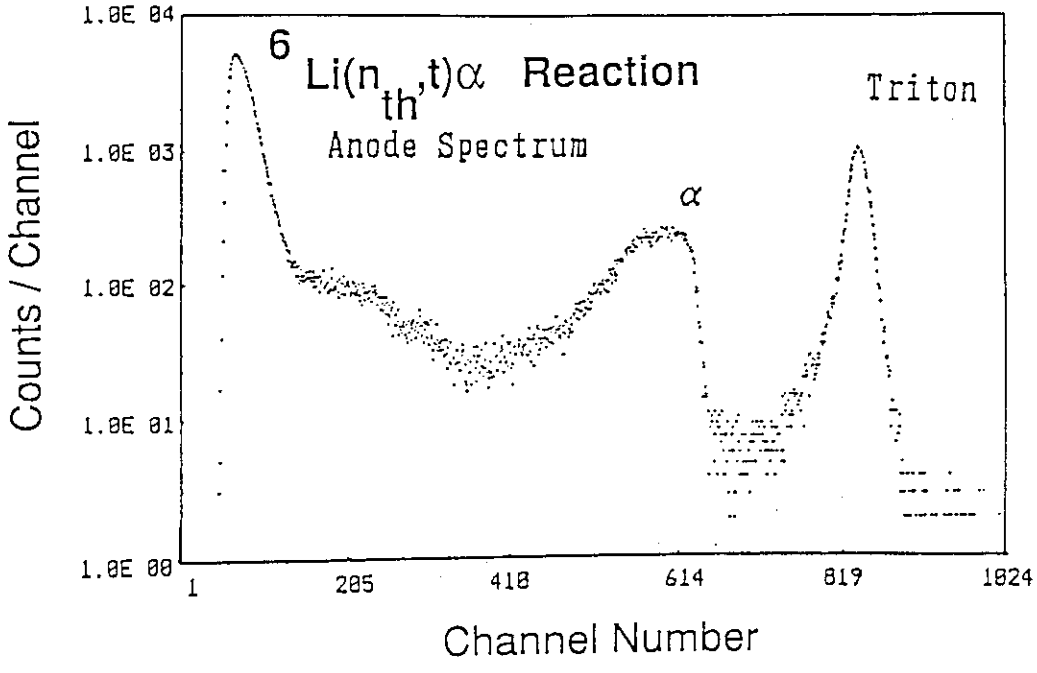

Fig. 3 Typical anode spectrum for the $^{6}Li(n_{th},t)\alpha$ reaction.

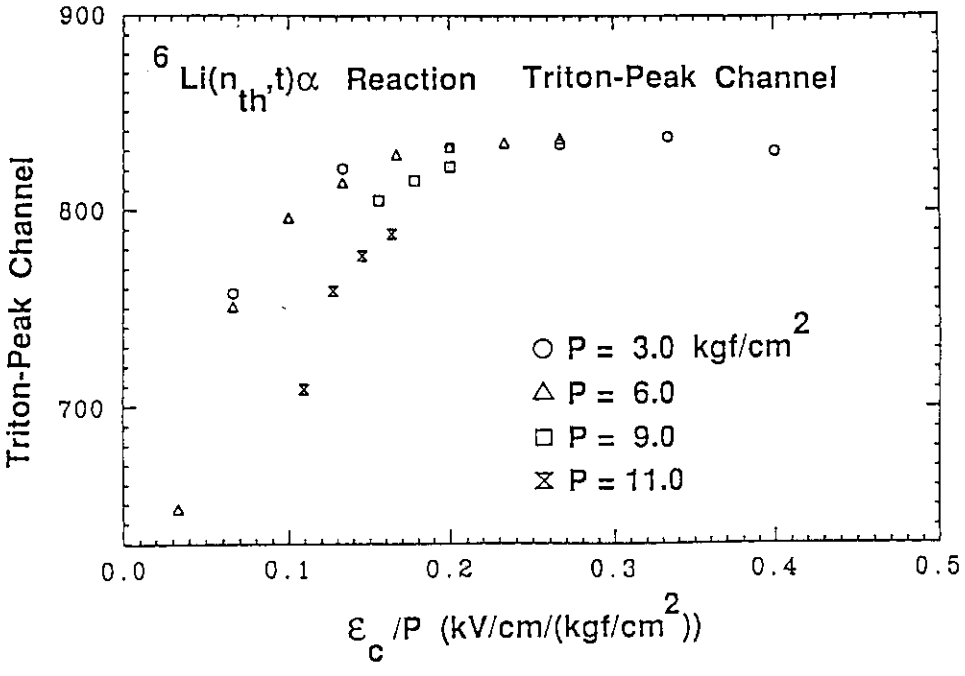

Fig. 4 Saturation property for triton; triton peak channels in anode spectrum shown in Fig. 3 are plotted as a function of ε_c/P. ε_c is a field strength between cathode and grid, and P is a gas pressure.

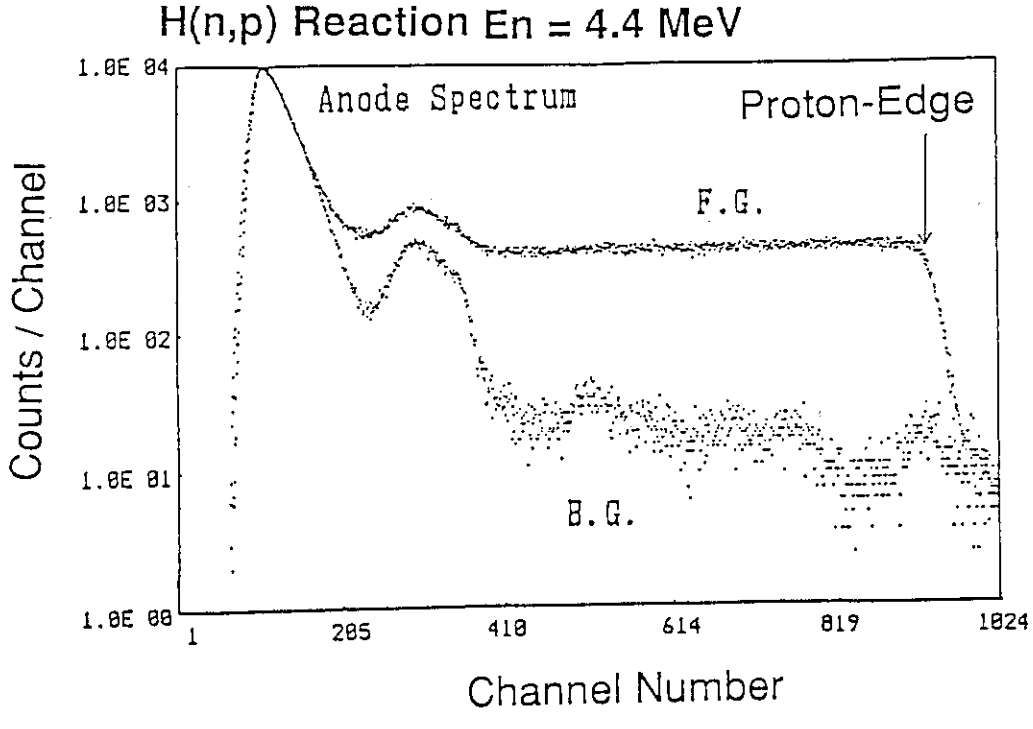

Fig. 5 Typical anode spectrum for the H(n,p) reaction at 4.4 MeV neutron energy.

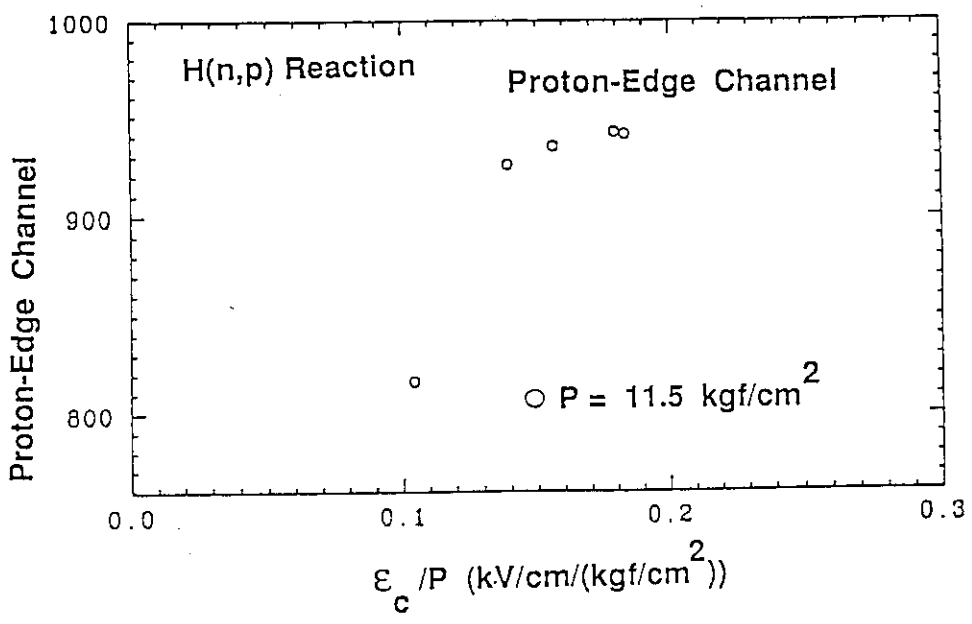

Fig. 6 Saturation property for proton; proton-edge channels in anode spectrum shown in Fig. 5 are plotted as a function of ε_C/P.

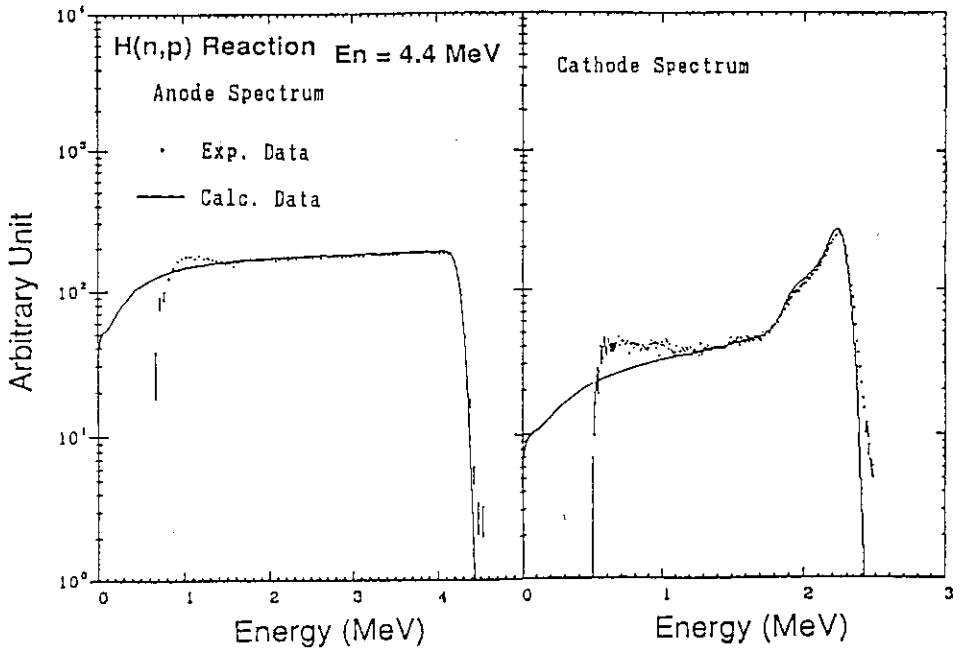

Fig. 7 Comparison of anode and cathode spectra with simulated spectra for the H(n,p) reaction. Energy loss of proton in the sample and the effect of grid inefficiency are considered in the simulation.

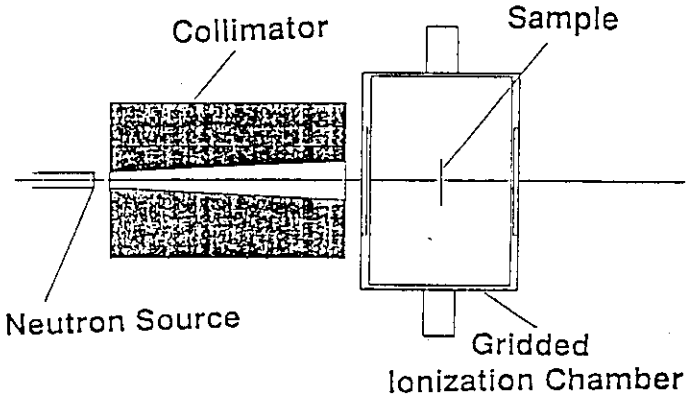

Fig. 8 Experimental arrangement for Ni(n,p) and Ni(n,α) cross section measurements.

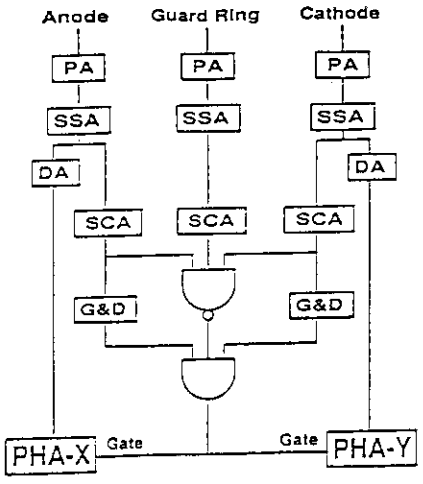

Fig. 9 Electronics block diagram of the measurement system.

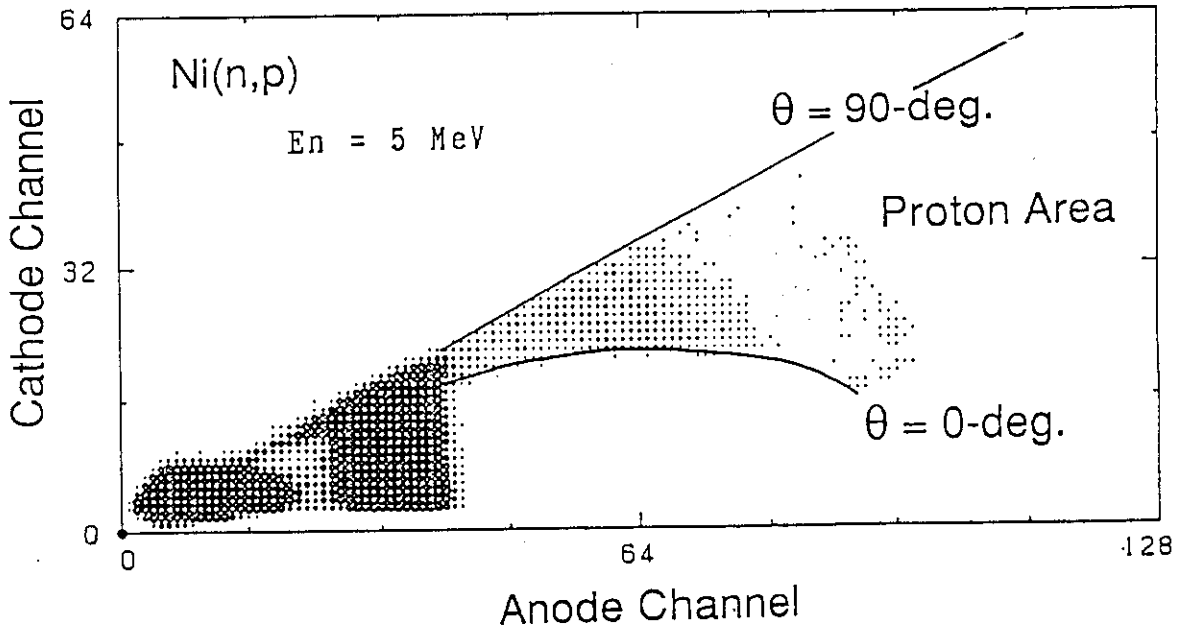

Fig. 10 Two-dimensional spectrum of anode versus cathode for the Ni(n,p) reaction at 5.0 MeV neutron energy. Straight and curved lines correspond to 0-deg. and 90-deg. of emission angle, respectively.

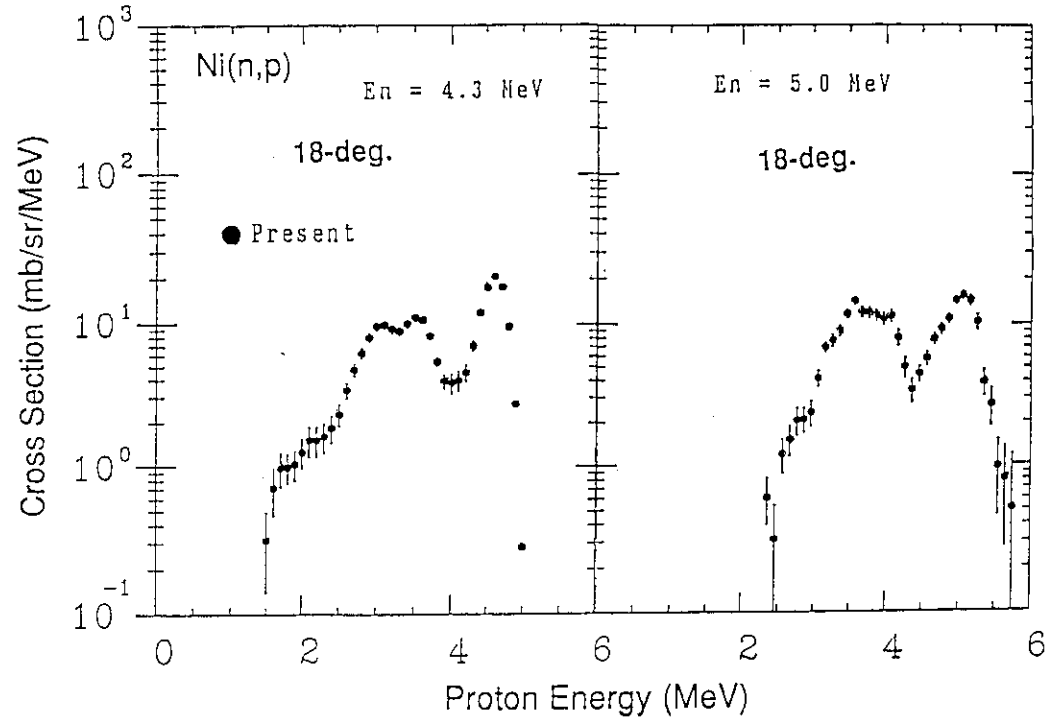

Fig. 11 Double-differential Ni(n,p) cross section at 4.3 and 5.0 MeV neutron energy.

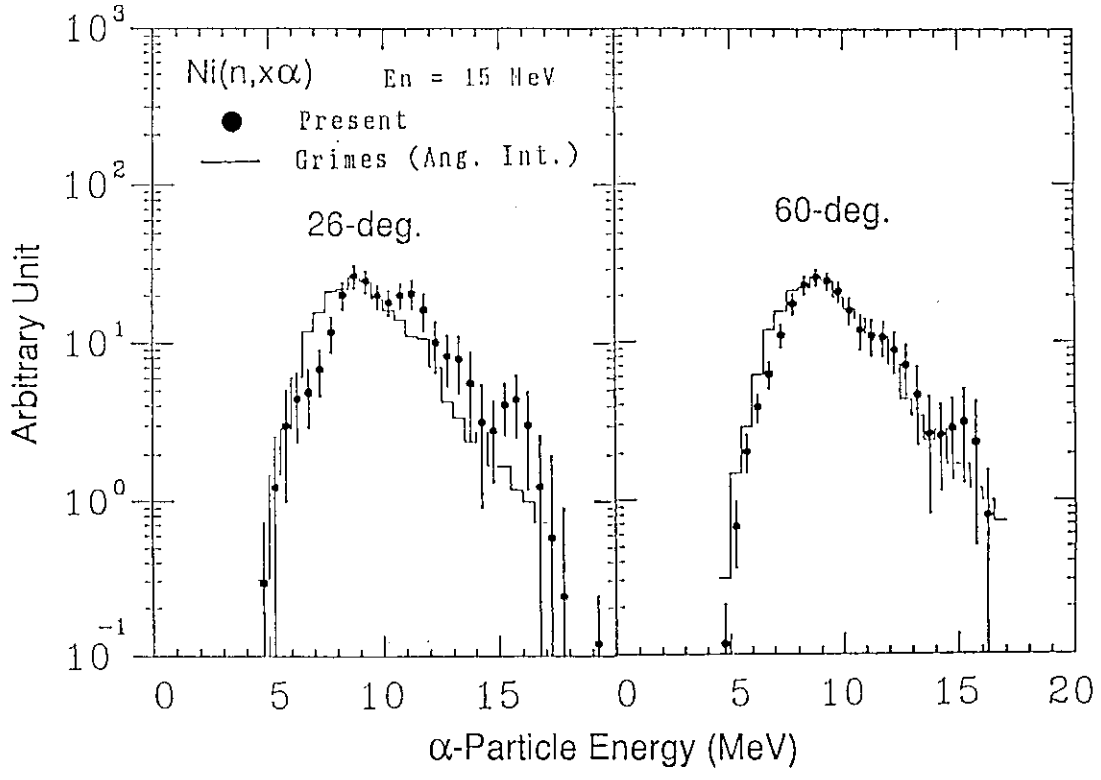

Fig. 12 α-particle energy spectra from the Ni(n,xα) reaction at 26 and 60 deg. for 15 MeV incident neutron compared with the angle-integrated spectrum from enriched ^{58}Ni by Grimes et al.[3]

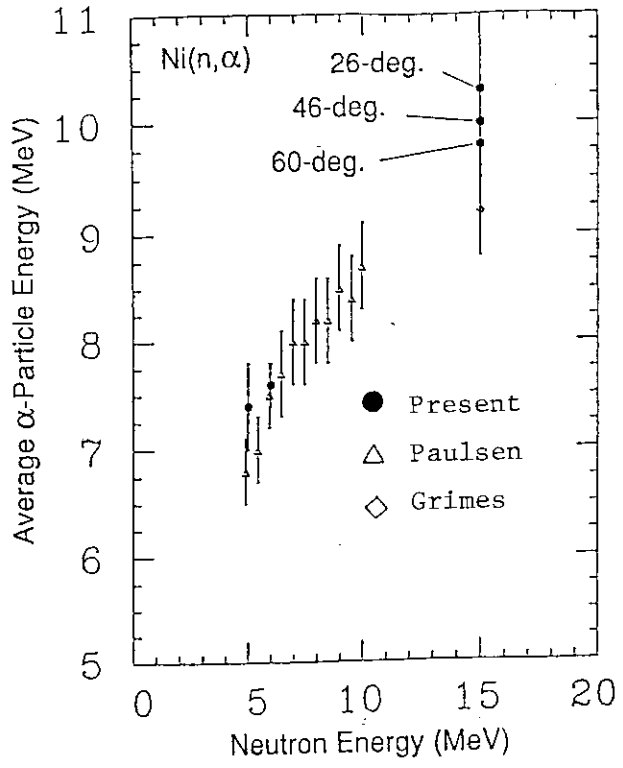

Fig. 13

Average α-particle energies for the Ni(n,α) and Ni(n,xα) reaction compared with those by Paulsen et et al.[4] and Grimes et al.[3]

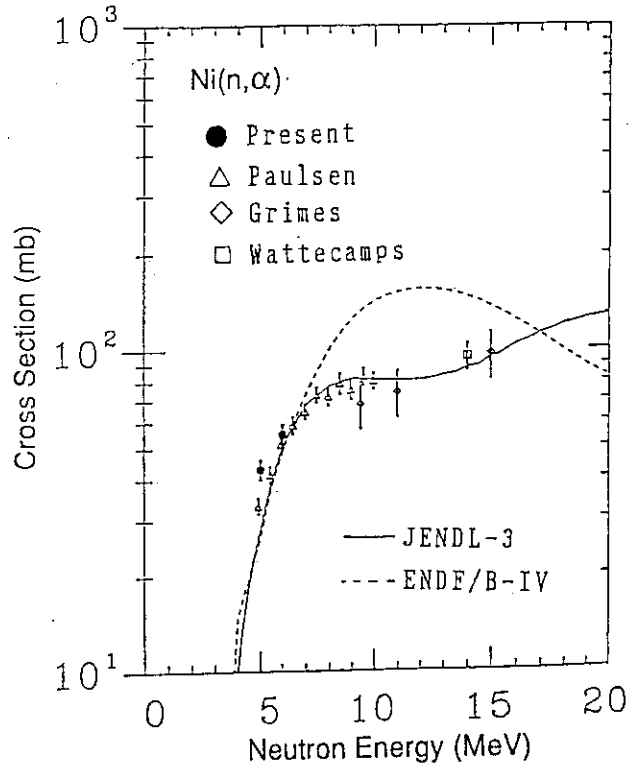

Fig. 14

α-emission cross section for Ni compared with the data by Paulsen et al.[4], Grimes et al.[3] and Wattecamps et al.[5] and with the evaluations of JENDL-3 and ENDF/B-IV.

3.14 Self-shielding Effect on Angular Neutron Flux Spectra Leaking from Thick Iron Slab

Yukio Oyama, Kazuaki Kosako and Hiroshi Maekawa
Department of Reactor Engineering,
Japan Atomic Energy Research Institute,
Tokai-mura, Ibaraki-ken, JAPAN

Leakage neutron flux measurement from thick iron assembly has been calculated by using DOT3.5 neutron transport code with self-shielding correction of iron cross section set. The calculated results were compared with the MCNP calculation and the experiment. The impact of group structure on self-shielding corrected calculation was also examined.

1. Introduction

Shielding performance of iron for 14 MeV neutrons is very critial issues to estimate safety factor of super conducting magnet design in a next fusion test device, such as ITER and FER. Recently several experiments were performed to examine a deep penetration property of DT fusion neutrons in iron. We had also measured angular neutron flux spectra leaking from the iron slabs with various thickness for 14.8 MeV neutrons.[1] The layout of the experiment is shown in Fig. 1. In analyses of the experiment using the Sn codes DOT3.5[2] and the Monte Carlo code MORSE-DD[3], large underestimation of angular neutron flux has been found at the range below 1 MeV. The MORSE-DD uses the double differential cross section (DDX) library. In contrast to those codes, the analysis by the ponit Monte Carlo code MCNP[4] showed fairly good agreement with the experiment. This fact suggests that the codes using the groupwise cross sections with infinite dilution which is assumed for both groupwise codes trend to underestimate low energy neutron flux due to self-shielding effect, because there exist many resonances in the energy range below 1 MeV for iron cross section.

In the present work, in order to examine the effectiveness of self-shielding correction for the problem, two kinds of cross section sets

with the correction were prepared and tested. The results are compared to the MCNP results and an impact of the self-shielding correction is dicussed.

2. Calculation

The reference cross section set used for DOT3.5 calculations is FUSION-J3[5] prepared for fusion neutronics experiment with 125 groups for neutrons and 40 groups for gamma rays. This is processed by MACS-N[6] code from the JENDL-3[7] nuclear data library with infinite dilution. To obtain the corrected cross section, two types of the cross section sets were made by reducing the JSSTD295 cross section set[8] of 295 groups using f-table for self-shileding correction. These sets includes all impurities in the iron assembly. The number of group of the reduced cross section sets are 125 and 191, respectively (named JSSTD125 and JSSTD191). The former set follows the group structure of FUSION-J3, and the latter set does the group structure of FUSION-J3 above 10 MeV and of VITAMINE-J below 10 MeV. Thus the latter sets is more fine for the range below 1 MeV by about twice. The calculations were performed for the case of 60 cm in thick.

3. Results and Discussion

Figures 2 and 3 shows the comparison between the DOT3.5/FUSION-J3 calculation and the MCNP/JNDL-3 calculations. One can see that the MCNP agrees very well with the experiment, but the DOT3.5/FUSION-J3 underestimate the flux in the range below about 1 MeV, except for the peak around 100 keV. The figure 3 also includes the result by DOT3.5/JSSTD125. The JSSTD125 improves the underestimation, but the result still underestimates the flux in the range of 500 keV to 1.5 MeV compared to the MCNP. Hence, to see the effect of group structure we compared both calculations using JSSTD125 and JSSTD191 sets. Figure 4 shows the calculations by both corrected cross section sets. It is remarkable from the comparison that the calculation with fine group does not improved much the descrepancy. Thus the descrepancy to the MCNP in the range of 500 keV to 1.5 MeV should be caused by the reason other than self-shielding, for example, angular treatment or so.

4. Conclusion

It was found from the present calculations that the case using self-shielding correction gave better results in the energy range below 1 MeV compared to the case using infinitely dilute cross section, but still not enough especially in the range of 500 keV to 1.5 MeV.

References

1) Y. Oyama, et al., presented at the Annual Meeting of Atomic Energy Society of Japan, Univ. of Tokyo, April 2-4 (1990)
2) W. A. Rhoades and F. R. Mynatt, ORNL/TM-4280 (1979)
3) M. Nakagawa and T. Mori, JAERI-M 84-126 (1984)
4) Los Alamos Radiation Transport Group (X-6), LA-7396-M (1981)
5) K. Maki and K. Kosako, private communication.(1990)
6) A. Hasegawa, private communication (1989)
7) K. Shibata, et al., JAERI 1319 (1990)
8) A. Hasegawa, private communication (1990)

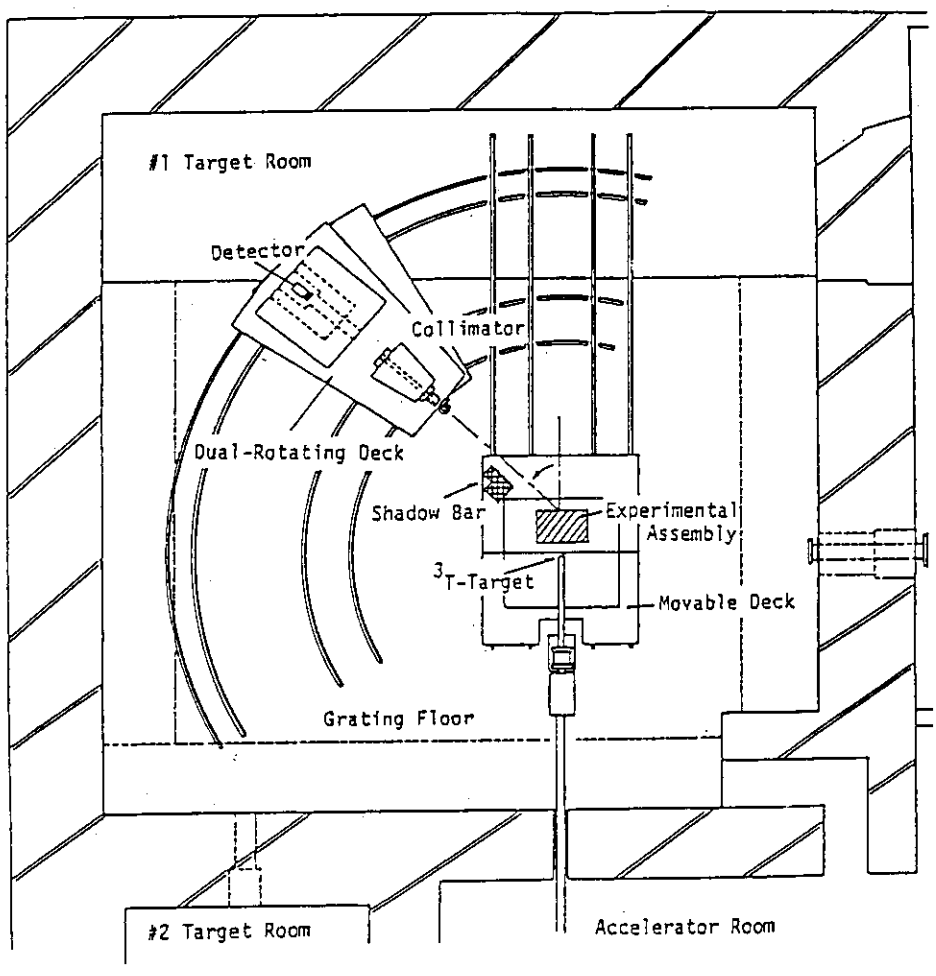

Fig. 1 Experimental layout of the angular neutron flux measurement

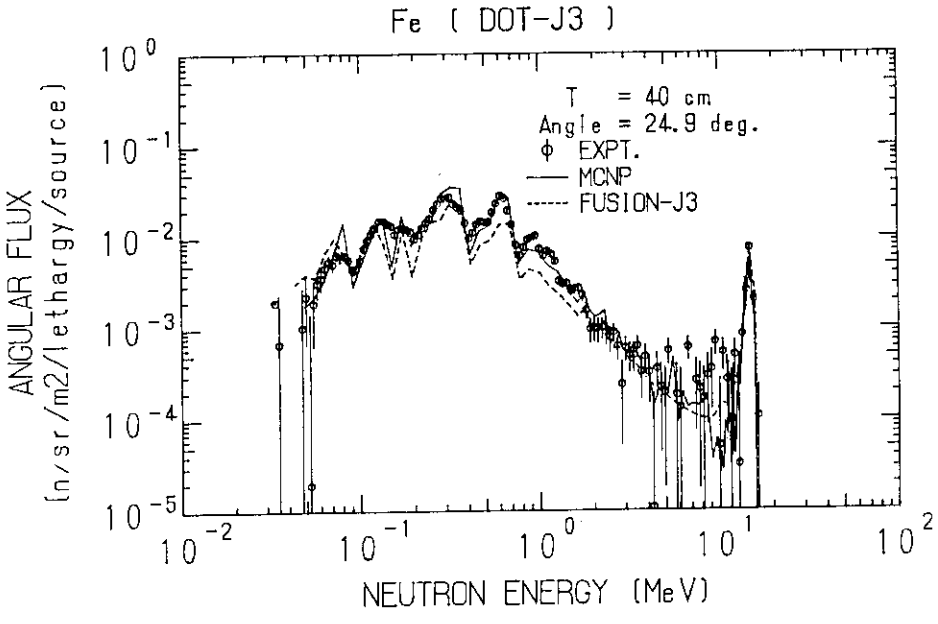

Fig. 2 The comparison between the DOT3.5/FUSION-J3 and the MCNP calculations for the 40 cm thick assembly

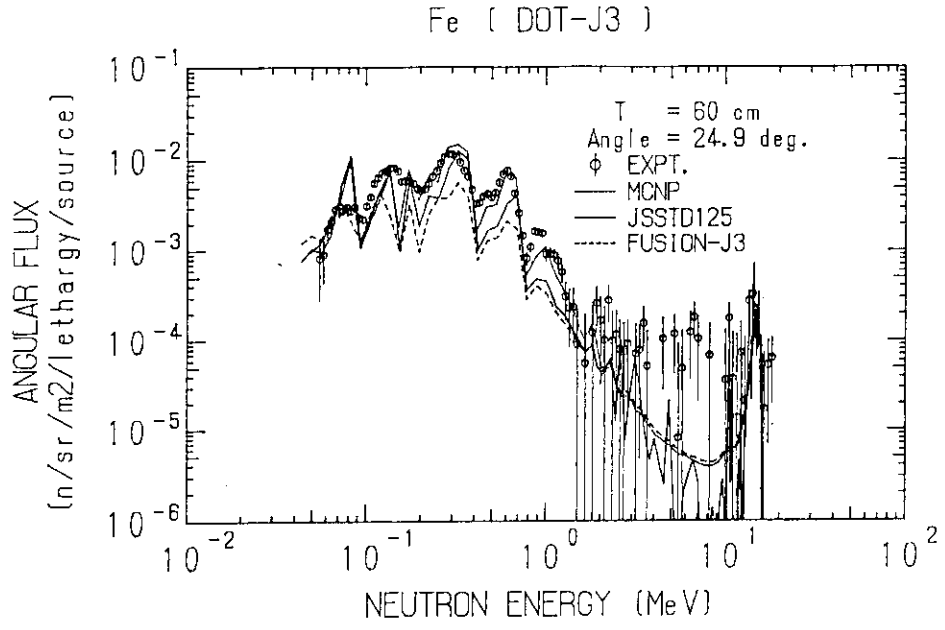

Fig. 3 The comparison among the DOT3.5/FUSION-J3, DOT3.5/JSSTD125 and the MCNP calculations for the 60 cm thick assembly

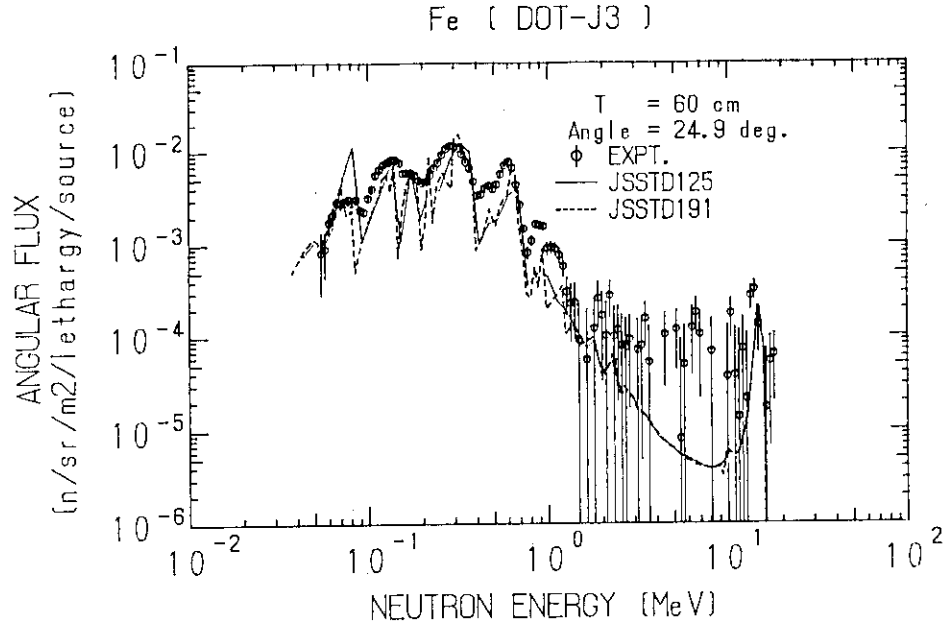

Fig. 4 The comparison between the DOT3.5/JSSTD125 and the DOT3.5/JSSTD191 calculations for the 60 cm thick assembly

3.15 Thick Target Neutron Yield by Heavy Ions

Kazuo Shin, Kagetomo Miyahara
Department of Nuclear Engineering, Kyoto University

Yoshitomo Uwamino
Institute for Nuclear Study, University of Tokyo

Abstract

This paper describes the systematic study of the thick target neutron yield by light and heavy ions.

Measurements of neutron yield data were made for combinations of several thick targets (C, Al, Cu, Fe, Pb) and projectiles (30-MeV p, 65-MeV alpha, 120-MeV $^{12}C^{5+}$, 153-MeV $^{16}O^{6+}$), and obtained neutron angular spectra were analyzed by the moving source model.

Through the consideration on the nuclear temperature, it was found that the multiplicity of equilibrium neutrons was proportional to target the mass number. Using this fact, a simple expression for systematics of equilibrium neutron yield was derived.

For nonequilibrium component, the neutron yield was proportional to the geometrical cross section, being consistent with the local hot spot model. The threshold for the nonequilibrium neutron production affected the yield for low energy projectiles.

I. Introduction

Inclusive neutron production data are fundamental ones for the application of ion accelerators to the engineering purpose. The thick target neutron yield data are indispensable as the neutron source data for the accelerator shield design. Unfortunately there are very few data existing./1/ Most data on secondary neutrons from heavy ion reactions were for the nuclear physics study and were exclusive ones to explore the reaction mechanism. Since experimental data on the inclusive neutron yield are very rare, it is important to study the systematics of the neutron yield for the assessment of unknown data.

We have continued measurements of the neutron production data from various thick targets bombarded by light ions./2,3,4/ The intranuclear

cascade evaporation calculations were tested through those measurements. The model is suited for the systematic generation of the neutron yield data. Therefore, it was desirable to extend the model to lower energy range. It was shown the total yield was reproduced even at the lower energies by the model within a factor of two, but the model failed to predict the angular and energy distributions of neutrons.

Nakamura and Uwamino/5/ proposed the two- or three-component exponential function fitting of the angular spectra. The method made very easy to reproduce the measured data for practical use. However, the systematic description of the neutron yield was still very hard by their method.

In this work, the moving source model, which has been used to analyzed the systematics of charged particle and neutron emission cross sections in heavy ion collisions, is applied for the analysis of our thick target data. The previous studies/2,3,4/ is extended to heavier ions, new measurements by $^{12}C^{5+}$ and $^{16}O^{6+}$ being added in this work. And systematics of the neutron yield is studied.

II. Experimental Procedure

The measurement made in this work is very similar to those in previous works/2,3,4/ except that projectile ions are $^{12}C^{5+}$ and $^{16}O^{6+}$. The experimental arrangement is shown in Fig. 1. The experiment was made at the SF cyclotron of the Institute for Nuclear Study at the University of Tokyo. The ion energies are about 10 MeV/u for the both ions. Targets of C, Al, Cu and Pb thicker than the ion stopping range were bombarded by the ions and neutron spectra were detected by an NE-213 at angles 0°, 15°, 30°, 60°, 90°, 135° for $^{16}O^{6+}$ and 0°, 30°, 75°, 120°, 150° for $^{12}C^{5+}$. The detector was located 2 m down from the target. The spectra were obtained by the unfolding method. Background data were taken by inserting an iron and polyethylene shadow shield between the target and the detector.

III. Results and Discussions

1. Moving Source Analysis

Measured neutron angular spectra of this work and the previous works (light ion data of 30-MeV p and 65-MeV alpha) were fitted by two-component moving source model of Eqs. (1) and (2);

$$\phi(E_n,\theta)=\sum_{i=1}^{2} M_i \frac{\sqrt{E_n}}{2(\pi\tau_i)^{3/2}} \cdot \exp\left(-\frac{E_s}{\tau_i}\right), \qquad (1)$$

$$E_s = E_n - 2\sqrt{\varepsilon_i} E_n \cos\theta + \varepsilon_i, \tag{2}$$

where M_i is the source intensity (neutron yield), τ_i the nuclear temperature, ε_i the source kinetic energy.

As is illustrated by Fig. 2, which is for the case of the $^{12}C^{5+}$ ion on the Pb target, the neutron angular spectra are very well reproduced by two sources, one with smaller ε_i (equilibrium neutrons: EN) and the faster one (nonequilibrium neutrons: NEN). The neutron yield is dominated by the EN. The contribution by the NEN is about one-tenth.

The systematics consideration on the neutron yield will be made below separetely for the EN and NEN using M_i values obtained by data fitting.

2. Equilibrium Neutrons

Fig. 3 summarizes the nuclear temperature of the EN. It shows that the nuclear temperature data for each target come on a unique curve and the shape of the curve resemble one another. Consequently, there is a simple relation between the nuclear temperature and the target mass number as,

$$A_T^{\frac{2}{5}} \tau^2 \sim \text{Const.} \tag{3}$$

The excitation energy E of the target-like fragment is

$$E = a\tau^2, \tag{4}$$

and the level density parameter a is written as

$$a = A_T/8, \tag{5}$$

then

$$E \sim \text{Const.} A_T^{\frac{3}{5}}. \tag{6}$$

For this excitation energy, we obtain that the neutron multiplicity $\bar{n}$ was approximately proportional to the target mass number A_T. Fig. 4 illustrates this relation, where "$E \propto A$" data in the figure are theoretically

calculated ones by Dostrovsky et al./6/, and those of "$E \propto A^{3/5}$" are reevaluated ones from Dostrovsky's data assuming the multiplicity being proportional to the excitation energy.

The neutron production cross section for the EN from the target nucleus in the central collision may be expressed as the target geometrical cross section times the nucleon number in the projectile times the neutron multiplicity;

$$\sigma_T = g \cdot A_P \cdot A_T^{\frac{2}{3}} \cdot A_T = g A_P A_T^{\frac{5}{3}}, \tag{7}$$

where g is a constant and A_p the projectile mass number.
The cross section for the projectile should be similar. So the total EN cross section may be,

$$\sigma_n = g(A_P A_T^{\frac{5}{3}} + A_T A_P^{\frac{5}{3}}) f. \tag{8}$$

In Eq. (8) we included correction factor f for the Coulomb barrier,

$$f = 1 - \frac{A_T + A_P}{A_T} \cdot \frac{V - Q}{E_P}, \tag{9}$$

where E_p is the projectile energy, V the Coulomb barrier, Q the effective Q value.

An example of the prediction by Eqs. (8) and (9) is given in Fig. 5, where the formula is compared with measured data of the neutron total production cross section by heavy ions given by Hubbard et al./7/ The dependence of the the neutron yield on the target and projectile mass numbers is very well reproduced.

The thick target neutron yield is given by Eq. (10), neglecting nuclear cascade by secondary ions,

$$Y = \int \sigma_n N \frac{dE_P}{\left(-\frac{dE_P}{dx}\right)}, \tag{10}$$

where N is the target atomic density.

The level density parameter a exhibits oscillation with A_T at low excitation energies due to the shell effect. This effect should be incorporated in Eq. (8) when E_p is not large. We simply assumed that σ_n was proportional

to the excitation energy which in turn was proportional to a. So the correction by this effect is

$$k=a/(A_T/8), \tag{11}$$

The results of the thick target neutron yield predicted by Eqs. (8) and (9) with the above level-density-parameter correction are compared in relative value in Fig. 6 with our measured yield data. The agreement is quite well.

3. Nonequilibrium Neutrons

Production of the NEN is understood by the local hot spot model. In the model, neutrons are generated from only a limited region where the target and projectile nuclei are contacting. Then, the neutron production rate should be proportional to the probability of contact (i.e., geometrical cross section),

$$\sigma_n \propto A_T^{\frac{2}{3}}, \tag{12}$$

The thick target yield of the NEN is given by inserting Eq. (12) into Eq. (10). This very simple description reproduced our 30MeV p data well, but failed in the case of 65-MeV alpha. The projectile energy in the latter case is 16.3 MeV/u, while the former is 30 MeV/u.

We considered that there was a threshold in the velocity of contacting nuclei to produce nonequilibrium neutrons. Only if the velocity is larger than E_Q in unit of nucleon energy, the NEN is produced. When we assumed E_Q = 2 MeV, the data of the 65-MeV alpha were reproduced well. This is demonstrated by the solid line in Fig. 7. The threshold did not give much effect to the 30-MeV p data.

IV. Conclusions

(1) The simple formula was proposed for the systematics of the EN production cross section. The proposed formula well reproduced the dependence of the EN neutron yield on the target and projectile mass numbers.

(2) The NEN neutron yield was reproduced by the geometrical cross section with the threshold of E_Q = 2 MeV for the relative velosity between the contacting nuclei.

References

1) T. Nakamura et al., "Bibliography of Published Papers on Neutron and Photon Emission from Thick or Thin Target Bombarded by Charged Particles," Report INS-TS-20, Insitute for Nuclear Study, Univ. Tokyo, (1981).
2)T. Nakamura et al., Nucl. Instr. Methods, 151, 493 (1978).
3)T. nakamura et al., Nucl. Sci. Eng., 83, 444 (1983).
4)K. Shin et al., Phys. Rev. C, 29, 1307 (1984).
5)T. Nakamura and Y. Uwamino, Phys. Rev. C, 29, 1317 (1984).
6) I. Dostrovsky et al., Phys. Rev., 111, 1659 (1958).
7) E. L. Hubbard et al., Phys. Rev., 118, 507 (1960).

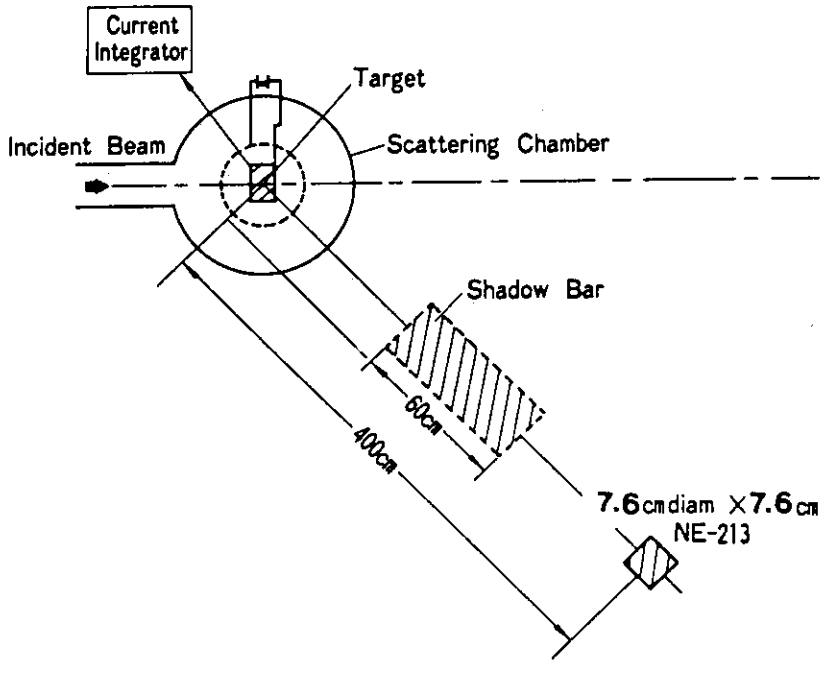

Fig. 1 Experimental arrangement

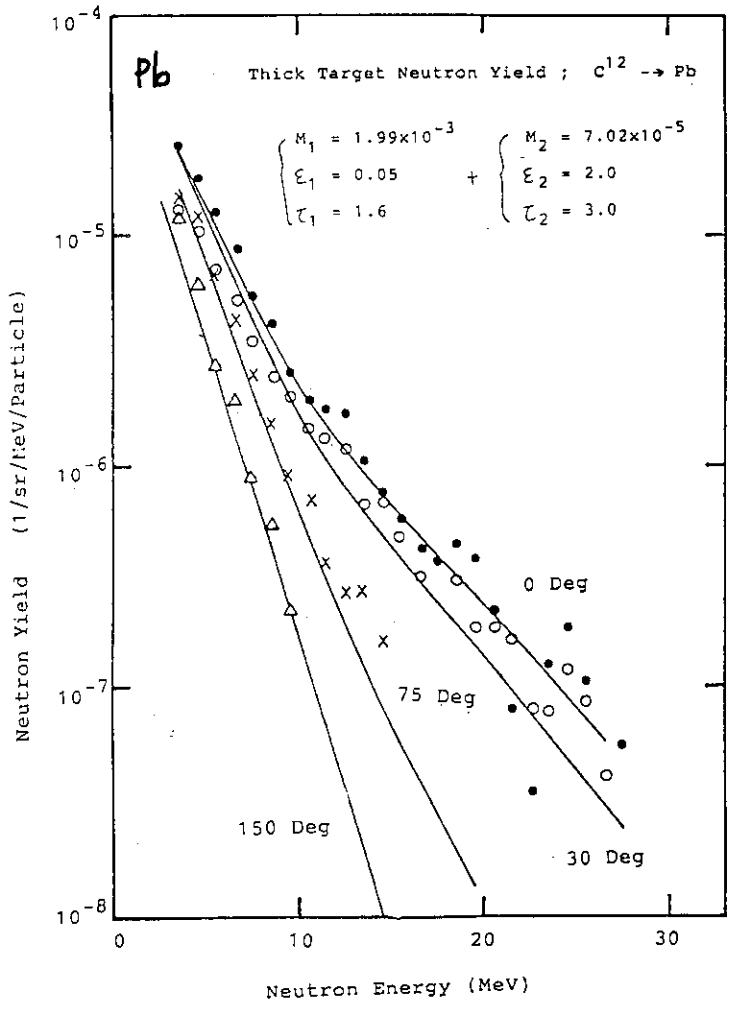

Fig. 2 Neutron angular spectra for the Pb target bombarded by $^{12}C^{5+}$ ions. The solid line shows two-component moving source fitting.

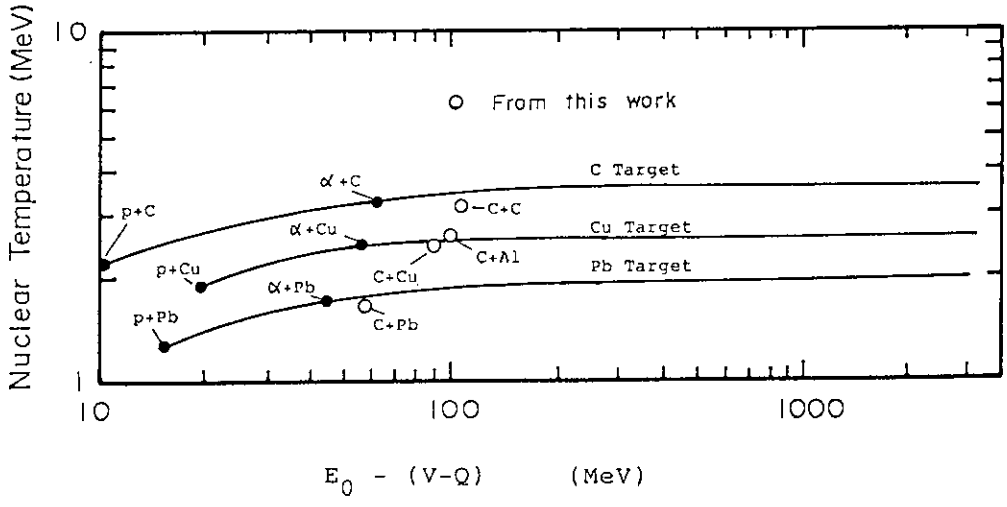

Fig. 3 Nuclear temperature of the EN

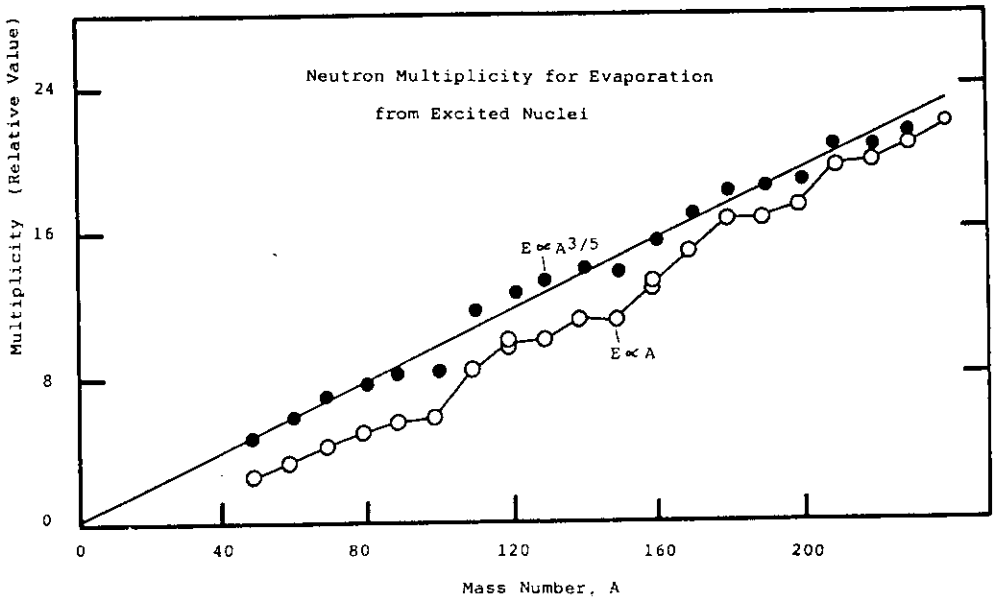

Fig. 4 Neutron multiplicity for the evaporation from excited nuclei

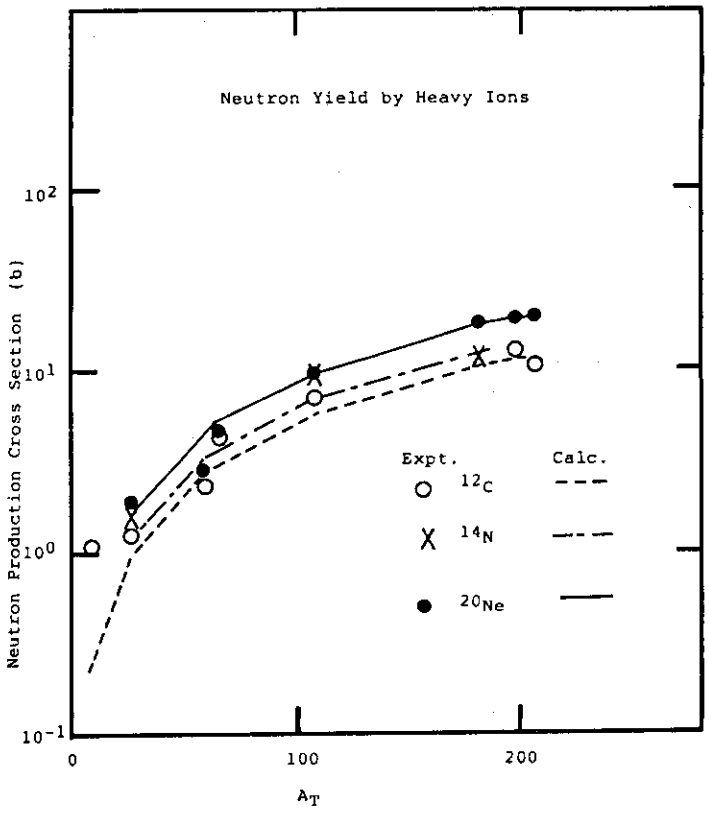

Fig. 5 Neutron total production cross sections from heavy ion reactions

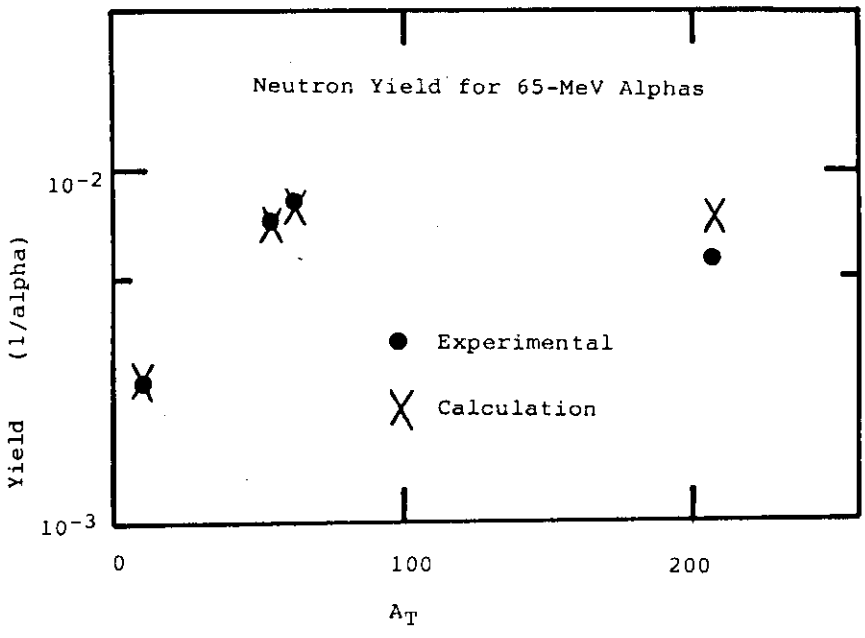

Fig. 6 Thick target EN yield for 65 MeV alphas

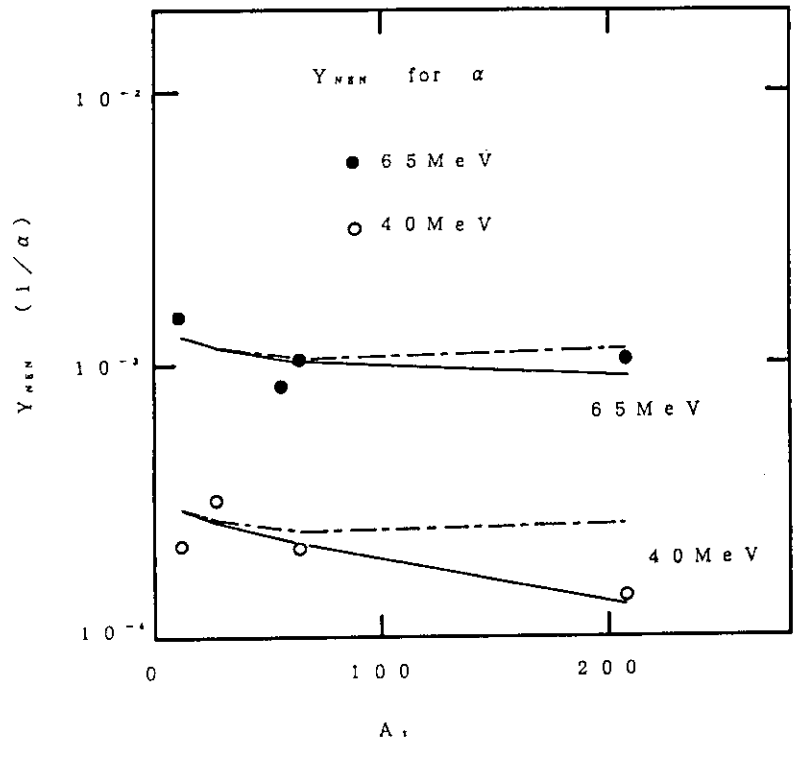

Fig. 7 Thick target NEN yield for 65 MeV alphas

3.16 Measurements of Neutron Emission Cross Sections of ^{nat}C and ^{nat}Fe for 14.1 MeV Incident Neutrons

K. Hata*, S. Shirato and Y. Ando

Department of Physics, Rikkyo University, Nishi-Ikebukuro 3, Toshima-ku, Tokyo 171, Japan

Double differential cross sections (DDX) for elastic and inelastic neutron scattering from ^{nat}C and ^{nat}Fe at 14.1 MeV were measured using the neutron time-of-flight (TOF) facility of the 300 kV Cockcroft-Walton accelerator of Rikkyo University. Angular distributions were measured at angles from 10° to 50° in 10° increments. The experimental layout is shown in fig. 1.

Neutron TOF spectra were obtained from the time signals of scattered neutrons and the associated α-particles produced in the $^3H(d,n)^4He$ reaction at 165 keV. Two well-shielded NE213 liquid scintillators of 2 in ϕ x 2 in and 10 cm ϕ x 30 cm were used as neutron detectors, while a thin (50 μm) NE102A plastic scintillator was done as an α-particle detector[1]. The time resolution (0.7 ns in FWHM) of the present TOF system using Hamamatsu R2083 photomultipliers was remarkably improved by the replacement of R1246X photomultipliers in our old system (1.35 ns)[2]. The cylindrical scattering samples of 3 cm ϕ x 3 cm were made of natural graphite and iron of 99.9 % purity.

The measured energy spectra of scattered neutrons are shown in fig. 2 for ^{nat}C and fig. 3 for ^{nat}Fe, where the curves

---

* Present address: Hitachi Seisakusho Co.

are predictions[3] based on JENDL-3T.

The measured differential cross sections for elastic scattering and inelastic one to the first excited state at 4.44 MeV from ^{12}C are compared with other experimental data[4,5,6,7] in figs. 4 and 5, respectively. The present data for ^{56}Fe are also compared with other experimental data[8,9,10] in fig. 6 for elastic scattering and in fig. 7 for inelastic one to the first excited state at 0.847 MeV.

The measured angular distributions for elastic scattering are in good agreement with optical model calculations using the computer code DWUCK4[11], as indicated by the solid lines in fig. 4 for ^{12}C and also in fig. 6 for ^{56}Fe. The optical potential parameters obtained by Gul et al.[7] for ^{12}C and by Hyakutake et al.[10] for ^{56}Fe were adopted in these calculations. These parameters are given in table 1. The dashed lines in figs. 4 and 6 show predictions of JENDL-3T.

The preliminary analyses of measured differential cross sections for inelastic neutron scattering from the first excited states of ^{12}C and ^{56}Fe were performed in DWBA calculations using the code DWUCK4, as shown in fig. 5 for ^{12}C and in fig. 7 for ^{56}Fe. In these calculations, the deformation parameters β_2 were assumed to be 0.90 for $^{12}C^*$(1st) in stead of 0.65 given by Olsson et al.[12] and to be 0.23 for $^{56}Fe^*$(1st)[10].

The details of the present work are described in ref. 13.

This report is written by summarizing the effort implemented under the Research-in-Trust in 1989 - 1990 fiscal years from the Japan Atomic Energy Research Institute (JAERI).

References

1) S. Shirato, S. Shibuya, Y. Ando, T. Kokubu and K. Hata, Nucl. Instr. Methods A278, 477 (1989).

2) Y. Ando, T. Motobayshi and S. Shirato, JAERI-M 86-080, 297 (1986).

3) T. Fukahori and I. Tazaki, JAERI-memo 62-453 (1988).

4) R. Bouchez, J. Duclos and P. Perrin, Nucl. Phys. 43, 628 (1963).

5) D. W. Glasgow, F. Purser, H. Hogue, J. Clement, K. Stelzer, G. Mack, J. Boyce, D. Epperson, S. Buccino, P. Lisowski, S. Glendinning, E. Bilpuch, H. Newson and C. Gould, Nucl. Sci. Eng. 61, 521 (1976).

6) G. Haouat, J. Lachkar, J. Siguad, Y. Patin and F. Cocu, Nucl. Sci. Eng. 65, 331 (1978).

7) K. Gul, M. Anwar, M. Ahmad, S. M. Saleem and N. A. Khan, Phys. Rev. C24, 2458 (1981).

8) J. H. Coon, R. W. Davis, H. E. Felthauser and D. B. Nicodemus, Phys. Rev. 111, 250 (1958).

9) B. E. Leshchenko et al., Soviet J. Nucl. Phys. 15, 5 (1972).

10) M. Hyakutake, M. Matoba, T. Tonai, J. Niidome and S. Nakamura, J. Phys. Soc. Japan 38, 606 (1975).

11) P. D. Kunz, University of Colorado Report, unpublished.

12) N. Olsson, B. Trostell and E. Ramstrom, Nucl. Phys. A496, 505 (1989).

13) K. Hata, S. Shirato and Y. Ando, JAERI-memo 02-308 (1990, in Japanese); to be submitted to JAERI-M.

Table 1 Optical potential parameters. [$U_C(r) = 0$]

	V (MeV)	W_s (MeV)	V_{so} (MeV)	r_0 (fm)	r_0' (fm)	a (fm)	b (fm)	Ref.
^{12}C	46.5	8.88	4.39*	1.28	0.86	0.39	0.39	7)
^{56}Fe	43.55	10.24	6.00*	1.25	1.242	0.673	0.47	10)

V: Real volume Woods-Saxon potentials with range parameters r_0 and a.

W_s = VI/4: Imaginary surface Woods-Saxon potential with range parameters r_0' and b.

* Note $V_{so} = V_{LS}/4$ in the $\underline{l}$-$\underline{\sigma}$ form.

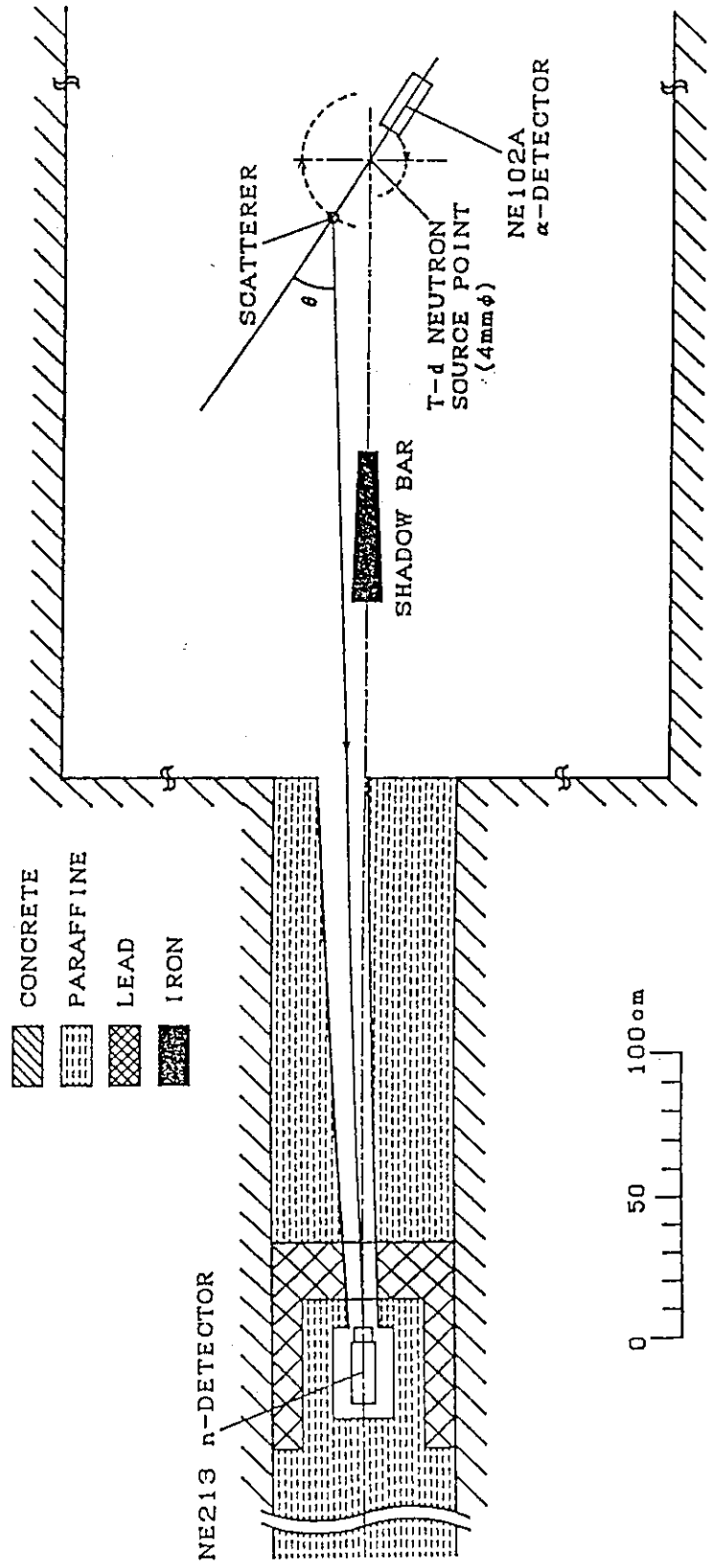

Fig. 1 Experimental layout

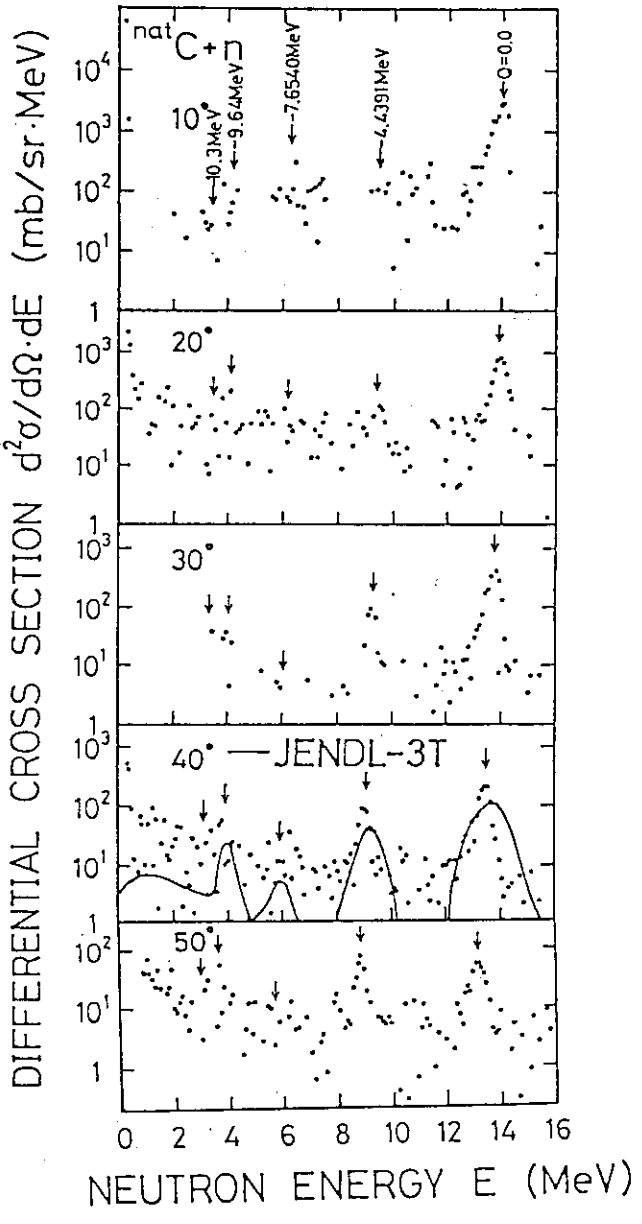

Fig. 2 Measured double differential cross sections for neutron scattering from ^{nat}C. The arrows indicate the energy states in ^{12}C.

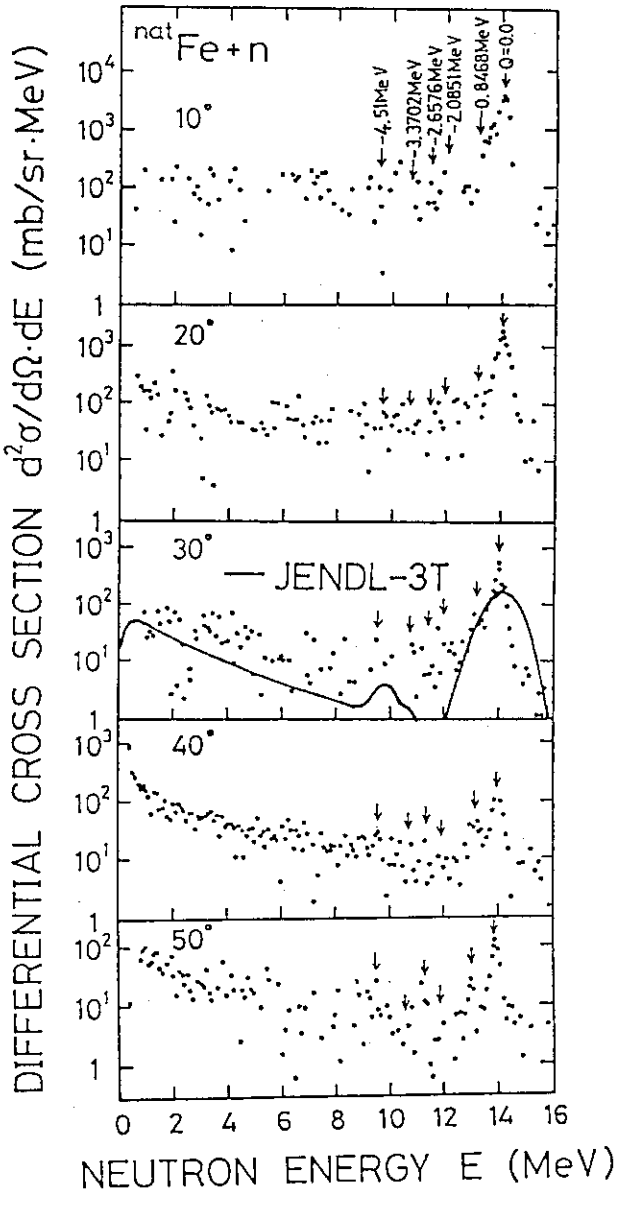

Fig. 3 Measured double differential cross sections for neutron scattering from ^{nat}Fe. The arrows indicate the energy states in ^{56}Fe.

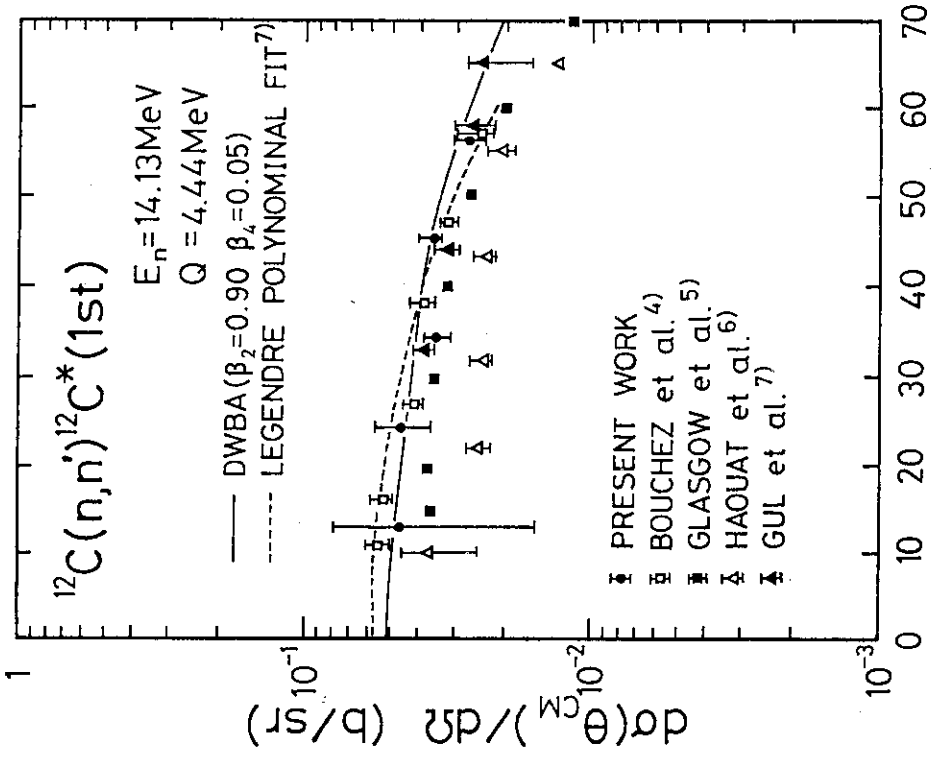

Fig. 5 Measured and calculated angular distributions for inelastic neutron scattering from $^{12}C^*$(1st).

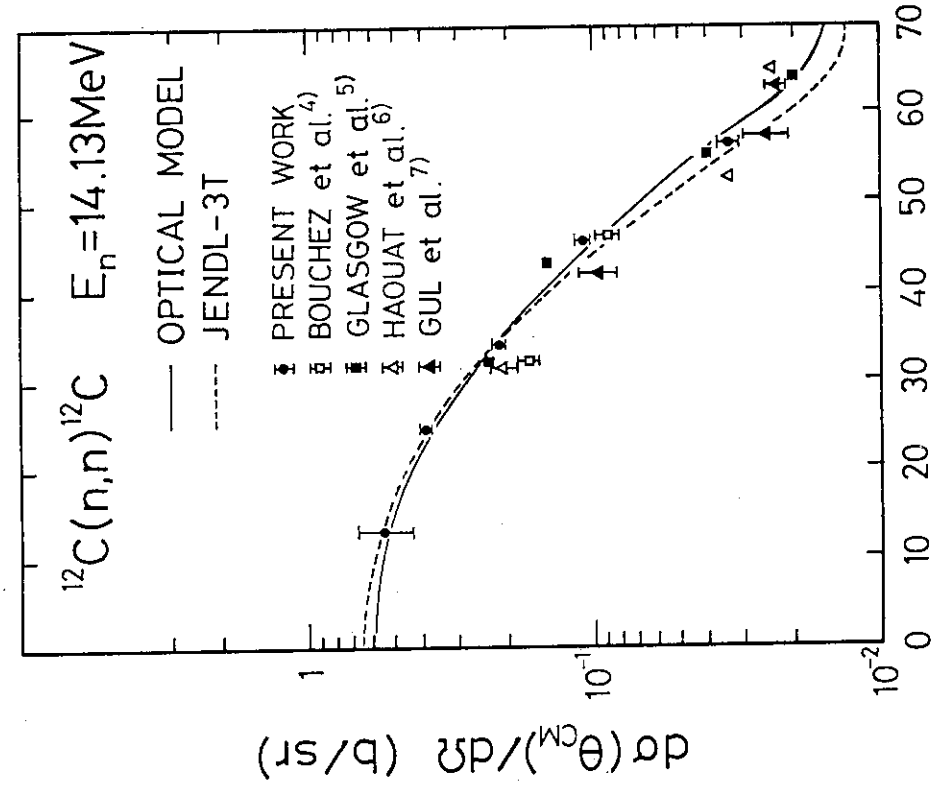

Fig. 4 Measured and calculated angular distributions for elastic neutron scattering from ^{12}C.

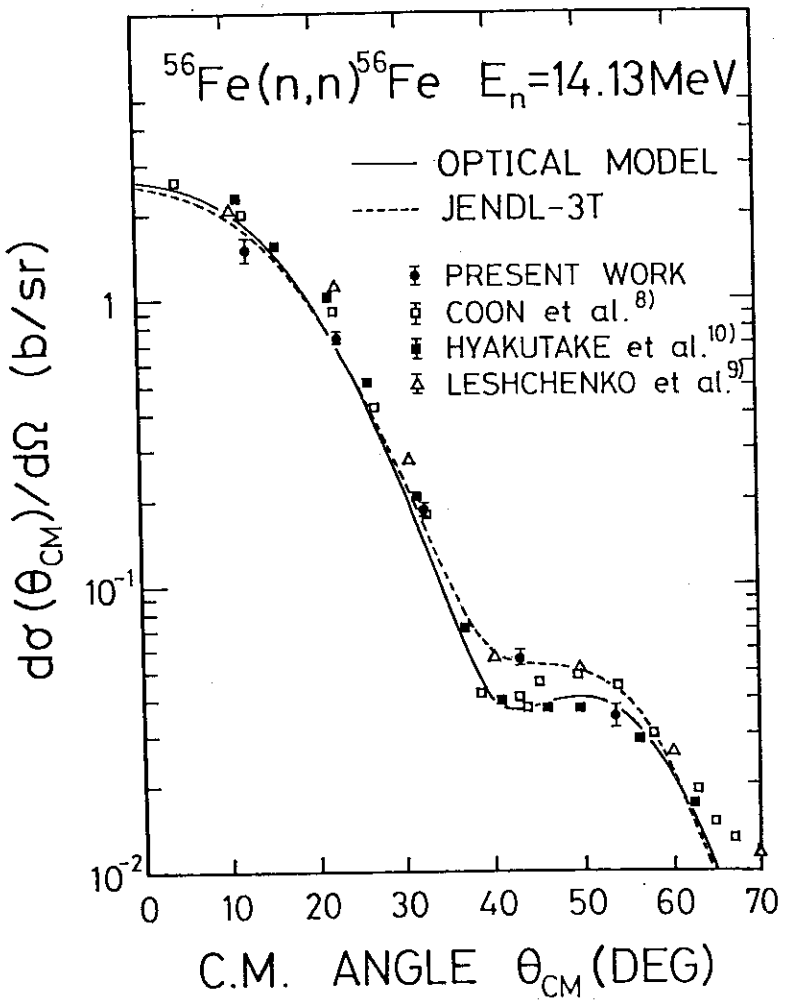

Fig. 6 Measured and calculated angular distributions for elastic neutron scattering from ^{56}Fe.

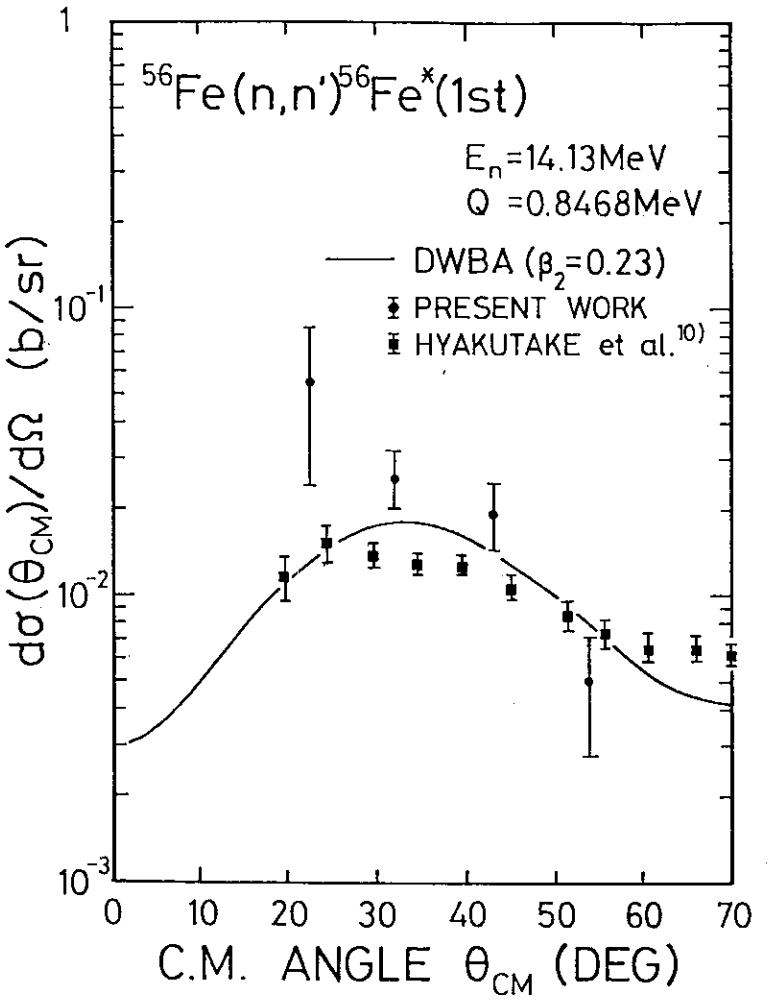

Fig. 7 Measured and calculated angular distributions for inelastic neutron scattering from ^{56}Fe*(1st).

3.17 Four Body Breakup Reaction on ^{12}C Induced by Polarized Proton

Y. Watanabe*, N. Koori**, H. Kashimoto*, H. Hane*, A. Aoto*
A. Nohtomi+, Susilo Widodo+, O. Iwamoto+, R. Yamaguchi+,
K. Sagara++, H. Nakamura++, K. Maeda++, and T. Nakashima++

** Department of Energy Conversion Engineering, Kyushu University, Kasuga, Fukuoka 816*
*** College of General Education, The University of Tokushima, Tokushima 770*
+ Department of Nuclear Engineering, Kyushu University, Fukuoka 812
++ Department of Physics, Kyushu University, Fukuoka 812

Double differential cross sections and analyzing powers were measured of protons and α particles emitted from the bombardment of ^{12}C with 14 and 16 MeV polarized protons. The measured energy spectra of protons and α particles are analyzed on the basis of the reaction model in which three or four-body simultaneous breakup process is taken into account. The calculated proton and α spectra show reasonable agreement with the experimental continuous spectra in low outgoing energy region.

1. Introduction

In the interaction of fast neutrons with carbon, the contribution of the $^{12}C(n,n')3\alpha$ reaction to the nonelastic cross section becomes dominant with increase in the incident energy. This four-body breakup reaction, therefore, is most important for estimation of radiation damage and neutron shielding in fusion reactor design and kerma factors needed for high-energy neutron radiotherapy. Double differential cross sections for the reaction is needed in more accurate calculations of neutron transformation and kerma factors as well as in understanding of the reaction mechanism. Several measurements on the $^{12}C(n,n')3\alpha$ cross section have been made in the high incident energy range between 14 and 60 MeV[1][2]. However, there are only a few direct measurements of both energy spectra of neutrons and α particles at the same incident energy[3][4].

So far, we have performed the study of neutron-induced reactions on Li-isotopes and several medium heavy nuclei through the experimental study of proton-induced reactions analogous to neutron-induced reactions[4][5]. In the present work, this approach is also applied to investigate the mechanism of the $^{12}C(n,n')3\alpha$ reaction. Double differential cross sections and analyzing powers have been measured of protons and α particles emitted from the bombardment of ^{12}C with 14 and 16 MeV polarized protons. The measured spectra of protons

and α particles are analyzed on the basis of the reaction model in which the simultaneous breakup process is taken into account. The aim of the present work is to establish a reliable model to evaluate the $^{12}C(n,n')3\alpha$ or $^{12}C(p,p')3\alpha$ breakup cross section.

2. Experimental procedure and data processing

The experiment was performed using 14 and 16 MeV polarized proton beams from the tandem Van de Graaff accelerator at Kyushu University. Details of the experimental procedure have already been reported elsewhere[4][5]. The experimental setup in a scattering chamber is illustrated in Fig.1. A ΔE-E counter telescope consisting of three silicon surface barrier detectors(E_1: 20 μm, E_2: 75μm, E_3: 2000μm) was employed to measure emitted protons and α particles up to as low energies as possible ($E_{p'}$>1 MeV and E_α> 1.5 MeV). A target was a self-supporting foil of natural carbon whose thickness was 0.116 mg/cm^2.

To measure α particles with low outgoing energy, the signals from E_1 detector were separately stored in anticoincidence with the signals from E_2 and E_3 detectors. It is possible to identify two particles (proton and α particle) by making use of the difference of maximum energy loss in the E_1 detector; the energy to be deposited in the E_1 detector is below about 1.1 MeV and about 4.3 MeV for proton and α particle, respectively, if the effect of energy loss straggling is neglected. At the forward angle, however, there is some contribution from the nucleus ^{12}C recoiled by the elastic and inelastic scatterings. The energy region of the α particles that can be measured using the present detecting system in low energy region is shown as the shaded portion in Fig.2. Note that the energy loss and the straggling effect of α particles in the target foil is neglected.

The absolute cross sections were determined by normalizing the elastic cross sections measured in the present experiment to those measured in the previous one[6]. The result is shown in Fig.3. Both the angular distributions show the same shape and hence the consistency of both the measured data was also confirmed.

3. Experimental results

Double differential α particle emission cross sections and analyzing powers measured at 30°, 80°, and 150° at 16 MeV are shown by solid circles in Figs.4 and 5, respectively. In Fig.4, two peaks observed at each angle correspond to the transtions to the ^9B(g.s.) and ^9B(2.36MeV) via the $^{12}C(p,\alpha)^9B$ reaction. Under those peaks, there is continuous component that is due to three α breakup process of our interest.

Measured proton spectra for the incident energy of 16 MeV are also shown by histograms in Fig.6. These data are those taken in our previous experiment[6], because the data processing for the proton spectra measured in the present experiment is now in progress. As

shown in Fig.6, the observed energy spectra exhibits a distinct continuum underlying the peak structure corresponding to single excited states of ^{12}C.

4. Theoretical analysis

Multiparticle breakup processes of ^{12}C induced by proton or neutron are mainly classified into the sequential breakup process via some intermediate states and the simultaneous breakup process[7]. Here we consider the following simultaneous breakup processes:

(i) $^{12}C + p \rightarrow p + \alpha + {}^{8}Be$
$\qquad\qquad\qquad\qquad\qquad\qquad\quad \hookrightarrow \alpha + \alpha$

(ii) $^{12}C + p \rightarrow p + \alpha + \alpha + \alpha$

The processes (i) and (ii) are referred to as three-body simultaneous breakup(3BSB) process and four-body simultaneous breakup(3BSB) process, respectively. In the 3BSB process, the sequential decay of ^{8}Be into two α particles occurs and finally three α particles are generated as the reaction products.

The energy spectra of particles emitted in the simultaneous breakup process can be easily calculated by using the phase space distribution $\rho_f(E_1)$ derived on the basis of the reaction kinematics as follows:

$$\frac{d^2\sigma}{dE_1 d\Omega_1} = \frac{2\pi}{h^2}\frac{m_p}{k_p}|M|^2 \rho_f(E_1) \qquad (1)$$

where m_p and k_p are the mass and the wave number of incident proton, respectively. $|M|^2$ is the square of the transition matrix element. The phase space distributions $\rho_f(E_1)$ for the 3BSB and 4BSB are given by the following expressions[8]:

$$\rho_f(E_1)_{3BSB} \propto \sqrt{E_1}\left[\left(\frac{m_2+m_3}{M}E^c_{tot} - E_1 + 2a_1\sqrt{E_1}\cos\theta_1 - a_1^2\right)\right]^{1/2} \qquad (2)$$

$$\rho_f(E_1)_{4BSB} \propto \sqrt{E_1}\left[\left(\frac{m_2+m_3+m_4}{M}E^c_{tot} - E_1 + 2a_1\sqrt{E_1}\cos\theta_1 - a_1^2\right)\right]^{2} \qquad (3)$$

where

$$E^c_{tot} = Q + \frac{m_t E_{in}}{m_p+m_t} \quad \text{and} \quad a_1 = \frac{\sqrt{2m_pE_{in}}}{m_p + m_t} \qquad (4)$$

In these expressions, the subscripts p and t refer to the incident particle and the target nucleus, respectively. The subscripts 1, 2, 3, and 4 refer to the four final particles. Particle 1 is the observed particle. The quantity m_i (i=1,2,3,and 4) is the mass and $M=m_1+m_2+m_3$ for the 3BSB and $M=m_1+m_2+m_3+m_4$ for the 4BSB. The quantity Q is the reaction Q value, E_{in} is the incident energy, and E_1 and θ_1 are the energy and angle of particle 1 in the laboratory system.

For simplicity, we assume that $|M|^2$ is an adjustable parameter independent of the angle

and the outgoing energy. Namely, the shape of energy spectrum is provided by the phase space distribution and the absolute value is determined by normalization to the experimental value. In the present analysis, this adjustable parameter was determined from analysis of proton spectra for 16 MeV so as to reproduce reasonably the continuum component. The same value was used as the normalization parameter in the calculation of α spectra.

A preliminary analysis was performed for the above 4BSB process (ii). The calculated 4BSB spectra for protons and α particles are shown by solid lines in Figs.4 and 6. Emitted three α particles in the process (ii) can not be distinguished by measurement using the present detector system, so that the right hand side of eq.(1) is multiplied by a factor of three and the obtained energy spectra are compared with the experimental data. The calculated proton and α spectra show overall agreement with the experimental ones in shape and magnitude as shown in Figs.4 and 6. Therefore, the 4BSB process seems to be responsible for emissions of protons and α particles with low outgoing energies. However, there is somewhat overestimation in the region around the threshold energy of three α breakup in both those proton and α spectra. From the analysis of the $^{12}C(n,n')3\alpha$ cross sections measured by using nuclear emulsions by Antolkovic et al.[7], they have concluded that the sequential decay process involving the n + α + $^{8}Be_{g.s.}$(or $^{8}Be_{2.9}$) system is the dominant reaction mechanism and the contribution of the 4BSB process is appreciably smaller than that of the 3BSB process. Therefore, the overestimation near threshold may be due to predominance of the 3 BSB process or the other sequential processes.

The energy spectra of proton emitted via the 3BSB process (i) were calculated using the reaction model in which the α-α final interaction was taken into account in the sequential decay from the ^{8}Be ground state and the 2.9 MeV state. As a result, it was found that the difference between the calculated 3BSB and 4BSB spectra appears obviously near the threshold energy as shown by dashed and solid curves in Fig.6, while both the spectra have similar shape in the low outgoing energy region. The calculation of α spectra for the 3BSB process has not yet been completed because the component of the sequential decay from ^{8}Be must be included. The question which process is dominant in the continuum underlying the peak structure, 3BSB or 4BSB process, will be discussed through comparison between the complete 3BSB spectra and the 4BSB spectra for α emissions.

5. Summary

The double differential proton and α particle emission cross sections were measured for $^{12}C(p,p')3\alpha$ reaction induced by 14 and 16 MeV polarized protons, with better resolution than several neutron induced experiments. The measured energy spectra of protons and α particles were analyzed in terms of the reaction model based on phase space distributions in which the three or four-body simultaneous breakup process was taken into account. Both the calculated

4BSB spectra of protons and α particles showed overall agreement with the experimental continuous spectra in low outgoing region under the assumption of a constant transition matrix element. However, overestimate was exhibited obviouly near the threshold energy. This may be due to the contribution of the 3BSB or the other sequential decay processes. Further analysis of the experimental data including the analyzing powers for 14 and 16 MeV will be required to know the details of the p + ^{12}C breakup reaction mechanism.

References

(1) Brenner, D.J., et al.: *Nucl. Scie. and Eng.*, **95**, 311 (1987).
(2) Brenner, D.J. and Prael, R.E.: *Atomic Data and Nuclear Data Tables*, **41**, 71 (1989).
(3) Haight , R.C., et al.: *Nucl. Scie. and Eng.*, **87**, 41 (1984).
(4) Koori, N., et al.: *JAERI-M* 89-167, (1989).
(5) Watanabe, Y.,et al.: *JAERI-M* 90-025, 216 (1990).
(6) Koori, N. et al.: *JAERI-M* 90-025, 208 (1990).
(7) Antolkovic', B., et al.: *Nucl. Phys.* **A394**, 87 (1983).
(8) Ohlsen, G.G.: *Nucl. Inst. and Meth.* **37**, 240 (1965).

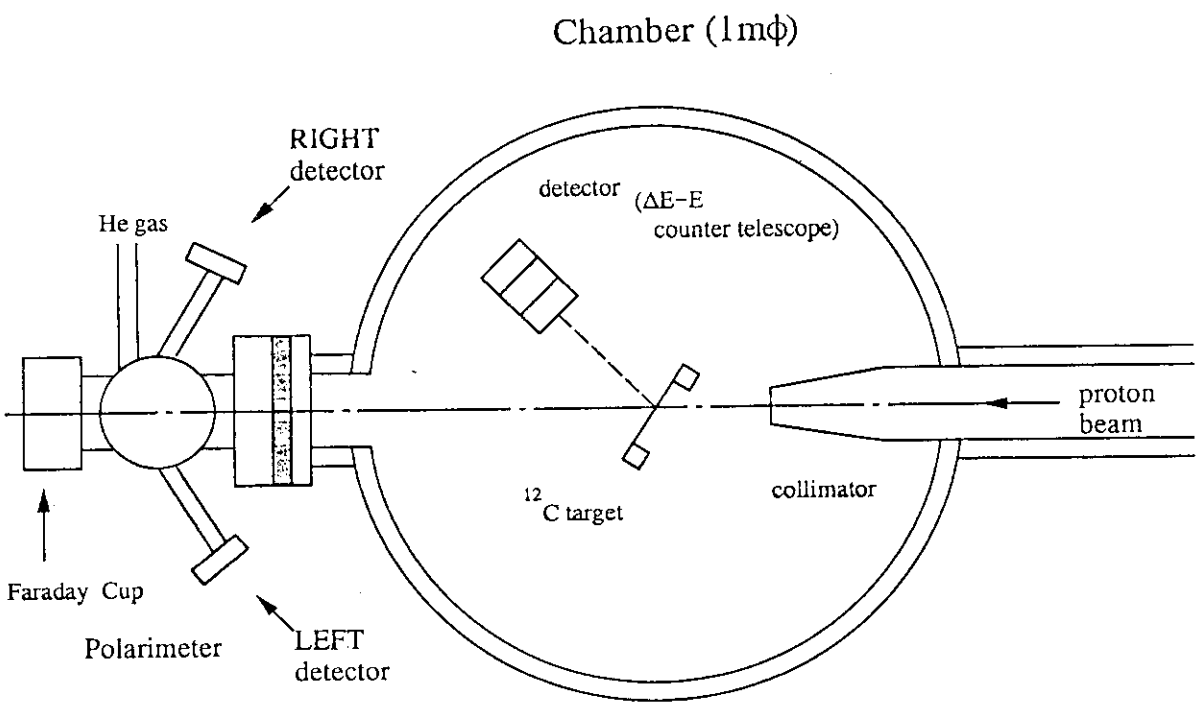

Fig. 1 Schematic layout of experimental setup inside the scattering chamber.

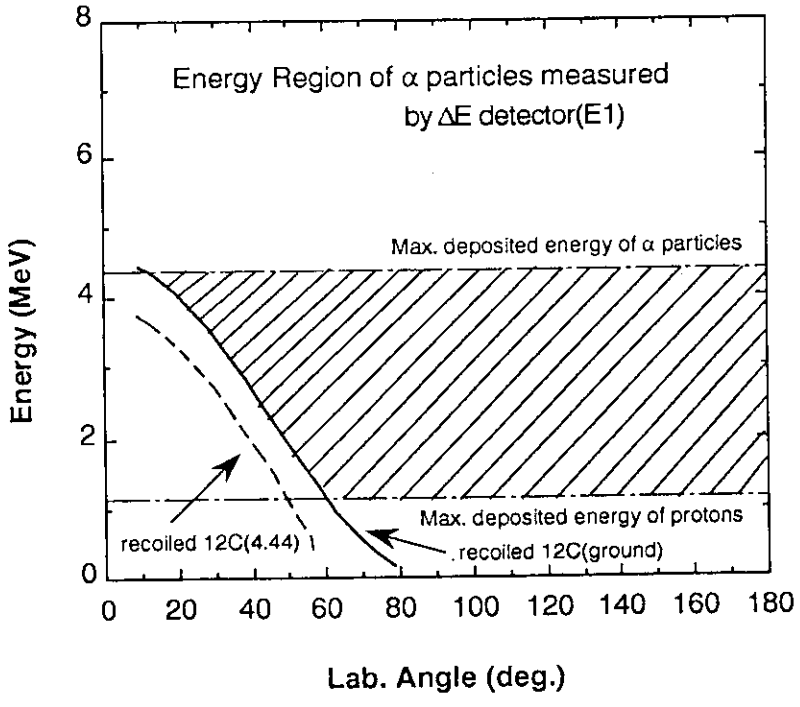

Fig. 2 Energy region of α particles to be measured by using the present α-detecting system in low energy region. The shaded portion indicates the energy region.

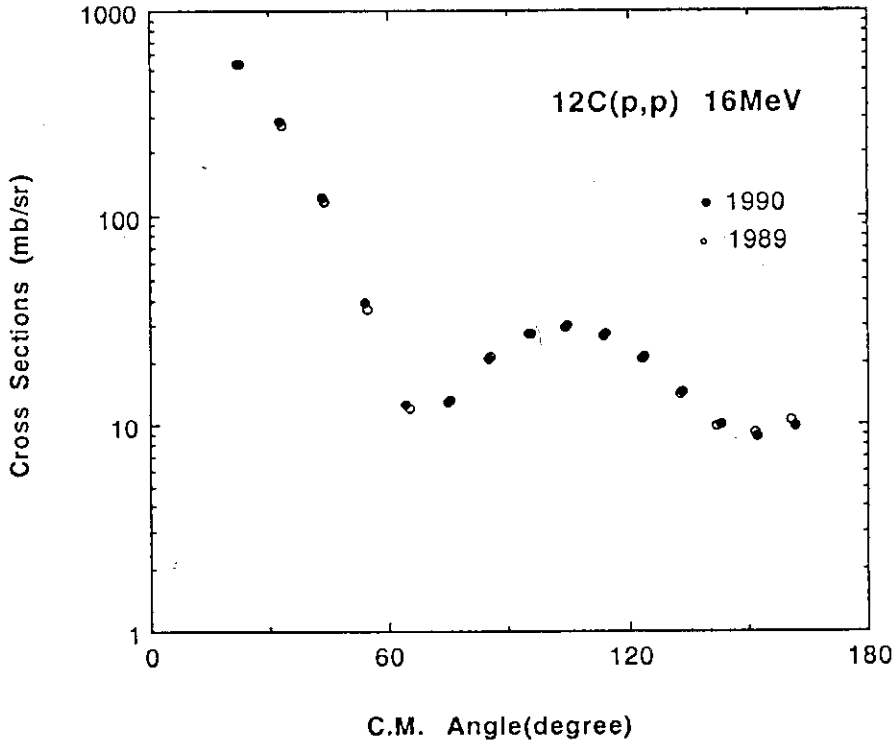

Fig. 3 Comparison of the differential elastic cross sections for ^{12}C at 16 MeV between our two experiments (1989 and 1990).

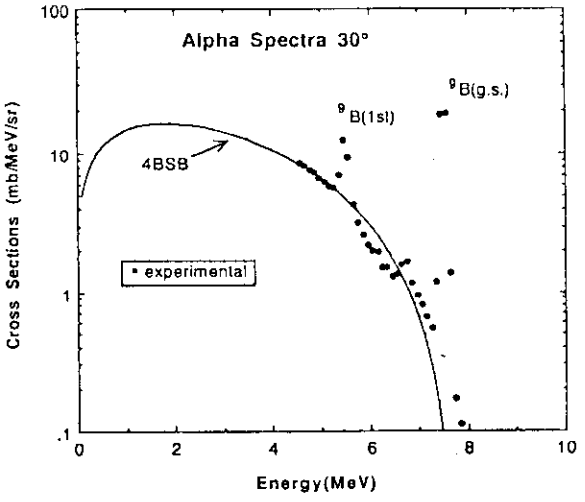

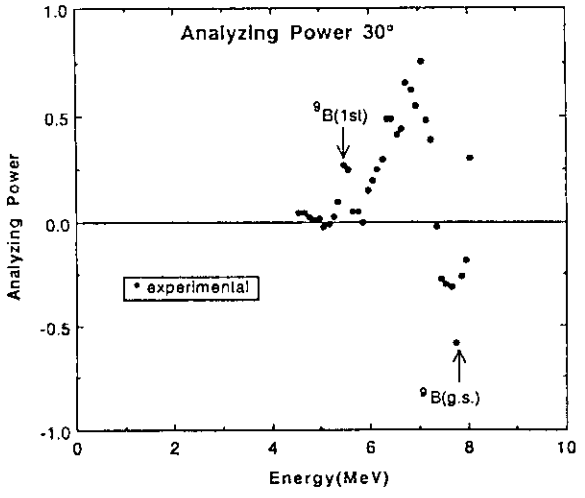

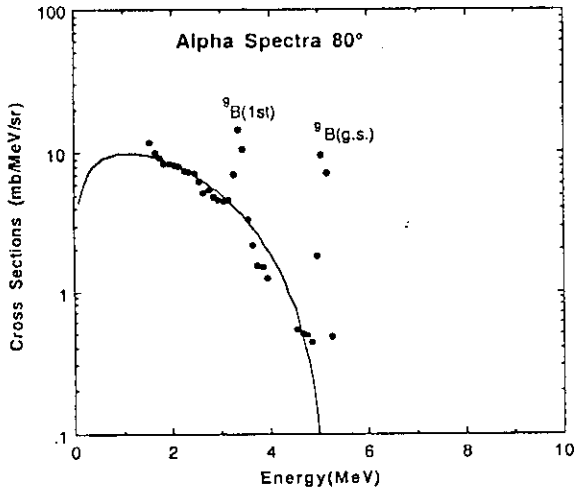

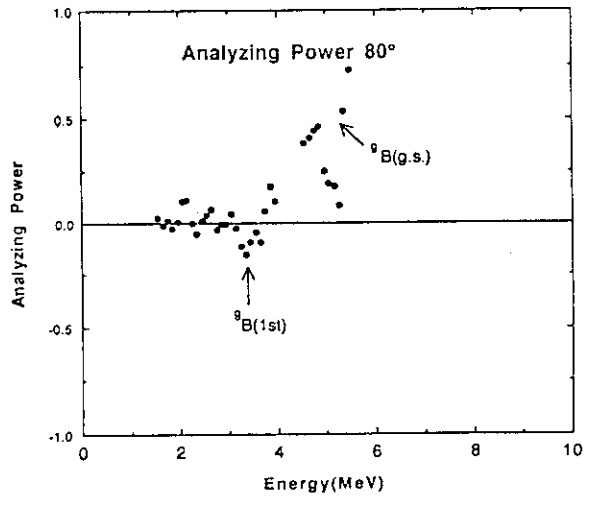

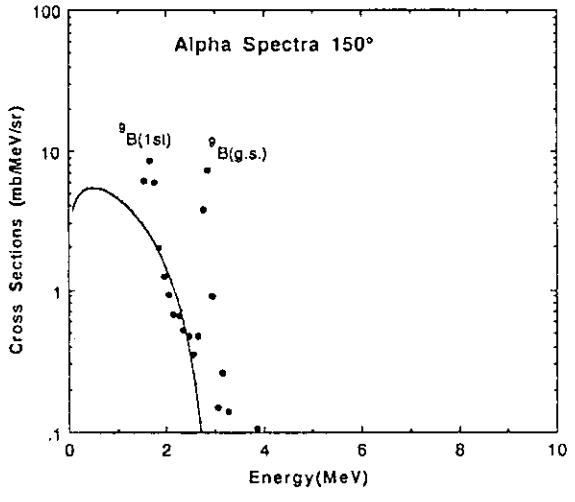

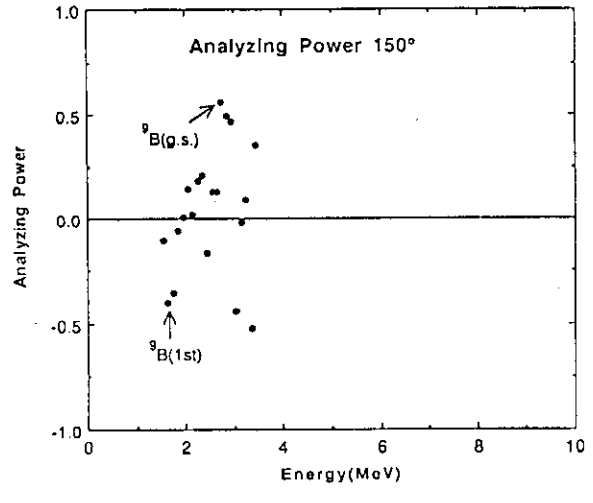

Fig. 4 Double differential α particle emission cross sections for the $^{12}C(p,\alpha)$ reaction at 16 MeV. The measured angles are 30°, 80°, and 150°. Solid circles are the experimental data and solid lines show the calculated 4BSB components.

Fig. 5 Experimental data on analyzing powers for the $^{12}C(p,\alpha)$ reaction at 16 MeV.

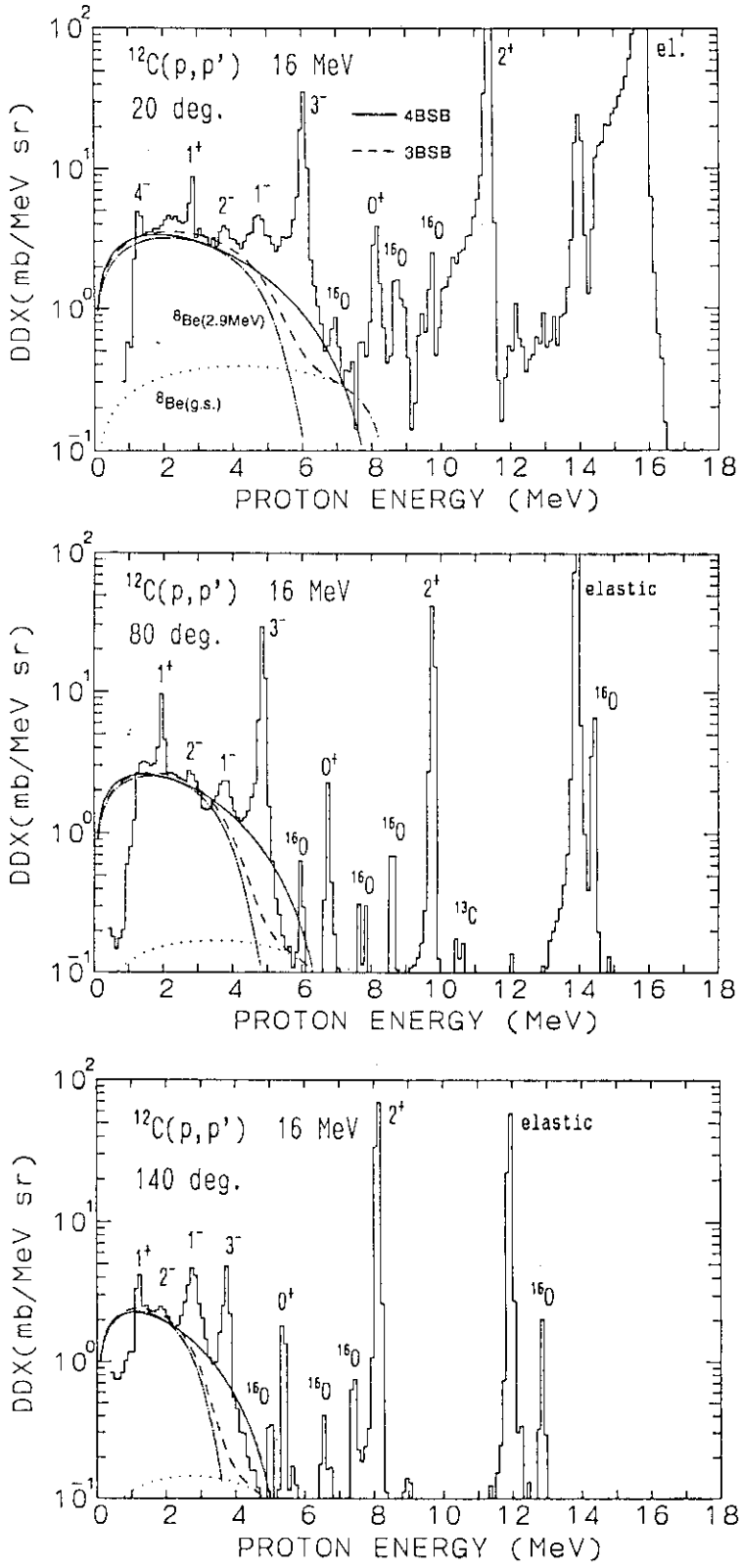

Fig. 6 Double differential proton emission cross sections for the $^{12}C(p,p')$ reaction at 16 MeV. The measured angles are 20°, 80°, and 140°. Histograms are the experimental data. Solid and dashed lines show the calculated 4BSB and 3BSB components, respectively.

3.18 The Extended Moving Source Model Analysis of the Cross Section for Proton Induced Spallation Reactions

Kazuhiko HIGO, Kenji ISHIBASHI, Shouichirou SAKAGUCHI,
Yuzuru MATSUMOTO, Yoshihisa WAKUTA
Department of Nuclear Engineering,
Kyushu University,
Hakozaki, Higashi-ku, Fukuoka, JAPAN
Hiroshi TAKADA, Takahiko NISHIDA, Yasuaki NAKAHARA, Yoshihiko KANEKO
Japan Atomic Energy Research Institute,
Tokai-mura, Ibaraki-ken, JAPAN

Abstract

The parameterization of the double differential cross section is made for the neutron emission from proton-induced spallation reaction. The neutron data for incident proton energy of 600 to 800 MeV are well analyzed by the moving source model. A new idea of a doubly moving source model is introduced in the incident energy region below several hundred MeV. The combination of the two models enables us to parameterize the double differential cross section of neutron emission for the incident protons of 80.5 to 800 MeV, and to find the systematic behavior of the parameters for a wide variety of target nuclei. The extended moving source model is also applied to the analysis of the proton emission cross section. The relationship is studied between the emission cross sections of neutrons and protons.

1. Introduction

The spallation reaction is applicable to such facilities as the intense spallation neutron source and transmutation of long-lived radioactive wastes. In spite of the usefulness for the engineering purpose, the accumulation of the neutron data is poor for the proton induced spallation reaction. Therefore, it is important to find the systematic behavior in the neutron data, and to parameterize them to extend to the other energy regions and target nuclei. Pearlstein[1] parameterized the experimental data at each emission angle by four-component evaporation model. The angle-based evaporation method requires quite many parameters to reproduce the angular distribution of the spectra.

On the other hand, a moving source (MS) model has been used by Shibata et al[2]. The fitting was satisfactory for the protons emitted by several GeV proton induced spallation reaction. Their model successfully expresses the angular distribution with a single parameter. When the present degree of the accumulation of neutron emission data is taken into account, the model may be better suited for reproducing the angular characteristics than the method by

Pearlstein. We extend the MS model to be applicable to the neutron emission data for the reaction that is induced by protons with energies down to 80 MeV. The emitted proton data for the proton induced spallation reaction may have a systematic structure similar to the neutron data. The proton data are considered to be helpful to find the systematic behavior in the neutron ones. We then analyze the proton data to compare them with that of neutron.

2. Moving source (MS) model

The MS model[2] is explained in Fig.1 (a), where a projectile particle interacts with the nucleus that is indicated by a circle. The illustration on the left hand side shows the collision phenomena in the laboratory frame. When this phenomena is observed in a moving frame of a certain velocity β, the particles can be seen to be evaporated isotropically with the Maxwell-type energy distribution of a temperature T(MeV). This situation is shown in Fig.1 (b). Since the velocity β is chosen on the basis of the isotropic angular distribution, the moving frame differs from the center of mass(cm) frame. The cross section in the laboratory frame is shown as

$$E_{tot}\left(\frac{d^3\sigma}{dp^3}\right) = \frac{1}{p}\frac{d^2\sigma}{d\Omega dE_{kin}} = \sum_{i=1}^{3} A_i \cdot \exp\left[-\left(\frac{E_{kin}+m-p\beta_i\cos\theta}{\sqrt{1-\beta_i^2}} - m\right)\Big/T_i\right], \quad (1)$$

where m is particle mass(MeV), θ the emission angle, p the momentum(MeV/c) of emitted particle, and E_{kin} the kinetic energy (MeV) of particle in the laboratory frame. The value of β is normalized by the light velocity c. The parameters A, T and β are adjustable in fitting the equation with the experimental differential cross section data. We designate A,T and β as amplitude, temperature and velocity parameters, respectively. Figure 2 shows the experimental neutron spectra for the 585 MeV proton incidence on lead target[3] together with the results of fitting by the MS model. For the spallation reaction, the neutron data can be reproduced by three components of the MS models successfully. The number of parameters used are smaller than in the case of the angle-based evaporation method[1]. The three components correspond to the intranuclear-cascade, the preequilibrium and the nuclear-evaporation (equilibrium) processes, respectively. The components of cascade, preequilibrium and evaporation processes are plotted by dashed curves for the spectrum of 150 deg. The agreement between the fitting and experiment was found to be excellent for the 585 MeV data[3] for a wide range of targets. Thus, the emitted neutron spectra are well analyzed by the MS model.

3. Introduction of the doubly moving source (DMS) model

The results of fitting by the above MS model are shown by the dashed curves in Fig. 3 for neutron emission cross sections for the iron target bombarded by 113 MeV protons[4]. In the forward directions of 7.5 and 30 deg., the dashed curves are in a poor agreement with the data of the neutron energy above several ten MeV. The neutrons in this energy range are emitted from the intranuclear-cascade process. When the fitting is made for targets having a mass number smaller than iron, the disagreement in the forward directions was more appreciable. In the incident proton energy region below a few hundred MeV, the MS model reproduced the experimental data unsuccessfully.

The particles emitted by the evaporation have Maxwell-type kinetic energy distribution $\exp(-E^*/T)$ in the moving frame. However, the disagreement in Fig.3 suggests to us that the energy spectra in the moving frame are different from the Maxwell-type, and are similar to the Watt distribution[5] which produces a shoulder in the spectra. The validity for use of the Watt distribution is explained as follow. For the incident energy above several hundred MeV, the typical collision phenomena was illustrated on the left-hand side in Fig. 1 (a). Since the incident energy is sufficiently high, the cascading may be developed further after the first collision in the nucleus. In addition, pions can be generated by the quasi-inelastic collision at this energy, and they have much shorter mean free path than nucleons. When the incident energy is above the threshold of the inelastic collision, therefore, the intranuclear cascade may produce some branches, as shown in Fig. 1 (a).

At the energy below 400 MeV, the situation may differ from the above: The cascading develops less extensively than in the case of the higher energy incidence. Besides, no quasi-inelastic scattering is allowed, and the quasi-elastic collision produces only two branches at each scattering, as indicated in Fig. 1 (b). When the moving frame is regarded as the center of mass (cm) frame in the primary collision, the two struck nucleons go away with the same kinetic energy, as shown in the left illustration in this figure. For simplicity, the angular distribution in the moving frame is assumed to be isotropic in the first collision in the nucleus. The struck nucleons are influenced by an additional interaction. The interaction may be due to the Fermi motion of the nucleons, or correlation potentials between nucleons. Such effects are produced before or after the first collision. In this study, however, the effects are included in a form of the residual interaction after the first collision, as deduced on the left-hand side in Fig. 1 (b).

The particles emitted from the residual are again treated by the MS model. These particles are considered to be isotropically evaporated with a temperature T_d if another moving frame is suitably chosen on the second level. Therefore, the particle emission coincides with Watt distribution[5] when it is observed in the original moving source. Taking this situation into

account, we call this model the doubly moving source (DMS) model. For the DMS model, the cross section is written in the laboratory frame by the equation as

$$E_{tot}\left(\frac{d^3\sigma}{dp^3}\right)=\frac{1}{p}\frac{d^2\sigma}{d\Omega dE_{kin}}=\frac{A}{p^*}\cdot\exp\left(-E^*_{kin}/T_d\right)\cdot\sinh\left(\frac{2\sqrt{E^*_{kin}\cdot E_d}}{T_d}\right) \quad . \tag{2}$$

The superscript * indicates the values in the original moving frame. The parameters T_d and E_d are designated a doubly-moving-source temperature and a doubly-moving-source energy, respectively. The value of E_d corresponds to the velocity of the moving frame of the second level relative to the original one. The Watt distribution produces an average kinetic energy $\overline{E}\cong 3/2T_d + E_d$, while the Maxwell distribution gives $\overline{E}\cong 3/2T$ in the original moving frame. The relationship between temperatures in the MS and the DMS models is approximately written as

$$\frac{3}{2}T=\frac{3}{2}T_d+E_d \quad . \tag{3}$$

The DMS model is applicable only to the first process, i.e. the cascade process, that directly induced by the incident protons. The two remaining processes are treated by the MS model. The solid curves in Fig.3 show the results of fitting by the combination of DMS and MS models. The DMS model was used for the first component, and the MS model for both the second and the third ones. The experimental data are expressed better by the solid than the dashed curves.

By the method mentioned above, parameter sets were obtained for the incident energy of 80.5 to 800 MeV[3),(4),(6),(7),(8),(9)]. The results on parameter T are shown for lead in Fig.4, where the subscripts 1 to 3 indicate the intranuclear-cascade, preequilibrium, and nuclear-evaporation processes, respectively. The values of T_d for 80.5 to 318 MeV data were converted by Eq.(3) into T_1 of the MS model, and is plotted together with T_1 at the other energy. The resultant values of T_1 exhibit a smooth dependence on the incident proton energy.

4. The emitted proton spectra

The emitted proton data from the proton induced spallation reaction may have systematics similar to the neutron data. Unfortunately, experimental data are not available for the emitted protons having energies below several ten MeV. The lack of data is mainly ascribed to the energy loss of emitted protons in the matter of target, and to the small yields of protons of lower energy due to existence of the nuclear coulomb barrier.

We compare the data of emitted protons with that of neutrons only in the energy region of the cascade process. Figure 5 shows both the neutron[3)] and proton[10)] spectra for

tantalum bombarded by protons of about 600 MeV. The yields of neutrons are appreciably larger than that of proton data. The neutron spectra can be reproduced by the MS model as mentioned above. For the proton data, however, the results of fitting by the DMS model have better agreement with the experimental data than that by the MS model. The difference in the applicability of the DMS model may be related to the quality of the experimental data. The cross sections were calculated with the microscopic point of view by use of a High Energy Transport Code(HETC). The nuclear calculation of this code is based on an intranuclear-cascade-evaporation model[11]. The results of HETC calculation are shown in Fig.6. One can see that the solid and the dashed lines are almost the same.

The experimental data[12],[13] for 90 MeV proton incidence are shown in Fig.7 together with the results of HETC calculation. In contrast to the data for about 600 MeV, the emission cross section is higher in the proton than the neutron emission data. The calculation results coincide with each other. For the difference of tendencies between the data in the region of 90 MeV and about 600 MeV, there may exist the special mechanism, which can not be included in the HETC calculation. In addition, the quality of the neutron data are worse than that of proton in general. This may be another possible explanation of the difference between the proton and neutron data.

As seen in Figs.6 and 7, the neutron spectra by HETC calculations are quite similar to the proton ones. The systematic data of emitted neutrons do not exist at the incident energy above 800 MeV. Figure 8 shows the experimental proton data[2] and the calculated spectra by HETC for both neutrons and protons for the 1.7 GeV proton incidence. The results of HETC calculation for neutron are similar to that for proton. When this similarity is taken into consideration, the parameters for the neutron data are considered to be predicable by parameter fits of the proton data.

5. Conclusion

The use of the moving source (MS) model with three components reproduced the experimental neutron spectra in the incident proton energy region of 600 to 800 MeV. At the energy below 400 MeV, the introduction of the doubly moving source (DMS) model for the cascade process were found to lead to the good agreement with the experimental spectra. The MS and DMS models were found to be applicable to the neutron data evaluation for a wide range of target masses and incident energies. In addition, the proton spectra for the incident proton energy of 600 MeV were well analyzed by the DMS model. For the HETC calculation, the neutron spectra were very similar to the proton ones. In the incident energy region above 800 MeV, the neutron spectra are predicable from the proton data to some extent.

ACKNOWLEDGMENT

The authors gratefully acknowledge Prof. A. Katase of Tohwa University and Dr. Y. Watanabe of Kyushu University for their useful discussions about this work.

REFERENCES

(1)PEARLSTEIN,S.,: Nucl.Sci. and Eng.,95, 116 (1987)

(2)SHIBATA,T.,-A., et al.: Nucl.Phys.,A408,525 (1983)

(3)CIERJACKS,S., et al.: Phys.Rev.C,36,1976 (1987)

(4)MEIER,M.,M., et al.: Nucl.Sci. and Eng.,102, 310 (1989)

(5)TERRELL,J.,: Phys.Rev.,113, 527 (1957)

(6)MEIER,M.,M., et al.: Rad.Eff.,92, 73 (1986)

(7)HOWE,S.,D., et al.: LANL-85-3360 (1985)

(8)MEIER,M.,M., et al.: LA-11656-MS (1989)

(9)TRABANDT,M., et al.: Phys.Rev.C,39, 452 (1989)

(10)KALEND,A.,M.,et al.:Phys.Rev.C,28,105 (1983)

(11)ARMSTRONG,T.,W.,et al.:Nucl.Sci. and Eng.,49, 82 (1972)

(12)CORDELL,K.,R., et al.:Nucl.Phys.A,352,485 (1981)

(13)WU,J.,R.,et al.:Phys.Rev.C,19,698 (1979)

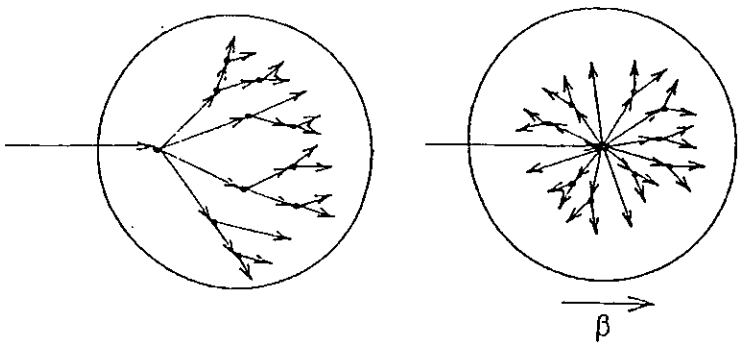

(a) moving source (MS) model

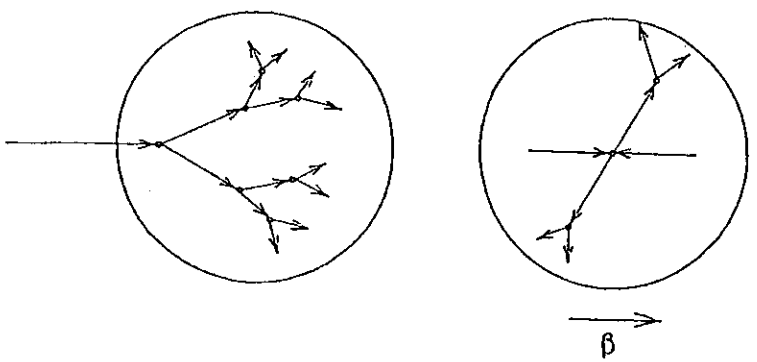

(b) doubly moving source(DMS) model

Fig.1 Illustrations of the moving source (MS) model (a), and the double moving source (DMS) model (b)

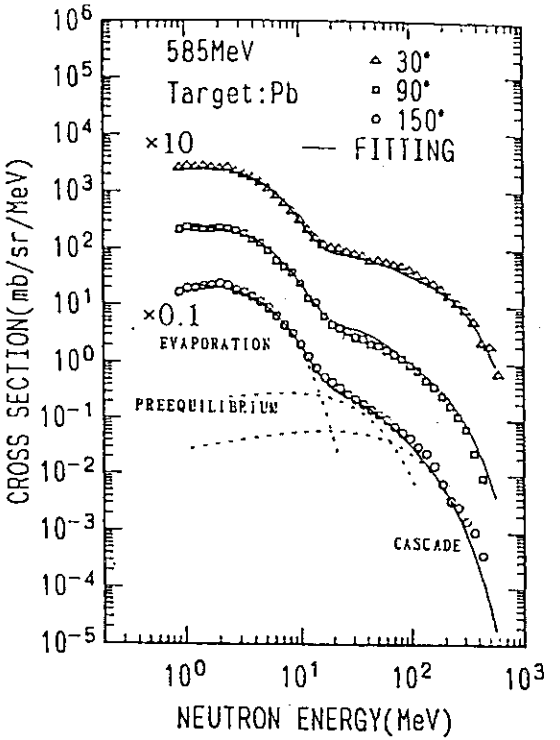

Fig. 2 Experimental neutron spectra and the results of parameter fits for 585 MeV proton incidence on lead. Marks show the experimental data[3]. The solid curves indicate the results of the parameter fits by the MS model. The dashed curves for the spectrum of 150 deg. express three components of cascade, preequilibrium and evaporation processes, respectively.

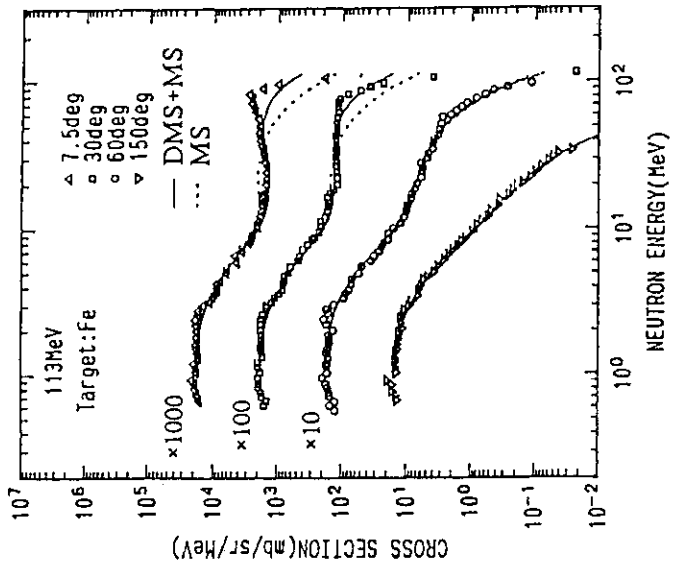

Fig. 3 Experimental neutron spectra and the results of parameter fits for 113 MeV proton incidence on iron. Marks show the experimental data[4]. The dashed curves indicate the results of the MS model, and the solid curves express that of the combination of the DMS and the MS models.

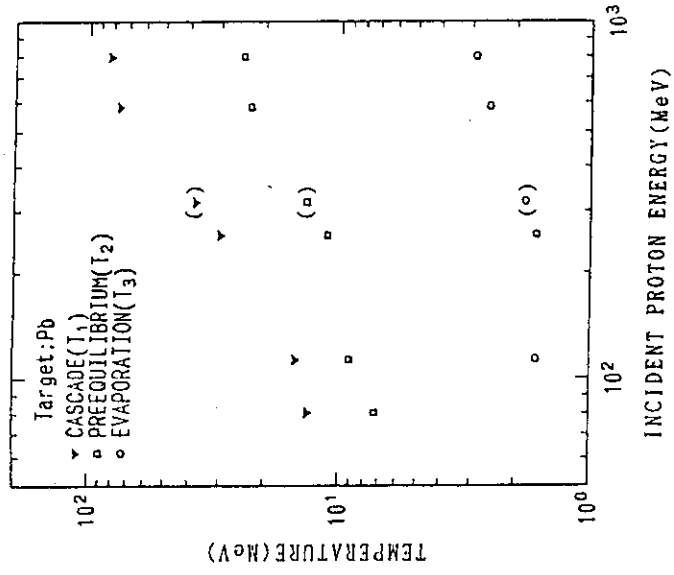

Fig. 4 Temperature parameter T for lead for the incident protons of 80.5 to 800 MeV.

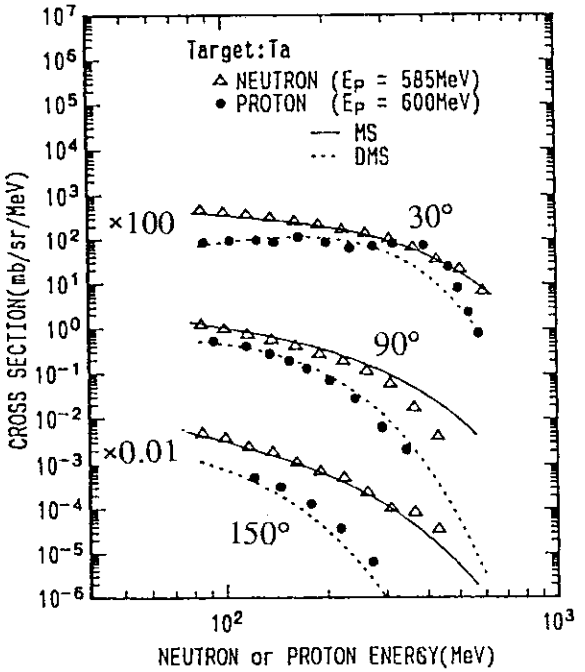

Fig. 5 Neutron and proton spectra for tantalum bombarded by protons of about 600 MeV. Triangular and circular marks show the experimental data for emitted neutrons[3] and protons[10], respectively. The solid curves indicate the results of the MS model for the neutron data, and the dashed curves show that of the DMS for the proton data.

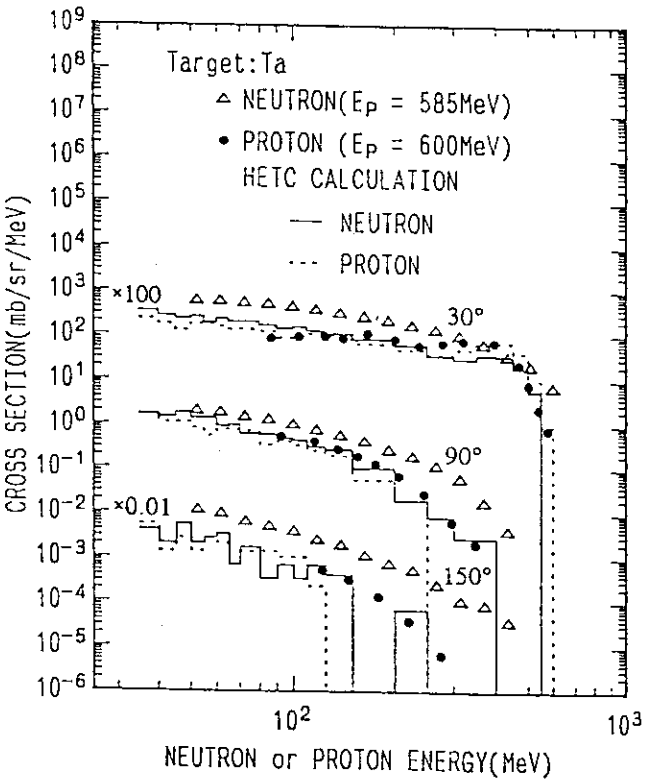

Fig. 6 Neutron and proton spectra by the HETC calculation for tantalum bombarded by protons of about 600 MeV. Triangular marks show the experimental data for emitted neutrons[3], while circular ones that of protons[10]. The solid and dashed lines indicate the calculation results of the HETC for neutrons and protons, respectively.

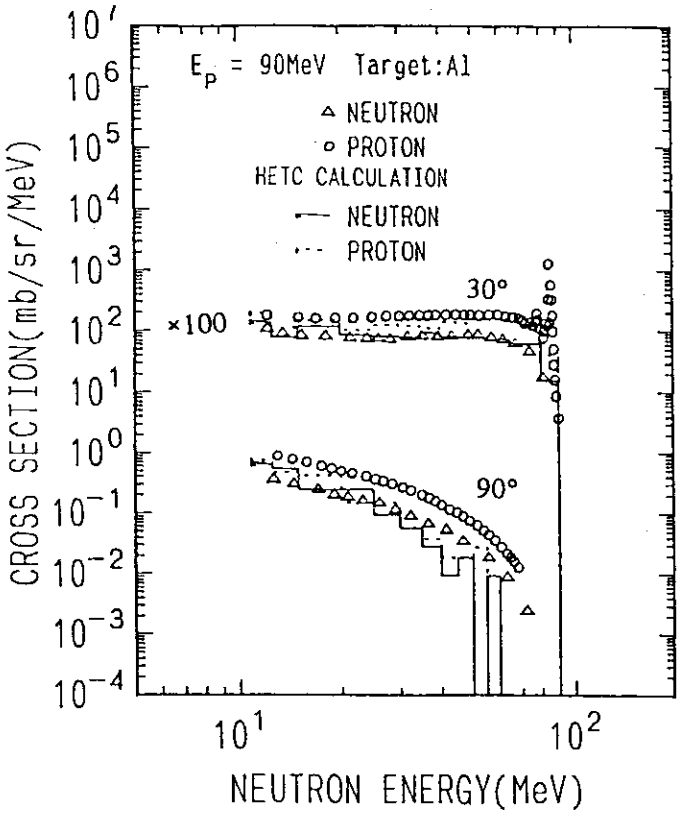

Fig. 7 Neutron and proton spectra for aluminum bombarded by protons of 90 MeV. Triangular marks show the experimental data for emitted neutrons[12], while circular ones that of protons[13]. The solid and dashed lines indicate the calculation results of the HETC for neutrons and protons, respectively.

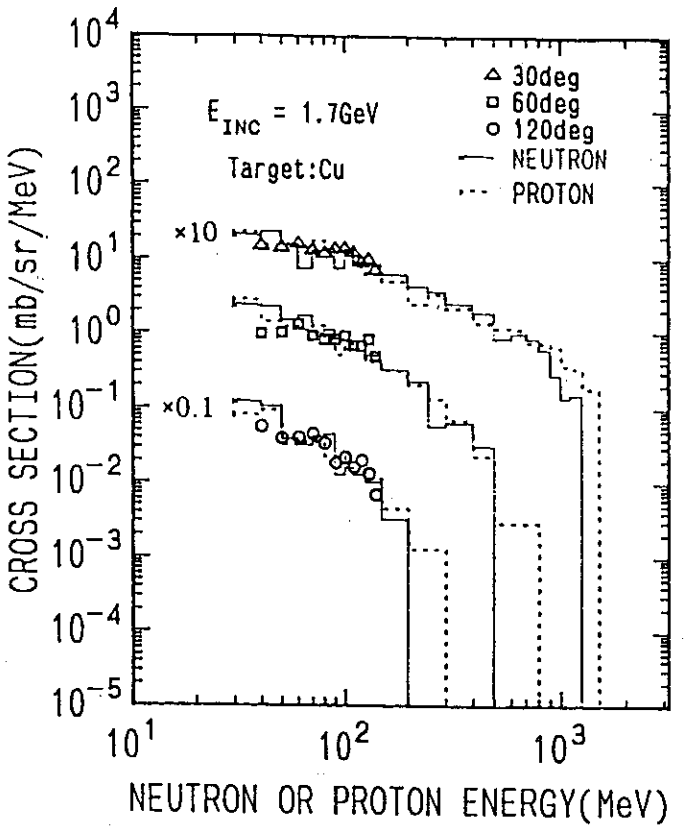

Fig. 8 Neutron and proton spectra for copper bombarded by protons of 1.7 GeV. Marks show the experimental data for emitted protons[2]. The solid and dashed lines indicate the calculation results of the HETC for neutrons and protons, respectively.

3.19 Estimation of Optical Model Parameters at Few-MeV Energy Region

T. Kawano, H. Tanaka, K. Kamitsubo, and Y. Kanda,

Department of Energy Conversion Engineering,
Kyushu University, Kasuga, Fukuoka 816, Japan

Abstract : Optical model parameters for ^{59}Co, ^{58}Ni, and ^{60}Ni have been estimated by statistical method based on the Bayes' theorem, and energy dependencies of the parameters have been investivated at few-MeV energy region. A successful reproduction of differential elastic scattering cross section and total cross section has been achieved by energy dependent potential.

The tendencies of estimated parameters are similar to those reported for the global parameters in high energy region, however, the parameters show large energy dependencies in low energy region.

1. Introduction

A statistical method which has been developed to estimate model parameters on the bases of the Bayes' theorem, is applied to estimate the optical model parameters (OMP). It founded on that the method is able to take account of correlations among parameters by setting prior parameters and their covariances, and that there are so many analyses of elastic scattering data that their results offer informations sufficient to infer prior parameters and their covariances.

Recently, accurate measurements of angular distribution for neutron elastic scattering have been performed. In these experiments, incident neutron energy intervals are narrow, and the large numbers of the data points are evenly distributed from forward to backward angles, so that they make it possible to estimate the OMP unambiguously. Accurate measurements have been also done for total cross sections, and calculation with the OMP derived by scattering data should also be consistent with them. Therefore, a quantitative treatment of both the elastic scattering and the total cross sections is necessary.

In this study, the spherical optical model (SOM) is adopted to reproduce the differential elastic scattering cross sections and the total cross sections of ^{59}Co, ^{58}Ni, and ^{60}Ni, and the OMP are estimated, and energy dependencies of the parameters are investigated.

2. Calculation

In order to use the total cross section as a data-base for estimation as well as

the differential elastic scattering cross section, experimental total cross sections are smoothed by a first order B-spline function[1]. Fluctuations are reduced by smoothing with 500 keV node intervals. Errors of the evaluated total cross sections are very small compared with the measured differential elastic scattering cross sections, and they are $\leq 0.5\%$. The experimental data of ^{59}Co comprise the measurements by Carlson and Barschall[2], Cierjacks *et al.*[3], Foster and Glasgow[4], Guenther *et al.*[5], and Harvey[6], and the experimental data of ^{60}Ni are the measurements by Boschung *et al.*[7], Stoler *et al.*[8], Smith *et al.*[9], and Fedorov *et al.*[10]. The available experimental data of ^{58}Ni are scarce, however it may be able to use the total cross section of ^{60}Ni in place of ^{58}Ni, because difference between them is expected to be small. The uncertainties for ^{58}Ni are estimated to 5% from the difference of the calculated total cross sections with the OMP of ^{58,60}Ni in Ref. 11.

The optical-statistical model calculation is carried out using the computer program ELIESE-3[12] with a conventional spherical optical potential that consists of a Woods-Saxon real part, a Woods-Saxon-derivative imaginary part, and a Thomas spin-orbit term. Below ≈3.5 MeV, compound elastic scattering cross sections are calculated with the Hauser-Feshbach-Moldauer theory. It is assumed that distribution of level width is equal to Porter-Thomas distribution. Above ≈3.5 MeV, compound nuclear process from a continuum region is significant, and the cross sections are affected by formulation of a level density and its parameters. Then the compound nuclear process is calculated with the Hauser-Feshbach theory with the level density formula by Gilbert and Cameron[13], and the cross sections are slightly adjusted so that the calculated values do not exceed the experimental ones at the minima of angular distributions. Above ≈6.5 MeV, the compound elastic scattering is negligible.

Sensitivity matrix $C = \left\{ c_{ij} | c_{ij} = \partial \left(\frac{d\sigma}{d\Omega} \right)_{\theta=\theta_i} / \partial x_j \right\}$ is requisite for the statistical method. This matrix can be replaced by the sensitivity of Legendre expansion coefficients (B_ℓ), as follows:

$$C = \left\{ c_{ij} \middle| c_{ij} = \sum_{\ell=0}^{\ell_{max}} \left(\frac{\partial B_\ell}{\partial x_j} \right) P_\ell(\cos\theta_i), \quad 1 \leq i \leq n, \quad 1 \leq j \leq m \right\}, \tag{1}$$

where n is number of angles, m is number of parameters, and $\mathbf{x} = \{x_j\}$ is a parameter vector composed of six OMPs (V, r_v, a_v, W, r_w, and a_w).

When prior OMP ($\mathbf{x}_0$) is obtained at a certain neutron energy, a posterior parameter ($\mathbf{x}_1$) for experimental data vector ($\mathbf{y}$) is given by following equations:

$$\mathbf{x}_1 = \mathbf{x}_0 + XC^{\mathrm{T}} \left(CXC^{\mathrm{T}} + R \right)^{-1} \left(\mathbf{y} - \mathbf{f}(\mathbf{x}_0) \right) \tag{2}$$

$$P = X - XC^{\mathrm{T}} \left(CXC^{\mathrm{T}} + R \right)^{-1} CX \tag{3}$$

where X, P, and R are covariance matrices for the vector $\mathbf{x}_0$, $\mathbf{x}_1$, and $\mathbf{y}$, respectively. The experimental data vector is composed of the measured differential elastic scattering cross sections and the evaluated total cross section at the same neutron energy. The matrix R contains both the experimental errors of the elastic scattering data and the evaluated error of the total cross section. The covariance matrix X are prepared on the assumption that the uncertainties of the prior parameters are 5%, and that correlation among them are zero.

The sources of differential elastic scattering cross section data are in Refs. 7, 11 and 14 to 19. Once the posterior parameters are obtained according to Eq.(2), they are used as the prior ones at the next energy, because variations of the OMP with energy are expected to be small. Here the prior covariance matrix is prepared in the above manner again, and the posterior covariance P obtained at the preceding calculation is ignored.

3. Results and Discussion

The estimated real and imaginary potential parameters are expressed as volume integrals par nucleon ;

$$J_{v,w} = \frac{4\pi}{A} \int_0^\infty \left\{V(r),\, W(r)\right\} r^2\, dr, \tag{4}$$

and J_v, J_w for ^{59}Co are shown in Figs. 1-(a) and (b). In these figures, the dotted lines represent the volume integrals deduced by Smith *et al.*[14] who considered mainly 4.5–10 MeV data. It is indicated in Fig. 1 that energy dependence of J_v is different below and above ≈4.0 MeV. At ≈4.0 MeV, J_v shows discontinuous drop. This energy dependence is not expected for the OMP, and this may be attributed to both experimental data and calculation of compound process. This anomalous energy dependence is shown in the potential depth and the radius parameter in Figs. 2–4. As seen in Fig. 2-(a) and Fig. 3, the tendency of V is opposite to r_v, because they are strongly anti-correlated. Above 5 MeV, the potential depth decrease with energy ($dV/dE \simeq -0.3 \sim -0.5$), and this value is slightly larger than that reported for the global OMPs. If the radius parameter is fixed at a certain value, the potential depth may show the same energy dependence with the global OMPs.

The volume integral of the imaginary potential J_w decrease with energy, as shown in Fig. 1-(b). As the incident neutron energy increases, more channels open and J_w would be expected to increase with energy at low energies. The estimated imaginary potential strength shows opposite tendency, and this energy dependence may be attributed to the vibrational character of ^{59}Co, as suggested by Smith *et al.*[14]. And relative small r_w in the 5–10 MeV region is also due to the vibrational character of this nucleus.

Figure 4 indicates that the diffuseness parameters a_v and a_w are approximately constant at higher energies, and they are not at low energies. As indicated by the dotted line in Fig. 6, a_v derived by Smith *et al.* is constant, because they extrapolated a_v obtained from 4.5–10 MeV data to the low energy region.

As shown in Figs. 3 and 4, the geometric parameters, a, r, change in behavior at ≈4.0 MeV, and this transition energy is different from the energy given by Smith (≈7.5 MeV). In this study, the six OMPs are estimated simultaneously, and the low energy data, $E_n \leq 4.0$ MeV are included explicitly. In addition, the total cross sections that strongly depends on a radius of nucleus, are included as the estimation data-base, and calculated total cross sections by the estimated OMPs are consistent with the evaluated ones, as shown in Fig. 5.

The volume integrals for ^{58}Ni and ^{60}Ni are displayed in Figs. 6 and 7, respectively, and differencies between them are small. It is known that ^{58}Ni and ^{60}Ni can be described by a vibrational model, direct inelastic scattering cross section for the low excited state is significant. This direct interaction is usually included implicitly in the imaginary potential at the spherical OM analysis. As mentioned above, the vibrational character brings unusual energy dependence of the OMPs, especially r_w which is estimated to relative small values compared with r_v.

At high energy region, volume integrals J_v for ^{58,60}Ni are larger systematically than the values derived by Guss *et al.*[11]. As the volume integral is approximately proportional to r_v^3, J_v is sensitive to r_v. In our study, radius parameter r_v is approximately constant in this energy region, and they are 1.2∼1.25 fm, while $r_v = 1.165$ fm[20] is employed in Ref. 11. Therefore the difference of J_v is attributed to the radius parameter, and it is difficult to avoid Vr^n ambiguity.

4. Conclusion

Spherical optical model parameters for ^{59}Co, ^{58}Ni, and ^{60}Ni were estimated by the statistical method developed by authors, and energy dependencies of the parameters were investigated at few-MeV energy region. Differential elastic scattering cross sections and total cross sections provided the data-base for parameter estimation.

The energy dependence of the volume integral, J_v for ^{59}Co is different below and above ≈4.0 MeV. The geometric parameters $a_{v,w}$, $r_{v,w}$ show energy depedency at low energy, and they are approximately constant and approarch to the values of global analysis at high energy. The imaginary radius r_w tends to be small compared with r_v.

References

[1] Y.Uenohara, M.Tsukamoto, and Y.Kanda :
J. Nucl. Sci. and technol. **20**, 787(1983).

[2] A.D.Carlson and H.H.Barschall : Phys. Rev., **158**, 1142(1967).

[3] S.Cierjacks, *et al.* : KFK-1000, 2(1969).

[4] D.G.Foster and D.W.Glasgow : Phys. Rev., **C3**, 576(1971).

[5] P.T.Guenther, P.A.Moldauer, A.B.Smith, and J.F.Whalen :
Nucl. Sci. Eng., **54**, 273(1974).

[6] J.A.Harvey : EXFOR12988 Data from NEA Data Bank, OECD(1986).

[7] P.Boschung, J.T.Lindow, and E.F.Shrader : Nucl. Phys., **A161**, 593(1971).

[8] P.Stoler, J.Clement, C.Goulding, and R.Fairchild : Proc. 3rd Conf.
on Neutron Cross-Sections and Technology, 311(Knoxvill,1971).

[9] A.B.Smith, P.T.Guenther, D.L.Smith, and J.F.Whalen :
Nucl. Sci. Eng., **72**, 293(1979).

[10] M.B.Fedorov, V.D.Ovdienko, G.A.Smetanin, T.I.Jakovenko :
Proc. 5th All Union Conf. on Neutron Physics, 1, 309(Kiev,1980).

[11] P.P.Guss, *et al.* : Nucl. Phys., **A438**, 187(1985).

[12] S.Igarasi : JAERI-1224(1972).

[13] A.Gilbert and A.C.W.Cameron : Can. J. Phys., **43**, 1446 (1965).

[14] A.B.Smith, P.T.Guenther, and R.D.Lawson : Nucl. Phys., **A483**, 50(1988).

[15] W.E.Kinney, and F.G.Perey : ORNL-4549(1970).

[16] J.C.Ferrer, J.D.Carlson, and J.Rapaport : Nucl. Phys., **A275**, 325(1977).

[17] C.Budtz-Jørgensen, P.T.Guenther, A.B.Smith, and J.F.Whalen :
Z. Phys., **A306**, 265(1982).

[18] W.E.Kinney, and F.G.Perey : ORNL-4807(1974).

[19] F.G.Perey, C.O.LeRigoleur, and W.E.Kinney : ORNL-4523(1970).

[20] J.P.Delaroche, *et al.* : Nucl. Phys., **A390**, 541(1982).

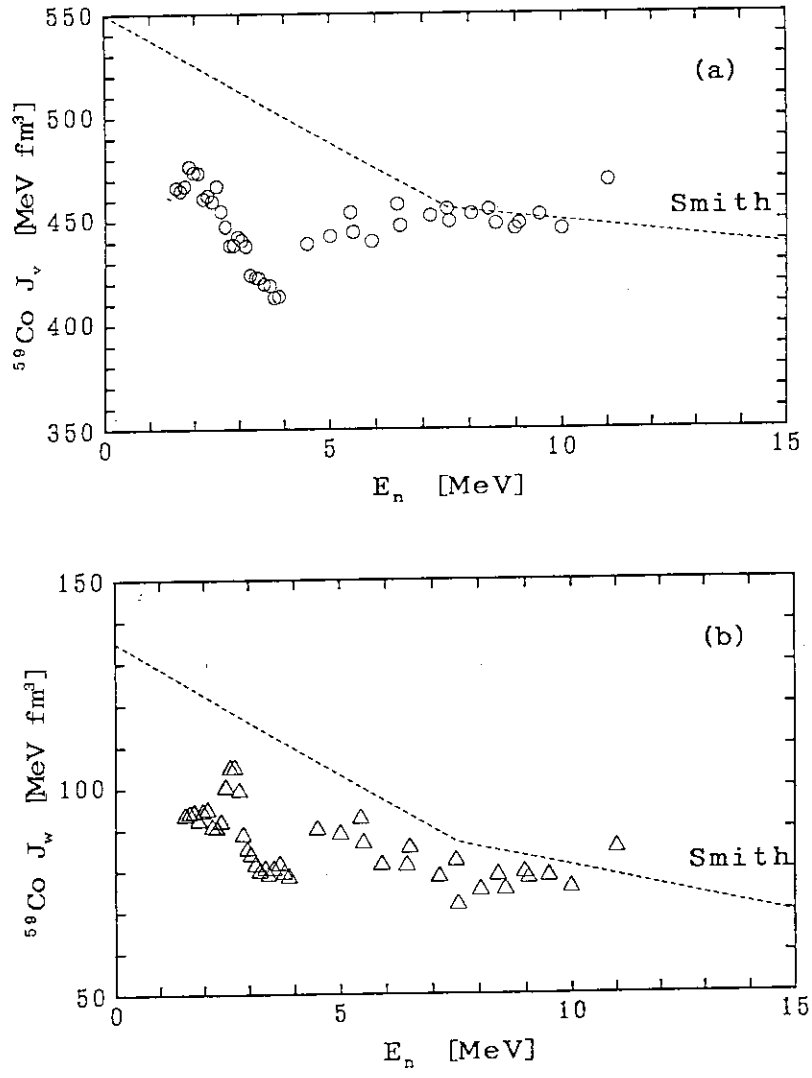

Fig. 1 Volume integrals as a function of incident neutron energy for n-^{59}Co. The dotted line is derived by Smith et al.[14]
(a): real potential, J_V
(b): imaginary potential, J_W

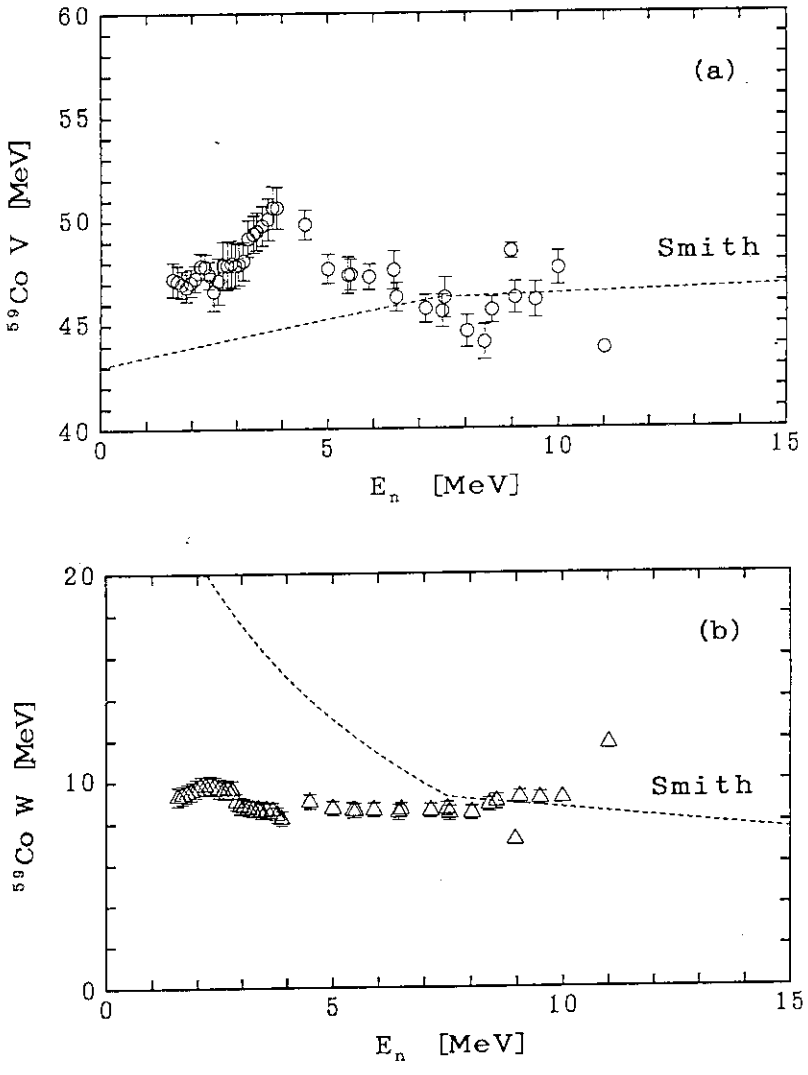

Fig. 2 Estimated potential depth as a function of incident neutron energy for n-^{59}Co. The dotted line is derived by Smith et al.[14]
(a): real potential, V
(b): imaginary potential, W

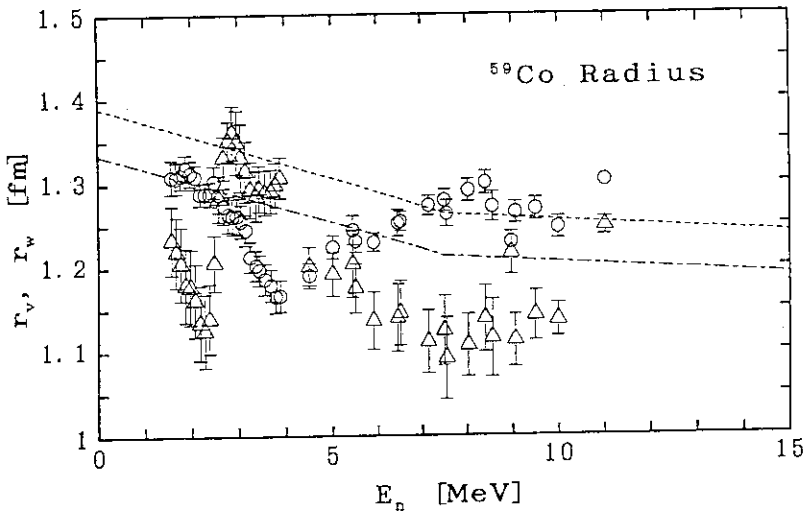

Fig. 3 Estimated radius parameters, r_V(○), r_W(△), as functions of incident neutron energy for n-^{59}Co. The dotted line is the real radius parameter, and the dot-dashed line is the imaginary radius, derived by Smith et al.[14]

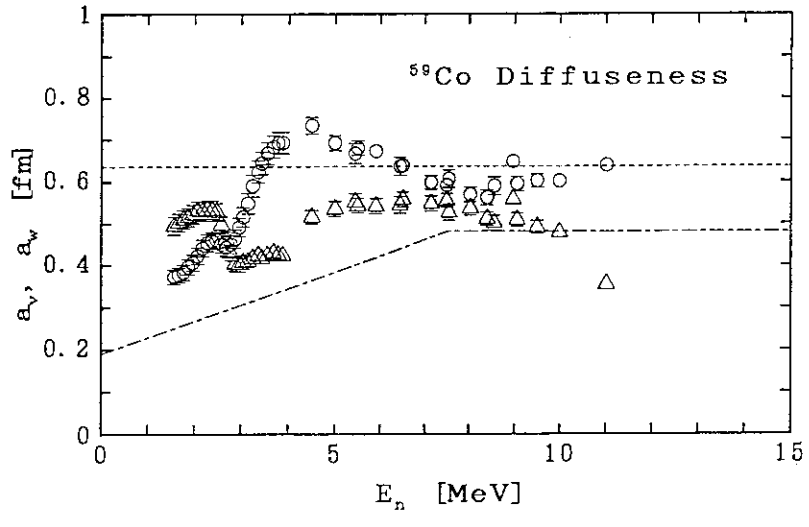

Fig. 4 Estimated diffuseness parameters, a_V(○), a_W(△), as functions of incident neutron energy for n-^{59}Co. The dotted line is the real diffuseness parameter, and the dot-dashed line is the imaginary diffuseness, derived by Smith et al.[14]

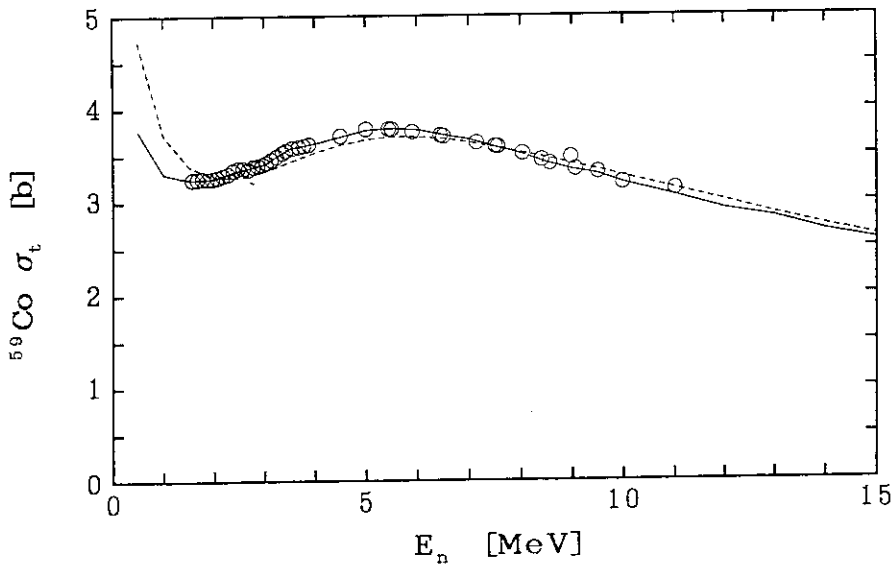

Fig. 5 Comparison of the total cross sections. The symbols are calculated using the estimated parameters. The solid line is evaluated data by the spline function. The dotted line is calculated using the parameters derived by Smith et al.[14]

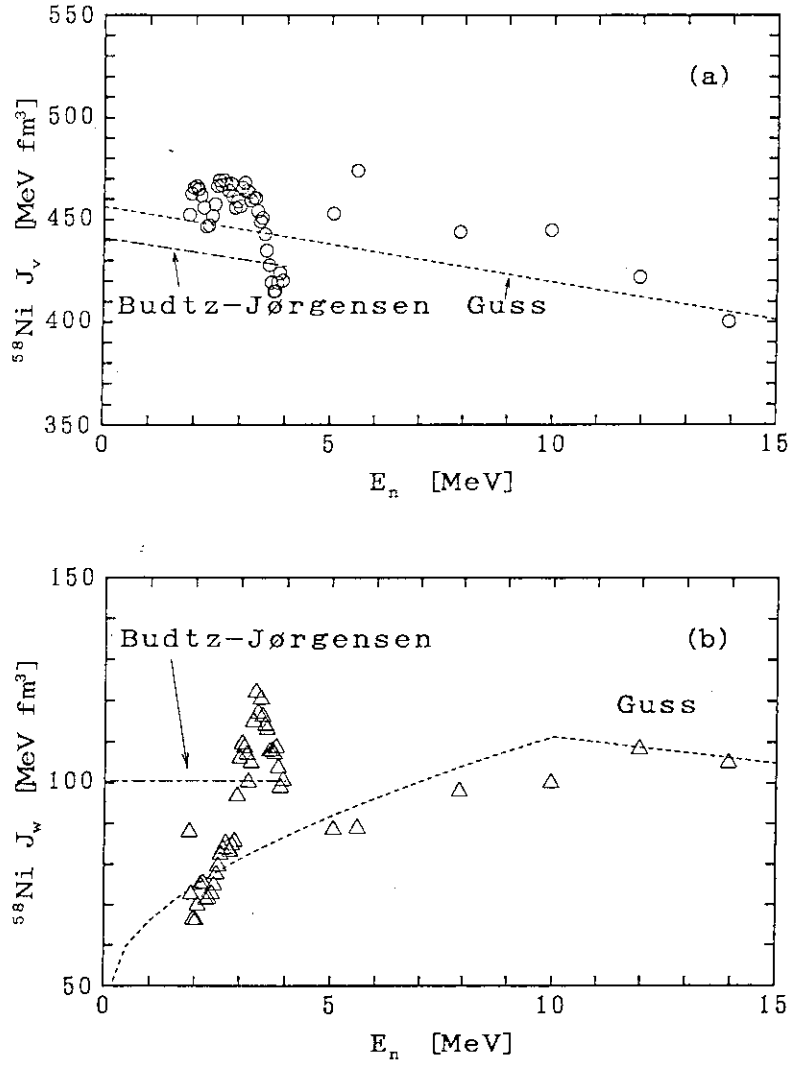

Fig. 6 Volume integrals as a function of incident neutron energy for n-^{58}Ni. The dot-dahsed line is derived by Bodtz-Jørgensen, et al.[17] The dotted line is derived by Guss, et al.[11]
(a): real potential, J_V
(b): imaginary potential, J_W

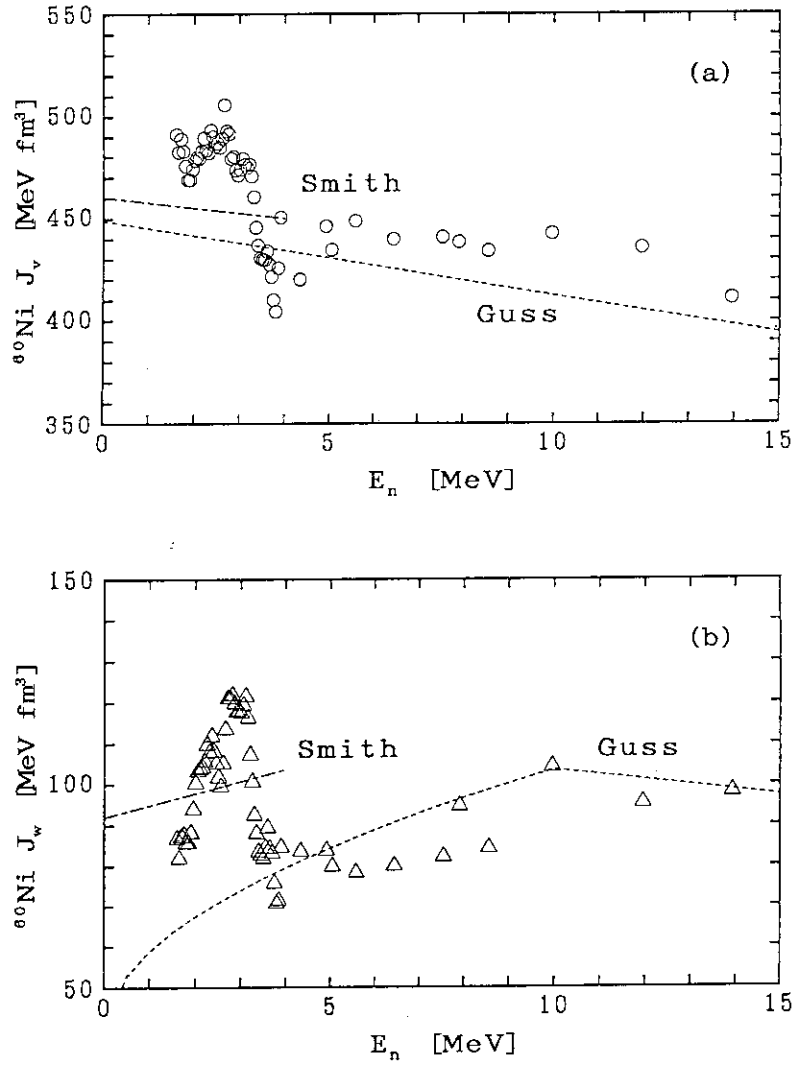

Fig. 7 Volume integrals as a function of incident neutron energy for n-^{60}Ni. The dot-dashed line is derived by Smith, et al.[9] The dotted line is derived by Guss, et al.[11]
(a): real potential, J_V
(b): imaginary potential, J_W

3.20 Object Model for the Evaluation of Nuclear Data in the Framework of Object Oriented Programming

S. Iwasaki and K. Sugiyama

Department of Nuclear Engineering
Tohoku University
Sendai 980, Japan

In order to construct an assisting system for the nuclear data evaluation process, a new framework of the knowledge base system have been proposed using the concept of the object-oriented programming(OOP), in which the knowledge can be modeled by the structure object and class, inheritance process, packaging of the data and method and message sending mechanism. The OOP based assisting system has high capability of modeling, and high maintenability and extensibility due to the modularity of the objects.

Nuclear data evaluation process has been modeled by the collection of the objects and interaction between these objects. Main objects and transaction classes have been described.

1. Introduction

Up to date, the concept of the assisting system for the nuclear data evaluation has not been established because there has been few discussions on this issues and very few studies on such system /1/ have been carried out.

In the evaluation process, the evaluator may encounter following questions: what is the necessary information of the given evaluation, how to get the information from where, what order to proceed tasks of the evaluation, how to determine, how to judge, and how to choose, etc. However, it is impossible to make such a system to cover all kinds of needs of evaluators because the evaluation procedures may varied from nucleus to nucleus, from evaluator to evaluator, dependent on various boundary conditions, and need very vast knowledge /2/.

There are two kinds of knowledge which play important role in the evaluation; the first type is a kind of the creative activity of human, i.e., idea, finding out, and innovation which belong to the future of the evaluator himself; and the other one is so called "heuristics" which are based on the experience of the evaluator, or facts and data which are past, published or presented (public). It is very difficult to deal with the former type knowledge at present, but there is a possibility of the representation of the latter type knowledge like as the knowledge engineering works have been done in the construction of expert systems in several domains.

But, if we stress only the later knowledge for the system, it becomes a sort of substitute system of the evaluators, or of automated evaluation system. These are often stereotype systems

which are lack of flexibility and may not be accepted by the evaluators.

Thus, the system should, on one hand, assist the basic, common way and routine like tasks of the evaluation processes which are based on the latter kind of knowledge, and should, on the other hand, be open and easy for users to customize, to revise it and to implement their new knowledge or methods into it by themselves.

In the present study, we newly propose a framework of the assisting system based on the object-oriented model(OOM)/programming (OOP)/3/ environment which has received much attention in recent years in many programming domains. It can be expected that the new framework has higher capability of the integration of the previous procedural programming resources, new type of knowledge bases and data bases.

In the following sections, general concept of the OOP and the environment used in the present study are described (sec.2), and a brief description of the object model of the nuclear data evaluation (sec.3) is given.

2. Concept of OOP and its Environment

2.1 OOP by NEXPERT OBJECT: General

Among several expert system shells of the secondary generation in which the representation of the frame/object and rule is supported, we have chosen NEXPERT OBJECT/4/ because of its several distinctive features besides those of the extended object-oriented concept discussed later; easily accessible rule- and object editors through which we can easily compile our concept and domain knowledge into the system; network representation of the compiled knowledge (rules and objects) to developer in a high level graphical technique; interfaces with the conventional procedural languages and several standard data base management systems.

As usual OOP, an object in NEXPERT OBJECT/5/ is an instance or a prototype, a structured description of an item corresponding to a precise reality. Objects are created either by using the editor, or directly from the incremental compilation of the rules in which they are used. An object can be created at any time, and is substantially incrementally compiled. Furthermore, at runtime, objects can be dynamically created/deleted by the rules (Create/DeleteObject operator in the rule/ method), or existing objects can be connected to other objects or classes by being modified throughout the inference(the same operator).

2.2 Object, Class and Inheritance

An object has a name, and belongs to one or several classes. It has a set of slots or properties to describe its qualities in symbolic or numerical terms. It may also have subobjects which constitute its components. For any given object, its class is a set of such objects, or a generalization, while the object to which it belongs (as a subobject) is closer to a construction with which it shares few properties.

The hierarchical relations between objects allow one to pass properties and their values from one object (parent) to another

(child) or vice versa (inheritance). Hence, a considerable economy of representation and declaration is made. Moreover, NEXPERT OBJECT supports multiple inheritance, which means that an object can have two or more parents. Objects can also benefit from class inheritance. This inheritancy is not only a mechanism for economy, but accounts for the overall reasoning power.

2.3 Methods

Procedures can be attached to the meta-slots of each property slot, 'Order of Sources' type(actuated when the slot value is required) and 'If Change' type (actuated when the slot value change) procedures, are called method. The methods are also inheritable and thus can be described at higher levels of the hierarchy.

The methods are various kinds of processing like as follows: *initial value= fixed value, *default value = taken if other methods fail to get value, *activation of a set of rules = (rule based method) if type of the property value is boolean (e.g., yes/no true/false), the property can be a hypothesis of rules; inheritance from parent objects, *retrieval from data base, *execution of an external routine= run an executable program, *question to users, *create object, *inheritance method,etc.

If all methods attached to a given property fail to get value, then the system automatically ask to user with an explanation window (option). Therefore the user can input the value determined by himself.

3. Object Model for Nuclear Data Evaluation

Using above described features, real domain world can be modeled and represented by the collection of many classes and objects which are for the realistic entities of the world and for the transactions of the processes in the world. Interaction mechanism toward the problem solving of the domain world can be described by the rules and message passing which evoke the method of objects.

3.1 Outline of the Data Evaluation Process

An orthodox procedure of the evaluation/2/ can be divided into following main processes as shown in Fig. 1.

(1) Processes on the nuclear data status and needs: first of all, the evaluator acquires various information relevant to the target element cross sections, information on the application areas and especially what cross sections are most important; listing up reactions and cross sections which should be considered in the evaluation; weighting of the cross section/reactions with respect to the application and model calculation; then, setting a goal of the evaluation, i.e., setting of bands of uncertainties of the respective cross section.

(2)Processes on the basic nuclear parameters: next task would be collection of the basic nuclear parameters related to the target nucleus and neighboring nuclei.

(3)Processes on the experimental data base: survey and retrieval of the experimental cross section data; rejection of

evidently unreliable data and select one (in some cases, multiple) reliable cross section set among the retrieved data; providing a basic experimental vector data for the comparison of the model calculation.

(4)Processes for the nuclear model codes: survey of development of the nuclear models and codes relevant to the evaluation in the target mass regions; understanding of the models and codes and their usage.

(5)Processes on the nuclear model parameters: survey of the methods or theories to estimate the model parameter values; survey of the previously determined or used parameter sets in order to find an initial set of the present evaluation.

(6)Processes on the model calculation and comparison: execution of the codes in proper order; making a set of cross section data vector from the calculation corresponding to the experimental data vectors (see (3));

(7)Processes of the fitting; comparison of both cross sections especially for the important reactions (see (1)); adjustment of the model parameters which would be sensitive to the cross sections showing poor agreement; changing of the initial parameter set, if one could not success to reach a satisfactory level of agreement;iteration of the process.

(8)Processes on the judgment of the evaluation: judgment for the finish the model calculations considering the goal of the evaluation, and conversion of the evaluated cross section to the ENDF/B format; or continuing of the evaluation by changing the cross section set as mentioned in(3), in some cases they have to change the method or change the model/code in order to get the satisfactory or tolerable level of agreement dependent on the situation and cross sections.

(9)Processes on the reevaluations: if there are some unsatisfied results in the comparison with the integral test, reevaluation will be undertaken by modifying the cross section sets, adjustment procedures, model parameters, and model codes, and changing the method of the evaluation. This process is out of the present scope.

Above mentioned main processes can be decomposed into elementary component which will be modeled by the objects.

3.2 Object Network of the Nuclear Data Evaluation

Object network representation of the above data evaluation procedure is shown in Fig. 2. In this model, two categories of objects are considered; one represents realistic things in the world called 'data object' which has a collection of data and/or status: e.g., for the nuclide, reactions, cross sections, nuclear model parameters, goal of the evaluation, etc.;the other one represents various tasks in the evaluation procedures, called 'transaction object': e.g., the setting of the goal, the preparation of the experimental data vector, the selection and adjustment of the model parameters, etc, in which the expertise of the evaluation process can be involved.

Actually, the transaction object is a class which usually possess only one property slot and its method to determine the value, and inherits the method down to the property of the data object when the property value is required object linked to this

class.

In the following section some main objects and their behavior are described in more detail.

3.3 Nuclide Related Objects

Nuclide object possesses the basic nuclear properties, such as, atomic_symbol, atomic_number, mass_defect, ground_meta, half_life, or abundance, spin and parity etc, all of which values are retrieved from a newly developed data base. Schematic relation between the class and their instance: object is shown in Fig.3.

A permanent class "nuclide" exists as a generic object. According to the target element of the evaluation given by the evalutator, all target nucleus's data are retrieved from a data base and each nuclide object 'dynamic object' would be created under the nuclide class as the instances. All stable nuclei of the nucleus objects are connected to the target_element_object as the subobjects. All nuclei including the unstable nuclei of the target element are connected to the target element Z class. Related elements to the evaluation are also retrieved and created like the target element and connected to the Z_1_nuclide, Z_2_nuclide class, etc., respectively.

Target_selectclass: the evaluator pick up a certain objective nucleus of the evaluation among the stable ones of the target elements and connected to the nucleus to A_Z_nuclide and so on.

Particle objects: these are belong to the nuclear object and also retrieved and created. As the incident particle, only neutron is taken for a while but extension to other particle is very easy and as the outgoing particles, i.e., n,p,d,t,h and are taken into account.

Nuclear_level and gamma_decay objects are belong to each nuclide objects and are created when their data retrieved from the ENSDF files as the subobjects.

Level_select object would be the appropriate levels whose spin, parity and their gamma decay branching rations are established are selected, and from which the input file of level structure and decay data for the code will be made.

3.4 Reaction and Cross Section Related Objects

Reaction object consists of a residual nucleus object and a emitting particle or gamma ray object. All objects of possible reactions on the A_Z_nucleus can be created assuming the maximum incident projectile (neutron,in the present case) energy and Q-value of the reactions

All cross section classes described in the nomenclature of the ENDF/B-VI format are created under a root class, Cross_Section, i.e., cross sections corresponding to simple reactions, production cross sections, such as, those of the n, p, helium, etc., activation cross sections, etc., are provided. Instances of the reactions and cross sections are created and connected to above corresponding classes if the energy condition is satisfied.

The cross section objects own key property slots: cross_section_name which can be used as key word for the retrieve the cross section values from the EXFOR data base described in the following section; reaction_Q_ value; weights with respect to the application area and the model calculation.

3.5 Experimental Cross Section Data and Selection

Objects for all important experimental cross sections, i.e., CrossSection objects are created after the access of EXFOR, etc. according to the key words of the cross section objects(3-4) whose weight are high and which will be used to fit by the theoretical model calculation(3-6).

There are three task classes as follows. Cs_retrieve class: with respect to the important cross sections, all candidate experimental cross section values are retrieved and corresponding instances(objects) are created under the each cross section class. Cs_select class: select the cross section set among the all cross section data in this process. Cs_prepare class: prepare the experimental data vector from the selected cross section data for the comparison using a certain statistical procedures for each selected cross section object.

3.6 Model Code and Calculation Related Objects

ModelCalcCode objects would be prepared for the codes which have been used in the evaluation process for the JENDL-3 and developed after that. A object code_A is characterized by the properties, such as, code name, original, models used, authors, revisions, corrections, years etc., and are consisted of three subobjects (executable code itself, input files, and output file).

There are two task classes. Code_run class checks input files ready, output files, and other status; runs the code. Prep_calc_CS class prepares the calculated cross section vectors from the output file.

3.7 Model Parameter Related Objects

CodeA's input object is CodeA_ParaSet which is a collection of the following three type card image objects :CodeA_StrPara objects contain the title of the calculation, CodeA_IntPara correspond to the various flag data for the options of the calculations and many CodeA_FloatPara objects are for the usual model parameters. Usually each parameter object or group of the parameters are connected to the corresponding each class when the value is required. Schematics of these objects is shown in Fig.4.

Two transaction classes are prepared for the model parameters: e.g., for a parameter x, Parameter_x_retrieve and Parameter_x_select classes. In order to calculate the cross section and get good agreement with the experimental cross sections, suitable model parameters should be selected among the previously obtained parameter sets, or estimated the initial values from the those for the neighboring nuclei by certain systematics or some theoretical consideration. In the former case, all related model parameters are retrieved into the system from the data base/6/ and corresponding dynamic parameter candidate objects are created by the parameters retrieve class. If you have multiple candidate sets of parameter objects, a method of the parameter selection class will be evoked; registered methods are like as choosing the newest one, one of more sophisticated model, one whose model/code being matched or consistent with the present code or one giving good agreement comparing with the experimental data, etc.

3.8 Comparison and Parameter Adjustment Related Objects

When the both cross section data vector objects, i.e., those of the experimental and calculated cross section are prepared, the both objects are connected to CS_compare class. The compare class provide the method of the comparison of the cross section; calculation of the index for the presentation of agreement between them, e.g., -squares values, or pattern matching based on the fuzzy logic, etc.

If some calculated indexes are over the predetermined values (bands of the fitting goals), the adjustment of the model parameters will be take place. The knowledge on what parameter should be altered by what amount is based on the experience or he calculation of the sensitivity analysis for the selected parameters.

3.9 Goal of the Evaluation Related Objects

Goal object is consisted of the six subgoal objects corresponding to the terms described above with status and level properties. The degree of attainment (levels) of respective subgoals is evaluated by the methods in the transaction class: Goal_attainment. If the evaluated value of the levels becomes larger than a certain set value,the status of each object become true. There might be several methods to evaluate each attained value, e.g., cumulative point of their goals (subsubgoal) over a threshold value. Usually the top goal status result in true when the all subgoals are satisfied.

3.10 Session Mechanism

In the system, the user's suggestion of hypothesis of a basic rule:

"if goal_object.attained true then EvalGoalReached"

triggers a top level object, the 'Goal_object', to be active whose properties are all the boolean type and present attainment of the subgoals corresponding to the grouped processes described above sections; sub_sub_goals under the subgoals are related to the elementary processes; then,the objects activated other objects by sending messages during the session, and the session would end when the aimed level of the evaluation is attained.

Our target system is, however, not an automated one, but is open to the users as mentioned before. If one develop a good method to determine a certain property value, one can easily implement the method to the meta-slot of the property.

4. Summary

A basic framework of the assisting system for the nuclear data evaluation process have been developed using the advantage of the feature of the Object-oriented programming. High comprehensibility of the system can be achieved by using the structured object-oriented knowledge system which are very similar to the human comprehension of the domain world.

Furthermore, if a system user want to customize the system, necessary work will only be an addition of new method in a object or transaction object, or to implement a few objects into the system, or modify the method of the object. Therefore the extensibility of the system can be enhanced comparing with the conven-

tional evaluation system.

In addition to the above system, various data bases for the nuclear data, model parameters /6/, data from BNL-325, etc, are designed in the framework of the object-oriented data base concept.

References

1. Iwasaki,S. and Sugiyama,K. , "Technological Problem Development of an Advanced Support System for Nuclear Data Evaluation" JAERI-M 90-025, p233 (1990).
2. Iwasaki,S. et al., "Development of a Supporting System for Nuclear Data Evaluation in a 32-bit Workstation Using Artificial Intelligence Technology (SENDAI)",JAERI-M 89-026, p313(1989).
3. L. J. Pinson and R. S. Wiener, Ed., "Applications of Object-Oriented Programming", Addison-Wesley Pub. Co., (1990).
4. NEXPERT OBJECT by Neuron Data Inc. CA, U.S.A.
5. NEXPERT OBJECT MANUAL, Neuron Data Inc.(1988).
6. Nakagawa,T. and Nucl. Data Base WG.; private communication.

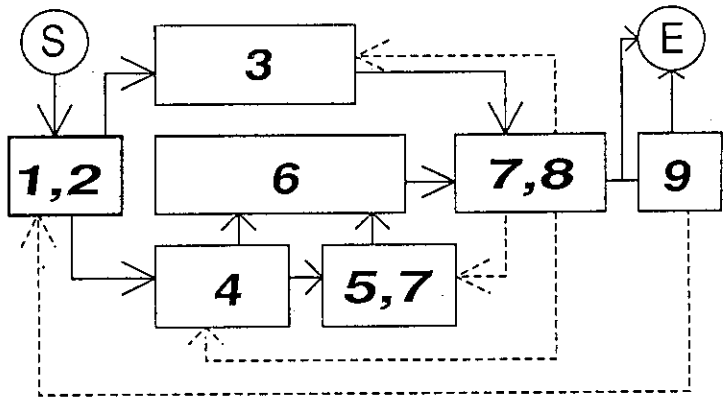

Fig. 1 Block diagram of the orthodox nuclear data evaluation procedure. Processes on (1) the nuclear data status and needs; (2) the basic nuclear parameters; (3) the experimental data base; (4) the nuclear model codes; (5,7) the nuclear model parameters; and adjustment; (6) the model calculation; (7,8) the comparison; and judgment of the evaluation; (9) the re-evaluations.

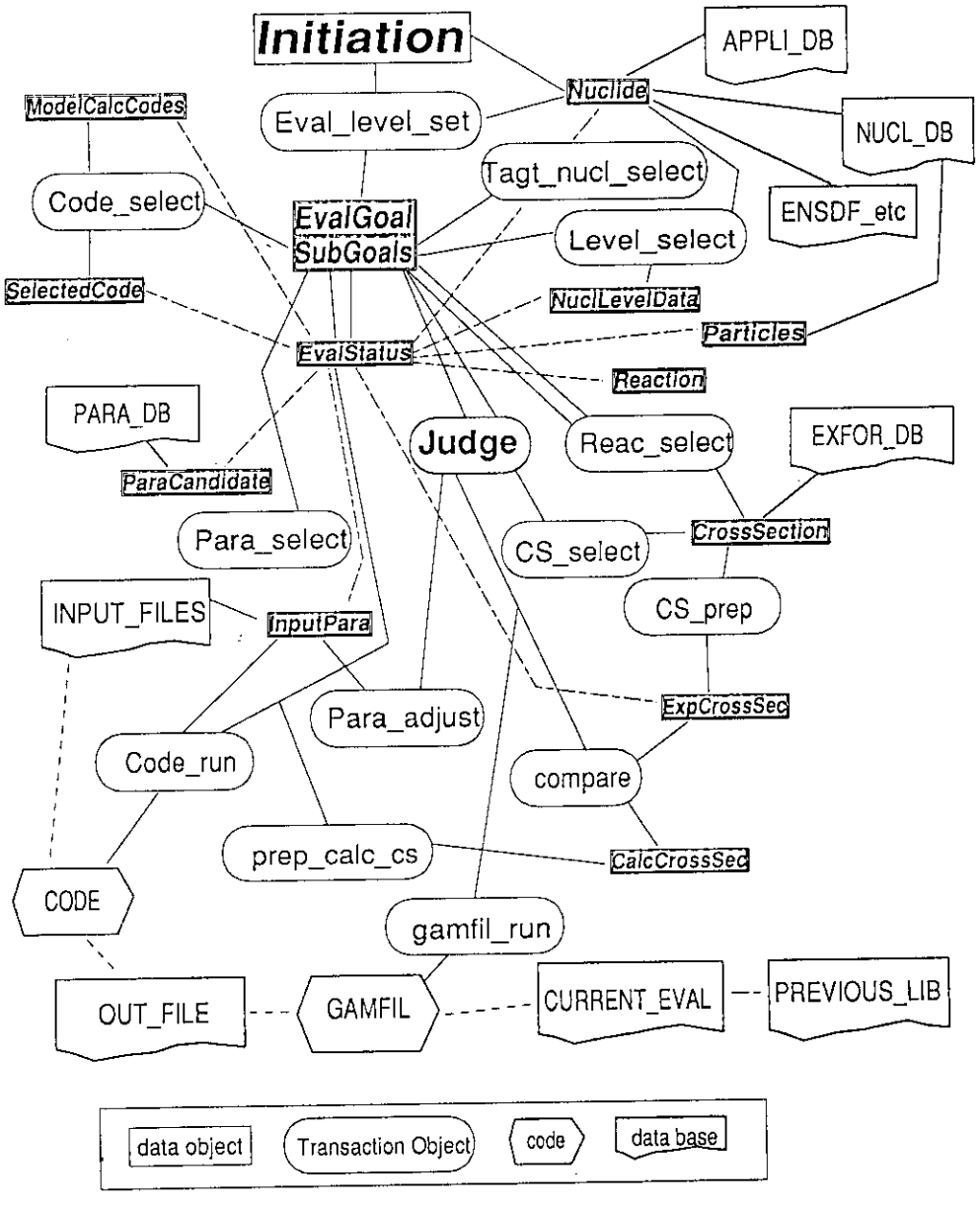

Fig. 2 Object network representation of the nuclear data evaluation procedure.

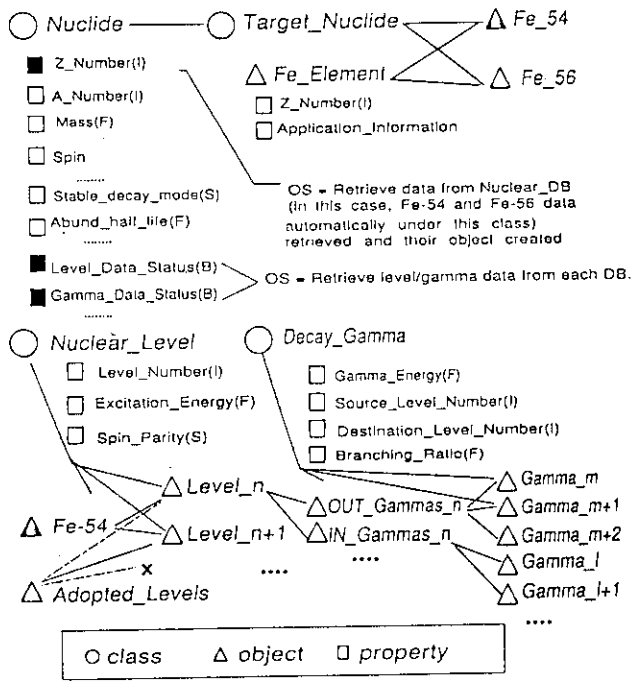

Fig. 3 Object model of nuclides.

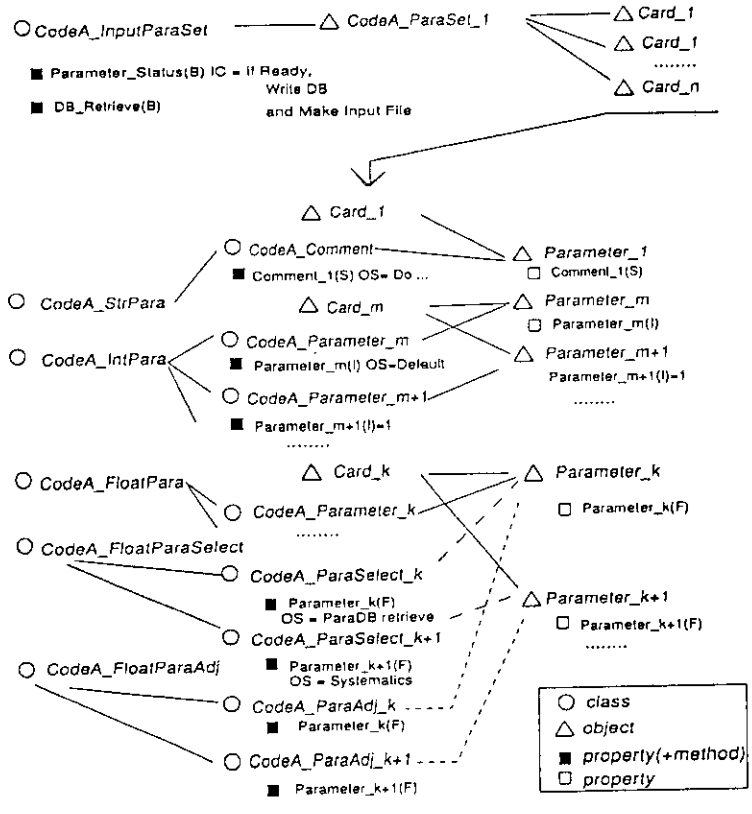

Fig. 4 Object model of the parameters for a CodeA.

3.21 Reevaluation of the DDX Data of ^{14}N in JENDL-3

Y. KANDA*, T. MURATA**, Y. NAKAJIMA*** and T. ASAMI****

* Department of Energy Conversion Engineering,
Kyushu University
** Nuclear Engineering Laboratory, Toshiba Corporation
*** Nuclear Data Center, Japan Atomic Energy Reserach Institute
**** Nuclear Energy Data Center

The neutron emission double differential cross-section data of ^{14}N in JENDL-3 were compared with the experimental ones, and the deffects were examined in deteil. The reevaluation of ^{14}N DDX data was made in refferring to the experimental data of Tohoku University and Ohsaka University. The reevaluated data for the neutron emission DDX at around 14 MeV-neutrons are in good agreement with the experimental ones generally, and the data were improved remarkably. The details on the reevaluation are discussed.

1. Introduction

It has been pointed out[1] that the neutron emission DDX(Double Differential Cross-section) data of ^{14}N in JENDL-3 deviate considerably in some parts from experimental data. The detailed comparison was made using both the experimental data of Tohoku University[2,3] and Ohsaka University[4], and several defects for the ^{14}N data of JENDL-3 (MAT=3071)[5] were found. The reevaluation for DDX data was made to remove these defects.

2. Problems on the ^{14}N DDX data of JENDL-3

The detailed comparison between the experimental and JENDL-3 data were performed using the figures plotted both the data superimposingly. The data plots were made with the computer codes of FAIR-DDX[6], DDXPLOT[7] and

SPLINT[8,9]. In this comparison, a part just below the elastic peak in the DDX data were excluded because of the ambiguity of the experimental ones.

As the results of the data comparison, we recognized that the inelastic scattering cross sections for some discrete levels and the continuum spectra for both the inelastic scattering and the other neutron emission reactions have some defects.

The main defects are summarized as follows:

1) The cross-section data for the 7th- and 8th-levels of the inelastic scattering (MF=3, MT=57 and 58) are higher considerably.

2) The neutron continuum spectrum data of the inealstic scattering are unreasonable in both its shape and magnitude (MF=3 and 5, MT=91).

3) The assumption of the isotropic angular distribution in the laboratory system is unsuitable for the neutrons from the reactions of (n,2n), (n,n'p), (n,n'd) and so on (MF=4, MT=16, 22, 28 and 32).

4) In the inelastic scattering, the 10th to 14th-level data (MF=3, MT=60 to 64) have no contributions from the direct processes.

3. Data reevaluation

The data reevaluation was made to remove these defects mainly in the following manner.

a) The cross-section data for the 7th- and 8th-levels of the inelastic scattering (MF=3, MT=57 and 58) were adjusted to fit to the experimental ones.

The integrated cross sections for the 7th- and 8th-levels were decreased uniformly by 70 and 80 %, respectively.

b) We decided that the neutron continuum of the inelastic scattering should be not handled in the present reevaluation in considering the difficulties of kinematic treatment for the continuum spectra. Hence, all the inealstic scattering data were given for discrete levels, including the direct contributions. Twenty-six discrete levels were added in the evaluation, and for the levels higher than 11.514 MeV the fictious levels spaced at a constant interval of 0.2 MeV were assumed to the excitation of 14.5 MeV (MT=78 to 90). The details of the reevaluation on the discrete-level data are shown in Table 1. For MT=65 to 77 the actual level data (excitation energy and spin-parity) and for MT=78 to 90 the fictious levels were given. For MT=78 to 90 the spin-parity value of +1 was

assumed.

For MT=51 to 77 the statistical components were calculated with a CASTHY code[10] and added to the direct components which were calculated with a DWUCK code[11]. For MT=78 to 90 only the direct components were taken. These data were adjusted to fit to the experimental ones of Tohoku university1,2).

c) The angular distributions for the continuum neutrons from the reactions of (n,2n), (n,n'p), (n,n'd) and so on were assumed to be isotropic in the center of mass system instead of in the laboratory system. In the data file the evaluated data were given as the equivalent ones in the laboratory system.

Except for these points to be revised, the ^{14}N data of JENDL-3 were adopted in remaining unchanged in this reevaluation, and the angular distributions of the inelastic scattering for the discrete levels were also left unchanged.

Figures 1, 2 and 3, as the examples, show the comparison of the reevaluated data with the JENDL-3 and the experimental ones induced by the 14.2-MeV neutrons, at the forward-(30 deg.), middle-(80 deg.) and backward-(150 deg.) angles, respectively. It is shown from these figures that the DDX data of the ^{14}N in JENDL-3 are improved remarkably on the whole though there are a few small deviation from the experimental data.

4. Discussion

The reevaluated data for the neutron emission DDX at around 14 MeV-neutrons are in good agreement with the experimental ones generally, and the data were improved remarkably. For further improvement, however, the angular distributiions of inelastic scattering would have to be examined carefully.

This work was done as a part of the activities of the JNDC working group on fusion nuclear data.

References

1) Maekawa, H. : JAERI-M 90-025 (1990) p.69.
2) Baba, M. : 85Santa Fe Vol.1, 223 (1985)
3) Baba, M. : Rad. Eff. 92, 223 (1986).

4) Takahashi, A. : OKTAV-A-87-01 (1987).

5) Shibata et al. : JAERI-1319 (1990) p.52.

6) Minami, K. and Yamano, N. : "FAIR-DDX:A Code for Production of Double Differential Cross Section Library", JAERI-M 84-022 (1984) (in Japanese).

7) Iguchi, T. and Yamano, N. : "DDXPLOT:A Program to Plot the Energy Angle Double Differential Cross Section", JAERI-M 84-033 (1984) (in Japanese).

8) Narita, T., Nakagawa, T., Kanemori, Y. and Yamakoshi, H. : "SPLINT:A Computer Code for Superimposed Plotting of the Experimental and the Evaluated Data", JAERI-M 5769 (1974) (in Japanese).

9) Nakagawa, T. : "SPINPUT:A Computer Code for Making Input Data of SPLINT ", JAERI-M 9499 (1981) (in Japanese).

10) Igarasi, S. : J. Nucl. Sci. Tech. 12, 67 (1975).

11) Kunz, P.D. : unpublished.

Table 1 Discrete-level data of ^{14}N for inelastic scattering

JENDL-3		Reevaluation				
MT	E_x (MeV)	MT	E_x (MeV)			
51	2.31	unchanged	79	12.0	1+	
52	3.95	unchanged	80	12.2	1+	
53	4.92	unchanged	81	12.4	1+	
54	5.11	unchanged	82	12.6	1+	
55	5.69	unchanged	83	12.8	1+	newly
56	5.83	unchanged	84	13.0	1+	evaluated
57	6.20	revised(MF=3)	85	13.2	1+	
58	6.44	revised(MF=3)	86	13.4	1+	
59	7.03	unchanged	87	13.6	1+	
60	7.97	revised(MF=3)	88	13.8	1+	
61	8.06	revised(MF=3)	89	14.0	1+	
62	8.49	revised(MF=3)	90	14.5	1+	
63	8.62	revised(MF=3)				
64	8.79	revised(MF=3)				
(91	8.91)	omitted				
		65	8.91	3-		
		66	8.96	5+		
		67	9.13	3+		
		68	9.17	2+		
		69	9.51	2-		
		70	10.23	1-		
		71	10.81	5+		
		72	11.05	3+		
		73	11.07	1+		
		74	11.24	3-		newly evaluated
		75	11.29	2-		
		76	11.357	1+		
		77	11.514	2+		
		78	11.8	1+		

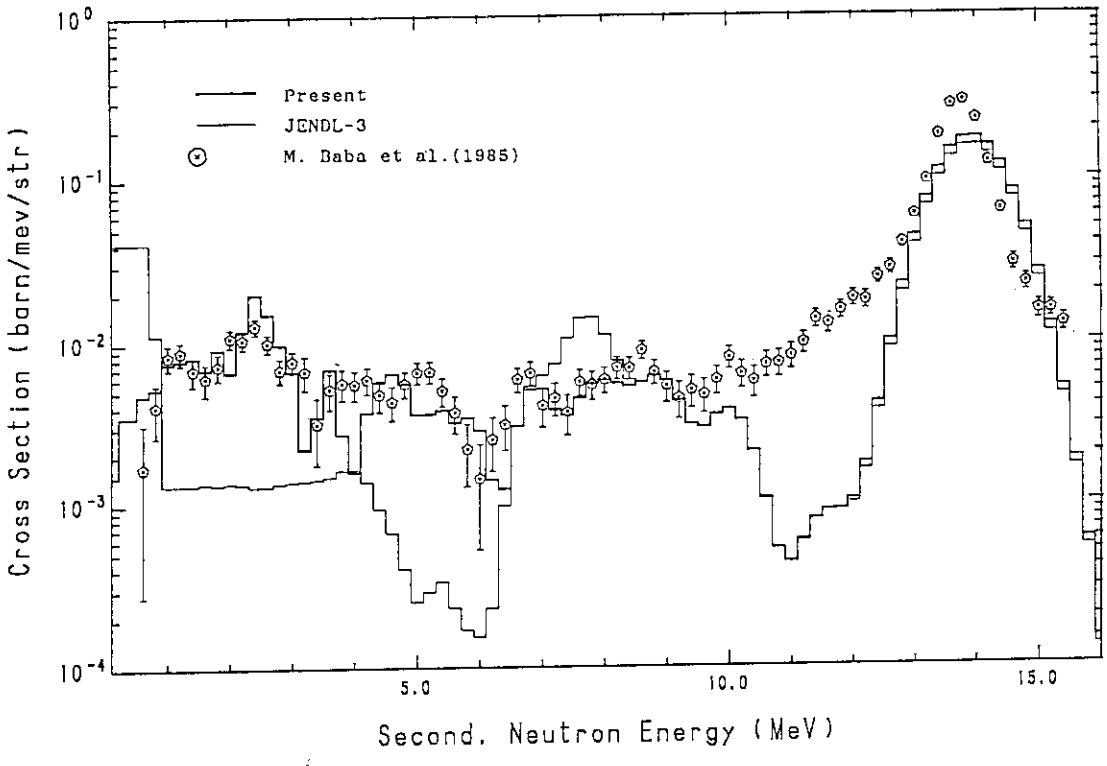

Fig. 1 The double differential cross sections of ^{14}N for the neutrons emitted at the laboratory angle of 30 deg., induced by the 14.2-MeV neutrons. The reevaluated data are compared with the JENDL-3 data and the experimental ones of Tohoku University[3].

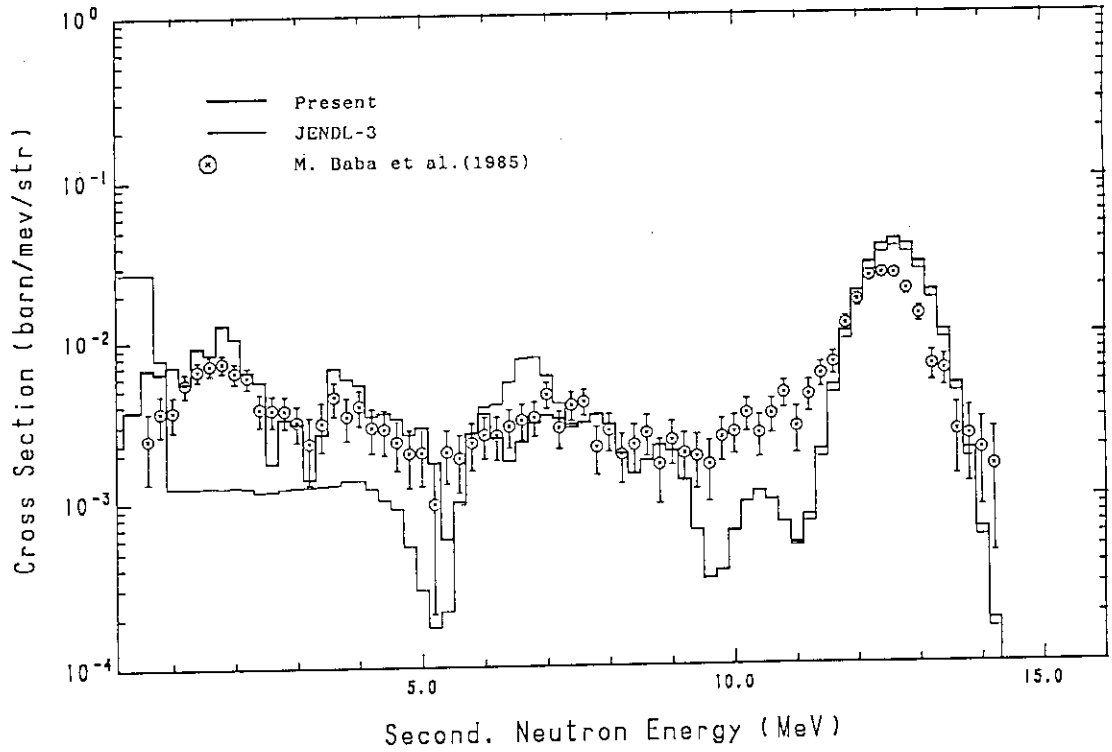

Fig. 2 The double differential cross sections of ^{14}N for the neutrons emitted at the laboratory angle of 80 deg., induced by the 14.2-MeV neutrons. The reevaluated data are compared with the JENDL-3 data and the experimental ones of Tohoku University[3].

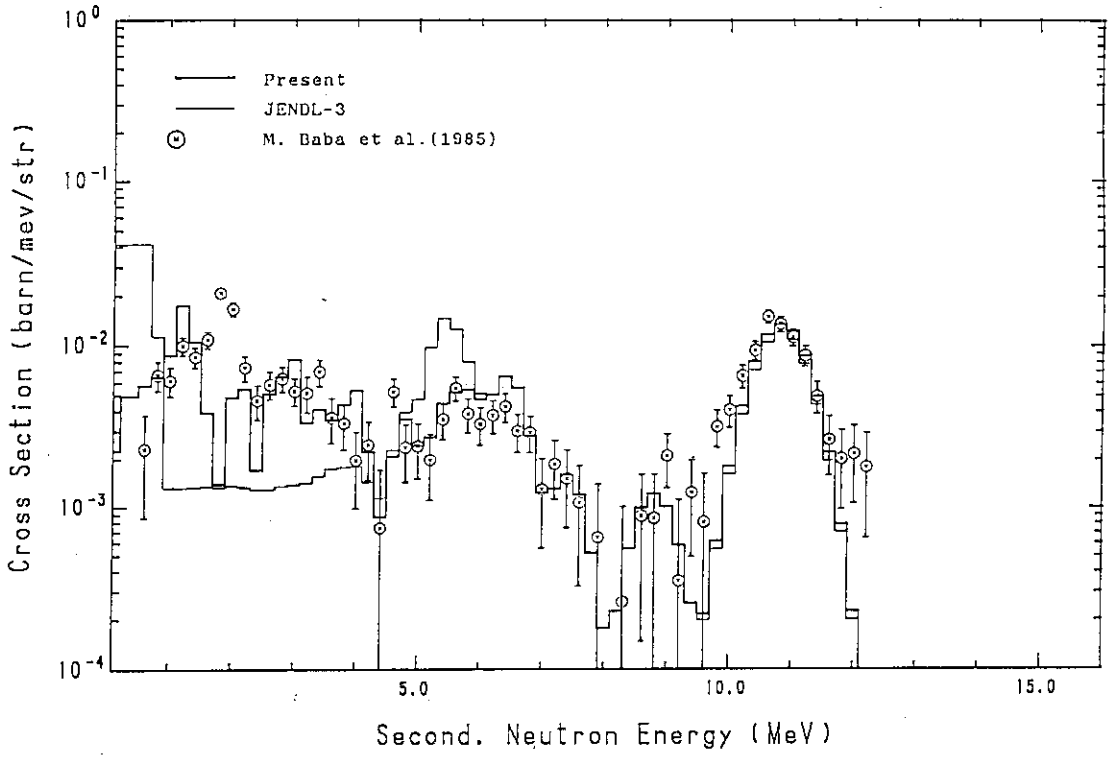

Fig. 3 The double differential cross sections of ^{14}N for the neutrons emitted at the laboratory angle of 150 deg., induced by the 14.2-MeV neutrons. The reevaluated data are compared with the JENDL-3 data and the experimental ones of Tohoku University[3].

3.22 An Improved Model for Fission Neutron Spectrum Calculation: Non-equitemperature Madland-Nix Model

Takaaki Ohsawa

Atomic Energy Research Institute, Kinki University
3-4-1 Kowakae, Higashi-osaka, 577 Japan

Abstract: An attempt was made to improve the Madland-Nix model for the calculation of the fission neutron spectrum. In the original Madland-Nix model, statistical equilibrium was assumed between the two fission fragments at the scission point. This was the ground for usinga single value of the maximum nuclear temperature for both fragments. However, this assumption seems questionable, since the deformation energies of the fragments at the scission point, which are generally different for the nascent fragments, eventually converts into the internal excitation energy. The author tried to take into account the difference in the nuclear temperature of the light and heavy fragments in a empirical manner. This non-equitemperature model was applied to analyze the fission neutron spectra for neutron-induced fission of U-235 and Pu-239 and spontaneous fission of Cf-252. It was found that *(i)* consideration of the temperature difference had greater effects on the spectral shape than the previous attempts, and *(ii)* this modification of the model gave better account of the experimental spectra for these nuclides.

I. Introduction

Exact analysis of nuclear characteristics of fast reactors requires exact knowledge of the fission neutron spectrum. According to a recent sensitivity analysis[1], the fission neutron spectrum of ^{239}Pu is one of the important factors that affect the calculated effective multiplication factor and control rod worths of a fast reactor. Study on extended burnup of LWR-fuels and of nuclear incineration systems add further

---

· This work is a result of the entrusted study by JAERI to Kinki University.

importance to the fission neutron spectrum data for many actinides at higher as well as at lower incident energies.

The Madland-Nix (MN) model[2] for fission neutron spectrum calculation was successfully applied for analysis and evaluation of important fissionable nuclides. The evaluation of fission neutron spectra for major actinides in the Japanese Evaluated Nuclear Data Library, Version 3 (JENDL-3) was also based on the model together with the parameters recommended by Madland and Nix.

However it has been recognized that the MN model underestimates the spectrum in the regions below ~0.5MeV and above ~7MeV. Several attempts have been made to improve the model.[3-5]

Walsh[3] examined the possibility of improving the calculated spectrum by taking into account the anisotropy of neutron emission in the center-of-mass system. He demonstrated that better agreement with experimental data could be obtained by assuming the anisotropy coefficient b (in the form $1+b\cos^2\theta$) to be 0.1. However, this value seems to be too largein view of the recent experimental data by Budtz-Jørgensen *et al.*[6](b=0.015), and by Bãtenkov *et al.*[7](b=0.04) both for ^{252}Cf(sf).

Madland *et al.*[4] presented a preliminary results of their efforts to improve and refine the model by replacing the average values of the fragment mass, charge, and kinetic energy with the distributions themselves on a point-by-point basis. This refined model yielded the spectrum in slightly better agreement with measured data but did not yet reproduce the experimental spectrum.

Another approach by Märten *et al.*[5] is to consider the mass dependence of the average excitation energy, the average kinetic energy of the fission fragment per nucleon, and the inverse cross section of compound-nucleus formation. This generalization resulted in better agreement with experimental data, at least atvery low and very high emission energies. A disadvantage of this method is that the mass-dependent quantities required as input are not always available for every fissionable nuclide.

One of the important assumptions of the Madland-Nix model is the triangular distribution of the nuclear temperature. This assumption is equivalent to assuming that the excitation energy distribution is uniform, which is appropriate at high excitaion energies but become less adequate at low excitation energies. So there may be some room for improvement in this respect.

Generally speaking, it is natural that using many empirical data as input leads to better results. From the point of view of an evaluator,

who is confronted with evaluations of nuclear data for many nuclides, it is desirable to have a model with a set of parameters systematics that provides acceptable results with less amount of input data within a short calculation time and that is applicable to estimate the spectra even for nuclides for which no or scarce experimental data are available. Also for the purpose of sensitivity analysis of integral experiments, it is useful to have a model with small amount of input parameters.

As an attempt in this direction, we tried to take into consideration the difference in the nuclear temperatures of the two fragments *not* at the scission point *but* at the time of prompt neutron emission, since it is physically reasonable to assume that the nuclear temperatures characterizing the neutron emission from the two fragments are different for different fragment masses due to different initial deformation energies and also due to different level density parameters.

II. The Non-equitemperature Assumption

In the original MN model, it is assumed that the same temperature distribution $P(T)$ applies to both the light and heavy fragments. This would be the case, if the nuclear system were in *statistical equilibrium* at the scission point, with the excitation energy and level density parameter of each fragment proportional to its mass number. Actually it is questionable if statistical equilibrium should be established at the scission point, since the fission process is not only a statistical but also a dynamical process. Even if equilibrium is established in partitioning of the internal excitation energy at the scission point, the total excitation energy available for neutron emission is composed of internal excitation energy $a_i T_{o\,i}^2$ and the deformation energy D_i at the scission point, the latter being eventually converted into the internal excitation energy. Thus, the average initial total excitation energy of the fragment i is expressed as

$$\langle E^*_i \rangle = a_i T_{o\,i}^2 + D_i \quad (i = \mathrm{L\ or\ H}) \tag{1a}$$

$$= a_i T_{m\,i}^2 \tag{1b}$$

where $T_{m\,i}$ is the maximum temperature for fragment i, L and H standing for light and heavy fragments, respectively. The deformation energy D_i at the scission point is strongly affected by the nuclear structure of the fragments so that the temperatures $T_{m\,i}$ for the two fragments are

generally not equal. The effecive nuclear temperatures for definite fragment masses deduced from the multi-parameter measurement of fission fragments and fission neutrons performed at Geel[6] (Fig.1) suggest that this is the case. In the case of ^{252}Cf(sf), the ratio of nuclear temperatures averaged over light and heavy fragments $\langle T_L \rangle / \langle T_H \rangle$ is 1.13.

In this respect, it is interesting to note that Wilkins *et al.*[9] have found that the fragment deformation $\beta(A)$ at the scission point show a saw-tooth behavior very similar to the neutron multiplicity $\nu(A)$ (Fig.2). This suggests that the deformation energy is greater than the excitation energy at the scission point, *i.e.* $D_i > a_i T_{0i}^2$. This fact accounts for the non-uniform (also saw-tooth-like) distribution of the nuclear temperature versus mass number A, as was observed in the Geel data.

III. Calculation with the Non-equitemperature Model

The present calculation is essentially based on the formalism of Madland and Nix[2]. The constant compound-formation cross-section model was used for the sake of simplicity. The maximum (sharp cutoff) nuclear temperature T_m is approximately related to the average total excitation energy $\langle E^* \rangle$ by

$$\langle E^* \rangle = \langle E_r \rangle + B_n + E_n - \langle E_k \rangle = a T_m^2 \qquad (2)$$

where $\langle E_r \rangle$ is the total energy release, B_n the neutron separation energy, E_n the incident neutron energy, $\langle E_k \rangle$ the total kinetic energy, and a the level density parameter given by $a = A/C$ (C = 8~11). The total energy release $\langle E_r \rangle$ of fission was calculated according to the seven-fragment approximation[2] using the mass formula of Tachibana, Uno, Yamada and Yamada (TUYY)[9], which was claimed to yield the appropriate mass even for nuclei far from the beta-stability line. The total kinetic energy of the fragments was taken from the work of Unik *et al.*[10]

The original formulas in the Madland-Nix formalism were somewhat modified so as to take into account the difference in temperature of the two fragments. Since the nuclear system is not in statistical equilibrium and the excitation energy is not proportional to the fragment mass number, we can write as follows:

$$\langle E^*_L \rangle = (A_L/C)T_{mL}^2 , \tag{3a}$$

$$\langle E^*_H \rangle = (A_H/C)T_{mH}^2 , \tag{3b}$$

$$\langle E^* \rangle = \langle E^*_L \rangle + \langle E^*_H \rangle = (A/C)T_m^2 . \tag{3c}$$

$$A = A_L + A_H \tag{3d}$$

(If the system were in statistical equilibrium, then the equality $T_{mL} = T_{mH} = T_m$ would hold.) Then we have

$$A_L T_{mL}^2 + A_H T_{mH}^2 = AT_m^2 . \tag{4}$$

Defining the ratio of the temperatures for the light and heavy fragments as $R_T = T_{mL}/T_{mH}$, we obtain

$$T_{mL} = [AR_T^2/(A_L R_T^2 + A_H)]^{1/2} T_m , \tag{5a}$$

$$T_{mH} = [A/(A_L R_T^2 + A_H)]^{1/2} T_m . \tag{5b}$$

IV. Results and Discussion

1. Effects of Changes in Input Data

Prior to performing the calculations with the non-equitemperature model, the sensitivity to changes in input parameters was analyzed on the basis of the original MN model. Different values of $\langle E_r \rangle$, $\langle E_k \rangle$, and a were used and the resultant spectra were compared. As can be seen from Figs.3a - 3c, it was found that in all these cases the calculated spectra shifted to one side, *i.e.*, when the high energy component was increased, the low energy component was decreased, and *vice versa*. It was not possible to increase *both* the high and low energy components *at the same time*, as required to improve agreement with experimental data.

2. Spectra Calculated with the Non-equitemperature MN Model

The non-equitemperature model was applied to analyze the data of the fission neutron spectra for ^{235}U(n,f), ^{239}Pu(n,f) and ^{252}Cf(sf). The quantities used as input data are summarized in Table 1.

Figure 4 compares the spectra for ^{235}U(n,f) for E_n = 0.53MeV calculated with different ratios R_T of the two temperatures. It can be observed that (*a*) if the temperature ratio was taken greater than unity, then both the low- and high-energy components were increased, and as a result, (*b*) the spectrum fits better with the experimental data. The value R_T=1.13 was taken from the Geel data[6]. This value was obtained for ^{252}Cf(sf) and not for ^{235}U(n,f), but since we do not have corresponding data for ^{235}U(n,f), we tentatively used this value. This value was found to give a spectrum in better agreement with the experimental data of Johansson[11]. The value R_T=1.34 was that suggested by Kapoor[12]. This value seems to be too large. Figure 5 shows the results for ^{252}Cf(sf). The experimental data were taken from the works of Poenitz and Tamura[13] and Batenkov *et al.*[14] Also in this case, better agreement was obtained by assuming non-equality of nuclear temperatures, although there still remain some discrepancies in the high and low energy ends of the spectrum.

The case for ^{239}Pu(n,f) is rather uncertain, because the two sets of experimental data, plotted in Fig.6, show different behavior in the region above 5 MeV. The data of Johansson *et al.*[15] are represented well with R_T=1.0, while those of Knitter[16] are represented with R_T=1.4.

V. Concluding Remarks

The main conclusionsto be drawn from the present preliminary analysis are as follows:

a) Taking into account the non-equality of nucleartemperatures for the two fragments had greater effects than other factors in improving the calculated spectral shapes, increasing *both* the low- andhigh-energy neutron components.

b) For ^{235}U(n,f) and ^{252}Cf(sf), reasonable choice of the temperature ratio R_T lead to better agreement between the calculated and experimental spectra. For ^{239}Pu(n,f), conclusion must be postponed until the discrepancies between experimental data are resolved.

c) The non-equitemperature model should further be tested onother nuclides and at higher incident energies. It would be interesting to know how the temperature ratio changes when the excitation energy of the fissioning system is increased.

References

1) T.Takeda, H.Matsumoto and Y.Kikuchi, J. Nucl. Sci. Technol. 27, 581 (1990)
2) D.G.Madland and R.J.Nix, Nucl. Sci. Eng. 81, 213 (1982)
3) R.L.Walsh, Nucl. Sci. Eng. 102, 119 (1989)
4) D.G.Madland, R.J.LaBauve and J.R.Nix, *Physics of Neutron Emission in Fission*, Proc. of a Consultants' Meeting, Mito, 1988, INDC(NDS)-220, p.259 (1989)
5) H.Märten and D.Seeliger, Nucl. Sci. Eng. 93, 370 (1986)
6) C.Budtz-Jørgensen and H.H.Knitter, *Physics of Neutron Emission in Fission*, Proc. of a Consultants' Meeting, Mito, 1988, INDC(NDS)-220, p.181 (1989); Nucl. Phys. A490, 307 (1988)
7) O.I.Batenkov, A.B.Blinov, M.V.Blinov, S.N.Smirnov, *ibid.* p.207 (1989)
8) B.D.Wilkins *et al.*, Phys. Rev. C14, 1832 (1976)
9) T.Tachibana, M.Uno, M.Yamada and S.Yamada, Atomic Data and Nuclear Data Tables 39, 251 (1988)
10) J.P.Unik, J.E.Gindler, L.E.Glendenin, K.F.Flynn, A.Gorski, and R.K. Sjoblom, *Physics and Chemistry of Fission*, Int. Symposium, Rochester, Vol.II, p.15 (1973)
11) P.I.Johansen and B.Holmqvist, Nucl. Sci. Eng. 62, 695 (1977)
12) S.S.Kapoor, R.Ramanna and P.N.Rama Rao, Phys. Rev. 131, 283 (1963)
13) W.P.Poenitz and T.Tamura, Proc. Int. Conf. on Nuclear Data for Science and Technology, p.473 (1983)
14) O.I.Batenkov, M.V.Blinov, G.S.Boykov, V.A.Vitenko, V.A.Rubchenya, Proc. IAEA Consultants' Meeting on the ^{235}U Fission Cross-Sections and the ^{252}Cf Fission Neutron Spectrum, Vienna 1983, p.161 (1983)
15) P.I.Johansson, B.Holmqvist, T.Wielding and L.Jeki, Proc. Conf. on Nuclear Cross Sections and Technology, Washington, Paper GB-8 (1975)
16) H.H.Knitter, Atomkernenergie 26, 76 (1975)
17) D.G.Madland, R.J.LaBauve and J.R.Nix, *Nuclear Standard Reference Data*, Proc. of IAEA/AG Meeting, Geel, 1984, IAEA-TECDOC-335 p.267 (1985)

Table 1 Input parameters used in the present calculation. The value marked with * is that calculated with the Moller-Nix mass formula, as used by Madland et al.[17] This value was chosen just for comparison purpose. The TUYY mass formula yielded 215.998 MeV.

Quantity	U-235		Pu-239		Cf-252	
$\langle E_r \rangle$	185.896	MeV	198.088	MeV	218.886	MeV*
$\langle E_k \rangle$	171.8	MeV	177.1	MeV	185.9	MeV
a	$A/9.6$	MeV^{-1}	$A/8.5$	MeV^{-1}	$A/8.0$	MeV^{-1}
A_H	140		140		144	
A_L	96		100		108	

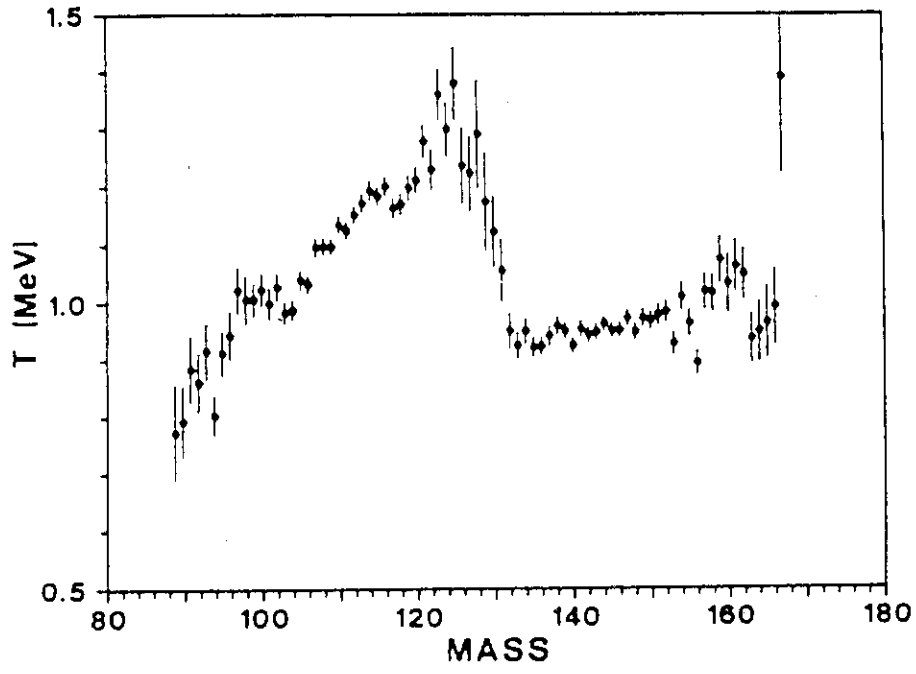

Fig. 1 The neutron temperature derived from neutron spectra plotted versus the fragment mass number (Budtz-Jørgensen et al.[6]).

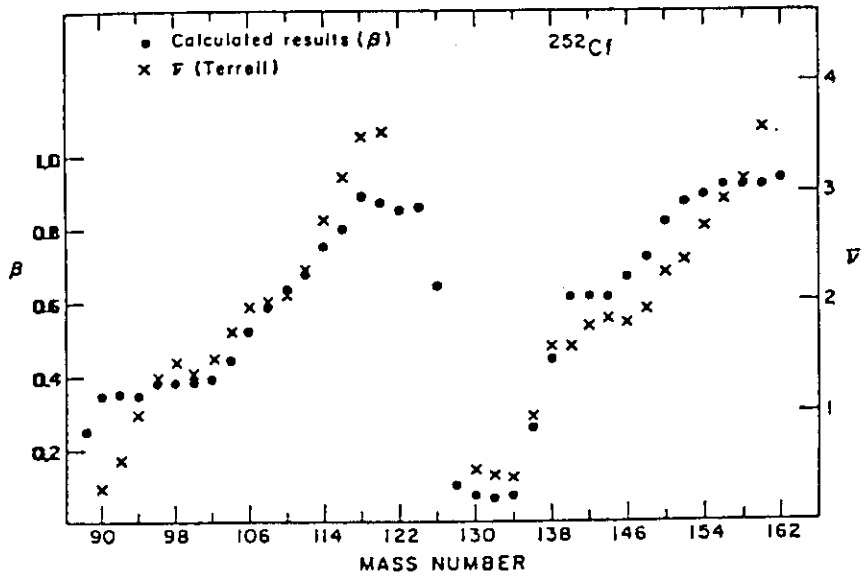

Fig. 2 The fragment deformation β(A) calculated for ^{252}Cf(sf) compared with the neutron multiplicity $\bar{\nu}$(A) (Wilkins et al.[9]).

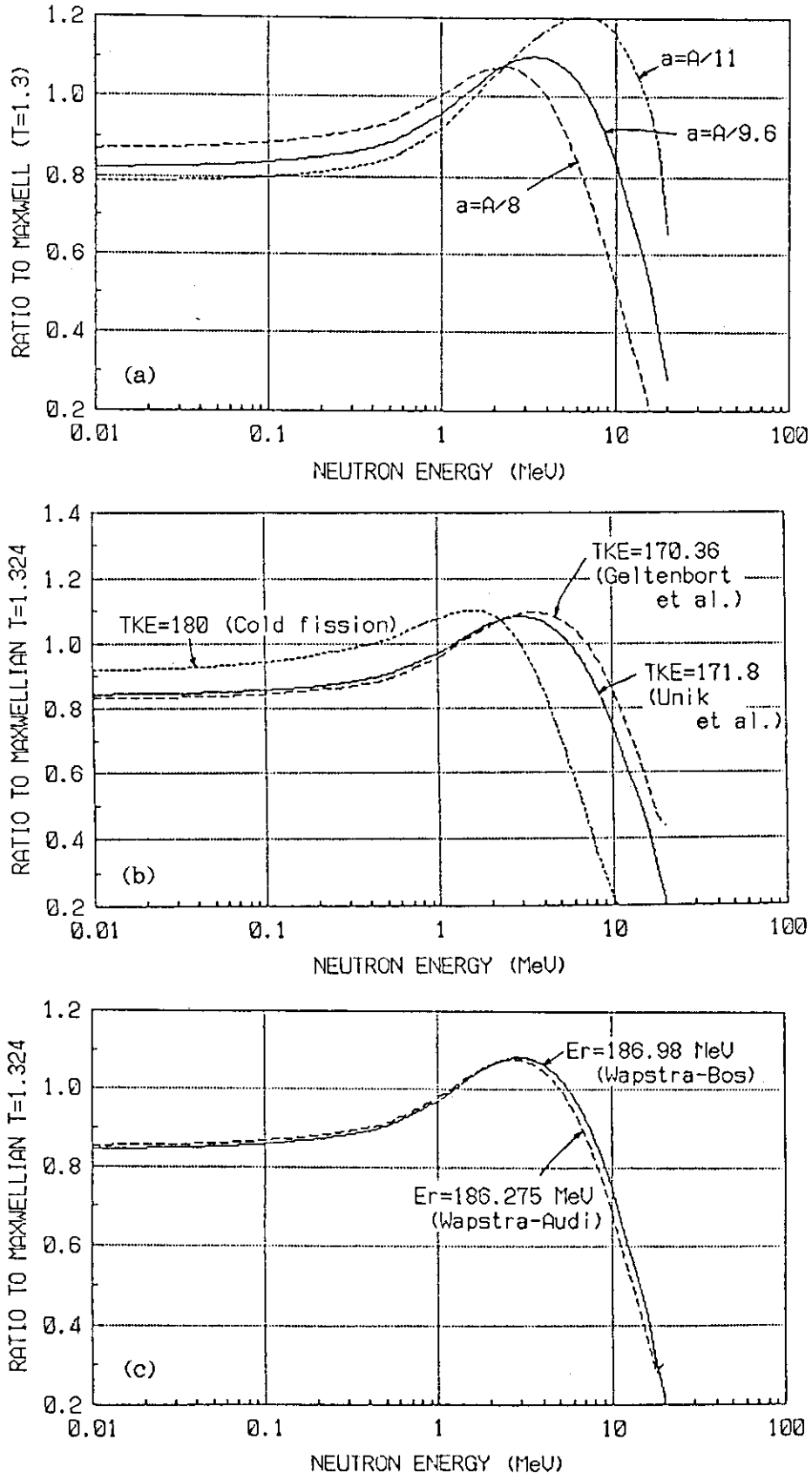

Fig. 3 Dependence on input parameters; (a) Level density parameter, (b) Fragment total kinetic energy, (c) Total energy release.

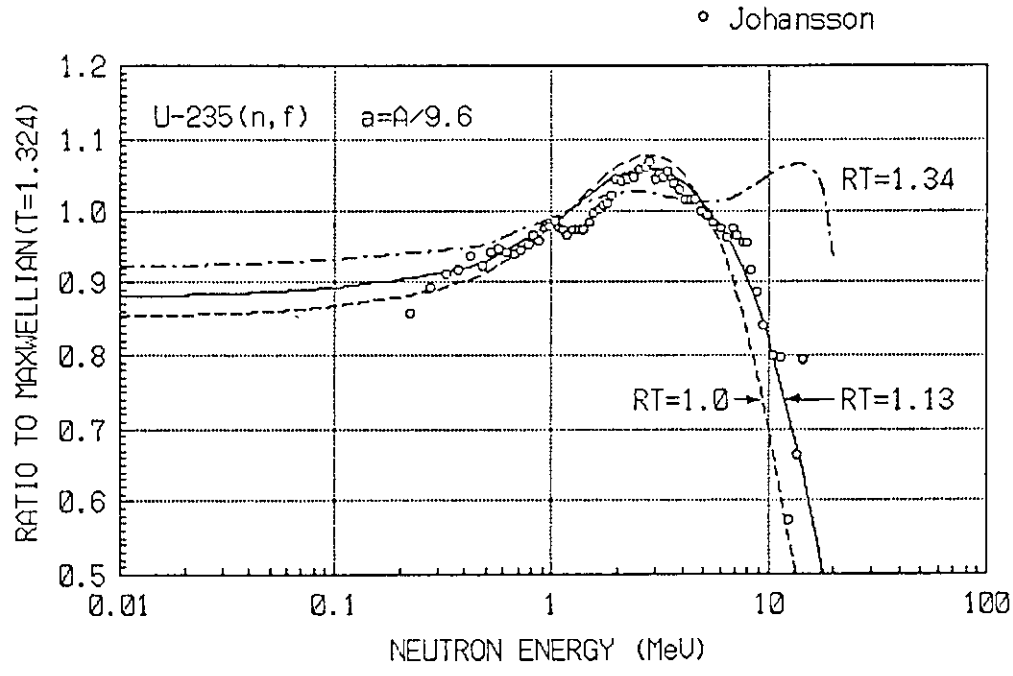

Fig. 4 Fission neutron spectra for $^{235}U(n,f)$ for E_n=0.53 MeV. The ratios to Maxwellian spectrum with T_M=1.324 MeV (the value adopted in JENDL-2) are plotted.

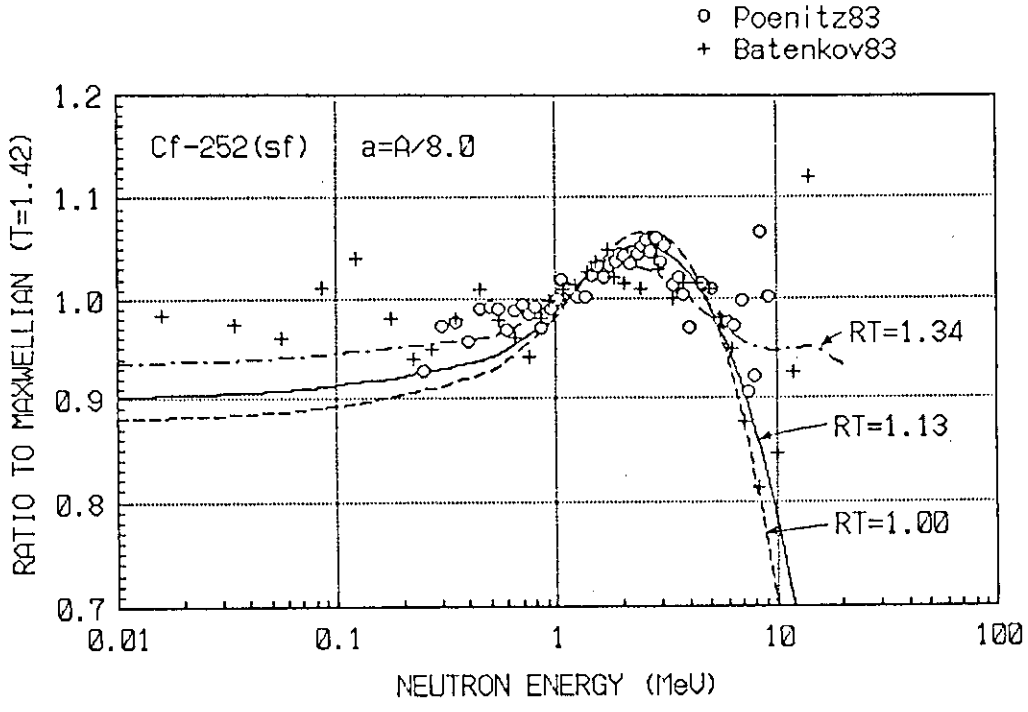

Fig. 5 Fission neutron spectra for $^{252}Cf(sf)$.

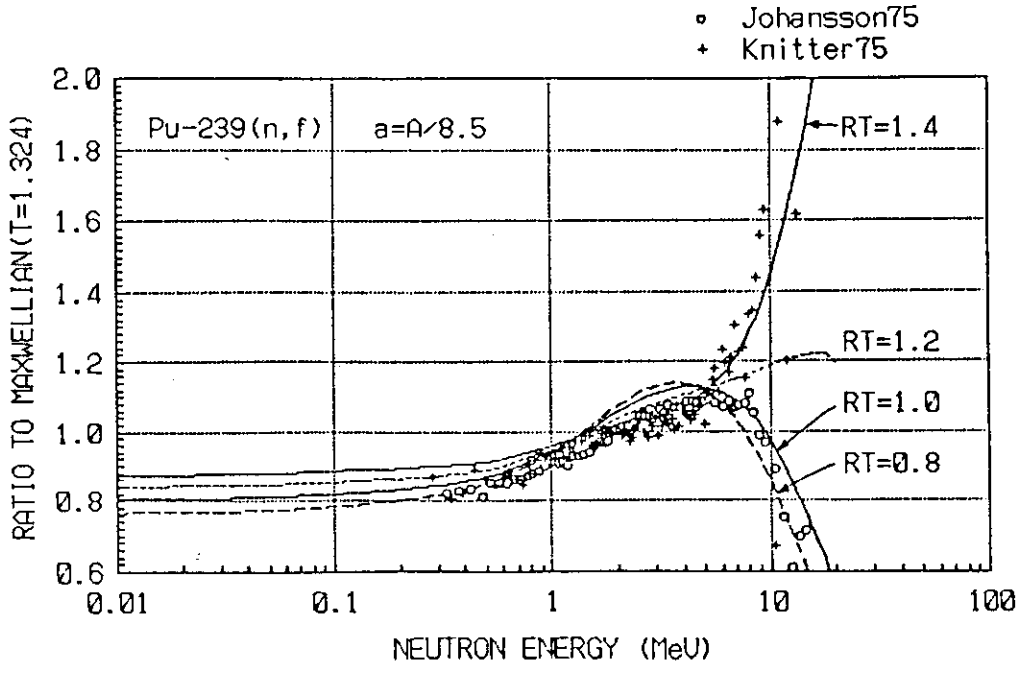

Fig. 6 Fission neutron spectra for $^{239}Pu(n,f)$ for E_n=0.53 MeV.

3.23 Semi-empirical Determination of Shell Energies

Takahiro TACHIBANA, Masatoshi TAKANO and Masami YAMADA

Science and Engineering Research Laboratory, Waseda University
3-4-1 Okubo, Shinjuku-ku, Tokyo, 169 Japan

ABSTRACT

A method is proposed for obtaining shell energies semi-empirically. First, single-particle levels are calculated for the Woods-Saxon potentials. Then, from the energies of particles put in these single-particle levels, a smooth part is subtracted by a new method. Since the remaining part shows excessive shell and submagic effects, a refinement including several parameters is made to yield shell energies to be used in mass formulas. Although the optimum parameters are not yet attained, a mass formula with these shell energies are discussed.

1. INTRODUCTION

Since 1975, our group has studied mass formulas with empirical shell terms.[1~6] Now they have reached so developed a stage that a major forward step will be possible only by a change of the policy. In this article we try to determine shell energies less empirically than before.

We start with a spherical shell-model potential, which is taken to be Woods-Saxon type. From the energies of particles put in this potential, we extract a certain kind of shell energies. Since these shell energies are too crude to be used in mass formulas, we refine them so as to include the effects of residual interactions, in particular, the pairing and deformation. Finally, a mass formula with these shell energies is discussed.

2. SHELL-MODEL POTENTIAL

We take the Woods-Saxon potential. Explicitly, our shell-model potentials for neutrons ($V_n(r)$) and protons ($V_p(r)$) are given as

$$V_{\rm n}(r)=-\left(V_{0\rm s}-\frac{N-Z}{A}V_{0\rm a}\right)\left[f(r)-\frac{\lambda}{2}\left(\frac{1}{m_{\rm n}c}\right)^2\frac{1}{r}\frac{{\rm d}f(r)}{{\rm d}r}(s\cdot l)\right], \tag{1}$$

$$V_{\rm p}(r)=-\left(V_{0\rm s}+\frac{N-Z}{A}V_{0\rm a}\right)\left[f(r)-\frac{\lambda}{2}\left(\frac{1}{m_{\rm p}c}\right)^2\frac{1}{r}\frac{{\rm d}f(r)}{{\rm d}r}(s\cdot l)\right]+eV_{\rm C}(r), \tag{2}$$

with

$$f(r)=\left[1+\exp\left(\frac{r-R}{a}\right)\right]^{-1}, \tag{3}$$

$$R=r_0A^{1/3}\left[1-\frac{1}{3}\left(\frac{\mu}{r_0}\right)^2A^{-2/3}\right]. \tag{4}$$

Here, the symbols used are either conventional ones or parameters mentioned below. The Coulomb potential $V_{\rm C}(r)$ is calculated from the Fermi distribution of charge $(Z-1)e$ with the radius parameter $R_{\rm C}=1.07A^{1/3}$fm and the surface diffuseness parameter $a_{\rm C}=0.55$fm.

The potential parameters should, in principle, be determined so as to give the best mass formula. Actually, however, the numerical calculation needed is so much that we have tested only a few sets of parameters. In order to choose a reasonable parameter set, we have approximately fitted the nucleon separation energies of single-particle nuclei to experimental values. The parameter set we refer to in this paper is as follows:

$$V_{0\rm s}=53.3{\rm MeV},\ V_{0\rm a}=35{\rm MeV},\ r_0=1.25{\rm fm},\ a=0.66{\rm fm},\ \mu=0.32{\rm fm},\ \lambda=35. \tag{5}$$

Owing to the Coulomb barrier, there are resonance states for the proton. In order to avoid this complication, we modify the proton potential outside the top of the barrier; there, the potential is taken to be constant, keeping the top value.

3. EXTRACTION OF CRUDE SHELL ENERGIES

The potentials in the previous section depend on Z and N. For each neutron (or proton) potential with specified Z and N, we calculate all bound states, from which we can obtain the minimum energy of a system of n particles put in the potential. This minimum energy $E_{\rm nsp}(n;Z,N)$ (or $E_{\rm psp}(n;Z,N)$) depends on n nonsmoothly, and gives a shell energy if an appropriate smooth part is subtracted. For such subtraction the Strutinsky method[7] is well known, but we found that this method is not quite appropriate for the Woods-Saxon potential. This potential can accommodate only a finite number of particles; we denote the maximum particle number by $n^q_{\rm nMax}(Z,N)$ (or $n^q_{\rm pMax}(Z,N)$), which depends on Z (or N) nonsmoothly. The Strutinsky method suffers from this nonsmooth dependence, occasionally giving false dependence of the neutron (or proton) shell energy on Z (or N).

In this paper we use a different subtraction method in two steps. In the first steps, we subtract a "classical" energy or sum of local Fermi-gas energies, which is explicitly defined as follows. We first calculate the single-particle level under which the phase-space volume

(including the doubling by spin) is $n(2\pi\hbar)^3$, and then, the "classical" energy $E_{i\mathrm{cl}}(n;Z,N)$ (i=n,p) is defined as the average energy of the system of n classical particles distributed uniformly in the phase space under this level. In this calculation the nucleon spin is also treated classically. This first step subtracts a large portion of the smooth part, but still a considerable amount of energy is left. A typical example of $E_{\mathrm{nsp}}(n;Z,N)-E_{\mathrm{ncl}}(n;Z,N)$ is shown in Fig. 1; the behavior in this figure can be understood from consideration of the uncertainty principle.The maximum of $E_{i\mathrm{cl}}(n;Z,N)$ (i=n,p) for given Z and N is denoted by $n^{\mathrm{cl}}_{i\mathrm{Max}}(Z,N)$ (i=n,p).

In the second step, we further subtract a smooth function $\Delta E_{\mathrm{nav}}(n;Z,N)$ (or $\Delta E_{\mathrm{pav}}(n;Z,N)$), for which we assume the following form;

$$\Delta E_{\mathrm{nav}}(n,Z,N) = \sum_i u_i(Z,N) n^{i/2} \ , \tag{6}$$

$$u_i(Z,N) = A^{1-i/2}\Big[u_{i1}A^{-1/3} + u_{i2}A^{-2/3} + u_{i3}A^{-1} + \left(u_{i4}A^{-1/3} + u_{i5}A^{-2/3}\right)(N-Z)/A\Big] \ , \tag{7}$$

$$\Delta E_{\mathrm{pav}}(n,Z,N) = \sum_i \left[u_i(N,Z) + v_i(N,Z)\ (Z-1)\ A^{-1/3}\right] n^{i/2} \ , \tag{8}$$

$$v_i(Z,N) = A^{1-i/2}\Big[v_{i1}A^{-1/3} + v_{i2}A^{-2/3} + v_{i3}A^{-1} + \left(v_{i4}A^{-1/3} + v_{i5}A^{-2/3}\right)(N-Z)/A\Big] \ . \tag{9}$$

Note that the charge symmetry is taken into account in the above form. $u_i(N,Z)$ in Eq. (8) means to interchannge Z and N in Eq.(7). The parameters u_{ij} and v_{ij} are determined so as to give the best weighted averages of $E_{i\mathrm{sp}}(n;Z,N)-E_{i\mathrm{cl}}(n;Z,N)$ (i=n,p) with five weight functions, $1/n$, $n[n_{i\mathrm{Max}}(Z,N)-n]^3$, $n[n_{i\mathrm{Max}}(Z,N)-n]$, $n^3[n_{i\mathrm{Max}}(Z,N)-n]$, and n^3, where $n_{i\mathrm{Max}}(Z,N)=\min[n^{\mathrm{q}}_{i\mathrm{Max}}(Z,N),\ n^{\mathrm{cl}}_{i\mathrm{Max}}(Z,N)]$. An example of this second subtraction is also given in Fig.1. Finally, we obtain crude shell energies as

$$E_{\mathrm{ncs}}(Z,N) = E_{\mathrm{nsp}}(N;Z,N) - E_{\mathrm{ncl}}(N;Z,N) - \Delta E_{\mathrm{nav}}(N;Z,N), \tag{10}$$

$$E_{\mathrm{pcs}}(Z,N) = E_{\mathrm{psp}}(Z;Z,N) - E_{\mathrm{pcl}}(Z;Z,N) - \Delta E_{\mathrm{pav}}(Z;Z,N). \tag{11}$$

It should be emphasized that the crude neutron shell energies $E_{\mathrm{ncs}}(Z,N)$ depend not only on N but also on Z. Similarly, the crude proton shell energies $E_{\mathrm{pcs}}(Z,N)$ depend not only on Z but also on N. The most remarkable dependence is seen when we approach the neutron drip line; the absolute magnitudes of $E_{\mathrm{ncs}}(Z,N)$ become considerably smaller.

We have also found that the crude shell energies are very sensitive to the spin-orbit interaction. When we used λ=28, we obtained crude shell energies quite different from those of λ=35.

4. REFINEMENT OF SHELL ENERGIES

Compared with the empirical shell energies,[1~6] the crude shell energies obtained in the last section are too large in absolute magnitude and have too marked submagic numbers. We refine them by taking into account the effects of residual interactions.

The high-energy part of residual interactions mixes a large number of high-energy configurations, each in a small amount. We assume that its effect on the shell energies is simply represented by a reduction factor k_r.

The low-energy part of residual interactions mixes low-energy configurations, each in a relatively large amount. Then, the Fermi surface becomes diffuse; i.e. the single-particle states near the Fermi level are partly occupied and partly vacant. Therfore, to the shell energy of (Z,N) nuclide, not only $E_{\rm ncs}(Z,N)$ and $E_{\rm pcs}(Z,N)$ but also $E_{\rm ncs}(Z,N')$ $(N'\neq N)$ and $E_{\rm pcs}(Z',N)$ $(Z'\neq Z)$ will contribute. We assume that important contributions come from such N' and Z' as $(1-\xi_{\rm n})N\leq N'\leq(1+\xi_{\rm n})N$ and $(1-\xi_{\rm p})Z\leq Z'\leq(1+\xi_{\rm p})Z$. Then, we denote an appropriate weighted averages of $E_{\rm ncs}(Z,N')$ and $E_{\rm pcs}(Z',N)$ by $E_{\rm ncs}(Z,N)$ and $E_{\rm pcs}(Z,N)$, respectively. In this paper, we take a simplest weight as illustrated in Fig. 2.

The configuration mixing brings about other kinds of energy change. Here, we consider two kinds, and assume that $\xi_{\rm n}$ (or $\xi_{\rm p}$) is composed of two parts as

$$\xi_{\rm n}^2=\eta_{\rm n}^2+\zeta^2, \tag{12}$$

$$\xi_{\rm p}^2=\eta_{\rm p}^2+\zeta^2, \tag{13}$$

in which η_i $(i$=n,p) is mainly responsible for pairing and ζ for deformation.

We assume the energy associated with η_i to be

$$E_{i\eta}=k_{i1}\eta_i^2-k_{i2}\eta_i^2(1-k_{i3}\eta_i). \tag{14}$$

Here, $k_{i1}\eta_i^2$ represents the change of the sum of single-particle energies caused by the configuration mixing, and k_{i1} can be estimated if a constant level spacing is assumed. The rest of the right-hand side of Eq. (14) is the interaction energy. In order to estimate k_{i2} and k_{i3}, we minimize $E_{i\eta}$ by changing η_i. The minimum and the value of η_i giving the minimum can be compared with results of the pairing theory, and from this comparison we can estimate k_{i2} and k_{i3}, although this estimation may not be accurate because our occupation probabilities of single-particle states are not the same as those of the pairing theory.

The energy associated with ζ is assumed to be

$$E_\zeta=k_{\rm s}\zeta^2-k_{\rm C}\zeta^2. \tag{15}$$

The main contribution to $k_{\rm s}\zeta^2$ is the increment of the average surface energy caused by deformation, and $k_{\rm C}\zeta^2$ is the decrement of the Coulomb energy. In order to estimate $k_{\rm s}$ and $k_{\rm C}$,

we put a correspondence between ζ and the degree of deformation as follows. In Fig. 3, the ellipse represents a deformed nucleus with uniform number density ρ, and its surface is divided into a number of parts by concentric spheres whose radii are $R(n) = \left[3(n+0.5)/4\pi\rho\right]^{1/3}$. For simplicity, we assume that the deformation is not very large (in Fig. 3, the deformation is exaggerated). Then, as far as the radius is concerned, the deformed nucleus may be regarded as a combination of fractional spherical nuclei having different nucleon numbers.[8] Here, each fraction is given by $\Delta\Omega(n)/4\pi$, where $\Delta\Omega(n)$ is the solid angle in which the radius lies between $R(n-1)$ and $R(n)$. Now we relate ζ to the degree of deformation by

$$<(N' - N)^2> = <(n - N)^2>. \tag{16}$$

On the left hand side of this equation, the average is taken over the distribution illustrated in Fig. 2 with ξ_n replaced by ζ, so that it is a function of ζ. On the right hand side, the average is taken with the weight $\Delta\Omega(n)/4\pi$. Once the correspondence between ζ and the degree of deformation is established, it is straight forward to estimate k_s and k_C, although small changes from these estimated values may be allowed when used in mass formulas.

Summing the above energies and minimizing the sum with respect to η_n,η_p and ζ, we get a refined shell energy of a (Z,N) nuclide:

$$E_{sh}(Z,N) = \min\left[k_r\overline{E_{ncs}(Z,N)} + k_r\overline{E_{pcs}(Z,N)} + \sum_{i=n,p}\left\{k_{i1}\eta_i^2 - k_{i2}\eta_i^2(1 - k_{i3}\eta_i)\right\} + k_s\zeta^2 - k_c\zeta^2\right]. \tag{17}$$

In Fig. 4 we show an example of $E_{sh}(Z,N)$ on the β-stability line.

5. INCORPORATION INTO A MASS FORMULA

Incorporation of the above-obtained shell energies into a mass formula is easy. For example, we can replace $M_s(Z,N)$ of the TUYY mass formula[5] by $E_{sh}(Z,N)/c^2$. The parameters in the gross part should be redetermined; if we use the shell-part parameters k's used in obtaining Fig. 4, the gross-part parameters are as given in Table I.

Unfortunately, the root-mean-square deviation of the above-obtained mass formula from experimental data is fairly large (972 keV). We hope that further search for a better set of parameter values and, in addition, use of a more variety of weights not restricted to that of Fig. 2 will considerably reduce the deviation.

6. CONCLUDING REMARKS

We have proposed a method for estimating shell energies semi-empirically. These shell energies are adopted in the TUYY type mass formula. The values of the parameters in the

gross term are readjusted. At present , the root-mean-square deviation between the calculated masses and the experimental masses is fairly large. There is a considerable freedom in our formalism, *e.g.*, in the parameters of the potential, and in the refinement of the crude shell energies. We are now exploiting this freedom to improve the mass formula.

REFERENCES

1 M.Uno and M.Yamada, Prog. Theor. Phys. **53** (1975), 987

2 M.Uno and M.Yamada, in *Atomic Masses and Fundamental Constants* 6, ed. J.A.Nolen,Jr. and W.Benenson (Plenum Pub. Co., New York, 1980), p.141.

3 M.Uno and M.Yamada, Prog. Theor. Phys. **65** (1981), 1322

4 M.Uno, M.Yamada, Y.Ando and T.Tachibana, Bull. Sci. Eng. Res. Lab., Waseda Univ. No. 97 (1981), 19.

5 T.Tachibana, M.Uno, M.Yamada and S.Yamada, Atomic Data and Nuclear Data Tables **39** (1988), 251.

6 T.Tachibana, M.Uno, S.Yamada and M.Yamada, in AIP Conf. Proc. 164, *Nuclei Far from Stability*, ed. I.S.Tonwer (A.I.P., New York, 1988), p.97.

7 V.M.Strutinsky, Nucl. Phys. **A95** (1967), 420; **A122** (1968), 1.

8 M.Yamada and T.Tominaga, Memoirs of the School of Science & Engineering, Waseda Univ. No.46 (1982), 453; Proc. 7th International Conference on Atomic Masses and Fundamental Constants, ed. O.Klepper (1984), p.450.

Table 1 Example of gross-part parameters (in MeV). The notation is the same as in Ref. 5.

i	1	2	3	4
a_i	−15.85858	17.13209	16.23738	−35.26787
b_i	(0.0)	(0.0)	(0.0)	25.22543
c_i	26.56847	−26.46991	−2.892673	(−30.0)

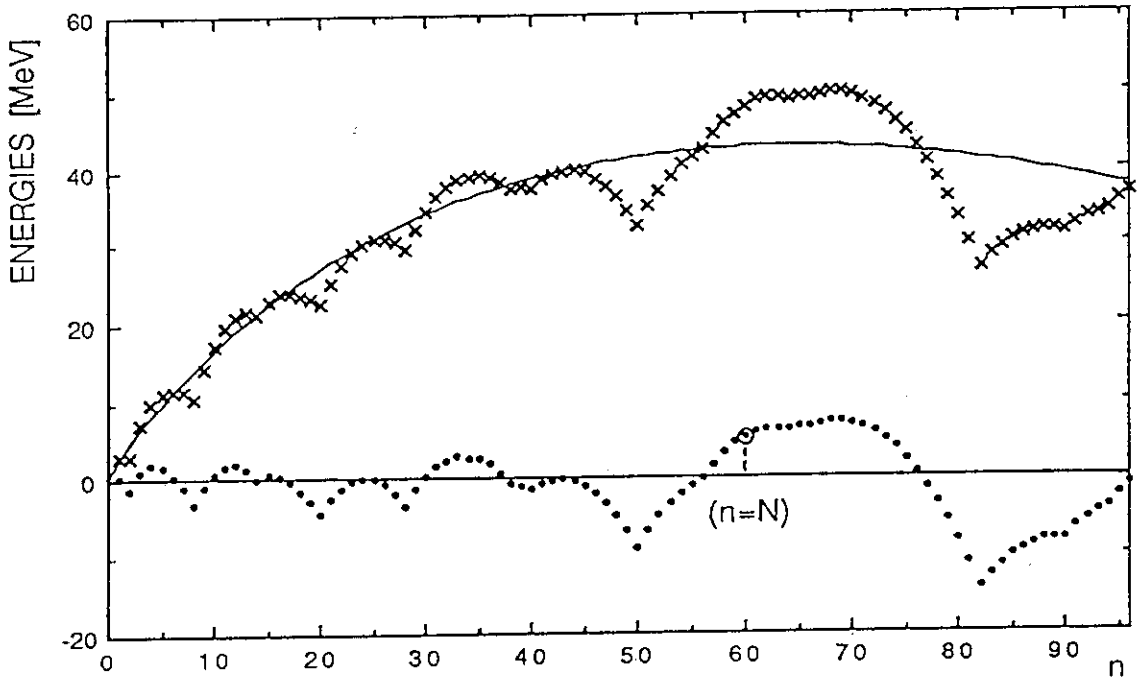

Fig. 1 Subtraction of the smooth energy to yield a crude neutron shell energy in the case of Z=50, N=60. Crosses represent $E_{nsp}(n;Z,N)$ $-E_{ncl}(n;Z,N)$, the solid line is $\Delta E_{nav}(n;Z,N)$, dots represent the differences, and the circled dot is the crude shell energy.

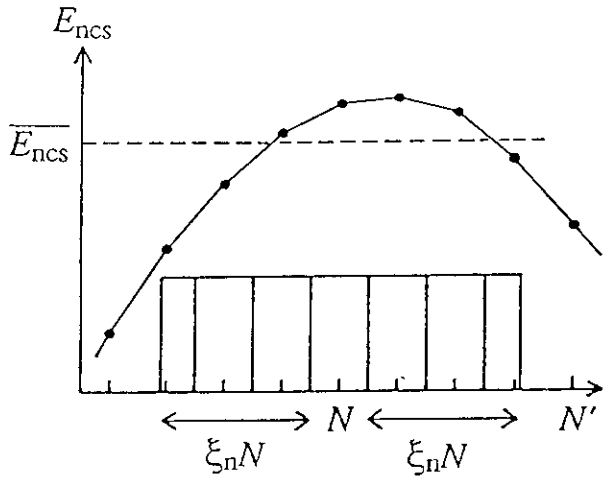

Fig. 2 Illustration of the weights giving $\overline{E_{ncs}(Z,N)}$. Each weight for a given value of N' is proportional to the area of the rectangle on that value of N'.

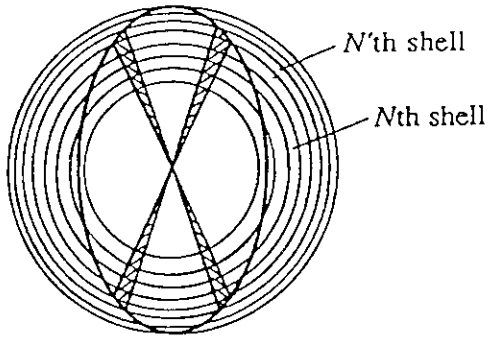

Fig. 3 Decomposition of a deformed nucleus into fractional spherical nuclei. The shaded part corresponds to the solid angle $\Delta\Omega(n)$.

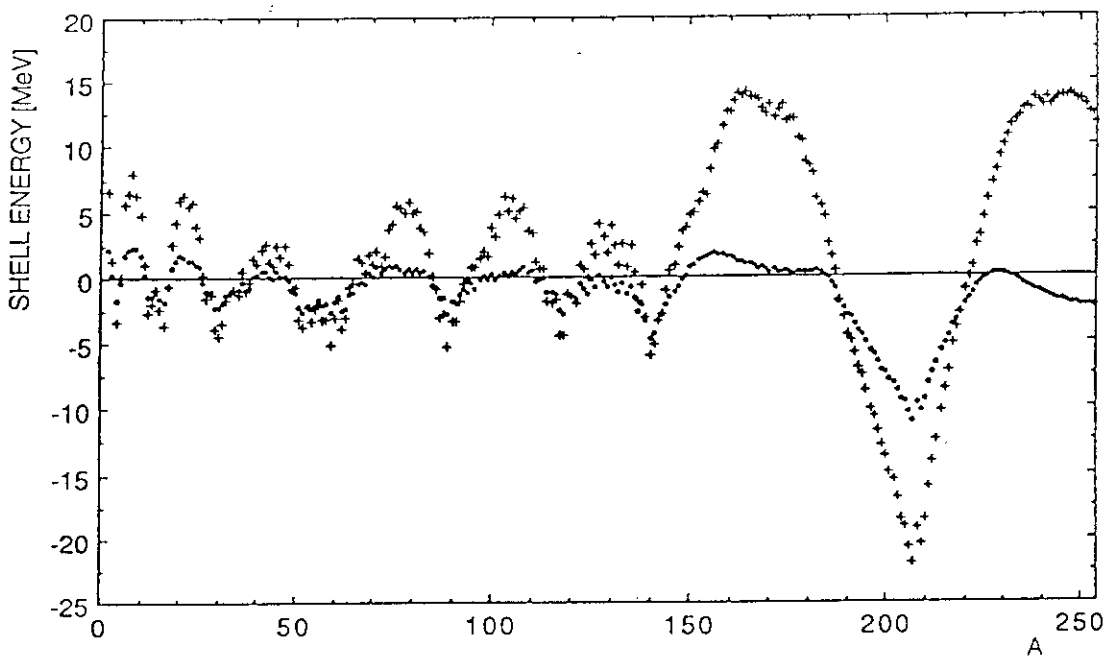

Fig. 4 Example of shell energies on the β-stability line. Crosses are crude shell energies ($E_{ncs}(Z,N)+E_{pcs}(Z,N)$), and dots are refined shell energies with the following specification of k's: k_r=0.5, k_{i1} is obtained from the single-particle level density for r_0=1.2fm (r_0 is the radius of the volume per nucleon), k_{i2} and k_{i3} correspond to the pairing coupling constant G=20/A MeV and the gap Δ=0.5 MeV, k_s corresponds to the surface energy $[19-29(N-Z)^2/A^2]A^{2/3}$ MeV, and k_C is obtained with a uniform charge density of r_0 =1.2fm.

3.24 The Calculations of the Bremsstrahlung Energy Spectra for Thick Targets Using Monte Carlo Method

Akifumi Fukumura and Kensuke Kitao

Division of Physics
National Institute of Radiological Sciences
9-1, Anagawa-4-chome, Chiba-shi 260 JAPAN

The bremsstrahlung spectra from 6 to 50 MV for thick targets were calculated by EGS4 (electron gamma shower version 4) Monte Carlo code. The calculated spectra were compared to the measured spectra. Some agreements between them were good within statistical errors but others were not good because of the different experimental conditions and a lack of information on geometries.

1. Introduction

In advanced radiation therapy, it is often to be used megavoltage photon beams produced by medical electron accelerators. They employ targets which are generally thick enough to absorb most of the incident electron energy to obtain high X-ray intensities.

The knowledge of the energy spectra of photon beams is essential for accurate dose calculations in patients and for estimations of photoneutron yields. However it is only in the case of electrons' impinging on thin targets that we can calculate bremsstrahlung spectra accurately.

We have calculated the energy spectra of bremsstrahlung from 6 to 50 MV for some thick targets using EGS4 Monte Carlo code[1]. Although we could hardly collect the experimental data with details about the geometry, we compared the results of our calculations with the experimental data.

2. Calculations

In our simulations some semi-infinite target slabs of materials are placed in a vacuum and pencil beam of electrons with total energy, E_0, are normally incident on the surface. The slabs are placed in the X-Y plane and the electrons are incident at the origin traveling along the Z-axis. We score the energy and the

direction cosine of each photon which comes out from the far side of the target. Using a 1 MIPS computer we calculated bremsstrahlung spectra for a few to 10 days.

3. Results and Discussion

Figure 1 shows calculated spectra of bremsstrahlung emitted in the forward direction for both thin and thick targets of platinum. The spectra for a thin target were estimated based on Schiff's formula[2][3] while the ones for thick targets were determined by EGS4 code. The thicknesses of the thick targets were 1.8 and 2.1 mm for E_0 = 32.511 and 52.511 MeV, respectively. This figure expresses that thick targets soften the bremsstrahlung spectra because of scatterings and attenuations of electrons and photons in them.

Figure 2 shows the calculated spectra and the measured ones[4] at E_0 = 10.511 and 21.411 MeV. A.A.O'Dell, Jr., et al. bombarded a 0.2 radiation length gold-tungsten converter and a 2.86 cm thick aluminum filter with electrons and measured bremsstrahlung emitted in the forward direction. They placed a secondary heavy-water target in the bremsstrahlung field, analyzed the photoneutrons produced by the D(γ,n)p reaction using time-of-flight techniques and then determined the bremsstrahlung spectra from the both neutron spectra and the cross sections for the deuteron photodisintegration process. Since we could not know the mixture ratio of the gold-tungsten converter, we assumed 0.07 cm thick tungsten target and 2.86 cm thick aluminum filter. We counted the photons with z-components of direction cosine from 0.9998 to 1 for 500,000 incident electrons in this simulations. It took about 2 and 3.5 days CPU time on

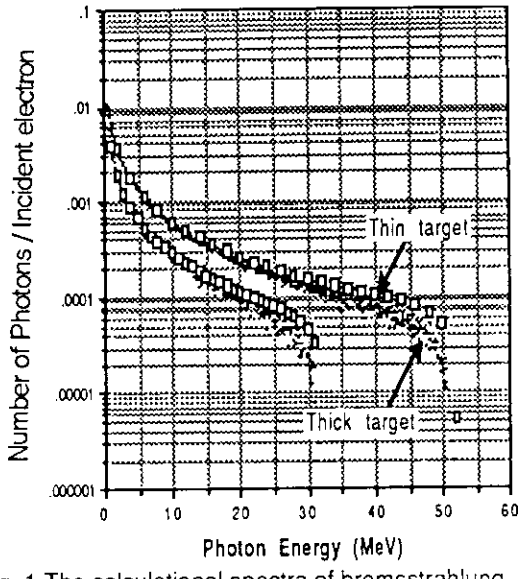

Fig. 1 The calculational spectra of bremsstrahlung for thin and thick targets of Pt

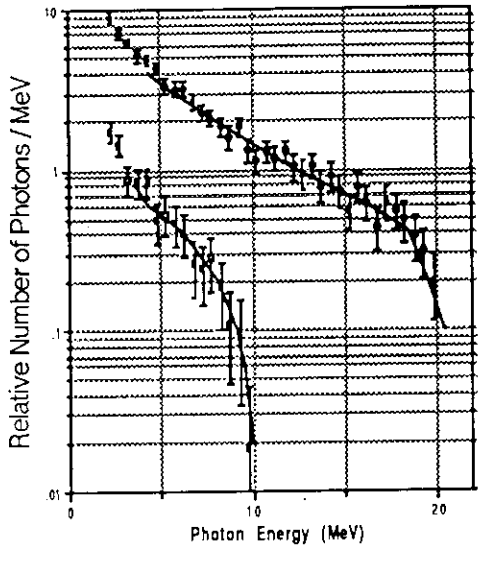

Fig. 2 The spectra of bremsstrahlung produced by 10 and 20.9 MeV electrons on W. The solid lines are the measured data and the dots with error bars are the calculated values.

μ-VAX II to calculate these spectra for E_0 = 10.511 and 21.411 MeV, respectively. This graph expresses the good agreements between the calculations and the measured results within statistical errors.

Figure 3 compares our calculations with the measured spectra[5] at E_0 = 15.511 MeV. The measurements were performed by H. Hirayama and T. Nakamura for 1.3-cm-thick iron and 0.7-cm-thick tungsten targets. The bremsstrahlung spectra were measured by activation detectors of gold, indium,

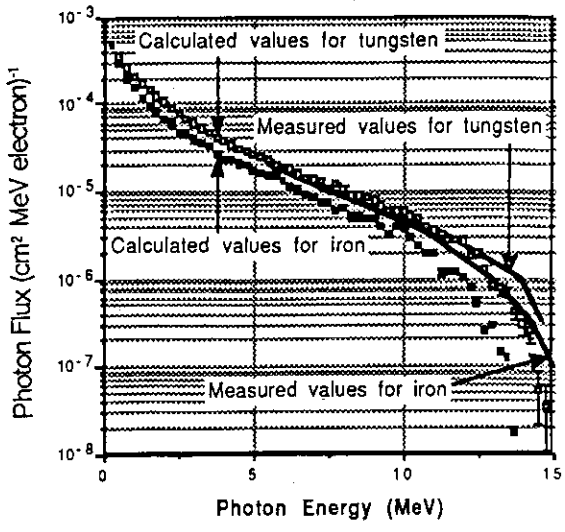

Fig. 3 The spectra of bremsstrahlung produced by 15 MeV electrons on W and Fe

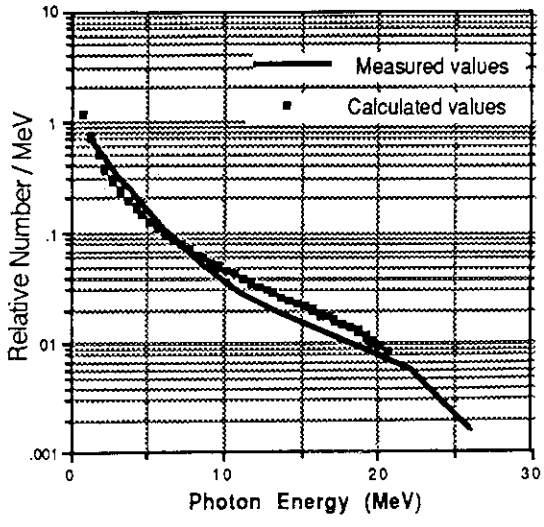

Fig. 4 The spectra of bremsstrahlung produced by 27 MeV medical LINAC

nickel, iron and chromium. The polar angle, θ, between the detectors and the center of the bremsstrahlung target was 9 deg. They measured the saturated activities of activation detectors induced by photonuclear reactions and determined the bremsstrahlung spectra by means of unfolding techniques with the cross sections of the photonuclear reactions. We counted the photons with the polar angle of 9 deg. for 1,000,000 incident electrons. We spent a week on this calculation. In general, it is difficult to estimate the photon spectra by the activation method because the some cross sections of photonuclear reactions are similar and may not be determined so accurate. This is the possible reason that the discrepancies exist.

Figure 4 shows our calculated spectrum and the measured one[6] at E_0 = 27.261 MeV. The experiment was performed by L. B. Levy et al. with the fully shielded NaI(Tl) scintillation detector. The primary beam was scattered once by a carbon scatterer for the purpose of decreasing the number of photons and the beam energy. The once scattered spectrum incident upon the detector was then converted to the primary spectrum incident upon the scatterer by means of Compton energy-angle relation and the Klein-Nishina formula. They used a

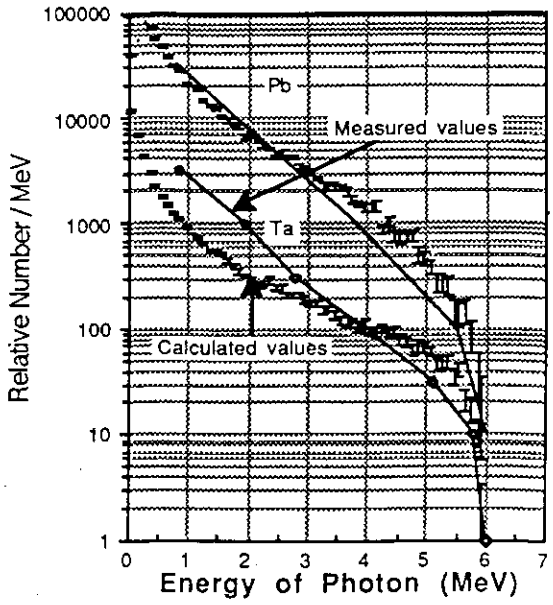

Fig. 5 The spectra of bremsstrahlung produced by 6 MeV electrons on Pb and Ta

medical linear accelerator in this experiment. We, however, could not get the information on the experimental geometries, such as collimator systems and a flattening filter, except for the target thickness in their paper. Then we did not take into account the attenuation and the scattering in those materials. So the measured curve is softer than the calculated one.

Including the experimental bremsstrahlung spectra[7] figure 5 shows the calculated ones which are generated by 1,000,000 incident electrons with E_0 = 6.511 MeV impinging on the 0.12 cm lead and 0.07 cm tantalum targets. V.S.Deshmukh and V.N.Bhoraskar analyzed Compton electrons scattered by photons from a thin aluminum foil and obtained the experimental spectra using the photons' cross section for giving a Compton electron. We could not get the information on the experimental geometries except for the target thickness in their paper, so we counted the photons with z-components of direction cosine from 0 to 1 in this simulations for 9 days. There are discrepancies between the experimental and the calculated data. It should be noted that the discrepancies may tend to increase at low energy and that this comparison is not strictly valid because of the difference of the geometries between the experimental and the calculated conditions.

4. Summary

We have calculated the energy spectra of bremsstrahlung from 6MV to 50MV for some thick targets using EGS4 Monte Carlo code . This code provided us with a convenient method for calculations of thick-target bremsstrahlung spectra but spent a long computing time. Although we could hardly collect the experimental data with details about the geometry, we tried to compare the results of our calculations with the experimental data. The level of agreements between them varies depending on the experimental conditions and geometries.

References

(1) W. R. Nelson, H. Hirayama and D. W. O. Rogers, SLAC **265** (1985)
(2) L. I. Schiff, Phys. Rev. **83** (1951).
(3) A. S. Penfold and J. E. Leiss, Univ. of Illinois (1958)
(4) A. A. O' Dell, Jr., et al., Nucl. Inst. Meth. **61** (1968)
(5) H. Hirayama and T. Nakamura, Nucl. Sci. Eng. **50** (1973)
(6) L. B. Levy, et al., Med. Phys. **3** (1976)
(7) V. S. Deshmukh and V. N. Bhoraskar, J. Radioanal. Nucl. Chem., Letters **103**(2) (1986)

3.25 Analysis on Neutron Beam Port of Medical Reactor Using JENDL-3 Library

Makoto Sasaki, Jituya Hirota, Satoshi Iwai
Mitsubishi Atomic Power Industries, Inc.
4-1, Shibakouen 2-chome, Minato-ku, Tokyo.

Shigeo Tamao
Mitsubishi Heavy Industries, Ltd.
4-1, Shibakouen 2-chome, Minato-ku, Tokyo.

Keiji Kanda
Kyoto University (KURRI)
Noda, Kumatori-Cho, Sennan-Gun, Osaka.

and

Yutaka Mishima
Kobe University (SINCT)
19-18, Naruko 2-chome, Kita-ku, Kobe-shi.

Abstract

A design study of a medical therapy reactor for "Boron Neutron Capture Therapy (BNCT)" is under way. The facility is to be used exclusively for the treatment of malignant melanoma and other cancers as well as for the further biomedical research. The MTR is fueled with UO_2, cooled and moderated by light water. As the therapeutic and experimental equipment to be provided, thermal and epithermal neutron beam ports are required. In this analysis, parametric survey of composition and arrangement of these neutron beam ports was performed with JSDTDL-100N/40G based on JENDL-3.

1. Introduction

Investigation of the medical therapy reactor for cancer therapy has been carried on since 1988, in cooperation with Mitubishi Heavy Industries, Ltd. and Kobe University. It is intend in this study to survey and investigate the

reactor concepts suitable for and to set up the main specifications of the reactor which is to be exclusively for the treatment of malignant melanoma and other cancers as well as for the further biomedical research.

The comparative study [1] of the core characteristics indicated that the UO_2 fueled core would be feasible for the BNCT reactor because of the higher epithermal neutron flux level, ability to operate without refueling and less excess reactivity requirement.

The main specifications of the core and fuel which have been so far selected [2], [3] are as follows. A cross sectional view of the core is shown in Fig. 1.

Thermal power	2 MW	Fuel enrichment	4 %
Moderator	H_2O	Outer diameter	
Coolant	H_2O	of fuel clad	9.50 mm
Reflector	Bi	Pitch of fuel rod	11.4 mm
Core height	~ 62 cm	Volume ratio of	
Core equivalent		moderator to pellet	~ 1.0
diameter	~ 51 cm	U loading	0.5 t
Fuel	UO_2	Fuel burn-up	~ 5,000 MWd/t

The therapeutic and experimental equipment to be provided is three horizontal beam ports, one vertical beam port and two neutron guide tubes for boron analysis as shown in Table 1. The three horizontal beam ports are a thermal(E_n < 1 eV) and an epithermal(1 eV < E_n < 1 keV) neutron beam ports and an experimantal neutron beam port, respectively. The vertical neutron beam port is changed to the thermal or the epithermal one with a rotational plug. The arrangement of these neutron beam ports is shown in Fig. 2. In this analysis, parametric survey of composition and arrangement of these neutron beam ports.

2. Analysis method

one-dimensional analytical models of the horizontal thermal and the horizontal epithermal neutron beam ports are shown in Fig. 3 and Fig. 4. The filter compositions used in design studies made in Japan and USA were of much help to our one-dimensional models. One-dimensional, neutron 100-group and gammma 40-group, coupled transport calculations were carried out using JSSTDL-100N/40G group cross sections[4] generated from JENDL-3. In these calculations, neutron production reaction by gamma ray in D_2O is considered. Taking into account of the calculated results, the compositions of the thermal

and the epithermal neutron filters were selected and two-dimensional(rz) analytical models were assumed including the collimeters, as shown Fig. 5 and Fig. 6. The two-dimensional neutron transport calculations were carried out using the 21-group cross sections collaped from the 100-group cross sections.

3. Results of Analysis

(1) The fast(E_n > 1 keV) neutron flux increases about 30 times and the epithermal neutron flux increase about 10 times at the outlet of the thermal neutron beam port , because of the neutron production reaction by gamma ray in D_2O region. It is very important to take into account of this effect by gamma ray, in the case of analyzing a model including D_2O.

(2) The thermal neutron flux available at the outlet of the horizontal beam port is 2 x 10^{10} n/cm^2 • s, as shown Fig. 5. The time interval needed for treatment is about 10 minutes, if it is assumed that the therapeutic thermal neutron fluence is 1.2 x 10^{13} n/cm^2.

(3) The epithermal neutron flux available at the outlet of thehorizontal epithermal neutron beam port is 1 x 10^{10} n/ cm^2 • s, as shown Fig. 6. The time interval needed for treatment is about 10 minutes, if it is assumed that the therapeutic epithermal neutron fluence is 0.6 x 10^{13} n/cm^2.

(4) The fast neutron contaminant in the epithermal neutron beam is 10 Gy/h at the horizontal beam port and the fast neutron dose during treatment is less than 2.0 Gy.

(5) The gamma contaminant in the thermal and the epithermal neutron beam during treatment is guessed to be less than about 0.3 Gy by the preliminary one-dimensional calculation.

References

<1> Mishima, M. : "INVESTIGATION OF THE NUCLEAR REACTOR FOR CANCER THERAPY (SINCT-REP-2)", (1989).

<2> Mishima, M. : "INVESTIGATION OF THE NUCLEAR REACTOR FOR CANCER THERAPY(2) (SINCT-REP-4)", (1990).

<3> Sasaki, M., Hirota, J., Tamao, S. et al. : "Design Study of a Reactor Facility for Boron Neutron Capture Therapy (in Japanese)", Preprint of 1990 Fall Mtg. of AESJ, B26, (1990).

<4> Hasegawa, A. : private communication, (1989).

Table 1 Requirement for neutron beam ports of BNCT reactor

Purpose	Position	No. of Facility	Thermal Port	Epithermal Port
Diagnosis and Treatment	Vertical	1 (Plug 1)	+++	-
		(Plug 2)	(+)	+++
	Horizontal	1 (tnermal port)	+++	-
		1 (epithermal port)	(+)	+++
Experiment	Horizontal	1 (filte 1)	+++	+
		(filte 2)	(+)	+++
Neutron guide tube		2	+++	-

(note) +++ : required, + : preferable, - : needless.

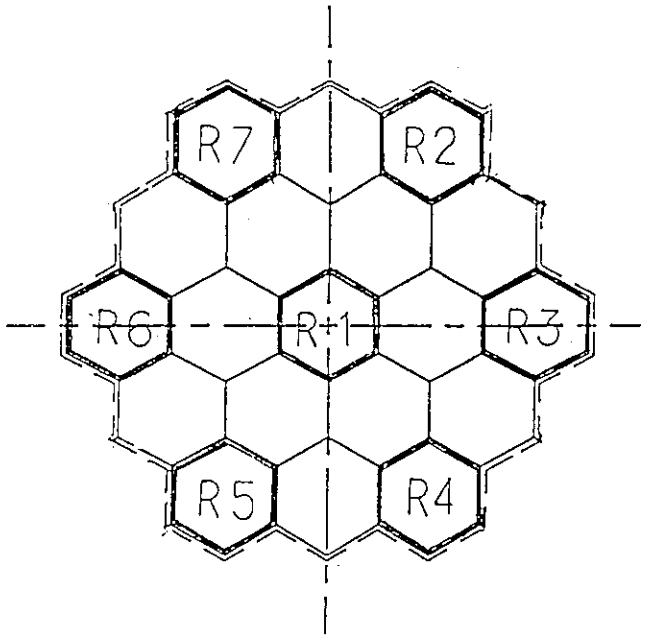

Fig. 1 Cross sectional view of core and control rod arrangement

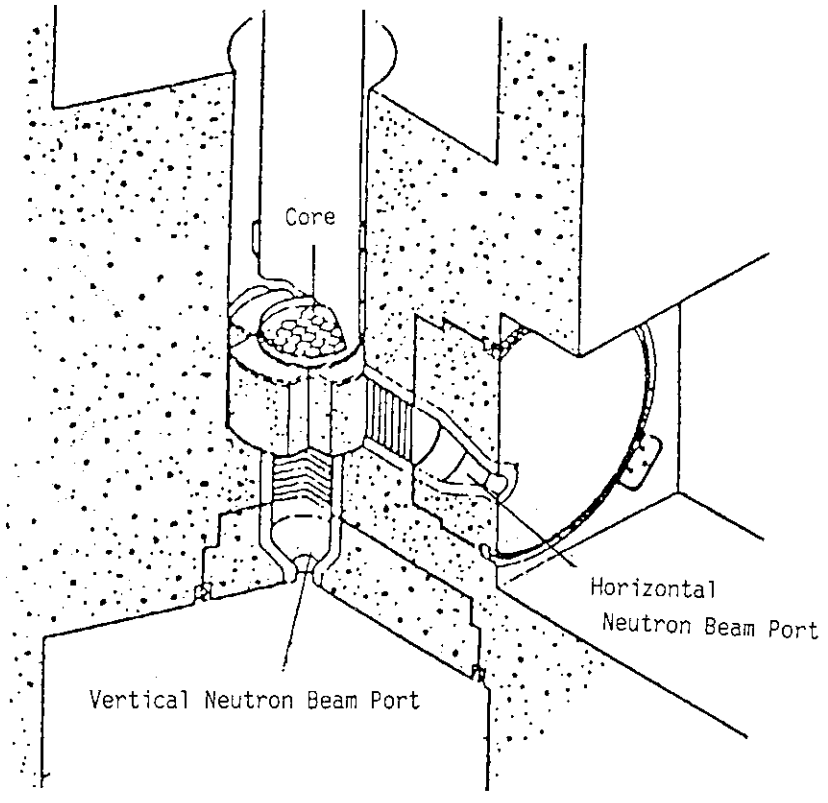

Fig. 2 Cut-away view of core and neutron beam ports

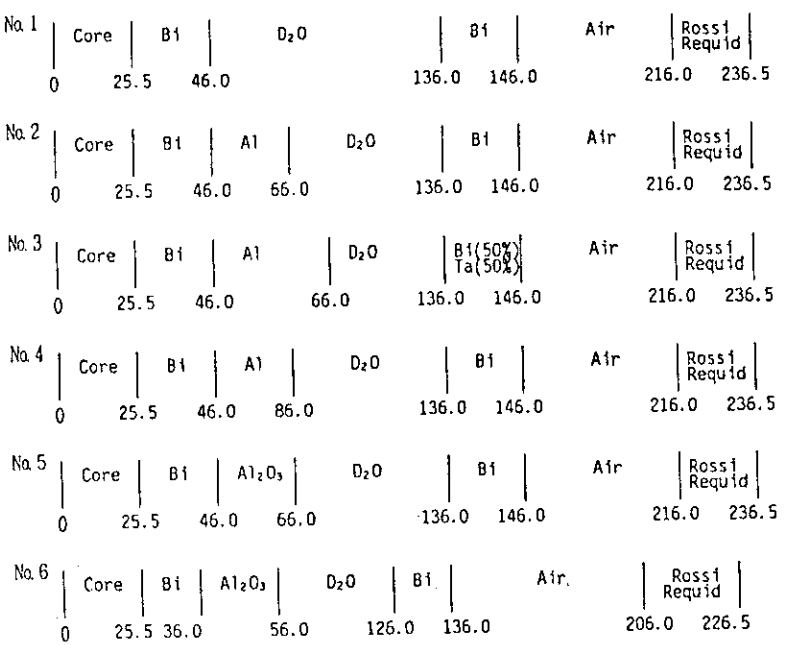

(note) Values mean distance from core center.

Fig. 3 Slab model of horizontal thermal neutron beam port

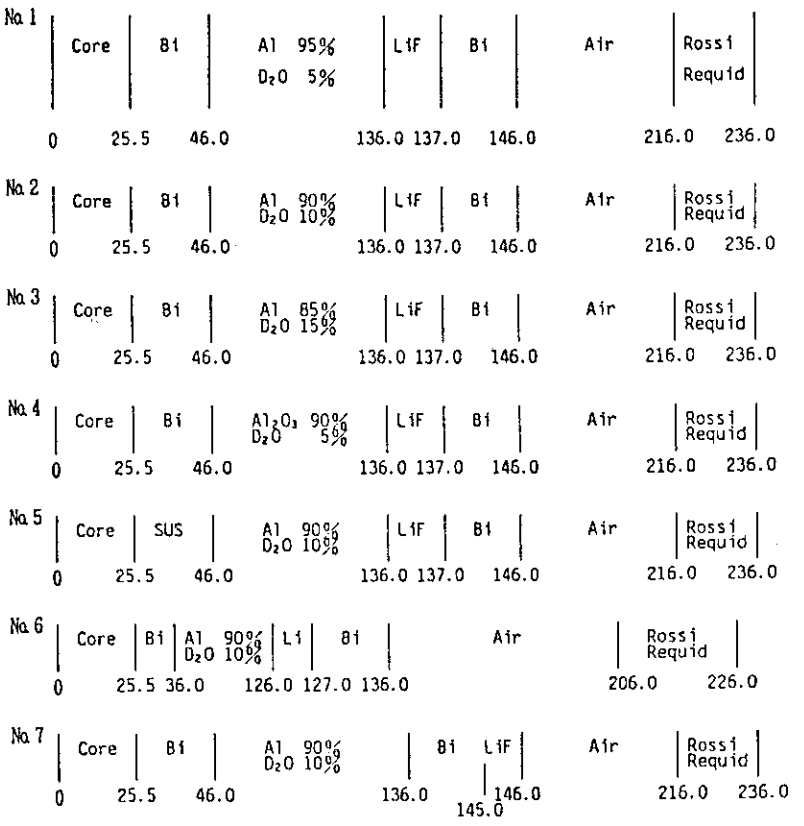

(note) Values mean distance from core center.

Fig. 4 Slab model of horizontal epithermal neutron beam port

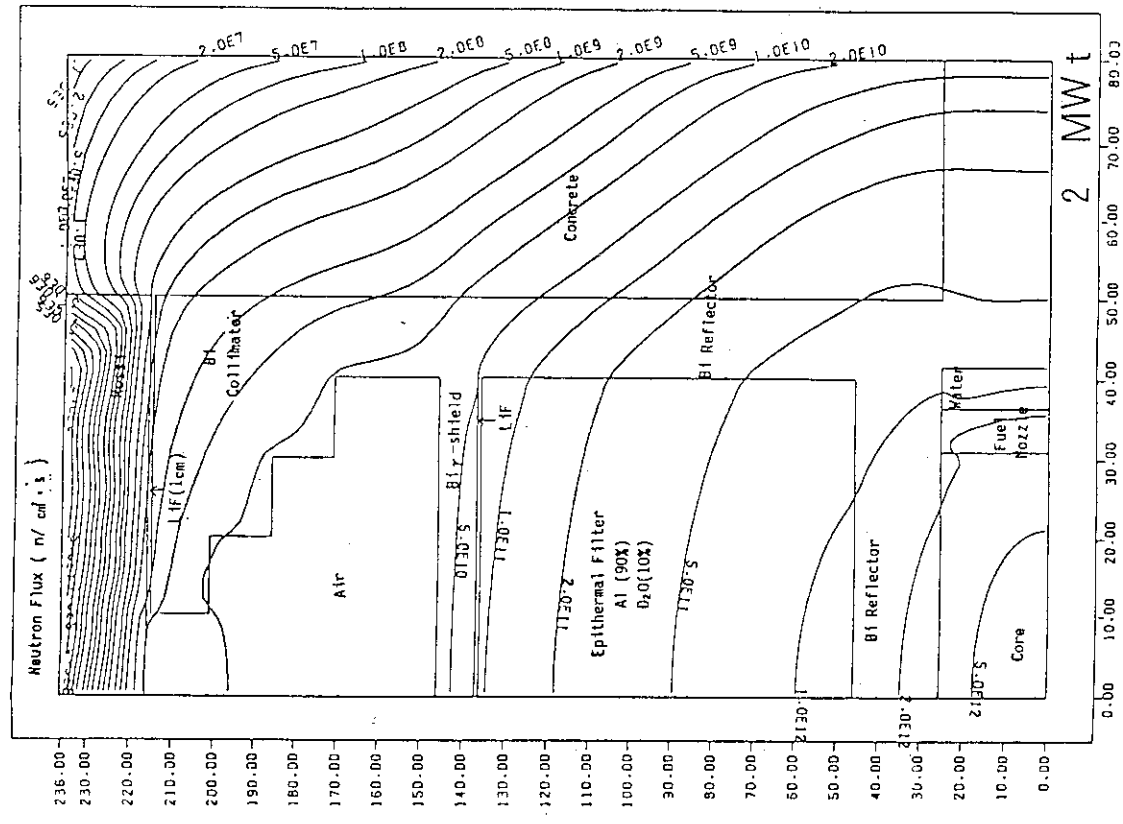

Fig. 6 Contour map of epithermal neutron flux in horizontal epithermal neutron beam port

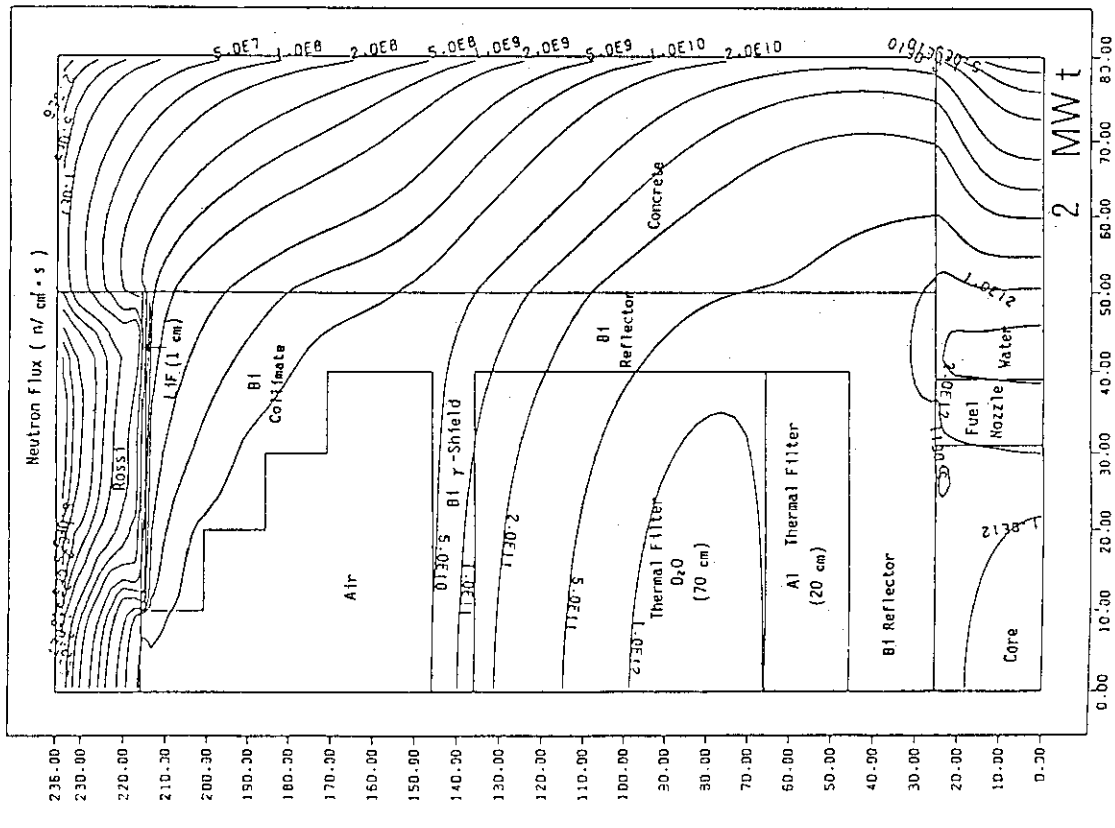

Fig. 5 Contour map of thermal neutron flux in horizontal thermal neutron beam port

3.26 14 MeV Neutron Transport in Thorium Metal Piles

C. ICHIHARA, S. A. HAYASHI, K. KOBAYASHI, and H. NAKAMURA
Research Reactor Institute, Kyoto University
Kumatori-cho, Sennan-gun, Osaka 590-04

S. KANAZAWA, and I. KIMURA
Dept. of Nuclear Eng., Fac. of Eng., Kyoto University
Yoshida-honmachi, Sakyo-ku, Kyoto 606

ABSTRACT

In order to examine the existing nuclear data for thorium, which is one of the most promising material for the fusion-fission hybrid reactors, the reaction rate distribution in the thorium metal piles was measured. The spatial distribution of the $^{197}Au(n,\gamma)$ and $^{27}Al(n,\alpha)$ reaction rates in three types of thorium metal piles was obtained by counting the γ-rays from ^{198}Au and ^{24}Na activities. The measured reaction rates and their distributions were compared with the theoretical calculations using MCNP Monte Carlo code with JENDL-3 and ENDL-75 evaluated nuclear data file. It was proven that the JENDL-3 evaluation gave superior prediction to the ENDL-75 one.

1. Introduction

Fusion reactor is expected as one of the dominant energy resources for the coming century. However, in spite of the rapid development of fusion related technologies in the past few decades, it seems not easy to create commercial fusion reactor plants by early 21st century. Fusion-fission hybrid reactors, which consist of the fusion core surrounded by various kinds of the "hybrid" blanket can take part in the nuclear energy cycle by producing energy and/or the nuclear fuel for both fission and fusion reactors, even before the fusion reactors become economically self-supported[1,2]. Thorium is one of the most promising hybrid blanket materials for breeding nuclear fuel for the fission reactors through $^{232}Th(n,\gamma)^{233}Th$ reactions and successive β-decays.

Several groups have carried out the experiments by combining 14 MeV neutrons and thorium material[3-5]. However, the agreements between experiments and calculations of their works are not always satisfactory. We have been conducting integral experiments to examine the nuclear data of thorium for further design of hybrid blanket designs[6].

The existing nuclear data for thorium differ considerably from each other. Particularly, the continuum part of the inelastic scattering cross sections and $(n,2n)$ cross sections have large difference as shown in **Fig.1**. This results in a large discrepancy of the calculated neutron spectra in the energy range from 0.01 to 10 MeV for the piles used for the present experiment. The **Figure 2** shows the calculated spectra with JENDL-3 and ENDL-75 for the bare thorium pile.

The $^{197}Au(n,\gamma)$ reaction rate in the present thorium piles originates mostly from the neutrons between 0.1 and 10 MeV, where the calculated spectrum is inconsistent. In the case JENDL-3 is used for the calculation, nearly 99% of the reaction rate comes from the neutrons between 0.01 and 1 MeV, and more than 70% between 0.1 and 1 MeV. In the case of ENDL-75, those values are 92%, and 46%, respectively. Also, the total $^{197}Au(n,\gamma)$ reaction rate from each data file differs by about 25 %. Therefore, the difference of each data file can be revealed by measuring the $^{197}Au(n,\gamma)$ reaction rate. In this paper, we describe the experimental results to measure reaction rate distributions of gold and aluminum foils in three kinds of thorium piles and the comparison between the experimented and calculated results. Particular interest is given to the examination of new version of Japanese evaluated nuclear data, JENDL-3[7].

2. Experimental procedure

We formed thorium piles by stacking the natural thorium metal plates, the size of which was 5.08 cm square by 1.27 cm and 0.32 cm thick. The dimension of the thorium pile was 32.8 cm × 25.5 cm × 25.5 cm (Type-I). In addition to this pile, 2 cm thick stainless-steel plates were put in front of the thorium pile (Type-II), and 2.54 cm thick beryllium plates were put in a similar manner (Type-III). A gold foil of about 70 mg was set on the front surface of the thorium section of each pile and four other foils were set 5.5 cm separated each other in the thorium section, except the thorium pile, where only three foils were irradiated. In addition to the gold foils, aluminum foils were irradiated in a similar manner to measure the fast neutron component. The **Figure 3** shows the typical experimental arrangement for the irradiation using Type-II pile. Neutron irradiation was performed with D-T neutrons from the neutron generator[8] at the Kyoto University Critical Assembly (KUCA). The bird-eye view of the neutron generator is shown in **Fig.4**. Typical irradiation time was about 8 hours at the neutron yield of about 10^9 n/sec.

The 411.8 keV γ-rays from the induced activities of ^{198}Au and 1368.6 keV ones from ^{24}Na were measured with a 50 cm^3 pure Ge detector and a 4096 channel multu-

channel analyser. From these γ-ray countings, the reaction rates were deduced after several kinds of corrections required.

3. Calculations

The theoretical calculations of the neutron energy spectra were performed with the three dimensional Monte Carlo continous energy neutron transport code, MCNP[9]. The continuous energy cross section libraries for thorium were taken from FSXLIB[10] processed from JENDL-3 and from ENDL-75[11]. The calclation geometry is taken from the actual size of the piles. The point source with an isotropic neutron distribution was given. Neutron histories were taken as 10^6.

Reaction rates were calculated from the neutron energy spectra and the activation cross section data, taken from ENDF/B-V dosimetry file[12].

4. Results and Discussion

The $^{197}Au(n,\gamma)$ reaction rates for the piles (Type -I to III) are shown in **Fig.5**. The prediction from JENDL-3 data gives a fair agreement with the experiment, while the prediction from ENDL-75 gives slightly higher value for all piles.

a) Type-I (Thorium) pile

In the **Fig.6**, are given the calculated-to-experimented (C/E) values of $^{197}Au(n,\gamma)$ reaction rate for Type-I pile. The prediction from JENDL-3 agrees with the experiment within exmerimental errors, while one from ENDL-75 overestimates by 12 to 30 %. This is because ENDL-75 give much softer spectrum than JENDL-3 as shown in Fig.3 and the $^{197}Au(n,\gamma)$ reaction rate becomes larger as the cross section increases according to lower neutron energy.

b) Type-II (SS + Thorium) pile

JENDL-3 prediction agrees well with the experiment within -4 to +10 %. However, ENDL-75 gives much overestimation by up to 40 % (**Fig.7**). Since the calculated spectra for this pile are not distinctive with the ones for Type-I pile as shown in **Fig.8**, the reason for the overestimation of ENDL-75 is the softer spectrum calculated.

c) Type-III (Be + thorium) pile

The **Figure 9** shows the C/E values for Type-III pile. The JENDL-3 prediction is again in good agreement with the calculation. ENDL-75 prediction overestimates experiments by up to 20 %, which is not so large as for other piles. This is probably because the

spectra from both data file become much softer than those of other piles due to beryllium slowing down effect (**Fig.10**), and consequently the fast neutrons which have more weight for $^{197}Au(n,\gamma)$ reaction rate decrease.

Acknowledgement

The present work has been partially supported by a Grant-in-Aid for Fundamental Research of the Ministry of Education, Government of Japan, and undertaken within the framework of the Visiting Researchers Program at the Research Reactor Instutute, Kyoto University (KURRI). The authors wish to thank the staff of the KUCA for their assistance in the experiment.

References

1) H. A. Bethe : "*The Fusion Hybrid*", Nuclear News, **21**, p.41, (May 1978).
2) E. Greenspan : "*Fusion-Fission Hybrid Reactors*", Advances in Nuclear Science and Technology, Vol. 16, p.289, Plenum Press (1984).
3) L. F. Hansen, *et al.* : Nucl. Sci. Eng., **72**, 35 (1979).
4) V. R. Nargundkar, *et al.* : Fusion Tech., **14**, 354 (1988).
5) A. Kumar, *et al.* : Fusion Tech., **15**, 1430 (1989).
6) I. Kimura (*ed.*) : "*The Fundamental Study of Thorium-Loaded Hybrid Reactor*", Research Result Report of Grant-in-Aid. Ministry of Education, Science and Culture, Japan (May 1990).
7) K. Shibata *et al.* : Japanese Evaluated Nuclear Data Library, Version-3 -JENDL-3-, JAERI 1319, (1990).
8) C. Ichihara, *et al.* : "*Characteristics of KUCA Pulsed Neutron Generator*", KURRI-TR-240 (1983).
9) F. Briesmeister (*ed.*) : MCNP-A General Monte Carlo Code for Neutron and Photon Transport, LA-7396-M, Rev. 2, (1986).
10) K. Kosako et al. : to be published on JAERI-M
11) "*LLNL Evaluated Nuclear Data Library*", UCRL-50400.
12) "*Evaluated Neutron Data File, ENDF/B-V*", ENDF/B Summary Documentation, Compiled by R. Kinsey, ENDF-201, 3rd Ed., BNL (1979)

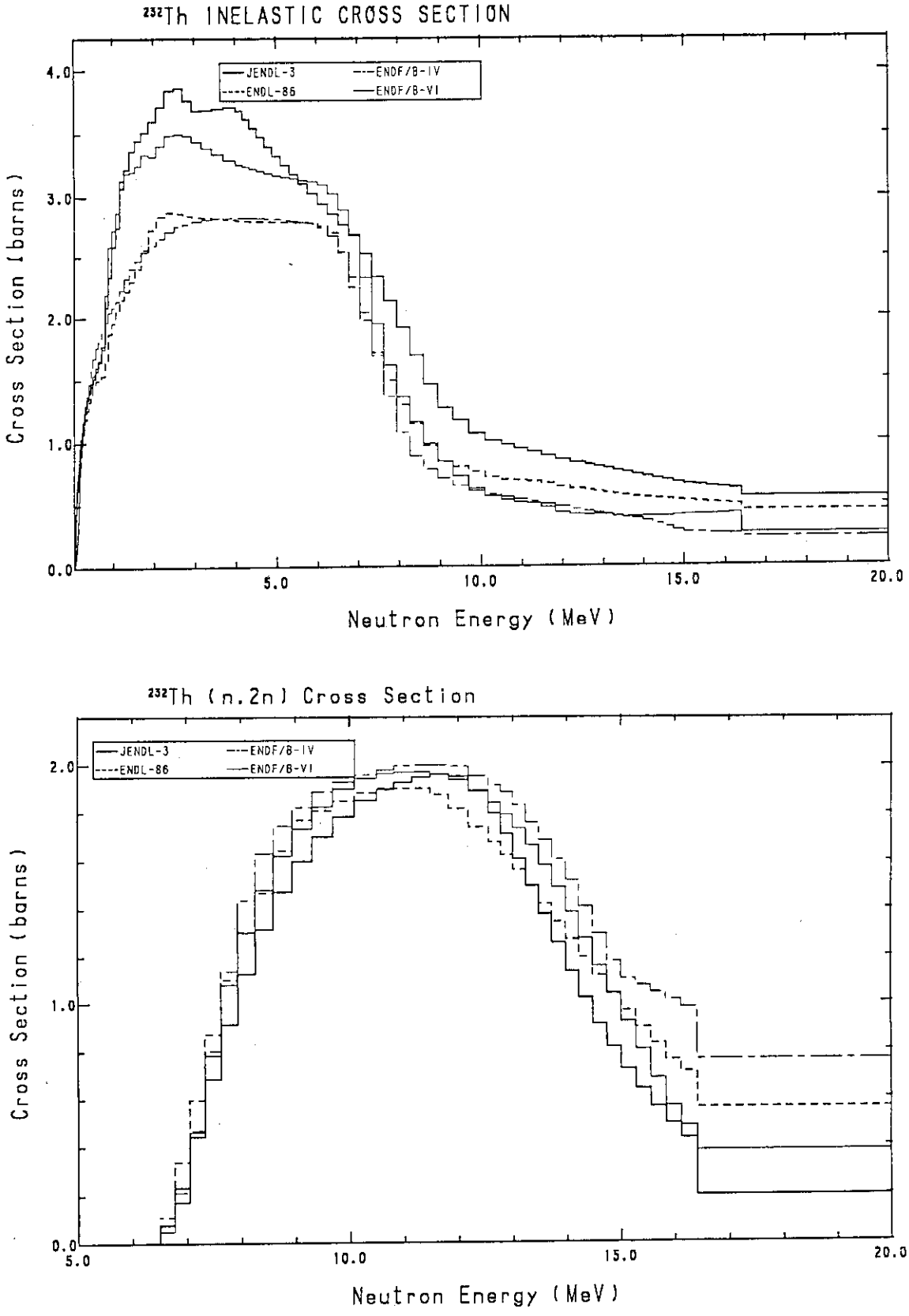

Fig. 1 Inelastic scattering and (n,2n) cross sections in various evaluated nuclear data files.

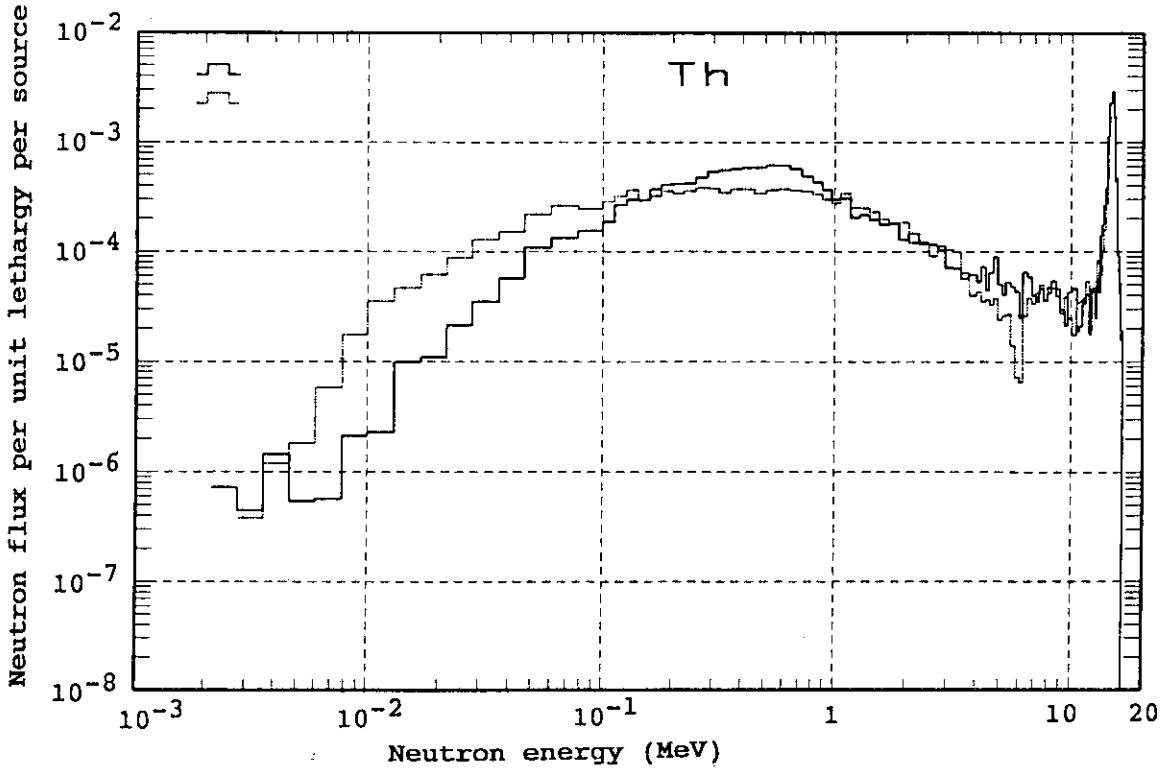

Fig. 2 Calculated spectrum for Type-I (thorium) pile at 11 cm from the front surface.

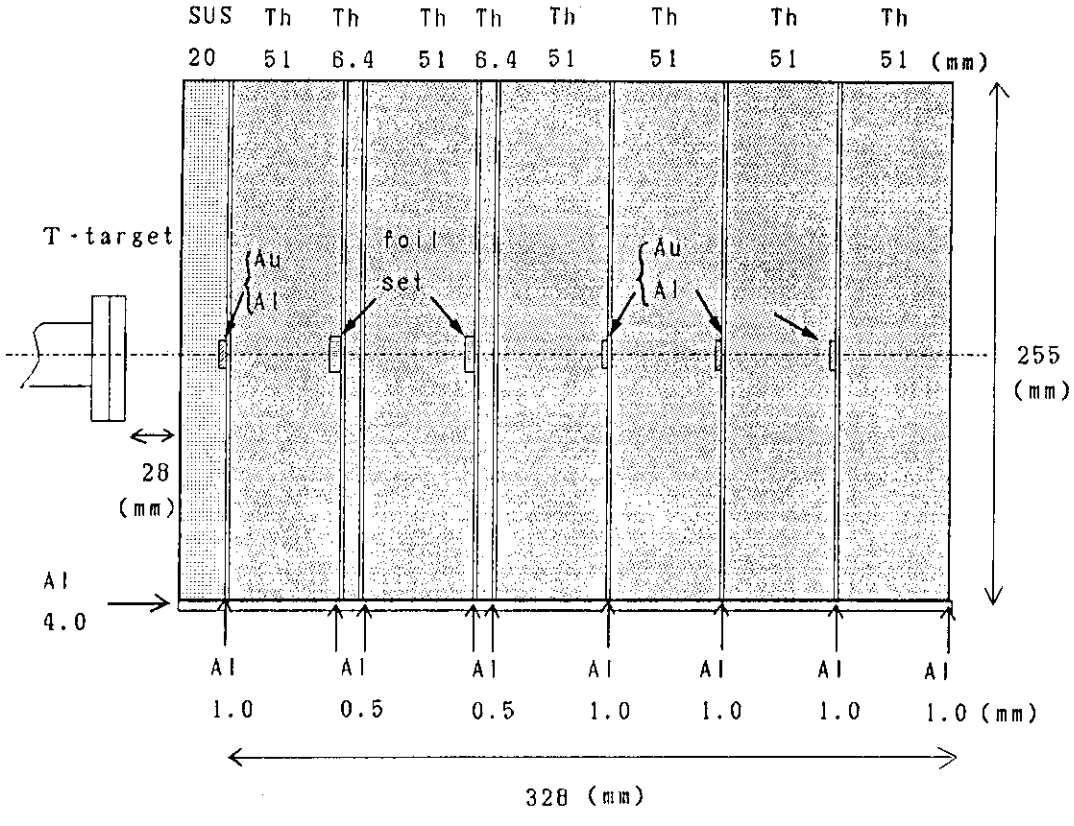

Fig. 3 Experimental arrangement of the Type-II (SS + thorium) pile.

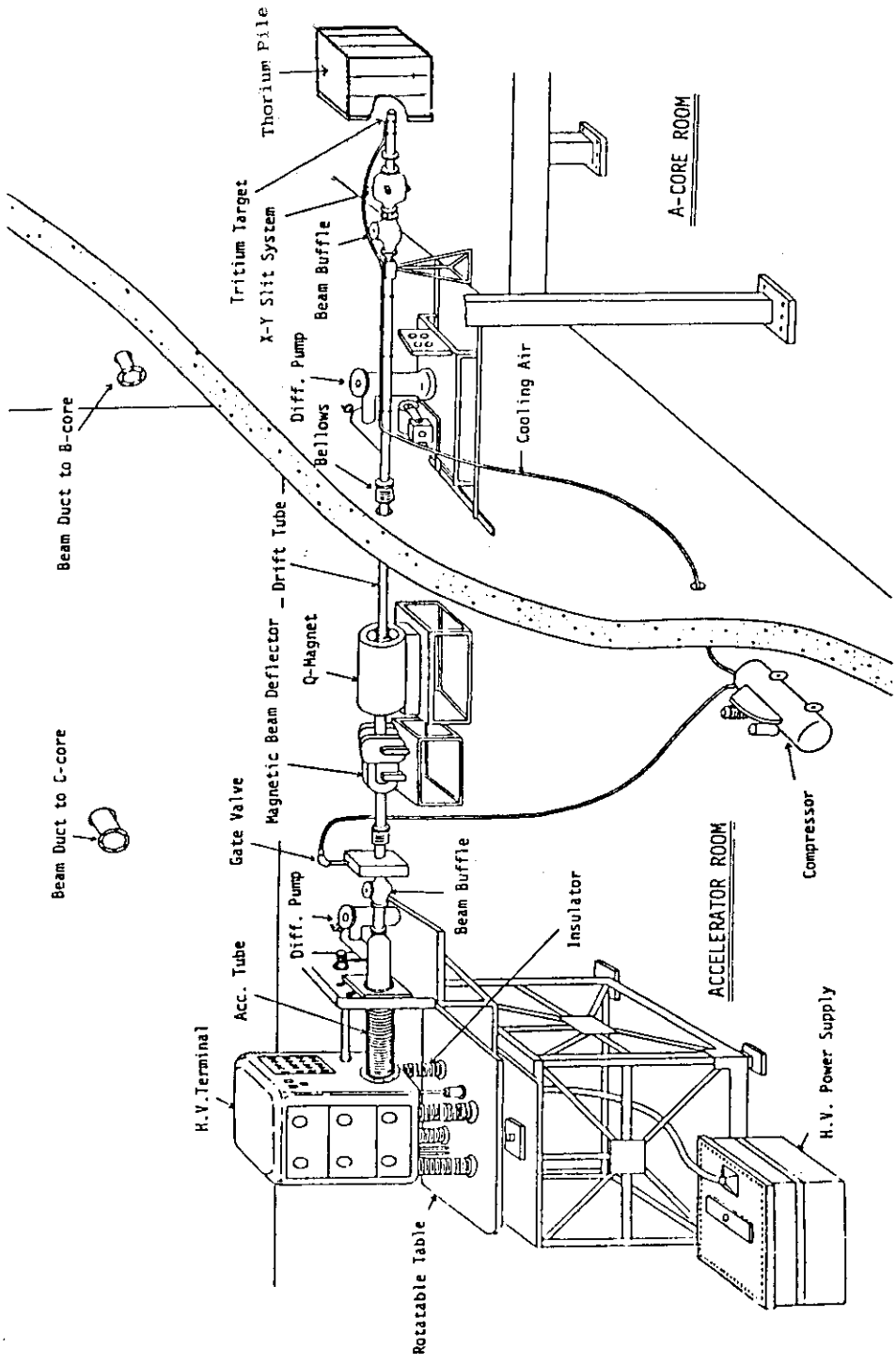

Fig. 4 Bird-eye view of the KUCA accelerator system.

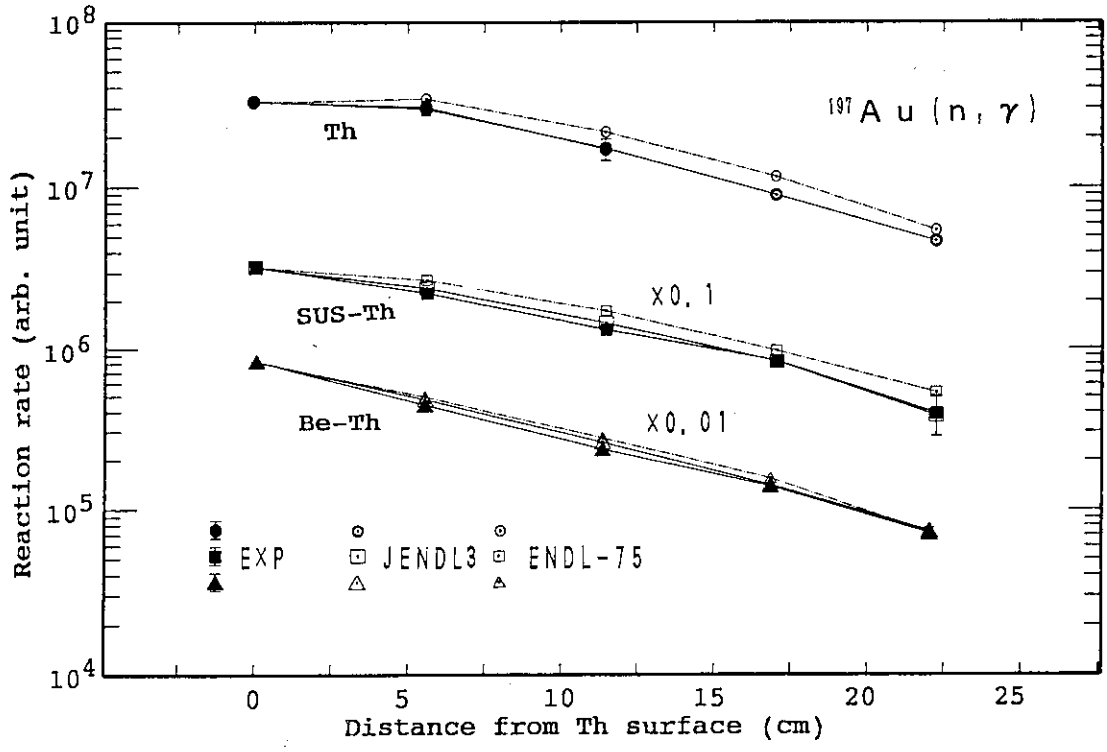

Fig. 5 Measured and calculated ^{197}Au(n,γ) reaction rate distribution for Type-I to III piles (normalized at the front surface of the thorium sections).

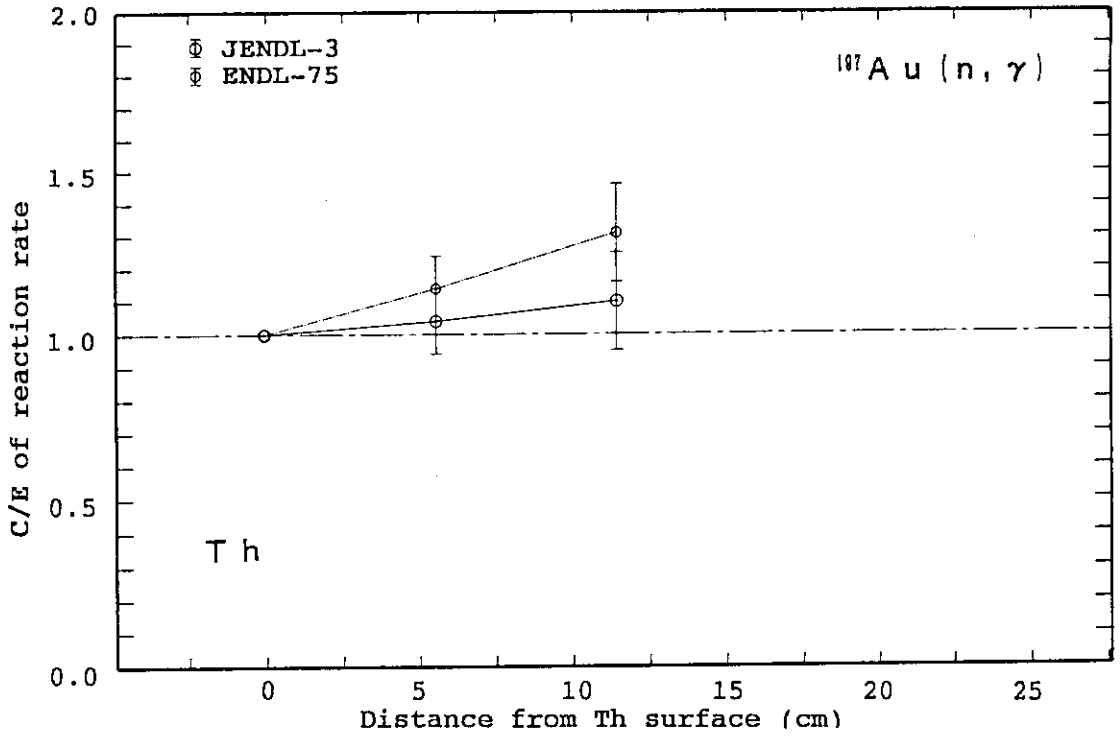

Fig. 6 Calculated-to-Experimented ratios of the ^{197}Au(n,γ) and ^{27}Al(n,α) reaction rates in Type-I pile.

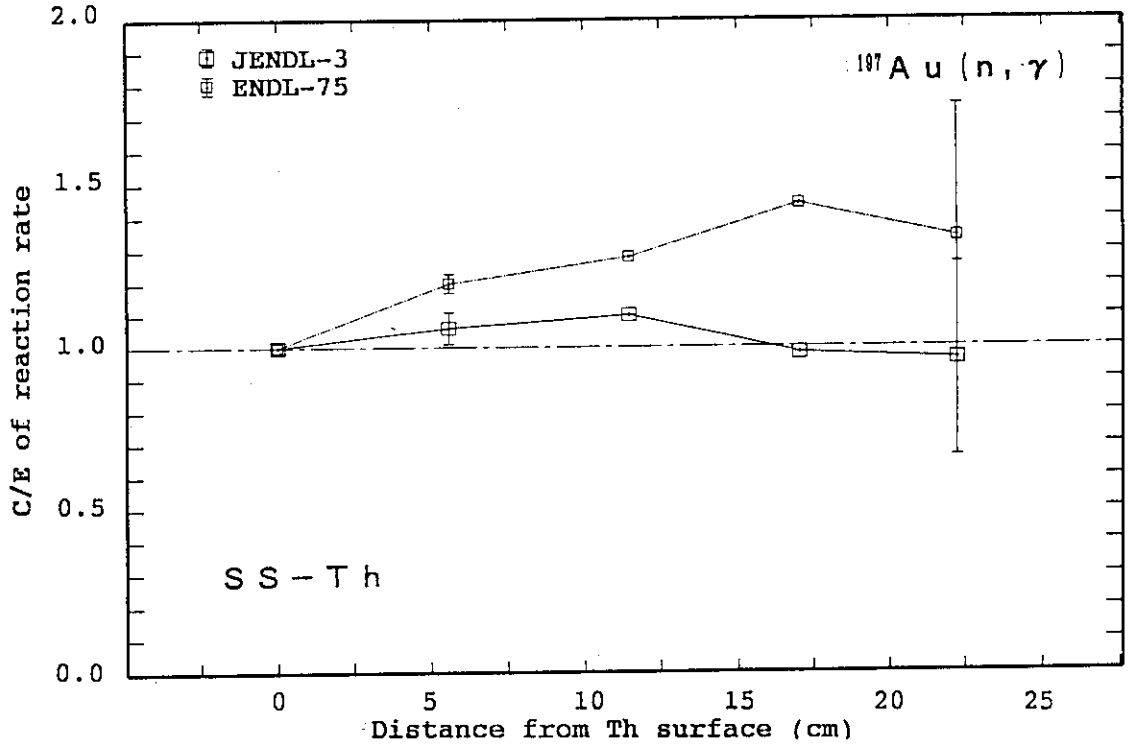

Fig. 7 Calculated-to-experimented ratio (C/E) values for $^{197}An(n,\gamma)$ reaction rates in Type-II pile.

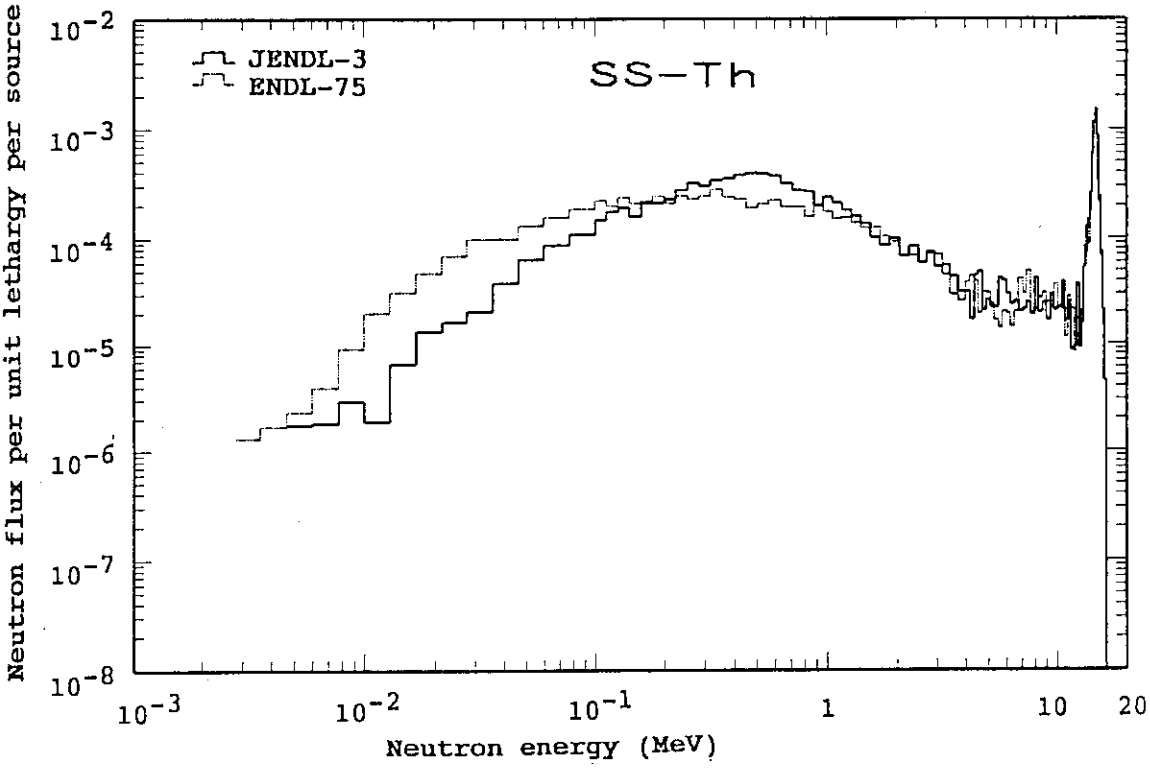

Fig. 8 Calculated spectrum for Type-II pile at 11 cm from thorium surface.

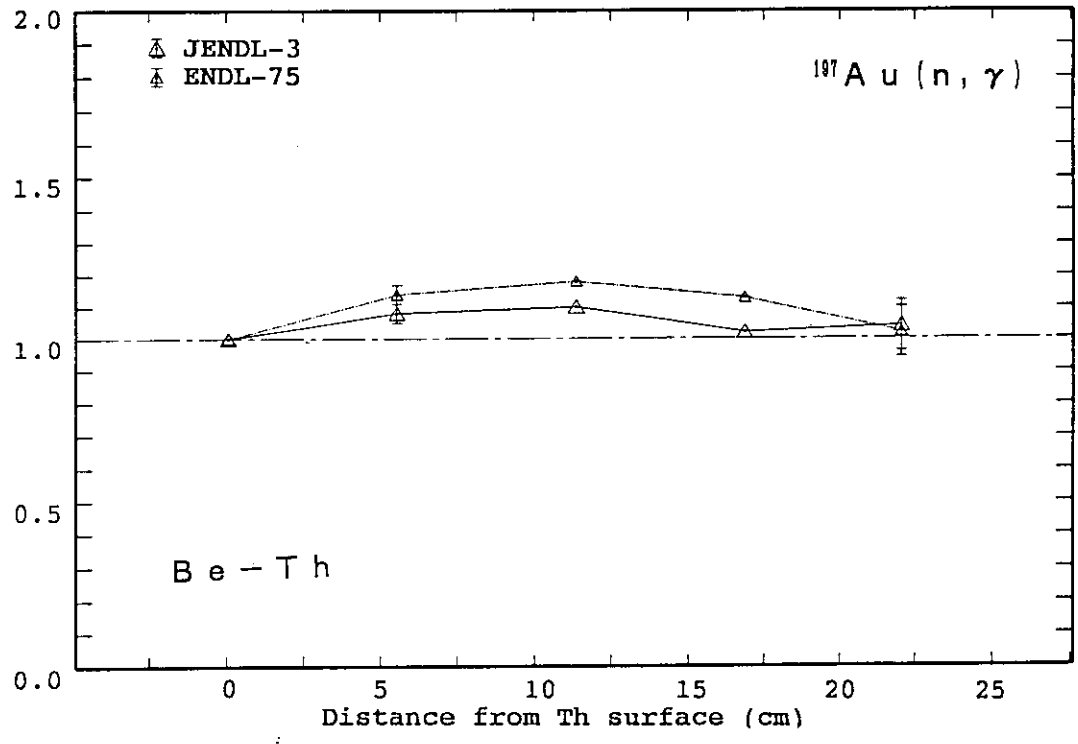

Fig. 9 Calculated-to-experimented ratio (C/E) values for $^{197}Au(n,\gamma)$ reaction rates for Type-III pile.

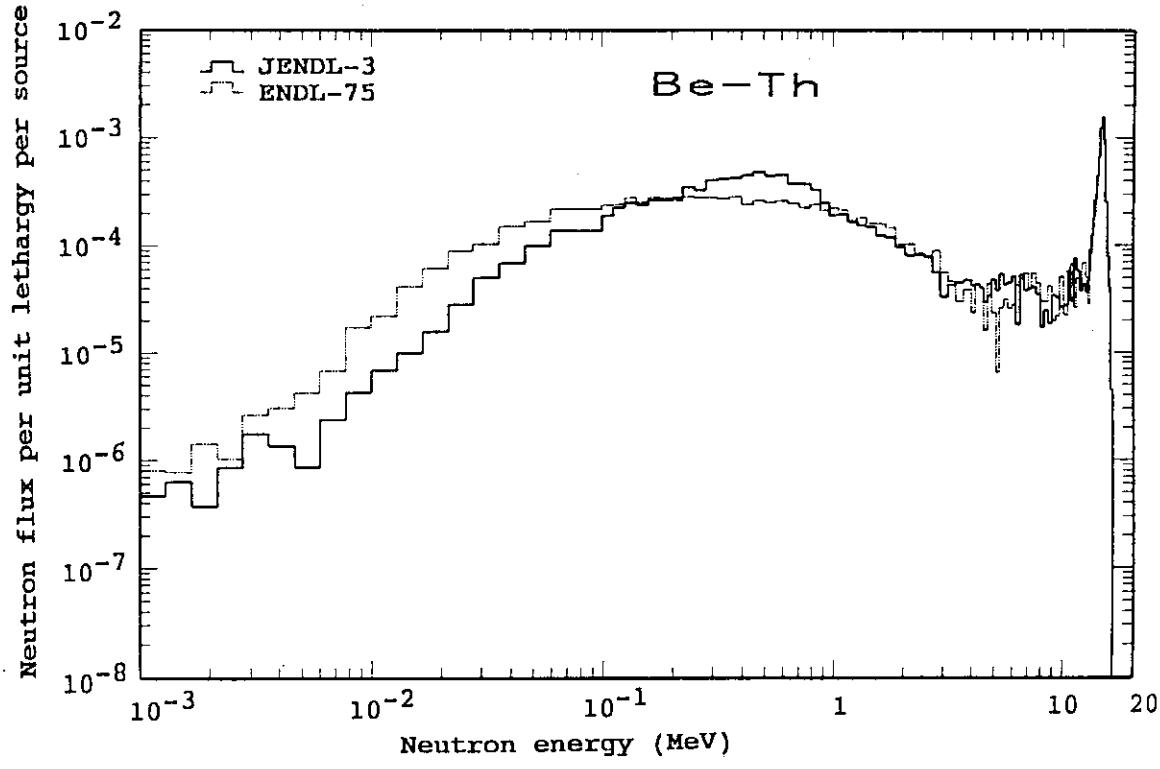

Fig. 10 Calculated spectrum for Type-III pile at 11 cm from thorium surface.

3.27 A Study on Cross-section Adjustment for Large LMFBR Cores

Toshio Sanda
Energy Research Lab., Hitachi, Ltd., Hitachi-shi

Takanobu Kamei
Nuclear Engineering Lab., Toshiba Corp., Kawasaki-shi

Takashi Kawakita
Mitsubishi Atomic Power Industries, Inc., Minato-ku, Tokyo

Masayuki Saito
Century Research Center Corp., Chiba-shi

Osamu Sato
Mitsubishi Research Institute, Chiyoda-ku, Tokyo

Makoto Ishikawa
Power Reactor and Nuclear Fuel Development Corp. (PNC)
Oarai-machi, Ibaraki-ken

Hideyuki Hayashi
The Japan Atomic Power Company (JAPC), Chiyoda-ku, Tokyo

Abstract

The cross-sections obtained from the JFS-3-J2 set were adjusted using C/E (Calculation/Experiment) values of integral physics parameters such as k_{eff}, reaction rate, and control rod worth in the JUPITER program. Remarkable improvement was observed in the C/E values. Furthermore the radial dependencies of C/E values of reaction rate distribution and control rod worth were significantly reduced, which is expected to be effective in improving prediction accuracy of core design parameters. The adjusted cross-sections were compared with the JENDL-3 library, as well as measured data, and it was found that the adjusted values were reasonable.

1. Introduction

In the core design of a large liquid metal fast breeder reactor (LMFBR), it is required to reduce the uncertainties for core design parameters. Critical experiments on large LMFBR cores were analyzed by a detailed neutronic analysis method, using a group constant set (JFS-3-J2)[1] based on the JENDL-2 library[2]. The C/E values for reaction rate distribution and control rod worth had tendencies to become higher gradually at farther distances from the core center[3] as shown in Figs. 1 and 2. Furthermore the C/E values of other physics parameters differed from unity. These gave difficulties in satisfying the required prediction accuracy in a large LMFBR core design. Cross-section adjustment for large LMFBR cores was studied as a possible effective means for improving prediction accuracy of core design parameters.

2. Cross-section adjustment method

Using Bayes theory, the adjusted cross-sections T and their covariance matrices M are expressed by [4]

$$T = T_0 + MG^t V^{-1} (R_e - R_c(T_0)) \quad (1)$$

$$M = (M_0^{-1} + G^t V^{-1} G)^{-1}, \quad (2)$$

where

T_0 = the cross-sections before adjustment

M_0 = covariance matrices of T_0

G = sensitivity coefficients of physics parameters

V = variances of experiment analysis values

R_e = measured physics parameters

$R_c(T_0)$ = physics parameters calculated using T_0

The variances of $R_c(T)$ due to the cross-section errors are expressed by $V_C = G\,M\,G^t$.

In this study, sensitivity coefficients were calculated by the generalized perturbation theory code SAGEP[5], and the adjusted cross-sections were obtained by the ABLE code[6] using Eqs. (1) and (2). Adjustment routines for inelastic scattering cross-sections and fission spectrum were added to the original ABLE code.

The 18 group cross-sections obtained from the JFS-3-J2 set were adjusted using C/E values for k_{eff}, reaction rate ratio, reaction rate distribution, control rod worth, and Na void worth from ZPPR-9, -10C, -17A, and -19B assemblies in the JUPITER program.[7] ZPPR-9,

-10C, and -19B are 600, 800, and 1000MWe size homogeneous cores, respectively. ZPPR-17A is a 650 MWe size axially heterogeneous core. Table 1 shows physics parameters and their uncertainties of experiment and analysis values to be used in the adjustment. Fission(f), capture(c), elastic(el), and inelastic(inel) cross-sections, ν and μ were adjusted for the main nuclides shown in Table 2. In addition to the individual cross-sections, the fission spectrum for ^{239}Pu and effective delayed neutron fraction β_{eff} were also adjusted. The fission spectrum was not given by the Maxwell distribution used in JENDL-2, but was adjusted for each energy group. As for the covariance matrices of the cross-sections, values from the COVERX file prepared by Drischler et al.[8] were mainly used, with others being provided by the Nuclear Data Center, JAERI as described in Table 2. Uncertainty of β_{eff} was evaluated as 4%, and that of the fission spectrum was evaluated by referring to the differences between the JENDL-2 and -3 libraries.

3. Adjustment results and discussion

Sensitivity coefficients were calculated before the adjustment. The following characteristics were found:

(1) Sensitivities are generally high for cross-sections of ^{239}Pu, ^{238}U, O, Fe, and Na, which are abundantly loaded in a core as shown in Fig. 3.

(2) Reduction of ^{238}U(n, γ) cross-section for 1-100 keV neutron energies is effective for reducing C/E radial dependency as shown in Figs. 4 and 5. The reduction of O, Fe, and Na elastic scattering cross-sections for 50-500 keV energies is also effective.

(3) Sensitivities of the Na void worth are high for ^{238}U(n, γ) and ^{239}Pu(n, f) cross-sections in the region of a few keV neutron energies, which corresponds to the resonance region of the Na(n, γ) reaction.

(4) Sensitivities of the ^{235}U cross-sections are high in ZPPR-19B because ^{235}U fuels are abundantly loaded in the core.

The cross-section adjustment was employed for a reference case and some test cases. As a reference case, 45 integral data for ZPPR-9, -17A, and -19B assemblies were selected. In the test cases, different data from the reference case were used in order to evaluate the effect of the data used in the adjustment. Table 3 shows C/E values before and after the adjustment in ZPPR-9. Remarkable

improvement was observed in C/E values of k_{eff}, C28/F49, reaction rate distribution, and control rod worth. In this table, GMG^t and $GM'G^t$ mean the uncertainties of physics parameters due to cross-section errors before and after the adjustment. These uncertainties were reduced remarkably. Figures 6 and 7 show C/E values of ^{239}Pu fission rate distribution and control rod worth, respectively. From these figures the C/E radial dependencies were found to be reduced after the adjustment remarkably. Table 4 shows the relative changes of cross-sections before and after the adjustment. The ^{239}Pu fission cross-section was decreased by 0.5-1.8% above 10keV and increased by 1.5-3.5% below 1 keV. The ^{238}U capture cross-section was increased by 2-8% above 2MeV and decreased by 5-9% below 40keV. The ^{238}U inelastic cross-section was decreased by 2-6% in the 400keV-2MeV range. The ^{235}U fission cross-section was decreased by 0.7-5% for all energies. β_{eff} was decreased by 1.3% and the fission spectrum changed slightly.

The adjusted cross-sections were compared with the JENDL-2, and -3 libraries, as well as measured data. The ^{239}Pu fission, ^{235}U fission, and ^{238}U capture cross-sections are shown in Figs. 8-10, respectively. Some adjusted cross-sections did not always approach values in the JENDL-3 library, but on the whole the adjusted cross-sections fell between the JENDL-2 and -3 libraries, and it was found that adjusted values were reasonable cross-sections.

In order to evaluate the applicability of the adjusted cross-sections, the FBR benchmark tests were performed for 21 international benchmark cores. Figures 11, 12, and 13 compare C/E values of k_{eff}, C8/F5, and F9/F5, respectively. The C/E values were satisfactory for intermediate and large scale cores with above 500 liter volumes. For uranium cores and small scale cores, they significently underestimated k_{eff}. The C/E values of the reaction rate ratios were improved slightly in comparison with JENDL-2 and -3 for intermediate and large scale cores. These results show the adjusted cross-sections are applicable to intermediate and large scale cores, though large assemblies with 4600-8500 liter core volumes were used in the adjustment.

Next, the results of the test cases were described in comparison with the reference case. Table 5 shows the relative cross-section changes before and after the adjustment for the reference case and

some cases using different data from the reference. In case 1, the elements of the covariance matrices of the cross-section were set to one half of the reference ones. In case 2, the non-diagonal elements of covariance matrices were set to zero. In case 3, uncertainties of experiment and analysis values were set to one half of the reference ones. Though C/E values after the adjustment improved for every case, the cross-section changes were considerably different, especially for ^{238}U capture. These results show that the adjusted cross-sections are very sensitive to the choice of the covariance matrices to be used in the adjustment, though C/E values are not sensitive. Other test cases with different integral data show that if only a few integral data are used, the adjusted cross-sections differ considerably, though the C/E values of the integral data approach unity. Therefore, it is desirable to employ various kinds of integral data in the adjustment.

4. Conclusion

Cross-section adjustment for large LMFBR cores was employed, which is expected to be effective in improving prediction accuracy of core design parameters. The 18 group cross-sections obtained from the JFS-3-J2 set were adjusted using integral data such as k_{eff}, reaction rate ratio, reaction rate distribution, and control rod worth from ZPPR-9, -17A, and -19B assemblies in the JUPITER program.

The main results from the adjustment were as follows.

(1) Remarkable improvement was observed in C/E values of k_{eff}, C28/F49, reaction rate distribution, and control rod worth. The uncertainties of the above parameters due to cross-section errors were also reduced.

(2) The radial dependencies of C/E values of reaction rate distribution and control rod worth were reduced remarkably; from 5 to 1% for reaction rate distribution and from 10 to 2% for control rod worth.

(3) The adjusted cross-sections are very sensitive to the choice of the covariance matrices to be used in the adjustment. Then it is desirable to employ various kinds of integral data in the cross-section adjustment.

(4) The adjusted cross-sections were compared with the JENDL-3 library, as well as measured data, and it was found that adjusted

values were reasonable cross-sections.

These are the results of the first year in our three year study. Based on the above results, we intend to revise the data used in the adjustment. This study is continuing regarding the following items.

(1) Improvement of the cross-section adjustment method.
(2) Revision of the covariance matrices of the cross-sections.
(3) Extension of experimental analysis data.
(4) Evaluation of the applicability of the adjusted cross-sections by benchmark data testing.
(5) Evaluation of the influence of the adjusted cross-sections on nuclear characteristics of large LMFBR cores.

Acknowledgments

The authors would like to thank T. Takeda (Osaka University) for providing the SAGEP and ABLE codes, Y. Kikuchi and T. Nakagawa (JAERI) for evaluating some covariance matrices of the cross-sections and comparing the adjusted cross-sections with the JENDL-3 library, and H. Takano (JAERI) for performing the benchmark tests. Acknowledgments are also due to K. Shirakata (PNC), T. Ikegami (JAPC) and any other members of the cross-section adjustment working group for their helpful discussions.

This paper is based on the results of the cooperative research between PNC and JAPC. (JAPC performed the work under the auspices of nine utilities and Electric Power Development Co., Ltd.)

References

(1) H. Takano, et al. : JAERI-M 89-141 (1989) (in Japanese)
(2) Y. Kikuchi, et al. : J. Nucl. Sci. Technol., 22 [8], 593 (1985)
(3) T. Kamei, et al. : J. Nucl. Sci. Technol., 22 [22], 1025 (1985)
(4) T. Takeda, et al. : Nucl. Sci. Eng., 103, 157 (1989)
(5) A. Hara, et al. : JAERI-M 84-027 (1984) (in Japanese)
(6) T. Takeda, Private Communication (1989)
(7) T. Sanda, et al. : J. At. Energy Soc. Japan, 31 [12], 1324 (1989) (in Japanese)
(8) J. D. Drischler, et al. : ORNL-5318 (1977)

Table 1 Uncertainties of experiment and analysis values used in adjustment

Physics Parameter	Uncertainties (%)	
	Experiment	Analysis
k_{eff}	0.04	0.2
Control Rod Worth		
Absolute Value	1.2	5.0
Relative Value	0.6	2.0
Reaction Rate Distribution*		
F9, F5, C8	1.0 (1.0-1.3)**	2.0 (4.0)
F8	2.5 (4.0-10.0)	3.0 (6.0)
Reaction Rate Ratio		
F5/F9, C8/F9	2.2	2.0
F8/F9	2.5	3.0
Na Void Worth	2.0	10.0

* F9 : ^{239}Pu fission rate, F5 : ^{235}U fission rate
C8 : ^{238}U capture rate

** Figures in parentheses were used for blanket.

Table 2 Adjustment cross-sections and their Covariance matrices

Nuclide	el	inel	f	c	ν	μ
^{235}U	–	◎	◎	○	◎	–
^{238}U	●	●	◎	○	◎	●
^{239}Pu	–	◎	◎	○	◎	●
^{240}Pu	–	–	–	○	◎	–
^{241}Pu	–	–	○	○	◎	–
^{12}C	–	–	–	○	–	–
^{16}O	◎	△	–	–	–	●
^{23}Na	○	–	–	○	–	●
Fe	○	–	–	○	–	●
Cr	–	–	–	–	–	●
Ni	–	–	–	–	–	●

△ :Only diagonal elements
◎ :Including correlations among other nuclides and reactions
○● :Including correlations among other energy groups (●:JAERI)

Table 3 Summary of C/E values and the uncertainties before and after adjustment in ZPPR-9

Physics Parameter	C/E		Uncertainty (1σ, %)	
	Before	After	GMG*	GM'G*
k_{eff}	0.997	1.000	3.4	0.2
F25/F49	1.02	1.01	2.8	1.4
C28/F49	1.05	1.02	7.1	1.6
F28/F49	0.97	0.97	17.7	2.3
F49 Distribution				
(IC, Outer)	1.03	0.99	4.1	0.6
(OC, Center)	1.05	1.00	5.0	0.8
CR Worth				
(Center)	0.92	1.02	5.9	3.2
(Ring 2)	0.99	1.02	6.2	2.9
Na Void Worth				
(Core Center)	1.28	1.15	19.2	6.1

Table 4 Cross-section changes due to adjustment in reference case (%)

Group No.	Upper Energy	Fission Spectrum	^{235}U Fission	^{238}U Inelastic	^{238}U Capture	^{239}Pu Fission
1	10.0MeV	0.0	-0.7	-3.0	8.4	-0.5
2	6.1	0.1	-0.7	0.3	7.7	-0.6
3	3.7	0.2	-1.1	-1.9	3.9	-0.9
4	2.2	0.0	-0.9	-6.4	2.5	-0.8
5	1.4	-0.2	-1.3	-4.5	0.4	-1.1
6	821keV	-0.2	-2.2	-2.8	1.0	-1.8
7	388	-0.5	-1.6	-2.5	1.2	-1.6
8	183	-0.4	-1.4	-1.4	-1.0	-1.1
9	87	-0.3	-1.1	-0.4	-1.5	-0.8
10	41	-0.1	-0.9	0.0	-5.2	-1.1
11	19	-0.1	-1.1	0.0	-6.9	-1.6
12	9.1	0.0	-4.7	0.0	-5.3	0.4
13	4.3	0.0	-4.9	0.0	-5.6	0.3
14	2.0	0.0	-4.5	0.0	-9.2	0.4
15	961eV	0.0	-2.4	0.0	-7.5	1.6
16	454	0.0	-2.1	0.0	-7.2	2.1
17	214	0.0	-2.1	0.0	-4.0	2.3
18	101	0.0	-0.1	0.0	0.0	3.4

Table 5 Comparison of cross-section changes due to several adjustments with different data from reference case

Group No.	^{239}Pu Fission				^{235}U Capture			
	Reference	Case 1	Case 2	Case 3	Reference	Case 1	Case 2	Case 3
1	-0.5	-0.3	-0.3	-0.4	8.4	1.7	0.1	15.0
2	-0.6	-0.5	-0.5	-0.4	7.7	3.5	0.3	10.5
3	-0.9	-0.8	-1.2	-0.5	3.9	1.9	0.5	5.0
4	-0.8	-0.7	-0.7	-0.4	2,5	0.7	0.3	4.2
5	-1.1	-0.9	-0.5	-0.7	0.4	-1.4	2.0	3.5
6	-1.8	-1.3	-1.7	-1.6	1.0	-0.5	3.2	3.0
7	-1.6	-1.1	-1.1	-1.3	1.2	-0.1	1.0	2.2
8	-1.1	-0.8	-1.0	-0.8	-0.1	-0.5	-0.1	-0.1
9	-0.8	-0.6	-0.9	-0.5	-1.5	-1.1	0.0	-1.8
10	-1.1	-0.8	-0.7	-0.9	-5.2	-3.5	-2.6	-7.0
11	-1.6	-1.2	-0.7	-1.6	-6.9	-4.6	-6.5	-8.9
12	0.4	0.0	-1.3	0.1	-5.3	-3.8	-3.2	-5.2
13	0.3	-0.1	-1.0	-0.1	-5.6	-3.9	1.0	-5.3
14	0.4	0.1	-2.2	-0.1	-9.2	-5.7	-10.1	-11.1
15	1.6	0.9	-0.1	1.7	-7.5	-4.5	-5.3	-9.2
16	2.0	1.2	-0.1	2.5	-7.2	-4.4	-3.2	-8.3
17	2.3	1.3	-0.1	2.8	-4.0	-2.4	-0.5	-4.6
18	3.4	2.1	0.2	4.4	0.0	0.0	0.0	0.0

Case 1 : The elements of covariance matrices of cross-sections were set to one half of the reference ones.

Case 2 : The non-diagonal elements of covariance matrices were set to zero.

Case 3 : Uncertainties of experiment and analysis values were set to one half of the reference ones.

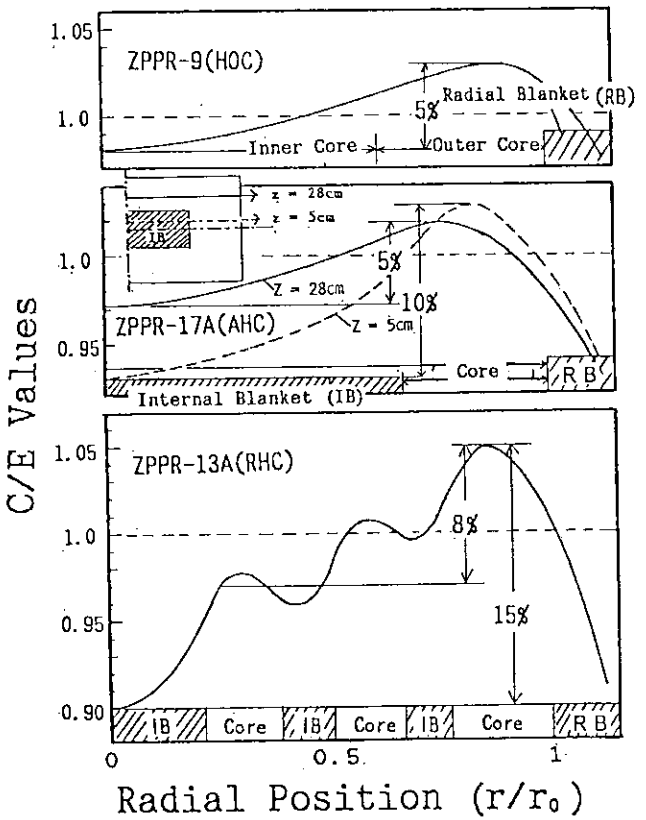

Fig. 1 C/E values of ^{239}Pu fission rate distribution in ZPPR-9, -13A and -17A

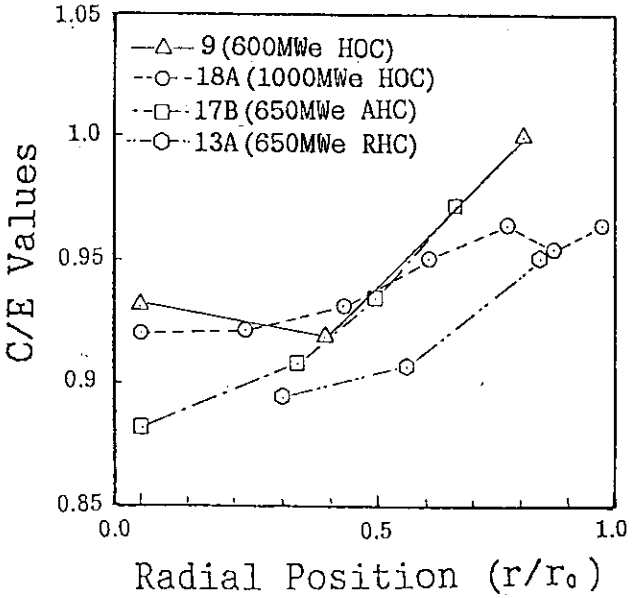

Fig. 2 C/E values of control rod worths in ZPPR-9, -13A, -17B and -18A

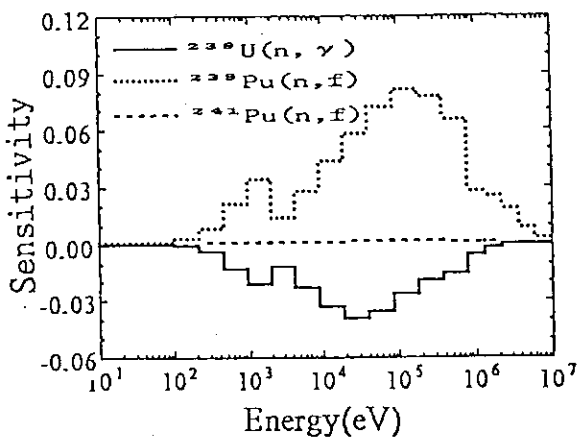

Fig. 3 Sensitivity coefficients of k_{eff}

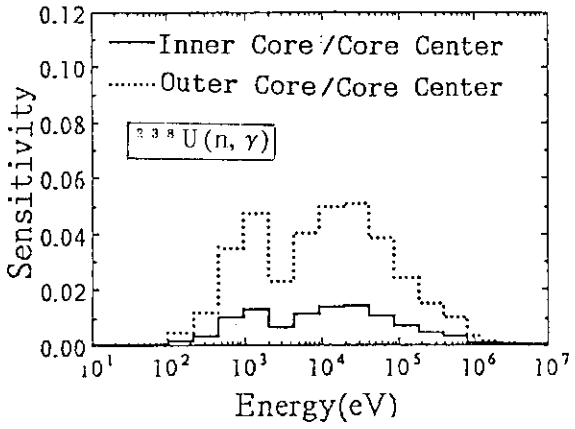

Fig. 4 Sensitivity coefficients of ^{239}Pu fission rate distribution

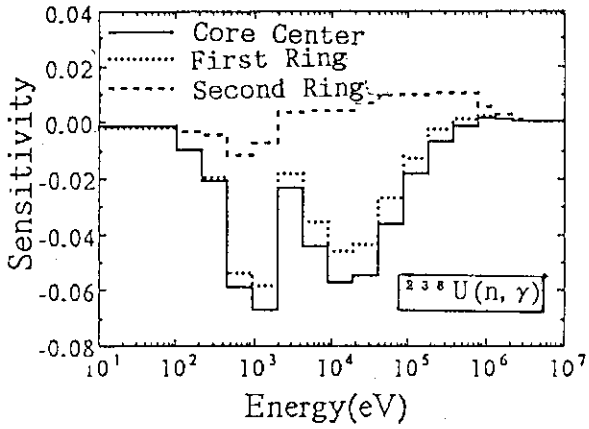

Fig. 5 Sensitivity coefficients of control rod worths

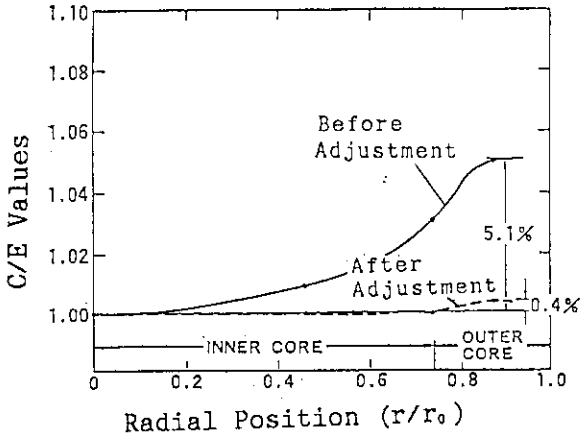

Fig. 6 C/E values of ^{239}Pu fission rate distribution in ZPPR-9

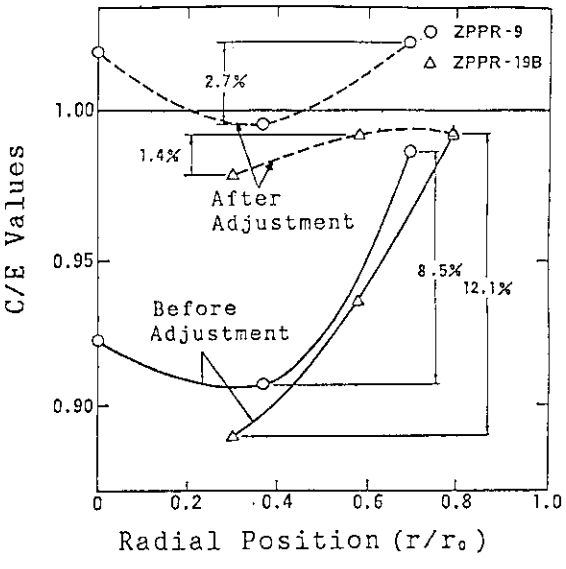

Fig. 7 C/E values of control rod worths in ZPPR-9 and -19B

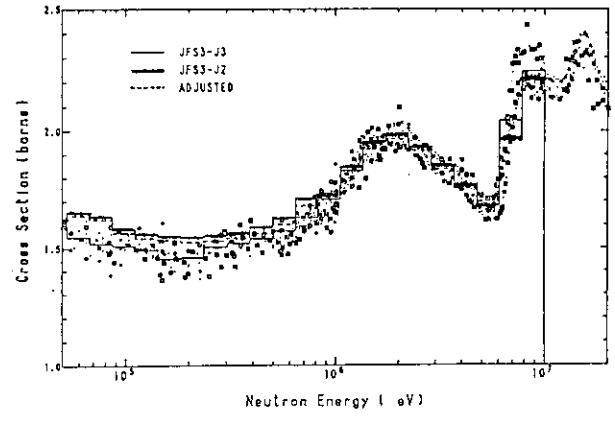

Fig. 8 Comparison of ^{239}Pu fission cross-sections

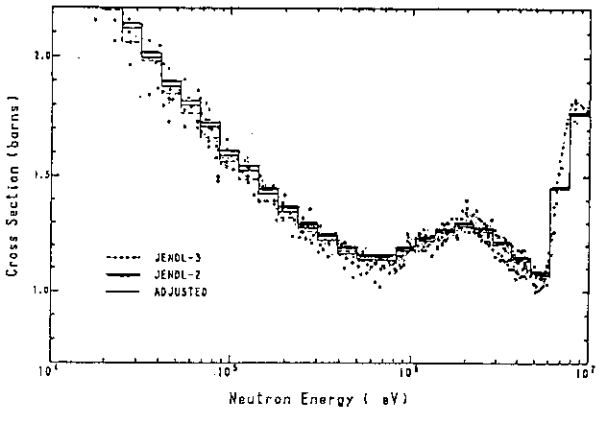

Fig. 9 Comparison of ^{235}U fission cross-sections

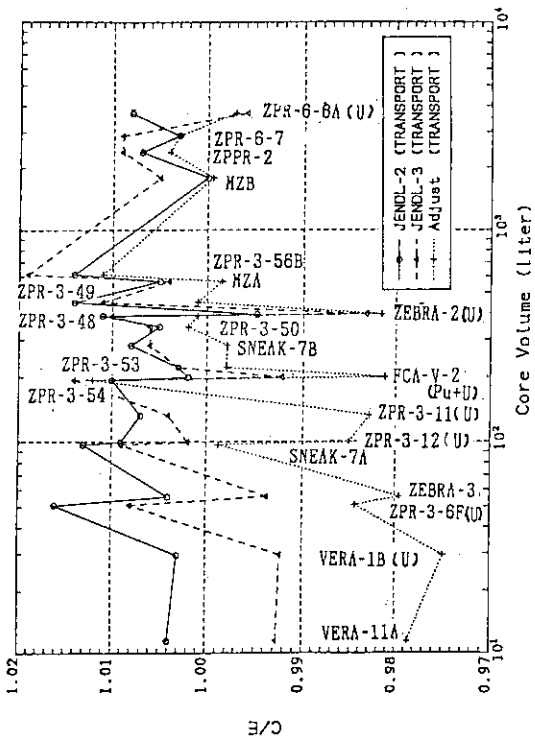

Fig. 11 Comparison of C/E values of k_{eff}

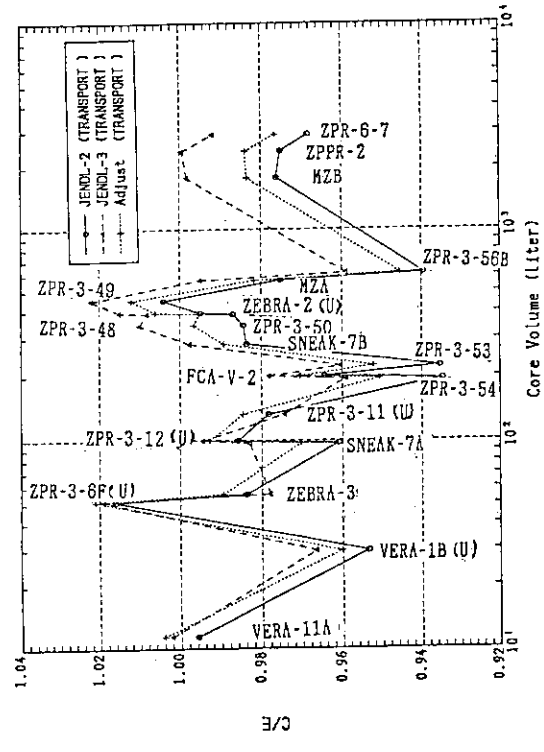

Fig. 13 Comparison of C/E values of F9/F5

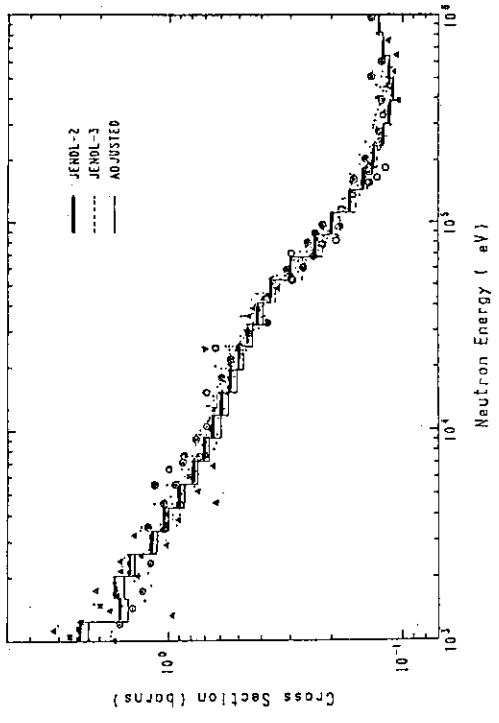

Fig. 10 Comparison of ^{238}U capture cross-section

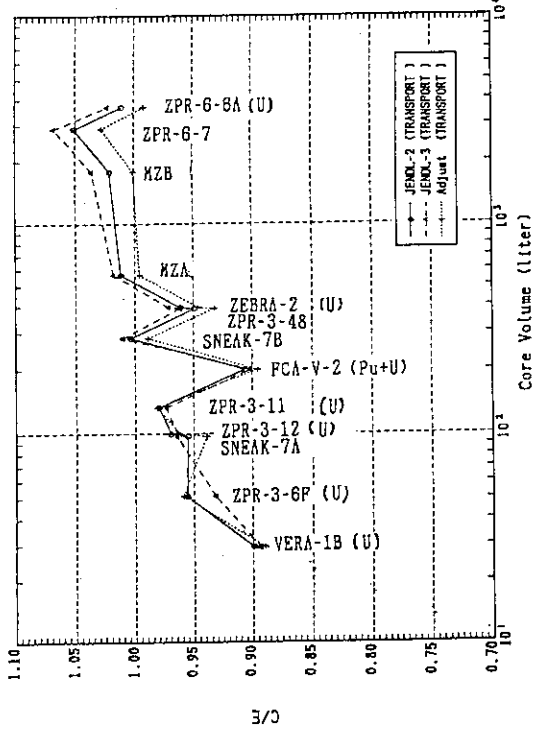

Fig. 12 Comparison of C8/F5

3.28 Systematics of (n,2n) and (n,3n) Reaction Cross Sections

WANG ZISHENG AND CAI DUNJIU
Instiute of Atomic Energy,P.O.BOX 275－41,Beijing,China

Abstract

Analyses of (n,2n) and (n,3n) cross sections are based on the compound decay,the preequilibrium emission and the direct reaction model.The results indicate that it is necessary to consider the odd even effect of neutron numbers in (n,2n) and (n,3n) cross sections .The (n,2n) and (n,3n) cross sections of many nuclides have been predicted and a good agreement with the measured data has been obtained.

Introduction

The (n,2n) and (n,3n) cross sections are of very importance for designs of the fission and fussion reactors. Many systematic studies have been done [1－5].But the contribution of the direct reaction and the odd even effect of neutron numbers have not all been considered in these works. However,with the incident neutron energy increasing,the contribution of the direct reaction is so important that it can not be ignored[1,2,4]. And the cross sections without considering the odd even effect of neutron numbers are not reliable for cascade reactions[5].for example,

. $^{158}Gd(n,2n)^{157}Gd(n,2n)^{156}Gd(n,2n)^{155}Gd(n,2n)^{154}Gd$

. $^{184}W(n,2n)^{183}W(n,2n)^{182}W(n,2n)^{181}W$

... ...

Systematic formulae

For the (n,2n) and (n,3n) reaction,the projectile neutron can be emitted from the direct reaction (D),the preequilibrium emission (PEQ) and the compound decay (EQ).In the calculation,it is neglected to emit two or more neutrons in the preequilibrium emition.It is assumed that only the inelastic scattering in the direct reaction is considered in the (n,2n) reactions and the direct reaction is neglected in the (n,3n) reactions.

We define the total cross section for (n,Xn) reaction (x = 1,2,3,…)as the follows,

$$\sigma_{n,M} = \sigma_{n,n} + \sigma_{n,n'} + \sigma_{n,2n} + \sigma_{n,3n} + \cdots$$

So the systematic formulae of $\sigma_{n,2n}$and $\sigma_{n,3n}$may be written as,respectively,

$$\frac{\sigma_{n,2n}}{\sigma_{n,M}} = \delta_d \left[\delta_p P_2^{PEQ} + (1-\delta_p)P_2^{EQ}\right] + (1-\delta_d)\left[\delta_{p'} P_{12}^{PEQ} + (1-\delta_{p'})P_{12}^{EQ}\right]$$

$$\frac{\sigma_{n,3n}}{\sigma_{n,M}} = \delta_{p'} P_{123}^{PEQ} + (1-\delta_{p'})P_{123}^{EQ}$$

where,

δ_d— the probability of the first projectile neutron emitted by the inelastic scattering process;

$\delta_{p'}$— the probability of the first projectile neutron emitted by the preequilibrium reaction process;

δ_p— the probability of the second projectile neutron emitted by the preequilibrium reaction process after the first emission of neutron in the inelastic scattering process;

P_2^{PEQ}— the emitted probability of the second projectile neutron in the preequilibrium reaction after the first projectile neutron in the inelastic scattering process;

P_2^{EQ}— the emitted probability of the second projectile neutron in the compound decay after the first projectile neutron in the inelastic scattering process;

P_{12}^{PEQ}— the emitted probability of the first projectile neutron in the preequilibrium reaction and the second projectile neutron in the compound decay;

P_{12}^{EQ}— the emitted probability of the two projectile neutron all in the compound decay;

P_{123}^{PEQ}— the emitted probability of the first projectile neutron in the preequilibrium reaction and the other two in the compound decay;

P_{123}^{EQ}— the emitted probability of the three projectile neutrons all in compound decay;

The calculation and simplification of expressions

(1) Calculation of $\sigma_{n,M}$

Based on experimental data,the total cross section may write as[1－5]

$$\sigma_{n,M} = \frac{\sigma_{n,M}}{\sigma_{n,\pi}} \sigma_{n,\pi} = \pi(0.12A^{\frac{1}{3}} + 0.21)^2 [1 - ke^{-m\frac{N-Z}{A}}]$$

where $\sigma_{n,e}$is the nonelastic cross section,A is nuclear mass in atomic mass unites,k and m are parameters to be fitted.

(2) Calculation and simplification of δ_d

In the Plane Born Approximation,the probability expression of the first projectile neutron in the inelastic scattering can be obtained

$$\delta_d = \frac{1}{4\pi R^2}\frac{k'}{k}\int\left|\int e^{-ik'\cdot r}V_{\beta\alpha}(r)e^{ik\cdot r}dr\right|^2 d\Omega$$

where

$$V_{\beta\alpha}(r) = \int\int\Psi_\beta^+ V\Psi_\alpha d\mathrm{n}d\mathrm{A}$$

$\Psi_\alpha$and $\Psi_\beta$are the internal wave functions for the inital and final nucleus,V is interaction potential,wich is given by[7]

$$V = (V_0 + V_1\sigma\cdot\sigma')\delta(\mathrm{r}-\mathrm{r}')$$

The target wave function is given by the Schrodinger equation,

$$\left[\frac{h^2}{2m}\Delta + V(\mathrm{r}) - \mathrm{C}(\mathbf{L}\cdot\mathbf{S})\right]\Psi = E\Psi$$

So the wave function has the following form,

$$\Psi = R_{n,l}(r)\Phi_{jm_l}(\theta,\varphi,S_z)$$

$$\Phi_{m_l} = \begin{bmatrix} \alpha_{lm_l}Y_{lm_l} \\ \\ \beta_{lm_l+1}Y_{lm_l+1} \end{bmatrix}$$

where, for $j = l + \frac{1}{2}$

$$\alpha_{lm} = \sqrt{\frac{l+m+1}{2l+1}}, \qquad \beta_{lm_l+1} = \sqrt{\frac{l-m_l}{2l+1}}$$

for $j = l - \frac{1}{2}$

$$\alpha_{lm_l} = -\sqrt{\frac{l-m_l}{2l+1}}, \qquad \beta_{lm_l+1} = \sqrt{\frac{l+m_l+1}{2l+1}}$$

Solving the Shrodinger equation,one can get

$$E = (N+\frac{3}{2})h\omega + C\frac{[j(j+1)-l(l+1)-\frac{3}{4}]}{2}$$

$$R_{n,l}(r) \propto r^l e^{-\frac{1}{2}\alpha^2 r^2} F\left(-n_r, l+\frac{3}{2}, \alpha^2 r^2\right)$$

The target nucleus excitation is caused by exciting valence nucleons in the different states according to the shell model.We only consider the neutron

excitations and make use of the particle number picture in the calculation of the single particle matrix elements.

For the sake of simplisity,we assume that the radial wave functions are

$$n_r = n_r' = 0, \qquad l' = l = 0$$

and the nuclear states are only changed by

$$\Delta l = 1, \qquad \Delta n_r = 0, \qquad or \Delta n_r = 0, \qquad \Delta l = -1$$

Therefore,the target excited states are only $\varepsilon_1$and ε_2.

$$for \quad j = l + \frac{1}{2}$$

$$\Delta l = 1, \qquad \varepsilon_1 = h\omega + \frac{C}{2} = 40A^{-\frac{1}{3}} + 10A^{-\frac{2}{3}}$$

$$\Delta l = -1, \qquad \varepsilon_2 = h\omega - \frac{C}{2} = 40A^{-\frac{1}{3}} - 10A^{-\frac{2}{3}}$$

$$for \quad j = l - \frac{1}{2}$$

$$\Delta l = 1, \qquad \varepsilon_1 = h\omega - \frac{C}{2} = 40A^{-\frac{1}{3}} - 10A^{-\frac{2}{3}}$$

$$\Delta l = -1, \qquad \varepsilon_2 = h\omega + \frac{C}{2} = 40A^{-\frac{1}{3}} + 10A^{-\frac{2}{3}}$$

The reduced mass is approximately equal to neutron mass.After averaging the the initial states and summing the final states,we can approximately get

for the odd neutron numbers

$$\begin{aligned}\delta_d = \frac{m}{4\pi h^2 R^2 \alpha^8}\{ & V_0^2[E_1^* d_{l,m_l}^2 (\alpha_{l,m_l}\alpha_{l+1,m_l} + \beta_{l,m_l+1}\beta_{l+1,m_l+1})^2 \\ & + E_2^* d_{l-1,m_l}^2 (\alpha_{l,m_l}\alpha_{l-1,m_l} + \beta_{l,m_l+1}\beta_{l-1,m_l+1})^2] \\ & + V_1^2[E_1^* d_{l,m_l}^2 (\alpha_{l+1,m_l+1}^2\beta_{l,m_l+1}^2 + \alpha_{l,m_l}^2\beta_{l+1,m_l}^2) \\ & + E_2^* d_{l-1,m_l}^2 (\alpha_{l-1,m_l+1}^2\beta_{l,m_l+1}^2 + \alpha_{l,m_l}^2\beta_{l-1,m_l}^2)]\}\end{aligned}$$

for the even neutron numbers

$$\begin{aligned}\delta_d = \frac{m}{2(2j+1)\pi h^2 R^2 \alpha^8}\{ & E_1^*[d_{l,m_l} V_0\sqrt{\frac{3}{4(j+1)}}(\alpha_{l,m_l}\alpha_{l+1,m_l} \\ & + \beta_{l,m_l+1}\beta_{l+1,m_l+1}) \\ & + d_{l,m_l-1} V_1\sqrt{\frac{3(2j-1)}{4(j+1)}}\alpha_{l+1,m_l}\beta_{l,m_l} \\ & + d_{l,m_l+1} V_1\sqrt{\frac{3}{8j}}\alpha_{l,m_l+1}\beta_{l+1,m_l+1}]^2\end{aligned}$$

$$+ E_2^* \left[- d_{l-1,m_l} V_0 \sqrt{\frac{3(2j+1)}{4j(2j-1)}} \left(\alpha_{l,m_l} \alpha_{l-1,m_l} + \beta_{l,m_l+1} \beta_{l-1,m_l+1} \right) \right.$$

$$+ d_{l-1,m_l-1} V_1 \sqrt{\frac{3(2j+1)}{8j(2j-1)}} \alpha_{l-1,m_l} \beta_{l,m_l}$$

$$\left. + d_{l-1,m_l+1} V_1 \sqrt{\frac{3}{8j}} \alpha_{l,m_l+1} \beta_{l-1,m_l+1} \right]^2 \Big\}$$

where,

$$E_1^* = (2E - \varepsilon_1) \sqrt{\frac{E - \varepsilon_1}{E}}, \qquad E_2^* = (2E - \varepsilon_2) \sqrt{\frac{E - \varepsilon_2}{E}},$$

$$d_{l,m_l} = \sqrt{\frac{(l+1)^2 - m_l}{(2l+1)(2l+3)}}$$

(3) Calculation and simplification of δ_p,$\delta_{p'}$

The probability of escaping the preequilibrium emission and the forming compound is D(n,C),so the probability in preequilibrium process is given by

$$\delta_p = 1 - D(2,C)$$

$$\delta_{p'} = 1 - D(3,C)$$

In the general case,we have

$$L < \lambda_{+2} \qquad (L \sim (0.2 - 0.4)\lambda_{+2})$$

So we can approximately get

$$\delta_p \approx 1 - exp\{ - \sum_{\substack{i=2 \\ \Delta i=2}}^{\bar{n}} \frac{L(i)}{\lambda_{+2}(i)} \}$$

$$\delta_{p'} \approx 1 - exp\{ - \sum_{\substack{i=3 \\ \Delta i=2}}^{\bar{n}} \frac{L(i)}{\lambda_{+2}(i)} \}$$

Only cosidering neutron and proton emission,we take it assumption that neutron formation cross section $\sigma_c$is constant and the proton formation cross section is $\sigma_c \left(1 - \frac{V_c}{E_b} \right)$.In terms of Marshell Blann formula[6], and setting $\bar{n} = i_0$ ($i_0 = 2,or\ 3$),we get

$$\sum_{\substack{i=2 \\ \Delta i=2}}^{\bar{n}} = \frac{L(i)}{\lambda_{+2}(i)} = 3G \frac{A^{\frac{2}{3}}}{\varepsilon} \left[\left(1 - \frac{B_2}{\varepsilon} \right)^2 + \left(1 - \frac{B_2 + V_c}{\varepsilon} \right)^2 \right]$$

$$\sum_{\substack{i=3 \\ \Delta i=2}}^{\bar{n}} = \frac{L(i)}{\lambda_{+2}(i)} = 4G \frac{A^{\frac{2}{3}}}{E + B_2} \left[\left(1 - \frac{B_2}{E + B_2} \right)^3 + \left(1 - \frac{B_2 + V_c}{E + B_2} \right)^3 \right]$$

where,$B_2$is the (n,2n) separation energy,G is a parameter,$V_c$is coulomb potential.

(4) Calculation and simplification of P_2^{PEQ}, P_2^{EQ}

The first step in the inelastic scattering process and the second step in the compound decay or the preequilibrium emission process can be schematically represented by

$$n(E) + A(0) \rightarrow A(E - E_1) + n(E_1)$$
$$\downarrow G_2(E, E_1, E_2)$$
$$(A - n)(E - B_2 - E_1 - E_2) + n(E_2)$$

where branching ratio $G_2(E,E_1,E_2)$ is the probability that the remaining nucleus only emits a neutron. $\varepsilon = E - E_1$ is the excited energy of the target. The Marshall Bann formula[6] is written as

$$\rho(\varepsilon \rightarrow E_2) = C_n E_2 (\varepsilon - E_2)(n^2 - n)$$

where $C_n = 1 / \varepsilon^n$ is normalizated constant in $[0,\varepsilon]$, $(\varepsilon = \varepsilon_1, \text{or} \varepsilon_2)$.

$$G_2^{PEQ} = \frac{L_n}{L_n + L_p} = \frac{1 - B_2 / \varepsilon}{(1 - B_2 / \varepsilon) + [1 - (B_2 + V_c) / \varepsilon]}$$

$$P_2^{PEQ} = \int_{W_3}^{W_2} \rho(\varepsilon \rightarrow E_2) G_2^{PEQ} dE_2$$

$$= G_2^{PEQ} \left[\left(1 - \frac{W_3}{\varepsilon}\right)^2 - \left(1 - \frac{W_2}{\varepsilon}\right)^2 + \frac{2W_3}{\varepsilon}\left(1 - \frac{W_3}{\varepsilon}\right) - 2\left(1 - \frac{W_2}{\varepsilon}\right) \right]$$

where, setting $\bar{n} = 2$.

For the compound decay, the projectile neutron energy distribution is approximately given[1－2] by

$$P_1(E \rightarrow E_1) = \frac{1}{\theta_1^2} E_1 e^{-\frac{E_1}{\theta_1}}$$

$$P_2(E \rightarrow E_2) = \frac{1}{\theta_2^2} E_2 e^{-\frac{E_2}{\theta_2}}$$

where E_1 and E_2 is the energy of the first and second projectile neutron, respectively.

$$\theta_1 \equiv \left(\frac{E}{a_A}\right)^{\frac{1}{2}}, \qquad \theta_2 \equiv \left(\frac{E - B_2 - 2\theta_1}{a_A}\right)^{\frac{1}{2}}$$

a_A is a level density parameter[1－3].

$$G_2^{EQ} = \frac{L_n}{L_n + L_p} = \frac{2\theta_2}{2\theta_2 + (2\theta_2 + V_c) e^{-\frac{V_c}{\theta_2}}}$$

$$P_2^{EQ} = \int_{W_3^*}^{W_2^*} P_2(E \rightarrow E_2) G_2^{EQ} dE_2$$

$$= G_2^{EQ}[(1 + X_{32}^*)e^{-X_{32}^*} - (1 + X_{22}^*)e^{-X_{22}^*}]$$

where,

$$W_i^* = \varepsilon - B_2, \theta_2^* = \sqrt{\frac{E}{a_A}}, X_{ij}^* = \frac{W_i^*}{\theta_j^*}, (i,j = 2,3)$$

(5) Calculation and simplification of P_{12}^{PEQ}, P_{12}^{EQ}, P_{123}^{PEQ}, and P_{123}^{EQ}

The processes of incident neutron n(E) being absorbed by target A(0), then emitting two or three neutrons can be schematically represented by

$$\begin{array}{l} n(E) + A(0) \rightarrow (A+n)(E+B_2) \xrightarrow{G_1(E,E_1)} A(E-E_1) + n(E_1) \\ \qquad\qquad\qquad\qquad\qquad\qquad\qquad\qquad \downarrow G_2(E,E_1,E_2) \\ \qquad\qquad\qquad\qquad\qquad\qquad\qquad\qquad (A-n)(E-B_2-E_1-E_2) + n(E_2) \\ \qquad\qquad\qquad\qquad\qquad\qquad\qquad\qquad \downarrow G_3(E,E_1,E_2,E_3) \\ \qquad\qquad\qquad\qquad\qquad\qquad\qquad\qquad (A-2n)(E-B_3-E_1-E_2-E_3) + n(E_3) \end{array}$$

For the preequilibrium emission, we use Marshall Blann formulae[6] fore the first two terms

$$\rho = 6C_3E_1(E-E_1) + 20C_5E_1(E-E_1)$$

where, $C_3 = 3/5E^3$ and $C_5 = 2/5E^5$ are normalizated constant in [0,E]

(I) For E $\langle B_3$,

$$\begin{aligned} P_{12}^{PEQ} &= \int_0^{W_2} \rho(E \rightarrow E_1) G(E,E_1) dE_1 \int_0^{W_2 - E_1} P_2 G(E,E_1,E_2) dE_2 \\ &= \frac{E^3}{E^3 + (E - V_c)^3} \frac{2\theta_2}{2\theta_2 + (2\theta_2 + V_c)e^{-V_c/\theta_2}} \{0.6Y_2^2(3 - 2Y_2) \\ &\quad - 3.6X_{12}^{-1}Y_2(1 - Y_2) + 3.6X_{12}^{-2}[(1 - X_{22} - 2Y_2 + Y_2X_{22}) \\ &\quad - (1 + X_{22})e^{-X_{22}}] + 7.2X_{12}^{-3}[(4 + X_{12} - 2X_{22}) \\ &\quad - (4 + X_{22} + X_{12})e^{-X_{22}}] + 0.4 - 2Y_2(1 - Y_2)^4 \\ &\quad - 0.4(1 - Y_2)^5 - 8X_{12}^{-1}Y_2(1 - 3Y_2) \\ &\quad + 8X_{12}^{-2}(1 - X_{22} - 6Y_2 + 3X_{22}Y_2) \\ &\quad - 8X_{12}^{-2}(1 + X_{22})e^{-X_{22}} + 16X_{12}^{-3}(12 - 6X_{22} + X_{12}) \\ &\quad - 6X_{12}^{-3}(12 + 3X_{22} + X_{12})e^{-X_{22}}\} \end{aligned}$$

$$P_{12}^{EQ} = \int_0^{W_2} P_1 G_1(E,E_1) dE_1 \int_0^{W_2 - E_1} P_2 G(E,E_1,E_2) dE_2$$

$$= \frac{2\theta_1}{2\theta_1 + (2\theta_1 + V_c)e^{-V_c/\theta_1}} \frac{2\theta_2}{2\theta_2 + (2\theta_2 + V_c)e^{-V_c/\theta_2}} \{1 - e^{-X_{21}}$$

$$- X_{21}e^{-X_{21}} - \frac{\theta}{\theta_1} X_{21}e^{-X_{21}}$$

$$+ \frac{\theta^2}{\theta_1^2}[(1 - X_{22})e^{-X_{21}} - (1 + X_{22})e^{-X_{22}}]$$

$$+ 2\frac{\theta^3}{\theta_1^2\theta_2}(e^{-X_{21}} - e^{-X_{22}})]\}$$

where, $W_1 = E, W_m = E - B_m, Y = W_m / E$ (m = 2,3,4)

$X_{ij} = \frac{W_i}{\theta_j}$ $(i = 1,2,3,4 \quad j = 1,2)$, $\theta = \theta_1\theta_2 / (\theta_1 - \theta_2)$

(Ⅱ) For E $< B_4$,

Assuming that the first and second projectile neutron is emitted at the same time, we get

$$P_{123}^{PEQ} = \int_0^{W_3} \rho(E \to E_1) G_1(E,E_1) dE_1 \int_0^{W_3 - E_1} P_2 G(E,E_1,E_2) dE_2$$

$$P_{123}^{EQ} = \int_0^{W_3} P_1 G_1(E,E_1) dE_1 \int_0^{W_3 - E_1} P_2 G(E,E_1,E_2) dE_2$$

The calculated result is obtained by replacing Y_2, X_{21}, X_{22} in P_{12}^{EQ} and P_{12}^{PEQ} with Y_3, X_{31}, X_{32}, respectively.

(Ⅲ) For E$>$ B_3,

In this region, we must consider the competion of $\sigma_{n,3n}$.

$$\sigma_{n,2n}(E > B_3) = \sigma_{n,2N}(E > B_3) - \sigma_{n,3n}(E < B_4)$$

$\sigma_{n,2N}$ is the sum of (n,2n) and (n,3n) cross sections.

(Ⅳ) For E$>$ B_4,

In this region, we must consider the competion of $\sigma_{n,4n}$.

$$\sigma_{n,3n}(E > B_4) = \sigma_{n,3N}(E > B_4) - \sigma_{n,4n}(E > B_4)$$

$\sigma_{n,3N}$ is the sum of (n,3n) and (n,4n) cross section.

The odd even effect of neutron numbers

Up to now, the odd even effect of neutron numbers have not been considered in systematics. Our study indicates that the odd even effect of neutron numbersis very important. It is that the calculated data are not agree with the experimental data in the odd neutron numbers. As shown in Fig 1－5 .

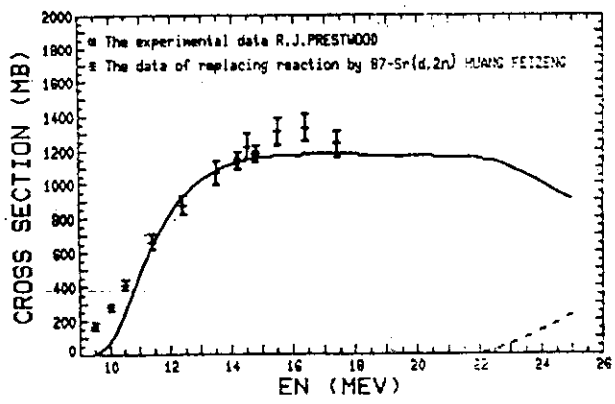

Fig. 1 39-Y-88(n,2n) and (n,3n) cross section

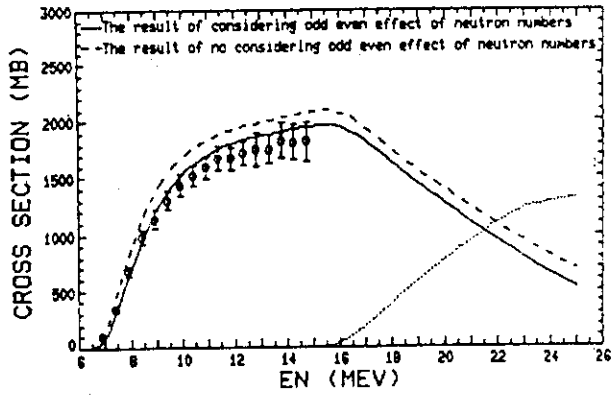

Fig. 2 64-Gd-157(n,2n) and (n,3n) cross section

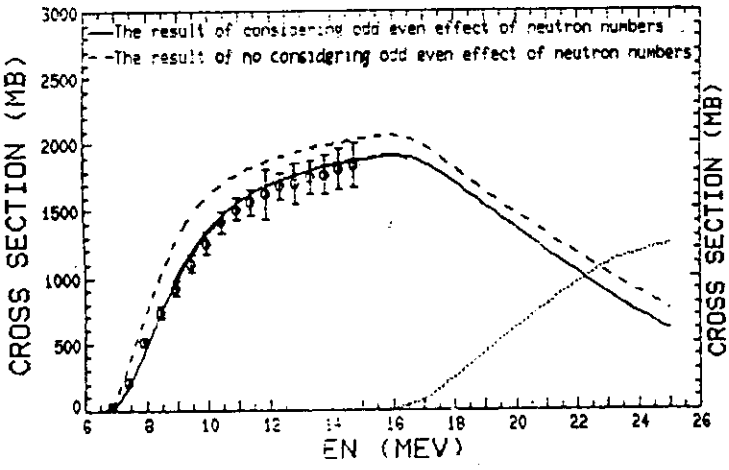

Fig. 3 64-Gd-155(n,2n) and (n,3n) cross section

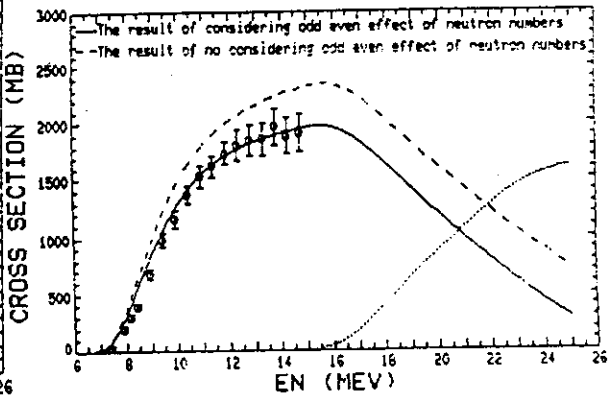

Fig. 4 82-Pb-207(n,2n) and (n,3n) cross section

The contribution of direct reaction to the (n,2n) cress section

In our study,we find that the calculated data are not agree with the experimental data with the incident neutron energy incressing,it means that the contribution of the direct reaction to the (n,2n) cross section in this region can not be ignored.As shown in Fig 6－10 .

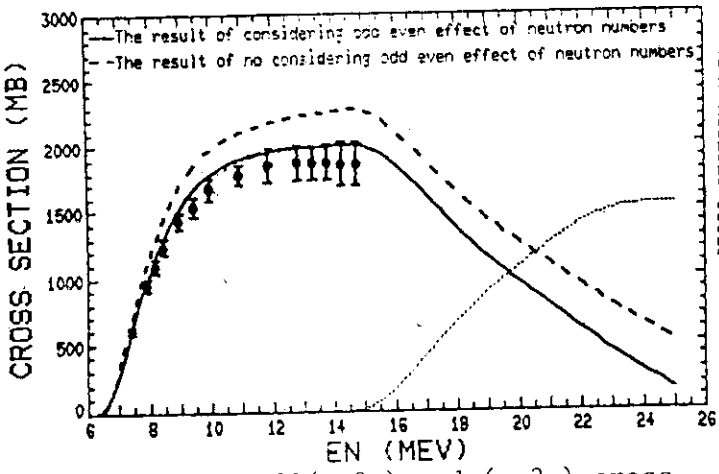

Fig. 5 74-W-183(n,2n) and (n,3n) cross section

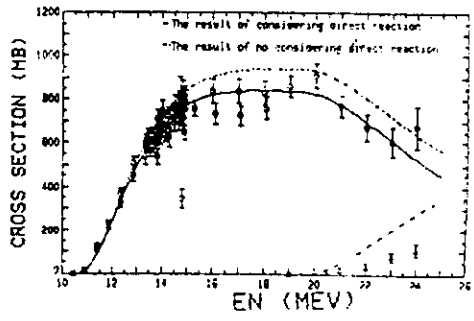

Fig. 6 27-Cd-59(n,2n) and (n,3n) cross section

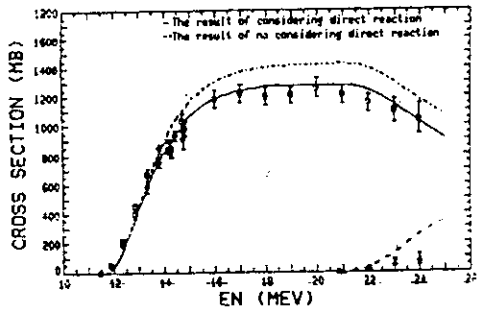

Fig. 7 39-Y-89(n,2n) and (n,3n) cross section

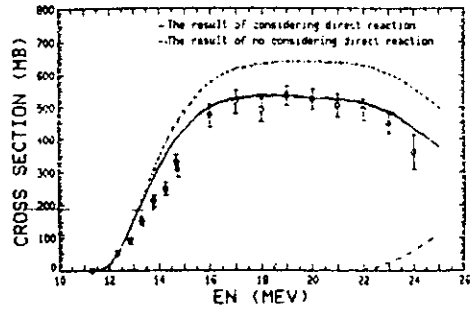

Fig. 8 21-Sc-45(n,2n) and (n,3n) cross section

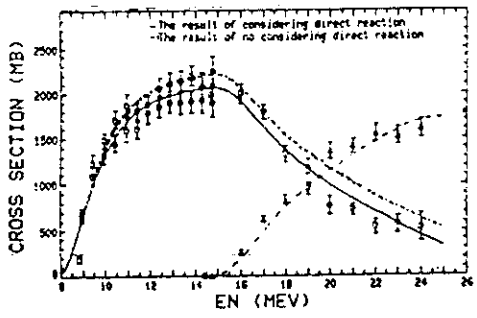

Fig. 9 71-Lu-175(n,2n) and (n,3n) cross section

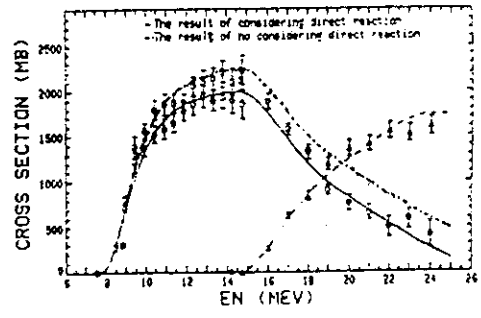

Fig. 10 73-Ta-181(n,2n) and (n,3n) cross section

Reference

1.M.SEGEV et.al Annuls of Nuclear Energy 5,239(1978)

2.M.SEGEV et.al Annuls of Nuclear Energy 7,577(1980)

3.S.PEARLSTEIN Nuclear Science and Energy 68,55(1978)

4.YAO LISHAN et.al MITO(Japan) 639(1988)

5.JIN ZHANG et.al IAEA－TECDOC－457 159(1986)

6.MARSHALL BLANN Physical review letters 21,1357(1968)

7.P.E.HODGSON Nuclear Reactions and Nuclear Structure Clarendon press oxford(1971)